Naoyuki Koide   *Editor*

The Liquid Crystal Display Story

50 Years of Liquid Crystal R&D that lead The Way to the Future

Springer

The Liquid Crystal Display Story

Naoyuki Koide

Editor

The Liquid Crystal Display Story

50 Years of Liquid Crystal R&D that lead The Way to the Future

Editor
Naoyuki Koide
Tokyo University of Science
Tokyo, Japan

Translator
Olaf Karthaus
Chitose Institute of Science
  and Technology
Chitose, Japan

Printed on acid-free paper

Preface

The 142nd Committee on Organic Materials Used in Information Science and Industry of the Japan Society for the Promotion of Science (JSPS) was established in November 1974. This committee has actively continued its research activities since then and now has entered its eighth research term (one term lasts 5 years). Meanwhile, the liquid crystal display (LCD) has been a wonderful achievement. When the committee was established, no one anticipated that the LCD could contribute so much to today's industrial field. In the transition of research and development during the early period, there was a growing opportunity that it would go beyond the contribution of this committee, which would become part of the history of the development of the LCD. The Technical Tradition Project arose accidentally from the University–Industry Research Cooperation Program (UICR) in JSPS. Fortunately, the project was adopted and was tentatively titled "Liquid Crystal—Past, Present, and Future".

The background that contributed to the innovation of the LCD, led worldwide by Japan, was the strong motivation for using liquid crystal materials as display elements. This story could hardly be told without the teamwork of university–industry research cooperation in different fields such as chemistry, physics, or electronics for development of the circuitry, the liquid crystal materials, and the liquid crystal-related elements.

I strongly requested that the early and later researchers should keep in mind, in writing about the development of liquid crystal materials or the related components of the LCD in advances from the electric calculator to the LCD: "A process and a way of thinking that preceded the invention and/or the discovery", and What brought about the breakthrough in industrialization of the LCD?

Chapters 1–8 of this book cover the topical research that provided a breakthrough in development of the liquid crystal display, from liquid crystals to devices. Because of the widespread field of diverse research activities in development of liquid crystal displays, the accomplishment of this aim would have been difficult with a single author trying to cover all aspects. Therefore, several knowledgeable authors who engaged in developing the field have been involved in writing the first eight chapters of the book.

Chapters 9–11 describe the story of the recent developments and the future perspectives in materials, physics, and functionality of liquid crystals, especially focusing on the contributions by Japanese research groups for the last decade.

On behalf of the editorial board, I wish to thank all the authors for their valuable contributions, their concerted efforts, and the time spent on this project, all of which made this book possible. Our special thanks go to Martin Schadt for his contributions in Sects. 1.2, 6.1, and 7.2. Last but not least, I wish to express our appreciation for having been granted generous financial support by the JSPS for this "Technical Tradition Project" for the UICR program. The grant enabled us to realize this book, *The Liquid Crystal Display Story: 50 Years of Liquid Crystal R&D That Lead the Way to the Future*.

Tokyo, Japan   Naoyuki Koide
December 2013

Contents

**Part II   Liquid Crystal Research Leading the Field
in the Twenty-First Century**

History of the 142nd Committee on Organic Materials Used in Information Science and Industry

Establishment

The announcement of the possibility of realizing a flat-panel display by applying an electric field to liquid crystal materials by G. H. Heilmeier et al. at RCA Laboratories in 1968 aroused considerable interest in liquid crystal research. The new display technique of controlling the transmittance and reflection of light was proposed, using organic materials of liquid crystal instead of the solid inorganic materials with a luminous phenomenon. This invention of the liquid crystal display (LCD) would match the needs of the watch and electronic calculator industry in Japan, and the "flower" of the LCD bloomed in Japan. The Sharp Corporation Group promptly took up the possibility of the LCD in a report of the RCA group. These circumstances are described by F. Funada in Sect. 1.1 in this book.

The Japanese industries was independently conducting research and development of the LCD, but the necessity for the domestic organization to grasp and solve the problem of whole organic materials synthetically from a scientific point of view was deeply felt. Therefore, the 142nd Committee on Organic Materials Used in Information Science and Industry of the Japan Society for the Promotion of Science (JSPS) was established with the aim of developing the technology for organic materials that would be especially relevant to the future of information science. The main projectors, Professor Masatami Takeda (Tokyo University of Science), Professor Shizuo Fujiwara (The University of Tokyo), and President Teru Miyazaki (Asahi Chemical Industry) have focused attention on information science based on organic materials. They anticipated that organic materials for the information industry would play an important role for future industry in Japan.

Installation was approved as a University–Industry Research Cooperation Program of JSPS, and the 142nd Committee on Organic Materials Used in Information Science and Industry was established in November 1974 for the purpose of research and development of organic materials supporting information science and technology. The membership of this committee has been limited to professors and senior research scientists from the industrial, administrative, and academic sectors.

Research Activity of the Committee

The committee created four subcommittees: liquid crystal materials, organic transducer materials, photosensitive materials, and multiple magnetic materials for information science. Membership in this committee from the time of its establishment has numbered 31 persons from academia and 50 from industry. The committee is currently conducting research by three subcommittees—liquid crystal materials, intelligent organic materials, and organic optical electronics—with 87 members from academia and 47 from industry. This committee has discussed and exchanged information by the leading researchers and the engineers from industrial, administrative, and academic sectors about the fundamental principles and applied technology for organic materials of information science. The committee has three major research activities: subcommittee meetings, joint meetings, and special meetings on special topics and current areas of interest. In order to grasp advanced information, the committee also offers lectures by researchers from overseas or makes reports on international conferences. These meetings play an important role in supporting scientific research in the interdisciplinary domain of information science and technology. Therefore, a committee symposium is held with a theme that is selected on present and future technical problems of developments for LCDs.

The committee has published the results of its work in Japanese once every 5 years (one term). The first result was published as a research report (1974–1979). The contents of the report for the liquid crystal materials subcommittee were as follows: (a) Applied technology of liquid crystal material (15 titles), (b) Molecular orientation of liquid crystal and its application (14 titles), (c) Chemistry of liquid crystal (8 titles), (d) Physics of liquid crystal (13 titles), (e) Various materials exhibiting liquid crystal (7 titles), (f) Electrochromism (3 titles).

The committee has also issued the following books in Japanese (translated titles here): *Liquid Crystal Term Dictionary*, *Liquid Crystal Device Handbook*, *Photoelectric Materials and Photoresist*, and *Materials for Intelligence Recording*. The *Liquid Crystal Device Handbook* was published by the Liquid Crystal Materials Subcommittee in September 1989. This book has been highly evaluated from all sides, worldwide. Until its publication, there were no books anywhere in the world giving a description from liquid crystals to the LCD using liquid crystal materials. These books published by the committee showed the high level LCD-related technology of Japan. Moreover, *The Liquid Crystal Term Dictionary,* published in 1989, contributed greatly to the standardization of liquid crystal terminology and the unification of the technical terms used in LCD technology.

The committee set up a liquid crystal symposium in 1975 as an annual meeting to provide a forum for exchanges among young liquid crystal researchers. The 1st Liquid Crystal Symposium was held at Kyushu University in the autumn of 1975, with the Chemical Society of Japan as a cosponsor. There were three special lectures: "Liquid Crystal Research for Chemistry," by Professor Narikazu Kusabayashi of Yamaguchi University; "Physical Phenomenon of the Liquid Crystal for the Application Side," by Professor Masanobu Wada of Tohoku University; and "Continuum Theory of Liquid Crystal," by Professor Kohji Okano of

The University of Tokyo. As well, there were 49 papers with more general titles. The symposium members have also organized mixers that have played a helpful role in information exchanges among young researchers from companies and universities. With the 17th symposium, the role of the Liquid Crystal Symposium was taken over by the inauguration of the Japanese Liquid Crystal Society. The last Liquid Crystal Symposium was held at Hokkaido University in 1991. There were two special lectures: "Molecular Geometry and Liquid Crystal Behavior — Revisited," by Professor Yoshio Matsunaga of Hokkaido University; and "Continuum Theory of Nematic and Chiral Smectic C Liquid Crystals," by Professor Tadashi Akahane of the Nagaoka University of Technology. Some 200 papers were presented with more general titles. We see, then, that liquid crystal research activity in Japan has made significant progress over the past couple of decades.

International Symposia

The 1st International Liquid Crystal Conference (ILCC) was held at Kent State University in the United States in 1965 with 42 participants. Thereafter, the ILCC has been held every 2 years. This committee organized the 8th ILCC in Kyoto in 1980 with 562 participants. Because there was no liquid crystal society in Japan at that time, the sponsoring body was this committee. The chairperson was Professor Masanobu Wada of Tohoku University, but he died suddenly before the conference and Professor Masatami Takeda of Tokyo University of Science served as the chairperson instead. I can well remember Professor Takeda's figure for the positive outcome of his negotiations with the JSPS or the Ministry of Finance in order to get duty-free authorization for deductions for contributions by companies. The state-of-the-art portable black-and-white LCD televisions exhibited at the conference by the Japanese electric companies were of special interest to participants. This exhibition emphasized the technical level for the LCD in Japan to all who attended, and the conference was a great success.

The 18th ILCC was held in Sendai in 2000, the second time the conference was convened in Japan. There were 813 participants (354 from overseas and 459 from Japan). The number of presentations was 886 (4 keynote lectures, 3 memorial lectures, 26 invited lectures, 86 general lectures, and 767 posters). Because the structure for cooperation by the taxation system of the JSPS differed then from that in 1980, preparations for the conference advanced comparatively smoothly. Surplus funds were contributed to both the International Liquid Crystal Society and the Japanese Liquid Crystal Society (JLCS), established in 1997. The money contributed to the JLCS was effectively utilized as "International Arts and Sciences Activity Assets" based on the initial fund.

The committee also organized the 4th International Conference on Ferroelectric Liquid Crystals in Tokyo in 1993. Many Japanese companies were very active in ferroelectric liquid crystals materials, especially a smectic C* liquid crystal phase in which is growing globally against a background of the next nematic liquid crystal, and the meeting was a great success.

This committee has organized a bilateral meeting, the Japanese–Italian Workshop on Liquid Crystals. The purpose of the workshop is to bring together members of the Japanese and Italian liquid crystal communities in order to present and discuss the latest results in research efforts carried out in these two countries. The workshops are hosted every 2 years by Japan and Italy in turn, with the host country providing support for the conference fees and the hotel expenses of the participants from the partner country. The sixth one of these biennial joint events was held in 2012 in Tokyo. The meeting was excellent both for the science and the friendly and collaborative climate between all the participants

Participation in Joint Research by This Committee

The research activity of the committee has been carried out through a national research project called "Research for the Future Program" supported by JSPS. The committee conducted a project entitled "Studies on Liquid Crystal Materials and the Stabilization of Orientation and Photopolymers" 1995–2000. There were nine research groups from universities and nine liquid crystal materials and device companies as supporting members of the committee.

In the JSPS Research for the Future Program, the committee supported and advanced research titled "Research and Development of Ultra-High-Speed and Ultra-High-Contrast Ratio Full Color LCD" for the realization of full-color LCD in which a movie display is possible. Professor Shunsuke Kobayashi of Tokyo University of Science in Yamaguchi (TUS) and head of the Liquid Crystal Research Institute of TUS were the chief examiners.

The contents of the project include: (1) Synthesis of liquid crystal materials and its evaluation, (2) Synthesis of liquid crystalline polymers (LCP) and its evaluation, (3) Synthesis of polymers for liquid crystal interfacial orientation and its evaluation (4) Preparation of the LCD cell and its evaluation, (5) Design and trial manufacture of a drive circuit, and (6) Trial manufacture of color sequential full color LCD.

This project has taken some advantage of the potential features of the ferroelectric liquid crystal (FLC) such as fast response speed and wide viewing angles. The project has succeeded in fabricating defect-free FLCDs that have given rise to a high contrast ratio of 700:1 by conducting a theoretical research and devising surface alignment method, and by adopting mesogenic polymer stabilization, achieving further success in fabricating FLCDs.

Activity Policy for Liquid Crystal Materials Subcommittee

Liquid crystals occupy a unique position as a condensed material in physics, because they appear as various types of existing matter. Liquid crystals will also bring great progress in technology as they are used for high-vision color LCD and

reflective color LCD. The Liquid Crystal Materials Subcommittee has discussed intensively the molecular design of low-molecular liquid crystal materials, the physical evaluation of liquid crystals, the control of orientation, and the evaluation of anisotropy for liquid crystal orientation film technology

The key subjects of the LCD at the present stage are (1) Development of new liquid crystal materials, (2) New orientation of liquid crystals, (3) High resolution and high quality of the LCD, and (4) Super low-power-consumption technology. In molecular design and the synthesis of new liquid crystal materials, the main topics of this committee are ferro- and anti-ferroelectric liquid crystals (1.6, 9.1, 9.2*), banana-type liquid crystals (9.4), liquid crystal polymers, liquid crystalline elastomers (10.2), and liquid crystalline gels for the establishment of synthetic technology and physical-properties analysis technology. Specific research subjects of the liquid crystal materials subcommittee are as follows:

1. Structure–property relationship of liquid crystal

   (a) A liquid crystal phase with novel molecular aggregation structure (9.1, 9.2, 9.4)
   (b) Physicochemical approach: supramolecular chemistry (9.3), computing science (10.5)
   (c) Molecular structure, an intermolecular interaction
   (d) Aggregation structure and macroscopic liquid crystal physical properties (10.4)

2. High-performance liquid crystal materials

   (a) Sophistication of operation speed and reliability
   (b) New liquid crystal materials corresponding to a new device mode

3. Interfacial orientation technique of liquid crystals

   (a) Breakthrough of the principle of liquid crystal interface from basic science
   (b) Next generation of oriented technique for liquid crystals

4. Development of novel LCDs (8.1, 8.2, 8.3)

   (a) Fast response, high brightness, wide-view angle, flexibility, memorization

5. Liquid crystal nano structure and its optical function

   (a) A hierarchical nano structure having liquid crystals
   (b) Photonic liquid crystals (11.3)
   (c) The nano structure formation utilizing the self-organization of liquid crystals, and its function (11.2)

6. Life science and liquid crystal

   (a) The elucidation of the reaction in the liquid crystal field
   (b) Bio-sensing devices
   (c) Drug delivery systems (11.5)

7. Environmental affairs and liquid crystal material

   (a) Electron- and ion-conductive liquid crystal material (11.4)
   (b) Waste disposal of LCDs

Thermotropic liquid crystals hold a dominant position in the field of the LCD; however, researchers have also to pay attention to another type of liquid crystals, lyotropic liquid crystals, from the aspect of the life science field. Essential properties of cell membranes originate from their liquid crystalline behavior. The point of view of biophysics exists in the liquid crystal discovery time inferred from the monograph of Otto Lehmann titled "The liquid crystal and life theory". In the experimental research of material science, the development of science cannot be expected without collaboration with a physicist, a physical chemist, and a synthetic chemist, as showing the history of research not only as that of liquid crystals but also of macromolecules and colloid science, among others. Because a considerable portion of a living organism (cell membrane, skin structure, etc.) is composed of liquid crystalline states, participation of researchers from many different fields is necessary for the bio-matter liquid crystal. I would hope to see the development of medical science, pharmacy, and foods by the full utilization of the potential of liquid crystal materials.

(*The numbers in parentheses indicate chapter and section numbers of the book.)

Part I
Breakthroughs in the Development of Liquid Crystal Displays

Chapter 1
Liquid Crystal Materials

Fumiaki Funada, Martin Schadt, Kazuhisa Toriyama, Haruyoshi Takatsu, Yasuyuki Gotoh, and Takashi Sekiya

F. Funada
SHARP Corporation, Nara, Japan
e-mail: funada61313@kcn.jp

M. Schadt
MS High-Tech Consulting, Seltisberg, Switzerland
e-mail: martin.schadt@bluewin.ch

K. Toriyama
Hitachi Ltd., Tokyo, Japan
e-mail: kazu-toriy@y4.dion.ne.jp

H. Takatsu
DIC Corporation, Saitama, Japan
e-mail: haruyoshi-takatsu@ma.dic.co.jp

Y. Gotoh
JNC Corporation, Tokyo, Japan
e-mail: y.gotoh@jnc-corp.co.jp

T. Sekiya
Advanced Technology Research Laboratories, Idemitsu Kosan
Co., Ltd., Sodegaura, Japan
e-mail: takashi.sekiya@idemitsu.com

1.1 Liquid Crystals for Dynamic Scattering Mode (DSM) Displays

Fumiaki Funada

1.1.1 Introduction: The Dawn of Development

The implementation of the black-and-white television broadcasting in the United States in 1939 was followed by color TV in 1953. Then, David Sarnoff, president of the Radio Corporation of America, had the next big dream to replace the furniture used to house cathode-ray tube TVs with picture frame that could be hanged on walls. He knew that the system development and element development needed an understanding of basic science as well as state-of-the-art technology and hired excellent researchers to work in the Princeton Institute of RCA in order to create the necessary new technologies.

It was under those circumstances that Richard Williams, who had joined RCA in 1958, started research on the necessary materials for flat-panel displays. He investigated the relatively unknown electro-optical effect of liquid crystals that had been reported by Glenn Brown et al. in a review in 1957 [1] and in George William Gray's book in 1962 [2].

Then, in 1962, Williams patented the light scattering type electro-optical effect by which a new type of flat-panel liquid crystal display (LCD) and electro-optical modulators can be operated [3]. He also published the scientific explanation for this effect in the following year [4]. But soon after Williams changed his research field and did not take part in the development to further implement this light scattering effect.

Right at that time, in 1962, George H. Heilmeier, a Princeton University PhD graduate who had received an RCA student fellowship joined the RCA research labs. There he showed interest in the liquid crystal research of Williams [5]. Heilmeier found that optically anisotropic dye molecules oriented in a liquid crystal matrix could be rotated in an electric field and that such guest–host systems showed a change in optical absorbance. He then investigated such systems for display applications, but because the difficulties in display clarity and lifetime/reliability issues could not be solved, the research was halted. Heilmeier instead decided to continue research on the Williams-type light scattering mode for LCD development.

Heilmeier became the leader of the new LCD development project and his project was strengthened as an important research project within the RCA company to actively advance the research and development.

As a result, on 28 May 1968 the executive vice president of the R&D made an extensive announcement on their achievement to the mass media. Moreover, because the press document clearly specified the possible applications for television, immediately companies around the world became interested in this new technology, which started a fierce competition in the global development.

Meanwhile, the management at Sharp, who had been worldwide the first company to develop the electronic calculator in 1964, also focused on such a development. At that time, a very important problem for the development of next-generation calculators was how to connect less power-consuming logic elements, such as the CMOS, with small displays, and RCA's achievement seemed to be a complete solution for the problem. Although the researchers at Sharp read about the LC research in publications and tried to test the reproducibility, no progress has been made due to the complete lack of commercially available LCs.

Sharp sold the first domestic black-and-white television sets just 1 month before the television broadcast started in Japan in February 1953. Thus, the Sharp management was intimately familiar with the top managements of RCA via TV patent license. Thus, just a few months after RCA's 1968 press conference, Sharp managers visited RCA and requested RCA to provide the LCD technology. However, RCA declined, saying that they could not provide such an LC technology, because it was still immature, and Sharp had to independently start their own R&D efforts. In 1970, they managed to fabricate the first in-house prototype display, in which the numbers were displayed in bright white because of the scattered light geometry of the device as in the RCA demonstration device. But the lifetime was extremely short and while watching, bubbles appeared in the device, the electrodes became damaged, and the image disappeared. It was clear from Heilmeier's papers [6] that under direct current conditions, the electrodes and liquid crystal material underwent oxidation or reduction reactions. Of course it was clear that by changing to alternating current (AC) driving, the redox reactions could be suppressed, but compared to a direct current (DC) device, an AC device performance was inferior, in addition to the fact that the AC current driver needed more complicated circuitry which would raise the manufacturing cost. Thus it was decided that performance and lifetime should be improved with sticking to the direct current design. Thus the tasks to consider were to increase the purity of the LC material and the stability of electrode materials. By autumn 1971 the lifetime of the devices had improved from minutes to thousand hours. However, lifetime improvement of more than one order of magnitude was required to further the development of the product, but which was like a large unsurmountable wall standing in the way. Other companies also faced this dire situation. At that time, RCA company itself recognized the difficulties in realizing a product and reduced its development group with their leading researchers, among them Heilmeier, leaving the company. This information has been transmitted to the outside and thus also to Sharp. Because of the inability to solve the lifetime issue, more and more companies stopped their development. Similar voice was also heard in Sharp.

1.1.2 Practical Development at Sharp

Going back in time a little bit, the specific research of LCDs was started in Sharp around April of 1969. The development of the flat cathode-ray tube was halted after the production and demonstration of a prototype in 1969. One of the engineers, Shunichi Shirokawa, started exploratory research of the LCD as the next research topic.

This topic was carried over to the group of Tomio Wada in 1970, and a prototype of a small LCD calculator was completed in the latter half of that year [7]. This LCD prototype display was bright and easy to see, its power consumption was of the order of μW, and all in all it showed the characteristics of a perfect calculator display. However, the not yet solved problem of display lifetime remained as a difficult situation. The search for solutions of the lifetime and reliability problems was intensified. Among researchers and engineers, voices were heard who said that "liquid crystals are organic materials and differ from semiconductors. It will be essentially impossible to create a long lifetime device."

Despite those circumstances, caused by the strong persuasion of Wada, the LCD R&D group was greatly expanded by six people, including the author of this chapter, to a total number of nine people, to become a full-scale research and development organization. A joint development framework with Dainippon Ink & Chemicals (DIC), who took the task of the development of liquid crystal materials, was established. A series of similar compounds were synthesized (among them N-(4-methoxybenzylidene)-4-butylaniline, MBBA) that showed a room temperature nematic liquid crystal phase [8]. A eutectic mixture of those compounds was made that showed an operating temperature from −15 to 68 °C.

In order to increase lifetime, the following aspects were examined: decreasing ionic impurities by increasing the purity of the LC material; using oxidation-resistant SnO_2 as a transparent anode material; using chemically stable Au/Pt alloys as the material for the reflecting cathode material; and using Ti/Pd as getters for hydrogen. The lifetime could be improved by over a thousand hours by these measures, and the in-house calculator division even came out with a lifetime of 10,000 h. However, for several months the "wall" of lifetime increase did not bulge, even though the study of the electrode material and purification of the liquid crystal material further advanced.

By autumn 1971, there was a growing body of in-house opinion that the display for next-generation electronic calculators should not be the short-lived LCDs, but reliable light-emitting diodes (LEDs) despite their high power consumption.

Because several influential domestic and international companies had abandoned LCD development, also within Sharp there were voices who want to review the LCD activities.

In this situation our eyes caught one paper. The Orsay LC group with its leader Pierre-Gilles de Gennes published a theoretical paper that the molecular motion of liquid crystalline molecules which cause the DSM effect could be generated even in AC-driven devices due to the anisotropy of the dielectric constant and the conductivity of the liquid crystal [9]. From this paper it became clear that if the AC driving cycle time is longer than the dielectric relaxation time of the ions in the liquid crystal, but shorter than the transit time of the ions passing between the electrodes, electrochemical reactions at the electrodes such as oxidation–reduction should be limited. We were thus convinced that a good light scattering effect similar to this in DC-driven devices could be obtained in AC devices.

By the way, in the paper Williams himself discussed in his 1962 paper both AC- and DC-driven devices. However, mainstream academia and industry were leaning towards the DC drive approach laid out in the paper on the DSM effect by Heilmeier in 1968. Companies thought positively on the relatively simple DC

drive rather than a slightly more complicated AC circuit for commercial liquid crystal displays. Thus DC driving of liquid crystals had become the norm. Generally, research was based on the belief that the issue of lifetime will be resolved by finding stable materials for the electrochemical oxidation–reduction reaction, such as in the DC-driven devices.

The liquid crystal material at that time had been raised to the maximum purity by repeated purification. Because of the decrease in residual ion concentration, the ionic conductivity of the liquid crystal decreased and the frequency conditions which the Orsay LC group had reported could not been met at all. Hence there was a situation for which good display characteristics in AC-driven devices could not be obtained.

Thus, the author, as well as the Orsay group, was willing to reproduce the requirements laid out in the proposal for AC-driven devices. But newly hired company employees hesitated to add ionic impurities to the highly purified liquid crystal materials, which cost up to several 10,000 yen (around several US$100) per gram, and thus research did not progress for quite a while.

Then, one day, good fortune struck. One morning I found that the lid of a sample flask that contained MBBA, which is a Schiff base, had not been closed the evening before. I thought that "maybe a hydrolysis reaction of the liquid crystal had occurred that would increase the ionic impurity to a level that would satisfy the Orsay group condition for ionic conductivity of the sample" and immediately went on to do AC experiments with that sample. As a result I found that good DSM characteristics could be obtained in the range of a few 10 Hertz, which is the necessary frequency for electronic calculators.

A deterioration of those characteristics did not take place up to voltages of several ten volts. Furthermore, aging experiments to determine the lifetime showed an improvement of stability and completely different characteristics than the DC-driven samples. We reported these results together with the background information of the Orsay LC group in a regular meeting in the department. There we suggested that highly pure liquid crystal materials that contained stable ionic compounds should become the focus in the development of AC-driven devices. The development of the trial product was carried out under this new policy to which all the groups agreed. The development of the ionic additive was carried out in cooperation with Dainippon Ink & Chemicals, too, and quaternary ammonium salts of organic acid showed the best results in terms of stability, solubility, and conductivity, and a joint patent application was made [10].

As a specific example of this invention, even at a low temperature of 0 °C, an AC frequency of 60 Hz can drive the liquid crystals that contain 0.05 wt% of para-aminobenzoic acid ammonium salt. Furthermore, a value of more than 10,000 h was predicted for its lifetime. Based on this discovery, liquid crystal materials for more practical DSM-LCDs were developed in about November 1971. Thus, the dual achievement of good display characteristics and device lifetime could be demonstrated to the electronic calculator division, and the adoption of LCD was decided.

When the decision was made, the concentrated resources of the whole company were used to put into practice the development of pocketable liquid crystal electronic calculator in 1972. The world's first mass production of liquid crystal

Fig. 1.1 The world's first mass production of portable electronic calculator with a liquid crystal display (Sharp EL-805)

electronic calculator EL-805, shown in Fig. 1.1, was shipped to the market in May 1973, which surprised many and triggered a lot of emotional responses from around the whole world.

1.1.3 Summary

For a future development, it should be important to note that the development of the LCD came naturally at that time, based on the available techniques, but putting it into practical use needed the presence of individuals who can read the social trends and needs of that time and overcome the various difficulties.

As social trends in the development of the LCD were concerned, there was the advent of the information society. Also, there was the presence of companies in Japan (Sharp, Suwa Seiko, and others) who were notable in leading the production of the LCD during the rapid progress of Japanese industry that supported consumer electronics technology. The presence of people with strong feelings who aim for the creation and commercialization of new products by utilizing state-of-the-art technology in those companies in particular was especially important.

It's also important to remember that semiconductors and liquid crystals originated from American and European military technology, but it was Japan that produced the first consumer electronic goods such as calculators and wristwatches.

A list of the important points for innovations are: (1) the progress of the scientific understanding of the science and physics of the liquid crystal of around 1960; (2) the development of integrated circuit according to Jack Kilby in 1959; (3) the discovery of the electro-optical effect in liquid crystals and the invention of the LCD by Williams in 1962; (4) the development of CMOS transistors by Frank Manon Wanlass in 1963; (5) the prototype presentation of the LCD by the research group of Heilmeier at RCA in 1968; (6) the synthesis of room temperature liquid crystal MBBA by Hans Kelker et al. in 1969; (7) the synthesis of the transparent ITO electrode by Yoshiyuki Katsube in 1969; (8) the proposal of a DSM theory by the Orsay LC group; and finally, (9) the decision to start the development of a simple calculator instead of a TV set in 1969.

This case study of LCD development also guides in terms of technology management for the innovation in the new fields in the future: (1) correct understanding of social trends; (2) understanding and utilization of the development status of key technologies; (3) appropriate setting of goals; and, finally, (4) the presence of a support system for human resources who contemplate challenges and motivation.
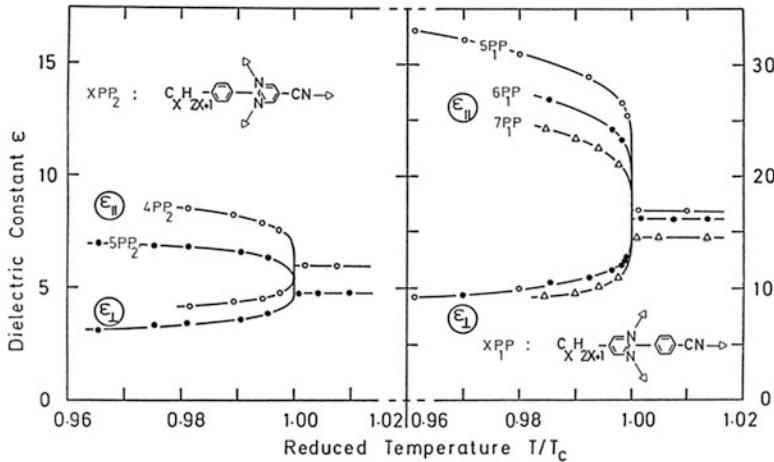
1.2   The First 35 Years of Positive Dielectric Liquid Crystal Material R&D for Field-Effect LCDs

Martin Schadt

1.2.1   Liquid Crystals for Field-Effect LCDs

Liquid crystal (LC) material research was in its infancy when Schadt and Helfrich [11] invented the twisted nematic effect in 1970 (Sect. 6.1). The few positive dielectric anisotropic liquid crystals known at that time were rather unstable and of poor electronic quality and they exhibited melting temperatures typically far above room temperature with much too narrow temperature ranges for practical use [12]. Except for the melting and clearing temperatures of LCs, only few of the approximately 20 anisotropic optical, mechanical, dielectric, and thermodynamic LC properties that are relevant for field-effect liquid crystal displays (LCDs) were known, and reliable experimental means for their investigation were hardly developed. Correlations between molecular functional groups, material properties, electro-optical performance, and LC quality were not attempted. Before Roche had abandoned its liquid crystal R&D in 1971 for 2 years, Schadt and his chemical colleagues had developed and patented new positive dielectric anisotropic liquid crystals for TN-LCDs (Sect. 6.1). These cyano-esters and Schiff bases were used by the author [13] for developing the first generation of room temperature TN mixtures with sufficiently fast response times and nematic operating temperature ranges extending from −20 to 65 °C. This first-generation TN mixtures was manufactured and sold by Roche after the company had reactivated its interdisciplinary liquid crystal R&D in 1973. Schadt was convinced that the prerequisites for the advancement of the new field-effect technology and potential future field effects were LC materials tailored to the effect-specific electro-optical requirements of LCDs. The author and his coworkers made strong efforts to compensate for their lost 2 years of LC material research and development (Sect. 6.1).

Ionic and polar organic impurities seriously hampered the lifetime of early TN-LCDs. Minute residual impurities irrelevant for pharmaceuticals caused deterioration of LCD alignment causing display failure. Apart from impurities introduced during LC manufacturing and contamination during display production, inherent molecular structural problems plagued the first commercial LC generation, especially the humidity-sensitive Schiff bases. Humidity diffusion through boundary seals of LCDs caused deterioration of nematic–isotropic transition temperatures and failure of surface alignment (cf. Fig. 6.4a in Sect. 6.1). To identify and get rid of sub-ppm LC impurities, new measuring techniques, accelerated lifetime tests, and new purification techniques had to be developed. A significant step towards structurally more stable nematic liquid crystals compared with the first LC generation of

Fig. 1.2 Temperature and molecular structural dependence of the dielectric anisotropy $\Delta\varepsilon = (\varepsilon_{\parallel} - \varepsilon_{\perp})$ of pyrimidine liquid crystals comprising differently positioned dipole moments in their rigid cores
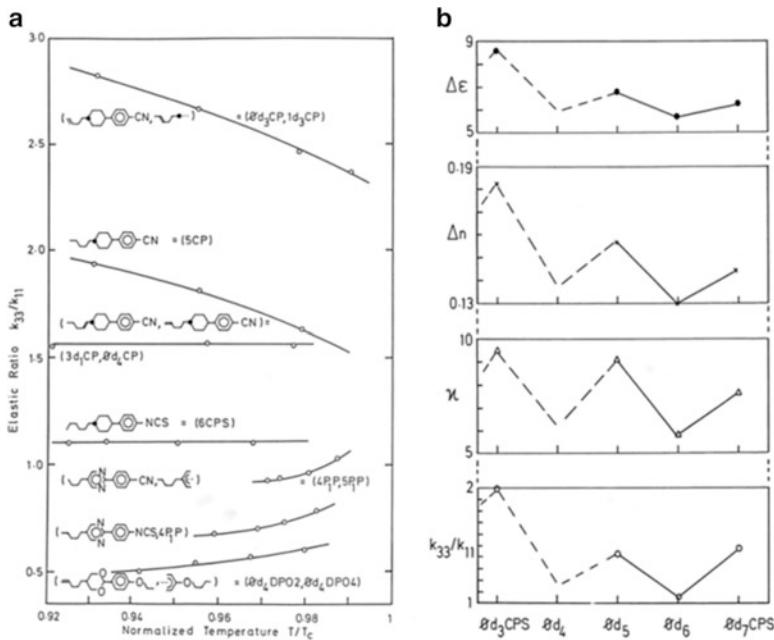
Boller et al. [13] at Roche was the invention of the second-generation LCs, i.e., the cyanobiphenyls of George Gray et al. [14], Hull University, in 1973. Gray published his biphenyls only a few months after Roche had reactivated its liquid crystal R&D. Schadt was impressed by their low viscosities, superior stability, and favorable thermodynamic properties. The author and coworkers immediately started investigating Gray's biphenyls and their compatibility with their own liquid crystals [13, 15]. The author was convinced that the more stable and faster responding biphenyls enable superior LC mixtures and started—together with the Roche TN-licensing team (Sect. 6.1)—licensing negotiations with the British Royal Signals and Radar Establishment (RSRE), Malvern, which owned the biphenyl patent rights. Roche and British Drug Houses were the only two LC manufacturers who reached a licensing agreement with RSRE. A few years later, BDH and its biphenyl license were acquired by Merck KGaA.

1.2.2 Molecular Structures, LC Material Properties, and LCD Performance

Until 1982 Schadt and coworkers successfully developed experimental techniques for reliably determining all relevant liquid crystal material parameters, i.e., optical $\Delta n = (n_{\parallel} - n_{\perp})$ and dielectric anisotropy $\Delta\varepsilon = (\varepsilon_{\parallel} - \varepsilon_{\perp})$, splay ($k_{11}$), twist ($k_{22}$) and bend ($k_{33}$) elastic constants, viscosity constants (η, γ_i), etc. This provided the basis for searching for correlations between molecular structural elements, LC material properties, and display performance [12, 16, 17]. Figure 1.2 illustrates an example

of this search for LC molecules with large positive dielectric anisotropy enabling mixtures for TN-LCD operation below 1.5 V battery voltage. They found that heterocyclic rings with strong lateral dipole moments—i.e., pyrimidine rings—in the rigid core(s) of LCs serve the purpose without unduly depressing liquid crystallinity and increasing viscosity [18]. Depending on dipole position in heterocyclic rings, large or small dielectric anisotropies $\Delta\varepsilon$ can be achieved (Fig. 1.2). Moreover, heterocyclic rings were found to reduce the splay/bend elastic ratio k_{33}/k_{11} of liquid crystals [16]. This led to the development of LC mixtures enabling steeper electro-optical characteristics of TN-LCDs, improved multiplexibility, and therefore increased information content [12, 17], enabling alphanumeric TN-LCDs for office equipment and portable calculators. The invention of the cyano-phenyl cyclohexanes (PCHs) by Eidenschink [19] et al. in 1977 led to a further reduction of LCD response. Equally important was the finding of Eidenschink that nonaromatic, directly linked rings in the rigid core of LC molecules are not detrimental to liquid crystallinity as was suggested by semiquantitative theories at that time. Moreover, PCHs enabled the development of stable LC mixtures with small optical anisotropy suitable for operation of TN-LCDs in the first wave-guiding minimum [20]. An interesting anecdote of a missed correlation between LC material properties and LCD performance is the first PCH patent of Merck. Initially Merck considered only those PCH components important that were "genuine" liquid crystals, i.e., LCs exhibiting liquid crystalline phases above their melting temperature T_m. Therefore, components with virtual nematic–isotropic transition temperatures below T_m—such as the short-side-chain phenylcyclohexane 5CP3 [21]—were not properly patent-protected. In 1976, i.e., before the PCHs of Merck, Schadt found that certain organic "solvents" serve as efficient viscosity reduction additives [22] in liquid crystal mixtures without unduly hampering mesophases. He filed a mixture patent on the viscosity reduction concept. Immediately after the PCHs became public his colleague Scherrer therefore synthesized short-chain PCHs. As expected, nonpolar, short-chain PCHs proved to be excellent additives for reducing the response times of LCDs without unduly depressing the nematic–isotropic transition temperatures of LC mixtures [21]. When Merck realized the value of their nonpolar PCHs, they negotiated a licensing agreement with Roche, enabling them to use their own short-chain PCHs for fast responding mixtures.
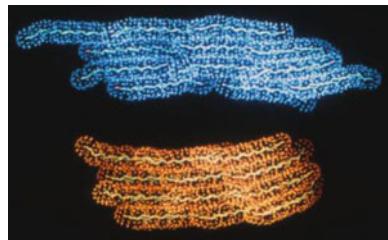
The replacement of polar cyano groups in positive dielectric nematic LCs by fluorine groups was first suggested by Sugimori [23] of Chisso Corporation in 1981. This was an important step towards liquid crystals with low ion solubility and large specific resistivity. With the advancement of thin-film transistor (TFT) addressing of TN-LCDs in the 1990s and subsequent TFT-addressed field effects for computer monitors and television, LCs exhibiting low conductivity became key [12, 17]. Initiated by the author, Roche and Dainippon Ink & Chemicals (DIC) founded in 1989 the joint venture company Rodic Ltd., Saitama, to mutually strengthen their nematic liquid crystal material business in Japan. The successful joint venture [24] was terminated when Roche decided to focus its business exclusively on life sciences and to divest its liquid crystal business (cf. M. Schadt, milestones in Physics (4), Communications of Swiss Physical Society SPS No. 43, to be

Fig. 1.3 (**a**) Dependence of the splay/bend elastic constant ratio k_{33}/k_{11} of different nematic liquid crystals on molecular structural elements versus normalized (reduced) temperature T/T_c. (**b**) Odd–even dependence of the material properties of a homologous series of Odi CPS alkenyl liquid crystals on side-chain double-bond position d_i ($i = 3,4,5,7$)

published) DIC was granted the right of continued use of those liquid crystal components of Roche that were commercialized by the joint venture during the collaboration, whereas the entire nematic liquid crystal material patent portfolio of Roche was sold to Merck KGaA in 1996.

The introduction of double bonds into specific side-chain positions of liquid crystal molecules by Schadt [25, 26] and coworkers in 1983 led to numerous important commercial liquid crystal classes in the years to come and provided new scientific and technological insights into correlations between molecular structural elements, LC material properties, and display performance [12, 17, 25–28]. Moreover, alkenyls rendered for the first time efficient molecular tuning of the elastic and viscoelastic constants of liquid crystals possible. The design of odd-positioned alkenyl LC mixtures with large bend/spay elastic constant ratios k_{33}/k_{11} enabled the development of LC mixtures with infinitely steep voltage-transmission characteristics in super twisted nematic (STN)-LCDs [12, 17, 29]. Today, nonpolar alkenyl LCs are key components in virtually all fast responding TFT mixtures. The measurements depicted in Fig. 1.3a illustrate the dependence of the elastic constant ratio k_{33}/k_{11} of different alkenyl liquid crystals on specific C=C double-bond positions [27]. The alkenyl double-bond odd–even effects depicted in Fig. 1.3b affect virtually all LC material properties [17, 27]. From experiments and molecular modeling Schadt and coworkers [26] attributed in 1989 the odd–even

Fig. 1.4 Computer model of the equilibrium conformations of two nano-ensembles of odd- (*top*) and even-positioned (*bottom*) alkenyl liquid crystals 1d$_3$CC (*top*) and Ød$_4$CC (*bottom*)

effects in alkenyl LCs to the formation of molecular nano-ensembles whose different shapes depend on double-bond position d$_x$, where d$_x$ specifies its position in the alkenyl side chain [26]. The Van der Waals representation in Fig. 1.4 illustrates the equilibrium conformations of two different alkenyl ensembles, namely a stretched, odd-positioned 1d$_3$CC nano-ensemble (top) and a bent, even-positioned Ød$_4$CC ensemble (bottom) [26].
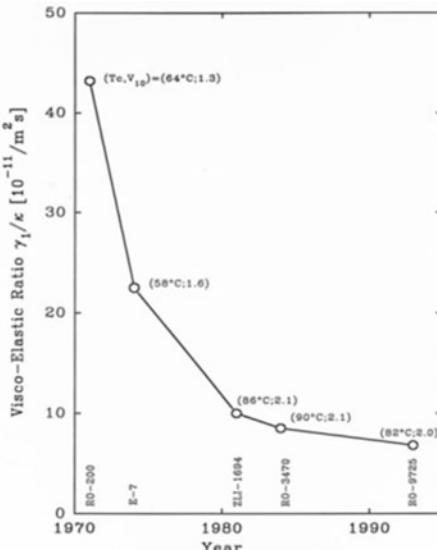
Figure 1.5 depicts a few important molecular structures of the hundreds of LC components which were invented, were commercialized, and have been used from the 1970s in LC mixtures, thus crucially advancing TN and subsequent field-effect LCDs [12]. Although negative dielectric and nonpolar LCs are equally important [30], the table focuses on typical positive dielectric anisotropic LC structures. The inadequate PEBAP on top of the list had been known from literature since the beginning of the twentieth century and was the primary positive dielectric aniso-tropic LC used for academic studies. Due to the lack of better LCs, PEBAP was also used by the author for his first twisted nematic experiments (Sect. 6.1). Because of the importance of the viscoelastic ratio γ_1/κ for TN-LCD response—small γ_1/κ values enable short response times [31]—Fig. 1.6 illustrates with this parameter the considerable LC material progress made during the first 35 years of field-effect LCD development. As shown in Fig. 1.6 the viscoelastic ratio γ_1/κ of commercial LC mixtures from Roche and Merck decreased during this period by about one order of magnitude. The timescale in Fig. 1.6 roughly correlates with the invention chronology of the LC families depicted in Fig. 1.5.
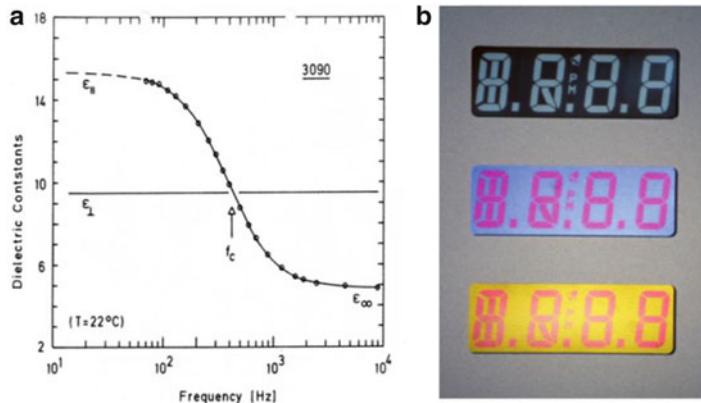
It is interesting to note the simplicity of the first commercial TN-LCD mixture RO-TN-200 developed and manufactured by Roche [13] in 1971. The mixture consisted—thanks to the excellent thermodynamic properties of its LC compo-nents—of just two Schiff-base homologues. Already the biphenyl mixture, E-7 developed by Raynes [32] 2 years later comprised five different LC components. To meet the numerous and often contradictory LCD requirements, modern LC mix-tures often consist not only of many more LC components but also of components belonging to very different liquid crystal families, enabling generating synergies between class-specific LC material properties. High-information content LCDs with short response times, operability over broad temperature ranges, etc., which are prerequisite for flat TV screens, monitors, iPhones, etc., would not have become possible without remarkable LC material progress.

1910	$C_7H_1 7O$-⬡-CH=N-⬡-CN	PEBAB (T_m, T_c = 106°C, 128°C)
1971	─⌐─⬡-CH=N-⬡-CN	Boller et al (Roche)
1972	─⌐─⬡-COO-⬡-CN	Boller et al (Roche)
1974	─⌐─⬡-⬡-CN	Grey et al (Univ. Hull)
1977	─⌐─⬡-⬡-CN	Eidenschink et al (Merck)
1977	─⌐─⬡-⬡-CN	Cereghetti et al (Roche)
1978	─⌐─⬡-⬡-CN	Eidenschink et al (Merck)
1981	─⌐─⬡-COO-⬡-F	Inukai et al (Chisso)
1983	─⌐─⬡-⬡-OR	Rich et al (Roche); Grey et al
1985	─⌐─⬡-⬡-CN	Schadt et al (Roche)
1991	─⌐─⬡-⬡-⬡-F	Takatsu et al (DIC and Roche)
1991 +	⬡-F ⬡-F,F ═══	Weitere Strukturelemente, etc, etc.

Fig. 1.5 Representatives of prominent LC classes whose discovery advanced field-effect LCDs

Fig. 1.6 Reduction of the viscoelastic constant ratio γ_1/κ of positive dielectric commercial LC mixtures developed from 1970 to the 1990s by Roche, BDH, and Merck. RO = Roche; E-7 = BDH and ZLI = Merck; γ_1 = rotational viscosity, $\kappa = (k_{11} - k_{22}/2 + k_{33}/4)$

Fig. 1.7 (**a**) Low-frequency relaxation of the parallel dielectric constant $\varepsilon_{\parallel}$ of a dual-frequency addressable nematic LC mixture. The dielectric anisotropy $\Delta\varepsilon = (\varepsilon_{\parallel} - \varepsilon_{\perp})$ changes sign at the crossover frequency f_{c}. (**b**) Three different color-switching guest–host LCD prototypes

1.2.2.1 Examples for Niche Application of Nematic Liquid Crystals

The above overview of nematic liquid crystal material development for field-effect LCDs from 1970 to 1995 is far from being complete. Many interesting and important aspects which advanced nematic liquid crystal R&D—especially those which have not made it into the nematic mainstream—are missing in this much too short review. The following two examples serve as an illustration for two R&D efforts made by the author that did not make it into the mainstream of LCD development.

The response times of nematic field-effect LCDs decrease with decreasing viscoelastic ratio of liquid crystals. Due to the angular momentum exerted on the dielectrically anisotropic LC director by applied electric fields, the turn-on time of an LCD decreases with increasing voltage, whereas its turn-off time is hardly affected by the field. To also actively reduce the turn-off-time the author [33] developed the concept of dual-frequency (2f) LCD addressing in 1982. 2f addressing is possible with LC mixtures exhibiting exceptionally low dielectric relaxation frequencies. This was achieved by combining polar components with long rigid cores with nonpolar, low viscous components [33]. Figure 1.7a shows the frequency dependence of a dual-frequency addressable LC mixture of Roche with its low dielectric crossover frequency f_{c} in the low audio frequency range [33]. 2f addressing of nematic LCDs enables the shortening of their turn-off times by more than one order of magnitude [33]. However, because of the temperature dependence of dielectric LC relaxation, 2f addressing is suitable only for applications with narrow operating temperature ranges [33].

The second example in Fig. 1.7b shows a photograph of a color-switching guest–host LCD prototype made by the author in 1979. The idea was to find a field effect

requiring neither polarizers nor color filters and whose contrast primarily depends on color perception [34] and not on light intensity modulation. Each of the three color-switching prototype LCDs in Fig. 1.7b comprises two different types of dichroic dyes. The dyes are characterized by different directions of their optical transition moments, namely parallel and perpendicular, to the long molecular axes of the nematic LC host. Color switching occurs upon electric field realignment of the dye molecules [24]. Due to limited dye stability and a too small contrast neither color-switching nor intensity-modulated guest–host LCDs succeeded.

1.3 TN Materials 2: Liquid Crystal Material for Multiplexed Liquid Crystal Display

Kazuhisa Toriyama

1.3.1 Historical Background in Relation to Multiplexed Liquid Crystal Devices

A multiplexing drive is the basic technology for liquid crystal displays (LCDs), and seen on a global perspective, its development was started in Japan [35]. Liquid crystal display development competition in Japan started in 1968 and it strongly motivated production cost reduction for the commercialized new LCD calculator. The large-scale integration (LSI) for device driving as part of the system (i.e., the LC calculator) must be and was coordinated with the development of the liquid crystal material. In 1968, G. Heilmeier of RCA Corporation announced the dynamic scattering mode (DSM) LCD [36, 37], and this event stimulated research and development of the drive circuits for LCD use. As we trace the history of the development of LC material for LCD calculators (small handheld), we must recall and see the so-called calculator war. In 1970, Tomio Wada, a researcher of Sharp Corp (his background was applied chemistry), who has described his progress vividly in the literature, embarked [38] on a research in his laboratory [39] (see also Part 1, Sect. 1.1.1). Many difficult obstacles were overcome and 3 years later, in 1973, the world's first calculator with a dynamic scattering mode LCD was commercialized. Even though it was the most advanced innovative technological achievement (the history of technology transfer from the RCA Corporation is detailed in Johnston [40]), some problem in the electric characteristics of the dynamic scattering mode, such as the high operating voltage of 10 V or more, the chemical instability of the liquid crystal material (a Schiff base), and further problems with response characteristics at low temperature [41, 42] could not make head against another new mode of LCDs, the TN mode (twisted nematic mode) [43]. Thus began the "calculator war." This is a keyword that represents the

characteristics of the industrial society in Japan at that time. More than 40 electronic companies competed in the race for the TN mode LCD technology development for the calculator market [44].
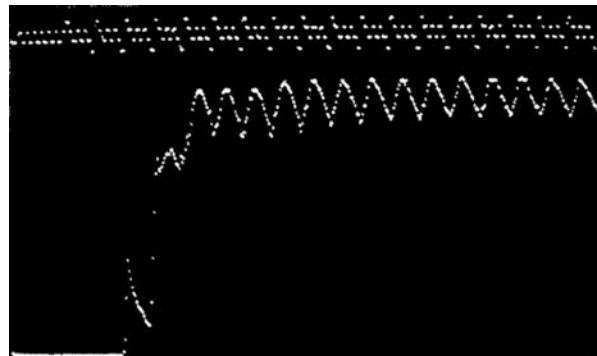
The development of multiplexing technology for wall-mounted TV was deployed simultaneously with the development of small liquid crystal device. It started from David Sarnoff (1891–1971), chairman of RCA, who predicted on the flat-panel screen in a lecture [38, 45] in 1956. Sarnoff did not envisage a LC display, but he was rather expecting that a solid-state crystal phenomena known as electroluminescence would be used. However scientists and engineers in Japan were working with strong expectations on the LCD by the end of the 1960s envisaging the future of liquid crystal. Four academic societies in the optics field (the Illuminating Engineering Institute of Japan, the Color Science Association of Japan, the Society of Photography and Imaging of Japan, and the Applied Optics Seminar) established a technical committee in October 1969 to forecast technological advancements from medium (1980–1990) to long term (throughout the twenty-first century) by the Delphi method [46]. The realization of the 1990s LCD color television among various types of related optical technologies had been predicted at that time. In order to meet these prediction, large electronics-related companies had to start early for the development of such a television. For example, in 1972, the Ministry of International Trade and Industry funded a 3-year joint research and development project with Hitachi, Asahi Glass Corp., and Dai Nippon Toryo Corp., to develop a dynamic scattering mode (DSM) large-scale matrix display [47] (40×50 cm display, 7×9 dots per character, 640 characters). The liquid crystal material was developed by Dai Nippon Toryo applying Schiff-base nematic liquid crystals doped with various ionic additives. The matrix LCD technology applied to the DSM mode was succeeded by the TN liquid crystal matrix LCDTV [48, 49]. The liquid crystal material was designed to optimize higher multiplex ability (early stage of development of the matrix LCD was adopted the DSM mode, one of the reasons why LC material for TN mode has not yet matured).

1.3.2 Concept of Multiplexing Drive

Multiplexing is a method to be employed to drive the dot matrix type liquid crystal display, in which a large number of pixels are aligned in rows and columns, and the signal voltage pulse and the scanning voltage pulse are applied synchronously during the display operation. An example of the waveform is shown in Fig. 1.8 in Sect. 2.1.2 engineered by Hideaki Kawakami. The biggest problem with multiplexing of liquid crystals is the so-called cross talk problem. Cross talk originates inevitably because of the matrixed circuitry consists with capacitive elements (i.e., pixels) of the LCD. Examples of the electro-optical response of a liquid crystal to the driving waveform (in TN mode) are shown in Fig. 2.1 in Sect. 2.1.1.

First, when the voltage is applied (Fig. 1.8 shows the example of a device using a Schiff base with ionic additives), the liquid crystal shows a successive and
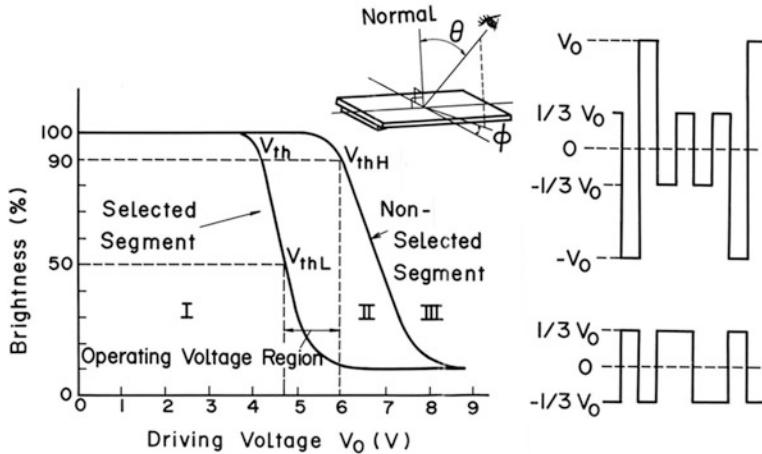
Fig. 1.8 Electro-optical
response waveform
that indicates the
rms-responding
characteristic and
accumulated response
for the optimized amplitude
selective addressing
scheme. 40 ms/div,
$N = 4$, $V_\mathrm{o} = 16$ V

accumulative electro-optical response in the dynamic scattering mode with an
initial rise time of 40 ms. This behavior is called "the accumulated response"
(Toriyama et al., private communication, 1972) [49] in which the scattering inten-
sity of the dynamic scattering mode saturates after three signal pulses as shown in
the figure. The (relative) brightness is uniquely governed by the applied effective
value of the voltage onto the LCD. In other words, the threshold voltage (V_th) that is
measured by the mean squared value is uniquely governed by the effective value of
the applied voltage, regardless of any of the waveforms adopted by a design. This
statement comes from that difference in the free energy of the LC in the cell before
and after the applied voltage is uniquely determined and is equal to the effective
value of applied voltage, where there is no energy loss in interaction between the
liquid crystal and external electric field [50]. There is no dependence on any
adopted field application process or an applied voltage waveform.

   Thus, two important concepts that are essential for the liquid crystal display can
be derived: the effective value dependence and the accumulated response. Thus, the
unique characteristic of the electro-optical effect of the liquid crystal material itself
should be and could be applied to the liquid crystal display driven by the optimized
addressing scheme that was designed to perform those two characteristics [51].

   From the standpoint of the molecular design of LC materials, the electro-optical
response, one must consider way to find a material that gives the best relation of
brightness to driving voltage (refer Fig. 1.9) and dynamic response (refer Figs. 1.8
and 2.1, respectively). Kawakami et al. collaborated with material scientist and have
studied [51] the driving method based on the root mean square dependence and have
concluded that the time-division multiplexing method of optimized amplitude
selective addressing scheme can be used. Equation (2.1) in Sect. 2.1.2 states that
the optimum condition for maximal contrast, the on/off voltage ratio ($V_\mathrm{s}/V_\mathrm{NS}$), is
unambiguously determined by the number of scanned lines, n. The contrast ratio
based on this rule applies in general to all liquid crystals regardless of their dielectric
anisotropy, elastic constants, etc. However, the threshold voltage is dependent on the
liquid crystal material. Furthermore, other circumstantial conditions and factors
such as operating temperature and viewing angle that might be considered in the
design of driving scheme depend on the liquid crystal material properties.

Fig. 1.9 Electro-optical response to the multiplexing drive of optimized amplitude selective addressing scheme with 1/3 duty and 1/3 bias

Taking into consideration the operating environment of the display and optimum conditions derived from the optimized amplitude selective addressing scheme, important parameters of the electro-optical characteristics of the device driving are induced with their definition as follows [52–54]: threshold sharpness characteristics of transmittance versus voltage (γ characteristic)

$$\gamma = V_{\mathrm{thL}}(0\,°C, \theta = 10°)/V_{\mathrm{th}}(0\,°C, \theta = 10°)$$

Viewing angle characteristics (β characteristics)

$$\beta = V_{\mathrm{thH}}(0\,°C, \theta = 40°)/V_{\mathrm{thH}}(0\,°C, \theta = 0°)$$

Temperature dependence characteristic (δ characteristics)

$$\delta = V_{\mathrm{thH}}(40\,°C, \theta = 40°)/V_{\mathrm{thH}}(0\,°C, \theta = 40°)$$

It is possible to define the operation margin α of the display using the above parameters with Eq. (1.1):

$$\alpha = \frac{V_{\mathrm{S}}}{V_{\mathrm{NS}}}(\beta/\gamma)\delta \qquad (1.1)$$

According to this equation, the operating margin α increases display quality when each of the three parameters, α, β and γ, is close to unity. Research and development of the liquid crystal could advance by investigating the liquid crystals refer with those parameter [53, 54].

1.3.3   Liquid Crystal Materials for Multiplexing Derive

Around the end of the 1960s, DSM (dynamic scattering mode) liquid crystal display was underestimated to be a high-performance display device, because of it's slow in their electro-optical response, and therefore high-speed multiplexing driving would be difficult. As discussed in the previous section, it was then discovered that a high-speed response could be achieved by the accumulated optical response by successive voltage pulses. These accumulated responses arise from dynamic behavior of charged species (which are from ionic additives to the liquid crystal material) under external electric field (i.e., applied voltage). For research works on the detailed mechanism, see [55–57]. The liquid crystal material used in those devices was the Schiff base MBBA (*N*-4-methoxybenzylidene-4-*n*-butylaniline), which was discovered by H. Kelker during his research on low melting point liquid crystals (Kelker, private communication, 1988). In 1975, a total design of the LCD electronic calculator, including the liquid crystal material design that fulfills the characteristic parameters for the dynamic scattering mode, was published in the IEEE Transactions on Electron Devices [58].

Since the announcement on the invention of TN-LCD [59] in 1970, the technological trend of LCDs for digital wristwatches and electronic calculators shifted towards the application of the twisted mode LCD (i.e., TN-LCD) because of a revelation of their superior characteristics. Research and development of nematic liquid crystal material for TN-LCDs was pushed forward in research organizations around the world, most prominently by the group of G. W. Gray (UK, Hull University) and RSRE (Royal Signals and Radar Establishment), Merck (West Germany), Hoffmann-La Roche (Switzerland), Chisso (Japan), and Dainippon Ink & Chemicals (DIC) (Japan). In 1973, Gray and others developed a biphenyl-based compound with para-positioned cyano groups that possess a positive dielectric anisotropy [60]. Those compounds showed superior chemical stability and low viscosity.

Until then, nematic liquid crystal molecules consisted of two aromatic groups that were connected by chemically labile structures, such as an azomethine group (–CH=N–) or an azoxy group (–N (O)=N–). The cyanobiphenyl molecules invented by Gray, on the other hand, linked the two aromatic rings directly and possess nematic liquid crystal phase with low viscosity at room temperature. By using biphenyls, the chemical stability was guaranteed. Eutectic mixtures of Gray's cyanobiphenyls (called eutectic 7, or E 7) were formulated by E. P. Raynes to commercialize LCDs used in clocks and electronic calculator. It needs to be mentioned here that those new nematic liquid crystals were synthesized in Europe and applied to the development of liquid crystal devices for the multiplexing drive. The timing of setting a symposium in 1975 was remarkable; the Brown, Boveri et Cie (BBC) Company held a symposium with the title "Nonemissive Electrooptic Display" that year. It was a small, 2-day symposium with less than 100 participants from Europe, the United States, and Japan, but this symposium considerably inflated the future development of the liquid crystal display. In the sixth and last session of the symposium, "Display Systems," chaired by Professor Shunsuke

Kobayashi, A. R. Kmetz (BBC) discussed [61] in his presentation entitled "Matrix addressing of nonemissive display" that there were few applications for a matrix addressing display though many non-emissive light electro-optical displays showed superior optical performance. The devices that use a voltage control (i.e., tunable) of birefringence LCD may be advantageous in multiplexing drive but suffer from poor appearance, especially in reflection. Dynamic scattering effect and the cholesteric texture change effect are obsolescent and may not be prominent in the future. At that time, in 1975, it was anticipated that the TN-LCD could be used for multiplexed displays for electronic calculators and clocks, but the breakthrough was not in sight and there was no optimism for a bright future.

The session in the symposium that was important for liquid crystal materials themselves had the title "Liquid Crystal Materials and Techniques" and was chaired by F. K. Kahn. Dietrich Demus (Halle University, East Germany) gave a lecture titled "Chemical Composition and Display Performance," in which the possibility for extremely superior display performance was outlined by using cyclohexane carboxylic acid phenyl ester liquid crystals (named ECH (Nakagomi 1997, private communication) liquid crystal later on in Japan). These types of compound show a wide temperature range of the LC phase, good chemical stability, and extremely low viscosity [62] (though they possessed small dielectric anisotropy that may cause higher driving voltage). It was important information for the R&D of LCDs brought from the other side of the Iron Curtain. Among the participants in this symposium, several key persons who may influentially contribute to liquid crystal material research were E. P. Raynes (RSRE, UK), D. Erdmann (E. Merck, West Germany), F. J. Kahn (Hewlett-Packard, USA), M. Schadt (F. Hoffmann-La Roche & Co. AG, Switzerland), and others. How did they run with that unexpected new information from Eastern Europe? What did the chemists, who attended at this symposium and who already knew about the low viscosity of cyanobiphenyls invented in 1973, think about new liquid crystal, cyclohexanecarboxylic acid phenyl ester system with low viscosity in the wide temperature range? Some thought of making mixtures of both types, biphenyl and ECH, and some thought about making molecules that hybridize both features. There are much more speculations that could be made, but the fact is that R. Eidenschink (E. Merck) in 1977 developed phenyl cyclohexane-ring containing compounds, particularly 4-*trans*-4-alkyl cyclohexyl benzonitrile [19]. This material was a low viscosity nematic liquid crystal that possessed positive dielectric anisotropy.

1.3.4 Development of White Liquid Crystals for Multiplexing Drive

The discovery of new liquid crystals and their continuing application to an early stage of liquid crystal display has been described in foregoing sections. In Sect. 1.3.2 it was outlined that difficult conditions had to be met for the application in multiplexing-driven devices. After the discovery by Gray of some

new kind of liquid crystal, the development strategy of these liquid crystal materials focused on meeting the condition mentioned above, not with a single liquid crystalline compound but in a mixture of various compounds. The method [63] conducted was based on classical thermodynamics, such as alloying liquid crystal compounds, expecting ideal behavior in the phase diagram [64], which evolved into a method to be applied to the next-generation calculator displays. Such a reductionist approach was followed by another approaches [65] of a molecular level model (such as association model [65]) based on liquid crystal molecular physics.

The first liquid crystal display for an electronic calculator with multiplexing drive was superior, but because it contained an azoxy compound [66] as the main component, it needed a color filter to prevent the photochemical deterioration, which was a perplexed problem for display quality. Biphenyl-based eutectic 7 (E 7) are colorless, but inferior to the former in terms of multiplexibility, and thus new mixtures are needed to be made. Mixed liquid crystals based on the cyclohexanecarboxylic acid phenyl ester system that was disclosed in the BBC symposium were adopted and developed by a Japanese electronics company [67]. This became the decisive factor to win the electronic calculator war, and it is credited as the major innovation of electronics and device engineering. By 1978, that is just 3 years after Demus' presentation at the BBC symposium, the white display calculators that were based on the novel technique of optimized amplitude selective addressing applying ECH mixtures of colorless LCs were leading the market for high-quality LCDs. Simultaneously, the molecular design of liquid crystals based on the microscopic-molecular model also advanced in the process of LC mixture design and contributed to the deepening of liquid crystal science.

1.3.5 Conclusions

Liquid crystal material for multiplexing drive was developed with an innovative drive technology called the optimized amplitude selective addressing scheme. This technology was developed to drive the dynamic scattering mode employing Schiff bases as the liquid crystal material. This was the first mode of the liquid crystal display in particular, and in a short term a technical achievement had been conducted. There was a discovery of the dynamic electro-optical phenomenon (the accumulative response phenomenon) that was a breakthrough for the high-speed multiplexing drive of the liquid crystal. This phenomenon opened the method to search liquid crystal material possessing optimized dynamic physical properties. The dynamic scattering mode, because of problems with reliability of the liquid crystal and the poor optical performance of the display, handed over the position to TN-LCD. The optimized amplitude selective addressing scheme that is based on the free energy conservation law was applied as a universal technique in TN cells. There was discovery of the new liquid crystal compounds in Europe that was the first half of material development, which was completed by the development of the alloying technology for LC material for display use in Japanese electronics and chemical

company in the latter half. The rapid progress of liquid crystal material development is persuaded with a sudden increase of the commercial market that ignited the electronic calculator war. Interdisciplinary corroboration between the basic research in the liquid crystal and the applications in display were effective and succeeded in building the strong basics for later liquid crystal display development.

1.4 Super Twisted Nematic Liquid Crystals

Haruyoshi Takatsu
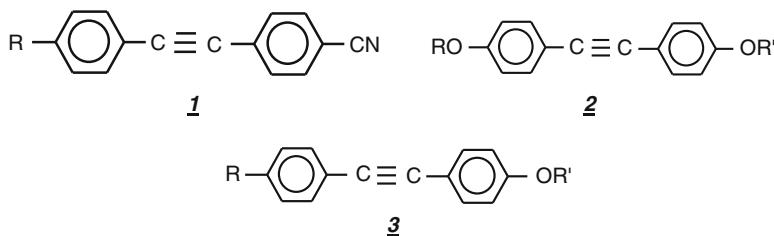
1.4.1 Introduction

By improving the multiplexibility of liquid crystal materials, it is possible to increase the number of scanning lines of an LCD. In case of the TN display, the ratio of the splay (k_{33}) and bent (k_{11}) elastic constants of the liquid crystal material needs to be minimal. However, in case of a STN display, a greater k_{33}/k_{11} is required, and thus the molecular design of the material and the design of the liquid crystal composition need to be changed greatly. In this section I describe how the liquid crystal material, comprising of a liquid crystalline tolan developed by DIC and a liquid crystalline alkenyl developed originally by Roche and industrialized jointly by DIC and Roche, became a mainstream material of STN liquid crystal displays by the synergy effect. And I also describe the drastic development of a liquid crystalline azine which has been used in a large screen monitor in 1997.

1.4.1.1 Liquid Crystalline Tolan

The limit of the optical anisotropy, Δn, of our material for a commercial calculator LCD in the 1970s was about 0.13. In the 1980s, the cell thickness of the LCD became gradually thinner, and the requirements of liquid crystal material were also diversifying. Hence, the development of liquid crystals with a large Δn was urgent. Because the π electrons of double bond increase the Δn, 1-cyclohexyl-2-phenylethylene or phenylethylene liquid crystals were synthesized that showed excellent characteristics. However, because of light-induced isomerization reactions, their chemical stability was not sufficient and they were disappointed as practical liquid crystals. Thus liquid crystalline tolan having a triple bond which does not undergo isomerization reaction became interesting.

We focused on 1,2-diphenyl acetylene, and some of the molecules with the general formula of *1*, *2*, or *3* in Fig. 1.10 showed liquid crystallinity and were known since 1973 [68]. Compound *1*, a 4-alkyl-4′-cyanotolan, could not be used as

**Fig. 1.10** Chemical structures of known liquid crystalline tolans
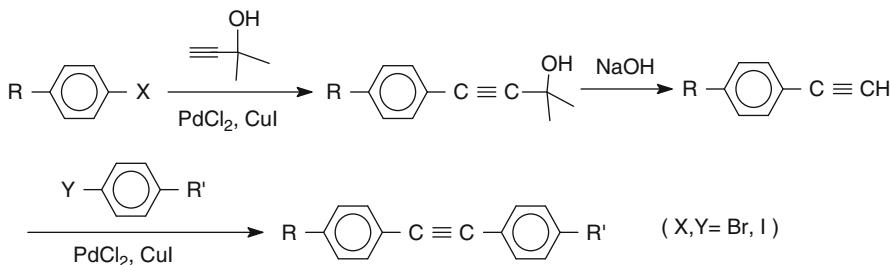
a practical liquid crystal cell, because of stability problems. However, compound *2*, a 4,-4′-dialkoxy tolan, and compound *3*, a 4-alkyl-4′-alkoxy tolan, were only known by their transition temperature, while other properties were not known at all. Furthermore, the synthesis and purification methods were insufficiently described in the patents and publications, and they were not considered useful candidates for practical use. Liquid crystalline tolan described above has not been noted at all for over 10 years for this reason.

STN-LCD has been mounted on a word processor for the first time in 1986. However, display performance such as contrast and switching speed was not very satisfactory. In particular, for applications in laptops or the like, improvement of the switching speed has been strongly demanded.
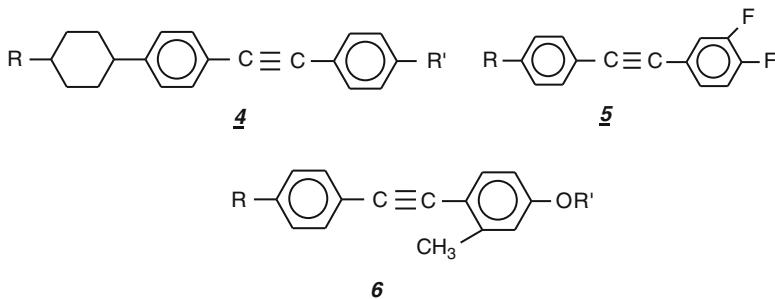
The response time (τ) is proportional to the product of the square of the cell thickness (d) and the viscosity (η) of the liquid crystal ($\tau \propto \eta \, d^2$). Therefore, when thinning the cell thickness by using a liquid crystal of low viscosity, a high-speed switching response is achieved with a large effect. Furthermore, it is necessary to set the product of cell thickness and Δn of the liquid crystal to a specified value in order to avoid interference fringes. Therefore, in order to reduce the cell thickness, a large Δn is required. That is, in order to achieve a fast response, the development of a liquid crystal material with large Δn and low viscosity has been awaited.

Properties that are always required for LC materials are a wide temperature range and a low viscosity. In order to broaden the temperature range, a liquid crystal compound with a high nematic–isotropic (NI) transition temperature is required. However, the NI temperature is generally correlated to viscosity. Compounds with a high NI transition temperature usually also have high viscosity. Furthermore, the liquid crystal with a larger Δn was considered to have a higher viscosity. Thus, a high NI transition temperature, a large Δn, and a low viscosity cannot be achieved in one compound. However, we were pleasantly surprised to find that liquid crystalline tolans have a large Δn of about 0.3, a NI transition temperature of about 70 °C, and a viscosity at 20 °C as low as about 20 mPa s.

However, these tolans synthesized by the conventional dehydrobromination reaction at first show low specific resistivity even if purified by utilizing distillation, columns and recrystallization, etc. Especially, due to the problem of heat stability, they tend to colorize at a high temperature, and the specific resistivity decreases by more than two orders of magnitude. We thought that at this level, tolans could not be used as a practical liquid crystal, and had no choice but to give up. At the end,

Fig. 1.11 Synthesis of liquid crystalline tolans by a coupling reaction
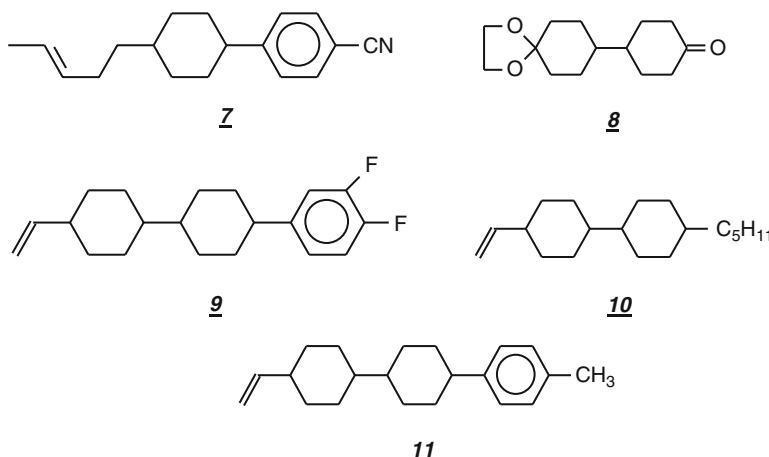
Fig. 1.12 Chemical structures of new liquid crystalline tolans

by using a newly developed coupling reaction for the synthesis of the tolan as shown in Fig. 1.11, we succeeded in the improvement of specific resistivity to the level more than 10^{13} Ω cm even after heating. Passing the stability test in a real LCD panel, we demonstrated that the liquid crystalline tolan can be used as a practical liquid crystal.

After the first hurdle had been taken, the subsequent development was fast. We developed a series of many useful liquid crystalline tolans *4*, *5*, and *6* [69], in Fig. 1.12, and prepared the liquid crystal mixtures having large Δn and low viscosity with high NI transition temperature such as DON-605: $\Delta n = 0.283$, viscosity at 20 °C $= 20.5$ mPa s, and NI transition temperature $= 100$ °C which can be a useful nonpolar host of STN liquid crystal.

The tolan liquid crystal drastically surpassed the other conventional liquid crystals having large Δn at that time such as a pyrimidine liquid crystal ($\Delta n = 0.196$, viscosity at 20 °C $= 37.7$ mPa s) or a biphenyl liquid crystal ($\Delta n = 0.195$, viscosity at 20 °C $= 52.8$ mPa s) in characteristics. By the synergy effect of the tolan and the alkenyl, the breakthrough of the trade-off relationship between the response and the contrast was achieved [70]. The STN-LCD, of which response time was improved from about 300 to 120 ms, was applied to a note PC, and the market was expanding. Now the liquid crystals including the liquid crystalline tolan are used widely in about 80 % of total liquid crystals for STN-LCD.
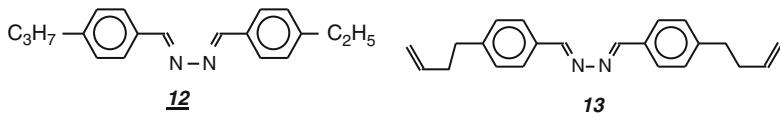
Fig. 1.13 Chemical structures of liquid crystalline alkenyls and the intermediate

1.4.1.2 Liquid Crystalline Alkenyl

At that time in 1986, the ratio of the bent and splay elastic constant ratio k_{33}/k_{11} did not improve and thus, the contrast of STN-LC displays could not be improved. There, Martin Schadt (Hoffmann-La Roche) introduced a new liquid crystal material. Around this time, Roche was in cooperation with DIC and supplied some LC materials, I visited the headquarters of Roche in Basel several times. The liquid crystalline allenyl *7* in Fig. 1.13 was introduced, which had a great characteristic. The double bond in the terminal group significantly changed the elastic constant ratio. After confirming the stability of liquid crystal, I was convinced that if we use *7* in conjunction with DIC's liquid crystalline tolan, we should be able to develop a state-of-the-art STN liquid crystal. In those circumstances that we negotiate with Roche about the use of *7*, the story progressed in an unforeseen direction: the establishment of a joint venture. After severe contract negotiations, Rodic started manufacturing and sales of the liquid crystal material in April 1988.

Collaborating with Schadt and his colleagues, we selected and commercialized the best suited liquid crystals from a large number of liquid crystalline alkenyls they had developed. However, the manufacturing cost of the original alkenyl liquid crystals was well above the market price of the liquid crystal material at that time, and the STN liquid crystal business of Rodic had a negative spread. Cost reduction became an urgent task, and we studied the process and synthetic route. We developed and mass-produced a key intermediate *8* in Fig. 1.13 and transferred the production of alkenyls to Japan. Then, we achieved a significant cost reduction. In addition to the liquid crystalline *7* having a cyano group [71], the fluorinated *9* and the hydrocarbon *10* and *11* in Fig. 1.13 improved the performance of the STN-LCD. Thus, alkenyl liquid crystals became the mainstream STN liquid crystals.

Fig. 1.14 Chemical structures of liquid crystalline azines

1.4.1.3 Liquid Crystalline Azine

In the LCD industry, there was a repeated battle between thin film transistor (TFT-LCD) and super twisted nematic (STN-LCD) technology for use in laptop computers. When in 1995 the sales of STN-LCDs had become recessive, the development of high-speed STN liquid crystals that contributed to the survival of STN-LCDs was strongly required from a leading LCD manufacturer. Without being bound by traditional stereotypes, there was a demand for high-speed liquid crystals that could compete with TFT-LCDs. The common sense at that time was that liquid crystals are to be colorless and transparent. However, if one looks at the beginnings of liquid crystal displays, the first room temperature liquid crystal, MBBA, and liquid crystalline azoxy have yellow color. In STN-LCDs, the color of the liquid crystal can be compensated by a retardation film. Thus azine liquid crystal which had been off-the-radar of development because of their color came up immediately. Azine liquid crystals show a superior hydrolysis resistance compared to the MBBA Schiff base. First, we considered liquid crystalline azine *12* in Fig. 1.14 that is described in a patent [72]. The sample met the demands of an improved response time and stability and cleared an internal evaluation procedure. Even though there were some great concerns and troubles because the unique properties of this new type of liquid crystal could not be understood, the joint work with LCD manufacturers could solve them. Finally, we developed a liquid crystalline azine *13* [73, 74] in Fig. 1.14 combining the azine and the alkenyl after the solution of some problems for a practical liquid crystal material. The liquid crystalline azine *13*, having 0.34 of large Δn and a nematic temperature range between 57 and 116 °C, surpassed the liquid crystalline tolan in the characteristics. The liquid crystalline azine shows more stable level than the tolan for the sun-test and has a sufficient stability for LCD application in spite of being colored yellow with 400 nm of the absorption edge wavelength.

The liquid crystalline azine *13* improved the trade-off relationship between the response and the contrast of the conventional STN liquid crystals comprising the tolan. By the serial development results for the STN-LCD, STN won a great victory over TFT in 1997 in a domain of large-sized LCD. Although all of the large-sized STN panels were replaced by TFT now, the liquid crystalline azine is used as an important component of the STN liquid crystals for a cellular phone and obtains high evaluation, being called "Golden liquid crystal" by customers in Taiwan and China in the 2000s.

1.5   Thin Film Transistor Materials: From Cyano Compounds to Fluorinated Compounds

Yasuyuki Gotoh
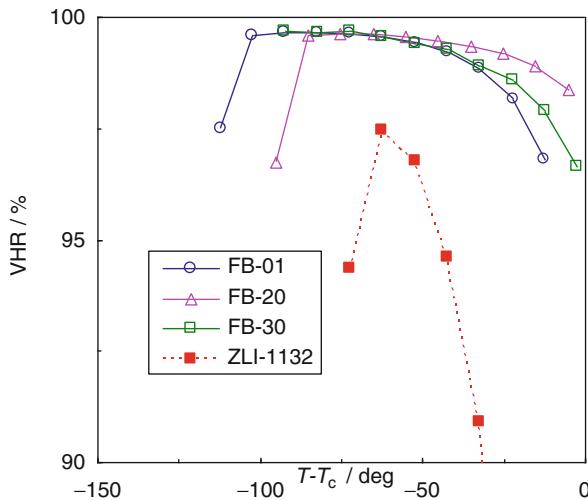
1.5.1   Introduction

There has been a remarkable development in the technology of liquid crystal display (LCD) devices in recent years. The driving method of LCDs can be classified into passive matrix (PM) and active matrix (AM) driving. For example, the former display drive is used in information displays, such as for audio sets in cars or in monochrome clock displays. The development of AM-LCDs came after the practical application of the PM-LCD and goes back to the end of the 1980s. The development of suitable liquid crystal materials occurred in parallel with the development of AM-LCDs.

The liquid crystalline benzonitrile-based cyano compounds that had been used in PM-LCDs were gradually replaced by fluorinated compounds developed in the 1980s. As the driving technology for displays has changed over time, liquid crystal compounds have also evolved. In this section, a partial overview of the developmental trends of AM-LCDs and trends in the physical properties of liquid crystal compounds and other materials are presented.

1.5.2   Discovery of Fluorinated Liquid Crystal Compounds and Liquid Crystal Material for the Initial Development of AM-LCDs

First, TN mode was considered for the development of AM-LCDs. There were attempts to directly make AM-LCDs by changing only the drive mode of PM-driven TN LCDs. However, display defects such as flicker occurred during durability tests, and it has been determined that long-term use would be impossible. Requests for improvements of the liquid crystal material were made very vaguely, and material manufacturers could not find a clear direction with respect to the development of AM-LCD liquid crystal materials for some time. In the 1980s a fluorophenyl cyclohexyl carboxylate was developed that showed a nematic liquid crystal phase near room temperature (see Table 1.3) [75]. Research in the 1950s showed that a fluorine group in the lateral position of a liquid crystal changes the layer structure of the liquid crystal phase, but nobody had the idea to replace the cyano group with a fluorine atom to introduce a large polarization in TN materials [76, 77]. At an early developmental stage, it was shown that fluorinated compounds

Fig. 1.15 Temperature dependence of VHR of fluorinated liquid crystal materials. FB-01: a compound of two types of molecules similar to chemical (f) shown in Table 1.3, but with different alkyl chain length. FB-20: a compound of two types of molecules similar to chemical (i) shown in Table 1.3, but with different alkyl chain length. FB-30: a compound of two types of molecules similar to chemical (c) shown in Table 1.3, but with different alkyl chain length. ZLI-1132: benzonitrile-based composition produced by Merck Inc.

have low viscosity, a small optical anisotropy, and a small dielectric anisotropy ($\Delta\varepsilon$), but that in spite of this small dielectric anisotropy, the driving voltage was lowered. During the development of AM-LCDs, Sharp Corp. proposed that a high voltage-holding ratio (VHR) is necessary [78].

At present, VHR is now well understood, but at that time, at the beginning of AM-LCD development, chemical manufacturers were groping in the dark as to how to achieve this goal of high VHR. It was found that the fluorinated compounds described above exhibited a high VHR, and thus its usefulness as a component for AM-LCDs was confirmed. This created the opportunity to develop fluorinated compounds. As shown in Fig. 1.15, the compounds that are fluorine-substituted at the end of the molecule show extremely high heat resistance in comparison with conventional compounds that are cyano-substituted, and as a result show a high VHR. Another reason for the use of fluorinated compounds in AM-LCDs is their excellent photostability and resistance.

1.5.3 Characteristics Required for LCDs

The required characteristics of LCDs differ greatly depending on application and environments. For example, PC monitors and TVs are commonly placed indoors where there is a constant power supply and the temperature fluctuation is not harsh.

Table 1.1 Relationship between response time of the LCD and rotational viscosity of liquid crystal materials (example: TN monitors)
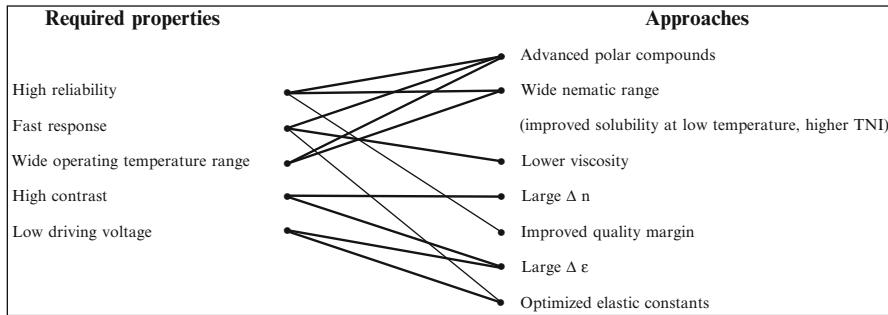
Period/year	~2000	2001–2003	2004–2007	2008–2011
Response time of LCD/ms	25	16	8	5
Rotational viscosity of LC materials/mPa s	100	80	60	45

On the other hand, for many small- and medium-sized devices, this might be different. The following two characteristics are the main requirements in common and conventional LCDs:

1. Low Power Consumption: In order to allow for long battery life, mobile phones and laptops frequently used in locations with no power environment must decrease power consumption by lowering the driving voltage.
2. Wide Operating Temperature Range: Because devices are exposed to widely varying temperatures depending on the season and region of use, it is essential to extend the operating temperature range.
   In recent years, other requirements have surfaced, especially for display of moving pictures on small- and medium-sized LCD TVs. Thus the following attributes related to display characteristics have to be obtained to a particularly high level.
3. Fast Response: LCDs used to display moving pictures have also been commercialized in recent years, but the low image quality that manifests in flickering and tailing is due to the slow response of LCDs. Table 1.1 shows the relationship between the response time of the LCD and the rotational viscosity of liquid crystal materials for the last 10 years. The response time was shortened to one fifth by reducing the rotational viscosity of the liquid crystal material to one half.
4. High Contrast: A high contrast is especially important when showing high-resolution images with higher definition. Small- and medium-sized displays are often taken from bright to low light environments. A high contrast is necessary in order to be able to show a variety of motion pictures independent of the variation of the environment. The role of the liquid crystal material to improve contrast will be mentioned in the latter part of this section.

1.5.4 Development of Fluorinated Liquid Crystal Compounds and Liquid Crystal Material Properties

The basic characteristics of LCDs, which is driving voltage, viewing angle characteristics, and response time, are often discussed, but the physical properties of the liquid crystal material have a close relationship with these characteristics. Optimization of the physical properties of the liquid crystal material is required to improve the display characteristics of the LCD, but one material property influences several display characteristics at the same time, and to improve one display characteristic,

Fig. 1.16 Matrix correlation—required properties and approaches

Table 1.2 Dependence of response time and threshold voltage for several driving methods

TN	$V_{th} = \dfrac{\pi}{2}\sqrt{\dfrac{k}{\varepsilon_0\,\Delta\varepsilon}}$	$\tau_{on} = \dfrac{\gamma_1 d^2}{\varepsilon_0\Delta\varepsilon\left(V_{on}{}^2 - V_{th}{}^2\right)}$	$\tau_{off} = \dfrac{\gamma_1 d^2}{\pi^2 k}$
IPS	$V_c = \dfrac{\pi l}{d}\sqrt{\dfrac{k_{22}}{\varepsilon_0\,|\Delta\varepsilon|}}$	$\tau_{on} = \dfrac{\gamma_1}{\varepsilon_0|\Delta\varepsilon|E_c{}^2 - \frac{\pi^2}{d^2}k_{22}}$	$\tau_{off} = \dfrac{\gamma_1 d^2}{\pi^2 k_{22}}$
VA	$V_{th} = \pi\sqrt{\dfrac{k_{33}}{\varepsilon_0\,|\Delta\varepsilon|}}$	$\tau_{on} = \dfrac{\gamma_1 d^2}{\varepsilon_0|\Delta\varepsilon|\left(V^2 - V_{th}{}^2\right)}$	$\tau_{off} = \dfrac{\gamma_1 d^2}{\pi^2 k_{33}}$

$d =$ cell thickness; $\varepsilon_0 =$ vacuum dielectric constant; $k = k_{11} + (k_{33} - 2k_{22})/4$, where $k_{11} =$ splay elasticity, $k_{22} =$ twist elasticity, $k_{33} =$ bend elasticity; $l =$ electrode distance; $\gamma_1 =$ rotational viscosity; $E_c =$ electric field

several material properties have to be changed. This complex relationship is illustrated in Fig. 1.16.

In addition, the properties required of the liquid crystal material for different driving modes are different. In order to achieve a fast response, low-voltage driving, high contrast, wide viewing angle, etc., the driving method has to be considered. The currently used driving methods are associated with the physical properties of the liquid crystal material and their relation to dependence of response time (τ_{on} and τ_{off}) and the threshold voltage are shown in Table 1.2 [79–82].

It can be seen from Table 1.2 that response time improvement requires large $\Delta\varepsilon$ and low rotational viscosity (η) for each driving mode.

The difference of the alignment film or thickness of the liquid crystal layer in the cell (d), even for the same driving mode, put various demands on the physical properties of the liquid crystal material. And on top of this, there are various driving modes. Thus a very wide range of characteristics are required for the liquid crystal material, which cannot be accomplished in a single compound. Therefore the liquid crystal material is usually prepared by mixing the 10–15 compounds. In order to meet the characteristic requirements, many useful fluorinated liquid crystal compounds have been developed after the initial development of fluorophenyl cyclohexyl carboxylate mentioned above. The concept of development was to

achieve both a large $\Delta\varepsilon$ and a low γ_1. It is no exaggeration to say that the history of the development of liquid crystal compounds was a fight to balance the large $\Delta\varepsilon$ and low γ_1 because there is a trade-off relationship between the two.

Table 1.3 shows representative compounds with positive $\Delta\varepsilon$ (the author refers to compounds with positive $\Delta\varepsilon$ as the first to third generations). The liquid crystal materials shown in Table 1.3 were developed to respond to the characteristics required for LCDs in the first half of the 2000 decade, as a basis for creating a solid alternative to the cathode-ray tube display. Improvement of response time in order to realize display of moving pictures was the objective. Development was achieved with low rotational viscosity materials using a variety of modes in order to satisfy the characteristics required. In the author's research group, it was found that there is a certain correlation between the measured viscosity and the calculated intermolecular interaction energy of the liquid crystal compound. Figure 1.17 shows the correlation of measured viscosities and calculated intermolecular interaction energies [83–86] (using MP-2 [87]/6-31G (d) ab initio molecular orbital calculation) of nine compounds having molecular skeletons with a large degree of freedom.
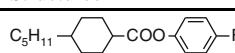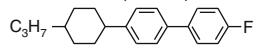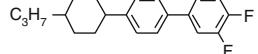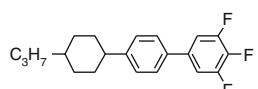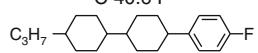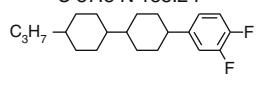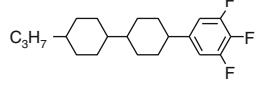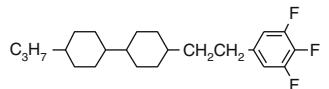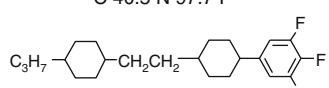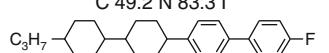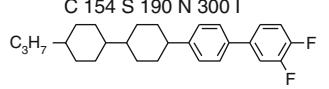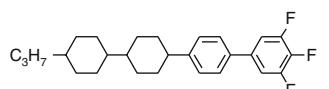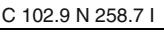
From a detailed analysis of intermolecular interaction energy, a relatively low viscosity is shown for a skeleton type of a liquid crystal compound that has not been reported so far: Ph–CF_2O–Ph (Ph = phenyl ring) [88]. So, producing a liquid crystal compound group with optimized molecular backbone structure that has excellent characteristics has become possible [89]. Figure 1.18 compares the physical properties of examples of the previous first- to third-generation and novel fourth-generation compounds.

Fifth-generation compounds having a molecular structure with four rings have been designed with the intent of further performance improvement, and compounds that have a positive $\Delta\varepsilon$ have come within the reach to be used for various driving modes [90]. The development of fluorinated liquid crystal materials that have been put into practical use in TN, IPS, and VA mode is described below.
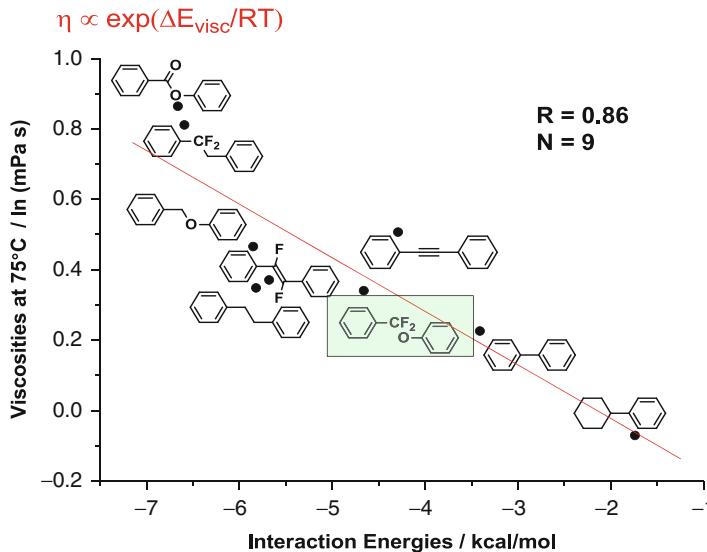
1.5.4.1 Liquid Crystal Material Development for TN Mode

Typical applications of the TN mode are monitors and notebook PCs. The most important characteristics required are fast response and low-voltage driving. As explained above, liquid crystal materials having a large positive $\Delta\varepsilon$ and a low rotational viscosity are required to satisfy the properties for these requirements. Liquid crystal compounds used in monitors have been developed from the third up to the fifth generations. Figure 1.19 indicates the improved level of response in notebook PC liquid crystal materials. $\Delta\varepsilon$ and γ_1/K_{eff} show a correlation. In the trade-off relationship, compared to the third generation, the use of compounds of the fourth and fifth generations shows a good balance between fast response (low viscosity) and low driving voltage (large $\Delta\varepsilon$).
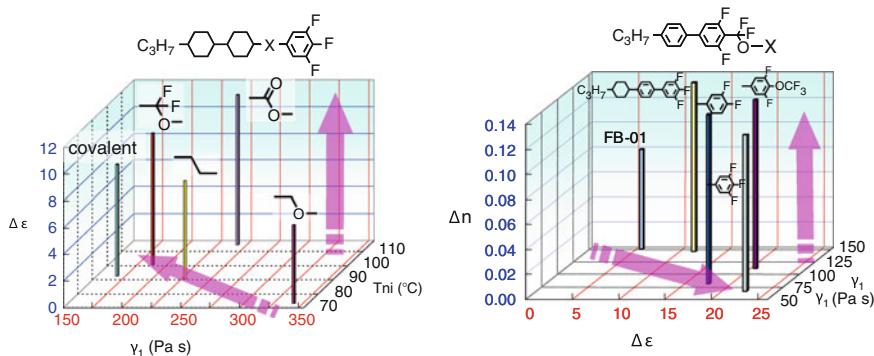
Table 1.3 Positive $\Delta\varepsilon$ of representative fluorinated compounds of the first to third generation

	Structures	$\Delta\varepsilon^a$	Δn^b	$\eta(mPa\ s)^c$
(a)	C₅H₁₁—⬡—COO—⬡—F	2.3	0.059	−6.0
	C 26.0 (N 23.1) I			
(b)	C₃H₇—⬡—⬡—⬡—F	4.3	0.164	19.6
	C 105.1 N 155.6 I			
(c)	C₃H₇—⬡—⬡—⬡(F)—F	8.3	0.149	19.1
	C 68.1 N 97.9 I			
(d)	C₃H₇—⬡—⬡—⬡(F)(F)—F	12.3	0.139	18.6
	C 40.6 I			
(e)	C₃H₇—⬡—⬡—⬡—F	3.8	0.089	19.1
	C 87.8 N 158.2 I			
(f)	C₃H₇—⬡—⬡—⬡(F)—F	5.8	0.084	18.6
	C 44.0 N 124.0 I			
(g)	C₃H₇—⬡—⬡—⬡(F)(F)—F	8.3	0.074	25.1
	C 64.3 N 93.9 I			
(h)	C₃H₇—⬡—⬡—CH₂CH₂—⬡(F)(F)—F	7.3	0.074	31.6
	C 40.5 N 97.7 I			
(i)	C₃H₇—⬡—CH₂CH₂—⬡—⬡(F)(F)—F	7.8	0.069	28.6
	C 49.2 N 83.3 I			
(j)	C₃H₇—⬡—⬡—⬡—⬡—F	1.0	0.179	67.3
	C 154 S 190 N 300 I			
(k)	C₃H₇—⬡—⬡—⬡—⬡(F)—F	5.7	0.166	62.0
	C 92.9 N 288.1 I			
(l)	C₃H₇—⬡—⬡—⬡—⬡(F)(F)—F	13.3	0.154	57.6
	C 102.9 N 258.7 I			

[a] 15 % (5 % for sample *j*) dissolved in FB-01; 25 °C, 1 kHz
[b] Same conditions, 25 °C, 589 nm
[c] Same conditions, 20 °C

$$\eta \propto \exp(\Delta E_{visc}/RT)$$
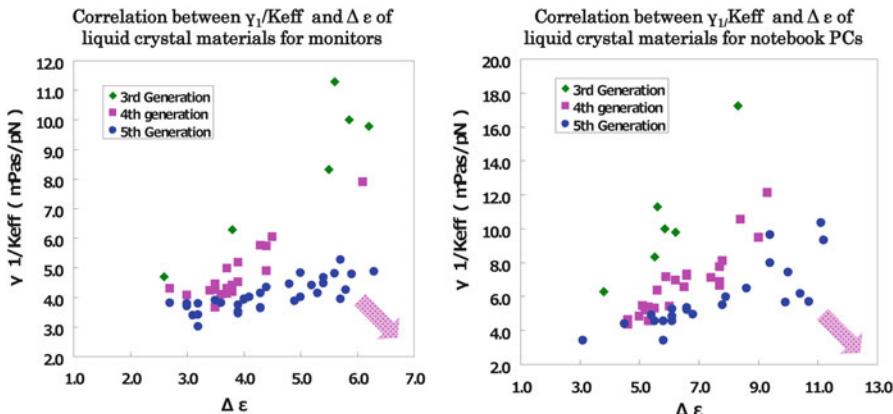
Fig. 1.17 Correlation of measured viscosities and calculated intermolecular interaction energies

Fig. 1.18 Physical properties of liquid crystal compounds having CF_2O unit

1.5.4.2 Liquid Crystal Material Development for IPS Mode

To make it possible for liquid crystal molecules to move in the direction of the electric field without them rising from the plane of the substrate, IPS type displays have a comb-type electrode structure that gives rise to only a small color change at different viewing angles and thus makes optical compensation films unnecessary. However, since the rotational direction of the liquid crystal is only in one direction, yellowish, greenish, or bluish tints are present when viewed from an oblique angle. By forming comb-like electrodes with an angle, reverse rotation direction of liquid
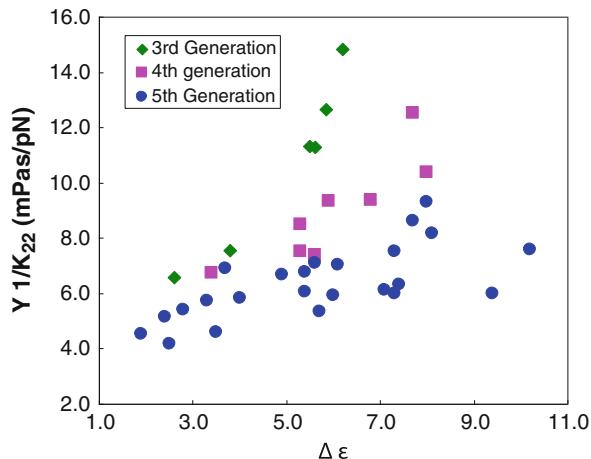
Fig. 1.19 Response characteristics of liquid crystal materials of third, fourth, and fifth generations used in monitors and notebook PCs in TN mode

crystal domains becomes possible, and color changes are reduced. Recently, panels with structures that improve transmittance using fringe field switching (FFS) [91] have been commercialized [92]. Originally, high resistivity of the liquid crystal, which is a strict requirement for the TN mode, was not necessary to obtain a high VHR. However, in order to respond to changing requirements to increase display quality further, fast response liquid crystal materials that contain fluorinated liquid crystal compounds are used at present. Because of low contrast as compared with the VA mode, the requirement for contrast improvement is strong with the IPS mode. In order to improve the brightness of the display, the need to increase the aperture ratio, that is, to increase the electrode spacing ℓ, is effective. This causes an increase in threshold voltage (V_{th}), as is apparent from the equations in Table 1.2. Increasing the $\Delta\varepsilon$ of the liquid crystal material is required to prevent this. Reducing the cell thickness (d) is effective for improving response time, but, in the case of IPS mode, that also leads to an increase in V_{th}. Therefore, it is necessary to select a liquid crystal material with a large $\Delta\varepsilon$ even when aiming at a fast response with a smaller d. From the above it becomes clear that it is important to develop liquid crystal materials that combine both a large $\Delta\varepsilon$ with low γ_1 for the IPS mode, as in the other modes.

IPS mode is useful not only for large TVs, but has also been used in many small- and medium-sized panels and touch panel display types, and the future will bring more useful applications. Figure 1.20 shows the correlation between $\Delta\varepsilon$ and γ_1/k_{22}, and the improvement of the response time of IPS mode liquid crystal materials that contain fluorinated liquid crystal compounds from the third to fifth generations of materials is very obvious.

Fig. 1.20 Response
characteristics of liquid
crystal materials of the
third, fourth, and fifth
generations used in TVs
in IPS mode

★   **Improvement of moving picture quality**

  False impulse response

    1) Baclight blinking (CCFL → LED), insertion of black screen

    2) Overdrive

⇩

  Properties required for LC materials
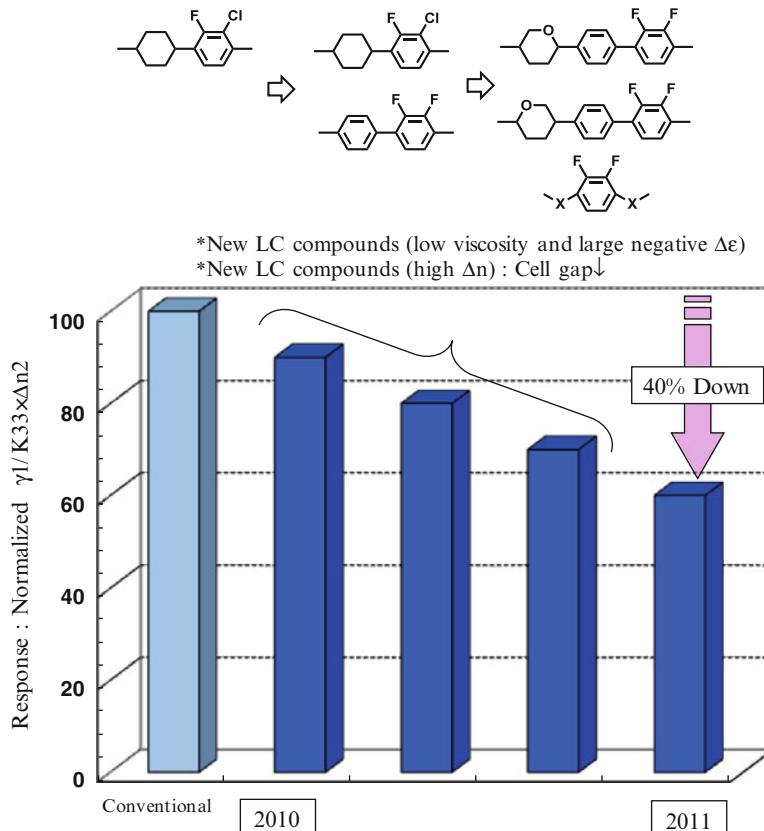
  Fast response (τon + τoff < 16ms)

  ⇒ Narrowing of cell gap

    Increasing birefringence of LC materials (high Δn)

  ⇒ Lowering of rotational viscosity coefficient

Fig. 1.21 Improvement of moving picture quality

1.5.4.3 Liquid Crystal Material Development for VA Mode

There are small displays such as for mobile phone applications that use the VA mode, but its main application is still for large TVs. The special feature of VA mode is that the liquid crystal molecules are oriented vertically to the alignment layer when no voltage is applied. Since it is necessary for the molecules to line up perpendicularly to the electric field, a liquid crystal material with a negative $\Delta\varepsilon$ is required. For this purpose, 2, 3-difluorophenyl groups have been in use for a relatively long time.

Fast response time for the display of moving pictures is the most important characteristic required for TV liquid crystal materials (see Fig. 1.21). In order to

*New LC compounds (low viscosity and large negative $\Delta\varepsilon$)
*New LC compounds (high Δn) : Cell gap$\downarrow$

Fig. 1.22 Improvement of performance of liquid crystal materials for VA mode

achieve fast response time, low viscosity and thin display thickness are required. The retardation is the product of the refractive index anisotropy (Δn) and cell thickness (d), and thus a relatively large Δn is required in order to keep the retardation constant. The author's research group developed a fluorinated liquid crystal compound that was designed based on a new concept [93]. As a result, as compared to 2009, the response time was reduced by 40 % by 2011, which is shown in Fig. 1.22 [94].

1.5.5 Towards Higher Contrast

In order for LCDs to expand into future applications, the major challenge is to increase contrast. This subsection provides an overview of directions for further contrast improvements. Moving picture quality performance improvement is shown in Fig. 1.22 for liquid crystal materials for VA mode. The contrast is defined as the ratio of black-and-white brightness. IPS, FFS, and VA modes are "normally black,"
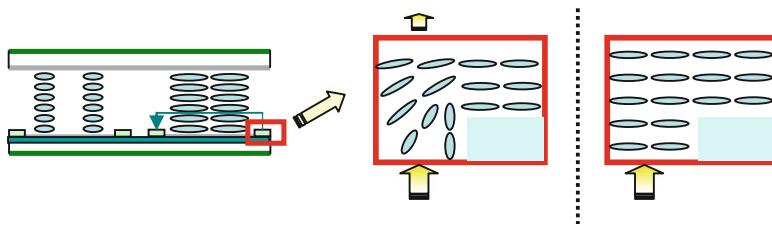
Fig. 1.23 Orientation of liquid crystal molecules in the vicinity of electrodes
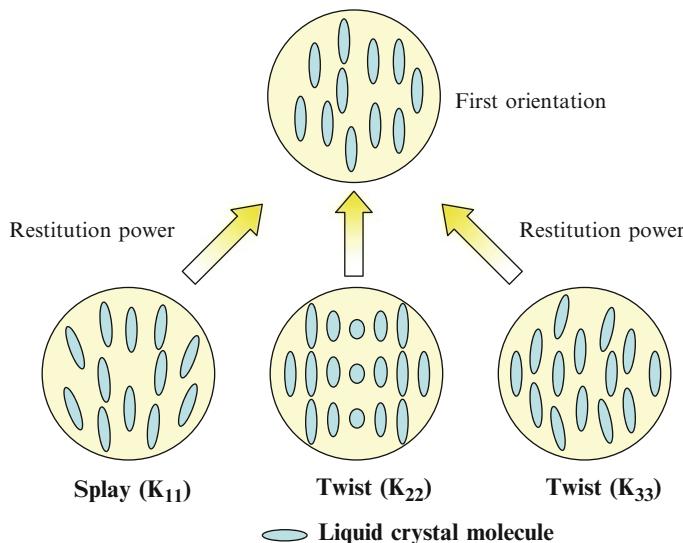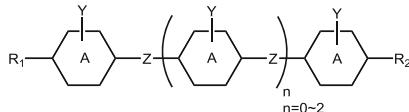
Fig. 1.24 Elastic constants of liquid crystal molecules

and the white brightness, during the application of a voltage, is largely dependent on the transmittance of the polarizing glass plate and the color filter, while the effect of the liquid crystal material is not that large. On the other hand, the contribution of the liquid crystal material cannot be ignored for the black off state. When adding up the effects of all LCD components, nearly 60 % of the black brightness comes from scattering by the liquid crystal, especially in the IPS and FFS modes [95]. This is due to the specific electrode structure of IPS and FFS modes. In order to form an electric field fringe type, the IPS mode must carry out processing using a two-layer electrode structure on the substrate. Rubbing of the alignment film is necessary to align the orientation of liquid crystal molecules in the IPS and FFS modes, and a disturbance of orientation occurs in a region adjacent to the electrode as shown in Fig. 1.23. The black luminance disturbance of the alignment causes light leakage. A parameter called the elastic constant is related to the alignment disorder of the liquid crystal molecules. The orientation of the liquid crystal molecules is modified as shown in Fig. 1.24 by a force such as an electric field. The elastic constant is the

Symbol	Skeletal structure	Interaction
R₁, R₂	Alkyl, alkenyl, etc.	· Hydrophobic interaction
		· Van der Waals force
A	Phenyl, dioxanyl, cyclohexyl, etc.	· π-π stacking
		· Hydrophobic interaction
Z	Single bond, ethylene, etc.	Intermolecular packing
Y	F, CL, etc.	Electrostatic interaction

Fig. 1.25 Interaction between liquid crystal molecules

force necessary to deform the molecular orientation. If a large force is needed to deform the orientation, the liquid crystal material elastic constant is large. Therefore, in order to solve the alignment disorder near the electrodes described above, a liquid crystal material with a large elastic constant is required.

Yuka Utsumi et al. announced that a scattering parameter SP_{cell}, which is an index of black luminance and includes contributions from the glass and the liquid crystal material, can be expressed by the following equation [96]:

$$SP_{cell} = \left[\{\Delta n(n_e + n_o)\}^2 \times d \right] / K_{ave} \tag{1.2}$$

where n_e and n_o are the extraordinary and ordinary refractive indexes, respectively, Δn is $n_e - n_o$, K_{ave} is the average value of the elastic constant, and d is the thickness of the liquid crystal layer. Increasing K_{ave} will reduce the SP_{cell} value in the liquid crystal material, as is apparent from the equation, that is, reducing the alignment disorder is effective to decrease black luminance.

Increasing the elastic constant of the liquid crystal material can be done by strengthening the interaction between the liquid crystal molecules. Usually, a liquid crystal material contains ten or more compounds, and the prediction of intermolecular interactions during the molecular design stage is difficult.

We have analyzed published data about the effective elastic constants of a wide variety of liquid crystal compounds (see Fig. 1.25) and attempted a systematic analysis in order to control intermolecular interactions.

Table 1.4 shows the physical properties of new liquid crystal materials having fluorinated liquid crystal compounds that have been designed from the viewpoint of intermolecular interaction control. Among the newly designed molecules are compound D, with van der Waals interactions (R₁, R₂ in Fig. 1.25), and compound E which is designed after considering electrostatic interactions (Y in Fig. 1.25). The elastic constant K_{ave} increases with increasing content of either D or E, indicating that D and E induce a strong interaction between the liquid crystal molecules. Unfortunately, the viscosity has increased to some extent due to the strengthened intermolecular interaction. Thus, new initiatives and technical

Table 1.4 Elastic constant of new developed liquid crystal mixtures

	Conventional	New LC material 1	New LC material 2	New LC material 3
TNI/°C	90	90	90	90
Viscosity/mPa s	85	87	90	90
Kave/pN	12.9	13.4	13.8	13.5
Content of compound D wt%	0	10	20	0
Content of compound E wt%	0	0	0	10

material development, to further decrease response time and increase contrast, are required in the future. It is imperative to solve the trade-off relationship between the elastic constants and viscosity balance.

1.5.6   Summary
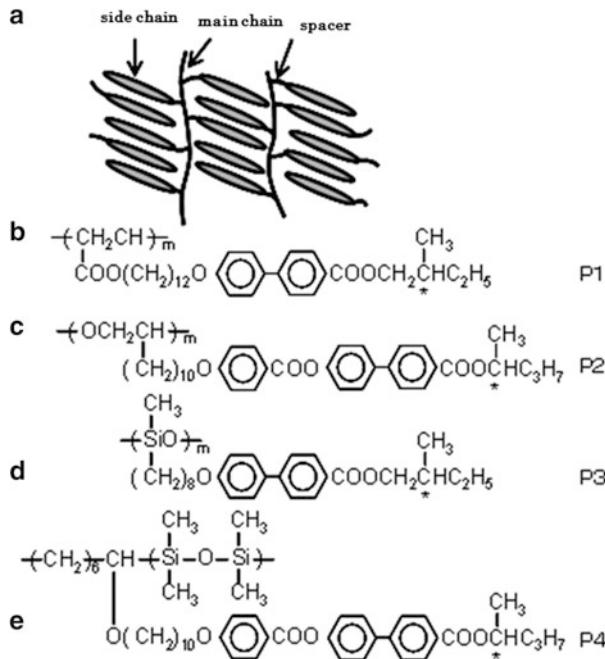
The present section focuses mainly on the approach of high contrast and fast response. The requirement for faster response, lower power consumption, and increased reliability still goes on. The relationship between molecular structure improvements and reliability of liquid crystal material has been omitted. LCDs are being used in a greater variety of applications than ever before, and with this the characteristics required will continue to expand. Along with expanded characteristics, the requirement to maximize the reliability of materials will also become more and more sophisticated. The continued creation of novel liquid crystal compounds is highly desirable not only in resolving this trade-off but also in furthering the development of the LCD industry.

1.6   Ferroelectric Liquid Crystalline Polymers: Properties and Applications

Takashi Sekiya

1.6.1   Introduction

In the 1980s, the interest in the basic physicochemical properties of ferroelectric liquid crystals (FLCs) was flourishing, and FLCs were eagerly studied for the next-generation liquid crystal materials that would replace the traditional nematic LCs, because of their excellent properties, such as microsecond-order high-speed

Fig. 1.26 Molecular structures of ferroelectric liquid crystalline polymers: (**a**) scheme of the molecular design, (**b**) polyacrylates, (**c**) polyoxyethylenes, (**d**) polysiloxanes, and (**e**) hybrid polymers
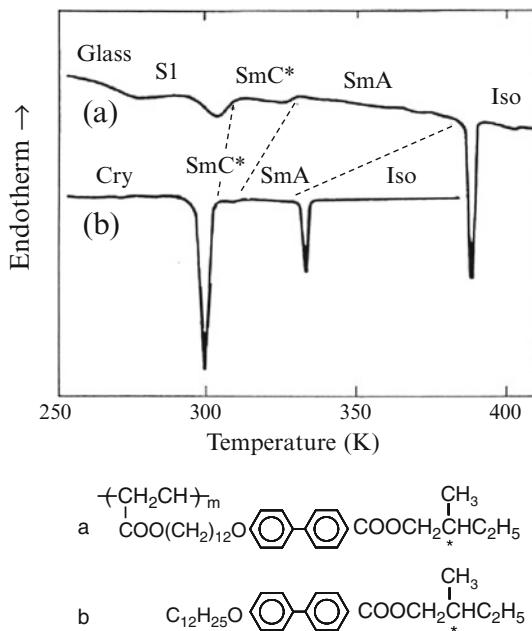
response and memory characteristics [97]. It is a well-known fact that the fierce competition in display development was fueled by the expectation that a super high-definition display would be realized by using the memory effect of the materials in a simple matrix display design. Unfortunately, viewing from the present standpoint, the high-definition liquid crystal display based on TFT-LCD technology has been declared victorious.

In those days, there are some technical difficulties in realizing FLC displays. One was that it was difficult to keep LC layer thickness being very thin of around 2 μm in order to utilize its memory effect. The other was that because of stiffness of ferroelectric smectic layer structure, defects in the alignment of the LC orientation could easily be produced by mechanical shocks.

The author's group thought that it might be possible to overcome these difficulties by incorporating small-molecule ferroelectric liquid crystals into a macromolecule [98, 99]. The molecular design was in such a way to introduce the mesogenic unit that resembles low-molar-mass FLCs as a side chain tethered through flexible spacer structure onto the polymer main chain (Fig. 1.26a).

From 1984 to 1987 there were several presentations of studies in which the similar approach was taken (see the references of 98 and 99). Valerii Shibaev et al. reported a spontaneous polarization of 0.8×10^{-5} C/m^2 for compounds that had the chiral group at the end of the side-group mesogen of an acrylate main chain

Fig. 1.27 Phase transition temperatures for a polyacrylate FLCP and its corresponding low-molar-mass FLC

polymer [100]. On the other hand, the group of the author introduced the chirality into the main chain structure in order to produce a main chain ferroelectric polymer liquid crystal [101].
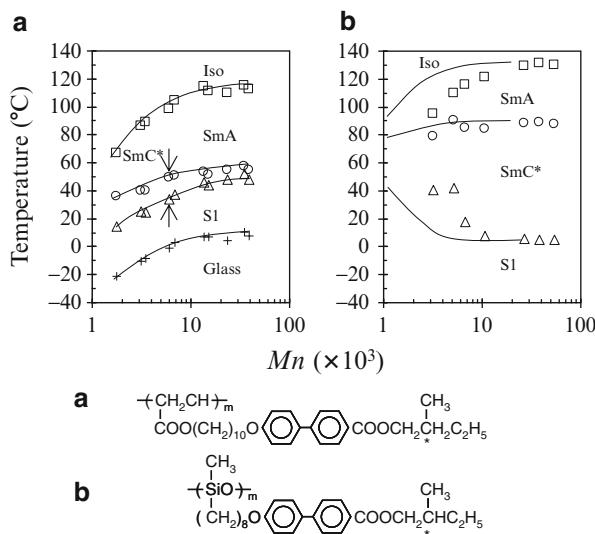
1.6.2 Ferroelectric Liquid Crystalline Polymers

1.6.2.1 Molecular Design and Properties

The author's group chose polyacrylate [102, 103], polyoxyethylene [104, 105], polysiloxane [103], and a polyacrylate/polysiloxane hybrid polymer [106] as the main chain according to the design in Fig. 1.26b–e. We attached various kinds of side-chain structures onto polymer main chains described above and checked the physical properties of these side-chain-type ferroelectric liquid crystalline polymers (FLCPs).

Figure 1.27 shows the phase transition behavior obtained from differential scanning calorimetry (DSC) measurements [102]. For the identification of the LC phase, we used optical microscopy and X-ray diffraction measurements. When comparing the FLCP with the corresponding low-molar-mass FLC compound, it became clear that the temperature range of the smectic phase was broadened. It is thought that smectic laminar structure is stabilized in FLCP because the side-chain ends are aligned forcibly by the main chain.

Fig. 1.28 Influence of the number average molecular weight M_n on the phase transition temperatures of acrylate (**a**) and siloxane (**b**) polymers

Fig. 1.29 Influence of the number average molecular weight M_n on the chiral pitch length p of the FLCP
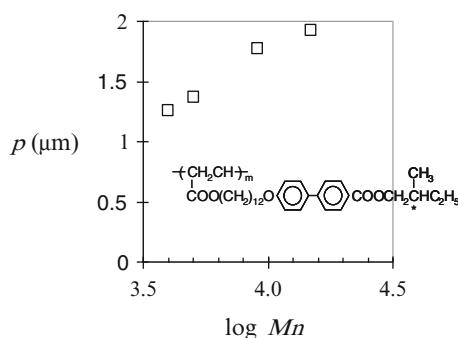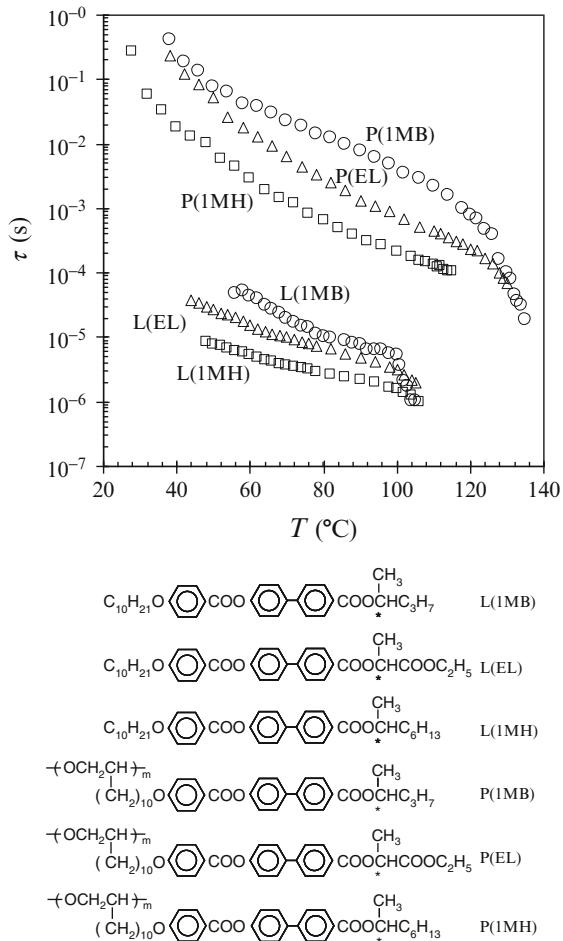
Figure 1.28 shows the relation of the number average molecular weight M_n with the phase transition behavior [102, 107]. With increasing molecular weight, the phase transition temperatures shift to higher temperature direction and saturated above M_n of around 20,000 (Fig. 1.28a). The temperature range of the ferroelectric SmC * phase narrowed significantly with increasing molecular weight of the acrylate main chain polymer, while the temperature range of a highly ordered smectic phase S1 (most likely a SmF * or SmI * phase) increased. On the other hand, the SmC * phase width increased with increasing molecular weight for the siloxane main chain polymer (Fig. 1.28b). This desired result shows the importance of the flexibility of the polymer main chain.

Figure 1.29 shows the relation of the chiral pitch p of FLCP with the number average molecular weight M_n [108]. The interaction between the LC side chains was weakened with increasing molecular weight and thus the pitch increased. Also in this case, saturation was seen at M_n of around 20,000.
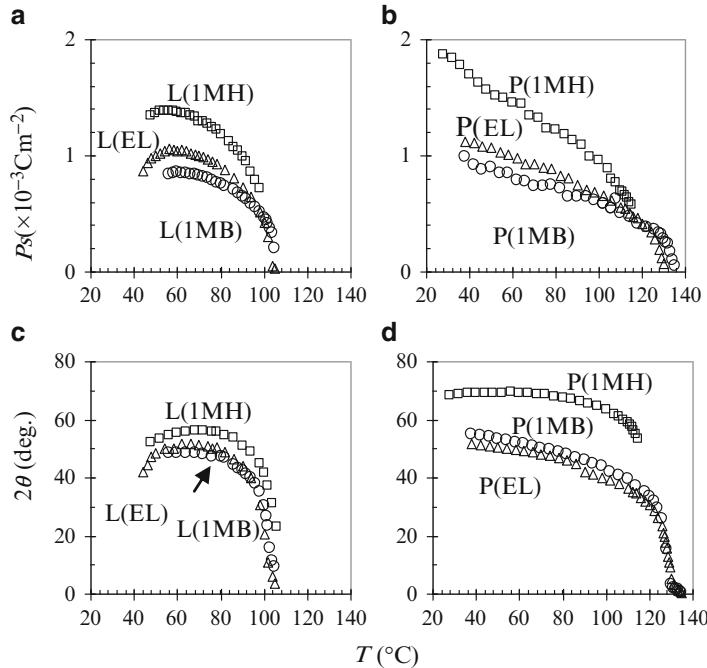
Fig. 1.30 Temperature T dependence of the electro-optical response time τ of three low-molar-mass L (FLC) and their corresponding polymers P (FLC). The notations of the chiral groups are 1 MB for 1-methylbutyloxycarbonyl; EL for ethyllactateoxycarbonyl; and 1MH for methylheptyloxycarbonyl. The applied electric field was $E = \pm 10$ MV/m

1.6.2.2 Electro-Optical Response and Molecular Structure

Figure 1.30 shows temperature T dependence of electro-optical response time τ (the time in which a 10–90 % change takes place for the electro-optical response when a square wave electric field $E = \pm 10$ MV/m is applied) for three different low-molar-mass FLCs that consist of three different chiral end groups respectively, and their corresponding FLCPs that consist of a common polyoxyethylene main chain.
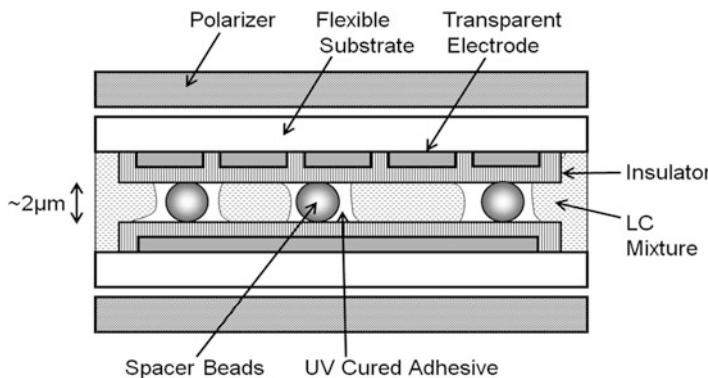
In addition, the temperature dependence of the spontaneous polarization P_s, measured by a triangular wave technique, and the cone angle 2θ, measured by

Fig. 1.31 Temperature T dependence of the spontaneous polarization P_s and cone angle 2θ of low-molar-mass L(FLC) and their corresponding polymers P(FLC); (**a**) and (**b**): P_s, (**c**) and (**d**): 2θ. Molecular structures of L(FLC) and P(FLC) are shown in Fig. 1.30

observing the extinction positions under a crossed Nicol prism in an optical microscope, are shown in Fig. 1.31 [99]. Figure 1.30 showed that, focusing attention on chiral end group, the ascending order of response time in polymers was the same as that in low-molar-mass compounds, but the response time values of polymers were two or three orders of magnitude larger than those of corresponding low-molar-mass compounds.

On the other hand, from Fig. 1.31, the spontaneous polarization and the cone angle seemed to depend mainly on the chiral end group, and both a polymer and a low-molar-mass compound showed the same values as far as they consisted of the same chiral end group. In addition, in both cases of a polymer and a low molar mass compound, a compound that possessed larger spontaneous polarization showed shorter response time. Therefore, in case of polymer, the increase in rotational viscosity coefficient is responsible for the increase in response time. We supposed that the following mechanisms led to an increase of rotational viscosity in polymers. Firstly, as a mesogenic side group is fixed to a main chain, its free motion is limited. Secondly, side groups which project from the main chain are placed next to each other, which lead to an increase of viscosity due to entanglement of side groups. This hypothesis was confirmed through the following experiment with siloxane FLCPs. Using a time-resolved FT-IR measurement, it became clear that

Fig. 1.32 Cross-sectional view of an FLCP panel

as side groups moved, the main chain was dragged by side group motion and moved simultaneously, too [109]. In addition, it was found that the rotational viscosity coefficient increased with increasing molecular weight [110].
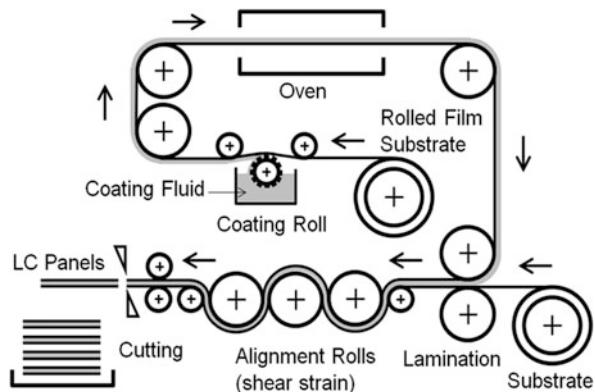
1.6.3   Applications of FLCPs

1.6.3.1   Application of Flexible Liquid Crystal Panel

An FLCP is excellent to guarantee a stable cell gap because of its high viscosity and resistance to shear stress makes the formation of defects more difficult. We realized that the obvious application that utilized such a characteristic would be the flexible liquid crystal panel. Because a pure FLCP did not match the needed response time and the temperature range, we designed a hybrid system consisting of a low-molar-mass FLC and several non-chiral low-molar-mass liquid crystals in addition to the basic FLCP (Fig. 1.26e) [106]. This hybrid system showed a response time of around 1 ms and a memory effect in a wide temperature range including room temperature. Because it became unfortunately difficult to maintain a stable cell gap in a liquid crystalline mixture containing low-molar-mass liquid crystals, we used an UV curable adhesive and spacer beads. Figure 1.32 shows the cross-sectional structure of the liquid crystalline cell which we developed.

Figure 1.33 shows the outline of the manufacturing process of the panel. The coating fluid consisted of a solvent, the liquid crystalline constituent, the UV curable adhesive, and the spacer beads. A reverse gravure coating was used to apply the coating fluid onto an unwound roll film coated with the transparent ITO electrode. After drying a uniform film with an approximate thickness of 2 μm was obtained, which gave, after laminating with the counter film, a liquid crystal panel. The liquid crystal was not oriented in this state. Liquid crystalline orientation of practical contrast had not been achieved by applying the normal rubbing alignment
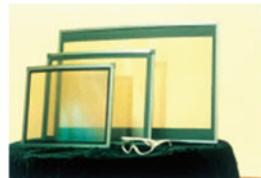
Fig. 1.33 Schematic view of the production process of FLCP panel

Fig. 1.34 A4 sized flexible dot matrix VGA panel

Fig. 1.35 3D FLCP shutter system. Screen sizes are 17″(4:3), 27″(4:3), and 36″(16:9)

technique. In order to obtain an alignment, the liquid crystalline cell was bent while applying a voltage between the electrodes. The difference in radius of the interfaces induced a shear stress and the liquid crystal orientation was achieved. After irradiation with UV light, the orientation was fixed by curing the adhesive. This gave enough strength and remained flexible for practical use afterwards. It can be said that this was the flexible liquid crystal panel based on an epoch-making roll process in those days.

Figure 1.34 shows one of the flexible liquid crystal panels which we produced experimentally. With a reflection type dot matrix panel, it maintained a memory state in a bent state. The characteristics of this panel were lightweight and flexibility. We produced experimentally a prototype of electronic paper based on this panel [106].

A panel with a solid electrode structure and a switching speed of order of 1 ms can even be used to fabricate a large-area high-speed liquid crystal shutter [106]. Figure 1.35 shows the example in which we applied this shutter to a 3D display unit (sold as the 3D indication system "SHADIO" in 1999).

This liquid crystal panel was used as an active retarder, so we attached it on the front of a CRT display and changed the direction of circularly polarized light. The merit of the system was that the audience only needed to wear glasses of simple passive retarder film. In addition, we applied this shutter to a high-speed color-switching panel which colorized high-definition monochromatic CRTs by using a field sequential method, and thus we realized a super high-definition display [106].

1.6.4 Summary

Combining FLCP with coating technique based on a flexible film substrate, it is possible to realize flexible, large area, and shock-resistant ferroelectric LC panels. On the other hand, they consist of macromolecules that exhibit problems such as a long response time and a large temperature dependence. The electric paper application based on this technology had been studied, but it did not lead to commercialization because of the limitation of monochromatic reflection type display. In addition, the shutters for 3D displays and super high-definition color CRT had not been able to appeal to market widely because of the costly hardware and the rack of software. We now feel that it was a too early technique when watching today's 3D and electronic paper boom.

Recently, a possible new panel technology has been suggested for high-speed response and grayscale reproduction that combine the latest photospacer and alignment film technologies with FLCPs [111]. As one of the persons who have been engaged in the development from an early stage on, it is my strong hope that FLCPs will appear in the market as the most advanced liquid crystal technologies.

References

1. G. Brown et al., Chem. Rev. **57**, 1067 (1957)
2. G.W. Gray, *Molecular Structure and Properties of Liquid Crystals* (Academic, New York, 1962)
3. R. Williams, U.S. Patent 3,322,485, (1962)
4. R. Williams, J. Chem. Phys. **39**, 384 (1963)
5. G. H. Heilmeier, IEEE. Trans. ED. **ED23**, 780 (1976)
6. G. H. Heilmeier et al., Proc. IEEE. **56**, 1162 (1968)
7. T. Wada, S. Takechi, H. Kuwagaki, SHARP. Gihou. **10**, 23 (1971)
8. H. Kelker et al., Angew. Chem. Int. Ed. **8**, 884 (1969)
9. O.L.C. Group, Phys. Rev. Lett. **25**(1642) (1970)
10. Y. Arai et al., Japan Patent 52-16468, 1972 (in Japanese)
11. M. Schadt, W. Helfrich, Appl. Phys. Lett. **18**, 127 (1971); Swiss Patent 532,261, 1970
12. M. Schadt, Jpn. J. Appl. Phys. **48**, 1 (2009); Naturwiss. Rundsch. **741**, 117 (2010); J. Eur. Acad. Sci. **1**, 1 (2011)
13. A. Boller, H.P. Scherrer, M. Schadt, P. Wild, Proc. IEEE. **60**, 1002 (1972)
14. G.W. Grey, K.J. Harrison, J.A. Nash, Elec. Lett. **9**, 130 (1973)

15. M. Schadt, C.V. Planta, J. Chem. Phys. **63**, 4379 (1975)
16. M. Schadt, P.R. Gerber, Z. Naturforsch. A. **37**, 165 (1982)
17. M. Schadt, Ann. Rev. Mater. Sci. **27**, 305 (1997)
18. A. Boller, M. Cereghetti, M. Schadt, H.P. Scherrer, Mol. Cryst. Liq. Cryst. **42**, 215 (1977)
19. R. Eidenschink, D. Erdmann, J. Krause, L. Pohl, Angew. Chem. **89**, 103 (1977)
20. C.H. Gooch, H.A. Tarry, J. Phys. D **8**, 1575 (1975)
21. M. Schadt, R. Buchecker, F. Leenhouts, A. Boller, A. Villiger, M. Petrzilka, Mol. Cryst. Liq. Cryst. **139**, 1 (1986)
22. M. Schadt, Phys. Lett. **57A**, 442 (1976)
23. S. Sugimori, Japan Patent 56-104844, 1981
24. H. Takatsu, K. Takeuchi, M. Sasaki, H. Ohnishi, M. Schadt, Mol. Cryst. Liq. Cryst. **206**, 159 (1991)
25. M. Schadt, M. Petrzilka, JSID. **26**(2), 117 (1985)
26. M. Schadt, R. Buchecker, K. Müller, Liq. Cryst. **5**, 293 (1989)
27. M. Schadt, Mol. Cryst. Liq. Cryst. **165**, 405 (1988)
28. C. Frech, B.F. Fung, M. Schadt, Liq. Cryst. **8**, 63 (1990)
29. F. Moia, M. Schadt, Proc. SID. **32**(4), 361 (1991)
30. M. Schadt, Liq. Cryst. **14**, 73 (1993)
31. M. Schadt, P.R. Gerber, Proc. SID. **23**, 29 (1982)
32. C.J. Alder, E.P. Raynes, J. Phys. D. **6**, L33 (1973)
33. M. Schadt, Mol. Cryst. Liq. Cryst. **89**, 77 (1982)
34. M. Schadt, J. Chem. Phys. **71**, 2336 (1979)
35. T. Numagami, *History of Liquid Crystal Display Technology* (Hakuto-Shobo, Tokyo, 1999). Chapter 10
36. R. Williams, Electro-optical elements utilizing an organic nematic compound, U.S. Patent 3,322,485 (9.11.1962) C.A. **68**, 34254e (1968)
37. G. H. Heilmeier, Dynamic scattering in liquid crystals. Appl. Eng. **2**, 21 (1968)
38. D. Dunmur, T. Sluckin, *Soap, Science, and Flat-Screen TVs – A History of Liquid Crystal* (Oxford University Press, New York, 2011)
39. T. Wada, in *Ekisho-Shinshi-Zuisoroku*, ed. by S. Matsumoto (Tekuno Taimusu Co., 2002)
40. B. Johnston, *We Were Burning – Japanese Entrepreneurs and the Forging of the Electronic Age* (A Cornelia and Michael Bessie Book, New York, 1998)
41. M. Tonedate, *Dentaku-To-Shinkansen* (Shincho-Sha, Tokyo, 1983), p. 97
42. H. Uni, in *Development of Liquid Crystal Display in Sharp, in Sengo Nihon-no Gijyutsu-Keisei – Moho-ka-Sozo-ka (Japanese Technological Achievement after World War II – Mimic or Creative?)*, ed. by T. Nakaoka (Nihon-Hyoron-Sha, Tokyo, 2002). Chapter 6
43. M. Schadt, W. Helfrich, Voltage-dependent optical activity of a twisted nematic. Appl. Phys. Lett. **18**, 127 (1971)
44. T. Numagami, *History of Liquid Crystal Display Technology* (Hakuto-Shobo, Tokyo, 1999). Chapter 8
45. E. Lyons, *David Sarnoff* (Pyramid Books, New York, 1966)
46. T. Ogawa, (Kagaku Asahi, 1970) pp. 65
47. K. Ono, A. Fujii, S. Furuichi, Large-scale liquid crystal display, Denshi. Zairyo. **14/34**(7), 65–66 (1975)
48. E. Kaneko, H. Kawakami, H. Hanmura, Liquid crystal television display. Proc. SID. (Society for Information Display), **19/2**, 55 (1978)
49. H. Kawakami, Y. Yoneda, F. Nakano, K. Toriyama, Driving method for liquid crystal display device. Paper for the meeting of the technical Group on Image-engineers, Institute of Electronics & Communication Engineers, 1973–1911, p. 85
50. H. Gruler, T.J. Scheffer, G. Meier, Elastic constants of nematic liquid crystals. Z. Naturforsch. **27a**, 966 (1972)

51. H. Kawakami, Y. Yoneda, F. Nakano, K. Toriyama, Multiplexing drive method for liquid crystal numeric display device. Paper for the meeting of the technical Group on Image-engineers, Institute of Electronics & Communication Engineers, IT72–43, 1973–03

52. K. Odawara, T. Ishibashi, K. Toriyama, M. Kanazaki, Liquid crystal display for calculators. Advances in Display Devices, Electro**76** Professional Program, Boston, 11–14 May 1976

53. K. Toriyama, K. Suzuki, T. Nakagomi, T. Ishibashi, K. Odawara, A design of liquid crystal material for multiplexed liquid crystal display. J. Phys. **C3–40**, 317 (1979)

54. K. Toriyama, K. Suzuki, T. Nakagomi, T. Ishibashi, and K. Odawara, Liquid crystal for multiplexed twisted nematic displays – its philosophy and practice, in *The Physics and Chemistry of Liquid Crystal Devices*, ed. by G.J. Sprokel (Plenum, 1980)

55. H. Kelker, R. Hatz, *Handbook of liquid Crystals* (Verlag Chemie, 1980). Chapter 14

56. F. Funada, K. Yamamoto, T. Wada, Sharp. Tech. J. **12**, 65 (1973)

57. K. Toriyama, Optical transient behavior of nematic liquid crystals in an electric field. Jpn. J. Appl. Phys. **9**, 1190 (1970)

58. K. Nakada, T. Ishibashi, K. Toriyama, A design of multiplexing liquid-crystal display for calculator. IEEE Trans. ED. **22**(9), 725 (1975)

59. M. Schadt, W. Helfrich, Voltage-dependent optical activity of a twisted nematic liquid crystal. Appl. Phys. Lett. **18**, 127 (1971)

60. G.W. Gray, K.J. Harrison, J.A. Nash, Elec. Lett. **22**, 130 (1973)

61. A.R. Kmetz, Matrix addressing of non-emissive display, in *Nonemissive Electrooptic Display*, ed. by A.R. Kmetz, F.K. von Willisen (Plenum, 1976)

62. D. Demus, Chemical composition and display performance, in *Nonemissive Electrooptic Display*, ed. by A.R. Kmetz, F.K. von Willisen (Plenum, 1976)

63. A. Muko, in *Liquid Crystal Device Handbook*, ed. by The 142-Committee (The Japan Society for Promotion of Science, 1989). Chapter 3, Section 3.3

64. D. Demus, S. Diele, S. Grande, H. Sackmann, Polymorphism in thermotropic liquid crystals, in *Advances in Liquid Crystals*, vol. 6 (1987)

65. K. Toriyama, in *Liquid Crystal Device Handbook*, ed. by The 142-Committee (The Japan Society for Promotion of Science, 1989). Chapter 3, Section 3.1 and references there in

66. A. Funada, H. Kuwagaki, Jpn Kokai. **57**, 2756 (1982)

67. K. Toriyama, T. Nakgomi, H. Sato, Y. Fujita, K. Morita, Y. Arai, U.S. patent 4,372,871, 1983

68. J. Malthete, M. Leclercq, M. Dvolaitzky, J. Gabard, J. Billard, V. Pontikis, J. Jacques, Mol. Cryst. Liq. Cryst. **23**, 233 (1973)

69. H. Takatsu, K. Takeuchi, Y. Tanaka, M. Sasaki, Mol. Cryst. Liq. Cryst. **141**, 279 (1986)

70. H. Ohnishi, H. Takatsu, K. Takeuchi, F. Moia, M. Schadt, SID 92 Digest 17 (1992)

71. R. Buchecker, M. Schadt, Mol. Cryst. Liq. Cryst. **149**, 359 (1987)

72. H. Mailer, S. Laskos, U.S. Patent 4196975, 1980

73. M. Negishi, S. Ogawa, M. Osawa, K. Takeuchi, S. Takehara, H. Takatsu, Jpn. Liq. Cryst. Soc. Conf. **3B01**, 418 (1998)

74. M. Negishi, S. Ogawa, M. Osawa, K. Takeuchi, S. Takehara, Y. Umezu, S. Kawakami, H. Takatsu, DIC Tech. Rev. **5**, 17 (1999)

75. S. Sugimori, U.S. Patent 4,340,498, 20 July 1982)

76. G.W. Gray, B. Jones, J. Chem. Soc. 2556 (1954)

77. G.W. Gray, B.M. Worrall, J. Chem. Soc. 1545 (1959)

78. T. Shimazaki et al., The Japanese liquid crystal society symposium lecture abstracts, 78 (1988)

79. E. Jakeman, E.P. Raynes, Phys. Lett. A **39A**, 69 (1972)

80. K. Tarumi et al., Jpn. J. Appl. Phys. **31**, 2829 (1992)

81. M. Ohe, K. Kondo, Appl. Phys. Lett. **69**, 623 (1996)

82. Y. Kubo, Denshizairyo. **5**, 48 (2007)

83. A.J. Stone, The theory of intermolecular forces (International Series of Monographs in Chemistry) (Clarendon Press, Oxford, 1996)

84. S. Tsuzuki, K. Tanabe, J. Phys. Chem. **95**, 2272 (1991)

85. S. Tsuzuki, T. Uchimaru, K. Tanabe, J. Mol. Struct. **307**, 107 (1994)
86. S. Tsuzuki, K. Tanabe, J. Phys. Chem. **96**, 10804 (1992)
87. C. Moller, M.S. Plesset, Phys. Rev. **46**, 618 (1934)
88. T. Matsushita et al., Proceeding of 19th ILCC, 777 (2002)
89. S. Matsui et al., Proceeding of 19th ILCC, 772 (2002)
90. T. Hiraoka et al., Mol. Cryst. Liq. Cryst. **509**, 89 (2009)
91. S.H. Lee et al., SID 2009 Digest, 202 (1999)
92. K. Kondo, SID 2005 Digest, 978 (2005)
93. Y. Gotoh, Mol. Cryst. Liq. Cryst. **542**, 16 (2011)
94. T. Aono, Y. Gotoh, Proceeding of 10th IMID, 21–1 (2010)
95. K.J. Kim et al., SID 2010 Digest, 34.1, 487 (2010)
96. Y. Utsumi et al., Jpn. Liq. Cryst. Soc. Conf. 418 (2008)
97. N.A. Clark, S.T. Lagerwall, Appl. Phys. Lett. **36**, 899 (1980)
98. T. Sekiya, K. Kawasaki, Koubunshi (Polymers) **40**, 454 (1991)
99. T. Sekiya et al., Liq. Cryst. **14**, 1255 (1993)
100. V.P. Shibaev et al., Polym. Bull. **12**, 299 (1984)
101. J. Watanabe et al., 14th Ekisho-Toronkai, 1B121, 56 (1988)
102. S. Uchida et al., Mol. Cryst. Liq. Cryst. **155**, 93 (1988)
103. K. Yuasa et al., Ferroelectrics **122**, 53 (1991)
104. S. Hachiya et al., J. SID. **1/3**, 295 (1993)
105. M. Ido et al., Ferroelectrics **148**, 223 (1993)
106. H. Kuma et al., SID 01 DIGEST (4.3/H. Kuma), 12 (2001)
107. K. Tomoike, Kino-zairyo (Funct Mater) **1**, 12 (1993)
108. H. Endo et al., Liq. Cryst. **9**, 635 (1991)
109. K. Kawasaki et al., Ferroelectrics **148**, 233 (1993)
110. H. Endo et al., Liq. Cryst. **12**, 147 (1992)
111. O. Sato et al., SID 10 DIGEST (27.4L/O. Sato), 394 (2010)

Chapter 2
Circuits and Drives for Liquid Crystal Devices

Hideaki Kawakami

2.1 Circuits and Drive Methods: Multiplexing and Matrix Addressing Technologies

Hideaki Kawakami

2.1.1 Introduction

The liquid crystal display (LCD) has been put to practical use in the early 1970s, and the following remarkable development progress led to today's prosperity. The LCD was driven from the early stage of practical use by complementary metal–oxide–semiconductor large-scale integration (CMOS LSI). In the early 1970s, the great market for electronic watches and electronic calculators was created. Then, CMOS LSIs and LCDs were developed as key components to realize low-power electronics.

The drive electronics was invented at the beginning of LCD development. The main drive electronics was followed from the passive matrix LCD (PM LCD) to active matrix LCD (AM LCD). Even if the main products moved to active matrix LCDs, the rms-responding characteristics peculiar to nematic liquid crystals remained as the drive electronics progressed.

B. J. Lechner of the American RCA Lab. suggested the AM LCD in 1971 [1]. However, we had to wait for the practical use of the AM LCD until the progress of Si film technology in the 1980s.

Here, I survey the progress of the multiplexing and the matrix addressing technologies.

H. Kawakami (✉)
Hitachi Ltd., Tokyo, Japan
e-mail: khideaki@tbb.t-com.ne.jp

2.1.2   Multiplexing Technologies

It was the electronic watches and electronic calculators that exploited the consumer market during the development of the CMOS LSI in the early 1970s. Because all those devices used button cells as power supply, the low power consumption of the display was important. In response to it, the segment-type LCD with a μW order power consumption was put to practical use at this time. There was limitation of the number of the output pins in the package of the LSI, and the multiplexing technologies of the LCD were developed to reduce the number of external terminals. This was the beginning of matrix addressing technologies of the LCD.

In the beginning of the1970, with solely nematic liquid crystals in use, the twisted nematic TN-LCD became mainstream for LCDs in electronic watches and calculators. The multiplexed LCD incorporates capacitors in their matrix circuits which led to crosstalk between the matrix elements. Therefore the amplitude selection method was developed to create a uniform bias voltage to control the crosstalk such as 3-to-1 or 2-to-1 amplitude selection. This model was known as the matrix addressing technology of inorganic electroluminescent devices. In order to apply this to TN-LCDs, the two next characteristics have to be considered.

(1) The accumulation response
     The electro-optical response when voltage pulses are applied to LCDs in a chronological order is cumulative and saturates after several voltage pulses.
(2) The rms-responding characteristics [2]
     The relative luminance that is reached in (1) depends on the effective value of the applied voltage to LCD.
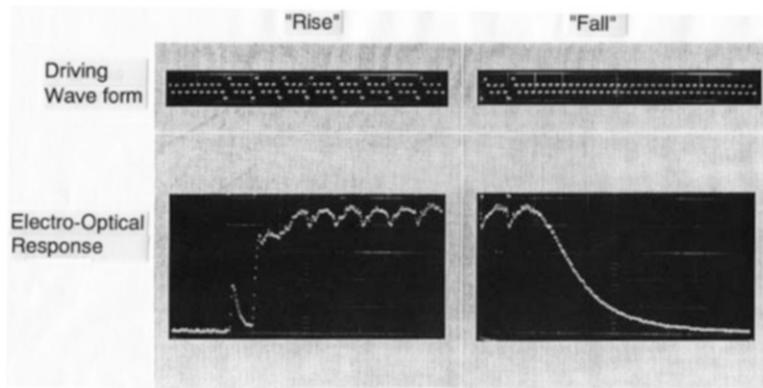
It was the two-frequency drive method on the basis of rms-responding characteristics that was proposed at first, but it was an immature drive method in those days and problems because of bad temperature characteristics did not lead to a practical use [3, 4].

On the other hand, the electro-optical response showed accumulated response on the temporal axes, and this slowed the electro-optical response (see Fig. 2.1). Hence the amplitude selection technologies were developed for driving LCDs. Regarding the driving spectrum, the amplitude selection technologies require that V_{th} is approximately constant in the bandwidth of driving frequency. In summary, it was clear that the transient response in electro-optical performance of nematic LCDs originally showed the accumulated response and the frequency response in the steady state of electro-optical performance required that V_{th} of LCD be approximately constant in the bandwidth of the driving frequency.

In the early amplitude selection, the number of scan lines was 2–4, and the frame frequency f_F was 50–60 Hz. Because of a frame inversion for the AC drive, the minimum driving frequency of the drive voltage applied to the LCD was 1/2 f_F, which means 30 Hz. The effective dielectric constant under such low frequencies fluctuated because the ionic conduction mainly fluctuated which led to malfunctions. More than 10^{10} Ω cm were required as the specific resistance of the bulk liquid crystal material.

Fig. 2.1 Example of an accumulation response in TN-LCDs, when 3-to-1 amplitude selection was used at 1/4 duty drive
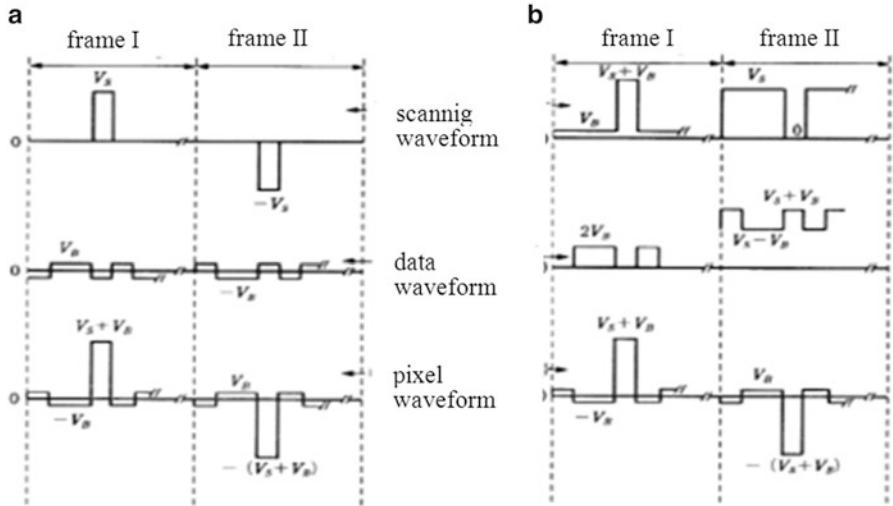
On 3-to-1 amplitude selection, the ratio of on-voltage V_S and off-voltage V_{NS} depends on the number of scanning lines, and $V_S/V_{NS} = \sqrt{(1 + 8/n)}$. The formula shows the margin allowing the deviation of V_{th}. At that time, deviation of V_{th} was caused by the deviation of the cell gap, molecular orientation factors, and others. Also, the margin suggested the demand on the material specifications of liquid crystalline materials that became a molecular design and production guideline.

2.1.3   Matrix Addressing Technologies for Passive Matrix LCDs

2.1.3.1   A-to-1 Amplitude Selection Technologies

From the first days of the LCD, there was the dream to make a flat panel LC TV, but the development of practical use active matrix LCD progressed too slowly. Development of the PM LCD became popular in the 1970s, and the necessary drive methods were developed. The basis in TN-LCDs, put to practical use in the early 1970s, was the root mean square value dependence (rms-responding) characteristics, and the drive methods were developed accordingly [5, 6].

For twisted nematic LCDs, the line inversion drive was used in the passive matrix display in which the number of scanning lines n was from 8 to 40. The driving frequency $f_F \times n$ for those devices was a few kHz. With the scale of the matrix growing bigger, and the number of scanning lines n reaching 200, the bandwidth of the driving frequency reached from a few 10 Hz to a few 10 kHz. The dielectric anisotropy $\Delta\varepsilon$ of nematic LCs used in TN cells was wide enough, and the threshold voltage V_{th} to trigger the electro-optical response was constant, and there was no upper limit level of the frequency bandwidth in principal.

Fig. 2.2 The optional amplitude selection technologies. Driving wave forms of a-to-1 amplitude selection, such as (**a**) Alt–Pleshko (AP) method and (**b**) amplitude selection (AS) method

In other words, the optimization of the amplitude selection was accomplished with the rms response in the frequency bandwidth where V_{th} was approximately constant (see Fig. 2.2).

When the ratio of on-voltage V_S and the off-voltage V_{NS} was maximum, the contrast was maximized, and for this optimization, the conditions are as follows:

$$V_S/V_{NS} = \sqrt{(\sqrt{n}+1)/(\sqrt{n}-1)} \qquad (2.1)$$

where n is the number of scan lines; V_S is the selection voltage (on voltage); and V_{NS} is the non-selection voltage (off voltage).

Under optimum condition that the contrast becomes high, the on-/off-voltage ratio V_S/V_{NS} depends on the number of scanning lines n and asymptotically reaches unity, which means that not enough contrast is provided when the number of scanning lines increases. This phenomenon is called the scanning limitation. Research and development of the advancement of the PM LCD continued in the 1980s and 1990s, but because of the scanning limitation by Eq. (2.1) we were defeated by this so-called iron law. Thus the use of the TN-LCD was limited to small LCDs at that stage.

In the 1980s, the research and development of AM LCDs were very active, but it had not yet opened great application. On the other hand, STN-LCD (super twisted nematic LCDs) for PCs and Japanese word processors were realized in the 1980s [7], and also colored STN-LCDs for PCs were developed. The electro-optical response increased steeply with increasing applied voltage for those cells and enough contrast was provided even if the number of scanning lines increased, and

the on-/off-voltage ratio became small. Its performance of STN-LCD was called threshold sharpness.

However, in the 1990s active matrix (AM) LCDs using thin-film transistors (TFT) with amorphous silicon films were put to practical use, and the superiority of the AM LCD for PC use became obvious once the reliability problems were solved. From there on, the market of the PM LCD was limited to small- to middle-sized LCDs. The root of this is the scanning limitation due to Eq. (2.1). The peculiar threshold sharpness of STN-LCDs gave enough contrast even if the number of scanning lines grew large to some extent. However, there was some difficulty to display half tone images. After some time, superior AM LCDs became mainstream after all.

2.1.4 Active Addressing and Multiline Addressing Methods

The topics of the 1990s for PM LCDs were the active addressing method and the multiline addressing method [8, 9].

$$D_j(t) = c\sum_{i=1}^{n} I_{ij}S_i(t) \tag{2.2}$$

where I_{ij} expresses the state of the pixel. On $= +1$, off $= -1$.

It is clear that on the basis of the rms-responding characteristics, the scanning signal $S_i(t)$, and data signal $D_j(t)$ are orthogonal [10].

This can be expressed by introducing a specific orthogonality function, e.g., Hadamard function into the scanning signal S (Eq. 2.2). By applying S to all lines at the same time, one field at a time scanning methods were developed. The schemes were called active addressing method and they have advanced to scan partial lines at the same time. Also, by scanning several lines at the same time, multiline addressing (MLA) methods were developed.

Techniques to integrate image compression algorisms such as JPEG2000 and MPEG-4 into the MLA have been developed to use STN-LCDs for mobile devices in research and development after 2000 [11].

References

1. B.J. Lechner et al., Proc. IEEE. **59**(1), 1566 (1971)
2. H. Kawakami, JP968570 (Application date: 1973/2/9)
3. P. Wild et al., APL. **19**(9), 335 (1971)
4. C.R. Stein et al., APL. **19**(9), 343 (1971)
5. P.M. Alt et al., IEEE Trans. ED. **ED-21**(2), 146 (1974)
6. H. Kawakami, JP1210998 (Application date : 1973/10/19)

 7. T.J. Scheffer et al., SID 1985 Digest, 120 (1985)
 8. T.J. Scheffer et al., SID 1992 Digest, 228 (1992)
 9. S. Ihara, T.N. Ruckmongatham et al., SID 1992 Digest, 232 (1992)
10. N.A. Nehring et al., IEEE Trans. ED. **ED-26**, 795 (1979)
11. A.A. Lawrence et al., SID 2001 Digest, 98 (2001)

Chapter 3
Alignment Films for Liquid Crystal Devices

**Shunsuke Kobayashi, Koji Kuroda, Makoto Matsuo,
and Michinori Nishikawa**

3.1 Liquid Crystal Surface Orientation Techniques

Shunsuke Kobayashi

3.1.1 Why Is the Orientation of the Liquid Crystal Necessary?

In order to do research on liquid crystals, to fabricate liquid crystal devices, or to mass-produce liquid crystal displays (LCDs), it is necessary to orient the liquid crystalline molecules in a liquid crystalline cell, except some in a few cases. The reason is that most liquid crystalline molecules are either rod like or disc shaped, and they have the natural tendency to orient each other. However, it is necessary to actively orient such molecules on a substrate in a cell for many practical purposes.

S. Kobayashi
Department of Electrical Engineering, Liquid Crystal Institute,
Tokyo University of Science in Yamaguchi, Japan
e-mail: kobayashi@rs.tus.ac.jp

K. Kuroda
Dai Nippon Printing Co., Ltd., Tokyo, Japan
e-mail: Kuroda-k2@mail.dnp.co.jp

M. Matsuo
Dai Nippon Techno Research Co., Ltd., Tokyo, Japan

M. Nishikawa
Display Materials Research Laboratories, JSR Corporation, Yokkaichi, Japan
e-mail: Michinori_Nishikawa@jsr.co.jp

There are then two reasons for the necessity to actively orient the molecules: first is to check all anisotropic physical properties such as the optical or electromagnetic anisotropy of the medium or the mechanical properties. It was already reported in 1911 by C. Mauguin and in 1951 by Chatelain [1] that by rubbing (or buffing) a glass substrate with paper in one direction, it was possible to measure the optical anisotropy of liquid crystalline molecules placed on top [1, 2].

Second, liquid crystal display technology began with the dynamic scattering mode (DSM), and it developed into twisted nematic (TN) [3], super twisted nematic (STN) [4], vertical alignment (VA) [5], and in-plane switching (IPS) [6, 7], and fringe field switching (FFS)-LCD [8] and polymer-stabilized V-shaped switching (PSV)-FLCD [9]. The orientation of the liquid crystalline molecules in one direction with an off-plane pretilt angle is necessary for those liquid crystalline cells.

If there is no pretilt angle, disclination defects appear that decrease the contrast ratio and homogeneity of displayed images for those LCDs. In other words, the realization of the "disclination-free" technique is necessary absolutely to mass-produce LCDs. These circumstances have not changed at all during the development of new types of LCDs and are valid even today [10].

TN-LCD has been used for digital clocks and electronic calculators from about 1973, and alignment films have been prepared from the 1970s to the 1980s by the oblique vapor deposition method of SiO_x [11]. However, this technology was not suitable for producing large-area LCDs. Alignment films based on polyimides (PIs) were invented in 1979 by Makoto Matsuo, Takashi Toita (both Dai Nippon Printing), Ichiro Tsunoda (Tokai University) [12]. Later, Hiroyoshi Fukuro (Nissan Chem. Ind.) and Shunsuke Kobayashi (Tokyo University of A&T) succeeded in developing practical PI films for producing large-area TN- and STN-LCDs in 1986 by synthesizing PIs with alkyl side chains and performing rubbing on these PI films [13, 14]. The details on this technology will be described in the next subsection.

3.1.2 Production of Defect-Free High-Contrast-Ratio TN-LCDs and STN-LCDs

Because TN-LCD has a lower power consumption than a DSM display, it came to be adopted rapidly in 1973. Therefore, defect-free TN-LCDs were required. Defect free means that it is possible to switch between constant levels of "black" and "white" in each pixel with an optical uniformity in an LCD. There are three types of defects that occur in TN-LCDs and STN-LCDs:

1. The reverse twist type in one pixel as shown in Fig. 3.1, which manifests as a bright line between crossed linear polarizers [15].
2. In addition, leaking of light as shown in Fig. 3.2 occurs when there is a reverse tilt of the molecules. This type of disclination lines disappears with increasing applied voltage [15].
3. Stripe domains in STN-LCD.
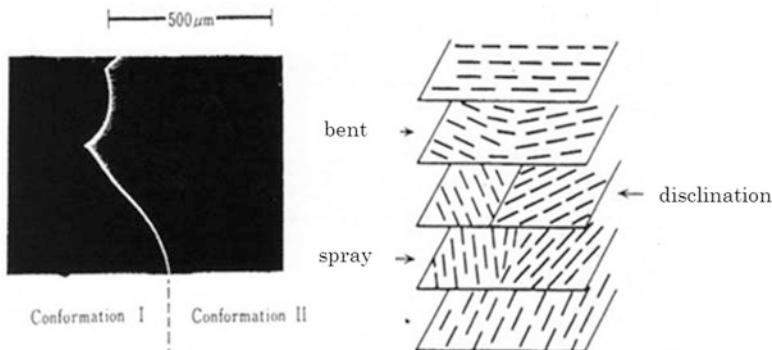
Fig. 3.1 Reverse twist disclination in a TN cell (©IEEE Tr.ED)

Fig. 3.2 Reverse-tilt disclinations in a TN cell (©IEEE Tr.ED)

What can be done to remove these defects?
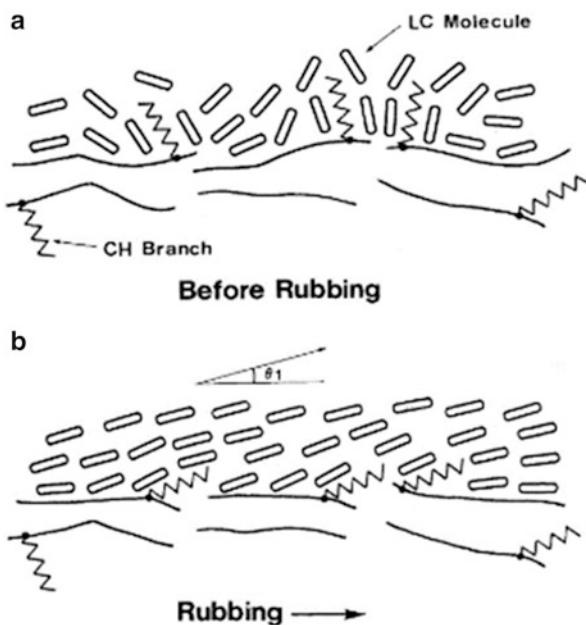
1. A TN cell without having reverse twist defect (disclination) will be fabricated by giving the twist angle of less than 90° [16] or by adding a chiral agent [17].
2. In addition, when an electric field is applied to a TN cell, liquid crystal molecules tend to tilt from a planar conformation. This situation will develop reverse-tilt disclinations when liquid crystal molecules do not have a pretilt angle. And this kind of defect can be eliminated by using rubbed alkylated polyimide (PI) films that produce pretilt. This concept is shown in the diagram in Fig. 3.3 [18]. The pretilt angle of 2–3° of LC molecules in a TN cell occurs practically naturally by rubbing PI, including non-alkylated ones. The mechanism of this structure formation is thought to be caused by stick–slip mechanism of friction.

Defect-free STN-LCDs need a high pretilt angle of 5–7°, because stripe domains, as shown in Fig. 3.4, will develop at lower pretilt angles. The synthesis of polyimide with alkyl chains produces a pretilt, which suppresses the outbreak of such a defect. The molecular formulas of the polyimides are shown in Figs. 3.5 and 3.6.
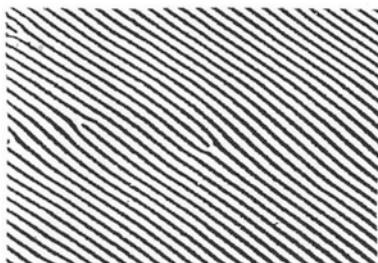
The resulting pretilt angles were 10° and 19°, respectively, as shown in Table 3.1, and as a result, we were able to manufacture defect-free STN-LCDs (see Sect. 3.3).

Figure 3.7 shows a rubbing machine that had been invented by Kobayashi et al. in 1971 and that had been used in 1986 to produce the tremendous defect-free
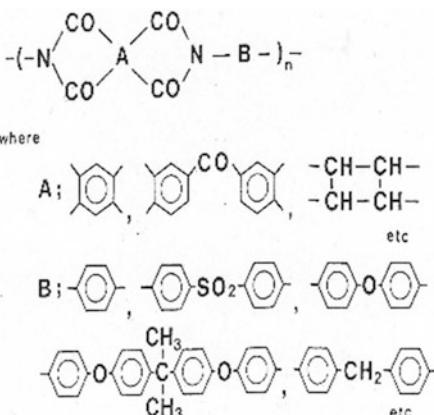
Fig. 3.3 Diagram of the pretilt angle formation by rubbing alkylated polyimides
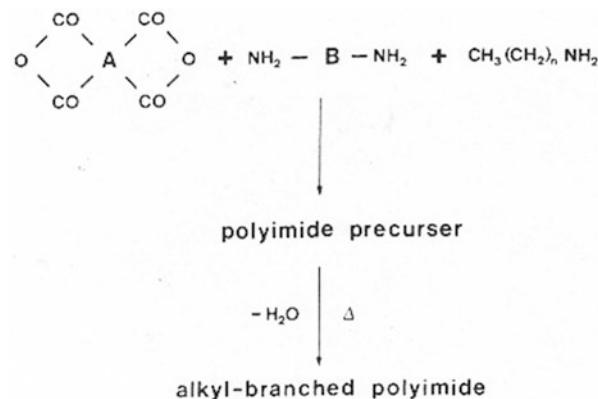
Fig. 3.4 Stripe domain in an STN-LCD with a low pretilt angle of 2–3°

Fig. 3.5 Basic chemical formula of polyimides
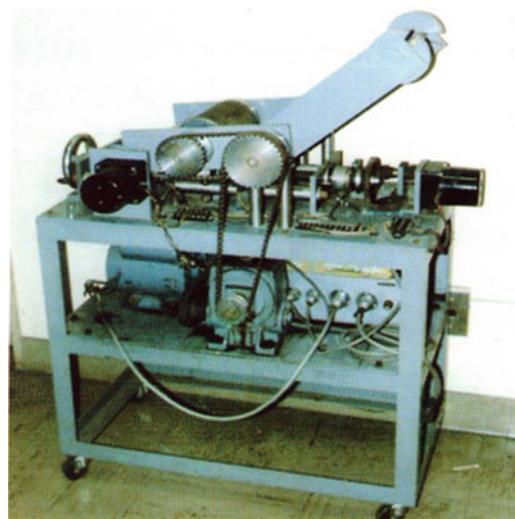
Fig. 3.6 Synthetic process of alkyl-branched polyimides

Table 3.1 Pretilt angles of polyimide alignment layers for STN-LCDs (©MCLC)

Reacted alkylamine	Alkylamine content in polymer (wt%)	Pretilt angle (°)
$CH_3(CH_2)_{11}NH_2$	10	10
$CH_3(CH_2)_{15}NH_2$	10	19

Fig. 3.7 A rubbing machine developed and constructed in 1971. It had the world's first dry wound cloth cylinder, and it was possible to adjust the intensity and the direction of rubbing
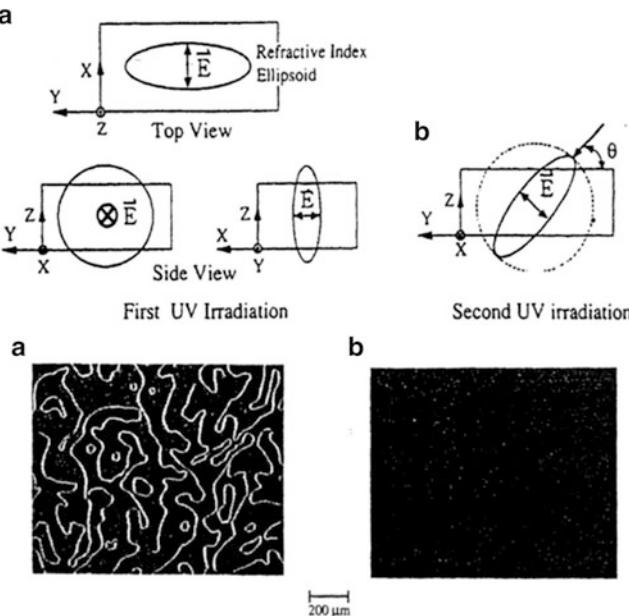
STN-LCD. The cylinder is wrapped with the rubbing cloth and was the first dry cloth machine. Up to then, the American RCA company and Jim Fergson at ILIXCO used a wet process with organic solvents and surfactants. The basic approach of rubbing machine shown in Fig. 3.7 is used as a standard technique in LCD factories today [10].

3.1.3 Mechanism of the Liquid Crystalline Interface Orientation

There is the opinion that the interfacial orientation of the liquid crystals a mystery, but there is not such a thing. Interface orientation is similar to the bulk orientation of the liquid crystal and can be regulated. In other words, the orientation between rod-like or board-shaped molecules can be explained by two effects that contribute equally: van der Waals attraction (Maier–Saupe) and the exclusion volume minimum effect (steric interaction) (Oseen) [19–21]. Rubbing extends the molecules in a polymer film in one direction and produces an optical anisotropy. Elongated molecules like those of liquid crystal in contact with such a film align parallel with such an optical anisotropy [19–21]. When these two anisotropic mediums, film and LC molecule, are below a distance of 10 nm, the thermal radiation emitted by one of those two molecules gets absorbed by the UV absorption edge of the other [22]. This is the mechanism of the attractive van der Waals or London forces [22]. The exclusion volume effect is to minimize the volume of an empty space (i.e., a bubble) in a liquid crystal, and thus, the free energy becomes the smallest [21]. As a result, liquid crystal molecules align along the branched tethered molecules on the interface or incline and form an asymmetry triangle at the interface which is the origin of the pretilt angle in Fig. 3.3 [18]. The tethered branched molecules or photopolymerized polymers lead to a perpendicular orientation (called homeotropic alignment) in order to use them as alignment films for vertical aligned LCDs (VA-LCDs), where the pretilt angle needs to be slightly lower than 90° [23]. There was the opinion that alkyl branches, which are attached to PI, may be thermally unstable to give a firm pretilt angle. But it is thought that both in STN-LCD and VA-LCD a stable LC molecular system may be developed as a whole system consisting of alkyl branches on the substrate, LC molecules near the surfaces, and LC molecules in the bulk region in an LC cell that has a narrow gap. In addition, Dwight W. Berreman's proposal that orientation occurs due to azimuthal anchoring in grooves is valid, too [24].

One often speaks of the strength of the alignment, but the formula for the surface anchoring energy of the aligned liquid crystal molecules per unit area can be given by the Rapini and Papoular approximation $F_s = A_s \sin^2\theta$, in which θ is the angle of liquid crystal molecules from the substrate surface [25]. This resembles an elastic energy in an elongated spring by x in it's length such that $F_x = -(1/2)\,kx^2$.

The LC molecules can align parallel to a completely smooth surface. This illustrates the minimum exclusion volume effect by Okano [26]. Generally, the anchoring energy A along the polar angle direction is extremely strong, $A_\theta = 10^{-3}$ J/m^2, for the planar orientation. The anchoring energy of the azimuthal direction is weak, $A(\varphi) = 10^{-4}$ J/m^2. The van der Waals energy is around 10^{-6} J/m^2 [22]. More detailed arguments for the strength of molecular alignment are outlined in the literature [27, 28].

Fig. 3.8 Defect-free TN-LCD by using photoalignment. (**a**) With defects, (**b**) Without defects (©SPIE)

3.1.4 Other Orientation Methods

3.1.4.1 Photoorientation

Defect-free interfaces for liquid crystal orientation can be attained by irradiation of poly(vinyl cinnamate) or polyimide with polarized UV light as reported by Shunsuke Kobayashi, Yasufumi Iimura, and others [29]. Figure 3.8 shows an example of the technology developed by the author's group for fabricating a defect-free TN-LCD by photoalignment [29]. Photoalignment has become an indispensable technology for producing large-area LCD with 4 K × 2 K or 8 K × 4 K pixels operated by VA or IPS mode. An example of this technology is that named UV^2 by Sharp [30].

3.1.4.2 Orientation by Using Langmuir–Blodgett Films

Orientation by using Langmuir–Blodgett films is possible even without rubbing. The transfer of the alignment film from the water surface onto the substrate creates an anisotropic film that can be used to align LCs [31].

3.1.4.3 Smooth PI Films

Defect-free polymer-stabilized V-shaped switching (PSV)-FLCD is realized by using a smooth PI alignment film [32], for example, the highly smooth PI (RN-1199) of Nissan Chemical Industries that has been widely used for in-plane switching (IPS)-LCD and fringe field switching (FFS)-LCD.

3.1.4.4 Amorphous TN-LCD

When a nematic liquid crystal is cooled down from the isotropic phase, oriented nematic droplets are physically adsorbed physics on the interface. As a result a TN-LCD cell with a wide viewing field is formed [33]. This device is called amorphous TN-LCD [30].

3.1.4.5 Alignment of LC Molecules on a Stretched Polymer Film

Stretch-drawn polymer films show an optical anisotropy; this film may be capable of aligning LC molecules in the direction of the stretching. Actually, the author's research group demonstrated the successful operation of a TN-LCD cell using stretched film of polyvinyl alcohol for the surface LC molecule alignment [34].

3.1.4.6 Surface-Stabilized FLCD

In a ferroelectric liquid crystal by reducing the cell gap of a cell to a critical value, the helix of the LC medium is unwound and the FLC medium takes a planar conformation due to the surface anchoring effect [35]. This device is called surface-stabilized (SS)-FLCD [35].

3.1.4.7 Effect of the Doping Nanoparticles into LCD on the Surface Effect

Doping nanoparticles into the host medium of an LCD or surface alignment films arouses the modification of surface anchoring effect and thus as an example a tremendous increase of contrast ratio of a TN-LCD is produced [10, 36, 37].

3.2   Development of Alignment Films that Supported the Liquid Crystal Industry

Koji Kuroda and Makoto Matsuo

3.2.1   Introduction

The "Most notable patents in the liquid crystal field" [38] section on the website of the Japanese Patent Office lists up seven Western and three Japanese innovations concerning twisted nematic liquid crystal display devices that count as "what is considered to be a specific technology that has supported a major position of the liquid crystal display field." Among others, the uniquely identifying material is polyimide alignment film—an invention that contributed to the development of the LCD industry. The first half of the 1970s was the time when the competition was extremely fierce to research and develop and industrialize alignment films that could align LC molecules completely uniform on the patterned electrodes in a stable manner.

3.2.2   Development of Liquid Crystal Alignment Films

3.2.2.1   Worldwide Competition for Liquid Crystal Display Device Industrialization

Followed by the invention of liquid crystal electro-optic effect by the RCA Corporation in the United States in 1962, the invention of the twisted nematic (TN)-type liquid crystal display by Hoffmann-La Roche in Switzerland in 1970, and the development of the integrated circuit (IC), the global race to develop electronic calculators and watches started. As the impedance matching is good between LCDs and ICs, an LCD can be driven directly from the IC with a button battery, combining the advantages of compactness with low power consumption.

For successful industrialization, the alignment films to produce a completely uniform display and the sealing technique to keep long life were the two major targets of development challenges. A wristwatch that was on the market by the Brown, Boveri et Cie company at that time had an alignment film made from obliquely evaporated silicon dioxide and sealed with low melting point glass and with solder at the inlet. It was a highly reliable watch with inorganic materials. But because of the low throughput of the vacuum evaporation process and the high-temperature sealing process it had a very low productivity. Therefore most Japanese companies focused on the development of polymer alignment film with organic resin sealing for high-throughput production by low-temperature processing.

3.2.2.2   The Development of the Alignment Film Was Decisive for the Liquid Crystal Display Industrialization

The effect of the alignment layer that used surfactant and polyvinyl alcohol is disclosed in the patent by the NCR company, filed in 1972. It was tested carefully in the laboratory, but the most important factors for industrialization, "orientation uniformity," "stability," and "high productivity" were still unsolved difficult problems.

Polyimide alignment film patent of Dai Nippon Printing Co., Ltd., filed in 1974, showed high weathering stability and uniform alignment and was recognized as one of the outstanding inventions to production stability. As the active development by material manufacturers continued, most domestic manufacturers adopted the polyimide alignment film.

3.2.2.3   Background of Practical Polyimide Alignment Film Development

The Liquid Crystal Development Strategy of Dai Nippon Printing Co., Ltd.

The technologies developed in the food airtight long-life packaging and thin-film printing can be applied, because an LCD is a kind of a highly defined packaged device. At that time Dai Nippon Printing Co., Ltd. (DNP) had a 50 % worldwide market share for shadow mask business which is one of the main components of the cathode-ray-tube-type color TV. The Central Research Institute embarked on the development of a liquid crystal display device in 1973, because they were determined that they had an advantage in the business development of precision electronic components for display field customers.

Stick on the Search of the Alignment Film Materials

In those days various display defects caused by irregular liquid crystal alignment were serious problems for industrialization. Various defects such as the chirality reversal (reverse twist) and the molecular rise direction reversal (reverse tilt) of the liquid crystal caused stripe defects or contrast abnormality depending on the viewing angle and rubbing direction were frequent. In addition these phenomena were caused by a number of factors, even depend on the combination of types of the liquid crystal structure and the alignment film materials. The selection of the most suitable alignment film material is essential for the production of stable LCDs and companies around the world were challenged by these issues.

DNP aimed at expanding their key packaging technology into all areas of industrial electronic components by their "extended print" route. Their central research institute proceeded to find a comprehensive selection method for functional materials, but in 1973 they still were at the level of material selection. There was quite some pessimism among experts on electronic components about the

Fig. 3.9 LCD with Polyimide and inorganic sealants (mass-produced module for the Swiss SSIH company in 1976)

use of unproven polymers, such as polyimide alignment film, but the background of DNP led to the invention of the polyimide alignment film [39, 40], which was fueled by the bold concepts of their inventor Makoto Matsuo in addition to the research by Takashi Toida who had a research background in heat-resistant polymers.

At that time polyimide was used in the coating of electric wires, because of its high durability and excellent insulation properties, but such a resin was considered unsuitable for clear display because of its dark brown color. However, Matsuo realized that polyimides are unique molecules which comprise a heat-resistant rigid skeleton of conjugated aromatic rings that form a straight chain. Upon hearing this idea, Toida utilizing his expertise, demonstrated that rubbed polyimide thin film could be used to uniformly align liquid crystals.

Furthermore, since polyimides can withstand fusing temperatures of low melting point glass, an LCD with inorganic hermetic sealing could be developed [41]. In 1975 SSIH in Switzerland mass produced LCD modules with DNP's inorganic hermetic sealing LCD with polyimide alignment film (Fig. 3.9) and they accomplished the feat of zero claims for 200,000 sold units, which demonstrated the merit of durability and display performance of polyimide alignment film for the international market.
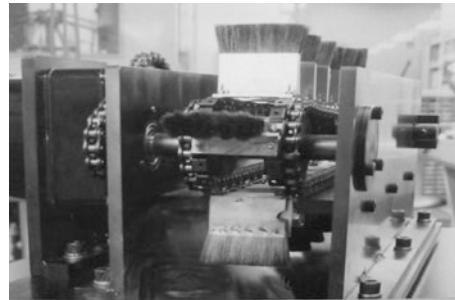
3.2.3 Industrial Superiority of the Polyimide Alignment Film and the Rubbing Method Development

3.2.3.1 Industrial Superiority of the Polyimide Alignment Film

Polyimide alignment films have the following excellent properties [42]:

(a) A polyimide surface allows for many different types of molecular interaction with liquid crystal molecules that lead to a stable homogeneous alignment of the molecules while being chemically inert.
(b) Polyimide forms uniform film on patterned LCD electrodes without any defects or irregularities. They are not influenced by the surface polarity change and

Fig. 3.10 Brush rubbing
machine (1975)

microscopic irregularities of the glass electrodes and can be coated by a variety
of techniques.

(c) Through the rubbing surface, polyimide leads to a uniformly well-aligned,
controlled orientation of the liquid crystal molecules.

(d) The alignment effect of polyimide by rubbing withstands the heat resistance
test of 500 °C for 5 min [43–45].

(e) As the tilt angle of the liquid crystal molecules against the rubbed polyimide
film surface is low, the threshold voltage slope is sharp and stable, polyimide
alignment is suitable for multiplex driving LCDs with a large number of lines.

3.2.3.2 Development of a Stable Rubbing Technique
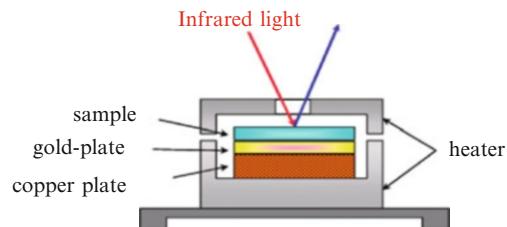
The next barrier to achieve the stable orientation of liquid crystals is a uniform
rubbing method. A commonly used cloth at that time was velveteen, but fibers
easily detached, pressure unevenness due to microscopic surface roughness irreg-
ularities on the electrode and damages by the corner edges of the glass substrates
caused various alignment defects. This required an extensive and time-consuming
inspection to weed out defect products.

We investigated many different materials for rubbing and found that raccoon
dog hair is particularly effective for rubbing. Electron microscopy showed that the
hairs are finely branched at their tips. Because of the elasticity of the hair, the
applied pressure during rubbing is dispersed evenly through the branched tips and a
homogeneous force is uniformly applied at the contact points. The hair of a rubbing
brush is aligned in bundles by the hands of a craftsman who adjusts them to the
precision of 0.1 mm in order to process evenly wide areas (Fig. 3.10).
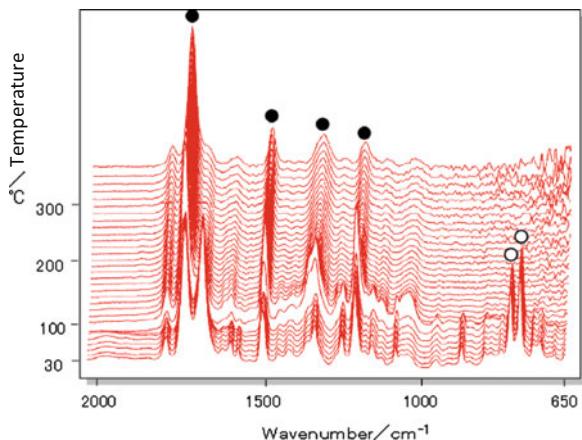
3.2.3.3 Later Research of Polyimide Alignment Film

There is no established mechanism to explain the stable horizontal alignment of
liquid crystals on rubbed polyimide (PI) films. There is a concentration range in
which a PI solution shows a lyotropic liquid crystalline phase. With the advance of
a PI solution drying, the concentration reaches to this liquid crystalline phase range

Fig. 3.11 Cast film heating measurement system

Fig. 3.12 Infrared spectroscopy of polyimide film formation process from solution with temperature rise
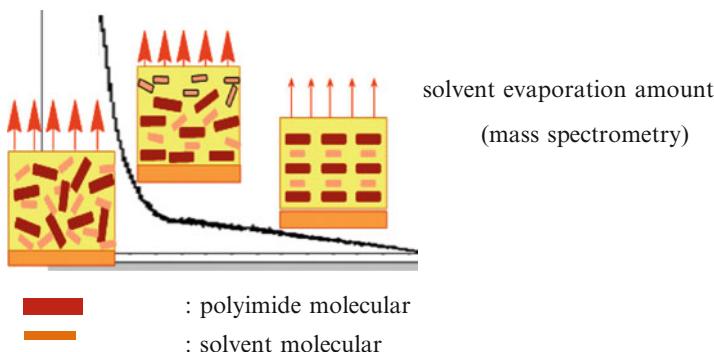
and the PI molecules adsorbed on the electrode surface act as a "command surface" influencing the molecular orientation over the bulk film. Koji Kuroda et al. of Dai Nippon Printing Co., Ltd. have reported the sudden horizontal alignment of PI molecules during the drying process [46].

They followed the drying process of a PI solution on a gold-plated copper during heating (10 °C/min) (Fig. 3.11) with infrared reflection absorption spectroscopy. When the polymer concentration reached about 10 %, the solvent's absorption peaks suddenly disappeared (Fig. 3.12).

Since the spectroscopy can only selectively detect vertically polarized vibrations, the uniformly oriented solvent's absorption peaks disappear when the whole molecular vibrations are arranged horizontally, which happens when the PI solution is in the lyotropic liquid crystal phase. The arrangement of the PI molecules is depicted in Fig. 3.13 which also explains the increase in elastic modulus of the coating and the decrease in volume change by solvent evaporation. In homogeneous solution, the evaporation of the solvent is proportional to the amount of the remaining solvent because of convection in the film. On the other hand, in organized solution with solvents, such as lyotropic LCs, solvent evaporation is limited with the solvent diffusion rate showing a fixed rate solvent decrease.

Masao Oe used sum-frequency generation vibration spectroscopy to investigate the molecular orientation effect and found that the macromolecular main chains of PI are aligned at a slight angle towards the actual rubbing direction [47].

solvent evaporation amount

(mass spectrometry)

: polyimide molecular

: solvent molecular

Fig. 3.13 Model of the solution structure and graph of solvent content of films during the drying process

3.2.4 Industrial Development of Polyimide Alignment Film Technology

3.2.4.1 Development from Wrist Watches, Electronic Calculators, and Word Processors Towards Flat-Screen TVs

The time-sharing multiplex drive that was used in watches and clocks was also applied to word processor displays that could display letters and other figures.

It was necessary to secure a suitable on-/off-voltage difference (margin) in those multiline displays and the PI alignment film stabilized the low inclination angle of liquid crystal molecules. After that, thin-film transistor electrodes were developed that enable minute gradation of the pixels. Color filters attached on the opposite electrode enabled large screen flat-panel color TVs were realized. But still, it is the polyimide alignment film on both electrodes that could achieve the stable orientation of the LC molecules.

During this time, the development of various types of LCD display products advanced, but in the long-term business development of the liquid crystal industry it was always the polyimide structure that could cope with new problems and challenges.

3.2.4.2 Business Development and Patent Strategy

In 1976, the number of patents and utility model exhibitions of Japan topped 1,200 cases according to a patent dossier at that time. The reason why many patents were applied for a few-layered device was the electronic companies' strong policy for developing LCD TV to their main business. As Dai Nippon Printing had the global top share for shadow masks in cathode-ray tubes their main customers were electronics makers. Since the company could not compete with the customers they decided to withdraw from the LCD market at the end of 1976.

On the other hand, in order to promote the inflection of the patents, that is, their accumulated intellectual assets, DNP announced license agreements with LCD makers that used polyimide alignment films. As for the polyimide alignment film patent applied for at the end of 1974, a US patent was established in 1976, but because of many formal objections, the examination was exceptionally prolonged in Japan.

In the meantime, Kuroda made full use of analysis technique and grasped the constitution and materials of LCDs. And he had been involved with the development of LCD technology (watches, calculators, LC materials, sealing materials, alignment films, and so on) from the very beginning, and through his efforts the patent was finally granted in 1989. As the long term of 15 years was spent on registering the patent, most of all electric companies commercialized LCDs with PI alignment film.

On the other hand, in order to facilitate the accumulation of proprietary rights, DNP announced license agreements with LCD makers that used polyimide alignment films. Newspapers picked up the issue that Dai Nippon Print claimed patent fees to customer companies that had used the technology and that a wave of US propatents had flooded Japan [48].

3.2.5 Expectations for the Technological Development in Japan Following the Liquid Crystal Display

The LCD business to develop a flat-panel TV had been dominated by Japan for nearly a quarter of a century, but other countries caught up because of the generalization of the materials, the equipments, and the technologies. And the development target has changed from hardware performance to human interface with interlocking software with hardware. Furthermore, the reduction of production cost, as well as strengthening the local support in overseas production bases, is necessary.

Japan faces some challenges in the future because of the aging society, shrinking markets, the decline in export competiveness due to the appreciation of the yen, and the issue of educating the next generation and keeping excellent work force.

We Japanese need to reflect on our unique creativeness in the development of fine technology. We have the sense to live in harmony with nature in our daily lives. Then, we can in put a new value into nurture future dreams.

3.3 A Brief History of the Alignment Film for STN-LCDs

Shunsuke Kobayashi

After the announcement of the twisted nematic liquid crystal display (TN-LCD) in 1971 [3], it quickly came to be used in calculators and digital watches. It had a so-called seven-segment display which was not a dot matrix. TN-LCD dot matrix displays were also made, but the number of scanning lines had been limited to

about ten. The reason is because it fulfilled the specification of a steep threshold of the scanning line that was required for the direct multiplexing of a 640×480 dot VGA matrix. There exists a prototype computer from around 1987 with TN-LCD, but with insufficient visibility.

Later, in 1986 a prototype of a super twisted nematic STN-LCD that allowed for 400 scanning lines had been developed, and this looked like a savior for this dilemma [4]. However, severe problems concerning the mass production surfaced immediately. It was not possible to make defect-free STN-LCDs with conventional rubbed polyimide (PI) alignment films (introduced in Sect. 3.1.2); instead, stripe domains (see Fig. 3.4 in Sect. 3.1) occurred. Hiroyoshi Fukuro and Shunsuke Kobayashi successfully developed polyimide (PI) films by synthesizing PIs with alkyl side chains and rubbing these films. The key point on this technology was to give a high pretilt angle to the LC molecules of 5–7° after rubbing. This paved the way to produce a defect-free STN-LCD with a very high pretilt angle in the range of 10–19° (Table 3.1 in Sect. 3.1) [49, 50].

Production of STN-LCDs was started simultaneously by several electronic companies in Japan using such PI alignment films. Some of these companies have made large investments in the vacuum deposition technology for STN-LCD production, but these equipments might not be useful anymore. The concept at that time is shown in Fig. 3.3 in Sect. 3.1. This idea was born in discussions between Shunsuke Kobayashi and Koji Okano, who had been a Tokyo University Professor at that time. The idea was that the pretilt angle could be generated by the minimum excluded volume effect of LC molecules aligning on the tiny asymmetric triangle structure orientated in a unidirectional direction on the substrates in an LC cell. This kind of structure was actually realized by unidirectional rubbing of a PI film with alkyl side chains.

Kobayashi illustrated this idea to Hiroyoshi Fukuro in a train to Chiba, where his laboratory was located. After that Fukuro had come as a research fellow to Kobayashi's group at Tokyo University of Agriculture and Technology from Nissan Chemical Industries, Co., Ltd. Such a PI was then synthesized by Nissan Chemical Industries, and the operation of a defect-free STN-LCD was demonstrated in Kobayashi's lab using such a PI [51].

The generation of high pretilt angle by such an approach led immediately to the development of vertically aligned nematic (VA)-LCDs using PI films with a very high pretilt angle of 89° on the basis of the research of PI-coated STN-LCDs.

It was also reported around that time that such a pretilt angle could happen if one lowers the interfacial energy, and the effect of the alkylated PI can be explained by the reduction of the interfacial energy [52]. Thereafter, a series of PIs that allow the generation of a stable pretilt, optical high transparent PIs, and cyclobutane polyamic acid (CBPA; patent opening 1992/6/1) were developed and manufactured by Nissan Chemical Industries, Ltd.

Also, JSR produced all kinds of useful PIs that were then introduced to the market including PIs alignment films for TFT driven TN-LCD. Later, PIs with a very low pretilt angle (very smooth ones) have been developed by Kobayashi and Fukuro for producing defect-free ferroelectric LCD and in-plane switching (IPS)-LCD and fringe field switching (FFS)-LCD.

3.4 Alignment Films for TFT-LCDs: Development of Organic-Solvent-Soluble Polyimides

Michinori Nishikawa

3.4.1 Introduction

Since the invention of the twisted nematic (TN)-type LCD in 1970, rubbed alignment films have been used for the alignment of the liquid crystal molecules [53, 54]. Until 1975, a wide variety of organic and inorganic materials had been developed in a trial-and-error fashion [55], but at present the use had been narrowed down to polyimide materials. In particular, in this chapter I want to review the developmental history of organic-solvent-soluble (soluble) polyimide alignment films that are currently widely used in high-definition LCD TVs.
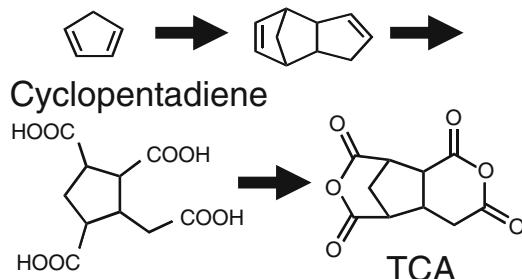
3.4.2 Development of Soluble Polyimide Alignment Films

3.4.2.1 The Alignment Film Business at JSR

Japan Synthetic Rubber Corporation (JSR) was established for the domestic production of synthetic rubber in 1957, but entered the diversified businesses that utilize rubber raw materials from around 1969. The first step was the development of a photosensitive material for semiconductors, and in search of new business, the LCD applications began to surface. Then the discussion started if it could be that new materials need to be synthesized for digital clocks, for example. LCDs at the time were TN-type monochrome displays, in which the alignment layer had to be heated to a high baking temperature of over 300 °C in order to transform the wholly aromatic polyamic acid precursor into polyimide.

The chance for JSR to enter the alignment film business was a pocket-size LCD TV color display that Suwa Seiko Corporation has announced for the first time to the world in 1983. In order to make a color LCD, red, green, and blue filters needed to be placed on each micropixel. The method of choice to produce patterned filters at that time was prepared by photolithography using natural gelatin, followed by dyeing using three colors. The high-temperature baking of the alignment film needed to be done on top of such a color filter, which caused problems because the dye and gelatin would undergo thermal decomposition and the original hue would change.

Fig. 3.14 Synthetic scheme of TCA

3.4.2.2 Development of Soluble Polyimide Material (1)

Wholly aromatic polyimide alignment films at that time needed a baking temperature of over 300 °C, but for color LCD applications it was necessary to make polyimide materials that can be cured at temperatures as low as 200 °C. In response to this request, we in JSR started research and development of new alignment film materials from 1980. It was supposed that a soluble polyimide could be made; a polyimide alignment film can be obtained by simply removing the solvent.
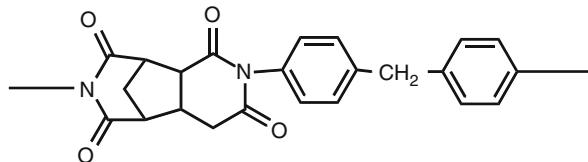
First we needed to trace down if wholly aromatic polyimides existed that could be baked at lower temperatures. In the patent literature, the most used solvents to dissolve polyamic acids were cresols. By using certain cresol derivatives it was possible to form soluble polyimides from polyamic acids, and soluble polyimides were thus obtained and introduced to several LCD manufacturers that use these materials up to today. As a result (it will be regarded as obvious by now), the production of a prototype LCD, let alone the mass production of LCDs, would not have been possible without the disinfectant-like smell of cresol. The concept and the application to use soluble polyimide materials for low-temperature bakeable alignment films was not by mistake, but their research and development hit a big wall.

3.4.2.3 Development of Soluble Polyimide Material (2)

While we were giving up the application of the traditional wholly aromatic polyimides, we received a surprising help from among the in-house research seeds. For the production of synthetic rubber, they used as raw materials the C4 fraction (called C4 fraction because of the number of carbon atoms in the compounds of carbon number 4) of the petrochemical industry: butadiene and isoprene. The C5 fraction was a by-product, which also contained cyclopentadiene.

In-house seed research had been used to make the best use of this component. Many derivatives had been synthesized by using this component, one of which was also tetracarboxylic acid that was a precursor to polyimides via its dianhydride (TCA) as can be seen in Fig. 3.14. It is believed that the introduction of the bulky component into a polyimide would improve its solubility in organic solvents.

Fig. 3.15 Chemical
structure of OPTOMER®
AL1051

However, unlike the aromatic tetracarboxylic acid dianhydride that was dominant at the time, a compound having a five-numbered ring structure aliphatic was highly unusual.

The question of how such a compound can provide the thermal stability required for LCD applications was raised, and a series of diamines were tested for trial-and-error imidization reaction conditions. One soluble polyimide that was born among them was the OPTOMER® AL1051 shown in Fig. 3.15.

3.4.2.4 Properties of Soluble Polyimides

The polyimide AL1051 is based on an aliphatic acid structure and can be dissolved in γ-butyrolactone which has a boiling point of about 200 °C. When the solvent is removed at 200 °C, a polyimide coating can be easily produced.

While examining the characteristics of this material, we found several useful properties [56]. Even though we initially were concerned about thermal stability, we found that it has a heat resistance of over 350 °C.
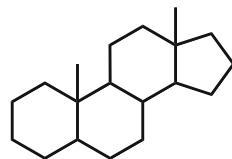
Further, when compared to the wholly aromatic polyimides that were mainly used at that time, AL1051 forms a highly transparent coating film, which is advantageous for optical applications, such as LCDs. Premarket testing from around 1984 told us that the films responded well to rubbing and could very well align liquid crystal molecules. The electric characteristic of the voltage-holding ratio [57], which is important for transistors in TFT-LCDs, was found to be excellent for the soluble polyimide AL1051.

As the LCDs changed from black and white to full color, the drive system also evolved from simple matrix to active matrix type. Soluble polyimides matched the needs of the LCD and were used as alignment films for TN-type LCD.

3.4.3 Highly Functional Soluble Polyimide Alignment Films

In order to improve the display quality of LCDs, we received requests to continue to develop alignment films. One of these requests was the control of the pretilt angle at the interface of the alignment film and liquid crystal molecules to match the needs for higher-definition TN-LCDs. AL1051 that had been developed by JSR shows a pretilt angle of about 1°. For high-definition LCDs, the reverse-tilt defect becomes more significant and pretilt angles of 3–5° are required. Another request concerns

Fig. 3.16 Chemical
structure of steroidal unit

the wide-viewing-angle mode of LCDs for TV applications. Alignment films in which the LC molecules are arranged vertically towards the alignment film have been actively promoted by LCD manufacturers. In order to meet these two requests, new techniques for controlling the pretilt angle of the alignment layer needed to be developed.

One approach to increase the pretilt angle of the alignment film is the introduction of fluorine-containing groups or long alkyl chains that increase the hydrophobicity of polyimides. But it was found that the pretilt angle becomes unstable and that the electric characteristics of the LCD deteriorate. By introducing the steroidal skeleton, an alicyclic biomaterial (see Fig. 3.16), into the polyimide, we have managed to achieve both good electric properties and excellent pretilt angle stability [58]. Alignment films that contain the steroidal skeleton are being employed in various LCD televisions and have become an essential material for improving the image quality of LCD TVs.

3.4.4 Conclusion

The alignment film is a film of only 100 nm thickness, but it is an indispensable material for manufacturing LCDs. I reviewed the history of the material design of the alignment film during the time when the display mode of the LCD changed. It is important not to miss the evolution of technologies in the development of new materials. Incorporating the material design technology in a timely manner will lead to seeds for future evolution of LCD technology. It is the mission of material manufacturers to diligently study new materials while expecting the evolution of LCD technology.

References

1. P. Chatelain, Acta. Cryst. **4**, 453 (1951)
2. C. Mauguin, Bull. Soc. Fr. Min. **34**, 71 (1911)
3. M. Schadt, W. Helfrich, APL **18**, 127 (1971)
4. T.J. Scheffer, J. Nehring, APL **45**, 1021 (1984)
5. M.F. Schiekel, K. Fahrenschon, Appl. Phys. Lett. **7**, 391 (1976)
6. R. Kiefer, B. Weber, F. Windscheid, G. Bayer, Proc. Jpn. Display. **92**, 47 (1992)
7. Oh-e, M. Ohta, S. Aratani, K. Kondo, Proc. 15th IDRC. 577 (1995)

8. S.H. Lee, S.-L. Lee, H.Y. Kim, Appl. Phys. Lett. **73**, 2881 (1998)
9. Y. Miyazaki, H. Furue, T. Takahashi, M. Shikada, S. Kobayashi, MCLC **364**, 491 (2001)
10. S. Kobayashi, *Progress in liquid crystal science and technology*, Part 1, in *Honor of Shunsuke Kobayashi's 80th Birthday*, ed. by H.S. Kwok, S. Naemura, H.L. Ong (World Scientific, 2013)
11. J. Janing, Appl. Phys. Lett. **21**, 173 (1984)
12. M. Matsuo, T. Tokita, in Section 3.2 in this book and Japanese Patent 1,541,667; T. Tokita, I. Tsunoda, 8th international liquid crystal conference (Kyoto, 1980)
13. H. Fukuro, S. Kobayashi, MCLC. **163**, 157 (1988); Japan Patent 1,832,762(H6/3/29), 1,924,246(H7/4/25)
14. K. Yoshida, H. Fukuro, S. Kobayashi, Proc. Jpn. Display. 396 (1986)
15. A. Miyaji, M. Yamaguchi, A. Toda, H. Mada, S. Kobayashi, IEEE Trans. **ED-24**, 81 (1977)
16. S. Kobayashi, F. Takeuchi, Proc. SID. **14/4**, 40 (1973)
17. E.P. Raynes, Elec. Lett. **10**, 10 (1974)
18. T. Sugiyama, S. Kuniyasu, D.-S. Seo, H. Fukuro, S. Kobayashi, Jpn. J. Appl. Phys. **291/10**, 2045 (1990)
19. S. Chandrasehar, *Liquid Crystals*, 2nd edn. (Cambridge University Press, Cambridge, 1992)
20. P.G. de Gennes, J. Prost, *The Physics of Liquid Crystals* (Oxford University Press, New York, 1994)
21. K. Okano, S. Kobayashi, *Liquid Crystals, Part I: Fundamentals, Part II: Applications* (Baifukan, Tokyo, 1985) (In Japanese)
22. K. Okano, N. Matsuura, S. Kobayashi, Jpn. J. Appl. Phys. **21/2**, L109 (1982)
23. H. Yoshikawa, H. Ushinohama, H. Furue, T. Takahashi, S. Kobayashi, Proc. IDW'99, 1087 (1999)
24. D. Berreman, Phys. Rev. Lett. **28**, 1683 (1972)
25. R. Rapini, M. Papoular, J. Phys. (Paris) **30–4**, 54 (1969)
26. K. Okano, Jpn. J. Appl. Phys. **22**, L-343 (1983)
27. S. Ishihara, J. Display. Technol. **1/1**, 30 (2005)
28. K. Takatoh, M. Hasegawa, M. Koden, N. Itoh, R. Hasegawa, M. Sakamoto, *Alignment Technologies and Applications of Liquid Crystal Devices* (Taylor and Francis, London, 2005)
29. S. Kobayashi, Y. Iimura, SPIE. **3015**, 40 (1997)
30. K. Miyachi, K. Kobayashi, Y. Yamada, S. Mizushima, SID2010 Digest of Tech. Papers, **41**, 579 (2010)
31. K. Ikeno, A. Oh-saki, N. Ozaki, M. Nitta, K. Nakaya, S. Kobayashi, SID1988 Digest of Tech. Papers, **19**, 45 (1988)
32. H. Furue, Y. Iimura, Y. Miyamoto, H. Endoh, H. Fukuro, S. Kobayashi, MCLC **328**, 193 (1999)
33. Y. Toko, T. Sugiyama, K. Katoh, Y. Iimura, S. Kobayashi, J. Appl. Phys. **74/3**, 2071 (1993)
34. H. Aoyama, Y. Yamasaki, N. Matsuura, H. Mada, S. Kobayashi, MCLC. Lett. **72**, 127 (1981)
35. N.A. Clark, S.T. Lagerwall, Appl. Phys. Lett. **36**, 899 (1980)
36. N. Toshima, S. Kobayashi, H. Shiraishi, H. Sawai, H. Kakiuchi, Japanese Patent 2013–149,635
37. Y. Shiraishi, S. Kobayashi, N. Toshima, Israel. J. Chem. **2012**(52), 908 (2012)
38. http://www.jpo.go.jp/shiryou/s_sonota/map/denki07/frame.htm
39. M. Matsuo, T. Toida, Tsunoda, Manufacturing method of the electrode panel for liquid crystal display, Japan Patent 1,541,667 (1974)
40. Electro-optical cell for field effect type liquid crystal display, USP3,994,567 (1974)
41. M. Matsuo, T. Toida, I. Tsunoda, Japan Patent 121,799, Liquid crystal display cell
42. T. Kuroda, I. Tsunoda, J. Soc. Fiber. Sci. Technol. Jpn. 11, 329 (1979)
43. T. Kuroda, I. Tsunoda, 26th meeting of the Japan society of applied physics and related societies, (1979), p. 114
44. T. Kuroda, I. Tsunoda, Special meeting of the 142nd committee on organic materials used in information science and industry for Japan society for the promotion of science, (1979)
45. T. Kuroda, T. Toida, I. Tsunoda, 8th international liquid crystal conference, Poster session (Kyoto, 1980)

46. Sakata, Takano, T. Kuroda, 3th discussion of polymer analysis, (1998), p. 111
47. M. Ohe, J. Vac. Soc. Jpn. **47**, 7 (2004)
48. The Asahi Shinbun 15 Apr (1992)
49. H. Fukuro, S. Kobayashi, MCLC **163**, 157 (1988)
50. S. Kobayashi, H. Fukuro, Japanese Patent 1,924,246 (25 Apr 1995)
51. K. Yoshida, H. Fukuro, S. Kobayashi, Proc. 6th IDRC, Japan Display'86, 396 (1986)
52. K. Okano, S. Kobayashi, *Liquid Crystals, Applications. Part II, P52-80* (Baifukan, Tokyo, 1985) (In Japanese)
53. Y. Takeuchi, Display. Imag. **4**, 213 (1996)
54. M. Nishikawa, J. Imag. Soc. Jpn. **41**, 58 (2002)
55. J. Cognard, Mol. Cryst. Liq. Cryst. **1**, 1 (1982)
56. Y. Yokoyama, M. Nishikawa, Y. Hosaka, Proc. Jpn. Display. 384 (1989)
57. T. Shimazaki, S. Mizushima, S. Minezaki, K. Yano, M. Hijikigawa, Proc. Jpn. Liq. Cryst. Soc. 78 (1988)
58. M. Nishikawa, J. Photopolym. Sci. Technol. **24**, 317 (2011)

Chapter 4
Filters and Films for Liquid Crystal Devices

Tatsuki Nagatsuka, Kunihiro Ichimura, Yoji Ito, Motohiro Yamahara, and Takehiro Toyooka

4.1 Development of Polarizers to Support the Development of the Liquid Crystal Industry

Tatsuki Nagatsuka

4.1.1 Introduction

The research on birefringence and polarization has a long history and began with the discovery of light polarization by the Dutch scientist Christiaan Huygens in 1690 when he was experimenting with two calcite plates. Then, Etienne L. Malus accidentally discovered that the light reflected at an angle from the windows of

T. Nagatsuka
Nitto Denko Corporation, Onomichi, Japan
e-mail: tatsuki_nagatsuka@gg.nitto.co.jp

K. Ichimura
Tokyo Institute of Technology, Yokohama, Japan
e-mail: kuni-ichimura@mue.biglobe.ne.jp

Y. Ito
FPD materials Research Laboratories, FUJIFILM Corporation, Ashigarakami-gun, Kanagawa, Japan
e-mail: youji_itou@fujifilm.co.jp

M. Yamahara
Sumitomo Chemical Co., Ltd., Osaka, Japan
e-mail: yamaharam@sc.sumitomo-chem.co.jp

T. Toyooka
JX Nippon Oil and Energy Corporation, Tokyo, Japan
e-mail: takehiro.toyooka@noe.jx-group.co.jp

Luxembourg Palace was polarized, which he reported in 1809, and in 1812 David Brewster announced the law of light polarization by reflection and refraction, which now takes his name. Furthermore, William Herapath discovered in 1852 that a synthetic crystalline compound, iodoquinine sulfate (also called herapathite), can polarize the light of all wavelengths in the visible region, a phenomenon that is now the underlying principle of current absorption-type polarizers.

Seventy-five years later, in 1938, Edwin Land invented the sheet polarizer, called H-film, that has been industrialized as the Polaroid filter. Attached to the windows of ships and trains these filters can act as blinds, and they also have been widely used in polarized sunglasses. There was a time when Polaroid filters were considered as antiglare systems for large-scale windshield and headlights of cars [1].

Polarizers thus had already a long history when they were reborn as the core technology to support the liquid crystal display industry when the twisted nematic liquid crystal display (TN-LCD) watch was released in 1975, along with the commercialization of the calculator. LCDs are now used in various kinds of electronic home appliances, such as calculators, mobile phones, notebook computers, and car navigation systems. In the last 10 years the boom in the development of innovative input and output information devices, for example, large LCD TVs and smartphones, has totally wiped out the cathode-ray tube and has become the symbol of industrial structure innovation in the twenty-first century.

By applying a weak electric signal to the liquid crystal material with a layer thickness of about 5 μm sandwiched between transparent electrodes, the LCD display principle involves the distortion of the optical properties of the liquid crystal material. That distortion is visualized by using two polarizers. Even though various types of liquid crystal displays have been developed that use different switching and alignment methods, the basic principle that two polarizers are needed has not changed at all. In other words, the polarizer is an optical film and an essential need for the LCD. Polarizers are the "face" of the display as they are at the outermost layer of the display and must provide easy visibility.

In this section, I would like to summarize my little efforts to the development of polarizers that supported the LCD industry.

4.1.2 Development of Polarizers for LCDs

4.1.2.1 Proposal of Adhesive Polarizers

When we talk about the history of polarizers for the LCD industry, we first have to mention the adhesive polarizers.

The first practical use of a TN-LCD was calculators and watches in 1975. The most important feature of this display was the low power consumption that could be driven even with a small button battery and a reflective display that utilizes the reflection of external light for illumination. At that time, not only the Polaroid
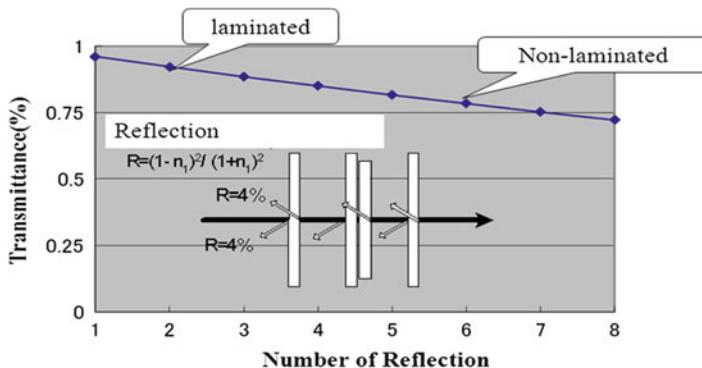
Fig. 4.1 Reflection loss and transparency at the air interface ($n = 1.5$)

company, but also a large number of small- and medium-sized manufacturers had been producing polarizers. The challenges at that time were both the thickness of the polarizers and the method to implement the plates to the display. The polarizer is placed on the front and on the back of the LCD cell, and the efficient transmission of "light" in particular needed to be addressed. Polarizers that were coated with a pressure-sensitive adhesive and bonded directly to the LCD cell have been made in order to solve this problem [2].

At each interface of materials with a different refractive index in the light path, there is a surface reflection as expressed in formula (4.1). Thus the amount of light that reaches our eyes is reduced, reducing the visual quality of LCDs by darkening them.

$$T = 1 - (n_1 - n_2)^2/(n_1 + n_2)^2 \tag{4.1}$$

Figure 4.1 shows the relation of the transmittance (T) and the number of reflections at the air interface by using $n = 1.5$ as a typical refractive index of the polymeric material. By placing two polarizers on both sides of the liquid crystal cell, one created six interfaces and a simple calculation shows a loss of 22 % of light intensity. The reflected light will lead to further deterioration of clarity and contrast of the display by stray light. Therefore, to reduce the number of interfacial reflections (e.g., by eliminating the air layer), the polarizers are bonded to the cell with an adhesive that has a refractive index of approximately 1.5. This significantly improves the light transmission efficiency, and it becomes easy to see a reflective LCD. The process of bonding with an adhesive layer will increase the number of processing steps at first glance, but because it contributes to the simplification of the implementation design of all the parts, it has become a common widely accepted technique. These methods have come in the spotlight again in recent years as the interlayer adhesion technology for 3DTV and smartphones.

4.1.2.2 Efforts of Nitto Denko Co., Ltd.

Commercialization of Adhesive Coatings for Polarizers

In 1975, Nitto Denko Co., Ltd. did not have their own production line for polarizers themselves, but they were responsible for the coating formulation and design of pressure-sensitive adhesives for customers who produced polarizers.

The mainstream method at that time of producing a pressure-sensitive adhesive tape was to coat the adhesive directly onto the substrate. However, there was no technology to precisely coat the adhesive material onto the polarizers that had a low scratch threshold and low heat resistance. There were very difficult problems of contamination and air bubbles, limits to the drying process, and the strict demand for small refractive index anisotropy. Slight uneven thickness of the adhesive will lead to defects in the display, even for pressure-sensitive adhesives. All this was completely different from the demands of customers of electronic adhesive tape so far. The aforementioned problems all led to visible optical distortions in the polarizer film. For this reason, the coating facility to apply the adhesive had to be installed in a clean room, the coating method of the pressure-sensitive adhesive transfer had to be studied, a stacked twist suppression technology had to be established, and the formation of microcrystals in the pressure-sensitive adhesive had to be suppressed, to satisfy customer requirements.

Development of Homegrown Polarizers

At first, we just provided the pressure-sensitive adhesive for TN-LCDs for clocks and calculators, but soon we started the development of homegrown polarizers in our company. As we embarked on the development we received a recipe to create a standard polarizer by Kuraray, which is a polyvinyl alcohol (PVA) manufacturer, and continued through "learning by doing." At that time, there already were a large number of manufacturers in Japan as well as in Europe and the United States for polarizers used in sunglasses.

We produced prototypes by dyeing and stretching PVA films at a speed of 10 cm per minute and could produce films with unexpected optical properties. But even though the PVA film had a width of merely 300 mm, the obtained polarizers were very uneven. Another big challenge was the improvement of the uniformity in appearance. The polarizer is laminated on both sides with a protective film in order to improve mechanical strength. At that time, triacetate and diacetate (TAC) films had been used as optically isotropic films. However, even though these films had an excellent optical uniformity, their moisture permeability posed a challenge to the reliability in humid conditions. We then proposed a method for coating an acrylic resin directly on the polarizer surface and such a film was commercialized as NPF-N.

The reliability was greatly improved, but because of its low glass transition temperature (T_g), we were not able to improve its mechanical strength and the dimensional stability during heat tests; FUJIFILM Corp. provided us with TAC

films and we restarted the development, resulting in the NPR-F-type films. It was extremely difficult to reduce streaks and slight dents that occur at the time of bonding. Even though we were familiar with the technologies and products for more than 30 years already, the pursuit of readability and ultimate beauty of LCDs is a challenge even today. The development from scratch was the start of our commercial success for polarizers. By relying on the wisdom and know-how of our predecessors, we have identified the problems, and while incorporating innovations in the production process along with the pursuit of principle we went on to finish a product for Nitto Denko.

In parallel with the development of homegrown polarizers, we have also started considering functions of semitransparent films by using reflections from the reverse side of the polarizer. In a joint development with an aluminum foil manufacturer, we developed reflecting films. Semitransparent films were produced by using our core expertise of adhesive tapes by coating polarizers with solutions that contain uniformly dispersed metals or metal oxides [3].

In those days, together with the engineers and manufacturers of raw materials, we created novel optical films not only for our customers but also for us. It is not an exaggeration to say that the production of TN-LCDs has started from these collaborations. Our customers at that time were not only in the domestic market, but also from the United States and the Soviet Union. We made our samples after the specifications from our customers, which led to plentiful orders.

Large transmissive STN-LCDs have been developed after the study on TFTs and were rapidly commercialized in the late 1980s. "Large" at that time meant 8 in. in size. Smaller TFT drives that employ STN-LCDs with a 3 in. diagonal, like LCD TVs or word processors, was started by over-the-counter electronics stores. When displays change from reflection type to transparent, the contrast reduction is a major challenge due to the lack of polarization characteristics. We have developed a polarizer with 10 times improved contrast ahead of our competitor companies. With increasing size of the display, a decrease in visibility due to the reflection of external light to the display surface has been a problem. Establishing the antiglare processing technology that made full use of precision coating technology and polymer compounding techniques to achieve easy viewing characteristics led to a timely commercialization again. Japan's LCD industry at that time succeeded in developing a transmission-type STN-LCD.

Our company has contributed to the advanced technology development of transparent and large displays by the threefold application of adhesive films, polarizers, and antiglare coatings.

Polarizers That Supported the Innovation of the LCD

Looking back at the LCD industry, through the infancy of reflective TN-LCDs, the LCD market began a major growth by establishing a transmission-type STN-LCD. Here, I want to have a look at this first period of growth from the infant state. The STN-LCD, a display with novel use of completely different organic materials,

became the driving force of the second growth period from the traditional electronic device, and of course there were many a challenge for engineers. The development of the optical compensation film (the phase difference plate) has played a major role in the success of the STN-LCD [4, 5]. In the beginning of the twenty-first century the TFT-LCD had been developed and in order to improve the display quality and performance of the LCD polarizers with an optical compensation function became necessary. We have developed a negative birefringence polymer, based on the optical design technology of polymer materials in our company, while we continued to commercialize coating X-Plates and positive optical compensation films. The details will be described in a separate chapter on compensation films.

The polarizer business of Nitto Denko, and its supporting R&D passed through the start phase of the LCD industry, has evolved into a system in which we anticipated the next half step of technology trends in the second growth phase. In other words, the primary growth period involved reflective LCD technology that is represented in small displays used for calculators and clocks. Those provided samples in a timely manner of how product specifications are going to be demanded by our customers, allowing us to brush up in material development in a short period of time that then led to commercialization. Then, in the second growth period in which large transmissive LCD technology represented by the word processor and small size TFT-TV became the driving force, we had started building the foundations to grow ahead of the proposed next developments. In the second half of the second growing period, we started the efforts to realize the next generation that would play a role in the LCD industry, thus contributing significantly to the growth of an industry that was superior to CRTs.
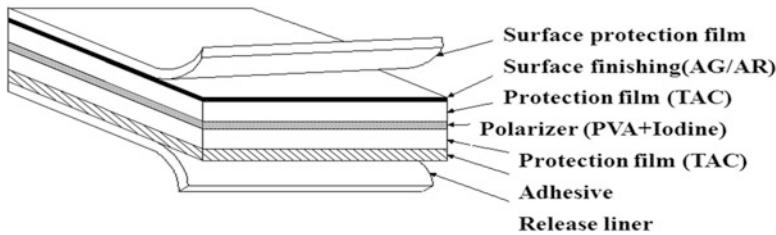
In addition, the polarizers are necessary materials for LCDs and they are capable of influencing the value of the merchandize. Laminating the polarizer onto a cell and equipping them with an external optical function is one of the concepts.

Because Nitto Denko was the developer of polarizers, we became the hub for our customers to collect their needs and act as the center of novel product creation. Our proposal to integrate the polarizer with a brightness enhancement film, which is one of the components of the backlight, contributed to the man-hour reduction of LCD development of low power consumption devices [6, 7].

So far, I explained why our polarizer business has grown while we were following up on changes in the LCD industry. From here, I will look back at the technologies and concepts that have supported the growth.
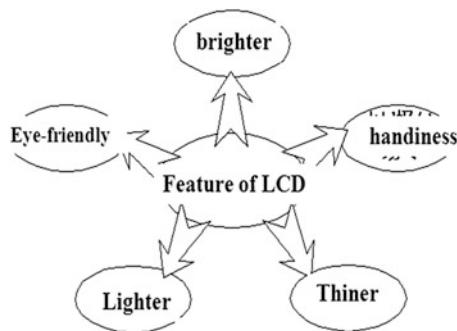
The structure of the polarization plate is shown in Fig. 4.2, and Fig. 4.3 shows the required characteristics. I will explain the special characteristics of each component material, the necessary LCD technology, and their impact on the market based on the basic technologies of our company.

The manufacturing technology of polarizers that are used in modern LCDs had been established already in 1930. As described above, polarizers were prepared by adsorbing iodine on PVA that was immersed in an aqueous iodine solution. This is the substrate that becomes the polarizer after stretch orienting the PVA. In order to give mechanical and physical strength, this stretched film of a water-soluble

Fig. 4.2 Structure of a polarizer

Fig. 4.3 The function
that is demanded from
a characteristic and
a polarizing plate of
the LCD

polymer is laminated between two protecting films of acrylate, diacetyl cellulose, or triacetate cellulose (TAC) that show low optical distortion. A variety of added features to this polarizer surface has led to important business opportunities. Here, I will introduce the efforts on our side to improve three features: becoming brighter, becoming easier to view, and becoming easier to handle.

Becoming Brighter

Two paths approach were carried out to increase brightness of a polarizer. As mentioned above, making adhesive polarizers has contributed greatly to increase the brightness. I might get reproached by my superiors on saying this, but the other approach was that several fortunate findings enabled us to accomplish industry standards.

In conjunction with the evolution of the LCD display modes, we have challenged the polarization characteristics to become an "exponential" innovation. We used the increase in contrast by a factor of ten as an indicator of product update cycle.

Since the invention by Land, the increase of a few percent in linear transmittance had been used as yardsticks, but have decreased to time for such a development to one tenth. In the mid-1980s, we were still a newcomer manufacturer, but we were matching the commercialization of the TFT-LCD by commercializing our G-type series polarizer. When I announced our findings at the most important conference of the Society for Information Display in 1985, I encountered great opposition [8].

Becoming Easier to See

The LCD is ease on the eyes, which means an increase in visibility, is an important point of a successful display. Polarizers are the "face" of the display as they are at the outermost layer of the display and must provide easy visibility.

In 1995, the LCD began to challenge the conventional CRT as a PC display. The PC displays must show a high brightness and a high contrast when seen from a distance of only a few ten centimeters. The "visibility that is easy on the eyes" is a keyword. It was a challenge to develop a treatment technology that results in an antiglare surface that, while reducing the reflection of external light, does not reduce the resolution. Technically, there is the antireflection (AR) and the antiglare (AG) treatment. Adhesive films that show AG properties were already being mass-produced at that time. Those films diffuse light by creating an uneven surface by applying silica particles that were dispersed in acrylic resin onto thin PET films. But this was not a method to satisfy the requirements of customers of large LCDs. Also, high-definition displays with pixels of 300,000 that are arranged in a screen with a diagonal of 8–9 in. need a different AG film. Therefore, we screened many different silica materials dispersed in the coating solutions and selected, contrary to common thinking, very fine particles that did not lead to surface irregularities even for very short viewing distances [9]. Fine particles easily aggregate in dispersions, and preparation of even surface structures depends very much on the state of the coating solution and the conditions of the coating process, but we could expand this new product to high-definition TFT-LCDs and market them in a timely manner. A further benefit developed after a conversation with a customer at a later time: the deposit of metal chromium on the glass surface of a TFT liquid crystal panel eliminated the light reflected from this surface. This finding has greatly contributed to the improvement of the legibility. Antiglare AGS1 films that increased the visibility of LCD screen were commercialized and became the standard "face" of notebook PCs.

On the other hand, AR is a technique that eliminates the surface reflections by optical interference in thin films. It is used in optical lens and glasses by coating the surface with a multilayer of compounds with different refractive index by sputtering or vapor deposition. There was the basic research in our company, but in order to offer a timely solution to our customer's problem, we started a joint development with the American OCLI company and mass-produced the large size (500 mm × 1 m) AR polarizer, which was a big breakthrough at that time.

With the help of those surface treatment technologies, we were able to promote our "face of the display" products. The coating technique to form uniform thin layers allowed us to now make AR and AG coatings as well as protect films made from liquid crystalline polymers, leading to a wide palette of products utilizing optical film technology processing.

Becoming Easier to Handle

At the start of the LCD industry 30 years ago, the display area of a cell for a watch was less than 1 cm^2. The process to apply a sticky polarizer with a film thickness of a mere 0.15 mm to a small cell was reasonable, but it was a challenging process for

Fig. 4.4 An example of the Labeler for polarizers

large surface as demanded by our customers. A product that contributed to solving the problem of cutting surfaces of self-adhesive films, which is one of the major challenges today, is the so-called labeler in Fig. 4.4 [10].

By utilizing our know-how that we had developed for cutting adhesive tape, we established a manufacturing technology that put the cut 0.15 mm thin film on a small piece of carrier film.

By using the labeler, we could avoid the problem of protruding adhesive surfaces at the cutting edge, and laminating the polarizer film has been efficiently implemented in the automated line.

Following this, we studied cutting techniques to produce various shapes and the post-processing of the cut surface, we solved the problems with packaging, and we continued to challenge further efforts to make our products more manageable. Thus, this labeler technology has led to revolutionary processes that are reviewed in the section about cemented large LCD TVs [11].

4.1.3 Expectations for Technology Development in the Future

The LCD-related optical film technology and business that was reviewed in this chapter dealt with the development and commercialization of optical films. Keywords were "phase plate," "NIPOCS," and "polarization" as starting points [12, 13]. A number of proposals were made to apply the changes of physical–optical properties of various liquid crystalline materials for the commercialization of LCDs, and it is not an exaggeration to say that polarized light is being used in all LCDs now. The only exception was the very first liquid crystal display that used light scattering without any polarizer.

The LCD industry was born in the US and has experienced significant growth through several technological breakthroughs in Japan. Now there is a major turning point because other countries are catching up on the commercialization due to the general purpose of the technology and equipment and the dawn of organic electro-luminescent devices.

Research on innovative alternatives to the polarizer using iodine that has been industrialized by Edwin Land can be seen [14], but has not reached the range of practical use yet. Presentation of academic research results delving further into Land's invention do not exist. Fortunately, the crystal structure of herapathite has been elucidated by Bart Kahr et al. in 2009 [15] and the anisotropic light absorption of the iodine complex can now be explained theoretically, 157 years after the artificial crystal had been discovered by William Herapath.

I consider that finding seeds of new industries by logical exploration to unexplored fields of classic technologies is another approach to create new industries.

In the LCD industry which has been thriving on generation of drastic changes for better, new changes are now needed for the next generation. Isn't it our specialty as Japanese to equip and spiral our intuitive understanding of and knack for manufacturing and scientific theory for further growth? We firmly believe that we will find new challenges there and new evolution will begin.

4.2 Color Filters

Kunihiro Ichimura

4.2.1 Introduction

The opportunity to develop color filters (CFs) for LCDs came from color strip filters for camera imaging tubes. Their manufacturing had been based on forming photolithographic patterns using a classic negative-type photopolymer prepared by dissolving ammonium dichromate in a native protein such as gelatin, followed by a staining step with anionic dyes. Since the beginning of the 1980s, this staining method is applied to the CF production for LCDs, which opened the door for full-color LCDs.

Based on this background, the Research Institute for Polymers and Textiles (RIPT) of the Agency of Industrial Science and Technology (AIST), Dai Nippon Ink Corp. (DNP), and Morohoshi Ink (which is now DNP Fine Chemicals Co., Ltd.) started a project in 1982 to replace the protein with synthetic polymers that could be dyed. The fight to find a staining-type manufacturing process lasted nearly a year and a half, and in mid-1983 the direction of the research took a sharp turn towards incorporating finely dispersed organic pigments. In August of the same year, we found that the transparency increases abruptly when particle sizes of milled pigments are below a certain size, and in 1987 the pigment-dispersed CFs entered the market [16]. At that time there was no clear concept of nanotechnology, and I want to explain the underlying nature of the finding that pigments can be transformed into transparent colorants once their diameter is below about 100 nm.

4.2.2 Origin

In the mid-1970s I as a researcher of RIPT had developed a water-soluble photopolymer, PVA-SbQ, that forms photodimers upon UV irradiation to work as a negative-working photoresist and applied to the production of screen-printing plates. PVA-SbQ is a polymer that contains few mol% of the photosensitive cationic group of styrylpyridinium attached to a polyvinyl alcohol (PVA) backbone as a side group. I routinely used staining with anionic dyes to visualize photopatterns made from the photopolymer. Meanwhile, instead of the gelatin, which posed serious challenges in terms of quality control, Makoto Matsuo of DNP, who had developed polyimide LC alignment films by rubbing, intended to develop dye-type CFs based on synthetic polymers. The two of us met at an editorial board meeting of "Polymers" (the monthly membership journal of the Society of Polymer Science, Japan) and our joint research immediately took off. Then, in January 1982, Toshio Komatsu of Morohoshi Ink was dispatched to RIPT.

4.2.3 Efforts to Stain Type Color Filter

The quaternized photodimer groups in photocrosslinked PVA-SbO film become the staining region, but the substitution ratio of the PVA OH groups with the styrylpyridinium groups is just a few percent and thus is lower than the basic amino acid content that determines the staining concentration of gelatin. Therefore, we further introduced the pyridinium groups to increase the dye ratio, and after 3 months we obtain a photopolymer having a color density comparable to that of gelatin. The development of a CF was started immediately by Satoshi Okazaki et al. at DNP, but unexpected pitfalls awaited. Defects during the high-temperature processing required for the cyclization of polyimide led to a color change.

To confirm if a chemical reaction of the PVA-SbQ by itself was responsible for the color change, we studied the addition of an antioxidant. However, nothing improved and we investigated the mechanism of coloration by going back to the foundation. As a result, we found that it is possible to suppress the color change during heating by binding anions to the PVA-SbQ. On the other hand, the dye concentration is reduced by the introduction of anionic groups, and we synthesized a variety of PVA-SbQs with different material parameters, such as different polymerization degree and degree of saponification of the PVA, and the substitution degree of the photosensitive group. However, the standstill of the progress lasted for many days and caused great headaches for the research members.

4.2.4   Paradigm Shift to the Pigment Dispersion Type

Project members met at RIPT on a regular basis and had repeated discussions about the measures and progress reports. At that time, the possibility of fading by a backlight or from the outside had become a hot topic for the dye-type CFs. Further, in the dyeing process, complex resist coating and dyeing steps had to be repeated for each of the three RGB colors. Abruptly, at a meeting which was held in mid-1985, I proposed to distribute organic pigments in advance into the photopolymer to dramatically increase lightfastness by first staining and then processing. It was a desperate measure for the development in this situation, but both involved companies agreed to start a new initiative with pigment systems. At a later date, at the stage where the prospect of pigment-dispersed CF was decided, officials of Morohoshi Ink revealed their real intention and they "were puzzled by the proposal of using a fine particle dispersion of organic pigments." This is because dispersions tend to become unstable when pigment particle sizes are reduced, something the ink industry at the time tried to avoid. I, the proponent and non-expert, may have had a beginner's luck concerning the pigment dispersion.

That the photopatterning of pigment-dispersed photopolymers is feasible was supported by the following two pieces of information and personal experiences. First, there was Dr. Yukimichi Nakao of RIPT who was studying the synthesis of stabilized gold colloids in a transparent fluid by the reduction of metal ions. His by-talk on transparent stained glasses doped with metal particles of sizes of less than several tens of nm was etched in my mind. I was thus led to the idea that if the particle size of organic pigments is less than about 100 nm, they would give a transparent, colored coating film. Second, around the same time I had a joint research with Nippon Kankoushi (the current Nikkan Co.) on second master technology. A second master is a negative image film for transferring an original drawing that was created in a silver halide film. We found that even a PET film coated with PVA-SbO dispersed with a large amount of a red pigment could be patterned by UV irradiation to overcome the light absorption by the pigment. This means that the subtle differences in the transmittance of the photosensitive group and an organic pigment and the so-called spectral window may be sensitive enough for the "first staining and then processing" approach. Note that the pigment particle size here is so large enough to bring about sufficient light scattering required for a photomask. This situation is essentially different from what CF is.

The transmittance of the first prototype of pigment-dispersed CF by Morohoshi Ink and DNP was almost zero. This was because the particle size of the organic pigment was comparable to those of conventional inks. However, the RGB patterning of such a pigment dispersion type was critical. I had just begun to carry out as an emergency alternative the color pattern formation in a two-layer film by applying a photosensitive layer on top of the pigment layer, but this study was discarded immediately.

The challenge to make finer organic pigment particles was taken up by Shuzaburo Kobayashi of Morohoshi Ink, who had been involved for many years

in pigment dispersions for offset printing inks, and Toshio Komatsu. They were lucky that PVA-SbQ did not only have a high photosensitivity, but it is also an excellent dispersion stabilizer. The cations of the photosensitive group probably led to electrostatic repulsion. They found that pigments that were roll-crushed and centrifuged before suspending them in PVA-SbQ showed high transparency suitable for CF performances. For the revival of the research project it was crucial that the pigment size is below a critical value.

In the wake of this, experiments in August 1983 went in a furious pace and, as a result, the CF patents on the transparent colored image-forming photosensitive resin and the transparent color image had been jointly applied by Morohoshi Ink, DNP, and AIST in December 1983. In the patent application, the contribution of intellectual property by DNP personnel is very large. My involvement stopped here, and the two companies continued development and subsequent market deployment.

4.2.5   Mass Production

In 1984, an LCD TV equipped with a dye-stained CF was launched from Seiko. I saw the product in stores in Akihabara around this time, and when I saw the faded bluish LCD color screen, I was convinced of the marketability of the pigment dispersion type. In fact, when DNP and Morohoshi Ink worked towards a joint development of LCD TVs with Toshiba in 1985, a prototype with a pigment-dispersion-type photopolymer had been developed. Dispersers like ball mills replaced a three-roll mill, but dispersions of pigments having particle diameters satisfying the required performance inevitably separated as supernatant fluids from milled dispersions so that the production efficiency was low. By the middle of that year the companies could make some samples, but it was trial-and-error dealt with by sheer force. The dispatched employees of DNP, who visited RIPT at that time, informed me that the yield of CFs was about 3 %. There is no conclusive evidence for the figure of 3 %, but we took it as it was. In the very same year, 1985, Toppan Printing Co., Ltd. had started a dye-stained CF production.

In 1985–1986 DNP and Morohoshi Ink supported the development for Toshiba products mounted with pigment-dispersed CF on the laboratory level. After that, the CF was added to Epson's viewfinder and NEC notebooks, and the operation of production lines began. Based on these results, Okazaki gave his first conference presentation about the pigment-dispersed CF in 1987 [17]. Conference presentations about photosensitive pigment-dispersed materials, the so-called color resists, followed in1989 by Komatsu and Ichimura [18].

Color LCD TVs equipped with this new CF were put on the market by Toshiba in 1988, and in 1990 the market began to expand rapidly by the appearance of the notebook PC. The Nikkei Sangyo Shimbun, dated 26 October 1990, reported about Toppan Printing's 14 in. and DNP's 15 in. screen prototypes that had been shipped to several electronics makers, as a step towards the support of wall-mounted TVs. However, they reported that Toppan Printing used the dyeing method, whereas

DNP used the pigment dispersion method. In fact, mass production started in June 1990, and 1 year later, the CF production of DNP soared. From there on, development efforts to optimize the color pastes and to overcome the depolarization effect stemming from the crystallinity of pigments were made.

Toppan Printing started mass production of the pigment-dispersion-type CFs in 1991. In the wake of this, the pigment dispersion type became the mainstream of CFs for LCD TVs, and mass production lines of DNP were added in 1995, 1996, 1999, and 2001. At the same time, manufacturing of organic pigments of ultra-fine particles, pigment dispersers, dispersion stabilizers, and dispersion methods have been developed, and characterization methods such as particle measurements and related technologies were making remarkable progress, which led to many business opportunities associated with the LCD-CF technology.

4.2.6   Patents

The base of the patents is that it has set a numerical range for the pigment particle size. Claims about the patents climbed to a record number unknown to the patent office. The claims stated that is a known fact that transparency goes up when reducing particle sizes of pigments. In those claims, the "Colorants Engineering Handbook (Asakura 1989)" was a commonly cited reference. In it is a description that "colorants with a strong opacity become transparent when its particles become finer. Titanium oxide and iron oxide with high transparency have been developed by applying this phenomenon." The original role of a pigment is to give a new tone by exhaustively covering the base substrate, and the argument is only about opacity. For this, the light source and the viewer are on the same side of the coating. On the other hand, in the CF, the projection light is located on the opposite side of the viewer across a pigment coating, and the positional relationship is substantially different. Owing to the extraordinary efforts of intellectual property officials at DNP, who developed these views, the patent could finally be registered.

After that written notices have been made to the concerned companies, but the licensing applications was almost absent. Measures against patent infringements were also discussed, but it was decided not to pursue them because of the costs. I often went to AIST, but it was not until it became an independent administrative agency that action was taken. The National Institute of Advanced Industrial Science and Technology was established in 2001, and the patent expired.

4.2.7   Summary

The market volume of the CFs and pigment-dispersed color resists is estimated at a cumulated four to five trillion yen until 2005. Three persons who were pioneers of the joint development applied for a couple of awards, but they were not selected.

Only Okazaki, who contributed to the mass production of CFs, was awarded the Special Recognition Award at the SID'95 conference in 1995 based on the evaluation on this research and development. This lack of recognition was very disappointing. However, after the main R&D efforts concluded in 1987, Matsuo's story of his experiences led me to develop the photoalignment of LCs, which was a special kind of bonus for me. Matsuo found that disclination lines will not occur in a 90° TN cell even without chiral dopants when a rubbed optically active polymer is used. Instantaneously, I had the idea to use photoreactive molecules that are fixed on the substrate to control the alignment of LCs by light. This idea led to the discovery of the command surface in 1987, and a new research area has been opened up. The needs of CFs for LCDs led to the seeds of LC photoalignment [19]. It is impressive that, although it took approximately 20 years, LC photoalignment film became a new orientation treatment method for LCDs.

4.3 WV Film: An Optical Compensation Film for TN-LCDs

Yoji Ito

4.3.1 Introduction

"The wide view film" (WV film) was developed by FUJIFILM Co., Ltd. (see Fig. 4.5) and released in December 1995. It is an optical compensation film for liquid crystal displays (LCDs). LC display modes are classified into several categories, but the most widely used mode for note PCs, monitors, and cell phones was the TN (twisted nematic) LCD because of its low power consumption.

One of the big problems of the TN-LCD was its narrow viewing angle. The image on the screen can clearly be seen from the front, but viewed at an angle, a

Fig. 4.5 The effect of WV films on the viewing angle. *Oblique view*: with WV film Z/O WV film. *On-axis view*: with WV film W/O WV film. Y. Ito, SPSJ 60th Aniversary Lecture (2012)

color change, a contrast drop, and a gray scale inversion (the screen displays a reverse image) occur. From the early to the mid-1990s, many alternatives were considered by LCD manufacturers to solve this problem. Some methods improved the viewing angle to a certain extent. However, they also increased the number of manufacturing steps, which gave rise to other problems. FUJIFILM succeeded in the development of the optical compensation film with a novel concept: the "WV film."

WV film can realize a wider viewing angle without increasing the manufacturing processes, and it has been adopted by LCD manufacturers worldwide. Current annual sales reached tens of billions of yen and WV film became one of the main products of FUJIFILM in 2010. As a developer of the WV film, I was involved from its very beginnings and am proud of being engaged in the project.

Many technical reports have been published about the WV film and the management of this technology had been analyzed in detail. But for this chapter I decided to add my own thoughts from the perspective of an engineer in charge. I would like the readers to feel the mood at the time of the development and I would be happy if this increases the motivation of the reader to develop a new product.
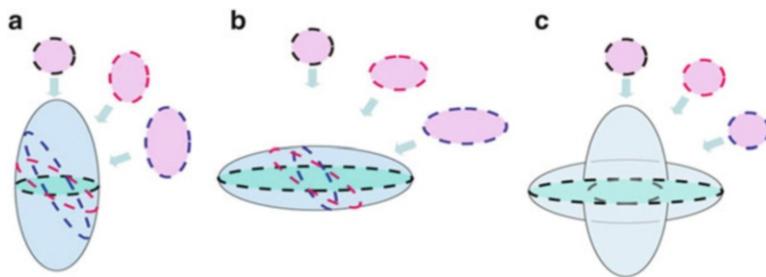
4.3.2   The Optical Design Concept of WV Films: An Amazing Discovery

4.3.2.1   Conventional Thinking About the Optical Compensation of TN-LCDs

In a TN cell, the rodlike liquid crystal molecules stand up when an external voltage is applied and lay down when the voltage is off. When the voltage is applied, the pixel turns black. Viewing the display from the front, this is the case, but when viewing at an angle, some light leaks out and colors the pixel.
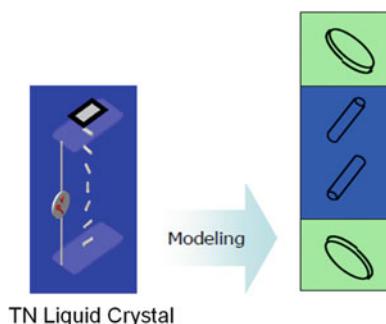
The liquid crystal cell can be regarded as an aggregate of rodlike liquid crystal molecules that are oriented uniformly. This aggregate could be modeled by assuming an oval, rugby ball shape. There is a difference in light refraction along the major and minor axes of such an ellipsoid, and this causes birefringence. In a sense, if you know the birefringence is a kind of transmittance, you could easily understand. When this ellipsoid is seen from straight above, the cross section becomes circular and thus does not produce birefringence (see Fig. 4.6a). At other angles, the cross section becomes elliptical and the birefringence increases with increasing angles. This angle dependence is the cause for the viewing angle dependence of LCDs.

On the other hand, viewing discotic compensator models, the cross section is also circular when viewed from above, but at oblique angles, the cross section is rotated by 90° compared to the rugby model (see Fig. 4.6b). If you combine the discotic compensator model with the rugby ball model, the cross section could be seen circle for all angles. That means no birefringence.

Fig. 4.6 Conceptual image of optical compensation. (**a**) Optical ellipsoid of rugby ball model. (**b**) Optical ellipsoid of disc-like model. (**c**) Combination of (**a**) and (**b**) [30]

Fig. 4.7 Conventional approach for optical compensation in LCDs

Previously, based on this optical compensation model, it was assumed that a liquid crystal cell contains obliquely oriented simple rugby ball model, and believed to be able to compensate with obliquely oriented simple discotic model which were arranged in a way that their optical axes were orthogonal [20, 21] (see Fig. 4.7).

It was a very simple and straightforward model. As an optical amateur, I could easily imagine what to do to realize this concept. My research group members devoted themselves to find a method to orient "discotic liquid crystals" (DLCs) and challenged various alignment methods such as the differential roller speed rubbing method [22] and the photoisomerization of azo compounds [23].

4.3.2.2   Reaching to the WV Film

The most superior viewing angle improvement could be obtained by a method for alignment of DLCs on a cellulose triacetate (CTA) film. It can be simply described as "a method for alignment," but it is a truly remarkable discovery to increase the viewing angle with this method. By comparing samples with a big viewing angle improvement with those having a small important, we discovered that the viewing
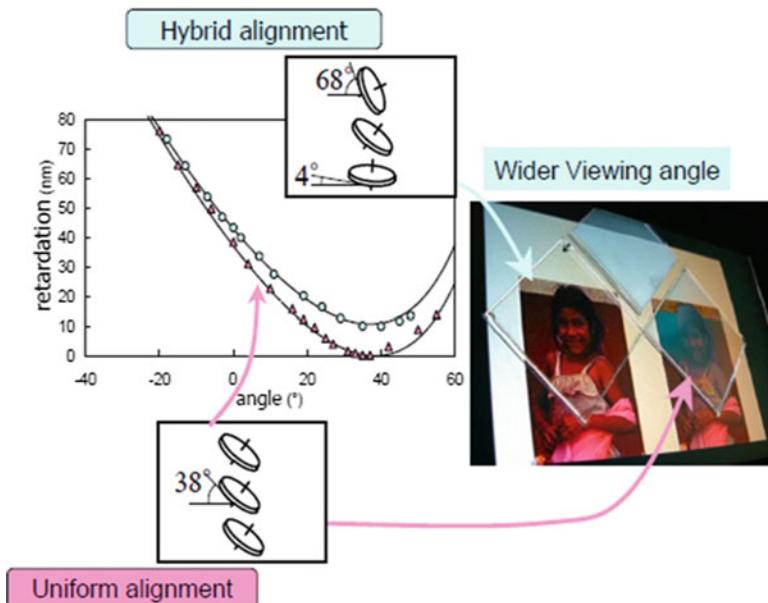
Fig. 4.8 The necessity for hybrid alignment [24]
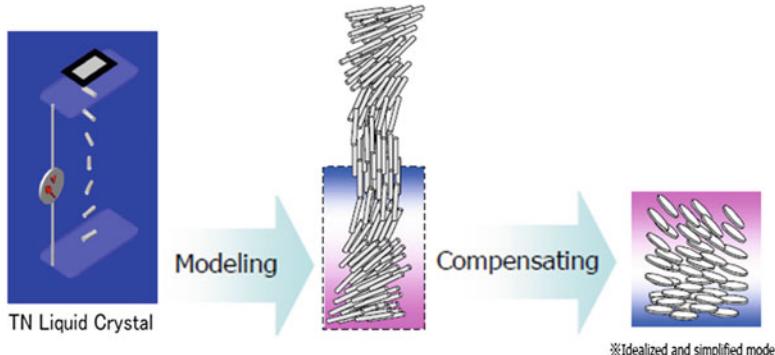
angle was improved by the "DLC hybrid alignment." As far hybrid structure, the viewing angle dependence is clearly different from the uniformly aligned conventional compensator, as shown in Fig. 4.8 [24].

We started out with a simple and beautiful concept for compensation films, but the best products have been obtained by a steady improvement, and thus we could reach a novel concept. In the following, I will explain the novel mechanism for the viewing angle improvement.
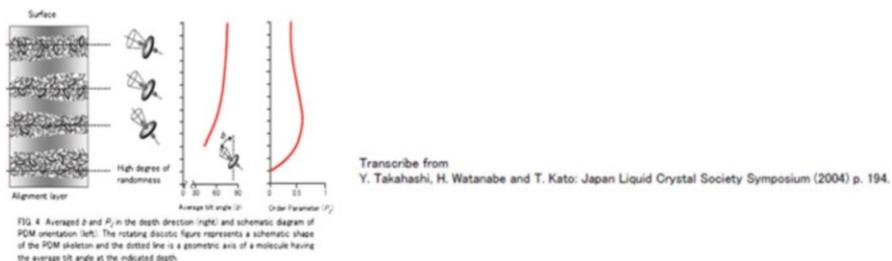
At the black state of TN-LCD, the liquid crystal molecules of the cell are almost standing up in the middle of the cell while being twisted in areas close to the electrodes.

The liquid crystal molecules thus do not have a homogeneous alignment along the z-axis of the cell, but rather form a complicated domain structure. As a whole of the cell, there is no optic axis. We examined the optical compensation on the molecular level for this complicated structure and reached the WV film having a hybrid alignment of the DLC molecules, which was not expected at first. The simplified model of the WV film is shown in Fig. 4.9. It is designed so that the optical compensation is realized on a molecular level for the complicated structure of the rodlike liquid crystal molecules in the cell precisely with the complicated hybrid structure of DLCs.

The light leakage can be improved by placing this WV film on the top and bottom sides of the liquid crystal TN cell so that "black" is seen as "black" from all angles. In the figure, the change of the molecular alignment along the vertical axis is shown simply, but the actual liquid crystal cell and WV film structure is much more complicated and is explained in the next subchapter.

Modeling   Compensating

TN Liquid Crystal

※Idealized and simplified model

Fig. 4.9 Unconventional approach to the compensation of LCDs: discotic liquid crystals [31]

Transcribe from
Y. Takahashi, H. Watanabe and T. Kato: Japan Liquid Crystal Society Symposium (2004) p. 194.

Fig. 4.10 Analysis of the molecular alignment in a layer of polymerized discotic material

4.3.3 Optical Control Techniques in WV Films

4.3.3.1 Control of DLC Alignment

To realize the concept described in Sect. 4.2, we reasoned that the nematic rodlike liquid crystal cell needs a nematic discotic liquid crystal with hybrid alignment as a compensator.

Thus we examined hundreds of nematic DLC compounds. We successfully found the way to control the hybrid alignment of DLC compounds as follows. (Fig. 4.10). Near a hydrophilic surface of alignment layer, DLCs tend to align horizontally; that means "face-on" towards the interface. The other interface contacts with air, which is hydrophobic, and the molecules orient "edge-on" with the discus surface perpendicular to the interface.

Furthermore, we could overcome the problem of heat resistance and durability, and we succeeded in developing DLCs meeting the target criteria for WV films in 1994. The inclination angle of the DLCs varies continuously between the interface

of the alignment layer and the surface towards the air, and this continuous change is called hybrid alignment. This variation of the alignment also occurs in the same way with the rodlike LC molecules in the LC cell [25].

We were able to produce such a complicated and precise alignment by a coating process. I admire all the members who challenged the task extremely difficult. Actually, by judging from my present knowledge, we might have given up before actual development. "Free of precedent," and "the feeling to finish" were our driving force to realize our dream.

4.3.3.2 Optical Control of the CTA Film

The control of the optical properties of the CTA film is also important for the WV film. Since CTA molecule has an acetyl group oriented in the vertical direction towards the main chain, it was known that the optical phase difference is very difficult to control by existing techniques. As we were manufacturers of CTA films named TAC, we could take advantage of our knowledge and review the state-of-the-art manufacturing processes [26, 27]. Thus, we were able to develop a new technique to stretch the films with novel additives in a way that we could freely control both of the in-plane phase difference and out-of-plane difference. Furthermore, we could control the wavelength dispersion by additives that contributed to a performance enhancement in various modes of LCDs [28].

4.3.4 A Long Struggle to Commercialize WV Films

In 1995, we launched theWVfilm. In traditional FUJIFILM research labs way at that time, researchers were usually looking towards the successful completion of the research topic, but here we, who have developed a newer market, encountered severe problems related to mass production. We had to solve problems with contaminations and unevenness of the WV film. From the LCD makers who considered their customer, the quality requirement for WV film gradually increased, and product specifications became stricter almost every month.

On the other hand, from a different viewpoint, the demands of LCD makers become a substantial source of know-how for us. Even though we as a material manufacturer were much troubled such demands it helped us to have a competitive edge. In other words, the solution the experience to Mura and defects could not easily be found, and we could solve the problems of the manufacturing processes one by one. Therefore, our competitors also needed a similar amount of time and experience to reach the level that we achieved in several years. The beautiful optical compensation concept was brilliant at a glance, and it was an important requirement, but in addition, I think that continuous improvement of such an unrefined technique needs a stable base of know-how in order to provide a product to the global market in large quantities in a manufacturing business that requires quick action, such as the LCD materials business.
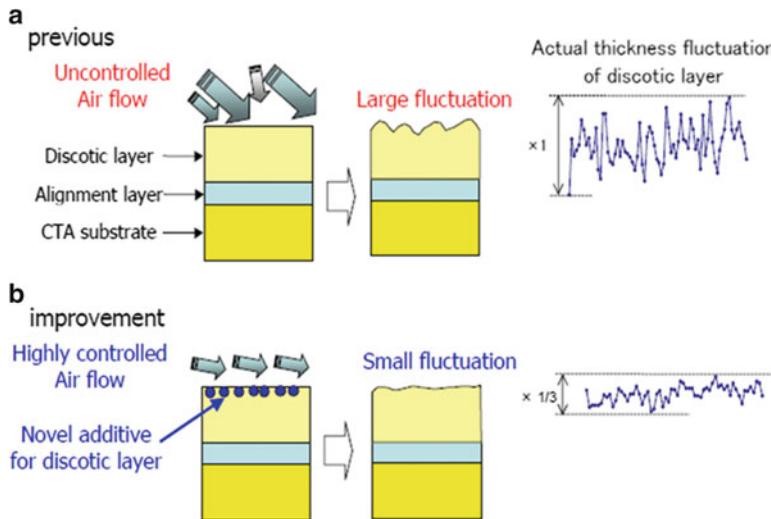
Fig. 4.11 Techniques to improve thickness fluctuations in WV films [31]

4.3.4.1 A Fight Against Heterogeneities
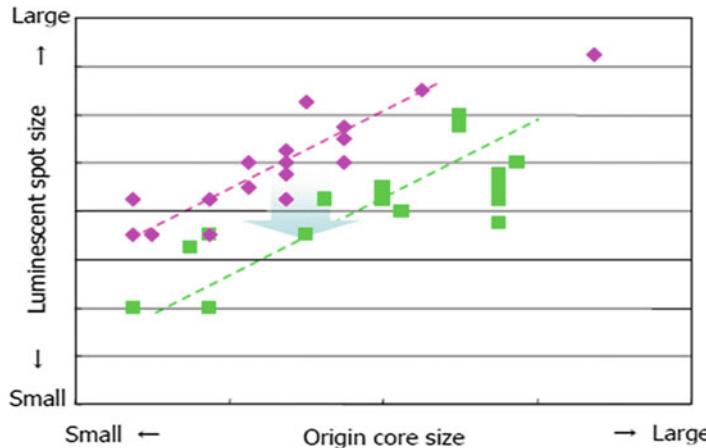
Just slight optical heterogeneities that were not detected in the very beginning had become visible with increasing the brightness of the LCD. We coated DLC solution which contains organic solvent onto a CTA substrate and after drying solvent, DLC became oriented. The WV film manufacturing is finalized by polymerizing DLC.

Thus, areas with a thickness deviation in the DLC layer occurred by this drying process and that caused an optical heterogeneity. We succeeded in largely improving the thickness evenness of the DLC layer by two approaches: control of the drying wind and the development of a new surface tension control agent. We succeeded in reducing the thickness unevenness in the DLC layer by these two techniques to about one third, compared to conventional drying techniques as shown in Fig. 4.11 [26].

Although the description of the techniques and know-how seems to be simple, actually hundreds of PDCA (plan, do, check, act) cycles of hypothesis ⇒ plan ⇒ enforcement ⇒ inspection, disproof ⇒ re-hypothesis ⇒ re-plan were needed to be completed to reach the present state.

4.3.4.2 Fight Against Small Defects (Dust)

At the beginning of the project, our customers allowed for a few defects per squire meter with a size of 100 μm in WV film, but their demands went up steadily and after several months the standard was raised to one defect per square meter, at which it stands now. In order to search for the origin of the dust, we measured the

Fig. 4.12 Improvement in the defect characteristics of WV films

air flow, air pressure, and other parameters in the production machine and solved the issues one by one. Let me just use one example: paint on walls. We ended up by not using paints at all, because paint deteriorates and produces debris. It might seem to be a straightforward solution to the problem, but we needed to go through every possible origin of debris in the production facilities before we found out that it had been the paint on building walls.

The production team, including me, was screening several hundred defects with a microscope every day. I became a specialist who can tell the origin and the process in which a defect would occur, just by looking at the shape and color of the nucleus. From the accumulation of such knowledge, we could associate the size of the nucleus of the defect with the size of the defect itself and found that the dependence varied according to the kind of the defect (Fig. 4.12). It goes without saying that this greatly advanced defect measures. It shortened the measurement cycle by collecting knowledge and know-how and made us meet customer demands that were becoming increasingly severe year by year.

4.3.5 Peculiars of the WV Film Development [29]

4.3.5.1 Historical Background: The Dawn of LCDs

The timing of the WV film commercialization was crucial for its soaring success in the LCD market. In other words, it was in 1992 that the development of products of WV started in. At that time, the LCD market was still small with annual sales around 200 billion yen. The LCD market flourished when LCD PC monitors replaced CRTs and it has currently reached around ten trillion yen. The WV film

was developed during the dawn of the LCD industry and the performance of the WV film has been improved in parallel with the commercial growth.

It is not too much to say that the success of the large screen LCDs is because WV could contribute to them. In the 1990s it was said that the screen size of the LCDs could not become larger than 10 in., and the bottleneck for an increase in size was the viewing angle and not the production of the LCD itself. In other words, the viewing angle problem becomes increasingly more urgent when increasing the display size. At that time, by using the WV film, the size of a TN-LCD could be increased to 23 in., with the prospect of further improvement. In a sense, I think WV films could remove the border between CRT and LCD.

4.3.5.2   The Early WV Film Project at FUJIFILM

Silver halide photosensitive materials for photographic purposes were the main products of FUJIFILM, and in the 1990s, future market projections did not hint any decline. Thus, silver halide photosensitive materials were mainstream materials in our company. As a result, less than 1 % of researchers developed optical films for LCDs. Our team had developed and commercialized an optical compensation film for super twisted nematic (STN) LCDs since 1987, but we were greatly defeated by competitions that had products with better performance, but we were greatly defeated by competitors that had products with better performance. Thus, in 1992 we faced the closing down of our unit.

Team members understood that, if they accepted the decision of the top management, they were placed in an unduly low position. So we even tried to develop unknown "WV film" with this strong will. In this project, I thought out "an optical compensation of LCD" in my all time. This has become a big asset now, after 20 years had passed. This has become a big asset now, after 20 years have passed.

Also, as mentioned above, the LCD market had not yet grown to its present scale, and the investment in production facilities was still small. Of course, when the LCD market grew, investments in production facilities progressed accordingly.

As the scale of the optical film market for LCDs was not so big, we did not have to invest in a large human capital and facilities. Furthermore, the top management had the foresight to invest resources. These were important factors of our success.

4.3.6   Future Development of the WV Film

The WV film went through several stages of development and the second generation integrated the WV film with the polarizer protection film [30], the third generation showed better durability and Mura improvement [26], and the fourth generation further enhanced the viewing angle performance [31] (Fig. 4.13). We have continuously developed these products hand in hand with the LCD makers, and we accomplished a joint, continuous display evolution, and we accomplished a
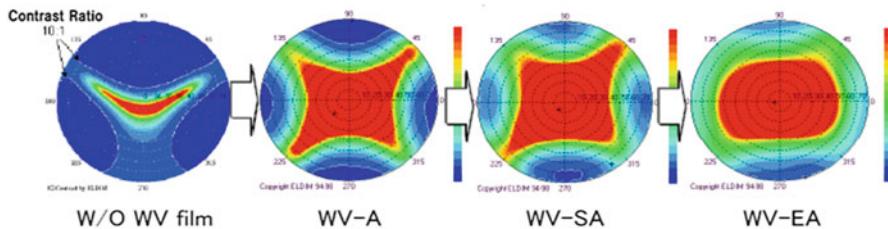
Fig. 4.13 Evolution of WN film [31]

joint, continuous display evolution. Just now, with this book in print, we are receiving positive feedback from the market about further viewing angle enhancement and increased contrast for the fifth generation.

I believe that there is still more room for the evolution on WV films and it is our mission to make further efforts for development of more beautiful displays for our customers. Furthermore, by increasing the technology for DLC alignment and the optical control of CTA films, we will improve the performance for all types of LCD modes and contribute to the society. That is my strong conviction.

4.3.7 Postscript

In this chapter I described the history of the WV film development faithfully. I believe that each person involved with the project has his own thoughts. I appreciate for your understanding if our view point might be different.
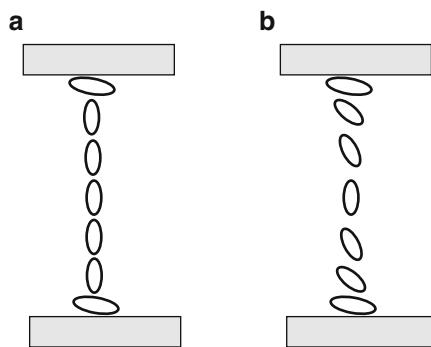
4.4 Development of Optics Films Which Contributed to the Progress of the Liquid Crystal Display

Motohiro Yamahara

4.4.1 Introduction

Nobody can talk about the evolution of the liquid crystal display (LCD) without mentioning the evolution of optical films which are essential for a wide viewing angle, high contrast, good antiglare properties and the improvement of viewing in a bright environment. I was in charge of optical design and material development of LCDs in Sharp Corporation and developed new techniques in cooperation with several material manufacturers which was a valuable experience. I want to discuss material development from the viewpoint of device development.

Fig. 4.14 Molecular orientation in a TN cell in the ON state. (**a**) Image in handbooks. (**b**) Simulation results
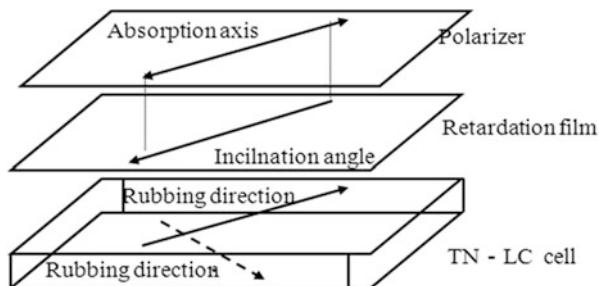
4.4.2 Development of Compensation Films for Wide-Viewing-Angle TN-LCD Application

A lecture given at the Fine Tech Japan exhibition in 2005 entitled "Innovation of the Retardation Film and Trend of the Compensation Film for Liquid Crystal Televisions" introduced the WV film which set fire to the competition wide-viewing-angle TN-LCDs [32].

In my first year at Sharp Corporation I already was given my own development topic of "the wide-field viewing angle for TN mode LCDs" from my supervisor in which I also optical simulations to test material properties [33]. As for the design of the wide-field viewing angle at that time, the optical compensation of white and black pixels was important, and most did not consider the optical compensation of the intermediate gray scales. However, I noticed that the grey tones had strong viewing angle dependence in normally white TN mode liquid crystalline cells and decided to confirm the orientation state of liquid crystal molecules by optical simulation. In many handbooks about LCDs, the molecular orientation when applying an electric field is shown in Fig. 4.14a: only molecules that are at the interface are horizontally aligned, whereas the bulk of the liquid crystalline molecules are oriented vertically. However, the result of my simulation is shown in Fig. 4.14b: even in the black state, only around half of the liquid crystal molecules, the ones close to the center of the cell, had a vertical orientation. Most liquid crystal molecules are slanted towards the glass substrate. By realizing this, it became clear that a compensation film containing birefringent molecules with an ellipsoid shape was needed to keep the clear black and white contrast. Figure 4.15 shows an image of the inclination of a birefringent ellipsoid in the retardation film that coincides with the rubbing direction of the TN cell, which leads to a wide viewing angle.

I examined the effect of such a structure described above by the liquid crystalline optical simulation. At that time there was no popular optical simulation software such as "LCD Master" made by Shintech, and it was common to use one's own software. The results of the simulation confirmed the graduation inversion and that the angle of the molecules deteriorated quickly when leaving the center of the cell.

Fig. 4.15 Part of the 1992 design

At first, we confirmed the wide-field viewing angle by using a mainstream "positive refractive index anisotropy" retardation film. However, later on it became clear that a "negative refractive index anisotropy" film that has the opposite optical property than the liquid crystalline molecules was easier to design for a wide-field viewing angle film, and we started the optimization of the optical characteristics of the retardation films. When I experimentally prepared the film with inclined refractive index ellipsoids, the tendency of a wider viewing angle was somehow confirmed. Therefore I asked material manufacturers to develop the phase contrast films with the simulated optical properties.

Because I belonged to a research institute my requests for the development of those films were turned down by several companies. Looking back at this situation now, it seems quite natural that a request for material development from a freshly hired employee without any credentials would be turned down. However, when I was looking for yet another material manufacturer, accidentally FUJIFILM Co., Ltd. introduced the concept of the inclination of a birefringent ellipsoid in the retardation film to Mr. Mizushima, who was the chief advisor of the Production Engineering Department at Sharp Corporation and now is the vice president of Sharp Corporation. He said "I introduced you to the researcher because he is a person who thinks about the same as you at our research institute." I then disclosed the most suitable optical design level and a joint development started between Sharp and FUJIFILM.

It would be commercialized in the summer of 1995, but the cooperation was not all comfortable. I examined every reliability experiment together with our polarizer manufacturer Sanritz Corporation and somehow we managed a prototype for mass production. Now my memories of examining films until late at night in Sharp Corporation, and also screening for quality after starting mass production at Sanriz production site were nice. Especially, I remember having been moved very much deeply when the development article is actually seen flowing with the line in the production trial.

When I checked the dates for the patent filings concerning the abovementioned presentation about the optical bases of WV films at the 2005 Fine Tech exhibition, I found that the Sharp patent was filed 1 month earlier.

In addition, in a liquid crystalline conference in 1995, FUJIFILM announced the WV film, but there was another company that announced a similar technique at the same time. FUJIFILM claimed that those rights were related to the patent application date after all. However, it may be said that FUJIFILM and our joint development were strangely lucky after all. It is often said that technical inventions and discoveries occur multiple times during the same period, and I really experienced this. I was also able to experience the importance of intellectual property that the difference among some of the filing dates impact on technical enforcement. A few years later, one person who worked for one of the companies which refused the request for film development said to me, "At that time, I think that what was necessary was just to have obeyed your request."

Moreover, I could also experience the decision of technical developments.

Later developments were that the WV film was directly attached to the polyvinyl alcohol (PVA) film of the polarizer, and the second generation design of WV films was developed in cooperation with FUJIFILM and Sanritz. The important experience for me was that the development of this WV film had formed the base for the whole R&D activity as well as the later wide-viewing-angle LCD development.

4.4.3 Development of Polarizers for Reflective/Transflective TFT-LCDs

The reflection-type TFT-LCD was first released in 1998 by Nintendo Co., Ltd. for their "Game Boy Color" console. For this reflective TFT-LCD the phase contrast film that is often called a "broadband $\lambda/4$ plate" was laminated directly onto the polarizer. This "broadband $\lambda/4$ plate" produces circularly polarized light having a phase difference of $\lambda/4$ for all wavelength λ of the visible light domain. Therefore, the refractive index anisotropic wavelength dispersion will have reverse wavelength dispersion than a normal polymeric film. In order to produce reverse wavelength dispersion, one needs to laminate $\lambda/4$ plate to $\lambda/2$ plate [34]. But because a liquid crystal layer between the polarizer and the reflector has a refractive index anisotropy and normal wavelength dispersion, instead of designing a perfectly circular polarizing film, the film should be shifted by the lamination angle and/or the retardation value.

Even if the polarizer for this reflection type lets the absorption axis be at right angles like two pieces of normal polarization films because it behaves as a circularly polarizing film as described above, light leaks out. Therefore, it cannot regulate the optical properties of the broadband $\lambda/4$ plate by the normal method. In addition, these optical properties do not correlate with the electro-optical properties of the reflective- and transflective-type LCDs, and this will hinder the causal elucidation of defective devices.

At that time, it is not the design of this reverse circular polarizing plate that the polarization emitted from broad band $\lambda/4$ board returns polarization conversely and

is returned to the original incident radiation and would normally be bright. This plate was then made by a polarizer manufacturer. Our reverse circular polarizing plate confirmed that there was a strong correlation of the optical properties of the film with the electro-optical properties of the LCD, which made it useful for polarizer inspection. However, during the trial mass production a high rate of defective reflection-type LCDs was found.

After investigating the cause, the polarizer manufacturer found that the broadband $\lambda/4$ plate selected one polarization orientation to pass the filter, but also reflected the oppositely circular polarized light and sent it back through the polarizer. Because the polarizer manufacturer could markedly decrease the amount of reflected light, the phase plates could, after all, be used for LCD inspection. It may be said that there would be no practical setup to measure the electro-optical properties, and thus a market opportunity, of the transflective- or reflective-type LCDs if the reverse circular polarizing plate had not been developed.

I have found a method to determine by the least number of parameter to describe the center line of the retardation value and lamination angle of their margins for reflective and transflective LCDs. A panel developer tried to further improve the optical properties by redesigning the polarization film, but it proved not to be possible. The manager in charge said that any further efforts to optimize the polarizer by changing the parameters would just lead to a decrease in optical properties. Receiving such a comment made me, the person in charge to develop those polarizing plates, extremely happy.

4.4.4 Development of Surface Treatments for TVs

The surface treatment of TVs now mostly employs general purpose antiglare (AG) films, but until recently antiglare low-reflection (AGLR) films had been used until models that had adopted antireflection (AR) and clear LR had a few technical problems and their manufacturers raised some objections. But now, some high-end models have been adopted for AGLR, and the surface treatment using clear LR is employed.

By the way, early LCD TVs used a high haze surface treatment with a haze value of 40 %. At that time, those films were made mainly by sputtering or vapor deposition of antireflective coatings, but the deposition of large areas is difficult and very expensive, and their use for televisions was impossible. Therefore, the real contrast in a bright room had been a problem, but in order to minimize the reflection of the surface, the design concept similar to the module for office automation (OA) had been incorporated. So, in 1999 Sharp Corp. announced "low-reflection black TFT" for medium-sized LCD modules, which combined LR and AG properties and had a haze value of 20 % or less. As the leader of the production unit, I
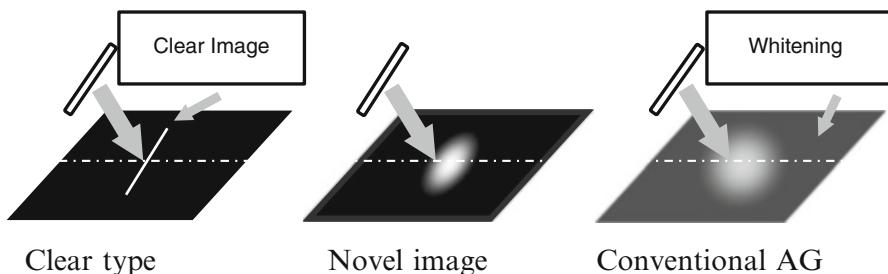
Fig. 4.16 Image of whitening suppression

was responsible for the development of this "low-reflection black TFT." This is the first use of the wet coating LR technique developed by Tomoegawa Paper Co., Ltd. With the advent of such a wet coating product, it became possible to conventionally produce large areas at comparably low cost. At that time, AG in low and medium haze films led to the problem of interference fringes, but not only that. Even though, in comparison with high haze films, the real contrast is not reduced, there is the tendency that the whole screen discolors. Even it was a low-reflection film, it was difficult to use under fluorescent lamp illumination.

Because in 1999 Sharp Corporation had declared "to replace all TVs with LCDs by 2005," the main development center was towards TVs. My opinion was that the observer when standing directly in front of the screen should not be reflected (antiglare), as well as a fluorescent tube at an oblique angle should only be blurred a little, and I thought that AG would be suitable for TV viewing. The whitening of a control image is shown in Fig. 4.16. I came up with my opinion when I saw the switching on of a light when viewing both a clear module and a high haze module. An LCD is bright when observed from the front, but at a higher viewing angle, the brightness is reduced. However, at that time, even high haze antiglare modules showed the tendency in a narrow domain of whitening from a normal direction. The more the viewing angle is inclined, the wider the domain of whitening becomes. It was also the case that it was impossible to watch images at an inclined viewing angle. Also when viewed from the front, the AG module can be viewed better than the clear one. Therefore, it was considered acceptable for viewing a video that a little blurring occurred when viewing from a slanted angle. At that time, in order to see the condition of reflection and surface texture, evaluation of AG was observed from an oblique angle. However, the rating of the influence on a video was not performed. So, I asked our manufacturers of surface treatment and polarizers to start this novel AG development.

When I showed a prototype of such an AG treatment to the person in charge of the TV development in the AV Division, he told me that they "were waiting for an AG like this," and it was adopted by Sharp. Thereafter, this type of AG surface treatment has spread and is now commonly used for liquid crystal televisions.

4.4.5   Conclusion

Through the development of polymeric optical films for LCDs, I met many people, who taught me many things and helped me in many ways. It made me realize that it takes the joint efforts of many and that I was very lucky to be in such a position. Some of my collaborators are still active in the R&D, some are retired, and some are deceased. I will always treasure my experiences and I am full of gratitude to everyone.

## 4.5   Development of the Liquid Crystalline Polymer Films "LC Film Series" for Optical Applications

Takehiro Toyooka

4.5.1   One More Type of Liquid Crystal: What Are Liquid Crystalline Polymers?

What comes to mind when we hear the word "liquid crystal"? Ordinary people think of a display, and scientists think of fluid substances that combine the characteristics of crystals and liquids. However, systems having no fluidity at all can also be liquid crystalline. Thus a liquid crystalline polymer is another liquid crystal. In analogy to the above explanation of an LC, a liquid crystalline polymer has both the characteristics of a liquid crystal as well the characteristics of a polymer.

The discovery of polymer liquid crystal lagged about 50 years behind the discovery of low molecular weight liquid crystals, but their applied research started from the 1960s. Low molecular weight liquid crystals are used as display materials, mainly because of their dynamic properties, whereas liquid crystalline polymers are also called super engineering plastics. Research and development of the application of liquid crystalline polymers for optical films has been carried out vigorously since 1980, and they have been commercialized as optical films and compensation films for LCDs by several companies from the mid-1990s. Typical examples are JX Nippon Oil & Energy's (formerly Nippon Oil Group) "LC Film Series" (Fig. 4.17), Nitto Denko's "NIPOCS," and Dejima's "Twister®." Furthermore FUJIFILM Corporation produced the "WV film" by cross-linking of low molecular weight discotic liquid crystal molecules, which is widely used as a key part of a modern liquid crystal display.

Fig. 4.17 Appearance
of the "Nisseki LC Film
Series"
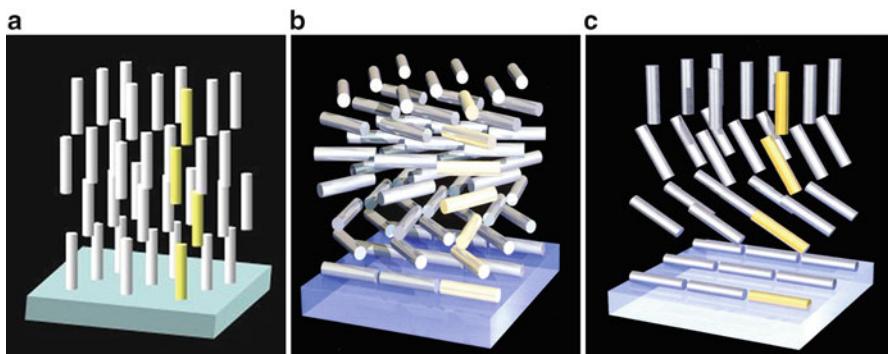
4.5.2   LC Film Series

The "LC film series" is a liquid crystalline polymer layer formed on a substrate film [35]. The thickness of the whole film is 50–100 μm, but most of which is due to the substrate film. The liquid crystalline polymer layer plays the role of a compensation film, but the necessary thickness of just a few micrometers cannot be reached by simply stretching the film. The thickness of the liquid crystalline polymer layer is an important parameter of the liquid crystalline polymer-based compensation film, and one of the key technologies for realizing high performance and good uniformity of product.

"LC film series" demonstrates a variety of optical functions by orienting the molecules in the liquid crystalline polymer layer. Three structures of liquid crystalline polymer layers are shown in Fig. 4.18. Stretching techniques cannot be used to change the orientation of the molecules in the vertical direction of the film, i.e., in the hybrid alignment and twisted alignment, which is the source of the advanced features of the "LC film series."

4.5.3   Two Breakthroughs in the "LC Film Series"

In order to use liquid crystalline polymers as commercial optical films, it is necessary to achieve both the immobilization of the liquid crystal molecular oriented structure and the orientation control of the liquid crystalline polymer. However, in the 1980s there was no technology that could satisfy both requirements and it was necessary to develop it ourselves. The key phrase at that time was "do not be bound by common sense."

Fig. 4.18 Molecular orientation in "Nisseki LC Film Series." (**a**) Twisted orientation, (**b**) hybrid orientation, (**c**) homeotropic orientation

4.5.3.1 Immobilization of the Liquid Crystal Molecular Oriented Structure

The conceivable immobilization methods for liquid crystal structures are immobilization by polymerization of oriented reactive low molar mass liquid crystals; immobilization by solvent evaporation of an oriented lyotropic liquid crystalline polymer; and immobilization by cooling an oriented thermotropic liquid crystalline polymer below its glass transition temperature. Because of the necessity for precisely control the orientation in the optical films (structural changes during immobilization should be as small as possible), we focused on the last method, thermotropic liquid crystalline polymer. The following properties are required for the liquid crystalline polymer materials for this approach: (a) it should show a nematic liquid crystal phase in a wide temperature range; (b) it should have the glass transition temperature in the low temperature region of the nematic phase, while it should not have higher-ordered liquid crystalline phases nor should it crystallize during the cooling process; and (c) it should have a low viscosity at the temperature at which the orientation process takes place.

In liquid crystalline polymers, the interaction between the molecules is small, and we have focused on low viscosity polyester. One decisive factor in the development of the materials was the introduction of nonliquid crystalline ortho-substituted aromatic units into the polymer main chain. Even though they might be rather disadvantageous to the liquid crystal phase expression, they slightly disrupt the molecular orientation and thus prevent crystallization or higher-ordered liquid crystalline phases while they increase the glass transition temperature so that the high-temperature stability of the nematic phase is guaranteed.

4.5.3.2 Orientation Control of Liquid Crystalline Polymers

It has been reported that liquid crystalline polymers can be oriented mechanically (shear and stretching) or by external fields (electric, magnetic), but was unsatisfactory for optical films.

Therefore, even though it had not been applied to liquid crystalline polymers, we used the anchoring effect at an interface that had been used for low molecular weight liquid crystals before. Low molecular weight liquid crystal materials can be oriented by placing it between two substrates. This method is problematic for polymers, because of the high viscosity that prevents filling of such a cell. As a solution for this problem, we adopted a process using only one alignment substrate. Specifically, a solution of a liquid crystalline polymer was dropped on a rubbed alignment substrate and the solvent evaporated. After a heat treatment step, the sample was cooled below its glass transition temperature and an oriented structure of the liquid crystalline polymer was produced. We think it is a simple process, but it was a considerable detour from the stereotypical approach of "filling of a liquid crystal cell" when looking at it in retrospect. Also, it is necessary to control the film thickness within a narrow range of ± 1 %, in order to make it useful as an optical film. Thus, ultra-precision coating of the solution is required to achieve this, and the polymer solution has to have a viscosity suitable from the viewpoint of workability.

4.5.4 Introduction to the Twisted Oriented Structure

Twisted oriented structures can be expressed, for example, by the addition of chiral dopants. This also applies to liquid crystalline polymer, but because the heat treatment is performed in an open system as described above (one film interface is the alignment substrate and the other interface is with air) an added low molecular weight chiral dopant does not distribute homogeneously within the film after the heat treatment, which made the control of the orientation difficult. This problem was solved by copolymerizing a chiral unit into the liquid crystalline polymer. By this copolymerization of a chiral unit, the twisted orientation structure is stable and it is possible to be controlled by the film thickness. Furthermore, by changing the ratio of chiral/non-chiral units, films having the desired twisted orientation and pitch can be produced.

4.5.5 Introduction to the Hybrid Oriented Structure

As described above, one side of the liquid crystalline polymer-based compensation film faces the textured substrate, while the opposite side faces air. By controlling the anchoring difference at both interfaces, the tilt of the molecule changes in the direction normal to the film, and a hybrid orientation structure can be formed.

Table 4.1 LCD operating mode vs. type of "LC film series"

LCD operation mode	Type of "LC film series"	Function of "LC film series"
Color reflective STN	Twisted oriented structure	Color compensation
Semi-transmissive TFT	Hybrid oriented structure	Color and viewing angle compensation
IPA, VA	Homeotropic oriented structure	Viewing angle compensation (compensation of polarizer)

We have measured the incident angle dependence of the retardation properties of the compensation film and have confirmed the hybrid oriented structure. Further, by controlling the anchoring energy on the alignment substrate, a structure in which the molecules are oriented normal to the film direction (homeotropic alignment) is also feasible.

4.5.6 Application for Liquid Crystal Displays (LCDs)

Table 4.1 summarizes which type of the "LC film series" is compatible for each LCD mode. Twisted oriented films can be used for color compensation of STN (super twisted nematic)-LCDs [36], in particular for color STN-LCDs in mobile devices. Because such color mobile STN-LCDs use only one polarizer, it is necessary that the combination of the compensation film and STN cell functions as a wideband $\lambda/4$ plate. Multiple films are required in order to achieve this condition for usual, stretched films, but by using the twisted oriented film this can be realized by just one film [37–39].

The hybrid alignment film is optimal for semi-transmissive thin film transistor LCDs (TFT-LCD) [40, 41]. In general, semi-transmissive TFT-LCDs need both a wide-viewing-angle film and a color compensation film. Hybrid alignment films have an appropriate retardation, and just one film combines the function of wide viewing angle and high contrast. This leads to a decrease in the number of device components which made it possible to expand the viewing angle characteristics of the semi-transmissive TFT-LCDs [42].

Homeotropic alignment films are used for enlarging the viewing angle of the vertical aligned (VA) and in-plane switching (IPS). Homeotropic alignment film made it possible to improve the viewing angle characteristics of the polarizing plate, and it achieves a wide-viewing-angle characteristics IPS method, the VA method both [43].

4.5.7 Conclusions

"Polymer is not arranged cleanly. Should you look for a different theme is good." We remember vividly even now that it has been pointed out at the time that we started to develop. However, we believed in the possibility of liquid crystalline

polymer and continued to develop, and finally were able to come out with a product somehow. It might be that were able to contribute slightly to the advancement of liquid crystal technology. Although it was omitted because of space limitation, very steady efforts such as "Mura" and defects (foreign matters) measures were also indispensable in the development of "LC film series".

The optical film using the liquid crystalline polymer from the diversity of the materials and the degree of freedom in orientation is different from that of the retardation film of he prior art, and it is an important member in a new liquid crystal display. In addition to LCD field, you are expected to continue expanding its application such as optoelectronics.

References

1. W.A. Shurcliff, Polarized Light and Its Application (Japanese) (Kyoritsu Shuppann Co., Ltd., Tokyo, 1965)
2. JPA 57-24896
3. USP 4268127
4. JP 2818983
5. Nagatsuka, Fujimura, Yoshimi, IEIEC EID91-43 (1991), p. 29
6. T. Kameyama et al., Proc. IDW'97, 407–410 (1997)
7. The Chemical Daily News (Japanese), May 9 (2003)
8. T. Nagatsuka, T. Shimomura, Y. Oishi, SID'85 DIGEST, 74 (1985)
9. S. Kobayashi, H. Shibata, Y. Takahashi, T. Hoda, IDW'99, 391 (1999)
10. JPA 62-014811
11. JP 4503689
12. N. Denko, R&D Report. **80**(38), P5–P32 (2000)
13. N. Denko, R&D Report. **84**(41), P21–P33 (2004)
14. M. Miyatake, Y. Fujimura, T. Miyashita, T. Uchida, JLCS Conf. 366 (1998)
15. B. Kahr, J. Freudenthal, S. Phillips, W. Kaminsky, Science **324**, 1407 (2009)
16. M. Tani, Electronic Materials (Japanese) (Kogyou Chosakai Publishing Co., Ltd., Tokyo, 2000), p. 44
17. T. Sugiura, J. SID. **1/2**, 177 (1993)
18. S. Okazaki, Preprint of Institute of Electronics, Information and Communication Engineers. Sect. Semicond. Mater. 1–293, S5–S7 (1987)
19. T. Komatsu, K. Ichimura, J. Photopolym. Sci. Technol. **2**, 237 (1989)
20. T. Mtsumoto et al., Liquid Crystal Display, unexamined Japan Patent 63-239421 (1988)
21. K. Arakawa, Y. Nishiura, Y. Ito, Optical anisotropic layer, and Liquid crystal display, Japan Patent 2565644 (1996)
22. K. Arakawa, Optical Anisotropic Layer, and Liquid Crystal Display, unexamined Japan Patent H7-98412 (1995)
23. Y. Ito, Optical Compensate Sheet, And Liquid Crystal Display, Japan Patent 3312063 (2002)
24. H. Mori, M. Nagai, H. Nakayama, Y. Ito, K. Kamada, K. Arakawa, K. Kawata, Novel optical compensation method based upon a discotic optical compensation film for wide-viewing-angle LCDs, SID'03 Digest, 1058–1061(2003)
25. Y. Takahash, H. Watanabe, T. Kato, Depth-dependent determination of molecular orientation for WV-film, 2004. JLCS. Conf. 194–195 (2004)
26. E. Aminaka, Y. Ito, M. Murayama, N. Fukagawa, M. Wada, H. Mori, K. Takeuchi, K. Mihayashi, Mura-improved thin wide view film for LCDs, IDW'03 Digest, 689–692 (2003)

27. Y. Ito, R. Matsubara, R. Nakamura, M. Nagai, S. Nakamura, Mori, K. Mihayashi, OCB-WV film for fast-response-time and wide-viewing-angle LCD-TVs. SID'05 Digest, 986–989(2005)
28. J. Takeda, H. Tooyama, I. Fujiwara, T. Ando, Y. Ito, K. Mihayashi, High performance VA-LCD compensation film made with environmentally friendly material for VA-LCD. SID'11 Digest, 50–53 (2011)
29. T. Fujimoto, K. Kuwashima, Japanese Process Industries: A Competitive Analysis of Their Manufacturing Systems (Yuhikaku Publishing Co., Ltd., Tokyo, 2009), pp. 332–357
30. Y. Ito, K. Kamada, K. Arakawa, M. Murayama, Y. Yabuki, New WV film: an optical compensation film for wide-viewing angle TN-TFT-LCDs, 52nd SPSJ Annual meeting, 109–110 (2003)
31. T. Ito, S. Yasuda, T. Oikawa, Y. Takahashi, Review of viewing angle compensation of TN-mode LCDs using WV Film. SID'08 Digest, 125–128 (2008)
32. K. Arakawa, Innovation of the retardation film and trend of the compensation film for liquid crystal televisions. Fine. Tech. Jpn. 21 (2005)
33. T. Katoh, N. Shimizu, T. Watanabe, T. Shiro, M. Yamahara, Chem. Today. **462**, 25 (2009)
34. H. Yoshimi, T. Nagatsuka, T. Araki, Japanese Patent Gazette. Patent No. 3174367
35. J. Mukai, T. Kurita, T. Kaminade, H. Hara, T. Toyooka, H. Itoh, SID '94 Digest, 241 (1994)
36. T.J. Scheffer, J. Nehring, Appl. Phys. **58**, 3022 (1985)
37. T. Sonehara, O. Okumura, Jpn. Display. 192 (1989)
38. A. Masaki, T. Uesaka, Y. Kumagai, Y. Kaminade, T. Toyooka, Y. Kobori, SID'01 Digest, 452 (2001)
39. K. Hosaki, T. Uesaka, Y. Kumagai, A. Mutoh, A. Masaki, T. Toyooka, Proc. Asia Display. IDW'01 Digest, 513 (2001)
40. M. Kubo, S. Fujioka, T. Ochi, Y. Narutaki, T. Shinomiya, Y. Ishii, F. Funada, IDW'99, 183 (1999)
41. Heume-Il, Y.-B. Kim, K.-S. Ha, D.-G. Kim, S.-B. Kwon, IDW'00, 41 (2000)
42. E. Yoda, T. Uesaka, T. Ogasawara, T. Toyooka, SID'02 Digest, 762 (2002)
43. Y. Takahashi, T. Uesaka, T. Hirai, H. Mazaki, SID'10 Digest, 491 (2010)

Chapter 5
Backlights

Kälil Käläntär

5.1 LCD Backlight Unit

Kälil Käläntär

5.1.1 Introduction

Liquid crystal displays (LCDs) now play a leading role out of various flat-panel electronic display devices, because of its excellent features such as a low profile, lightweight, large area, low operating voltage, low power consumption, and a full-color capabilities and higher resolution.

An LCD is a spatial light modulator based on the electro-optical effect. In order to recognize the image on the LCD display a backlighting apparatus, i.e., backlight unit (BLU), is required. The light generated in BLU is transmitted through the LCD and is spatially modulated by each pixel in the panel which is recognized as an image. LCDs are lightweight, have thin structure, and have low power consumption. Therefore, LCDs are widely applied as display devices for products as cell phone, netbook, video camera, digital still camera, car navigation system, personal computer, desktop monitor, and a flat-screen TV.

Mainly two structures are being used in BLUs for illuminating the LCD panels. The first one is the edge-lit (edge light) or side-light type that uses a light-guide plate (LGP) and the second one is direct-view type that uses a light chamber. Light-guide plate is an important component in light direction controlling in an edge-lit BLU, and in the same manner a light chamber is important component in direct-view type BLU.
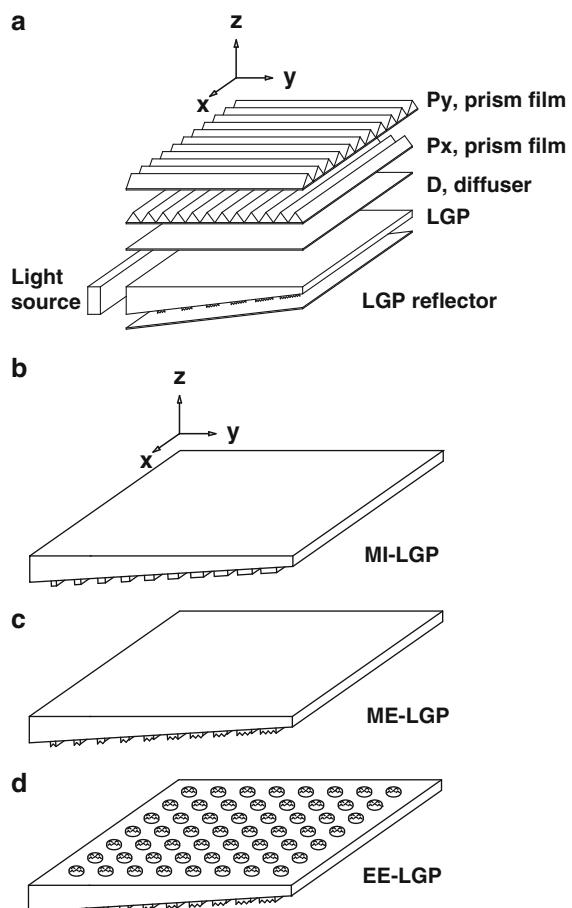
K. Käläntär (✉)
Japan Global Optical Solutions, Hachioji, Japan
e-mail: azerogli1953@yahoo.co.jp

Fig. 5.1 (**a**) Structure of a
conventional BLU and
(**b**–**d**) are the LGPs with
light diffusing elements.
(**b**) LGP with light
scattering printed dots.
(**c**) LGP with replicated
light scattering dots.
(**d**) LGP with replicated
light scattering dots on the
front and back surfaces

By using an LGP in an edge-lit BLU one can obtain a thin BLU with high
luminance uniformity than the direct-view BLU. In the early period of LCD panel
the direct-view BLUs were used. However, the demand for thinner structures
boosted the usage of LGP, i.e., the edge-lit type. Currently the mainstream of the
BLU for LCDs is the edge-lit type, and direct-view type is used in large sizes.

5.1.2 LCD Structure and LGP Materials

The basic structure of an edge-lit type backlight is shown in Fig. 5.1a. In this type of
BLU the light control medium that is the LGP is a transparent resin which is made up
of polymethyl methacrylate (PMMA), poly carbonate (PC), or cyclic olefin polymer
(COP). The LGPs are formed into a slab shape or wedge shape. The light-emitting
diode (LED) or cold cathode fluorescent lamp (CCFL) are being used as light
sources near to one to four sides for inserting the light into the LGP [1].

5.1.3 Light Diffusing White-Ink (Silkscreen) Printed LGP

The conventional light-guide patterning is a silkscreen method to print spots on the back surface of the LGP as shown in Fig. 5.1b. Here the surface of the LGP without any element taken as "mirror" (M) and the ink-printed surface are taken as "ink" (I), so that the LGP is named "MI-LGP" as shown in the figure [1, 2].

In general the ink used in the pigment of printing of the LGP is titanium dioxide (TiO$_2$) that possesses high refractive index. The pigment includes drying solvent as the main medium. Another option is to use curable ultraviolet medium with the pigment. For obtaining high reflection, irregular sizes of spherical beads are used in the pigment. High luminance uniformity is achievable by changing the size of the printed dots, i.e., having a size gradation in which the dot becomes large at distances far from the light sources. The shape of printed dot can be a circle, square, rectangle, or diamond. These dots are being positioned at the corners of hexagon shape, in which the maximum fill factor can be obtained. For example, in a 6 in. LGP with 3 mm thickness, the dispersing element is a circle with a size of 200 μm on the back surface of the LGP near to the light sources and 600 μm at a position far from the light sources. When the size of light-dispersing element is large, it can be recognized from the front surface of the LCD depending on the thickness of the LGP. Recognition of the dispersive spots can be seen in the early types of the LCD displays.
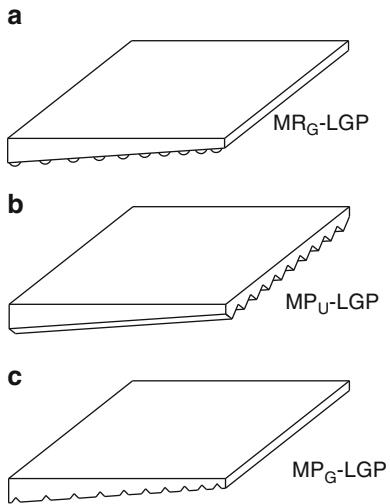
In this type of the LGP the propagating light inside the LGP repeats the internal reflection on the inner surfaces of the LGP and is dispersed by hitting the dots that leads to wavelength dispersion. When a light source with three primary colors or a pseudo-white is used, the white light is extracted on the LGP near the light sources and reddish light at positions far from the light source. The short wavelength components such as blue and green scatter more strongly by the printed spots. Thus, these colors are removed from the propagating light. This phenomenon is the so-called sunset light dispersion that exists in the light diffusing LGPs.

5.1.4 Light Diffusing Etched-Dot Replicated LGP

In order to avoid the printing process, more efforts have been put in the mold tool etching in which an optical flat surface of a mold is designed to have a pattern with etched (E) elements. The mold is used in a cavity on an injection machine. The hot resin is shaped in the cavity and the pattern is transferred onto the resin that makes an LGP [1, 2]. As shown in Fig. 5.1c, the etched elements are transferred onto the back surface of the LGP, and the front surface of the LGP is flat and "mirrorlike," so that the LGP is named "ME-LGP." To extract more light from the LGP a uniform replication pattern of an etched mold is transferred onto the front surface of LGP. If both sides of LGP are a replication of the etched elements, the LGP is named "EE-LGP."

The size of a light-dispersing etched element is about 200 μm and all the elements have the same size. For making uniform luminance on the BLU, a density gradation is applied in which the distance between the elements decreases as

distance from the light sources increases. This is shown in Fig. 5.1d. In case of "EE-LGP," the front surface pattern is uniform, i.e., the distance between the etched dots is constant. However, to avoid interference between the LGP pattern and the prism films that are used on the LGP, the dot position is randomized frequently. By using the precise etched molds and replication process, the time spent for printing can be reduced. In addition, the issues regarding the pigment differences or diffusing element size can be avoided. To increase the diffusing function of the LGP, diffusing beads are added to the material of the LGP. Another option is to make fine diffusing dots on the front surface of the LGP. This can be realized by replication of a diffusing mold pattern onto the LGP's front surface [3].

The LGPs explained above are light diffusing types in which single side or double sides of an LGP are the replication of the etched dots. In a diffusing LGP the direction of the dispersed light is not controlled, thus resulting in light loss in the BLU.

To enhance luminance a light direction control LGP that can collimate the extracted light into a narrow light cone is required.

5.1.5 LGP with MR Elements

LGPs with optical micro-reflectors (MRs) are shown in Fig. 5.2 [1, 4–6]. An MR element has a shape of a micro-lens or microprism with optical surface. The MR elements are structured on the back surface of an LGP [7–16]. Each MR element reflects light based on the total internal reflection (TIR). To provide a uniform extracted luminance on the BLU, an array of MR elements are fabricated on a mold with an optical surface. The pattern of the mold is transferred onto an LGP in an injection molding. The MR element is often a concave or convex lenslet with round, square, elliptical, or diamond geometrical shape [1, 8]. An MR element reflects

substantial portion of the rays that are incident on the inner surface of the element. A portion of the light rays that could not satisfy the TIR condition is refracted on the inner surface of the element. The refracted light leaks towards the back surface of the element. A reflector film is used near to the elements to reflect back the leakage light into the LGP (Fig. 5.1).

Since the front surface of the LGP is "mirrorlike" (M) and the back surface is a gradation (G) of the MR elements, the LGP is named "MR_G-LGP." In case of uniform the pattern elements with constant pitch, the LGP is "MR_U-LGP." To enhance the TIR function of the elements, the tangent of the concave surface or the angle of reflection should be kept constant, i.e., the surface should be as close as to a prism surface.

To collimate the extracted light a uniform line prism pattern with constant pitch is structured on the back surface of the LGP. In this case the LGP is named "MP-LGP." The feature of the MR elements is to reflect the propagating light without any optical loss and direct the extracted light into a light cone. By controlling the reflection angle of the element the emergent light cone angle is controlled resulting in an increase of luminous flux and luminance on the BLU.
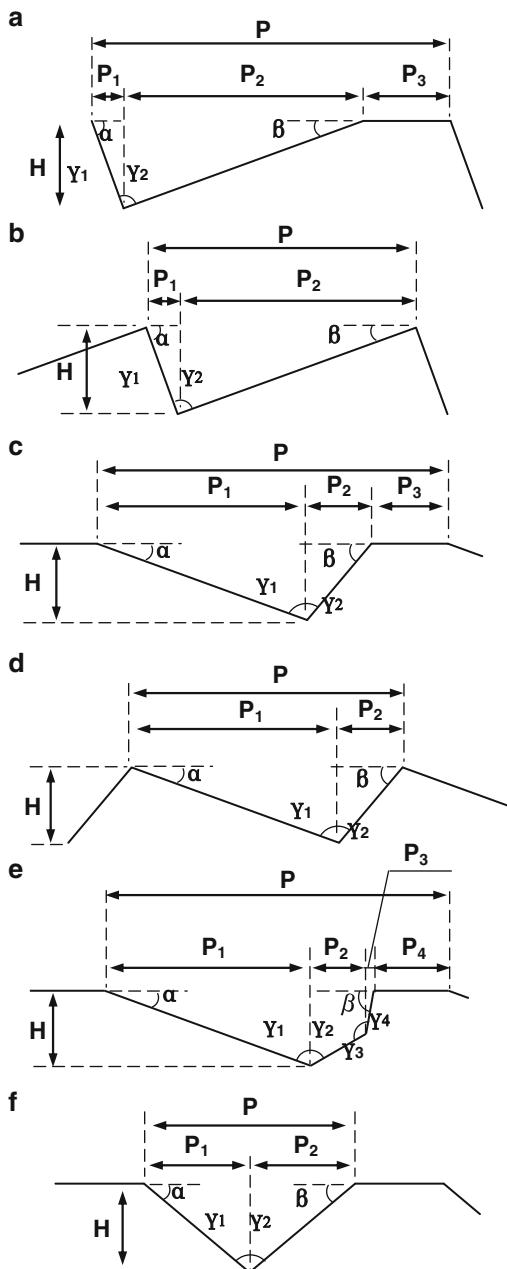
The size of the MR element is about few microns, and in comparison with diffusing printing or etching elements, the MR elements are small and not recognizable from top of the BLU or LCD. Figure 5.3 shows cross sections of the MR elements that are often used to extract the light. Depending on the shape of the prism, the polar angle of extracted light rays increases. When the prisms shown in Fig. 5.3a, b are used, the emergent light have a large zenith angle (the angle between the z-axis and the emergent ray direction) on the LGP. Therefore, a prism film with total internal reflection, the so-called inverted prism, is required on the LGP to direct the emergent rays towards the normal surface of the LGP [17]. The prism structure shown in Fig. 5.3c–f extracts the reflect light rays towards the normal in which the polar angles are reduced. To provide a uniform luminance, two methods are mainly used. In the first method the prism angle is fixed and the pitch is varied. In the second method the pitch is fixed and the angles varied. The parameters given in the figure are important for fixing the shape of the prism or making a gradation of the prisms. By using a diffuser film with low haze on the LGP, a BLU without prism film can be made.

When the MR elements are used as light extraction, the light diffusion or wavelength dispersion is absent in the LGP. The light cone of such an LGP is narrower than the light diffusing type LGP.
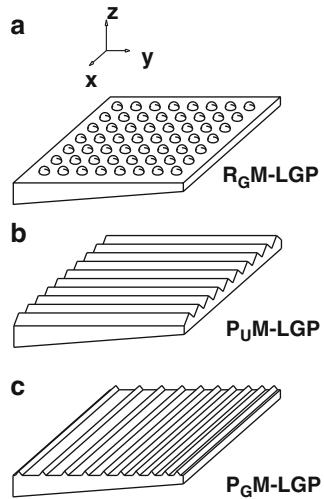
5.1.6 LGP with MD Element

To provide a direction controlled light cone on the front surface of an LGP the MR elements shown in Fig. 5.3 are structured on the back surface of the LGP [1]. Figure 5.4 shows the light guides with the microdeflector (MD) elements on the front surfaces. The MD elements are being fabricated on the mold tools similar to that of MR elements and are being transferred to an LGP using injection mold.
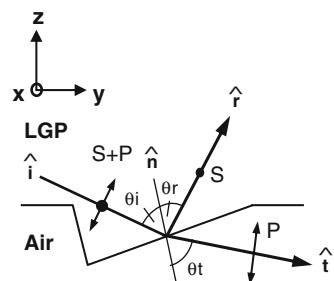
Fig. 5.3 Prism structures
for light extraction. (**a**, **b**)
Prisms that extract the light
in a way that the zenith
angle of the emerged light
increases with respect to
the surface normal. (**c–f**)
The prisms that extract the
light in a manner that the
zenith angle decreases with
respect to surface normal

Fig. 5.4 LGPs with light deflecting elements. (**a**) Omnidirectional elements, (**b**) uniform unidirectional light deflecting elements, and (**c**) position-graded light deflector elements on the front surface of the LGPs

Fig. 5.5 Light polarizing element. The polarizing elements separate the S-wave and P-wave on reflection. These are structured on the back surface of the LGP
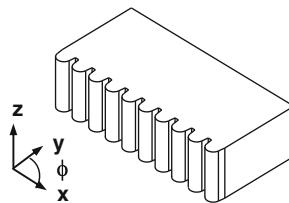
In a MD-LGP a light ray repeats total internal reflections before hitting a single MD element. When a ray is incident on the inner surface of a MD element, the ray is deflected (on refraction) and directed on the MD element. To form the emergent light cone and control its direction the geometrical shape of the micro-deflector element should be designed and adopted to the MR element.

In the design of an LGP the emergent light is assumed and the micro-reflector and micro-deflectors are designed, respectively, in which the combination can provide the required light cone on the LGP. A proper gradation of the element positions can be designed and structured.

5.1.7   LGP with Light Polarizing Element

A microprism shaped on the back surface of LGP dispatches the internally reflected propagating light and the refracted light [1]. As shown in Fig. 5.5 depending on the angle of an incident light onto the prism surface, the light is being polarized into

Fig. 5.6 Micro-optical elements on the light introduction surface of the light-guide plate. These structures widen the spatial light distribution of the inserted light inside the LGP

S-polarization, perpendicular to the incident surface, and P-polarization, parallel to the incident surface. The reflection factors for these polarizations are different. However, when the reflection factor of the P-polarization approaches to zero, the incident angle is the so-called Brewster angle. By defining the incident angle θ_i, the reflection angle θ_r, and the refraction (transmitted) angle θ_t, under the Brewster condition, the reflected ray is perpendicular to the refracted light ray, i.e., the angle between these two rays is $90°$ ($\theta_r + \theta_t = 90°$). The Brewster angle is given by $\theta_B = \tan^{-1}[1/n(\lambda)]$, where the refractive index of the prism material is $n(\lambda)$. In case of PMMA, the refractive index $n_D(\lambda)$ is equal to 1.492 at D-line ($\lambda = 589.3$ nm) of the sodium and the Brewster angle is about $\theta_B = 33.8°$. The Brewster polarization angle is defined for a single light ray. Therefore a portion of the propagating light rays can satisfy the polarization condition. The prism with Brewster angle can be designed by considering the propagating ray angles.
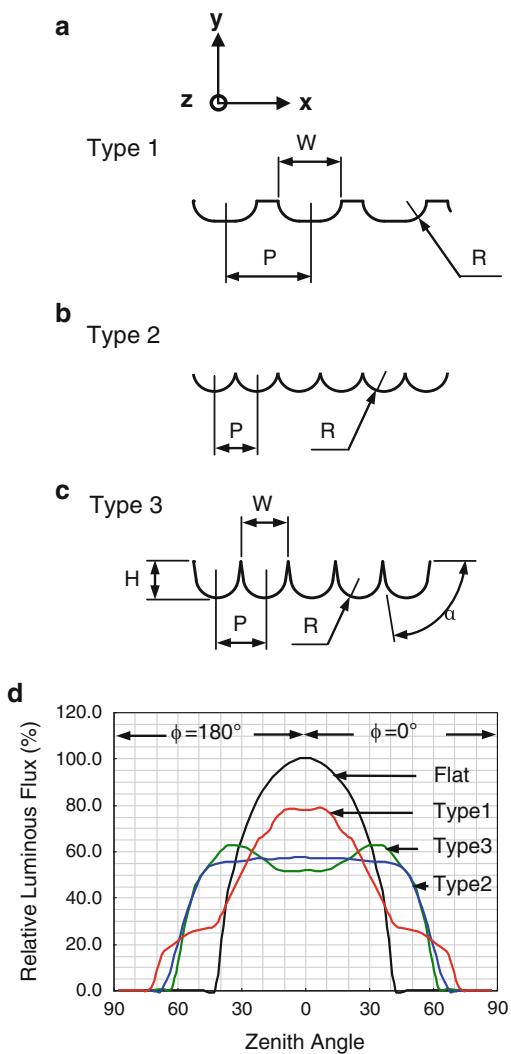
5.1.8 Light-Shaping Element

5.1.8.1 Shaping Light in an LGP with Microstructures on the Light Incident Plane

In an edge-lit type BLU few LEDs or tens of LEDs are used near to the light introduction surface (one of the sides) of an LGP depending on the application, the size, the amount of luminance, or an optimized angular luminance distribution [18].
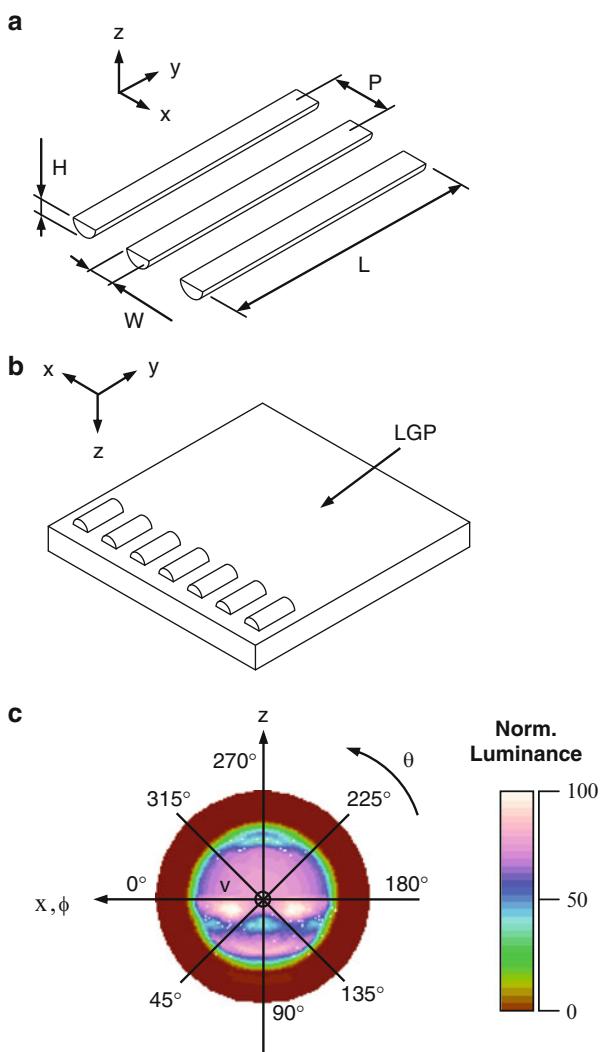
When the light introduction surface of an LGP is flat, the introduced light of the LED is being refracted and as a result the rays are being deflected towards the surface normal. The maximum possible angle of an introduced ray is corresponding to the critical angle $\theta_C = \sin^{-1}(1/n_{LGP})$, where n_{LGP} is the refraction angle of the LGP. The light distribution inside such an LGP is limited within the critical angles and a dark zone appears between two internal distributions (between two LEDs). The zone contributes in the nonuniformity of the luminance distribution on the BLU. To reduce or eliminate the nonuniformity, an array of microstructures are fabricated on the light introduction surface to widen the internal light distributions as shown the structures in Fig. 5.6. The array of microstructures widens the light

Fig. 5.7 Structures used on the light introduction surface of an LGP for light shaping inside the LGP. (**a–c**) The cross section of the three-type elements. (**d**) Light intensity distribution in an LGP using the structures shown in (**a–c**). Flat is the surface without microstructure that is shown for comparison

distribution inside the LGP that results in reducing the dark zone and increasing uniformities. The internal light distribution is limited to about $\pm 42°$ ($n_{\mathrm{LGP}} = 1.492$, PMMA) when the light introduction surface is flat. However, when the microstructures are used on the light introduction surface, the distribution is widened to $\pm 7°$ (Fig. 5.7). By providing the microstructures the inserted light in coupling surface increases that result in reducing the Fresnel loss and an increase in coupling efficiency by 5 %.
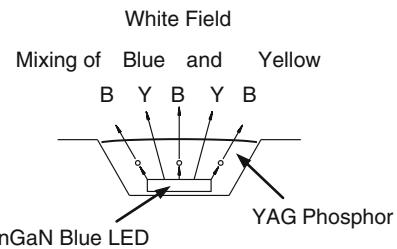
Fig. 5.8 Incoherent diffraction grating on the back surface of the LGP, near the light introduction surface, for forming the light inside the LGP. (**a**) Incoherent diffraction gratings, (**b**) The light-guide plate with rear gratings. (**c**) Light intensity distribution in the LGP observed on the y-axis (observing the far field pattern of the propagating light from a point against the light introduction surface)

5.1.8.2 Light Shaping in the LGP using Incoherent Diffraction Gratings

To shape and to control the direction of the light inserted into the LGP, an incoherent diffraction grating is structured on the back surface of the LGP near to the light introduction surface as shown in Fig. 5.8. As an example a grating of pitch $P = 240$ μm, a width of $W = 120$ μm, a height of $H = 32$ μm, a radius of $R = 72$ μm, and a length of $L = 2$ mm has been designed in an LGP with a micro-reflectors and a thickness of $t = 0.8$ mm that is used in a cell phone BLU. The thickness or the number of the LEDs is the parameters in designing of the gratings where the size

Fig. 5.9 A pseudo-white
LED. A blue light-emitting
chip (InGaN) is covered
with the yellow fluorescent
agent, YAG. The additive
complementary color
mixing results in white
color light

can be few microns to tens of microns. In addition, the shape can be "V" prism or
rounded prism depending on the distribution of the inserted light on the inner
surface of the light introduction surface. Due to the shape of the gratings the light
can be directed towards the sides of the LGP or towards the surface against the light
source. The gratings shape the propagating light, and as a result it shapes the
emergent light on the LGP. Therefore, the dark zone reduces and decreases, leading
to an increase in the bright area and finally an increase in uniformity.

5.1.9 Light Sources for Backlight

5.1.9.1 Pseudo-White LED
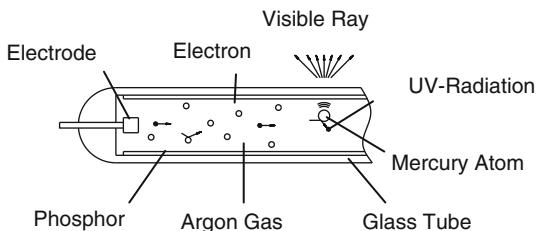
An LED is a solid-state lighting element that is based on the PN junction of gallium
nitride (GaN)-based compound semiconductor light-emitting material [1]. A
pseudo-white LED is a combination of indium GaN that has a light-emitting
quantum well structure and YAG phosphor layer that covers the semiconductor
chip (Fig. 5.9).

A pseudo-white LED is based on phosphor excitation and wavelength conversion.
The chip emits blue light that excites the surrounding phosphor layer of yellow light.
The blue light is scattered and absorbed by the phosphor. Since the blue and yellow
lights are complementary colors, the result of color combination is a white color.

In recent years, the pseudo-white LEDs are widely used in the backlights of the
handy terminals, such as cell phones, netbooks, and notebook computers. Top-view
LEDs are used in car navigation systems and side-view LEDs are used in notebook
PCs and netbooks. By using these small pseudo-white LEDs, thin and lightweight
units and modules are realized. The LEDs are being merged into the display
backlight of various sizes. Therefore, the demands for higher-efficiency LEDs
with different packages are widely highlighted.

In recent years, high-efficiency monochromatic LED light sources of red (R),
green (G), and blue (B) have been developed and used as primary colors in LCD
backlighting unit. Blue and green are the chips of compound semiconductors of
InGaN, and red LED is a compound of four semiconductors, i.e., AlInGaP (alumi-
num, indium, gallium, and potassium). These LEDs are used in a backlight and a

Fig. 5.10 Structure of a CCFL. Small amount of mercury (0.5–1.0 mg) and inert gas (argon) are encapsulated in the tube

white point is obtained based on the additive color mixing. Because of the large dependency of the LEDs on the temperature, a light sensor is installed in the BLU to stabilize the BLU. The three primary used BLUs have wide color production gamut that can be used in the applications of image editing and design. However, the tolerances between some color LEDs or low electro-optical conversion efficacy and high-cost LEDs are the barriers in employing the primary LED colors in displaying backlights. Despite great attempt to use primary colors in BLUs, Sony Corporation announced all LED display in Las Vegas Consumer Electronic Show in 2012.

5.1.9.2 Cold Cathode Fluorescent Lamp

A CCFL that is used in large-sized LCD displays is made up of two electrodes mounted at each side of the fluorescent glass tube, of any shape, filled with mercury (0.5–1.0 mg) and an inert gas (argon). The fluorescent materials include three-wavelength phosphor that is coated on the inner wall surface of the tube [1]. When a high voltage is applied between the electrodes, the electrons are drawn towards the electrodes present inside the tube as shown in Fig. 5.10. The electrons collide with mercury molecules in the tube and as a result of collision ultraviolet light is emitted. The ultraviolet light excites the phosphor that leads to white light conversion. Large TV sets or monitors use CCFLs of 3 mm in diameter. However, recent movements on prohibition of the mercury which is a toxic material and recent development of high-efficacy pseudo-white LEDs boost the usage of the LEDs in the display BLUs.

5.1.10 Conclusions

A backlight is functioning at the rear of liquid crystal panel and plays an important role in reducing power consumption and improving the display characteristics. The advances in light-emitting devices, their driving methods, and the function of a light-guide plate that configures a backlight are explained in this section.

A light-guide plate is used not only to make a uniform luminance but also for dispersing, reflecting, deflecting, or shaping the emergent light. A backlight unit with wide angular luminance distribution can be realized by using a light-dispersing LGP. A backlight unit with controlled angular luminance distribution can be

obtained by employing an LGP that is featured by micro-reflector elements. The angular luminance can be squeezed by combining the light deflecting elements and light reflection micro-deflectors in a light-guide plate. A variety of light-shaping BLUs can be realized by selecting proper light reflector and deflector elements.

In the near future, the divergence applications of versatile LCD terminals are expected. Therefore, a thin and highly functional LGP that results in realization of low power consumption BLU is necessary.

References

1. K. Käläntär, *LCD backlight technology*, Tokyo, Japan (Supervisor, CMC Publishing, 2006)
2. K. Käläntär, Monthly Display, June issue (2003)
3. Y. Koike, The 41st meeting of the Society of Polymer Science, Spring 1992, Paper No. IL-27
4. K. Käläntär, *Digest-C5 Fine Process Technology Japan 1997 7th Seminar*, (1997), pp. 11–18
5. M. Ohe, Flat Panel Display '93, (1992/11), p. 137
6. A. Tanaka, in *Proceeding of the 4th International Display Workshops (IDW)* (1998), pp. 347–350
7. K. Käläntär, SID99 Technical Digest, (1999), pp.764–766
8. K. Käläntär et al., IEICE Trans. Electron. **E84-C**(11), 1637–1645 (2001)
9. K. Käläntär et al., SID00 Technical Digest (2000), pp. 1029–1030
10. K. Käläntär et al., in *Proceeding of the 7th International Display Workshops (IDW)* (2000), pp. 463–466
11. K. Käläntär, in *Proceeding of the 9th International Display Workshops (IDW)* (2002), pp. 549–552
12. K. Käläntär, Monthly Display **7**(1), 6–72 (2001)
13. K. Käläntär, JSAP, AM-FPD 2008 (2008), pp. 101–104
14. K. Käläntär, EKISHO **12**(1), 31–38 (2008)
15. T. Uchida, "Display" Supervisor, Industrial Commission (2006), pp. 96–100
16. *"Kogaku Jitsumu Shiryou Shuu" Digest of Practical Optics*, Chap. 15 (Johokiko Co., Ltd, Tokyo, 2006), pp. 338–360
17. Guidelines of prism sheet for LCD backlight, technical art S/M16X Diamond Series (Mitsubishi Rayon Co., Ltd.) https://www.mrc.co.jp/press/p07/070524.html
18. K. Käläntär, SID2007 Technical Digest, 33.3L (2007) pp. 1240–1243

Chapter 6
Modes for Liquid Crystal Devices

Martin Schadt, Hidefumi Yoshida, Kenji Okamoto, Hidehiro Seki, and Akio Sasaki

6.1 Invention of the Twisted Nematic Effect and Subsequent Field Effects

Martin Schadt

6.1.1 State of the Art of Liquid Crystal Displays in 1970

The first observation of a liquid crystalline phenomenon was made in 1888 by the Austrian botanist Reinitzer, in Graz. He noticed an opaque appearance in liquid cholesterol benzoate upon melting which turned into the common transparent liquid state when further increasing temperature. Only decades later it was realized that liquid crystals are not suspended solid-state microcrystals but represent a novel class of materials exhibiting long-range molecular order within their liquid

M. Schadt
MS High-Tech Consulting, Seltisberg, Switzerland
e-mail: martin.schadt@bluewin.ch

H. Yoshida • K. Okamoto
Sharp Corporation, Nara, Japan
e-mail: hidefumi.yoshida@sharp.co.jp; LX13010097@partner.sharp.co.jp
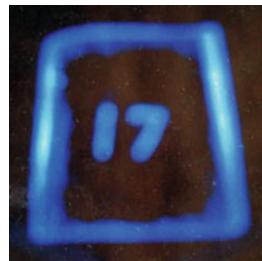
H. Seki
Graduate School of Engineering, Hachinohe Institute of Technology, Hachinohe, Japan
e-mail: seki@hi-tech.ac.jp

A. Sasaki
Kyoto University, Kyoto, Japan
e-mail: sasakiak@muh.biglobe.ne.jp

crystalline temperature range. As a consequence of long-range order, liquid crystals exhibit unique anisotropic optical, dielectric, and mechanical properties. In 1918 Björnstahl [1], Uppsala, published the first study of an electro-optical liquid crystal effect. Upon current flow through a thin, negative dielectric liquid crystal (LC) film of *p*-azoxyanisole he observed light scattering. In 1935 Zwetkoff [2] reported analogous results in sandwich cells using also *p*-azoxyanisole, i.e., the standard LC used by virtually all scientists between 1900 and 1960. In the mid-1960s, industrial research groups in the United States and in Europe became interested in liquid crystals for potential electronic display applications. At that time the few compounds known to exhibit liquid crystallinity were unstable, and their melting temperatures were typically far above room temperature and/or extending over much too narrow temperature ranges for practical use. Only few of the numerous anisotropic optical, mechanical, and dielectric properties of liquid crystals (LCs) were known, and reliable experimental means for their investigation had hardly been developed [3–5]. Correlations between molecular functional groups, display-relevant LC material properties, and electro-optical properties which are prerequisite for advancing LC materials and LCDs hardly existed.

Most engineers considered liquid crystals to be exotic organic materials with questionable stability and of primarily academic interest. In 1963, i.e., 45 years after Bijörnstahl and 28 years after Zwetkoff, Williams [6], RCA Princeton, rediscovered light scattering in transparent layers of negative dielectric nematic liquid crystals. He filed one of the first liquid crystal display device patents. In 1968 Heilmeier and Zanoni [7] extended the work of Williams towards practical liquid crystal displays and denominated their display dynamic (light) scattering (DS)-LCD. Helfrich [8] and Carr [9] attributed dynamic scattering to current-induced molecular turbulence caused by ion conduction in negative dielectric LCs. The work of Heilmeier and his group triggered strong interest in liquid crystal displays, and attempts were made to commercialize DS-LCDs in early digital electronic watches and pocket calculators. However, DS-LCDs suffered from serious drawbacks such as current-induced electrochemical decomposition, large driving voltage, high power consumption, and poor optical contrast.

Spurred by scientific curiosity and by the rapidly advancing semiconductor industry, research groups around the globe started to search for operating principles enabling flat-panel digital displays in the late 1960s. Operating principles with fast response, large optical contrast, broad field of view, and compatibility with the low driving voltage and small power consumption of the emerging complementary metal oxide (CMOS) semiconductor technology were some of the goals. However, none of the electro-optical effects known at the time met the requirements. In the late 1960s scientists and engineers therefore followed very different research strategies. The rapidly emerging inorganic light-emitting diodes (LEDs) of Hewlett-Packard and others were most advanced. Other research candidates were electro-chromic and electrophoresis effects, displays based on electroluminescence, field emission, plasma discharge, and flat cathode-ray tubes (CRTs). Even exotic ideas such as displays based on organic light-emitting diodes (OLEDs)—the first primitive OLED prototype was made by the author and patented by Williams

Fig. 6.1 Instant color Polaroid photograph of the OLED prototype display made by the author at the CNRC in 1969. The 22×22 mm, 2-digit display consists of a 1 mm thick anthracene single crystal comprising solid-state hole- and electron-injecting electrodes

and Schadt at the Canadian National Research Council, Ottawa, in 1969—were considered [3–5, 10, 11]. Figure 6.1 shows a picture of the OLED prototype made by the author. With their reputation of being unstable and poorly visible, dynamic scattering LCDs were one option among many.
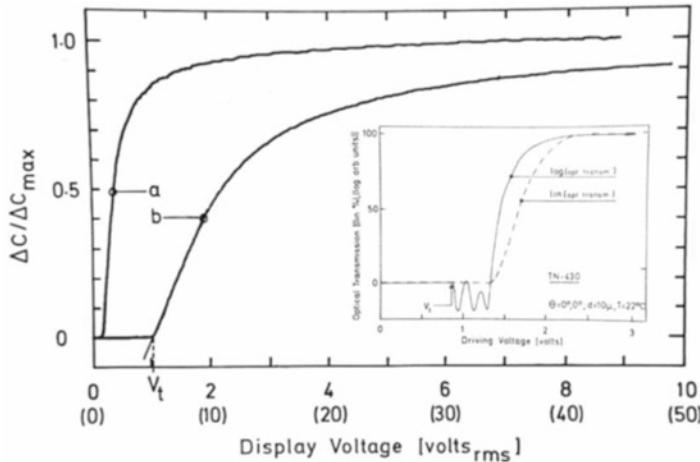
6.1.2   Invention of the Twisted Nematic (TN) Field Effect

Triggered by the DS work of Heilmeier et al., the pharmaceutical company F. Hoffmann-La Roche, Basel, Switzerland, established a liquid crystal research group in 1969. This was part of Roche's strategy of business diversification at the time. It included collaboration with former Brown, Boveri et Cie company (BBC, now ABB) for jointly developing DS-LCDs for medical electronics equipment. After Wolfgang Helfrich had left RCA in 1970 and joined the Roche liquid crystal group he met his colleague, the experimental physicist Martin Schadt.
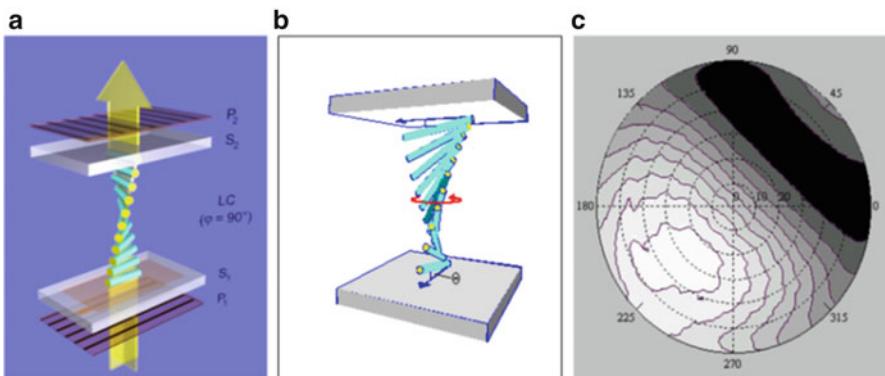
Intrigued by a mechanical twist observation made with a negative dielectric (azoxyphenole) twisted liquid crystal film sandwiched between crossed polarizers and published in 1911 by the French crystallographer Mauguin [12], Helfrich had the idea that a voltage could realign the long axes of initially twisted positive dielectric nematic liquid crystal molecules perpendicular to the cell substrates, thereby blocking light transmission. Contrary to the management of RCA who was not interested, Schadt was immediately attracted by Helfrich's idea and began to design and perform a series of electro-optical experiments for investigating its feasibility. Schadt first used the high-melting, positive dielectric liquid crystal PEBAB known from literature (Sect. 6.1.2), which he asked his colleague, chemist Hanspeter Scherrer [13], to synthesize. The author used uniaxial mechanical brushing for surface-aligned ITO-coated cell substrates. Because of the high melting temperature of PEBAP (106 °C), he performed the initial experiments—which mostly failed [3–5]—at 110 °C. Retrospectively, failure was due to a combination of inadequate LCs with unknown ionic and polar organic contamination, weak and irregular molecular surface anchoring, erratic wave-guiding caused by inadequate

cell gaps, and non-defined bias tilt angles between substrates and long molecular axes. In the late fall of 1970, Schadt for the first time succeeded in reproducibly switching and observing polarization changes in a twisted nematic LC configuration under his microscope. Now, as so often happens in physics, new surprising findings were made. Other than initially thought and after numerous experiments, he showed that it was not necessary for the electric field applied to surface-aligned twisted nematic molecular configurations to fully unwind the liquid crystal helix, i.e., to realign the long molecular LC axes vertical to the cell substrates. To his great surprise, Schadt discovered that a few volts were sufficient to fully block light transmission of the TN configuration. This was more than one order of magnitude below the saturation voltage which Helfrich and Schadt had initially expected to be required for complete vertical alignment of the long LC axes. Moreover, further experiments excluded another initial concern, namely, that weak surface anchoring would render vertical LC alignment feasible but would prevent repetitive switching due to elastic fatigue of surface alignment. Moreover, the experiments of Schadt suggested that it is sufficient for the electric field to *deform* only the central part of the TN helix for suppression of wave-guiding. Schadt and Helfrich immediately filed a Swiss patent and published the surprising results in the February issue of Applied Physics Letters [14]. In this first publication of the twisted nematic effect, they adapted the equation for the *magnetomechanical* twist threshold derived by Eric Leslie [15] for estimating the *electromechanical* threshold of the twist configuration. However, since Leslie's elastic model did not treat optical properties, the *electro-optical threshold* of the TN helix and its electro-optical response *above* mechanical threshold were not predictable. A theory describing the complex electro-optics of twisted nematic LC configurations did not exist at the time; it was only developed by Berreman [16] at Bell labs 3 years after the first publication of the TN effect. In 1973 Berreman's 4×4 Jones matrix approach enabled for the first time computer simulations of the anisotropic electro-optical response of TN-LCDs. It is interesting to note that even 1 year after the publication of the TN effect, renowned scientists who attempted to reproduce Schadt's experiments failed and attributed their results to electro-hydrodynamic instabilities [17]. This is a further confirmation of the saying of Niels Bohr that nothing exists before it is measured.

Figure 6.2 illustrates the remarkable difference between the optical and the mechanical response of a $90°$ twisted nematic helix versus applied voltage. The capacitance chance $\Delta C \propto (\varepsilon_{\parallel} - \varepsilon_{\perp})$ of graphs *a* and *b* versus applied voltage is proportionate to the mechanical helix deformation from its planar off-state to full vertical (homeotropic) LC alignment. The inset in Fig. 6.2 shows the corresponding optical change of the TN-LCD transmission. From Fig. 6.2 it follows that ~45 V is required for complete mechanical unwinding of the helix, whereas only 2.5 V is needed to reach maximum optical contrast. The computer model in Fig. 6.3 visualizes the experiments of the author in Fig. 6.2 for the off-state (Fig. 6.3a) and the 50 % optical on-state (V_{50}) of a twisted nematic director deformation (Fig. 6.3b). Figure 6.3 a, b shows the twist configurations of the two states. Figure 6.3c depicts the azimuthal angular contrast dependence of a partially switched TN-LCD [3-5] at V_{50}. The photograph in Fig. 6.4a shows one of the three seven-segment TN-LCD prototypes made by the author in 1971. Figure 6.4b depicts the off-state of one of the

Fig. 6.2 Electromechanical nematic director deformation of a TN-LCD helix (graphs *a*, *b*) and corresponding voltage-dependent optical TN-LCD transmission between parallel polarizers (inset)
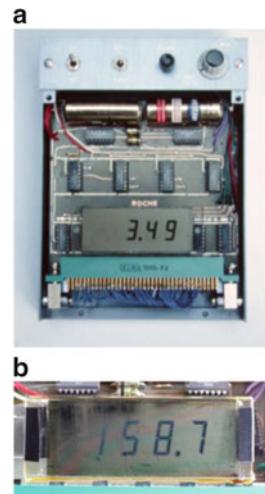
Fig. 6.3 (**a**) Wave-guiding in the off-state LC director configuration of a 90° twisted TN-LCD between crossed polarizers P. (**b**) Twist configuration of a TN-LCD at V_{50}, i.e., 50 % optical transmission. (**c**) Azimuthally angular contrast dependence of a partially switched TN-LCD at V_{50}

prototypes whose surface LC alignment started deteriorating due to poor surface anchoring after 2-year operation.

Helfrich and Schadt filed their Swiss TN patent application on 4 December 1970 and published their TN field-effect results in the February 1971 issue of Applied Physics Letters [14]. The reason for their rush filing and submission of a short manuscript with preliminary results in a fast publishing US journal was an information leak at Brown Boveri. During a November visit of BBC by Al Saupe, Kent State University, the project manager of the dynamic scattering group at BBC had mentioned key features of the TN experiments of the author. He asked for Saupe's opinion without informing him of the confidential nature of the

Fig. 6.4 (**a**) Seven-segment TN-LCD prototype made by the author in 1971. (**b**) TN prototype made at the same time exhibiting partly degraded surface alignment after 2 years of continued operation

information. This violated the nondisclosure agreement between Roche and BBC, and Ferguson—who also worked at Kent State University—learned of the TN experiments of Schadt. More than 5 months after the Swiss TN priority date, Ferguson filed a TN patent in the United States [18]. Ferguson's US patent triggered years of legal actions between Roche and Ferguson and gave insights into the sequence of events which triggered the controversy. The patent interference conflict was eventually settled out of court when Ferguson decided to sell his US patent to Roche [19].

Other field-effect research attempts made by Helfrich and Schadt at the time led to the discovery of field-induced curvature electricity in banana-shaped, bent-core nematic LCs [20]. However, the birefringence of the effect proved to be too weak for displays. This did not apply to their discovery of the alignment-free pre-transitional electro-optical Kerr effect in strongly positive dielectric LCs which showed remarkably large birefringence [21]. However, due to the narrow pre-transitional operating temperature range of nematic liquid crystals and despite very fast response, nematic liquid crystal displays based on the Kerr effect were only of scientific interest at the time [22]. In retrospective it is interesting to note the recent renewed interest in LCDs based on the Kerr effect [23] which is spurred by remarkable progress made with blue-phase liquid crystals and display geometrics [23–25] since 1985.

6.1.3 Subsequent Field-Effect LCDs Spurred by the TN Invention

The publication of the twisted nematic effect by Schadt and Helfrich in the February 1971 issue of Applied Physics Letters [14] spurred a strong interest of the scientific community in the new effect and in the development of positive

dielectric liquid crystal materials. However, the potential of TN-LCDs and liquid crystal displays in general continued to be questioned by many for years to come [3–5]. One of the internal skeptics of the Roche liquid crystal research project was the new general manager of its Central Research Labs who joined the company in 1971. He declared liquid crystals to be "überflüssige Kristalle" and stopped liquid crystal research. The collaboration with BBC was also terminated. As a consequence Helfrich left the company and became professor at the Freie Universität Berlin where he discontinued work on thermotropic liquid crystals and LCDs. Professor Pletscher, member of the board of directors of Roche and head of global Roche research, convinced Schadt to stay with the company. Thus, the author started searching for new research topics of interest, namely electro-optical effects and charge transport phenomena in the field of biophysics, i.e., lyotropic liquid crystal black lipid membranes. In the next 2 years this led to the development of an electronic analogy model of the photoresponse of doped artificial lipid bilayer membranes [26]. In collaboration with medical research he discovered correlations between neurotransmitter transport, selective ion conduction across ionophore-doped cell membranes, and heart activity [27].

In the mean time, leading Japanese watch and electronics companies had started research on TN-LCDs realizing the potential of the new field effect. In the spring of 1973 Dr. von Graffenried, then head of the legal and patent department of Roche, asked Schadt to explain the content and relevance of the pending Swiss TN-LCD patent. The reason was a visit of Mr. Hamamoto, advisor to the president of Suwa Seikosha, who had approached Roche to buy the TN patent rights. Schadt outlined its potential which in his opinion went far beyond digital watch displays. He suggested not to sell the TN patent but to make it nonexclusively accessible to all interested parties. Roche decided to reactivate its liquid crystal research, and the author was given the opportunity to establish an interdisciplinary liquid crystal research team consisting of physicists and synthetic chemists. He envisaged numerous device and material R&D problems to be resolved for advancing TN-LCDs. Moreover, he planned to continue his search for new electro-optical field-effects and find solutions remedying the drawbacks of TN-LCDs. One intriguing puzzle was the delicate LC alignment at the display boundaries and bias tilt generation [3–5]. It was still not known whether the interactions between LC molecules and substrates remained indeed stable under continued operation and stress (cf. Fig. 6.4b); mechanical surface alignment was a sort of black magic (Sect. 7.3). Moreover, display-related liquid crystal material research was in its infancy (Sect. 6.1.2). Schadt was convinced that much better liquid crystal molecules and LC mixtures had to be invented and tailored to the electro-optical requirements of TN-LCDs and potential future field effects. Therefore, and to support Roche LC production, he started the development of new analytical tools and research into correlations between molecular structures, material properties, and display performance.

Parallel to reactivating liquid crystal research, Roche established a TN patent and licensing team for nonexclusively licensing and defending the TN patent worldwide [19]. For the first time in its history, Roche also entered into

manufacturing of non-health-related functional chemicals, i.e., liquid crystals. This enabled commercialization of the first room temperature TN liquid crystal mixtures which the author and his chemical colleagues had already started developing prior to the R&D stop [3–5, 13]. Strong efforts were made by the author and his team to compensate for the lost two crucial years at the beginning of field-effect LC material development. One target was generating intellectual property on new liquid crystal materials for continued supply of new products for the Roche LC production and for supporting the emerging TN-LCD industry with LC materials.

In the following decade and after settlement of eight complex TN patent opposition cases in different countries, including Japan, the Roche licensing portfolio covered worldwide 20 TN-LCD patents based on the Swiss TN patent of Helfrich and Schadt [14] plus Ferguson's US TN patent. The first TN-LCD licensing agreement was negotiated between Roche and Mr. Hamamoto of Suwa Seikosha. A few months later, Mr. Odawara of Hitachi and Dr. Sasaki of Sharp independently reached licensing agreements with Roche, followed by all other companies worldwide which started TN-LCD production. This was the beginning of a fruitful and long-lasting R&D relationship between the author and the emerging LCD and LC material industries up to the present [3–5].

In retrospective and in view of the numerous potentially competing display technologies under development in the early 1970s, it was a far-sighted decision of leading Japanese companies to enter into TN-LCD development and manufacturing. The invention of the twisted nematic effect, subsequent R&D progress in device physics and LC material development, and the early engagement of the Japanese watch and electronics industry caused a paradigm change towards flat-panel field-effect liquid crystal displays. The parallel development of new LC materials by Roche, by George Gray at Hull University, British Drug Houses, and Merck KGaA in Europe—followed by Dainippon Ink and Chisso in Japan—strongly contributed to this development (cf. Sect. 6.1.2). First portable products comprising TN-LCDs were digital watches, electronic calculators, and games. They paved the way for the new technology and confirmed its reliability. The development of subsequent field effects, time multiplex, and thin-film transistor (TFT) addressing led to today's high-quality and high information content of field-effect LCD's annual turnover of over $130 billion.

6.1.4   TN-LCD and Subsequent Field Effects
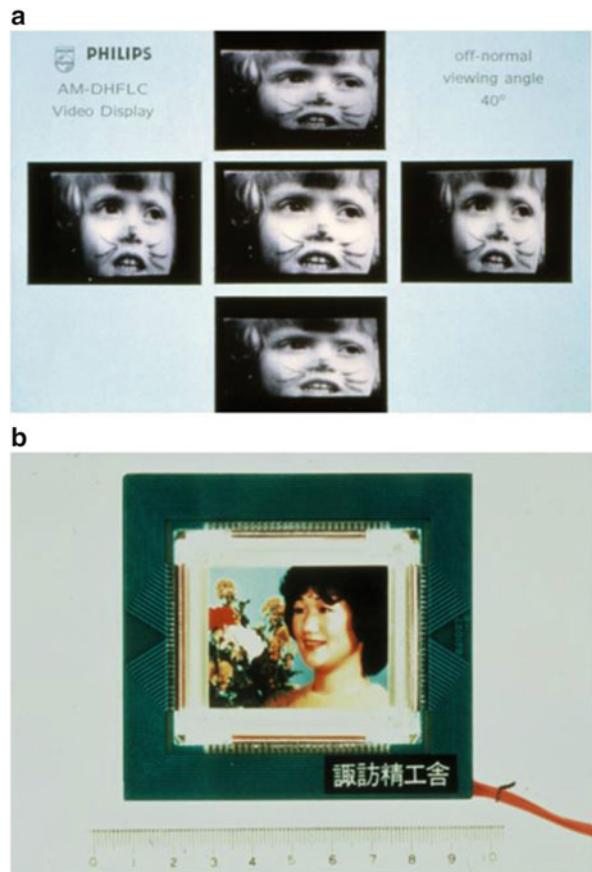
The range of flat-panel display applications from initially reflective black/white TN-LCDs rapidly broadened. Backlighting, brighter polarizers, polarized reflectors, color filters, optical retarders, and wide-view films were developed and integrated into TN-LCDs. Progress made in device physics and LC materials enabled medium information content TN-LCDs with increased fields of view for games, office equipment, and digital car dashboards [3–5]. A further step towards

LCDs with larger information content was the independent development of time multiplex addressing of matrix electrode patterns by Kawakami et al. [28] and Alt and Pleshko [29]. In the mid-1980s TN-LCD manufacturing and LC material development had reached a stage where higher information content field-effect solutions became feasible [3–5, 30]. The development of more than 90° twisted nematic configurations, i.e., super twisted nematic (STN)-LCDs by Scheffer and Nehring [31], Waters and Raynes [32], and Schadt and Leenhouts [33] enabled—strongly supported by the development of infinitely steep and fast-responding alkenyl STN-LC mixtures by the author and coworkers (cf. Sect. 6.1.2)—a drastic increase of the number of multiplexible lines of LCDs [3–5]. As a consequence, the rising information content of liquid crystal displays started to challenge simple cathode-ray tube (CRT) monitors. However, insufficient contrast, colored off-state appearance due to residual elliptical polarized light leakage, the initial lack of optical compensation films, and inadequate cell gap control still hampered STN-LCDs [3–5]. Moreover, despite improved information content of super twisted LCDs, their slower response times prevented the development of fast-responding flat TV LCD screens and high information content LCD monitors. Dual-frequency addressing developed by the author [34] did not solve the response time problem either (cf. Sect. 6.1.2). Parallel to thin-film transistor (TFT) development, this spurred the search for electro-optical effects with improved field of view based on planar field-effect LC configurations. One solution was the in-plane switching (IPS) effect published independently by Kiefer and Baur [35] and by Kondo et al. [36] in 1992. Further important developments of field-effect LCDs [3–5] are the fast-responding Pi-cell of Bos et al. [37], the optically compensated birefringence (OCB)-LCD of Uchida et al. [38], and the fringe field switching (FFS)-LCD of Lee et al. [39].

Until the mid-1990s and after 20 years of intense research on nematic field-effect LCDs it was still uncertain whether LCDs and LC materials could indeed meet the short response time requirements and the optical quality required for LCD television. Therefore, parallel to nematic LCD research, strong efforts were made to find effects based on the inherently faster responding ferroelectric liquid crystals (FLCs). Unfortunately, FLCs proved to be difficult to surface-align, rendering them up to now commercially applicable only for niche products such as electronic eye shutters or time sequential LCD projection. FLC examples are the surface-stabilized ferroelectric (SSF)-LCD of Clark and Lagerwall [40] which initiated FLC-LCD development and the deformed helix ferroelectric (DHF)-LCD of Beresnev et al. [41]. In 1995 a TFT-addressed black–white DHF-LCD television prototype with 20 μs response time and broad field of view was developed by the author and coworkers in collaboration with Philips [42] (Fig. 6.5a).

Peter Brody et al. [43] at Westinghouse were the first to realize the compatibility of TN-LCDs with thin-film-transistors (TFTs). In 1974 they realized the first TFT-addressed TN-LCD prototype whose negligible current consumption (field effect) and therefore large voltage holding ratio [3–5, 30] enables pulse-sequential matrix addressing of its picture elements. TFT addressing circumvented

Fig. 6.5 (**a**) Broad field of view of fast-responding (32 μs), diode-matrix-addressed, *black–white* DHF-LCD prototype with gray scale of 1995. (**b**) Early TFT-TN-LCD color television from Seiko Epson of ~1985

time-multiplexed matrix addressing of LCDs with its requirement for steep electro-optical LCD characteristics for displaying large information contents [3–5]. However, apart from small TFT-TV-LCDs (Fig. 6.5b), it took research and industry more than twenty more years of R & D until TFT addressing had reached a stage in the 1990s justifying large-scale investment into TFT-LCD production [3–5]. TFT-addressed TN-LCDs replaced the slow super twisted nematic LCDs in high information content displays. At the end of the 1990s, TFT-addressed in-plane-switched (IPS)-LCDs followed [3–5, 36]. Moreover, in the late 1990s multi-domain pixelation [3–5] combined with TFT addressing enabled the broadening of the narrow field of view of the vertically aligned (VA) field effect [44, 45] known since 1973 (Sect. 7.3). Large-sized TFT-addressed TV-LCDs based on in-plane switching and on multi-domain vertical aligned (MVA) configurations became feasible [3–5] (cf. Sect. 7.3).

6.2 VA Technique

Hidefumi Yoshida
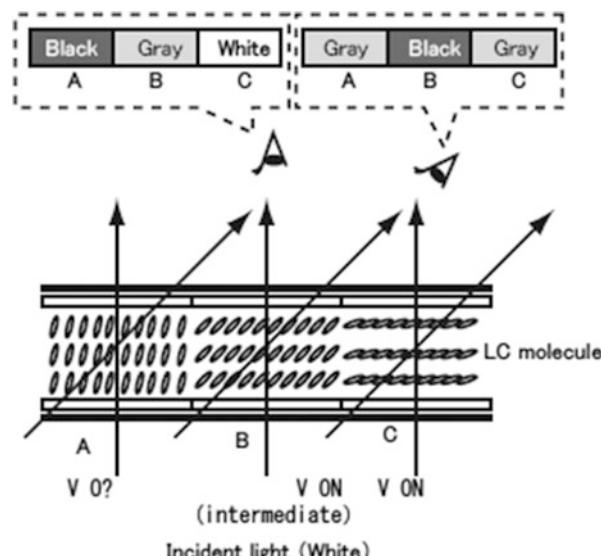
6.2.1 Basic Principles

In the vertically aligned mode (VA mode), the long axis of rodlike liquid crystal molecules is oriented perpendicular to the glass substrate. In general, nematic liquid crystals with a negative anisotropy of the dielectric constant are used.

The liquid crystal is oriented vertically when no voltage is applied and tilts under an electric field. With a pair of polarizers whose absorption direction is perpendicular to each other (referred to as crossed Nicols), a so-called "normally black" display is realized, in which the display is black when no voltage is applied and white with an applied voltage (Fig. 6.6). This mode has been reported in 1971, at around the same time as the twisted nematic (TN) mode [46].

This VA method was introduced a few times at liquid crystal conferences under different names, such as ECB type and VAN type.

The VA mode uses a monodomain orientation, having a narrow viewing range especially when showing gray scale display image and it cannot be used as such. The ECB-type VA mode was announced in the liquid crystal conference in 1988 by Mr. Kinoshita from Toshiba [47], and the first question during the presentation was about the viewing angle characteristics. The questioner might have been noticed

Fig. 6.6 The reason why the gray scale image is reversed in the oblique viewing direction

that problem in his own experiments already. Essentially, the question was phrased as "Doesn't the display deteriorate when viewed even at a slightly lower viewing angle?" One of the authors (Yoshida) was young and recollected to think "He is right. Vertical alignment (VA) technology might not be useful at all." Now I (Yoshida) think that I should have had a more positive approach that would have led to a wonderful solution of the posed problem.

One of the key methods to improve the viewing angle characteristics is to divide the pixel into sub-pixels, which had first been proposed for the TN type. Later, it had been applied to the VA and IPS type. Let us first touch on this domain-dividing technology.

6.2.2 Domain-Dividing Technology

If one looks at a TN or VA mode screen from vertically above or below the screen normal, the images show a remarkable negative–positive reversal, and the cause is shown in Fig. 6.6. We focus on the liquid crystal molecules near the center of the liquid crystal layer, because they show large orientational changes upon voltage switching. The liquid crystal molecules are almost vertically oriented when no voltage is applied as shown in Fig. 6.6a, but are almost horizontally oriented as in Fig. 6.6c when a large voltage is applied and occupy an intermediate state when an intermediate voltage is applied as seen in Fig. 6.6b. The three pixels appear black, gray, and white, respectively, when viewed from the front. When observed at an oblique angle, the pixel at an intermediate voltage appears black because the molecular long axis direction of the liquid crystal molecules is inclined obliquely as shown in Fig. 6.6b. Vertical (Fig. 6.6a) or horizontal (Fig. 6.6c) states appear gray. From this, it becomes clear that black becomes gray, gray becomes black, and white becomes gray, which amounts to a negative–positive reversal. That is, the image of black hair becomes white, and whitish skin becomes black.
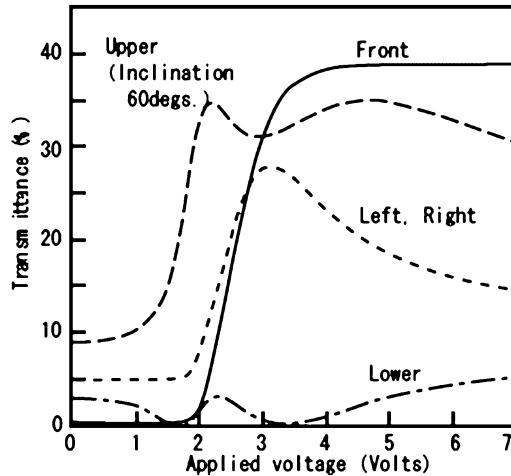
Mr. Tanuma was measuring the viewing angle characteristics of TN-type liquid crystal cells day by day. Since PCs were still not common at that time, the voltage–transmittance characteristics were measured while he was staring at chart papers. Everyday he was measuring the transmittance–voltage characteristics from various inclination and azimuth angles (see Fig. 6.7).

After he looked at these chart many times, he got an idea that just by adding all values at a certain angle and dividing the result by the number would lead to the best results. In any case, the idea that rubbing the alignment layer in different directions would give good results was filed as a patent.
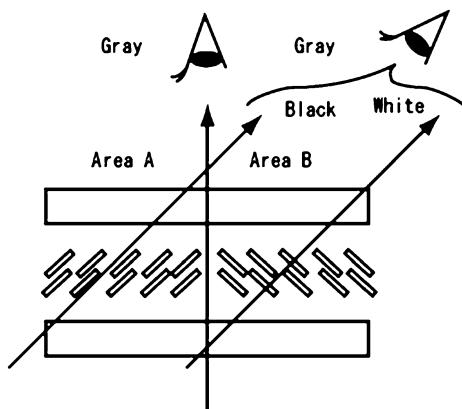
That is the opportunity how the domain-dividing method started. One pixel would be divided into two or more segments in which the liquid crystal molecules had different orientations towards each other.

Pixel area A becomes black when viewed from an oblique angle and also becomes white when viewed from the other oblique angle as can be seen in Fig. 6.8. Because the average brightness of the two regions in the entire pixel

Fig. 6.7 The viewing angle characteristic of TN (twisted nematic)-LCDs (transmittance–voltage characteristics)
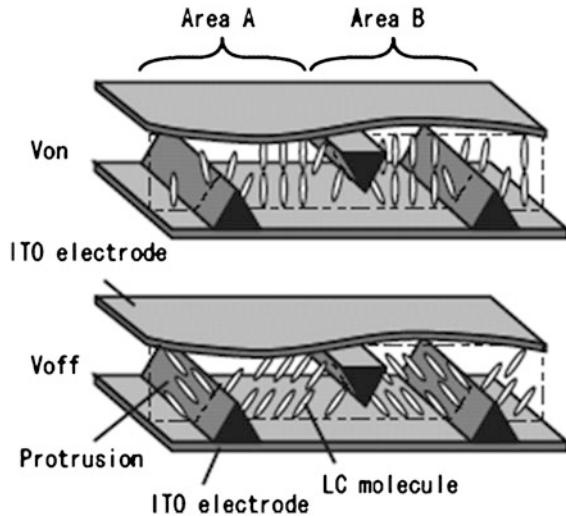

Fig. 6.8 The basic principle of optical compensation through the domain-dividing technology (TN-LCD)

is dimmed, the pixel will be seen as gray from an oblique angle as well as from the front. This technique was put into practice by Mr. Kamada, Mr. Koike, and Dr. Okamoto et al. and a display with the most wide viewing angle at the time was produced.

We will omit details of further technologies relating to TN-LCDs here, but interesting ideas were developed on the way. One example is the irradiation of the rubbed alignment layer with UV light, which leads to a change of the rotational orientation in a TN cell by controlling the molecular pretilt angle [48, 49]. Furthermore, by incorporating the domain dividing, this technology of stable alignment is currently widely used in the IPS mode and the vertical alignment mode.

Fig. 6.9 The principal
configuration of MVA-LCD
(dual-domain configuration)
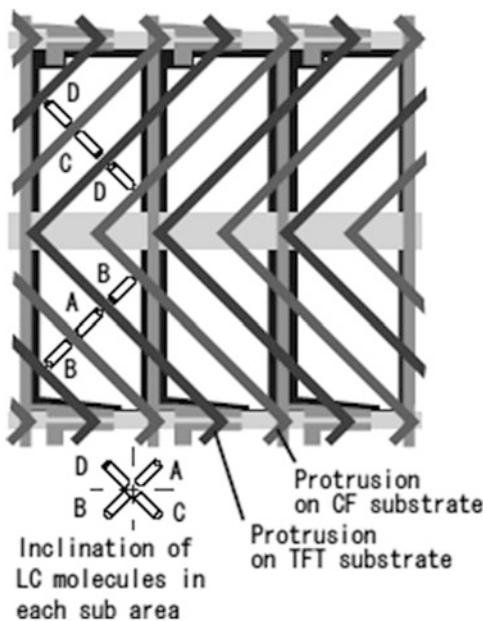
## 6.2.3 Vertical Alignment and Domain Dividing: MVA Liquid Crystal Display Mode

In the vertical alignment mode, based on the experience in TN-type displays, a wide viewing angle characteristic was tried to develop from the beginning on the assumption of using the aforementioned domain dividing.

The orientation of the molecules can be controlled by providing a protrusion of the resist on the TFT substrate side and/or the CF counter-substrate side [50]. Figure 6.9 shows that such resist protrusions on the ITO transparent electrode can control the LC molecular alignment using the pretilt. The resist structures cause an oblique electric field, which matches the pretilt or inclination direction. Figure 6.10 schematically shows the actual TFT pixel. Bank-like protrusions are formed in a zigzag, and the liquid crystal molecules are divided into four areas A, B, C, and D. A and B are complementary to each other, as well as C and D. Thus, as a whole, the liquid crystal molecules tilt in four directions. The optical axis of the polarizer is in the vertical and horizontal direction, and a good black display image is obtained in the vertical and horizontal viewing directions. At present, further improvement is reached by replacing the TFT side protrusions with slits, using the oblique electric field in the vicinity of the slit for stable alignment [51].
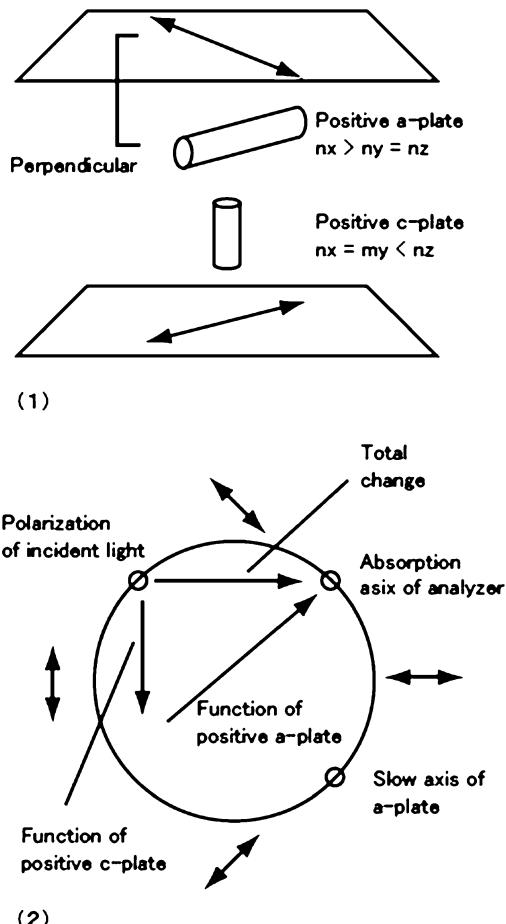
Here, we will introduce the start of the MVA technology. At the very first stage for developing VA-LCDs, we have struggled considerably with the rubbing techniques [52], but we could not achieve the level necessary for monitor quality due to the line-shape mura. The issue with defect lines due to rubbing was difficult to resolve. Mr. Takeda was given the task to develop an orientation technology that does not require rubbing. Such a rubbingless technology had been developed by

Fig. 6.10 The principal configuration of MVA-LCD (four-domain configuration)

IBM by fabricating slits on the CF side of the substrate [46]. We thought that partially covering the electrode with a dielectric material will partially shield the electric field and proceeded by trial and error. We initially used a negative resist for the dielectric layer. However, our factory refused to use such an unproven material. In response to advice from one of the authors, the developing team focused on positive resists that are commonly used in semiconductor processes. However, those tend to dissolve in the solvents used to coat the alignment film. By chance we had a visit to Mr. Okubo, the former supervisor of Mr. Takeda, who with his strong background in chemistry advised Mr. Takeda to bake the material to prevent solution. The good relations with a large number of people in the network of contacts paid off and with their advice, the team was able to achieve the ideal design of the structures: protrusion with slant edge. There was also initial ridicule that we would end up with a bright red display since the resist was red, but we produced a prototype, anyhow. The display wasn't reddish. The resist turned brown during annealing, and the voltage for the LC layer on the protrusion portion was decreased due to the protrusion (dielectric layer), and the disclination was formed in the protrusion portion. No light leakage was observed. In this initial prototype, the width of the protrusion and the protrusion spacing was a serious problem. At that time there was no simulation software for two-dimensional calculations, and we simply depended on the intuition getting through some experimental results. It is very impressive that the initial design through the intuition was later proved to be the appropriate one or the same as the best design that was introduced through additional many experimental results.

Fig. 6.11 The basic
principle of optical
compensation on the
viewing angle
characteristics with
VA-type LCDs

Perpendicular

Positive a-plate
nx > ny = nz

Positive c-plate
nx = my < nz

(1)

Total
change

Polarization
of incident light

Absorption
asix of analyzer

Function of
positive a-plate

Slow axis of
a-plate

Function of
positive c-plate

(2)

6.2.4 Viewing Angle Improvement of the Black State in MVA Mode Liquid Crystal Displays

The contrast in the front direction of the MVA mode displays is higher than that of the other liquid crystal displays like TN-LCDs. However, at an oblique direction, especially by observation from the 45° diagonal azimuth direction, there is the problem that the contrast is reduced by leaking light in the black state. Figure 6.11 shows that the orientation of crossed Nicol polarizers is no longer perpendicular to each other when viewed obliquely, increasing the light transmission or light leakage [52, 53].

Figure 6.11a shows the polarization state of light for this case plotted on Poincaré sphere. We optimized the c-plate ($n_x = n_y > n_z$) and a-plate ($n_x > n_y = n_z$)
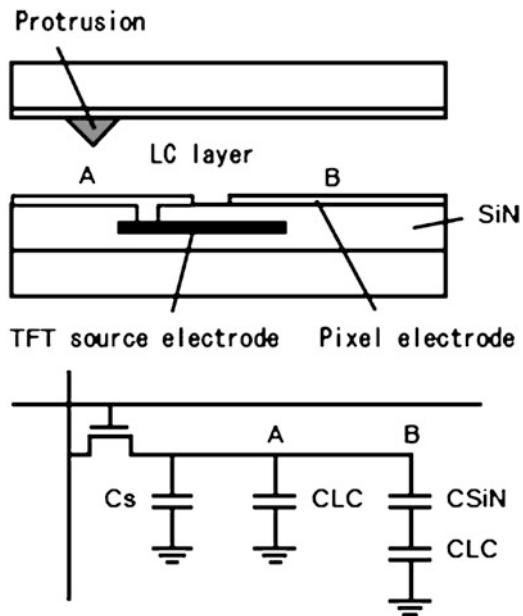
and let the polarization of the linearly polarized incident light be varied to match the absorption axis at the exit. In the vertical alignment mode LCDs, the birefringence of a vertically aligned liquid crystal layer that can be deemed as a positive c-plate is too large and needs to be corrected to an appropriate value by a stacked negative c-plate. The biaxial films (definition is $n_x \neq n_y \neq n_z$, and for VA films: $n_x > n_y > n_z$) can work as both of a- and c-plate. Stretched films of norbornene resins with a small optical elastic modulus and the stretched TAC films are widely used as the biaxial films. Examples in the simplest configuration are the TAC (triacetylcellulose)/PVA (polyvinyl alcohol)/TAC//liquid crystal layer//biaxial film/(TAC)/PVA/TAC. The configuration TAC/PVA/biaxial TAC//liquid crystal layer//biaxial TAC/PVA/TAC has been widely used as a symmetric structure.

The development of this technology was with a continuous struggle. Mr. Sasabayashi's calculation showed that the simplest configuration needed a stretched TAC polarizer film. He, together with the two of us, visited the polarizer manufacturer. However, we faced opposition because their machinery will be contaminated by gas generated from the TAC film. So, we tried another configuration. The large phase difference in non-stretched TAC films can be used as just a c-plate to compensate the phase difference stemming from the vertical direction of the liquid crystal. We commissioned the mass production of bonded polarizers: additional c-plate and a-plate were stacked.

At that time, polarizer manufacturers just started to understand the principle of optical compensation. We explained the film configuration and the optical principles. Then, prototypes were fabricated and mass-produced polarizers were manufactured. It was a situation where we, one by one, fostered the understanding of optics among the technicians of each manufacturer. Biaxial films show a phase difference both in the vertical direction and in the plane of the optical film. This contributes to cost reduction since the manufacture of films with good viewing angle characteristic is completed in one step. However, the control of the phase difference was difficult. The period to develop commercial products was long because of the unevenness of the films. However, while the MVA-type display became more familiar, those aspects changed gradually. The unevenness or nonuniformity problem was gradually improved by the development of a norbornene resin film that was being used for a $\lambda/4$ plate. While the VA type is the standard for large-sized liquid crystal displays, technologies were developed by many manufacturers entering the market. Polarizer manufacturers started proposing their own new film configuration and developed polarizers, which were then evaluated by panel manufactures. Panel manufactures became evaluators instead of proposers.

It is a little ironic that at present the stretched TAC films that had generated so much resistance from polarizer manufacturers at the beginning have become the standard.
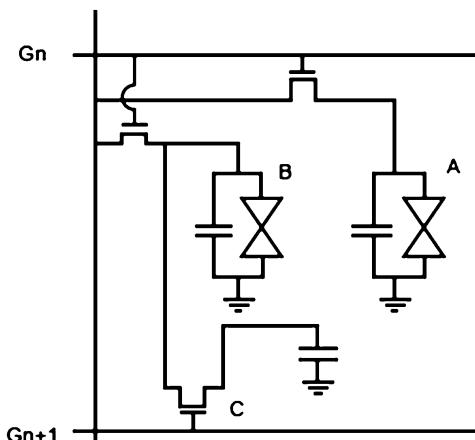
Fig. 6.12 The control of
voltage applied on the LC
layer by using capacitance-
coupling method

6.2.5 Viewing Angle Improvement of MVA Mode Liquid Crystal Displays Through Halftone Technologies

We described viewing angle improvement of screen images with gray scale by
using the domain dividing in the previous sections, but with increasing market
share of large-sized LCD TVs, a further improvement of the viewing angle was
desired. There was a peculiar problem that flesh colors became whitish and, in
general, colors faded when viewing from an oblique angle. This is because the
gradation of the RGB pixels to achieve skin color has a different change in the
amount of transmitted light at oblique viewing angles for each RGB color. Hence,
the originally quartered pixels were further divided into two, resulting in 8 -
sub-pixels in which the display image could be controlled by changing the
applied voltage. Figure 6.12 shows the basic structure of a capacitive coupling
method as a way of changing the voltage that is being adopted in current mass
production [54]. The signal is applied from the source electrode directly to
sub-pixel A and through the SiN layer capacitance to sub-pixel B. Therefore, a
lower voltage is applied to the liquid crystal layer of sub-pixel B than to sub-pixel
A. As a result, even in the gray scale display state, sub-pixels A and B can avoid
an intermediate state at the same time. Other methods using the capacitance have
been put into practical use, for example, a method that controls the voltage after a
voltage pulse [55]. As shown in Fig. 6.13, the capacitance of the previous frame
will lower the voltage.
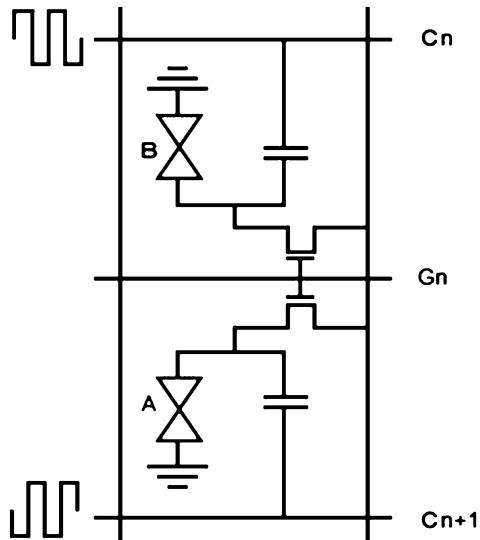
Fig. 6.13 The control of voltage applied on the LC layer by discharging the electric charge with the LC cells

Mr. Kamata played a large role in these technological developments. Dr. Yoshida (one of the authors) was struggling for improving the viewing angle characteristics of gray scale images after improving that with black display image (see Sect. 6.2.4). He (I) had believed the display would become cleaner by mixing bright and dark sub-pixels. However, it was difficult to demonstrate this. Mr. Kamata simulated a display with a reduced resolution by mixing several pixels instead of dividing one pixel into sub-pixels. He sent the simulated image to all persons, from his superior to his colleagues, who had an interest in this, and he urged them to see the effect by changing the angle on the monitor in front of them. The reaction of the recipients, who saw the improved viewing angle with their own eyes on their own VA monitors, was immediate, and development began at once. In conjunction with Mr. Suzuki, the circuit technician wrote a modified circuit by programming the measured characteristics into a γ table. Initially, only the capacitive coupling was studied (Fig. 6.12); however, it could suffer from the image sticking problem. In one of the regular vivid brainstorming sessions at Fujitsu, Mr. Ueda commented "Can we differentiate or change the voltage on the LC cell after applying a voltage to each pixel?" The equivalent circuit shown in Fig. 6.13 came to Kamata's mind at this time. After a computer simulation, the pixels were carefully designed. This method was to be announced in an invited talk at SID05. However, the announcement was canceled because Fujitsu Display Technologies, Inc. was sold to Sharp Co., Ltd. Thereafter, similar practical techniques have been announced by several companies.

Meanwhile, a method of varying the applied voltage to each sub-pixel by changing the common potential had been developed in Sharp around 2004, in which pixels were addressed by low and high voltage. One concern that has been discussed at that time was the crosstalk that occurred because of the capacitive coupling between the pixel electrode and the data signal lines. Through the discussions among technical personnel on that crosstalk, Mr. Shimoshikiryo got the idea

Fig. 6.14 The control of
voltage applied on the LC
layer by swinging or
changing alternately the
common voltage

of intentionally using the crosstalk to differentiate the applying voltage on each
pixel. He proposed to change or swing the voltage of the common electrode rather
than the data electrodes [56]. The development advanced immediately when the
circuit team and pixel design team worked together at that problem, and the
resulting equivalent circuit is shown in Fig. 6.14. Voltage is applied to the pixel
while swinging the common electrode, but so that the phase difference at each
sub-pixel is superimposed, and as a result the different voltage is applied to each
sub-pixel.

By introducing these methods, a high contrast VA-type LCD with maximum
viewing angle characteristics has been developed that is now used in standard
large TVs.

6.2.6 Conclusions

We were allowed to tell some anecdotes related to the development of the VA-type
LCD and the MVA-type in particular. We found that a group of talented persons
can steer the aggressive development of a technology. Due to limited page, a
limited number of engineers are referred in this section. However, in the stage of
development, we suppose, ten times of engineers were in charge, and in the stage of
mass production, hundred times of engineers tried to put the products into market.
For the technology related to VA-type LCDs, other than the MVA-type, please refer
to Sect. 7.2.

6.3   OCB Mode

Hidehiro Seki

6.3.1   Introduction

The key features of liquid crystal displays (LCDs) are low-voltage driving, low power consumption, and a slim profile. Thus LCDs are used in a variety of applications. Research and development is being carried out to increase contrast ratio, viewing angle, screen size, etc. So far, those challenges have been overcome, and R+D has produced results that started with the TN mode and led to the VA and IPS modes.

On the other hand, the response time of the liquid crystal (LC) material is generally around 100 milliseconds, and this slow response has been a concern for a while. The electro-optical characteristics of the LC depend on the behavior of molecules in the electric field and the distortion of their orientation, and increasing the switching speed has been a barrier of high-speed response. It was for this purpose that the optically compensated bend (OCB) mode had been developed [57]. In this chapter, the birth of the OCB mode and its application will be described.

6.3.2   The Birth of the OCB Mode

For high-speed response, thinning the LC layer is one conceivable method. Thus it is necessary to increase the optical properties of the LC materials, which in turn necessitates future material development. Ferroelectric LCs use the interaction of the electric field with the spontaneous polarization of the LC molecules for high-speed switching, but the problems are the stable molecular alignment in thin-gap cells and the increase of the speed of the current supply of the drive elements because of the relatively high dielectric constant of ferroelectrics, as compared to a nematic LC.

The OCB mode uses basic nematic LCs which are readily obtained and easy to handle. It is possible to remarkably increase switching speed, because the LC molecules have to bend by half a turn along their main axis in the direction perpendicular to the cell, as shown in Fig. 6.15. This bend alignment cell was proposed in 1983 by P. J. Bos et al. and was named π cell [58]. The electro-optical properties of the molecules allow it to operate in the birefringence mode. Bos et al. used the two-state on–off of the π cell as the polarization switching element of a multicolor oscilloscope [59]. The cell has been reported to show high-speed response and wide viewing angle based on the self-compensation from the symmetric structure in the center of the LC layer.
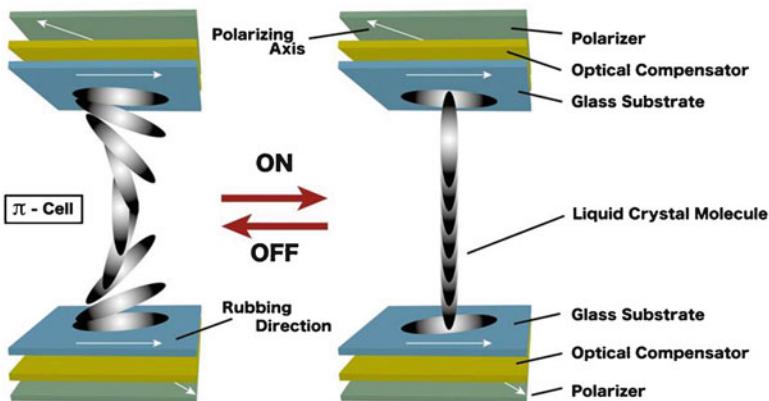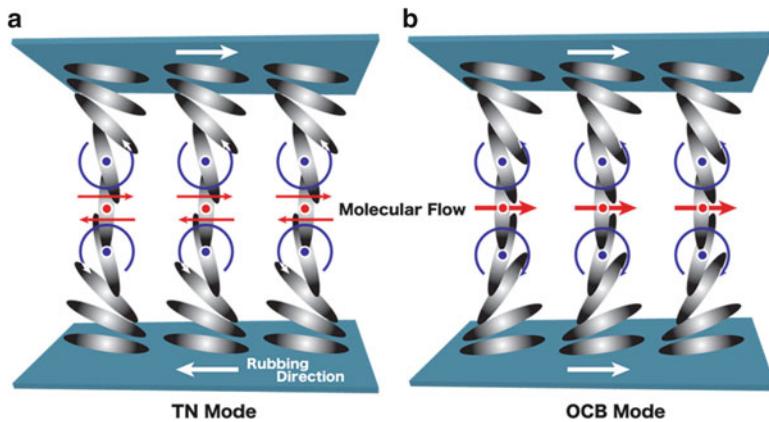
**Fig. 6.15** Operation Principle of the OCB Mode of Liquid Crystal

Bos et al. proposed an LC cell that is sandwiched between two negative uniaxial polarizers [60]. In this case, rather than compensating the retardation vertical to the cell, the compensation is satisfied in the oblique direction, for which a high voltage of 32 V was necessary to achieve the black state.

Furthermore, since a transmittance of 5 % remained in the black state, an even higher voltage was required to obtain a better contrast. On the other hand, T. Uchida et al. showed that it is possible to realize a display using the OCB mode [61] by using LC cell consisting of a π cell sandwiched between two polarizers and two biaxial retardation films, with which they achieved a wide viewing angle halftone image at a low voltage (2–6 V). This is because a satisfactory three-dimensional optical compensation can be achieved in the black state. Furthermore, it was shown by analyzing the free energy of bend and splay alignment state that it is possible to stabilize the bend state at a higher voltage than the threshold voltage [62–65].

6.3.3 Fast Response Is Achieved by the Acceleration Effect of LC Flow

One of the main features of the OCB mode is a high-speed response, which is due to the rotation of the LC molecules that resulted from the flow of the molecules. Figure 6.16a shows the asymmetric molecular orientation of a conventional nematic LC cell. It shows the movement of the LC molecules when the voltage is switched off. The molecules near the center of the cell experience a torque in the reverse direction in which they should move, due to the flow caused by the rotation of molecules in upper and lower layers. This slows down the response. Meanwhile, in the OCB mode, the molecular orientation is symmetrical as shown in Fig. 6.16b,
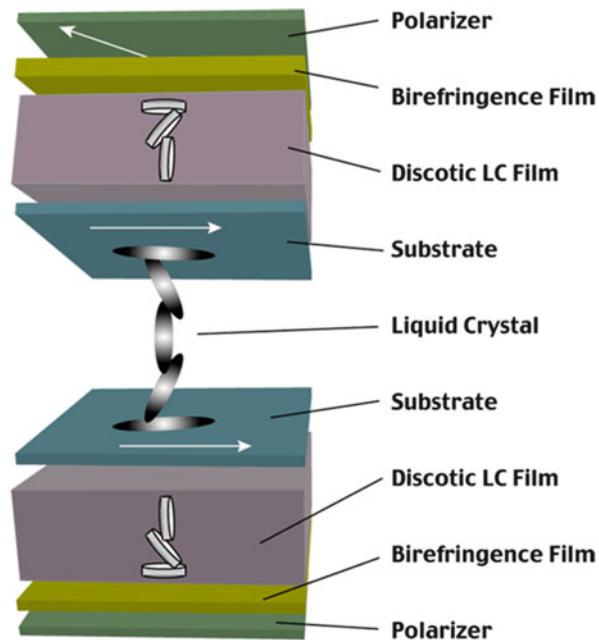
Fig. 6.16 Accelerating effect of the flow in the OCB mode of liquid crystal

the vertical flow of molecules will accelerate the lateral movement of the central molecules [66–68]. As a result, the molecular flow in the OCB mode results in a high-speed response of the LC molecules. In fact, the response time of the twisted nematic mode in general is in the order of 10 ms and even slows down to 10–100 ms for gray scale display. The response time of a typical OCB cell is around 1–5 ms, with the potential of further decrease by improving the design and conditions of the LC molecules. Furthermore, this high-speed response due to the flow effect has been shown to be effective even at low temperatures [69].

6.3.4   Wide Viewing Angle Based on the Self-Compensation Effect

In order to achieve a wide viewing angle in the OCB LC display, a wide viewing angle is necessary for each component. The OCB mode is based on the electric field-controlled birefringence effect. Bos et al. [58] have reported that the wide viewing angle in the π cell type is due to a self-compensation effect caused by the symmetrical molecular orientation [70]. That means that each component above and below the LC cell mutually compensates their optical properties, as shown in Fig. 6.15. However, the compensation in the vertical plane has not been considered. T. Ishinabe et al. address this in their paper in which they study the improvement of the viewing angle in the vertical direction. Given the structure of a π cell, two biaxial films in the plane of the molecular orientation should be considered. For the black state, two other biaxial films lead to a three-dimensional compensation. This method leads to high contrast and wide viewing angle in a low-voltage region and can solve the problem of the problematic viewing angle characteristics of crossed

Fig. 6.17 Viewing angle compensation in the OCB mode of liquid crystal

linear polarizers and improve performance by using two biaxial films. As a result, a high contrast and wide viewing angle which is practically satisfactory can be obtained.

The OCB mode uses a bend structure and from an oblique angle the molecules show an effective twist. Bos and H. Mori have proposed a method of using a discotic LC film in the diagonal direction of the bend structure of the OCB mode [71]. A viewing angle of over 160° has been achieved in this way. In addition, T. Uchida et al. have developed a new method to analyze precisely the birefringence properties of the discotic LC film and have established a method of designing the OCB mode LC display as shown in Fig. 6.17. As a result, a contrast ratio of at least 100:1 is obtained for wide viewing angles in all directions. Similar properties are also obtained experimentally, and a contrast ratio of at least 1000:1 is obtained in the vertical direction [57].

6.3.5 Alignment Transition from the Splay State to the Bend State

In the OCB mode, LC molecules show a splay orientation in the electric off-state, which is the low free energy state, and thus a stable orientation, as shown in Fig. 6.18a. Therefore, it is necessary to change the alignment from splay to bend orientation before driving, as shown in Fig. 6.18b. Such a state is obtained by
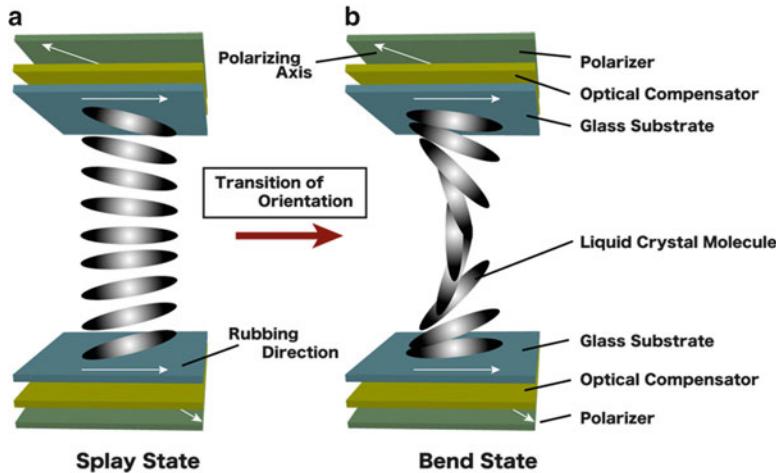
Fig. 6.18 Orientational transition in the OCB mode of liquid crystal

rubbing the upper and lower substrates in the same direction but with the resulting pretilt angle of the LC molecules in opposite directions. The resulting structure can be considered as one of the three orientation types: bend, splay, or 180° twist state. The splay state is more stable than the bend state in the absence of an electric field. On the other hand, at high voltages, the free energy of the bend state is lower compared to the splay state, and the states easily transfer. However, in order to take into account the practical applications at lower voltage, some transition kernels are required in order to lower the energy barrier of the alignment switching [72]. Spacer and dust particles can act as accidental kernels, but the reproducibility is not satisfactory. In order to form kernels, a high pretilt angle [73, 74] or partly rubbing in orthogonal directions in combination with a chiral dopant has been proposed [75]. When analyzing the details of the mechanism that causes the transition, it has been found that a twist angle of >90° is required for kernel formation [76].

6.3.6 Ultralow-Power Field Sequential Color OCB LCD

Here, the application of the high-speed response that is a key feature of the OCB mode will be described as an example. Fast response results in improved video display performance, but furthermore it is a key device that can achieve ultralow-power consumption of the LCD. One of those devices is the field sequential color LCD.

A serious problem for LCDs in general is their very low utilization efficiency of light in a few percent. One of the reasons for this is the color filter. To achieve a color display, color needs to be made by independently mixing the three primary colors, red, green, and blue. The three primary color filters are fabricated in a planar substrate. This means that in order to obtain a colored light, unwanted components

Fig. 6.19 Fifteen inch
liquid crystal display
prototype of field sequential
color OCB

from the white backlight need to be absorbed, which translates in a loss of light in
the color filter. Thus, in the field sequential color system, the backlight for each of
the three colors is blinking sequentially by a high-speed driving. With this tech-
nique, color filters that account for two thirds of light absorption become
unnecessary.

The flame of this method is composed of three fields with three primary colors
RGB linked sequentially. Moreover, since it uses neither sub-pixels nor color
filters, the transmittance is several times higher and the resolution is increased
threefold [77]. Figure 6.19 shows a 15 in. panel that with improved clarity of video
images, light efficiency, and color reproducibility [69, 78–82]. The subfield fre-
quency in this case was set to 180 Hz or 360 Hz. The pixel shape is different from
displays using color filters, and the square pixels display full color, using amor-
phous silicon (a-Si) in the channel of the TFT. Polycrystalline or single crystal
silicon has some advantages for the required high-speed operation of the field
sequential method, but we considered the possibility of a-Si because of its low
cost and the simplicity of the fabrication process. The display shows the excellent
characteristics of sharp video images with high contrast, high resolution, high
definition, and high color purity and thus has all the features of a high-quality
display. Additionally, because it works without color filters which absorb about 2/3
of the backlight, this LC panel reduces power consumption. In addition, because of
the rapidly flashing LED backlight by this method, a clear video is displayed
without blur.

6.3.7 Conclusion

The history of the development of LC display is a repetition of breakthroughs to
overcome the walls of technology. A fast response has been the weak point of LC
displays from the very beginning. The OCB mode achieves faster switching by the

effective use of the flow effect based on the precise characterization of the response time of the LC element. In addition, this type of display mode uses the anisotropy of birefringence, and one achieves a wide viewing angle by optimizing the angle compensation effect of the optical compensation film. The ultralow-power consumption and high definition has led to the features of a high-value-added display.

6.4 Thermo-optic and Electro-thermo-optic Effects of Liquid Crystals and Their Applications to Display

Akio Sasaki

6.4.1 Introduction: Why Are These Effects Interested?

In a liquid crystal display, the change in the light transmission by applying an electric field has been studied in detail. Why it was decided to investigate light transmission variations by applying heat under these circumstances should be noted in their historic context.

Heilmeier et al. [83] at Princeton RCA Laboratories announced the possibility of realizing a flat-panel display by applying an electric field to a liquid crystal in 1968. The research and development of semiconductor materials at that time focused on the search for new materials other than single-crystalline silicon (Si). GaAs and amorphous Si are two representative examples that have been studied, and the application development was intensively interested. A heating thin film of Si becomes a single-crystalline state after gradual cooling, but returns to an amorphous state after rapid cooling or quenching. Thus this material has been proposed for the use of a memory storage device because of the two different atomic arrangements of Si. At present, the material other than Si has been put into practical use in optical disks (compact disk, digital versatile disk, etc.).

It was under the above situation that the liquid crystal (LC) appeared on the stage. The application of an electric field causes the change in the molecular arrangement, which leads to the attention of researchers to use this to control the change in the light transmission. However, in our laboratory, we were interested to see how the reaction of a liquid crystal upon a temperature change would compare to amorphous Si. We immediately started the investigation of the thermo-optic effect of LCs. Our results and their applications to displays are a part of the "Heritage of Technology Achievement" of LCs in Japan. We measured those optic effects of nematic, nematic/cholesteric mixtures, smectic, and smectic/cholesteric mixtures.

6.4.2   Thermo-optic Effect
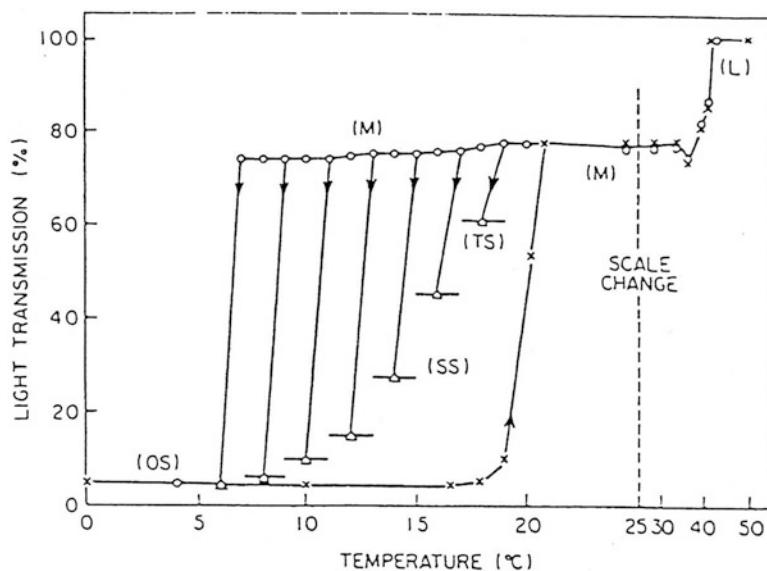
A temperature change in a liquid crystal cell causes changes in the light transmission. The LC cells used in the experiments are typically several tens of µm thickness and have an area of a few square centimeters.

6.4.2.1   Nematic Liquid Crystal

4-Methoxy-4/-n-butyl-benzylideneaniline (MBBA) was used as the LC material. The intermediate phase (liquid crystal phase) of MBBA ranged from 21 to 48 °C. At first, the cell is fully filled with the LC of the opaque solid state, and then, after irradiating a part of the cell with a laser beam, its temperature increases partially, as shown in Fig. 6.20 [84, 85]. At that time, the material goes from the opaque solid state through the intermediate phase to the liquid phase. After the laser is switched off, the sample cools down and goes through the intermediate phase to the supercooled intermediate phase. The supercooled intermediate phase is transparent. However, since the periphery of the irradiated portion remains the opaque solid state, a transparent supercooled image is influenced by the opaque solid state. Since it is a supercooled state, it would eventually return to the original opaque solid state. As the material temperature is lower, the irradiated portion is returned to the lower transparent state. When the material temperature is higher, the transparency can be increased by mixing more with a transparent intermediate state, as shown by the triangular mark in Fig. 6.20. Furthermore, when heating the whole LC cell, a stable transparent supercooled state can be obtained.
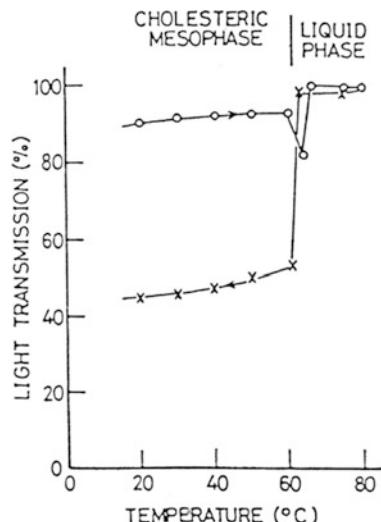
6.4.2.2   Nematic–Cholesteric Liquid Crystal Mixture

Figure 6.21 [86] shows the thermo-optic properties of the LC mixture containing MBBA, EBBA (4-ethoxy-4/-n-butyl-benzylideneaniline), and CN (cholesteryl-nonanoate) in the weight ratio of 45:45:10. The nematic phase of EBBA is between 37 and 80 °C, while the temperature range of the cholesteric phase of CN is 78–98 °C. After heating the whole cell, the mixture becomes a transparent LC phase, which turns turbid upon cooling. The temperature was changed with the rate of a thermal equilibrium. Upon cooling, the LC texture becomes the focal conic [86]. On the other hand, if the temperature change is caused by a laser beam to only a part of the LC cell, a rapid temperature drop occurs after the laser is switched off. The LC molecules result in heterogeneous and irregular arrangements which cause a low light transmission. The thermo-optic property is same as the case of thermal change in the whole cell.
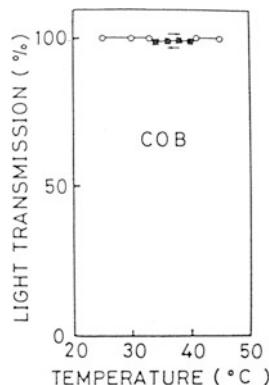
Fig. 6.20 The thermo-optic effect of MBBA. The temperature range for the nematic (liquid crystal) phase is 21–48 °C. The light transmission variations are shown for the temperature change of a part of the liquid crystal (LC) cell. The temperature is changed by the laser beam irradiation. The (SS) and (TS) do not occur to the cell for the temperature change of a whole area [84, 85]. As for the transmission reference, the transmission through a cell in an isotropic phase is taken as 100 %. This reference is applied for results hereafter. *OS* opaque solid state, *M* meso (nematic)-phase, *SS* semitransparent solid state, *I* isotropic (liquid) phase, *TS* transparent solid state

Fig. 6.21 The thermo-optic effect of nematic–cholesteric LC mixture: MBBA:EBBA: CN = 45:45:10 in weight ratio [86]. On cooling the cell, the LC texture shows the focal conic and the transmission becomes opaque. The transmission characteristic is same for the temperature change of either a part of or a whole area of the cell

Fig. 6.22 The thermo-optic
effect of smectic liquid
crystal COB. The
transmission change does
not occur by the
temperature change.
However, it decreases when
the temperature is changed
to a part of the cell by the
laser beam irradiation.
Then, the irradiated portion
becomes the light scattering
center

6.4.2.3 Smectic Liquid Crystal
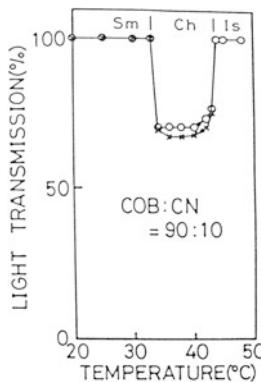
Cyano-octyl-4-4/-biphenyl (COB) was used as a liquid crystal material. During the
temperature rise, as well as while lowering the temperature, there was no change in
light transmission even when the sample passed through the smectic $\leftrightarrows$ nematic $\leftrightarrows$
liquid phases, as can be seen in Fig. 6.22 [87]. However, when a part of the sample is
heated by a laser beam, the center of the irradiated portion transforms into the
disordered liquid phase, surrounded by a bent nematic phase. The central portion
shows a honeycomb structure upon cooling. The light scattering of this structure
yields a black spot. By using this effect, a laser addressed large-scale display can be
demonstrated [88].

6.4.2.4 Smectic–Cholesteric LC Mixture

The temperature dependence of the light transmission of a mixture of COB and
CN in the weight ratio of 90:10 is shown in Fig. 6.23 [87]. The addition of the
cholesteric liquid crystal CN leads to the smectic $\leftrightarrows$ cholesteric $\leftrightarrows$ liquid phase
change. The cholesteric phase shows a focal conic texture, and the light trans-
mission is decreased. The temperature is changed with a laser beam, and then the
smectic phase shows the honeycomb and the focal conic textures that remain as a
light scattering center. By using this effect, static figure can be displayed. With
regard to the texture change, see [86]. The texture change upon rapid cooling has
also been reported [89].

6.4.3 Electro-thermo-optic Effect

Various changes occur in the light transmission of a liquid crystal cell by changing
the temperature and simultaneously by applying an electric field. In general,
dynamic scattering yields when applying a low-frequency electric field to a nematic
LC. In a cholesteric LC, a focal conic texture yields light scattering centers and then

Fig. 6.23 The thermo-optic effect of smectic–cholesteric LC mixture. The transmission variations are caused by mixing of cholesteric LC. By the laser beam irradiation on to a portion of the cell, the light scattering is observed in the smectic phase, and it remains in the honeycomb + focal conic texture. It can be applied to the display of static figures. *Sm* smectic phase, *Ch* cholesteric phase, *Is* isotropic phase
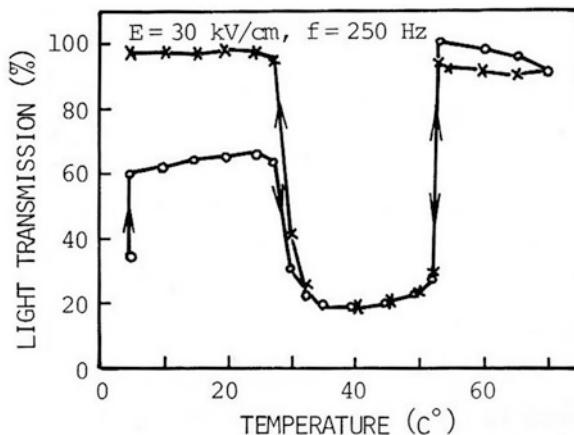
the light transmission decreases. On the other hand, when applying a high-frequency electric field to the LC cell, these light scattering centers are erased, and the cell becomes transparent. In these experiments, in order to obtain an enhanced light transmission change, a small amount of a cholesteric LC was added to either a nematic or a smectic LC.

### 6.4.3.1 Nematic–Cholesteric Liquid Crystal Mixture
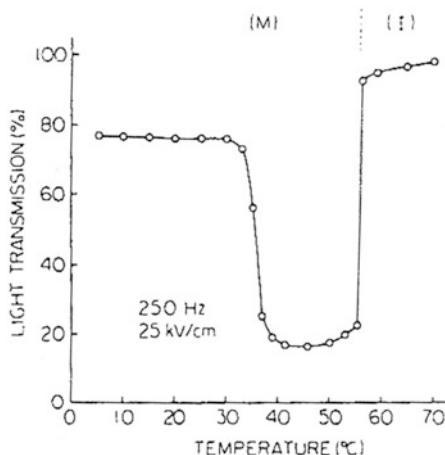
As in the case of thermo-optic effect (Sect. 6.4.2), the LC material was a mixture of MBBA, EBBA, and CN (45:45:10). The light transmission change with the temperature under the electric field of 30 kV and 250 Hz is shown in Fig. 6.24 [90]. The marks ○ and × indicate the initial temperature up and down processes, respectively. Then, both processes of the temperature up and down are shown by the mark ×. The light transmission decrease here is due to the focal conic texture of the cholesteric phase. The temperature range of a low light transmission becomes narrower with a higher frequency of the applied field. In the cooling process after the liquid and cholesteric phases, the light scattering center (opaque state) disappears by the electric field application and becomes transparent. This characteristic of the opaque ⇆ transparent states under the electric field application can be applied to display a dynamic figure.

6.4.3.2 Smectic–Cholesteric Liquid Crystal Mixture

The LC material used for the measurement is the mixture of COB and CN (90:10) which is same as used for the thermo-optic effect. The cell is 25 μm in thickness and 20 × 20 mm in area. The result is shown in Fig. 6.25 [91]. When compared with the

Fig. 6.24 The electro-thermo-optic effect of nematic–cholesteric LC mixture: MBBA:EBBA: CN = 45:45:10. The material here is same with the thermo-optic effect [90]. The transmission variations are enhanced by the electric field application. The scattering centers in the nematic phase are turned to a clear state with the electric field application and then the irradiated portion becomes clear. Thus, the dynamic figures can be displayed

Fig. 6.25 The electro-thermo-optic effect of smectic–cholesteric mixture: COB:CN = 90:10. The light transmission is greatly decreased by the electric field application [91]. The light scattering centers are created in the smectic phase by the irradiation on to a part of the LC cell, and they are erased by the electric field application and become clear. This characteristic can be applied to a dynamic display. *M* mesophase, *I* isotropic phase

results of the thermo-optic effect in Fig. 6.23, the decrease in the light transmission becomes greater by applying an electric field. Thus, such a characteristic can be used to display dynamic figures in the same way as that based on the results shown in Fig. 6.24.

6.4.4 Applications to Display

It was revealed by the thermo-optic and electro-thermo-optic effects that the light transmission of an LC cell can be easily changed by temperature variations with or without an electric field application. Therefore, a new application that projected figures drawn by a laser beam onto an LC cell was conceived. In this case, it is necessary to consider that the light transmittance change is different for two types of thermal treatments: changing the temperature of the whole LC cell in the thermal equilibrium state and irradiating a part of the LC cell by a laser beam.
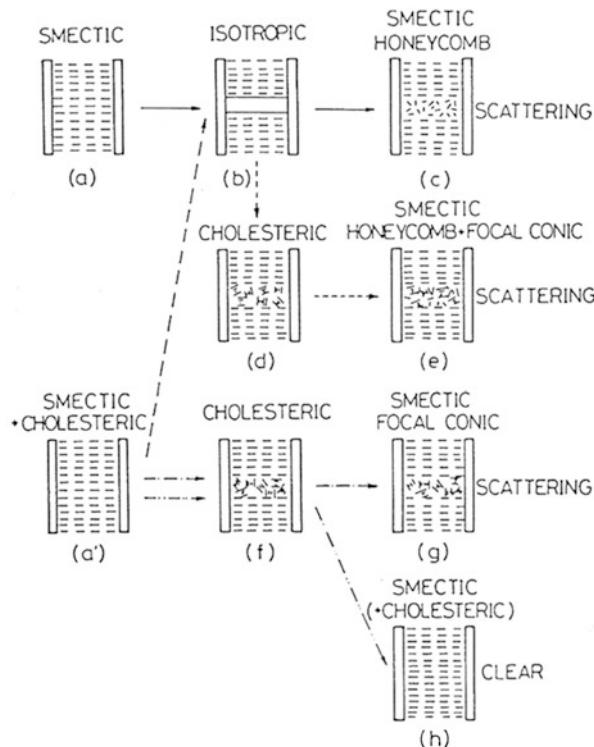
6.4.4.1 Principles and Results

The principle behind the display applications is shown in Fig. 6.26 [92]. Basically, the principles for both of the nematic—cholesteric mixtures and the smectic—cholesteric mixtures are the same. The processes shown in the figure are the following:

(a) → (b) → (c): the thermo-optic effect as shown in Figs. 6.20 and 6.22
(a) → (b) → (d) → (e): the thermo-optic effect as shown in Figs. 6.21 and 6.22
(a) → (f) → (g): same as above, but the temperature increase does not reach the liquid phase
(a) → (f) → (h): the electro-thermo-optic effect as shown in Figs. 6.24 and 6.25 or those which the temperature is increased to reach the liquid phase

These devices are called liquid crystal light valves (LCLVs), and projection LC display systems used in the LCLV are shown in Fig. 6.27 [93]. In drawing figures, the option of YAG: Nd lasers, GaAs semiconductor lasers, or Ar or He–Ne gas lasers can be used. As a projection light source, the option of halogen, xenon, mercury arc lamps, or the like can be used. The size of the screen can be as large as 2.5 m × 2.5 m.

The actual projection in the experiment is shown in Fig. 6.28 [94]. Here, a static diamond figure is drawn by using the thermo-optic effect. With the switched-on electric field, a dynamic figure can be displayed with holding the static figure. The 90:10 mixture of COB and CN was used, and the surfactant of cetyltrimethylammonium bromide (CTAB) was added for a homeotropic arrangement. The cell thickness was 12 μm, and the electric current flows through transparent conductive thin films that were coated onto glass plates. The cell temperature was maintained at
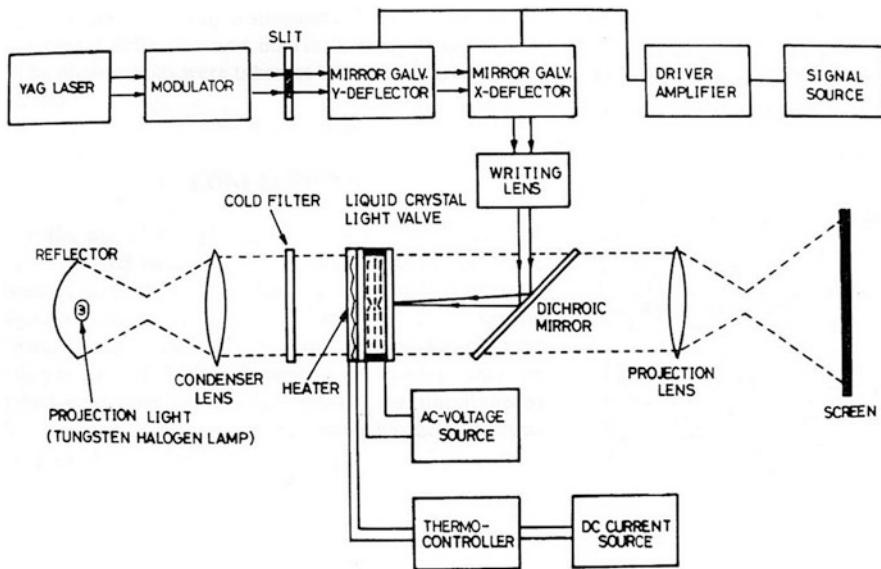
Fig. 6.26 The operation principles of laser addressed display used the thermo-optic and the electro-thermo-optic effects [92]. In the figure, the operation by a nematic LC can be expected same by a smectic LC. The LC cell used as a light valve can be applied to a large-scale projection display
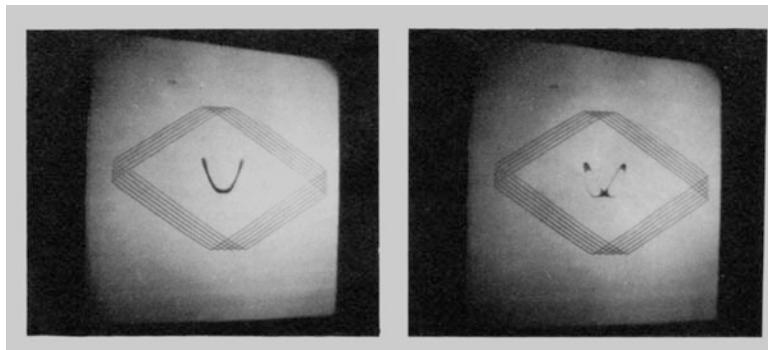
just below the transition temperature to the cholesteric phase, which improves the writing speed [93]. A dichroic glass was suggested for the effective absorption of the laser light.

6.4.4.2 Other Developments

The effect of dye mixing into the LC material has been reported. (i) It is possible to make a colored display by adding dyes [95]. (ii) Dyes improve also the writing speed by absorbing effectively the energy of the laser beam [96]. (iii) With dye addition, the resolution of the display can be improved by suppressing heat diffusion to the surroundings, since the light absorption is concentrated to the dyes added [97]. Thus, by incorporating dyes, new features and various improved characteristics can be expected. By laser beam addressing, a high-resolution figure with a
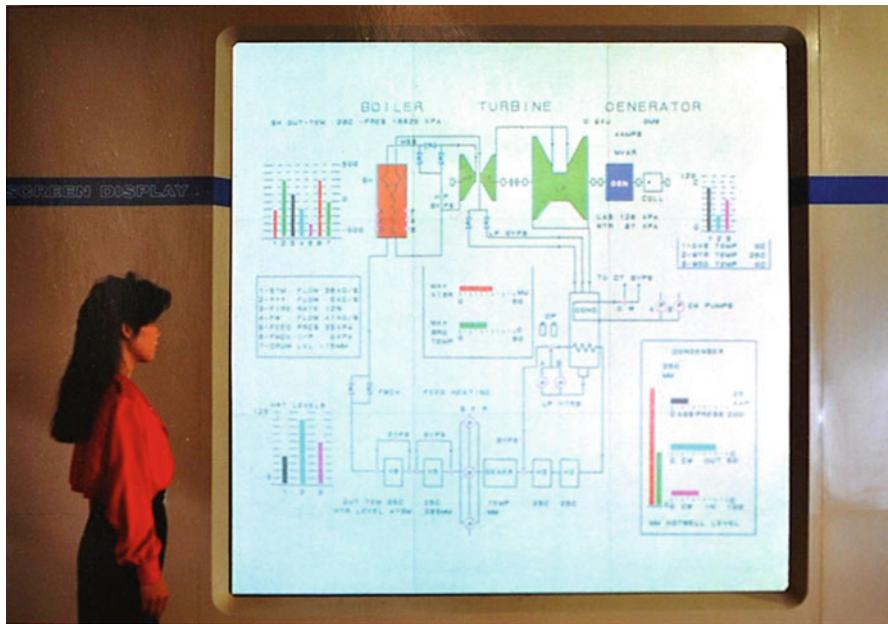
Fig. 6.27 The projection display system [93]. The LC cell is used as a light valve and figures are projected on to a screen

Fig. 6.28 The simultaneous display of static and dynamic figures by the thermo-optic and the electro-thermo-optic effects [94]. The liquid crystal used is COB:CN = 90:10. The static figures are displayed by the light scattering centers, and, holding them, the dynamic figures are displayed with the electric field application. *Two photographs* show dynamic display, as the *right photograph* was taken at 1/4 s after the *left photograph*

smaller pixel can be written into a liquid crystal cell and can be projected onto a large-scale screen.

The research and development by domestic and foreign companies led to various applications of such displays for integrated circuit designs, power control
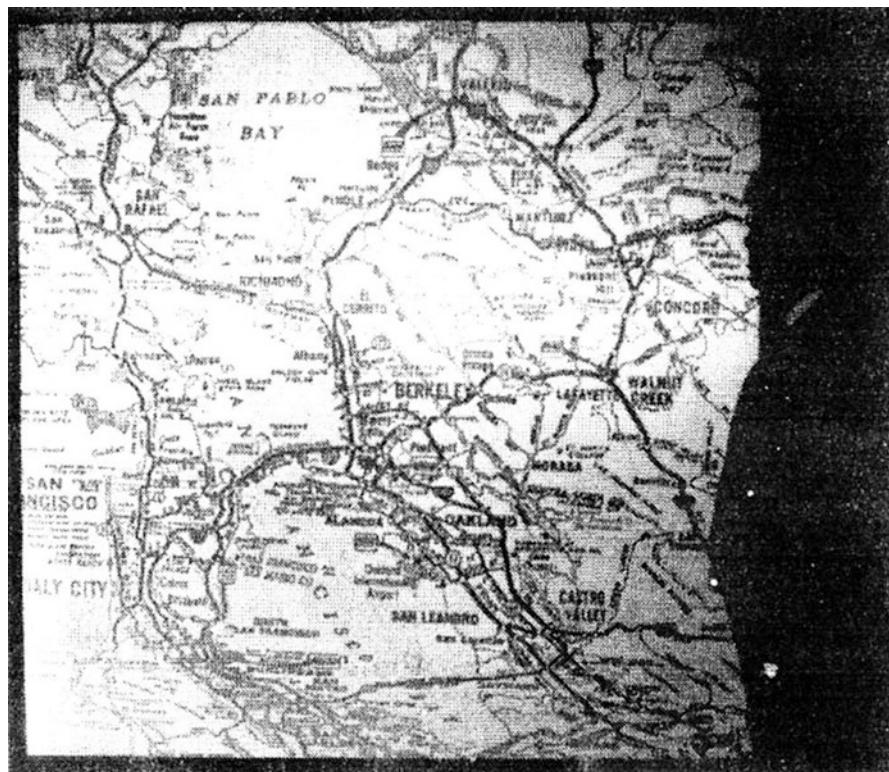
Fig. 6.29 The example of the large-scale display by a laser addressed projection system. The figure shows the power control system board (Courtesy of Hitachi)

boards, newspaper editions, and the projection of large maps. In Japan, Hitachi, NEC, and Sony led these efforts, and in particular, Hitachi has demonstrated the display of the power control panel, and NEC demonstrated the large map display as shown in Figs. 6.29 and 6.30, respectively. More examples of large displays that use the thermo-optic effect or the electro-thermo-optic effect are listed in literature [87].

6.4.5   Summary

Initially, I started with the characterization of thin-film liquid crystals based on the idea that they share some properties that may correspond to amorphous silicon thin films. The change in the light transmission due to thermally induced changes of the liquid crystal material (thermo-optic effect), and changes under the influence of an electric field application (electro-thermo-optic effect), has been revealed. Compared to thin silicon films, liquid crystal cells are more restricted since they need to be sandwiched between two glass plates. However, since the light transmission change can be easily obtained, these liquid crystal cells are possibly used as light valves, which open the road towards large projection displays. Both of

Fig. 6.30 The example of the large-scale display by a laser addressed projection system. The figure shows the map near San Francisco Bay (Courtesy of NEC)

domestic and foreign companies have developed practical applications. Companies in Japan focused on large display power systems, navigation maps, or the like. Large display of this kind can be widely used, but depending on the purpose, the scanning speed needs to be improved to display dynamic figures, and full-color video display needs to be realized.

References

1. Y. Bijörnstahl, Ann. Phys. (Leipzig) **56**, 161 (1918) (in German)
2. W. Zwetkoff, C. R. Acad. Sci. USSR **4**, 131 (1935) (in French)
3. M. Schadt, Jpn. J. Appl. Phys. **48**, 1 (2009)
4. M. Schadt, Naturwissenschaftliche Rundschau **741**, 117 (2010)
5. M. Schadt, J. Eur. Acad. Sci. **1**, 1 (2011)
6. R. Williams, J. Chem. Phys. **39**, 384 (1963)
7. G.H. Heilmeier, L.A. Zanoni, Appl. Phys. Lett. **13**, 91 (1968)

8. W. Helfrich, J. Chem. Phys. **51**, 4092 (1969)
9. E.F. Carr, *Ordered Fluids and Liquid Crystals* (American Chemical Society, Washington D. C, 1967), p. 76
10. M. Schadt, D.F. Williams, J. Chem. Phys. **50**, 4364 (1969)
11. D.F. Williams, M. Schadt, Proc. IEEE **58**, 476 (1970)
12. C. Mauguin, Bull. Soc. Fr. Minéral. **34**, 71 (1911) (in French)
13. A. Boller, H.P. Scherrer, M. Schadt, P. Wild, Proc. IEEE **60**, 1002 (1972)
14. M. Schadt, W. Helfrich, Appl. Phys. Lett. **18**, 127 (1971); Swiss Patent 532,261 (4 Dec 1970)
15. F.M. Leslie, Mol. Cryst. Liq. Cryst. **12**, 57 (1970)
16. D.W. Berreman, J. Opt. Soc. Amer. **63**, 1374 (1973)
17. C.J. Gerritsma, W.H. de Jeu, P. van Zanten, Phys. Lett. **36A**, 389 (1971)
18. J. Fergason, U.S. Patent 3,918,796 (22 April 1971)
19. G. H. Buntz, *Information der Internationalen*, vol 118 (Treuhand AG, Basel, 2005), p. 1 (in German). cf also the English translation authorized by G. Buntz [http://www.lcd-experts.net]
20. D. Schmidt, M. Schadt, W. Helfrich, Z. Naturforsch. A **27**, 277 (1972)
21. M. Schadt, W. Helfrich, Mol. Cryst. Liq. Cryst. **17**, 355 (1972)
22. M. Schadt, J. Chem. Phys. **67**, 210 (1977)
23. Z. Ge, L. Rao, S. Gauza, S.T. Wu, J. Display Tech. **5**, 250 (2009)
24. P.R. Gerber, Mol. Cryst. Liq. Cryst. **116**, 197 (1985)
25. H. Kikuchi, M. Yokota, Y. Hisakado, H. Yang, Nat. Mater. **1**, 64 (2002)
26. M. Schadt, Biophys. Acta. **323**, 351 (1973)
27. M. Schadt, G. Häusler, J. Membrane Biol. **18**, 277 (1974)
28. H. Kawakami et al., Jpn. Inst. Electron. Inf. Eng. **73** (1974)
29. P.M. Alt, P. Pleshko, IEEE Trans. ED **21**, 146 (1974)
30. M. Schadt, Annu. Rev. Mater. Sci. **27**, 305 (1997)
31. T.J. Scheffer, J. Nehring, Appl. Phys. Lett. **45**, 1021 (1984)
32. C. W. Waters, V. Brimmel, E. P. Raynes, in *Proceedings of the SID84*, 261 (1984)
33. M. Schadt, F. Leenhouts, Appl. Phys. Lett. **50**, 236 (1987)
34. M. Schadt, Mol. Cryst. Liq. Cryst. **89**, 77 (1982)
35. R. Kiefer et al., in *SID Proceedings of the IDRC92*, 547 (1992)
36. M. Ohe, et al., in *Proceedings of the SID Japan Display'95*, 577 (1995)
37. P. J. Bos, K. R. Koehler, in *SID Proceedings of the Japan Display'83*, 478 (1983)
38. T. Miyashita, C-L. Kuo, M. Suzuki, T. Uchida, in *SID Proceedings of the International Symposium Digest of Technical Papers*, 797 (1995)
39. S. H. Lee, S. L. Lee, H. Y. Kim, T. Y. Eom, in *SID Proceedings of the International Symposium Digest of Technical Papers*, 202 (1999)
40. N.A. Clark, S.T. Lagerwall, Appl. Phys. Lett. **36**, 899 (1980)
41. L.A. Beresnev, V.G. Chigrinov, D.I. Durgachev, E.P. Posiadaev, J. Fünfschilling, M. Schadt, Liq. Cryst. **5**, 217 (1989)
42. A.G. Verhulst, G. Cnossen, J. Fünfschilling, M. Schadt, in *SID Proceedings of the IDRC94*, 377 (1994)
43. T. F. Brody, F. C. Luo, D. H. Davies, E. W. Greeneich, in *SID Proceedings of the SID74*, 166 (1974)
44. M. Schiekel, K. Fahrenschon, Appl. Phys. Lett. **19**, 391 (1971)
45. F. Kahn, Appl. Phys. Lett. **20**, 199 (1972)
46. M.F. Shiekel et al., Appl. Phys. Lett. **19**, 391 (1971)
47. Kinoshita et al., Electro-optical characteristics of VAN type LCD. Dig. Liq. Cryst. Conf. **2B107**, 72 (1988)
48. K. H. Yang et al., IDRC91 Digest, (1991) pp. 68–72
49. T. Kamada et al., Dig. Jpn. Display **92**, 886 (1992)
50. A. Takeda et al., SID 98 Digest, 1077 (1998)
51. Y. Tanaka et al., SID 99 Digest, 206 (1999)
52. K. Ohmuro et al., SID 97 Digest, 845 (1997)

53. J. Chen et al., SID 98 Digest **212**, 315 (1998)
54. Y. Yoshida et al., Digest of Asia Display/IMID'04, (2004), pp. 198–201
55. Ueda et al., Japanese opened patent 2006-133577 (2006)
56. Shimoshikiryo, Japanese opened patent 2005-99746 (2005)
57. T. Uchida, in *Proceedings of 12th International Display Workshops/Asia Display*, LCT2-1, (2005), p. 33
58. P. J. Bos, P. A. Johnson Jr., K. Rickey Koehler/Beran, SID Symposium Digest, (1983), p. 30
59. P. A. Johnson, R. Vante, P. J. Bos, SID Symposium Digest, (1983), p. 28
60. P. J. Bos, J. A. Rahman, SID Symposium Digest, (1993), p. 273
61. Y. Yamaguchi, T. Miyashita, T. Uchida, SID Symposium Digest, (1993), p. 277
62. T. Miyashita, P. Vetter, M. Suzuki, Y. Yamaguchi, T. Uchida, Conference Record of Eurodisplay, (1993), p.149; J. SID, **3**, 29 (1995)
63. C.-L. Kuo, T. Miyashita, M. Suzuki, T. Uchida, SID Symposium Digest, (1994), p. 927
64. C.-L. Kuo, T. Miyashita, M. Suzuki, T. Uchida, Jpn. J. Appl. Phys. **34**, L1362 (1995)
65. C.-L. Kuo, T. Miyashita, M. Suzuki, T. Uchida, Appl. Phys. Lett. **68**, 1461 (1996)
66. T. Miyashita, T. Uchida, IEICE Trans. Electron. **E79E-C**, 1076 (1996)
67. S. Onda, T. Miyashita, T. Uchida, Mol. Cryst. Liq. Cryst. **331**, 383 (1999)
68. T. Uchida, in *Proceedings of IDMC*, We-05-01. (2003)
69. K. Wako, H. Yaginuma, T. Kishimoto, T. Ishinabe, T. Miyashita, T. Uchida, SID Symp. Digest **P-179L**, 666 (2005)
70. T. Ishinabe, T. Miyashita, T. Uchida, SID Symposium Digest (2000), p. 1094
71. H. Mori, P.J. Bos, Jpn. Appl. Phys. **38**, 2838 (1999)
72. N. Koma, T. Miyashita, T. Uchida, K. Yoneda, SID Symposium Digest (1999), p. 28
73. N. Nagae, T. Miyashita, T. Uchida, Y. Yamada, Y. Ishii, IDRC (2000), p. 26
74. N. Nagae, Y. Yamada, Y.Ishii, T. Miyashita, T. Uchida, in *Proceedings of the Asia Display/ IDW* (2001), p. 363
75. I. Inoue, T. Miyashita, T. Uchida, Y. Yamada, Y. Ishii, Conference Record of Eurodisplay (2002), p. 179; J. SID, **11/3**, 571 (2003)
76. K. Kuboki, T. Miyashita, T. Ishinabe, T. Uchida, Record of IDRC (2003), p. 80
77. T. Uchida, K. Saitoh, T. Miyashita, M. Suzuki, Conference Record of IDRC (1997), p. 37
78. K. Sekiya, K. Wako, T. Ishinabe, T. Miyashita, T. Uchida, in *Proceedings of IDW* (2003), p. 1731
79. T. Ishinabe, T. Miyashita, T. Uchida, K. Wako, T. Kishimoto, K. Sekiya, SID Symposium Digest (2004), LP-10
80. K. Sekiya, K. Wako, S. Nakano, T. Ishinabe, T. Miyashita, T. Uchida, in *Proceedings of the IDW*, No.LCT5-5L (2004), p. 97
81. K. Wako, H. Yaginuma, T. Kishimoto, T. Ishinabe, T. Miyashita, T. Uchida, SID Symposium Digest, No.P-179L (2005), p. 666
82. H. Seki, K. Wako, K. Sekiya, T. Ishinabe, T. Miyashita, T. Uchida, in *Proceedings of the SPIE* (2006), No.6030
83. G.H. Heilmeier, L.A. Zanoni, L.A. Barton, Proc. IEEE **56**, 1162 (1968)
84. A. Sasaki, K. Kurahashi, T. Takagi, *Conference Record of the 1972 I.E. Conference on Display Devices* (IEEE New York, 1972)
85. A. Sasaki, K. Kurahahi, T. Takagi, J. Appl. Phys. **45**, 4356 (1974)
86. A. Sasaki, M. Inoda, T. Ishibashi, Mol. Cryt. Liq. Cryt. **65**, 39 (1981)
87. A. Sasaki, M. Inoda, T. Ishibashi, Mol. Crst. Liq. Cryst. **74**, 149 (1981)
88. H. Melchior, F.J. Kahn, D. Maydan, D.B. Fraser, Appl. Phys. Lett. **21**, 392 (1972)
89. N. Nawa, Jpn. J. Appl. **29**, 2465 (1990)
90. A. Sasaki, T. Morioka, T. Ishibashi, T. Takagi, in *Proceedings of the 7th Conference on Solid State Devices, Tokyo 1975*; Suppl. Jpn. J. Appl. Phys. Suppl., **15** 121 (1976)
91. A. Sasaki, T. Morioka, T. Takagi, T. Ishibashi, IEEE Trans. Electron Devices (Sept 1975), pp. 805–806
92. A. Sasaki, Mol. Cryt. Liq. Cryst. **139**, 103 (1986)

93. A. Sasaki, T. Ishibashi, M. Inoda, K. Kawahata, Write-in speed of laser beam address in liquid-crystal large-scale display. Trans. Inst. Electron. Comm. Eng. **63-C**, 368 (1980) (in Japanese)
94. A.Sasaki, M.Inoda, T.Ishibshi, in *Proceedings of the Society of Information Display*, 21 (1980)
95. C. Tani, T. Urabe, Appl. Phys. Lett. **32**, 275 (1978)
96. A. Sasaki, N. Hayashi, T. Ishibashi, Proc. Soci. Infom. Display **25**, 95 (1984)
97. T. Urabe, K. Arai, A. Ohkoshi, J. Appl. Phys. **54**, 1552 (1983)

Chapter 7
Latest Liquid Crystal Technology

Koji Okano, Jun Yamamoto, Hidefumi Yoshida, Kenji Okamoto, Martin Schadt, and Masanori Matsuda

7.1 Nematodynamics as a Unified Hydrodynamic Theory: Theory That Provides Physical Basis of Liquid Crystal Display Technology

Koji Okano and Jun Yamamoto

7.1.1 Physical Basis of Liquid Crystal Display Devices

Among the characteristic physical properties of liquid crystals, what are of critical importance to display devices (LCDs) are those of macroscopic spatiotemporal scale; there, the theories of liquid crystals as continuous media play essential roles. The basis of static continuum mechanics of nematic liquid crystals was established by

K. Okano
Tokyo University, Tokyo, Japan

J. Yamamoto
Kyoto University, Kyoto, Japan
e-mail: junyama@scphys.kyoto-u.ac.jp

H. Yoshida • K. Okamoto
Sharp Corporation, Nara, Japan
e-mail: hidefumi.yoshida@sharp.co.jp; LX13010097@partner.sharp.co.jp

M. Schadt
MS High-Tech Consulting, Seltisberg, Switzerland
e-mail: martin.schadt@bluewin.ch

M. Matsuda
Fine Chemicals Technology Section, Fine Chemicals Product Department,
Sekisui Chemical Co., Ltd, Osaka, Japan
e-mail: matsuda015@sekisui.com

Oseen [1] and Frank [2] far before the development of LCD technology. The dynamic continuum theory of nematics, which is frequently called the nematodynamics, was developed by Ericksen [3] and Leslie [4] (hereafter referred to as E–L theory) based on the classical mechanics just in time for the upsurge of LCD technology. In conjunction with the electrodynamics of continuous media, the static and dynamic continuum mechanics of Oseen–Frank and E–L theory provided theoretical tools to analyze quantitatively key phenomena, e.g., Freedericksz transition of various configurations and associated optical switching characteristics. For the details of E–L theory [5–7] and its development [9, 10], please refer to the articles cited.

However, from the point of view of modern physics, in particular statistical physics, the E–L theory based upon classical mechanics is not fully satisfactory:

1. The concepts of symmetries and continuous broken symmetries are not adequately taken into account. As a result, the fundamental reason why director n, instead of scalar order parameter, plays the leading role in nematodynamics is not definitely demonstrated.
2. It does not rely on the thermodynamics of irreversible processes and as a consequence reversible and irreversible variables have not been clearly separated. The authors of classical continuum theory seem still quite reluctant to accept Onsager reciprocal relations [8].

Motivated by these criticisms, a unified hydrodynamics theory (hereafter referred to as UHT) of condensed matter [11–13] has been developed based on the theoretical framework of fundamental physical concept which is succinctly called "the grand synthesis" by Lubensky [14]. From its nature, the UHT is applicable to a wide range of "hydrodynamics" including various phases of liquid crystals, spin systems, even crystals, and so on. In the following, we briefly review the UHT of nematodynamics.

7.1.2 Unified Hydrodynamics

In a macroscopic condensed matter, most disturbances or excitations from a thermodynamic equilibrium state decay rapidly to equilibrium state in microscopic time, say 10^{-10} to 10^{-14} s. in ordinary liquids. There exist, however, a few variables that relax very slowly as the wavelength of excitations becomes long. We take the excitations of the form $\exp(i\omega t - i\mathbf{q} \cdot \mathbf{r})$, where $\mathbf{q}$ is a wave vector, $\mathbf{r}$ the position vector, and ω the angular frequency.

When the longitudinal sound wave is excited in ordinary liquid, we have the dispersion relation of the form from classical hydrodynamics:

$$\omega = \pm cq + i\frac{1}{2}\Gamma q^2, \qquad (7.1)$$

where c is the speed of sound and Γ is the attenuation constant. Equation (7.1) shows that as the wavelength becomes long (q becomes small) the decay time becomes long, or

$$\omega(q \to 0) \to 0. \tag{7.2}$$

For a thermal excitation, from the Fourier's equation, we have the relation

$$\omega = -iD_{\mathrm{T}}q^2, \tag{7.3}$$

where D_{T} is the thermal diffusivity, which shows that the thermal relaxation is also a slow process that satisfies (7.2). In condensed matter physics, the unified theoretical framework that describes the dynamics of slow long-lived modes characterized by the property (7.2) is called UHT, irrespective of material flow. The pertinent variables associated with the slow long-lived modes are called hydrodynamic variables or slow variables.

7.1.3   Hydrodynamic Variables

Hydrodynamic variables are singled out by invoking the following fundamental physical principles.

(a) The density of local physical quantities that obey conservation laws:
   Mass density $\rho(\mathbf{r}, t)$, momentum density $\mathbf{g}(\mathbf{r}, t)$ and energy density $\varepsilon(\mathbf{r}, t)$. For small wave number excitations, restoring forces are very weak due to the pertinent conservation laws. Thus, abovementioned variables satisfy (7.2), and they are hydrodynamic variables. By a local variable $f(\mathbf{r})$ we mean that $f(\mathbf{r})$ is unchanged when both $\mathbf{r}$ and all the microscopic particles within the physically infinitesimal region around $\mathbf{r}$ are translated by the same amount. The angular momentum density employed in E–L theory is discarded in UHT, since there is no "local" angular momentum density [11–13].
(b) The variables related to the spontaneously broken continuous symmetries:
   Nematic director $\mathbf{n}$ is typical of this category. The director breaks the continuous rotational symmetry of isotropy into lower symmetry $D_{\infty h}$. Homogeneous rotation of director does not change the energy of the system and there arises no restoring force. This fact is consistent with (7.2), and the director is a hydrodynamic variable. Slow modes associated with the variables of broken continuous symmetry are called Nambu–Goldstone modes.

7.1.4 Conservation Laws and Thermodynamics

7.1.4.1 Conservation Laws of Mass and Momentum

Conservation law of mass is just the equation of continuity:

$$\frac{\partial \rho}{\partial t} = -\nabla \cdot (\rho \mathbf{v}), \tag{7.4}$$

where ρ is the mass density and $\mathbf{v}$ the velocity vector. The mass flux density is the momentum density, $\mathbf{g} = \rho \mathbf{v}$.

Conservation law of momentum is embodied in the Euler's equation of motion:

$$\rho \left[\frac{\partial v_i}{\partial t} + v_j \nabla_j v_i \right] = \nabla_j \sigma_{ij}, \tag{7.5}$$

where σ_{ij} is the stress tensor, and in what follows, the spatial differential operator is denoted as ∇_i and the summation convention for repeated indices is used. Equation (7.5) can be expressed in the canonical form of the conservation law of momentum density $g_i = \rho v_i$:

$$\frac{\partial g_i}{\partial t} = -\nabla_j \Pi_{ij}, \tag{7.6}$$

where

$$\Pi_{ij} = \rho v_i v_j - \sigma_{ij}, \tag{7.7}$$

is the momentum flux density. The nonlinear term of momentum flux density can be neglected in the usual application to LCD; then the conservation law of momentum becomes

$$\frac{\partial g_i}{\partial t} = \nabla_j \sigma_{ij} \tag{7.8}$$

7.1.4.2 Thermodynamics and Conservation Law of Energy

Since temporal change of hydrodynamic variables is very slow compared to any microscopic time, at any instant on the hydrodynamic timescale we can assume that in each volume element the microscopic degrees of freedom have reached their thermodynamic equilibrium, and we can apply equilibrium thermodynamics there. Thus in the moving fluid, the (internal) energy density in the laboratory frame is given by

$$\varepsilon = \varepsilon_0 + \frac{1}{2\rho} g^2, \tag{7.9}$$

where ε_0 is the energy density in the rest frame, i.e., in the frame moving with the velocity v_i relative to the laboratory frame. For nematics there is the contribution from Frank's curvature elasticity $\varepsilon_F(\nabla_j n_i)$ and ε_0 are expressed as

$$\varepsilon_0 = u(\rho, s) + \varepsilon_F(\nabla_j n_i), \tag{7.10}$$

where $u(\rho, s)$ is the energy density in the uniformly oriented nematics, s being the entropy per unit mass. As is well known, ε_F is given by

$$\varepsilon_F = \frac{1}{2} K_1(\nabla \cdot \mathbf{n})^2 + \frac{1}{2} K_2(\mathbf{n} \cdot \nabla \times \mathbf{n})^2 + \frac{1}{2} K_3(\mathbf{n} \times \nabla \times \mathbf{n})^2, \tag{7.11}$$

where K_1, K_2, and K_3 are the Frank elastic constants. Equation (7.11) can be rewritten as

$$\varepsilon_F = \frac{1}{2} K_{ijkl} \nabla_j n_i \nabla_l n_k, \tag{7.12}$$

where

$$K_{ijkl} = K_1 \delta_{ij}^{\perp} \delta_{kl}^{\perp} + K_2 n_p \varepsilon_{pij} n_q \varepsilon_{qkl} + K_3 n_j n_l \delta_{ik}^{\perp}. \tag{7.13}$$

Here we used the projection operator $\delta_{ij}^{\perp} \equiv \delta_{ij} - n_i n_j$, and ε_{ijk} is the Levi–Civita symbol. In the nematodynamics the Frank constants K_i ($i = 1, 2, 3$) should be adiabatic ones; however, since ε_F is the homogeneous quadratic form of $\nabla_j n_i$ the adiabatic and isothermal constants are the same [12]. In this section, we shall consider the case where the external electric and magnetic fields are absent. By virtue of local equilibrium, we have the following thermodynamic equations in laboratory frame:

$$d\varepsilon = T d(\rho s) + \mu d\rho + v_i dg_i + \phi_{ij} d(\nabla_j n_i), \tag{7.14}$$

$$\rho \mu = p + \varepsilon_0 - T\rho s - \frac{1}{2\rho} g^2, \tag{7.15}$$

where μ is the chemical potential in the laboratory frame and p is the pressure. The variables ϕ_{ij} conjugate to $\nabla_j n_i$ are defined by

$$\phi_{ij} = \left(\frac{\partial \varepsilon}{\partial \nabla_j n_i} \right)_{s, \rho, g} = K_{ijkl} \nabla_l n_k. \tag{7.16}$$

The conservation law of energy is expressed as

$$\frac{\partial}{\partial t} \left(\varepsilon_0 + \frac{1}{2\rho} g^2 \right) = -\nabla_i Q_i, \tag{7.17}$$

where the vector $\boldsymbol{Q}$ is the energy flux density. Flux densities on the right-hand side of equations of conservation laws (7.4), (7.8), and (7.17) are split into reversible and irreversible parts: The former are related to the entropy conserving processes and the latter give rise to the entropy production. In UHT the reversible part of a flux is called the reactive one; the reactive and dissipative parts of the flux are denoted by superscripts R and D, respectively. Momentum density (mass flux density) (7.4) is essentially reactive and $g^{D} = 0$.

Reactive Dynamics of the Director

It is appropriate to discuss here the reversible dynamics of the director which is not explicitly demonstrated in E–L theory. The basic idea is that a deformation of the volume element of the nematic continuum automatically causes the change of director orientation: when the flow pattern $\nabla_k v_i$ is decomposed into a symmetric part A_{ik} and antisymmetric part Ω_{ik} as

$$A_{ik} = \frac{1}{2}(\nabla_i v_k + \nabla_k v_i), \quad \Omega_{ik} = \frac{1}{2}(\nabla_i v_k - \nabla_k v_i). \tag{7.18}$$

It is natural to consider that when external fields are absent the director will rotate together with the rigid body rotation of the volume element, which gives rise to angular velocity $\Omega_{ik} n_k$. In addition, a shape deformation of the volume element (whose rate is A_{ik}) also causes a change of orientation without any viscous process. Thus introducing a nondimensional parameter λ, we have

$$\left(\frac{\partial n_i}{\partial t}\right)^{R} = \lambda \delta_{il}^{\perp} n_k A_{kl} + \Omega_{ik} n_k. \tag{7.19}$$

For rodlike molecules, the value of the reactive parameter λ is expected to be close to $+1$, and it must be close to -1 for disk-like molecules. Introducing a tensor of reactive parameter λ_{ijk}, which depends only on $\mathbf{n}$, we have

$$\lambda_{ijk} = (\lambda - 1)\delta_{ij}^{\perp} n_k + (\lambda + 1)\delta_{ik}^{\perp} n_j. \tag{7.20}$$

Then, (7.19) is rewritten as

$$\left(\frac{\partial n_i}{\partial t}\right)^{R} = \frac{1}{2}\lambda_{ijk}\nabla_j v_k. \tag{7.21}$$

7.1.4.3 Entropy Production and Flux Densities

The rate of increase of total entropy is given by

$$\dot{S} = \int \frac{\partial}{\partial t}(\rho s)\mathrm{d}\mathbf{r}. \tag{7.22}$$

Substituting (7.14) we have

$$\dot{S} = \int \left\{ \frac{1}{T} \frac{\partial \varepsilon}{\partial t} - \frac{\mu}{T} \frac{\partial \rho}{\partial t} - \frac{v_i}{T} \frac{\partial g_i}{\partial t} - \frac{1}{T} \phi_{ij} \nabla_j \left(\frac{\partial n_i}{\partial t} \right) \right\} d\mathbf{r}. \qquad (7.23)$$

By recalling conservation laws (7.4), (7.8), and (7.17), the integrand of (7.23) is expressed by respective fluxes as

$$\dot{S} = \int \left\{ -\frac{1}{T} \nabla_i Q_i + \frac{\mu}{T} \nabla_j (\rho v_i) - \frac{v_i}{T} \nabla_j \sigma_{ij} - \frac{1}{T} \phi_{ij} \nabla_j \left(\frac{\partial n_i}{\partial t} \right) \right\} d\mathbf{r}. \qquad (7.24)$$

Integrating by parts, and separating a total divergence term including fluxes, which is removed by converting it to a surface integral and assuming the fluxes vanish at the boundary, we have

$$\dot{S} = -\int \left\{ \frac{1}{T^2} [Q_i - (\varepsilon + p)v_i] \nabla_i T - \frac{1}{T} [\sigma_{ij} + p\delta_{ij}] \nabla_j v_i \right.$$
$$\left. - \frac{1}{T} \left[\left(\frac{\partial n_i}{\partial t} \right)^R + \left(\frac{\partial n_i}{\partial t} \right)^D \right] \nabla_l \phi_{il} \right\} d\mathbf{r} + \{\text{higher order terms}\}. \qquad (7.25)$$

In what follows, we will be concerned with the small deviation from equilibrium and discuss explicitly the linearized nematodynamics, although this restriction is not mandatory in UHT. Then, we neglect all terms higher than quadratic in deviation of variables and retain only explicitly expressed terms in (7.25). From (7.25), the reactive part of fluxes is obtained as

$$Q_i^R = (\varepsilon + p)v_i \qquad (7.26)$$

$$\sigma_{ij}^R = -p\delta_{ij} - \frac{1}{2} \lambda_{kji} \nabla_l \phi_{kl} \qquad (7.27)$$

where (7.21) was used for $\left(\frac{\partial n_i}{\partial t} \right)^R$

Equation (7.26) shows that the reactive part of energy flux density is just the enthalpy flux density. The vector $\nabla_l \phi_{kl}$ in (7.27) is called the molecular field by de Gennes [5] and usually denoted by $\mathbf{h}$,

$$h_i \equiv \nabla_j \phi_{ij} = \nabla_j \left(\frac{\partial \varepsilon}{\partial \nabla_j n_i} \right). \qquad (7.28)$$

$\mathbf{h}$ acts as a field that tends to orient the director parallel to it. In the linear approximation (7.27), the Ericksen stress $\phi_{kj} \nabla_j n_k$ [5] has been dropped out.

Due to the presence of the second term on the right-hand side of (7.27), the tensor σ_{ij}^{R} is not symmetric. Since in the equation of motion only its divergence $\nabla_{j}\sigma_{ij}^{R}$ matters, we can construct a symmetric stress tensor that gives exactly the same value of divergence [11, 12, 15]. The symmetric stress tensor guarantees the conservation of local angular momentum. Therefore asymmetry of σ_{ij}^{R} is not really a problem in nematodynamics.

The dissipative parts of the flux densities are set up as the linear constitutive relations of thermodynamic forces, $\nabla_{j}v_{i}$, $h_{i} = \nabla_{j}\phi_{ij}$, and $\nabla_{i}T$, based on the recipe of irreversible thermodynamics:

$$Q_{i}^{D} = -\kappa_{ij}\nabla_{j}T, \tag{7.29}$$

$$\sigma_{ij}^{D} = \nu_{ijkl}A_{kl}, \text{ (the Harvard notation [16])} \tag{7.30}$$

$$= \eta_{ijkl}A_{kl}, \text{ (the MPP notation [11])} \tag{7.31}$$

$$\left(\frac{\partial n_{i}}{\partial t}\right)^{D} = \frac{1}{\gamma_{1}}\nabla_{l}\phi_{il} = \frac{1}{\gamma_{1}}h_{i}. \tag{7.32}$$

The respective tensor of transport coefficients is determined by the symmetry $D_{\infty h}$ of nematic and the Onsager reciprocal relations. Thermal conductivity tensor has two independent components $\kappa_{||}$ and $\kappa_{\perp}$, and

$$\kappa_{ij} = \kappa_{||}n_{i}n_{j} + \kappa_{\perp}\delta_{ij}^{\perp}. \tag{7.33}$$

Due to the symmetry property of σ_{ij}^{D} and A_{ij}, the four-rank viscosity tensor must be $\nu_{ijkl} = \nu_{jikl} = \nu_{ijlk}$, and the Onsager reciprocal relations require that $\nu_{ijkl} = \nu_{klij}$. For Harvard notation (7.30) we have

$$\begin{aligned}
\sigma_{ij}^{D} = &\ 2\nu_{2}A_{ij} + 2(\nu_{3} - \nu_{2})\left[A_{ik}n_{k}n_{j} + A_{jk}n_{k}n_{i}\right] + (\nu_{4} - \nu_{2})\delta_{ij}A_{kk} \\
&+ 2(\nu_{1} + \nu_{2} - 2\nu_{3})n_{i}n_{j}n_{k}n_{l}A_{kl} \\
&+ (\nu_{5} - \nu_{4} + \nu_{2})\left[\delta_{ij}n_{k}n_{l}A_{kl} + n_{i}n_{j}A_{kk}\right].
\end{aligned} \tag{7.34}$$

MPP notation is slightly different from (7.34):

$$\left.\begin{aligned}
\nu_{2} = \eta_{2}, \nu_{3} = \eta_{3}, \nu_{4} = \eta_{4}, \nu_{5} = \eta_{5} \\
2\nu_{1} = \eta_{1} - \eta_{2} + \eta_{4} - 2\eta_{5}.
\end{aligned}\right\} \tag{7.35}$$

When $n_i = \delta_{iz}$, in matrix form we have a transparent form:

$$
\begin{bmatrix}
\sigma_{xx}^{\mathrm{D}} \\
\sigma_{yy}^{\mathrm{D}} \\
\sigma_{zz}^{\mathrm{D}} \\
\sigma_{yz}^{\mathrm{D}} \\
\sigma_{zx}^{\mathrm{D}} \\
\sigma_{xy}^{\mathrm{D}}
\end{bmatrix}
=
\begin{bmatrix}
\eta_4 + \eta_2 & \eta_4 - \eta_2 & \eta_5 & & & \\
\eta_4 - \eta_2 & \eta_4 + \eta_2 & \eta_5 & & 0 & \\
\eta_5 & \eta_5 & \eta_1 & & & \\
& & & 2\eta_3 & & \\
& 0 & & & 2\eta_3 & \\
& & & & & 2\eta_2
\end{bmatrix}
\begin{bmatrix}
A_{xx} \\
A_{yy} \\
A_{zz} \\
A_{yz} \\
A_{zx} \\
A_{xy}
\end{bmatrix}
\tag{7.36}
$$

The dissipative coefficient γ_1 on the right-hand side of (7.32) is called the rotational viscosity and plays a major role in the dynamics of Freedericksz transition. Since entropy production is positive, we have

$$
\nu_2 = \eta_2 \geq 0, \nu_3 = \eta_3 \geq 0, \nu_4 = \eta_4 \geq 0,
$$
$$
2(\nu_1 + \nu_5) - \nu_4 + \nu_2 = \eta_1 \geq 0, \gamma_1 \geq 0
$$
$$
\nu_4(2\nu_1 + \nu_2) \geq (\nu_5 - \nu_4)^2, \eta_1 \eta_4 \geq \eta_5^2.
$$

Although we have set up linear relations for the flux densities and conjugate thermodynamic forces based on the formalism of irreversible thermodynamics, the fluxes are not linear in hydrodynamic variables, the director **n** in particular, since the constitutive tensor ν_{ijkl} explicitly depends on **n**. When we apply UHT formalism to normal (isotropic) fluid constructing four-rank isotropic tensor for ν_{ijkl}, we have the viscous constitutive equation with two independent coefficients:

$$
\sigma_{ij}^{\mathrm{D}} = 2\eta \left(A_{ij} - \frac{1}{3}\delta_{ij}A_{kk} \right) + \zeta \delta_{ij}A_{kk}
\tag{7.37}
$$

where η and ζ are shear and bulk viscosities. Equation (7.37) amounts to putting

$$
\nu_1 = \nu_2 = \nu_3 = \eta, \nu_4 = \frac{1}{3}\eta + \zeta, \nu_5 = -\frac{2}{3}\eta + \zeta
\tag{7.38}
$$

in (7.34).

7.1.5 Equations of Motion

Substituting the explicit expression of fluxes derived so far into conservation laws, we have the linearized equations of hydrodynamic variables:

$$
\frac{\partial}{\partial t}\delta\rho = -\rho\nabla_i v_i
\tag{7.39}
$$

$$\rho \frac{\partial v_i}{\partial t} = -\nabla_i p + \lambda_{lij} \nabla_j \nabla_k \phi_{lk} + \nu_{ijkl} \nabla_j \nabla_l v_k \tag{7.40}$$

$$\frac{\partial}{\partial t} \delta n_i = \lambda_{ijk} \nabla_k v_j + \frac{1}{\gamma_1} \nabla_j \phi_{ij} \tag{7.41}$$

$$\frac{\partial}{\partial t} \delta \varepsilon = -(\varepsilon + p) \nabla_i v_i + \kappa_{ij} \nabla_i \nabla_j T \tag{7.42}$$

where attached δ denotes the deviation of the variables from the equilibrium state. In order to compare the above UHT results, we reproduce here the linearized version of the equations of motion of E–L theory. When E–L theory is referred to, almost exclusively the incompressible nematic is implied [7], and the terms connected with div $\mathbf{v} = A_{kk}$ have been eliminated from the viscous constitutive relation:

$$\nabla_i v_i = 0 \tag{7.43}$$

$$\rho \frac{\partial v_i}{\partial t} = \nabla_j \sigma_{ij} \tag{7.44}$$

$$\sigma_{ij} = -p\delta_{ij} + \sigma'_{ij} \tag{7.45}$$

where

$$\sigma'_{ij} = \alpha_1 n_k A_{kl} n_l n_i n_j + \alpha_2 N_i n_j + \alpha_3 n_i N_j + \alpha_4 A_{ij} + \alpha_5 n_j A_{ik} n_k + \alpha_6 n_i A_{jk} n_k \tag{7.46}$$

$$N_i = \frac{\partial n_i}{\partial t} - \Omega_{ij} n_j. \tag{7.47}$$

The six coefficients $\alpha_1 \sim \alpha_6$ are called the Leslie coefficients and have been widely used. As for the director,

$$h_i = \gamma_1 N_i + \gamma_2 A_{ij} n_j \tag{7.48}$$

where

$$\gamma_1 \equiv \alpha_3 - \alpha_2, \ \ \gamma_2 \equiv \alpha_2 + \alpha_3 = \alpha_6 - \alpha_5. \tag{7.49}$$

The last equality of γ_2 is a consequence of Onsager reciprocal relations [17], which reduces the number of independent Leslie coefficients to five. Although it has been stated that the linearized versions of E–L theory and UHT are essentially identical [5], there remain some subtle points to be remarked.

7.1.6 Additional Remarks and Conclusion

7.1.6.1 On the Equation of Motion of the Director

The equation of motion of the director in E–L theory (7.47) together with (7.48) can be rewritten as

$$\frac{\partial n_i}{\partial t} = \Omega_{ij}n_j - \frac{\gamma_2}{\gamma_1}A_{ij}n_j + \frac{1}{\gamma_1}h_i. \tag{7.50}$$

Putting $-\frac{\gamma_2}{\gamma_1} = \lambda$, (7.50) reduces to exactly the same equation as (7.41) in UHT. This means that the change in orientation of the director due to the flow field is not dissipative; rather, it is reactive. γ_1 is a truly dissipative coefficient as shown in (7.32). The parameter γ_2 in E–L theory, although it is called viscosity, has nothing to do with entropy production.

7.1.6.2 On the Incompressibility Approximation

Ordinary liquids and liquid crystals are nearly incompressible. In ordinary fluid dynamics the incompressibility approximation under the constraint div $\mathbf{v} = 0$ has frequently been utilized. In a soft elastomer such as vulcanized rubber, where shear modulus is very small as compared with bulk modulus, the incompressibility approximation has also been usefully employed. The constraint of the incompressibility approximation, div $\mathbf{v} = 0$ for ordinary fluids or divergence of displacement vector for elastic (isotropic) materials, does not modify any other terms of the equations of motion: div $\mathbf{v} = 0$, or divergence of displacement vector, is a solution of the equations of motion, provided that pressure p is chosen as an appropriate harmonic function ($\nabla^2 p = 0$). However, for anisotropic matters, such as liquid crystals or anisotropic solids (crystals), since the div $\mathbf{v} = 0$ or its elastic version cannot be a special solution of equations of motion, the incompressibility approximation requires a careful consideration [12, 18].

In E–L theory [3, 4], and even in an excellent textbook [5] and also in the pioneer paper of UHT [16], all contributions A_{kk} have been eliminated from the constitutive equations, which amount to putting

$$\nu_4 = \nu_2, \ \nu_5 = 0. \tag{7.51}$$

This "tosses out" of (7.34), the term $\delta_{ij}n_kn_lA_{kl}$ which is not a purely compressional term [18]. A more reasonable approach would be to employ (7.34) as it is and to determine the pressure by the equation

$$\frac{\partial}{\partial t}\text{div } \mathbf{v} = -\nabla^2 p + \nabla_i\nabla_j\sigma_{ij} = 0, (\text{div } \mathbf{v} = 0 \text{ at } t = 0). \tag{7.52}$$

Then, we have [12]

$$
\begin{aligned}
\nabla^2 p = {} & +\lambda n_k \nabla_k (\text{div } \mathbf{h}) + \left(2\nu_3 - \nu_2 - \nu_4 + \nu_5\right) n_k n_j \nabla_j \nabla^2 v_k \\
& + 2(\nu_1 + \nu_2 - 2\nu_3) n_i n_j n_k n_l \nabla_i \nabla_j \nabla_k v_l.
\end{aligned}
\tag{7.53}
$$

7.1.7 Concluding Remark

Contrary to the opinion [9] that UHT of nematics is restricted to the small perturbations of a uniformly aligned nematic, the framework of the UHT itself has wider range of applicability than a linearized version outlined in this review: what is essential to UHT of nematodynamics is that the local thermodynamic equilibrium is attained for each nonequilibrium $\mathbf{n}(\mathbf{r})$, which is not necessarily a uniform ground state. For explicit expositions of full version of UHT, please refer to excellent descriptions [12, 15].

Finally, it is quite impressive to recognize that at the very base of LCD technology, there lie such fundamental physical principles as symmetries and broken symmetries, conservation laws, and the microscopic reversibility.

7.2 New Modes
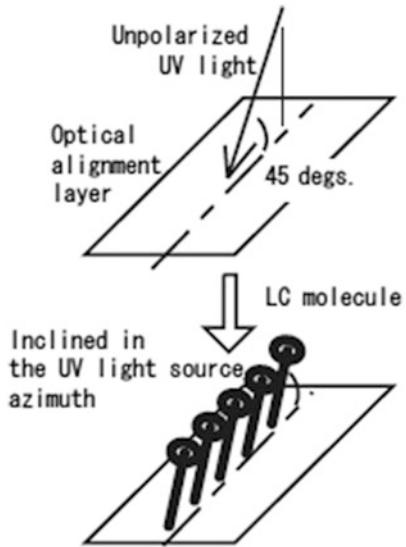
Hidefumi Yoshida and Kenji Okamoto

7.2.1 Introduction
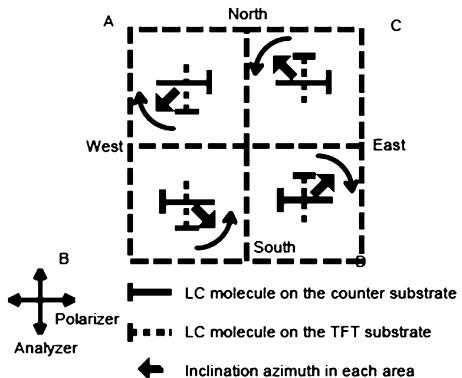
In Sect. 6.2, we introduced the development of the protrusion-type multi-domain vertical alignment (MVA)-type displays and in the present chapter we will focus in particular on the recent VA-type display.

At the international liquid crystal conference in 2002, one of us, Yoshida (at that time at Fujitsu, now at Sharp), gave an invited presentation about new liquid crystal display technologies including the MVA [19], the quadrant split photo-alignment technology, and the transverse electric field-driven vertical alignment technology (VA-IPS). Nine years later, in an invited presentation at the 2011 SID conference, Mr. Yamada (Sharp) reported on the practical use of similar technologies, the ultraviolet-induced multi-domain vertical alignment (UV2A) and the transverse birefringent alignment (TBA) [20]. Despite the differences of nearly a decade, the UV2A technology is similar to the abovementioned photo-alignment technique, and TBA is similar to VA-IPS. In this chapter, we will show why the technology that has been introduced in 2002 did not lead to practical use and why it flowered in 2011. In addition, we introduce the polymer-sustained alignment (PSA) as a new orientation technology.

Fig. 7.1 Basic alignment
through UV irradiation

Fig. 7.2 Principle optical
alignment with multi-
domain configuration

7.2.2 Optical Alignment LCD Systems

Here, we describe the optical alignment as a display mode. Please refer to Sect. 7.3
for the mechanisms of the photo-alignment itself.
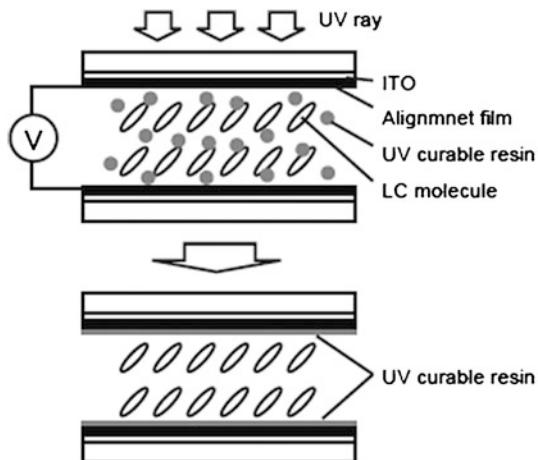
It has been shown that the oblique irradiation of an alignment film by ultraviolet
light can control the alignment direction of the liquid crystal molecules, as shown
in Fig. 7.1 [21–23]. In Sect. 6.2 we discussed quadrant division alignment [24].
We adopted the domain-dividing technology to photo-alignment as shown in
Fig. 7.2. UV light is irradiated through a shadow mask from two directions onto the
TFT substrate and the CF substrate sides to produce the four quadrants with different
molecular alignment. Figure 7.2 shows the example in which the A and B quadrants of
the TFT substrate side are irradiated from one side and the C and D quadrants from the

other side. The opposite substrate, the CF side, is irradiated in such a way that A and C quadrants have the same molecular orientation and B and D quadrants the opposite orientation. Thus, the pixel is divided into four quadrants in which the molecules tilt in different directions (the thick arrows in Fig. 7.2). This cell shows a high light transmittance and the only disclination line has a swastika shape in the pixel center.

One of us, Dr. Yoshida, attended domestic conferences to explore promising technologies when he met the enthusiastic Professor Shunsuke Kobayashi who was working on photo-alignment. The horizontal photo-alignment, as announced by another company, was plagued by an unstable orientation and weak anchoring. Other groups in the Fujitsu Co., Ltd. considered the rubbing method for vertical alignment technology, but they had been struggling that the uniformity did not improve by rubbing (see Sect. 6.2). Strong anchoring for molecules is not necessary for the vertical alignment and the idea to use photo-alignment was born quite naturally. We needed an ultraviolet irradiation device, but had not enough time to purchase a new one. Instead, we used an ultraviolet irradiation device that was kindly provided at no charge by Ushio at their Yokohama Office to irradiate substrates with ultraviolet light. Within 1 week we were able to formulate the experimental design for the devices: substrate cleaning, alignment film coating, irradiation with the Ushio device, injection of the liquid crystal into the empty cells, and final investigation of their characteristics. The liquid crystal cells had a thickness of around 2 mm. I stocked the LC cells used for experiment, stacking them together. Finally, their total thickness was around 1.5 m. Around 750 LC cells ($=1.5$ m/2 mm) were fabricated. We had a great spirit of tenacity. We checked the basic LC molecular alignment, and it was possible to achieve a uniform alignment by the combination of radiation from orthogonal orientations, and we thought to use this type of orientation for alignment division technology. We also came up with the idea to irradiate the samples with light from opposite directions (Fig. 7.2). Then, in order to suppress the deviation of the irradiation position when the optical mask is bent due to its own weight, it is irradiated with ultraviolet rays in a parallel orientation with the light-shielding pattern of the straight line of the optical mask. Thus the configuration of Fig. 7.2 was determined to be excellent. We also investigated the materials in parallel with the discussion of the apparatus and the ultraviolet irradiation method. We also examined the material for vertical alignment provided by foreign material manufacturers. However, their properties were far from satisfactory.

Because of the strong competition with protrusion-type MVA, we were required to launch our products early, and the available time was short. Therefore, we took a polyimide as an alignment film for volume production. It was possible to widen the margin of the amount of ultraviolet irradiation for realizing the predetermined pretilt angle and achieve an alignment film showing a satisfactory voltage holding ratio. However, the required UV dose could not be reduced below about 1 J/cm^2. This sensitivity level is completely different from that with photo-alignment films which are used today. We were calculating the cost for mass production, but the investment into the ultraviolet irradiation device, the ultraviolet lamps, and the cost with repairs was too high, and the slow throughput of the technology led to the decision not to mass-produce in Fujitsu unfortunately.

**Fig. 7.3** Basic fabrication process of PSA technology
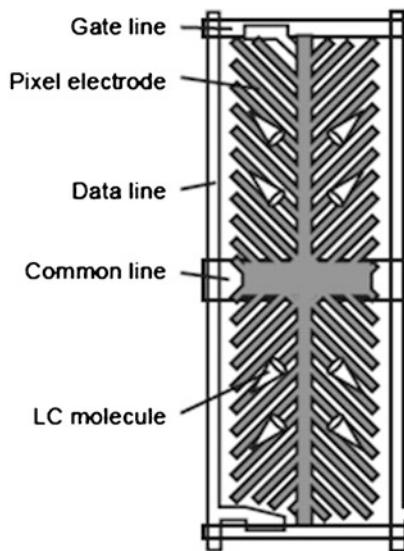
However, at Sharp Mr. Yamada and Mr. Miyachi adopted the photo-alignment technology, which they call ultraviolet-induced multi-domain vertical alignment (UV2A) for mass production of large TV sets [25]. What did they do different? The improvement of MVA technology at Sharp was based on the tenaciously carried out development, particularly by human resources that allowed the development of new materials. When the photo-alignment technology was investigated in Fujitsu, MVA which was investigated by another team in Fujitsu was a rival for photo-alignment technology. In order to differentiate the photo-alignment technology from protrusion-type MVA, the team needed a quick start-up and decided to look into orientation control by using polyimide films not by using new material that needed additional principal investigation. It can be said that Fujitsu had engineers who were good at physics, and Sharp had engineers who were good at chemicals. Thus the difference in advancing with photo-alignment materials was the networking with contacts within chemical manufacturers. Fujitsu engineers played an important role in the start-up phase, but other engineers of Sharp were required to complete the development. The technique of this photo-alignment itself is described in Sect. 7.3. There the author shows that tact time during production poses no problem.

7.2.3   Polymer-Sustained Alignment (PSA)-Type Liquid Crystal Displays

In this method, an amount of monomer is added to the liquid crystal and its photopolymerization stabilizes the liquid crystal orientation (Fig. 7.3) [26]. In the manufacturing process, first the liquid crystal is oriented by applying a voltage to transparent electrodes in a hairline-bone pattern with a width of three to four micrometers (Fig. 7.4). The liquid crystal molecules are aligned in parallel to the

Fig. 7.4 Pixel example
of 4-domain PSA-LCDs

Gate line

Pixel electrode

Data line

Common line

LC molecule

slits' extending direction, which means they tilt towards the center of the pixel. Then, the monomer is photopolymerized by irradiation with ultraviolet rays in this state. The polymers adsorb onto the alignment film interface, and thus the polymer controls the alignment direction of the liquid crystal. This alignment has as key features a high transmittance and a high contrast ratio. Hence, this method has led to wide practical use in large TVs or in mobile applications.

How had this PSA type been developed? Mr. Kataoka had reported at a monthly meeting a technique to stabilize the orientation by adding a liquid crystal polymer, but the good point of this technique was initially not understood. However, one of us, Dr. Okamoto, intuitively felt that it is an interesting technology and instructed Mr. Koike, Kataoka's superior, to think about the advantages of this method. Meanwhile, a technique for controlling the directional tilt of liquid crystal molecules using micro slits had been examined, but the technology did not work well. Liquid crystal molecules can be aligned in a parallel orientation within a micro slit, but for long slits, the liquid crystal molecules tend to tilt in opposite directions along the trench. There, Kataoka had the idea to combine those two techniques. He knew that molecular tilt orientation becomes uniform by slowly applying the voltage. Then, this alignment can be stabilized by irradiation with ultraviolet light. However, this technique did not lead to practical use easily. Inhomogeneities are caused by the photopolymers that tend to be adsorbed and accumulated on the alignment layer during the LC filling process in a special position and thus decrease the voltage holding ratio.
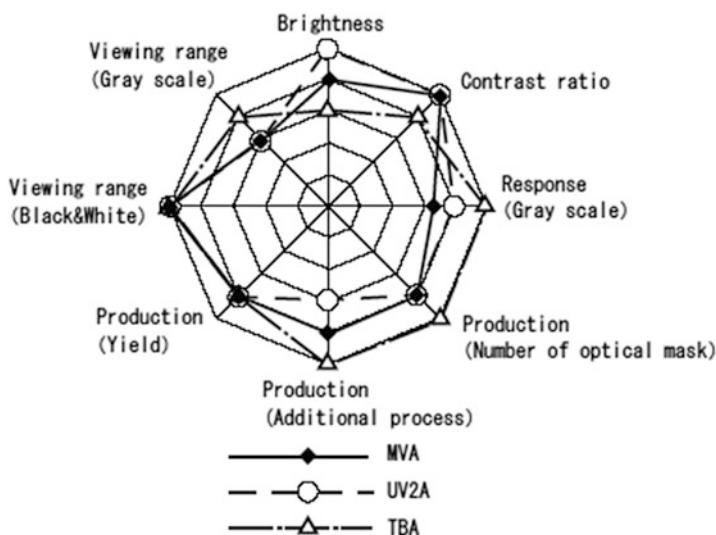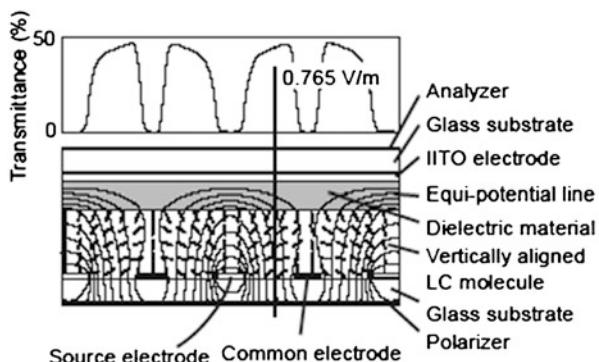
But because of the molecular pretilt, the switching response is fast. Because it did not use any protrusions like MVA display (see Sect. 6.2), the display has a high transmittance. Thus, Dr. Okamoto determined it to be a promising technique as the successor to the MVA technology and increased the number of engineers working on the new technology. Mr. Hanaoka became in charge of the experimental

work, while Mr. Nakanishi was devoted to development while writing patents. The development was continued even after Fujitsu LCD section (Fujitsu Display Technologies Company Co., Ltd.) was absorbed by Sharp. This development culminated in mobile applications. It was decided to be employed in applications where a high-speed response was needed, such as in game machines. Furthermore, it was used by AUO Corporation and Samsung Electronics for TVs and now is one of the main technologies for liquid crystal TVs.

7.2.4 Vertically Aligned In-Plane Field Switching (VA-IPS), or TBA Type

However, in the vertical orientation, liquid crystals having a positive dielectric anisotropy can be used for in-plane switching (for details, we refer to the cited literature [27]). Since the electric field is concentrated near the electrodes, low gray levels can be displayed by just driving only a part of the liquid crystals. Fast response is also realized. Furthermore, summing up the areas having different threshold voltages, a wide viewing angle is achieved. Yoshida used a two-dimensional simulation software and tried to develop a novel display mode through combinations of various electrode designs. We first studied the structure for applying an electric field in the plane provided from comb electrodes as in the IPS type in advances vertically aligned liquid crystals. Black disclination lines occurred between the electrodes, and overall, the display was not bright or rather dark. The cause for this was the high symmetry of the device. Therefore, we tried several layouts that break the symmetry, such as providing a common electrode in the opposing substrate only at positions of the common electrode in the TFT substrate. Another design was providing a counter electrode on the entire surface of the counter substrate. This display was very dark, too. The electric field was in the direction perpendicular to the substrate and only concentrated near the source electrode in the TFT substrate. In order to flip the liquid crystal molecules horizontally, we thought about coating a dielectric layer on top of the counter electrode to change the electric field (Fig. 7.5). After we had confirmed the design by calculations, we asked our colleague Mr. Nakanishi to prepare a cell. We told him that a cell which is free from dark disclination lines should be realized. At first glance, Mr. Nakanishi thought that the microscopic observation of the prototype showed some indeed disclination lines. It was wrong. Then he found that the disclination happens only on top of the metal electrodes, and none between the electrodes. Mr. Nakanishi was so fascinated. There, the formal active cooperation was started to manufacture TFT-LCD prototypes in cooperation with the factory for mass production [27, 28]. The response speed was fast (especially in the low gradient regime it was ten times faster than a MVA device), and the viewing angle characteristics were good with very little color change. The results of our calculations in Fig. 7.5 show only a small distortion of the electric field lines that are

Fig. 7.5 Basic cross-sectional view of VA-IPS or TBA LCDs

Fig. 7.6 Specification of LCD modes

nonuniform in the gap. Therefore, the electric field has become asymmetric and thus acting differently on the liquid crystal molecules depending on their position, automatically resulting in the configuration with multiple threshold voltages (V_{th}). However, once again, there was the decision to make which design to mass-produce. Product evaluation was based only on monitors. Figure 7.6 shows the characteristics of three different display types. Here, the lower brightness was the decisive disadvantage of the VA-IPS type.

This VA-IPS type (also called as TBA type later by Sharp Corporation) has not been put into practical use by Fujitsu, but again, Sharp mass-produced it [29]. Sharp had various applications in the automotive sector, mobile phones, and photo frames. Among these, it was possible to stimulate demand for photo frames because of the tight demands of the black state and the wide viewing angle characteristics,

including for halftones or gray scale images. Currently, further applications utilizing the advantage of the response speed are being examined.

7.2.5 Summary

The authors were writing Sects. 6.2 and 7.2. Many episodes have the tint of funny nostalgic memories. We would like to note here that many of the examples of epoch-making inventions have been made as soon as the person in charge just had been transferred to another team with a different theme. We think that the new environment gives an important new input for new ideas.

Liquid crystal display has been plagued with the problem of viewing angle, but this problem has been solved by the joint efforts of engineers and researchers, and display characteristics have been improved significantly.

With their excellent display quality and the advantage of being thin, lightweight, and low power consumption, LCDs became popular as large TV screens. We believe that liquid crystal displays fulfill a central role in various fields in the future.

## 7.3 Photo-Alignment/Pattering of Liquid Crystals and LCDs by Side-Chain Photopolymers

Martin Schadt
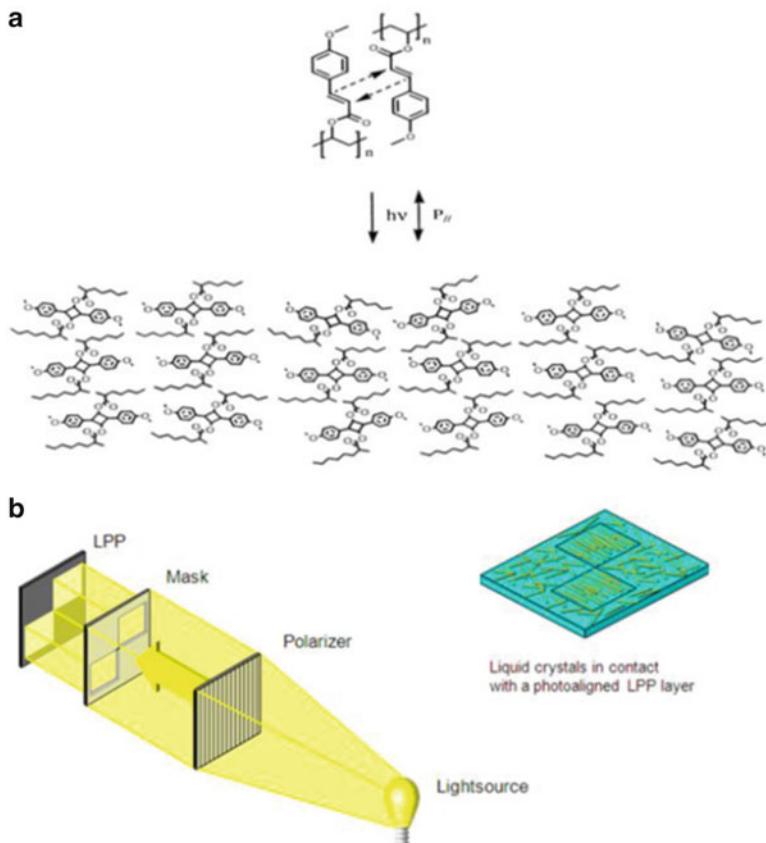
7.3.1 The Beginnings of Liquid Crystal and LCD Photo-Alignment

Uniaxially, surface anchoring energy and bias tilt angle between the nematic LC director(s) and display substrate(s) define the alignment boundaries of field-effect LCDs [30]. Prior to photo-alignment by side-chain photopolymers [30, 31], LCD substrates were mainly aligned by mechanically buffed polyimide films [32]. Since buffing is a macroscopic process, LCD alignment was possible only in one direction; microscopic alignment pattering with arbitrary azimuthal angles and/or different bias tilt angles could not be achieved. Moreover, brushing generates electric charges, dust, and alignment defects which are detrimental for display manufacturing and LCD performance. Despite the relative simplicity of mechanical brushing, its surface interactions are not really understood; brushing is more of a craft than a science. The origin of the complex anisotropic forces causing liquid crystal molecules to align on surfaces has intrigued Schadt since his early twisted nematic (TN) experiments [33] (cf. Sect. 6.1). His findings that some molecular functional

groups and molecular LC configurations align well, whereas others—such as super twisted nematic [34, 35], ferroelectric [36, 37], and phase-change cholesteric configurations [38]—are delicate to align often, proved frustrating. In his search for correlations between molecular structural elements, their influence on macroscopic LC order, LC material properties and electro-optical LCD performance, and from the few observations reported for brushed main-chain polymer films [39], he suspected that—apart from the rather well-understood topological [40, 41] and steric LC surface interactions—anisotropic Van der Waals interactions play an important role in LC alignment. However, and apart from perfect vertical alignment with fatty acids and siloxanes [42], it was unknown how LC alignment could be realized by molecular means. Parallel to his nematic research, Schadt started at the end of the 1980s several new projects with his liquid crystal research division at Roche. One was collaboration with the research group of the late Professor Titov, NIOPIK, Moscow, with the aim of strengthening the search for fast-responding ferroelectric electro-optical effects and functional organic materials. During a brainstorming session at NIOPIK, Kozinkov presented photo-alignment samples which he had made using two different photosensitive materials known from literature, namely azobenzene and polyvinyl cinnamate (PVMC). Kozinkov was inspired by the linear polarized light switching experiments of Ichimura [43] et al. which had shown that *cis–trans* isomerization of azobenzene changes the direction of LC alignment in free-standing monolayer films. At about the same time Gibbons [44] et al. investigated rewritable optical storage devices using azobenzene photo-aligned liquid crystal cells. The reversible *cis–trans* LC aligning mechanism of azobenzene caused by steric conformational change was understood [43], whereas the mechanism causing LC alignment on PVMC was mysterious.
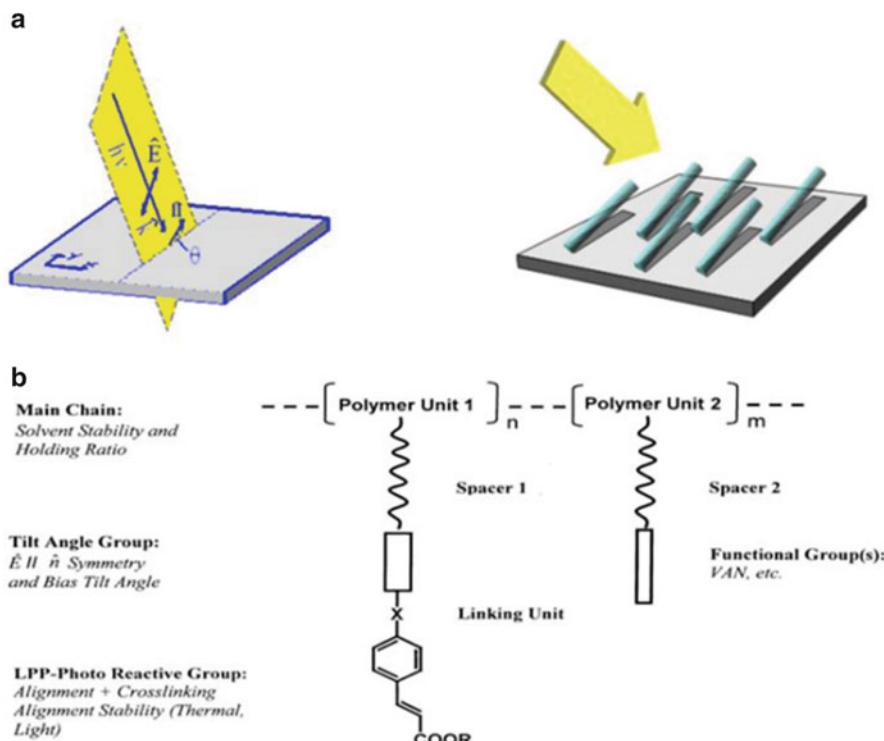
7.3.2 Photo-Alignment of Monomer Liquid Crystals by Directional Photosensitive Side-Chain Polymers

Although the optical and thermal stability of PVMC photo-aligned cells were poor and alignment quality inferior to azobenzene, Schadt attempted to elucidate the underlying photo-mechanism and developed a quantitative molecular LC alignment model for photosensitive side-chain polymers comprising dichroic cinnamoyl moieties [31]. The model is based on the idea that photochemical excitation of π-electrons in double bonds of nearest neighbor cinnamoyl moieties should be *directional* dependent, i.e., the reaction probability is largest for bonds lying parallel to the plane defined by the electric field vector E and the propagation direction of incident polarized UV light [31]. As a consequence of polarized excitation and due to 2+2 cyloaddition of prepolymer pairs, he assumed directional photoisomers to result, thus converting the initially isotropic distribution of non-cross-linked prepolymer molecules into an anisotropic distribution of photoisomers and depleted non-cross-linked prepolymer molecules with respect to the

Fig. 7.7 (**a**) Photo-alignment of LCs by directional side-chain photopolymers (LPPs): directional crosslinking under linear polarized UV light of double bonds in PVMC generating anisotropic van der Waals surface interactions and uniaxial LC alignment. (**b**) Photo-pattering of LC alignment through photomask

polarization direction [31]. Moreover, the author expected that the resulting anisotropic molecular distribution would generate anisotropic van der Waals surface interactions enabling adjacent LC molecules to uniaxially align [31] (Fig. 7.7). Last but not least, simultaneous *fixation* of the anisotropic molecular distribution via an increase in the glass transition temperature of the LPP film due to UV crosslinking was expected to occur. With his coworkers at Roche, Schadt started a series of photo-alignment experiments which confirmed his linear photopolymerization (LPP) model and showed that the double bonds of cinnamoyl moieties in PVMC indeed undergo directional crosslinking under linear polarized UV light and that uniaxial LC alignment is indeed caused by anisotropic van der Waals interactions [31] (Fig. 7.7a). Moreover, the experiments confirmed that 2+2 cyloaddition stabilizes LC alignment, thus enabling alignment patterning by sequential polarized UV exposure of the substrate through photomasks [30, 31] (Fig. 7.7b).

Fig. 7.8 (**a**) Non-cylinder symmetry and uniaxiality of LPP photo-aligned long molecular LC axes under oblique polarized UV exposure. (**b**) Generic molecular LC aligning functions of directional photo-aligning side-chain copolymers
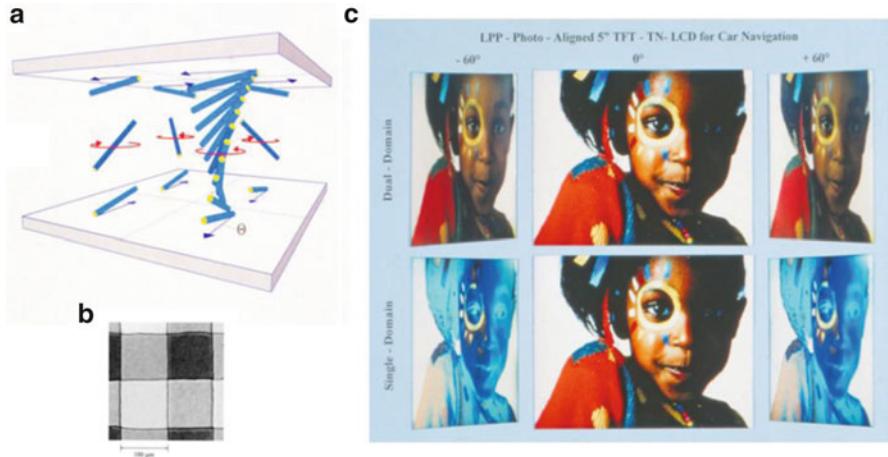
However, thermal and light stability as well as surface LC anchoring of PVMC proved to be poor and inadequate for practical use. From the poor initial stability results it was questionable whether stable directional photosensitive side-chain polymers could be developed. Moreover, LC alignment on PVMC occurred *perpendicular* to the polarization direction of incident polarized UV light [31], i.e., in the same direction as caused by the *cis–trans* isomerization of azobenzenes [43–45]. Due to the cylinder symmetry of the process, it was impossible to simultaneously generate uniaxiality *and* bias tilt with PVMC [31]. At this stage the collaboration with NIOPIK was terminated. However, Schadt continued the search for stable, non-cylinder symmetric photo-aligning polymers with his coworkers at Roche and later at Rolic even though the odds were against his conviction that optically stable photo-materials with *non-cylinder symmetry* are feasible. He was convinced that the demanding alignment stability and non-cylinder symmetry required for LCD alignment cannot be realized by the *cis–trans* azo mechanism pursued by most groups [46]. Four years later, the author [47] and coworkers discovered the first side-chain photopolymer material which combined non-cylinder symmetry and uniaxiality upon oblique polarized UV

exposure (Fig. 7.8a). This paved the way for stable photo-alignment and alignment patterning of field-effect LCDs, enabling markedly improved fields of view of LCDs [47, 48] and novel anisotropic optical liquid crystal polymer thin films [30, 49]. The findings justified further development of side-chain photopolymers with the goal of covering the full range of possible bias tilt angles (0–90°), thus enabling photo-alignment and photo-patterning of all types of field-effect LCDs1 [47–49]. Figure 7.8b schematically depicts different molecular LC alignment functions of a side-chain photo copolymer [50].

In 1994 Roche decided to focus its core business exclusively on life sciences, terminating or selling all its non-pharmaceutical business activities, including its nematic liquid crystal material business. The nematic liquid crystal material business was sold to Merck KgaA, Darmstadt, including 64 basic nematic liquid crystal chemical patent families. Thanks to the strong photo-alignment device and material patent position as well as liquid crystal polymers (LCPs) which Schadt had developed with his interdisciplinary research team since the late 1980s, the foundation of the spin-off company Rolic Ltd. (Roche liquid crystals) became possible in 1994. Forty-four basic patent families covering photo-aligned LCDs, optical LCP thin-film devices, polymer side-chain photo-aligning materials, and LCP materials, each filed in 10–12 countries, were transferred from Roche into the new company. Analogous to the TN-licensing business of Roche 30 years before (cf. Sect. 6.1), Rolic's photo-alignment IP portfolio provided the basis for the licensing business of the new company. The author agreed to act as the first CEO, head of research, and delegate of the board of directors of Rolic until 2002. He and his coworkers continued R&D on photo-alignment and started licensing the new technologies and collaborating with LCD manufacturers and optical film companies worldwide. In line with the Roche exit strategy, Rolic was sold to Karl Nicklaus, a Swiss investor in late 1996.
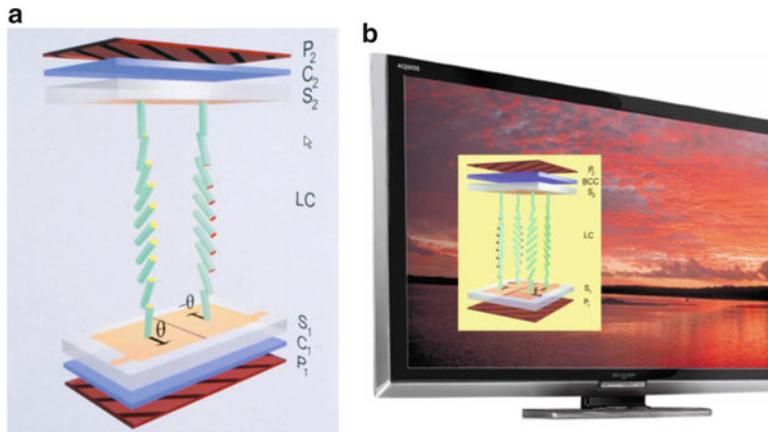
7.3.3   Photo-Alignment/Patterning of LCDs by Directionally Photosensitive Side-Chain Polymers

LPP photo-alignment enables generating multi-domain field-effect LCDs with broad fields of view. This was first demonstrated by Schadt and coworkers in 1996 with a photo-aligned four-domain TN-LCD [47]. Figure 7.9a schematically depicts the LC director configuration of a partially switched picture element (pixel) of such a display. The four reverse twist domains in the sub-pixels—each rotated by $\pi/2$—result from different bias tilt angle directions at the two display substrates, where the different tilt directions were realized by sequential UV exposure under different angles of incident polarized UV light through a photomask [47]. Figure 7.9b shows a microphotograph of the angular dependence of four sub-pixels whose angular-dependent contrast averages in the eyes of the viewer, thus enlarging the field of view [47]. Figure 7.9c shows an actual photo-aligned dual-domain TFT-addressed TN-LCD with its markedly improved field of view compared with its conventional single-domain counterpart [51].

Fig. 7.9 (**a**) LC director configuration of a partially switched four-domain TN-LCD pixel. (**b**) Microphotograph of its four sub-pixels. (**c**) Fields of view of two-domain photo-aligned/photo-patterned TFT-addressed TN-LCD (*top*) and conventional single-domain counterpart (*bottom*)

In the late 1990s multi-domain LCD alignment, thin-film transistor (TFT) development, and LC material progress opened up the possibility to base TFT-LCD manufacturing not only on the twisted nematic effect [33] and in-plane switching [52] but also on vertically aligned nematic (VAN) configurations whose single-domain version [53, 54] was known since the 1970s. However, poor viewing properties, fluctuations of contrast and color due to cell gap and birefringence variations as well as inadequate negative dielectric anisotropic LC materials prevented their commercialization for more than 30 years [30]. In the late 1990s progress enabled increasingly large-sized TFT-TN-LCDs for computer monitors and first LCD TVs which spurred the demand for larger sized TFT-LCDs (Sect. 6.1). This required increased off-state contrast and broader fields of view beyond those of optical film-compensated TN-LCDs [55]. The realization of multi-domain vertical aligned (MVA)-LC configurations in 1998 by LPP photo-alignment [48] and independently by lateral fringe fields [56] enabled the development and manufacturing of TFT-addressed MVAN-LCDs. Due to almost homeotropic LC alignment in the off-state—i.e., optical uniaxiality—MVAN-LCDs exhibit large contrast [30, 48]. Figure 7.10a depicts the slightly off-vertical LC director configuration of a partially switched LPP photo-aligned dual-domain VAN-LCD developed by Seiberle and Schadt [48] in 1998. In the same year, Takeda et al. at [56] published a multi-domain MVAN-LCD based on fringe field electrode patterning. Fringe field patterning adds complexity to the electrode structure of TFT substrates, induces additional LC dislocations, reduces LCD brightness, and increases response time [30]. However, since electrode patterning was a continuation of established manufacturing processing, fringe field patterned
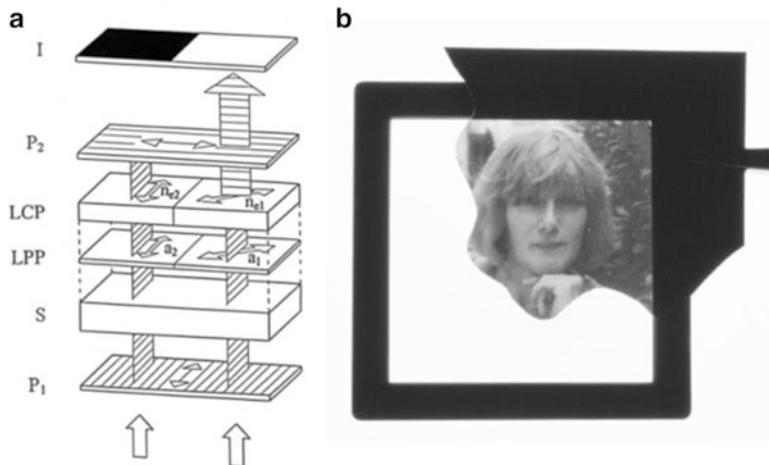
Fig. 7.10 (**a**) Partially switched, slightly off-vertical LC director configuration of LPP photo-aligned dual-domain VAN-LCD. (**b**) LPP photo-aligned, 40″ Sharp TFT-MVAN-LCD TV; partly switched 4-domain MVAN director configuration (*inset*)

TFT-MVAN-LCDs for large-sized television LCDs were introduced first by Sharp, Samsung, and others in 2000. In order to reduce LCD power consumption and response time and simultaneously increasing display brightness, Sharp changed in 2009 to LPP photo-alignment in its gen10 Sakurai plant and renamed the technology UV2A. Figure 7.10b shows an LPP photo-aligned, 40″ Sharp TFT-MVAN TV; the inset depicts a partly switched, LPP photo-aligned 4-domain MVAN director configuration [48].

### 7.3.4 Photo-Alignment/Pattering of Liquid Crystal Polymers (LCP) on Single Substrates
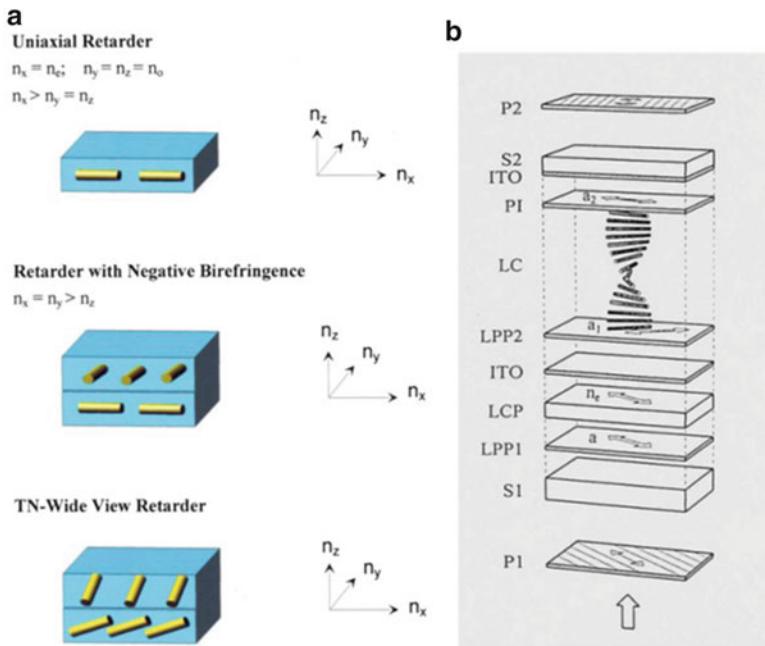
The LC molecules of field-effect liquid crystal displays are surface-aligned by *two* substrates; i.e., they are confined in a sandwich configuration which exerts uniaxial aligning forces to bottom *and* top adjacent LC layers (Fig. 7.9a). During his research on photo-alignment of LCDs, the author wondered whether and to what extent anisotropic photo-aligning forces could be transferred into the bulk of a liquid crystalline film deposited on a *single* aligned substrate. Moreover, he wondered whether not only monomer LCs but also liquid crystal polymers (LCPs) could be photo-aligned on single substrates. If feasible without optical defects he envisaged interesting liquid crystal polymer configurations and anisotropic optical thin-film devices [49]. However, in 1995 it was unknown how far the aligning information on a single aligned surface would extend into a prepolymer LCP film whose top surface is exposed to air. It was also not known whether adjacent photo-patterned pixels exhibiting different aligning directions would maintain their respective surface

Fig. 7.11 (**a**) Photo-aligned/photo-patterned LCP retarder on substrate S between crossed polarizers. (**b**) LCP retarder image visible only between crossed polarizers

alignment information in the bulk of the LCP film. Director coalescence due to interfering elastic deformations at the pixel boundaries [57] and thermal disorder were likely to occur. Moreover, it was questionable whether photo-patterned prepolymer configurations would survive subsequent polymerization without destruction of macroscopic order causing optical defects. Based on the above LPP photo-alignment technology, the author started the development of photo-alignment of liquid crystal polymer films on single substrates with his coworkers in the early 1990s [30]. The target was photo-alignment and optical patterning of liquid crystal polymers on single substrates of glass, plastic, metal, silicon, paper, etc. The author and coworkers first achieved copying the molecular surface alignment information (uniaxiality and bias tilt) and transferring it into the bulk of adjacent prepolymer LCP films via long-range LC order in the mid-1990s [58, 59]. Fixation of liquid crystal prepolymer configurations by subsequent polymerization at room temperature by unpolarized UV light without optical defects proved feasible. Moreover, due to optical bias tilt generation, the direction of the slow optical axes of LCP films enabled arbitrarily 3D director alignment in space [60]. The concept is illustrated by the following few examples.
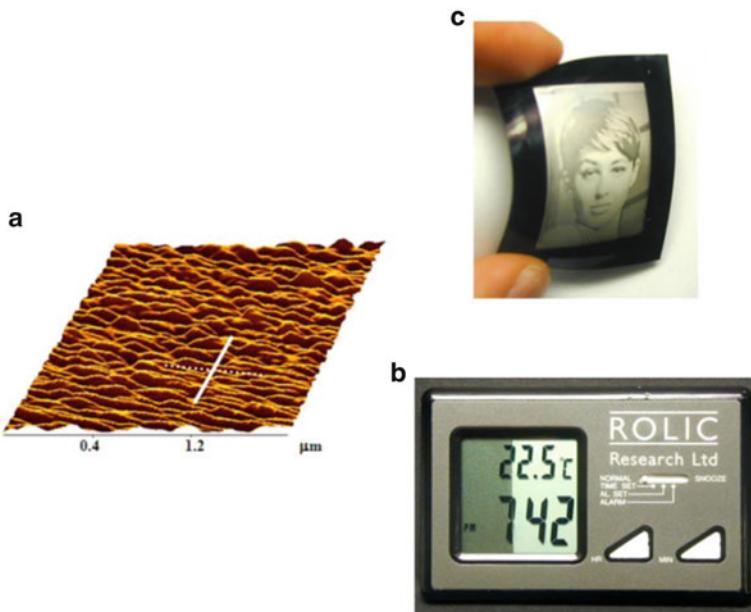
The two LPP-aligned and photo-patterned LCP pixels in Fig. 7.11a schematically depict the operating principle of a 1 μm thin photo-aligned/photo-patterned half-wave retarder on the transparent substrate S viewed between crossed polarizers [58]. The LCP director in the right pixel defines the slow optical retarder axis ne1 of the birefringence ellipsoid. The direction of ne1 copies the underlying photo-aligning direction a_1 of the photo-patterned, 40 nm thin photo-alignment film. The angle between a_2 and a_1 is 45°. Therefore, incident linear polarized light P_1 is rotated by $\pi/2$ in the right pixel rendering it transmissive. Since the alignment direction a_2 and the slow optical axis n_{e2} in the left pixel are parallel to P_1,

Fig. 7.12 (**a**) Photo-aligned LCP retarder integrated onto the substrate of a photo-aligned LCD. (**b**) Black–white super twisted nematic (STN)-LCD with integrated color compensating a-plate LCP retarder

the polarization state of the left pixel is not affected and appears black between crossed polarizers (Fig. 7.11a). By combining the optical LCP retarder patterning concept of Fig. 7.11a with photo-alignment through digital photomasks, not only high-resolution retarder images with gray scale reproduction became feasible but also photo-patterned retarders for 3D LCDs [49, 59]. Figure 7.11b shows an early example of a photo-patterned LCP retarder image between partly crossed polarizers made by the author and coworkers in 1995. Since optical retarder images are only visible in polarized light, photo-aligned/photo-patterned LCP films enable transmissive and reflective optical security elements [49].

Due to the large optical anisotropy of LCP molecules, alignment and photo-patterning of LCP films enables very thin, complex, chiral, and non-chiral optical polymer retarder films and LCP film stacks with photographic resolution, patterned dichroic guest–host polarizers, loss-free polarization interference filters for projection optics, etc. [49]. Moreover, due to LPP bias tilt generation the direction of the slow optical axes of LCP films can be arbitrarily photo-aligned in space and different films can be stacked [60]. Examples for different LCP director configurations in optical retarders are depicted in Fig. 7.12a. Figure 7.12b shows a photo-aligned LCP retarder which is directly integrated onto the substrate of a photo-aligned LCD [58]. The integrated a-plate retarder converts the

Fig. 7.13 (**a**) AFM profile of a uniaxial aligned nano-corrugated LCP surface topology. (**b**) Reflective TN-LCD clock whose conventional diffuse reflector is replaced by a high-gain metalized diffuse directional MC reflector (*right*). (**c**) High-resolution directional diffuse MC reflector image on plastic substrate

interference colors of a super twisted nematic (STN)-LCD into a black–white STN-LCD.

Last but not least, the above optical generation of anisotropic surface interactions on single substrates and their transfer into adjacent liquid crystalline materials developed by the author and coworkers also enables anisotropic phase separation and anisotropic surface diffusion in liquid crystalline mixtures consisting of monomer and cross-linkable prepolymer components. In 2001 Ibn-Elhaj and Schadt have shown that anisotropic 3D phase separation can optically be induced in films of liquid crystal mixtures coated on uniaxial aligned/patterned surfaces. In principle monomer corrugation (MC) mixtures consist of a monomer liquid crystal (LC) and a liquid crystal prepolymer (LCP), where only the latter is photo-cross-linkable [61]. After film coating, directional phase separation is induced in the MC mixture by crosslinking its LCP component with flush UV light. Subsequent removal of the (liquid) LC component leaves uniaxial aligned nano- and micro-corrugations in the remaining cross-linked solid LCP film. The AFM profile in Fig. 7.13a depicts a uniaxial aligned nano-corrugated LCP surface topology, exhibiting elongated grooves aligned parallel to the underlying LPP photo-alignment direction of the substrate [61]. Photo-aligned and patterned nano- and micro-topologies on substrates enable interesting optical thin-film devices, such as efficient diffuse directional broadband reflectors which preserve polarization, high-resolution directional diffuse reflectors, diffractive

polymer film topologies, uniaxial polymer nano-topologies enabling liquid crystal alignment via minimizing the elastic deformation energy of adjacent LC films [41, 61], etc. The photograph in Fig. 7.13b shows a digital clock with a TN-LCD whose conventional diffuse reflector (right) is replaced by a much brighter metalized diffuse directional MC reflector [61]. Figure 7.13c shows a photo-aligned and photo-patterned high-resolution directional diffuse MC reflector image on a plastic substrate [61].

7.4 Sealants for One Drop Fill (ODF) Process
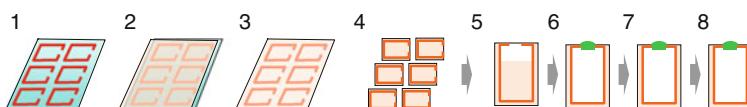
Masanori Matsuda

7.4.1 Introduction
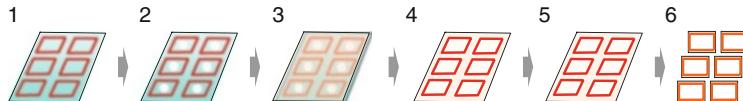
In recent years the LCD market has seen a rapid growth because of a variety of technological innovations, the *one drop filling* (ODF) method being one of the most important innovations. During the dawn of the LCD era, cells were produced by vacuum injection, a method for injecting the liquid crystal material inside cell inside pressure is reduced [62]. The ODF method was developed to challenge the problems in the production of LCDs with large cell sizes and increased display dimensions. The ODF method started from the production of fourth-generation LCDs [63] and has now been adopted in almost all plants from the second- to the tenth-generation LCD.

7.4.2 Characteristics of the ODF Technique

In order to fill an LC cell with an LC material in the conventional vacuum filling technique the following steps are necessary: (1) application of the thermosetting sealant, (2) sealing with substrate, (3) thermal curing of the sealant, (4) cutting, (5) filling with LCs, (6) filling the injection port, (7) UV curing, and (8) thermal curing (Fig. 7.14). In the vacuum injection method, the injection time becomes longer with increasing cell size, reaching 20 h for sizes of 20 in. or so [64].

Fig. 7.14 Process of vacuum injection method. (1) Sealant dispensing. (2) Sealing. (3) Thermal curing. (4) Cutting. (5) LC filling. (6) End filling. (7) UV curing. (8) Thermal curing

Fig. 7.15 Process of one drop filling (ODF) method. (1) Sealant dispensing. (2) LC dropping. (3) Sealing under vacuum. (4) UV curing. (5) Thermal curing. (6) Cutting

On the other hand, some steps in the manufacturing processes can be combined and the overall process significantly simplified by the ODF method: (1) application of ODF sealant, (2) dropping of the LC, (3) sealing with substrate in vacuum, (4) UV curing, (5) thermal curing, and finally (6) cutting (Fig. 7.15). Furthermore, the injection time increased exponentially with cell size for the vacuum injection method, but the ODF method has a constant filling time regardless of cell size. Thus productivity is shortened to 1–2 h per substrate.

The ODF method is thus characterized by a very high productivity, but the usual thermosetting sealant cannot be used and thus, a new ODF sealant was required. Whereas in the vacuum injection method the liquid crystal material is in contact with the sealant after complete cure, the impact of ODF sealant on the display quality of the LCD can be very large [65]. ODF sealant comes into contact with the LC in an uncured state and before the heat curing stage (5), making it possible for uncured material to seep into the LC material. Looking at each process, we aimed at reducing as much as possible the effect on the display quality.
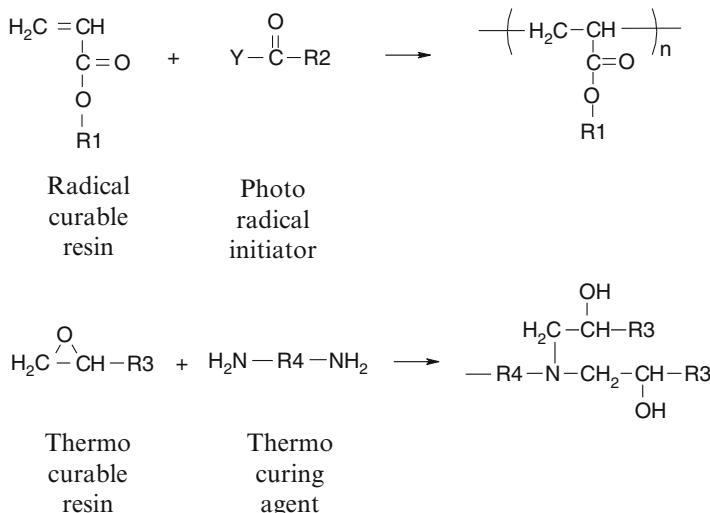
7.4.3 Composition and Role of ODF Sealant

To minimize the negative impact on display quality as described above the following points are important for ODF sealant: (a) disconnection prevention during thermal curing and (b) high enough adhesive strength during thermal curing.

Therefore, in general, a thermal curing resin contains a radical curable function that is activated by light and a hardening agent. Acrylic resins such as urethane acrylate and epoxy acrylate are mainly used for the radically curable resin, and an epoxy resin is mainly used for thermal curing. The reaction mechanism due to the heat and UV irradiation are shown in Fig. 7.16.

The display quality of the LCD depends not only on the liquid crystal and the quality of the alignment film but also on the photo initiator, thermal curing agent, and the blending ratio of each material. Because it is the main material of the ODF sealant, the dispensing properties, adhesion, low contamination, and reliability of the UV-curable resin are important ingredients affecting the LCD.

The photo-radical initiator requires a UV irradiation apparatus that can be used in the LCD manufacturing process. Because it is used in combination with metal halide lamps and low wavelength (320–380 nm) cut filters, the absorption

Fig. 7.16 Reaction mechanism of ODF sealant

wavelength region of the photo-radical initiator is important. Latent curing agents are commonly used as hardeners and the thermal curing temperature greatly differs depending on their molecular structure. The combination of the resin and thermo-curing agent is also important because many heat curing agents affect pot life.
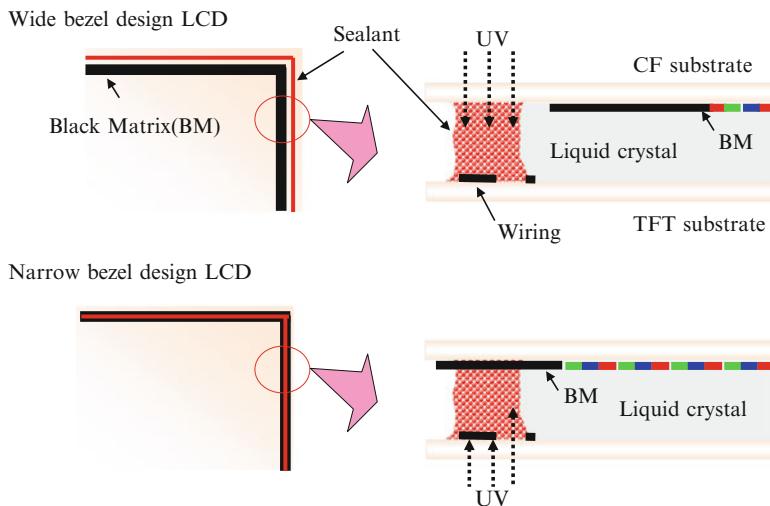
7.4.4   Quality Requirements

Next, I describe the main quality requirements of ODF sealants.

7.4.4.1   Dispensing Properties

The ODF sealant is dispensed by a dispensing machine after mixing with gap material and conductive material and filled in a syringe under vacuum by the LCD manufacturer. The viscosity and the thixotropic index of the ODF sealant depend largely on dispensing properties, and the optimal combination of resin and fillers is important, too.

The demands for optimal dispensing properties have been increasing in recent years due to narrower bezels of the LCD, which requires the dispensing of thinner lines of the ODF sealant. Furthermore, the dispensing properties depend on the pot life of the ODF sealant. If pot life is short, constant dispensing becomes difficult because the viscosity of ODF sealant increases over time. Depending on the production status of the user, a pot life of 48 h or more is required after syringe filling. Therefore, the selection of the thermo-curable resin and curing agent is important in order to prolong pot life.

Fig. 7.17 LCD bezel design and UV irradiation side for sealant

7.4.4.2 UV Curing Property

The purpose of UV irradiation is to prevent breakage of the ODF sealant and elution of its components at curing temperature. The irradiation beam typically has an intensity of 100 mW/cm^2 for 30 s, which equals 3,000 mJ/cm^2 at a wavelength of 365 nm. This dose can be several times larger for small displays as mobile devices with large shaded area. Also, the presence or absence of a mask to protect the liquid crystal during UV irradiation affects the UV dosage. Covering the ODF sealant line by a mask greatly reduces its reaction rate.

Optimum sealant and UV condition are necessary for manufacturer processes. The influence of the ODF sealant on display quality depends on the LC material, the alignment layer, and the ODF sealant, but it has to be noticed that the influence of the panel design, because the ODF sealant is applied to the bezel part of the panel [66].

In a wide bezel design, such as in TVs, it is possible to ensure a space between the ODF sealants that can be fully exposed to the UV outside the black matrix (BM), for example. On the other hand, in narrow bezel panels, such as **UV** for mobile applications, the ODF sealant would be applied directly below the BM and cannot be cured by UV from the color filter substrate side. Therefore, it needs to be cured by UV radiation from the TFT substrate side, but because of the metal wiring on the TFT substrate, curing by UV irradiation may be insufficient (Fig. 7.17). So a well UV-curable ODF sealant under a large shaded area is necessary for narrow bezel and TFT substrate side UV irradiation panels. Thus, the product development and combinations of UV-curable resins and photo initiators need to match the panel design process of LCD manufacturers to provide the best products.

7.4.4.3 Thermo-curable Property/Pot Life

The goal of the thermal curing may be summarized in two points: improved adhesion and improved reliability. Typical thermal curing conditions are 120 °C for 1 h, regardless of the specifications of the LCD in general. This can be controlled to some extent by a combination of heat curable resin and a hardener. By lowering the melting point of the thermal curing agent, and by increasing the solubility to the resin, the curing time can be shortened. But the pot life decreases because the viscosity of the ODF sealant increases by reactions that proceed at room temperature. On the other hand, if one focuses on pot life, higher heating temperatures and longer curing times are required.

Strictly speaking, the pot life depends on the dispensing equipment and the magnitude of the allowable range for the viscosity of the ODF sealant. LCD manufacturer wants long pot life ODF sealants and we have developed one which can be used for 1 week at room temperature.

7.4.4.4 Contamination Control

Because the uncured ODF sealant is in contact with the liquid crystal, it is necessary to use a material that has an as small as possible impact and that does not elute into the liquid crystal. Because eluted components may also contaminate the alignment film, it is necessary to use a material with little effect on the alignment film.

Among the ODF sealant components, solubility in the liquid crystal is relatively high for thermo-curable resin compared to the radically curable resin. Therefore the blending ratio of the thermo-curable resin and radical curable resin is important in order to suppress elution into the liquid crystal. Our product is a formulation which suppresses the elution of the liquid crystal by increasing the ratio of the radical curable resin as much as possible. Further, since the photo-radical initiator has a higher contamination effect, both contamination and reactivity are important.

7.4.4.5 Adhesion

Adhesive surfaces of the ODF sealant are ITO, alignment films, BM, and insulating films. In general, the ODF sealing compound has a high adhesive force with respect to ITO, but there is a tendency of low adhesion onto the alignment layer, especially for vertical alignment. There is little overlap of the ODF sealant with the alignment film in the case of a large TV, but 50 % of the seal line width overlaps with the alignment layer when it comes to narrow frame designs in mobile displays. High adhesion has been required by thinner glass substrates for weight reduction and thinning of the seal line due to the narrower frame of the mobile in more recent years.

Optimizing the filler and resin content in the ODF sealant for high adhesive strength runs contrary to other characteristics.

So we also think it is worth to approach from modifying of surface of substrates for adhesion. If peeling occurs, it is important to analyze which surface is peeled off. For example, if the ODF sealant is present on the BM or the insulating film, the peeling seemingly occurred at the sealant/BM or sealant/insulating film interface. But actually it may occur at the BM/ITO or insulating film/ITO interface.

7.4.4.6 Reliability

The reliability of ODF sealant concerns the deterioration over time of display quality and adhesive strength after LCD manufacture. Elution of components of the ODF sealant to active areas and invasion of moisture from outside to the display deteriorate display quality. In order to raise reliability, it is important to raise the reaction rate, lower moisture permeability, and increase adhesive strength of ODF sealants.

7.4.5 Summary

ODF sealant technology was fighting with display quality problems from the beginning of its development. ODF sealants have many constituent materials compared to the vacuum injection method. The curing mechanism is also complex and the contact of the uncured material with the liquid crystal was the main cause of problems. Initially, product development focused on the solubility in the liquid crystal material. But, we found out that defects could be reduced by strengthening UV curing ability, and we developed the new type ODF sealant. So this technology became mainstream for current products.

However, in recent years we saw the introduction of new narrow LCD and a further reduction in LCD frame size. Those new devices are difficult to make with conventional products, and thus it is necessary to further improve quality of ODF sealant.

References

1. C.W. Oseen, Trans. Faraday Soc. **29**, 883 (1933)
2. F.C. Frank, Discuss. Faraday Soc. **25**, 19 (1958)
3. J.L. Ericksen, Arch. Rat. Mech. Anal. **4**, 231 (1960); **9**, 371 (1962)
4. F.M. Leslie, Quart. J. Mech. Appl. Math. **19**, 357 (1966); Arch. Rat. Mech. Anal. **28**, 265 (1968)
5. P.G. de Gennes, J. Prost, *The Physics of Liquid Crystals*, 2nd edn. (Clarendon, Oxford, 1993)
6. S. Chandrasekkar, *Liquid Crystals*, 2nd edn. (Cambridge University Press, Cambridge, 1992)
7. I.W. Stewart, *The Static and Dynamic Continuum Theory of Liquid Crystals, A Mathematical Introduction* (Taylor & Francis, London/New York, 2004)

8. A.M. Sonnet, E.G. Virga, *The Dissipative Ordered Fluids, Theories for Liquid Crystals* (Springer, New York, 2012)
9. T. Carlsson, F.M. Leslie, Liq. Cryst. **26**, 1267 (1999)
10. D. Dummur, T. Sluckin, *Soap, Science, and Flat-Screen TVs* (Oxford University Press, New York, 2011)
11. P.C. Martin, O. Parodi, P.S. Pershan, Phys. Rev. A **6**, 2401 (1972)
12. H. Pleiner, H.R. Brand, Hydrodynamics and Electrohydrodynamics of Liquid Crystals, in *Pattern Formation in Liquid Crystals, Chapter 2*, ed. by A. Buka, L. Kramer (Springer, Berlin, 1996)
13. P.M. Chaikin, T.C. Lubensky, *Principles of Condensed Matter Physics* (Cambridge University Press, Cambridge, 1995)
14. T.C. Lubensky, Symmetry and the Physical Properties of Liquid Crystals, Part 2, Chapter 1, in *Progress in Liquid Crystal Science and Technology, In Honor of Shunsuke Kobayashi's 80th Birthday*, ed. by H.-S. Kwok, S. Naemura, H.L. Ong (World Scientific, Singapore, 2013)
15. L.D. Landau, E.M. Lifshitz, *Theory of Elasticity*, 3rd edn. (Pergamon Press, New York, 1986)
16. D. Forster, T.C. Lubensky, P.C. Martin, J. Swift, P.S. Pershan, Phys. Rev. Lett. **26**, 1016 (1971)
17. O. Parodi, J. Phys. (Paris) **31**, 581 (1970)
18. D. Forster, Ann. Phys. (NY) **85**, 505 (1974)
19. H. Yoshida et al., Abstract of ILCC, I10 (2002)
20. Y. Yamada et al., SID 11 Digest, 160 (2011)
21. M. Schadt et al., Jpn. J. Appl. Phys. **31**, 2155 (1992)
22. Y. Iimura et al., J. Photopolym. Sci. Technol. 257 (1995)
23. H. Yoshida et al., Jpn. J. Appl. Phys. **36**, L428–L431 (1997)
24. Y. Tasaka et al., Digest of AM-LCD'98, 35 (1998)
25. K. Miyachi et al., SID 10 Digest, 579 (2010)
26. K. Hanaoka et al., SID 04 Digest, 1200 (2004)
27. H. Yoshida et al., SID 00 Digest, 334 (2000)
28. Y. Nakanishi et al., Digest of AM-LCD 2000, 13 (2000)
29. T. Sakurai et al., SID 10 Digest, 724 (2010)
30. M. Schadt, Jpn. J. Appl. Phys. **48**, 1 (2009); Naturwissenschaftliche Rundschau **741**, 117 (2010); J. Eur. Acad. Sci. **1**, 1 (2011)
31. M. Schadt, K. Schmitt, V. Kozinkov, V. Chigrinov, Jpn. J. Appl. Phys. **31**, 2155 (1992). US Patent US 5,389,698 (1991)
32. J. Cognard, Mol. Cryst. Liq. Cryst. Suppl. **1**, 1–74 (1982)
33. M. Schadt, W. Helfrich, Mol. Cryst. Liq. Cryst. **17**, 355 (1972)
34. T.J. Scheffer, J. Nehring, Appl. Phys. Lett. **45**, 1021 (1984)
35. M. Schadt, F. Leenhouts, Appl. Phys. Lett. **50**, 236 (1987)
36. N.A. Clark, S.T. Lagerwall, Appl. Phys. Lett. **36**, 899 (1980)
37. J. Fünfschilling, M. Schadt, Digest SID **99**, 308 (1999)
38. M. Schadt, P.R. Gerber, Mol. Cryst. Liq. Cryst. **65**, 241 (1981)
39. L.T. Creagh, A.R. Kmetz, Mol. Cryst. Liq. Cryst. **24**, 59 (1973)
40. J.L. Janning, Appl. Phys. Lett. **21**, 173 (1972)
41. D.W. Berreman, Phys. Rev. Lett. **28**, 1683 (1972)
42. A.M. Lackner, J.D. Margerum, L.J. Miller, W.H. Smith Jr., Mol. Cryst. Liq. Cryst. **199**, 37 (1991)
43. K. Ichimura, Y. Suzuki, T. Seki, A. Hosoki, K. Aoki, Langmuir **4**, 646 (1988)
44. W.M. Gibbons, P.J. Shannon, S.T. Sun, B.J. Swetlin, Nature **351**, 49 (1991)
45. M. Dumont, Z. Sekkat, SPIE **1774**, 188 (1992)
46. V.G. Chigrinov, H.-S. Kwok, H. Hasebe, H. Takatsu, H. Takada, J. SID. **16/9**, 897 (2008)
47. M. Schadt, H. Seiberle, A. Schuster, Nature **381**, 212 (1996). US Patent US-6,215,539 (1995)
48. H. Seiberle, M. Schadt, SID Proc. Asia Display'98, 193 (1998); J. SID. **8/1** Soc. Inf. Disp. 67 (2000)
49. M. Schadt, Ann. Rev. Mater. Sci. **27**, 305 (1997)
50. M. Schadt, Mol. Cryst. Liq. Cryst. **364**, 151 (2001)

51. E. Hoffmann, H. Klausmann, E. Ginter, P.M. Knoll, H. Seiberle, M. Schadt, Proc. **SID98**, 737 (1998)
52. R. Kiefer et al., SID Proc. IDRC92, 547(1992);. M. Oh-e et al., Proc. SID Japan Display'95, 577 (1995)
53. M.F. Fahrenschon, K. Schiekel, Appl. Phys. Lett. **19**, 301 (1971)
54. F.J. Kahn, Appl. Phys. Lett. **20**, 199 (1972)
55. J. Chen, K.C. Chang, J. DelPico, H. Seiberle, M. Schadt, Proc. SID99, 98 (1999)
56. A. Takeda et al., Proc. SID98, 1077(1998)
57. E.P. Virga, M. Schadt, Jpn. J. Appl. Phys. **39**, 6637 (2000)
58. M. Schadt, H. Seiberle, A. Schuster, S. Kelly, Jpn. J. Appl. Phys. **34**, 3240 (1995)
59. M. Schadt, H. Seiberle, A. Schuster, S. Kelly, Jpn. J. Appl. Phys. **34**, L764(1995). US 5,602,661 (1993)
60. C. Benecke, H. Seiberle, M. Schadt, Jpn. J. Appl. Phys. **39**, 525 (2000)
61. M. Ibn-Elhaj, M. Schadt, Nature **410**, 796 (2001); Jpn. J. Appl. Phys. **42** (2003). EP-1230319 (1999)
62. T. Yukinari, Electronic Materials and Parts, **58** (1992)
63. Y. Sato, '04 Newest Liquid Crystal Process Technology, 78 (2008)
64. T. Ishizu, 2nd New JSPMI Prize (2004)
65. T. Asano, Monthly DISPLAY, 46 (2006)
66. M. Matsuda, Japanese Liquid Crystal Society Forum (2008)

Chapter 8
Next-Generation Liquid Crystal Displays

**Hideo Fujikake, Hirotsugu Kikuchi, Toru Fujisawa,
and Shunsuke Kobayashi**

8.1 Flexible Displays

Hideo Fujikake

8.1.1 Role of Liquid Crystal Displays in Information Society

8.1.1.1 Possibilities for Liquid Crystal Displays

The development of information industry in recent years is largely attributable to
the eminent development of flat-panel display technology as an interface between
people and information. The innovation of flat-panel displays will pioneer the
possibility of new information services in the future. Even though there are many
different display types including plasma display panels and organic light-emitting

H. Fujikake
Tohoku University, Sendai, Japan
e-mail: fujikake@ecei.tohoku.ac.jp

H. Kikuchi
Kyushu University, Fukuoka, Japan
e-mail: kikuchi@cm.kyushu-u.ac.jp

T. Fujisawa
DIC Corporation, Saitama, Japan
e-mail: toru-fujisawa@ma.dic.co.jp

S. Kobayashi
Liquid Crystal Institute and Department of Electrical Engineering,
Tokyo University of Science in Yamaguchi, Japan
e-mail: kobayashi@rs.tus.ac.jp

diodes, the liquid crystal display evolved from small to large area and used many different optical operation modes, such as projection, reflective, and semi-transmissive displays.

The evolution and adaptation of a liquid crystal display for various applications is due to the basic principle of being a non-emissive display type. Because the two basic functions of light source and light modulation are separated, the individual performance can be optimized depending on the requirements and applications. In addition, elements of both technologies are rich in diversity, and by integration and combination, the degree of freedom in display design is large and extremely flexible systems can be achieved.

For example, large screen liquid crystal display currently have been developed that use glass substrate panels with a diagonal of more than 100 in. Such ultra-large screen displays become part of the wall and evolve into highly realistic video systems to even influence the lighting and atmosphere of the room. High resolution is also progressing with large screen liquid crystal panels, beyond the current high-definition ($1,920 \times 1,080$ pixels), towards ultra-high-definition panels (4 K system; $3,840 \times 2,160$ pixels and 8 K systems; $7,680 \times 4,320$ pixels) for next television broadcast services.

Liquid crystal displays are evolving in terms of image quality. Contrast characteristics have been improved by the innovation of the panel components and sophistication of the liquid crystal alignment control. A drastic improvement of contrast ratio is possible by dimming control of the backlight. In addition, dynamic and local control of the backlight has become an effective method to save power and its importance has increased recently. Also in terms of color reproduction, the use of light-emitting diodes in backlights in recent years and the introduction of laser diodes in the near future will further enhance color gamut of liquid crystal displays. The quality of the video images has been greatly improved by increasing driving frequency and frame rates of the liquid crystal panels.

On the other hand, the current panel manufacturing technology has reached a mature stage and a paradigm shift is required in order to promote industrial development and new applications. In that sense, flexible displays are the most promising next-generation technology of a new concept. Displays turned from box-type cathode-ray tubes to thin flat-panel displays. The next step is to evolve into flexible structure at last. It can be said that the display is a human interface for communicating information and its appearance is going to be less and less felt.

8.1.1.2 Impact of Flexible Liquid Crystal Displays

In science fiction novels and movies that deal with the near future, alongside with three-dimensional holographic displays, displays that can be folded have appeared frequently as future technology items. However, the specific path for the realization of such a flexible display has become clear as recent flat-panel display technology is maturing. At present, the term "flexible display" is becoming more widely used, and it becomes essential as a next-generation display technology.
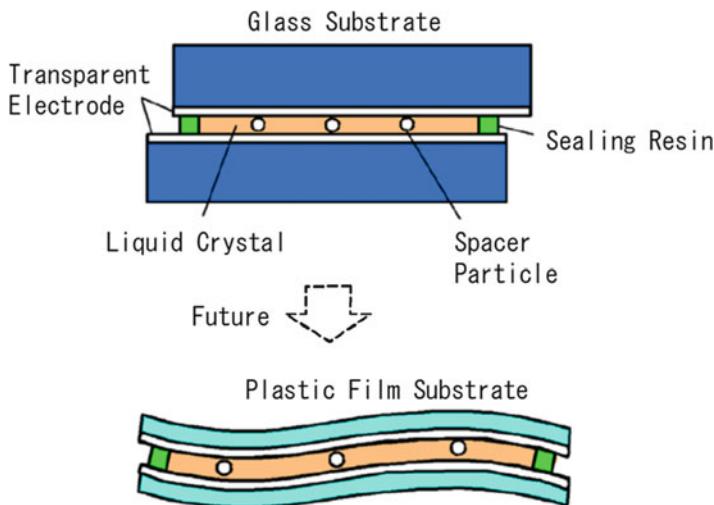
Fig. 8.1 Possible applications for various flexible displays

By making displays flexible, the freedom of display design becomes spread borderless, based on their excellent portability, storability, and installability. As a result, a flexible display can create a variety of new human interfaces (Fig. 8.1). Therefore, it can be said that flexible displays form the ultimate evolution of flat-panel displays.

For example, by carrying a display panel, in conjunction with a wireless network technology, it is possible to easily enjoy various information contents and to promote a ubiquitous information society. In the recent past, even medium-sized displays have required a bag to carry, but flexible displays can be stored in a pocket. The effect of flexible displays is particularly prominent on the video service field, using portable tablet devices to enjoy realistic images. The advantages of flexible displays are enhanced for large displays. Superlarge screen displays used for the next-generation Super Hi-Vision with a diagonal of 100 in. or more can be easily installed in the home by carrying a roll through the door. In addition, space-saving curved screens can be effectively used in room corners.

Such large and flexible displays will influence our daily necessities in a variety of living conditions. Therefore, we expect that the technology infrastructure provides a vast amount of real-time information services in the future to present necessary and appropriate information.

Fig. 8.2 From hard to soft substrates in liquid crystal display panel structure evolution

Below, we will explain the basic structure and operating principle of flexible liquid crystal displays, their panel production method, design of the flexible backlight, demonstration of full-color display panels, and introduction of active matrix drive technology.
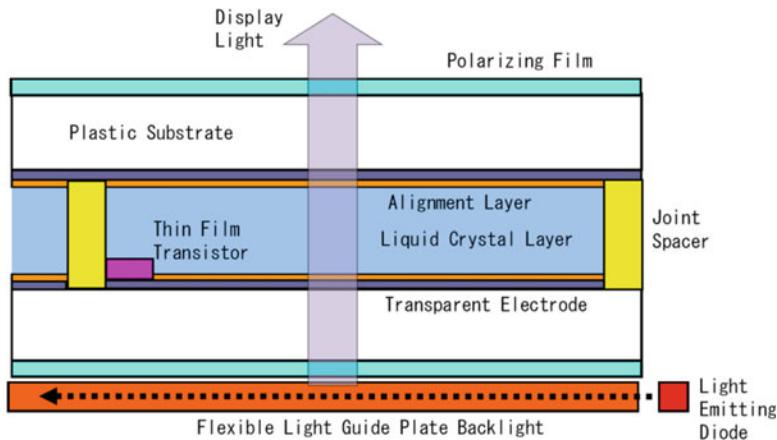
8.1.2 Towards the Development of Flexible Liquid Crystal Displays

8.1.2.1 Advantages of Liquid Crystal Method

The large degree of freedom in system design is a big driving force for the evolution of flexible displays. One important tool to adapt flexibility for liquid crystal displays is a plastic substrate.

Currently, the thickness and weight of the liquid crystal displays have been reduced by polishing the two glass substrates. The introduction of a plastic substrate is its logic extension. Thereby, it is possible to realize a display panel that does not crack even though it is very thin and has light weight. By using a filmlike thin plastic substrate, it becomes possible to freely bend a liquid crystal panel (Fig. 8.2). Efforts towards flexible displays have been made not only in the field of the liquid crystal displays but also in the field of organic light-emitting diode. Various flexible display types have been proposed, and the liquid crystal method shows important advantages especially in the following three points:

1. Panel manufacturing and drive technology that have been accumulated for glass-substrate liquid crystal displays can also be used for plastic substrate, which will accelerate the development of large-area and high-resolution panels.

**Fig. 8.3** Fundamental device structure for flexible display
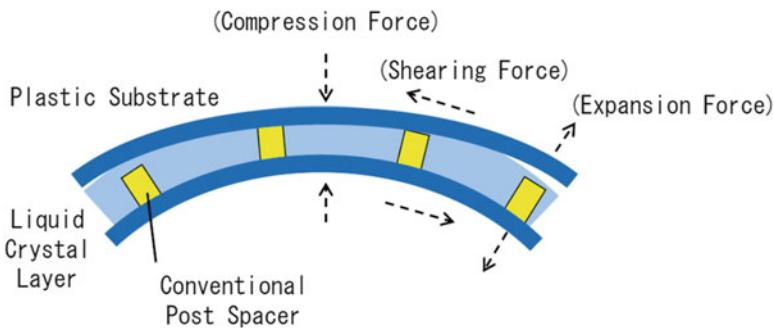
2. The time degradation of liquid crystal materials without electronically excited molecular states is not recognized in contrast to materials for organic light-emitting diodes. Therefore, stable display operation is guaranteed.
3. The backlight control can adapt to the illumination situation in various environments. Furthermore, power-saving displays are also possible.

On the other hand, the drawback is the complex panel structure that consists of several components, such as the two plastic substrates, two polarizers, and a backlight system, which is disadvantageous for ultrathin and ultrasoft panels.

### 8.1.2.2   Technology Issues to Be Overcome
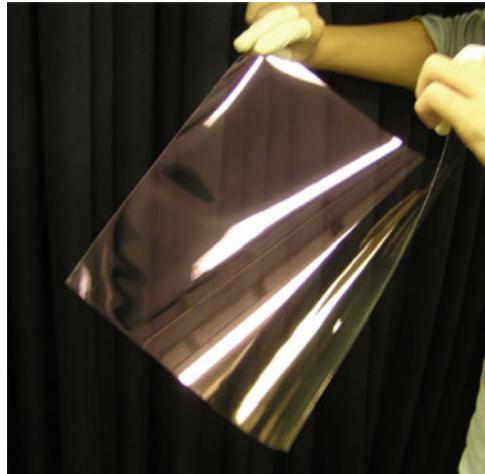
During researching device structure and fabrication (Fig. 8.3), concrete technical problems have been encountered. Main breakthrough technologies that are required include thin-film transistors to be formed at low temperature, spacer technology for stabilizing the gap between the substrates sandwiching the liquid crystal, flexible backlight, and the plastic substrate. Among them, the most pressing issue is the construction of a new spacer to improve the panel structure that holds the flexible plastic film substrates.

If you configure the flexible display by replacing the glass substrates with plastic substrates, fatigue fracture of the liquid crystal layer will not occur during bending, but the liquid crystal layer needs to be kept in a uniform thickness between the two substrates [1]. In flexible liquid crystal displays using plastic substrates, the thickness of the liquid crystal layer changes in response to a variety of external forces, and the light modulation characteristic is changed, which leads to distorted display images. In conventional rigid panels, particle spacers and post spacers have been used (Fig. 8.4) to tolerate compression force on the panel, but a new spacer concept is needed to tolerate both compression and expansion forces upon bending.

Fig. 8.4 Deformation of plastic-substrate-based liquid crystal panel using conventional post spacers

**Fig. 8.5** Photograph of flexible plastic film substrate
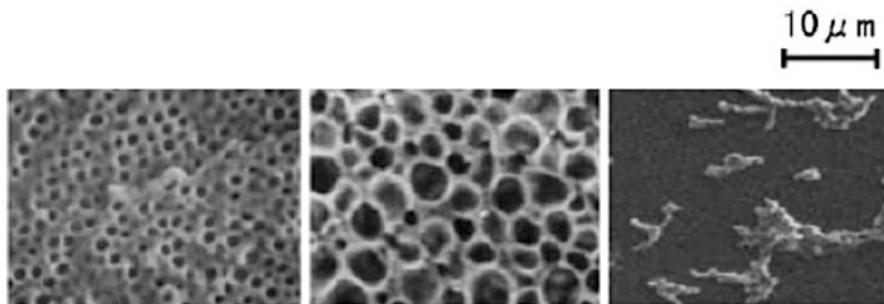
8.1.3 Spacer Technology Using Polymer Dispersion

8.1.3.1 Liquid Crystal Polymer Composite Film

Therefore, a flexible liquid crystal panel consisting of two thin plastic substrates needs joint spacers to keep the plastic substrates in a constant and determined gap.

In order to realize a flexible video display with a large screen, we have investigated a flexible liquid crystal display using a microstructured polymer. The plastic film substrates (Fig. 8.5) of display panel are supported by a liquid crystal/polymer composite film that is a self-holding elastic sheet. This composite film is used as an adhesive and spacer and is also responsible for light modulation. Since the entire surface bonds the two substrates, it can withstand shearing as well as expansion force, and seal resin breakage of the panel outer periphery by stress concentration can be prevented.
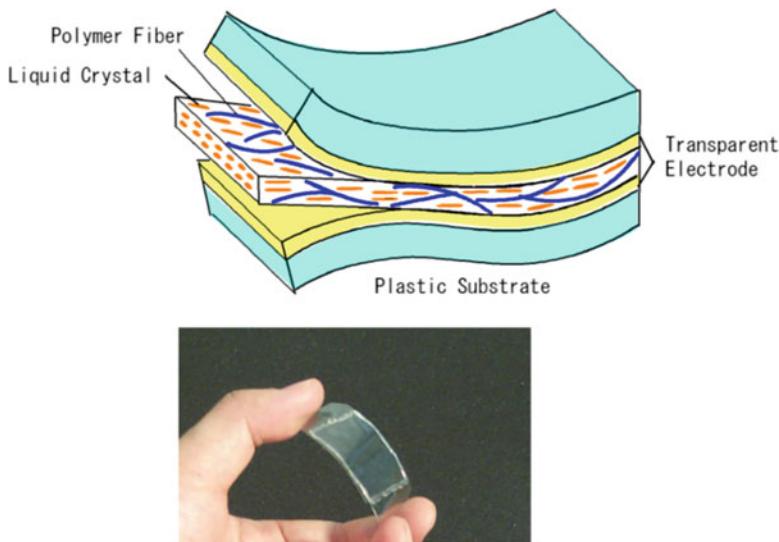
Fig. 8.6 Morphological control of segregated polymers

In this composite film, the polymer structure must not disturb the liquid crystal alignment. That is, it needs to maintain the highly ordered liquid crystal alignment (that is indispensable for the high-contrast light modulation) in the dispersion structure of the polymer. Therefore, the composite film preparation uses the phase separation of polymer and liquid crystal materials with molecular alignment, as described below.
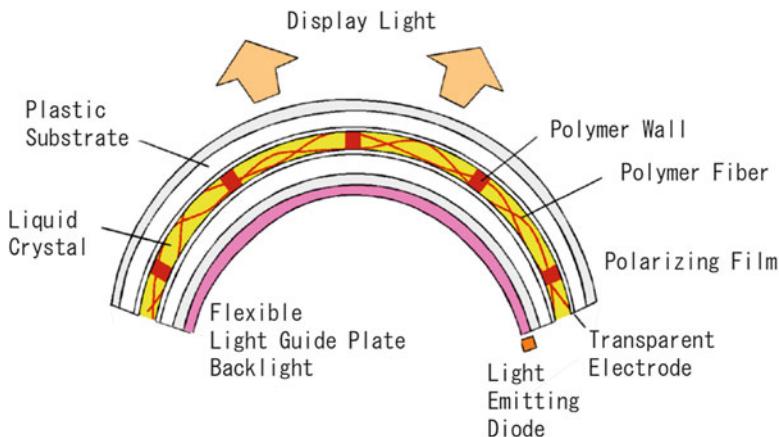
Recently, a method of forming a liquid crystal/polymer composite film has been invented in which a homogeneous mixture of the monomers and liquid crystal is polymerized. During polymerization, a phase separation occurs, because the polymer components become insoluble in the low molecular weight liquid crystal solution and aggregate.

Photopolymerization by irradiation with ultraviolet light irradiation [2] in particular is known as a method having excellent controllability of polymer dispersion structure. With decreasing monomer concentration, the aggregating morphology from phase separation changes from liquid crystal droplets to bubble-shaped cellular polymer structure and to polymer fiber networks, as shown in Fig. 8.6.

Thus we used a nematic phase mixture solution consisting of low molecular weight liquid crystals and liquid crystalline monomers (photo-curable monomer in which the acrylate group was directly and rigidly attached to the mesogen of liquid crystal molecular skeleton) that could easily be oriented between the alignment layers on substrates. Photopolymerization resulted in a phase-separated structure with a high purity liquid crystal and submicron polymer networks (Fig. 8.7). Thus, it is possible to construct the hard polymer fiber networks along the liquid crystal alignment direction, and the polymer networks also have a stable substrate spacing function [3]. Because the polymer networks are grown so as not to inhibit the molecular flow in the nematic phase solution with one-directional molecular alignment during the ultraviolet irradiation, fibers extending in the direction of the liquid crystal alignment are formed. In addition, after the polymer has cured completely, the networks play the role to stabilize the liquid crystal molecular alignment. Thus, a flexible liquid crystal device having good contrast characteristics becomes possible.

Fig. 8.7 Flexible liquid crystal device containing polymer fiber networks (*top*, structure; *bottom*, photograph)

Fig. 8.8 Total flexible display system using liquid crystal with polymer walls and fibers

8.1.3.2 Introduction of Polymer Walls

In order to enhance the bending resistance of the display panel as shown in Fig. 8.8, we decided that, in addition to a network of polymer fibers, lattice-shaped polymer "walls" [4] should be introduced. Furthermore, we developed an easy method in which two fine polymer elements of wall and fiber are separately formed from a
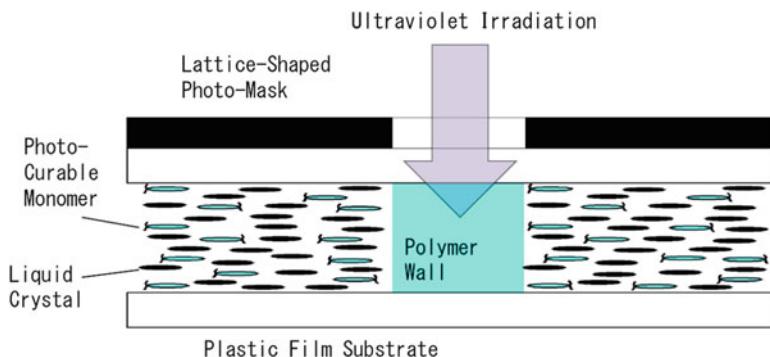
Fig. 8.9   Forming principle of polymer walls in liquid crystal layer
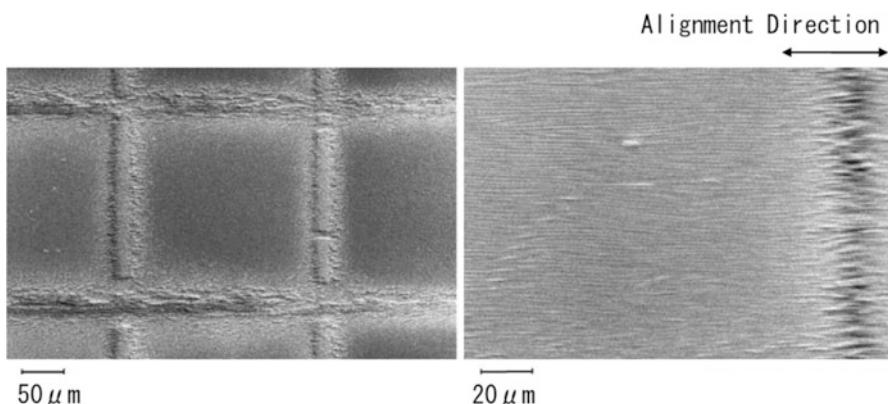
Fig. 8.10   Scanning electron micrographs of polymer walls (*left*) and polymer fibers (*right*)

single monomer material. The polymer formation method utilizes two-stage exposure using ultraviolet light as follows.

The same monomer in the solution is used for both the wall and the fiber structures. Therefore, the concentration of monomer has to be increased. First, the wall-patterned exposure of ultraviolet light is made through an orthogonal lattice-like photomask (Fig. 8.9). The suspended monomer diffuses in the illuminated solution region and continues to aggregate. As the result, both substrates are connected by the segregated dense polymer wall.

Then the second ultraviolet exposure is performed after removing the optical mask. The concentration of remaining monomers which was left in the unexposed area leads to the formation of low-density polymer fiber networks in the display area of the device. Figure 8.10 shows the formation of the polymer networks and walls (the width of the wall is approximately 20 μm). From the figure, it becomes clear that the polymer surface morphology of the fibers and walls shows a significant anisotropy and an alignment in the rubbing direction of the polyimide alignment layers coated on the substrate.

This is because the polymer fibers and walls are formed in the molecular-aligned solution by oriented polymerization in the rubbing direction. Therefore, no birefringence of the formed polymer occurs under crossed Nicol polarizers, and a good contrast characteristic is easily obtained with suppressed black level in the off-state.

Incidentally, the use of polymer fibers and walls as spacer is not limited to future flexible display application; the spacer technique for bonding and fixing substrates is also useful in the practical usage field of superlarge glass-substrate liquid crystal displays. Those display screens are prone to a gap variation between the substrates due to the large weight of the glass substrates, which leads to image display distortions. If those screens could be made with the above adhesive spacers, this problem would be solved.

8.1.4 Introduction of Various Liquid Crystal Materials

8.1.4.1 Ferroelectric Liquid Crystal

It is possible to use a liquid crystal material in various ways depending on the application in flexible display. In order to stabilize the substrate spacing, polymer walls and fibers allow also the application of ferroelectric liquid crystal, whose molecular alignment structure is conventionally known to be fragile and called as smectic layers.

For realizing a fast response display with excellent moving image quality, the ferroelectric liquid crystal [5] is thought to be an ideal liquid crystal material, but it is difficult to form stable and uniform liquid crystal alignment. We have found that the smectic layered structure is stabilized against thermal shock and mechanical shock and shows a self-recovering ability, when ferroelectric liquid crystal is dispersed in dense rigid polymer fibers with a surface anchoring force. Thereto, the molecular switching in the low molecular weight ferroelectric liquid crystal is not bound or restricted by the molecular structure of the polymers by a clear phase separation. The fast response time for rise and decay operation is ensured to be 1 ms or less for obtaining high moving image quality.

The surface-stabilized ferroelectric liquid crystal in a conventional contrast was limited to binary display operation. In order to display a natural color image including gradation, it is necessary to obtain grayscale capability. Therefore, we realized the grayscale-capable display by two methods with polymer dispersion. First, we formed a polymer composite film by dispersing nonliquid crystalline monomers of low concentration (3 % by weight). The fine dispersion structure to reach the molecular order exerts a subtle alignment control effect to the liquid crystal; the polymer thereby changes spatially threshold voltage for switching the liquid crystal molecules. Therefore, the spatial distribution of switching domains is induced, in order to vary continuously according to the applied voltage intensity, and the area ratio of the microscaled binary domains exhibits a spatial grayscale function.

Because it is based on the bistable liquid crystal switching, the device in this device also has the memory function of the halftone levels.

Subsequently, in order to keep the grayscale display reproducibility and to obtain mechanical stability for holding the substrate, by adding the liquid crystal-line monomers of high concentration (20 wt%), the molecular-oriented polymer fibers (sub-μm diameter) were finely dispersed in ferroelectric liquid crystal. The formed polymer fibers with molecular alignment were segregated through phase separation of liquid crystal and polymers, in order to exert a strong anchoring force from short range for ferroelectric liquid crystal. The cone angle of liquid crystal switching reaches full angle of 90°, and the rotation of the liquid crystal molecules is monostable into fiber alignment direction. As a result, the electro-optical properties obtain the V-shaped curve symmetrical to 0 V. The V characteristic is useful in the same manner as the conventional nematic liquid crystal displays, for bipolar voltage driving scheme using thin-film transistors, to prevent unstable display operation such as image sticking or afterimage.

Further, by achieving hardening of the polymers by high strength ultraviolet irradiation as well as reducing the polymer concentration to 15 wt%, it was possible to lower the drive voltage until normal operating voltage of prevailed thin-film transistors. For the composite structure mingled at the molecular level, where the high-concentration polymers of such do not phase-separate the liquid crystal in macroscopic scale, the tangled fixed polymer chain inhibits movement of the liquid crystal molecules, and low-voltage operation cannot be expected.

8.1.4.2   Nematic Liquid Crystal and Cholesteric Liquid Crystal

For wide range applications of flexible display, selecting a liquid crystal material according to each application is desirable. Therefore, besides the ferroelectric liquid crystal above with the aim of moving image display with high quality, flexible low-cost displays using nematic liquid crystal are also useful.

For example, with the aim of inexpensive simple display, a twisted nematic liquid crystal device [6] is resistant for variation of substrate spacing. Formation of twisted-alignment polymer walls is useful to hold two substrates and can have good contrast ratio. This is because the light leakage from the walls is suppressed to be small.

Further, two thick rigid polarizing films spoil device flexibility to be unnecessary. Therefore, guest–host twisted liquid crystal devices with dichroic dyes [7] were fabricated to absorb the all-polarization-angle incident light. In this device, a nematic liquid crystal with low birefringence is introduced, and optical rotation effect is suppressed in the twisted liquid crystal layer. The contrast ratio of the display is inferior, but the guest–host nematic liquid crystal of twist orientation is suitable for simple text display.

In addition, we have proposed and fabricated a device dispersing polymer walls in cholesteric liquid crystal [8] having the wavelength selective reflection for electronic paper applications. In this case, the control of the changing twist pitch (deciding the wavelength of the reflected light) will be the developing technical point when the polymer walls are segregated and formed.

8.1.5   Development of Peripheral Technology

8.1.5.1   Printing Process and Transfer Process

We also introduced flexographic printing method for the coating process of a liquid crystal monomer solution during the forming of the composite film. In this printing method, the mixed solution thickness is controlled with high accuracy, and we can accurately select the coating area by relief structure on a printing drum. Furthermore, the coated solution film is sandwiched by the substrate of another one by using a conventional film laminator with a pressing roller. The printing and laminating processes such as above are extremely useful in large-area fabrication of the flexible liquid crystal panel.
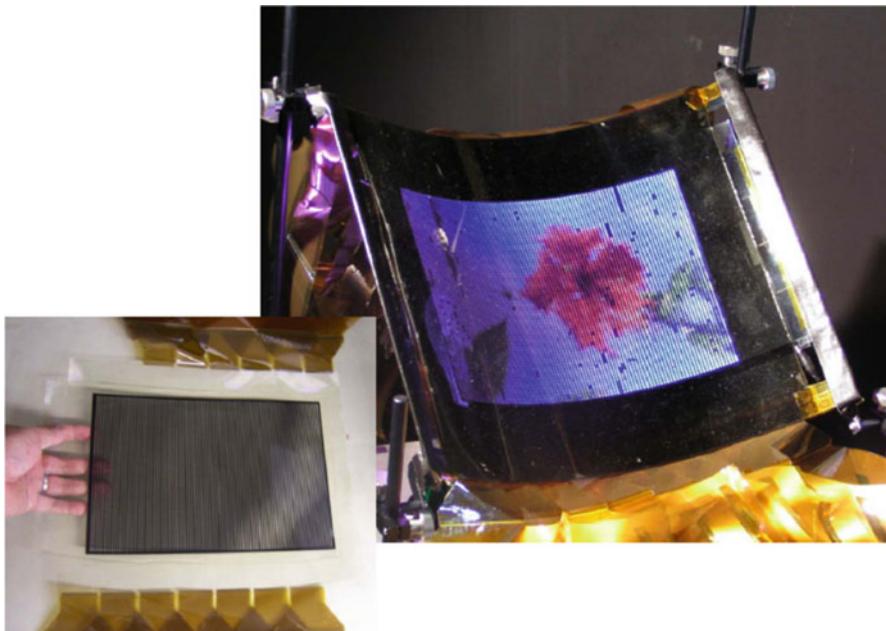
Also, to configure the display, a fine pixel structure including metal wiring, transparent electrodes, and black matrix must be accurately formed on a flexible plastic substrate. The dimensional stability of plastic substrates to solvent exposure and heating process is generally inferior to that of glass substrates, in the conventional photolithography for forming a high-precision fine pixel structure in large area. So we applied the transfer method from the glass substrate. That is, after the pixel pattern is precisely formed in reverse order on the glass substrate by photolithography, the pattern is peeled off from the glass substrate by bonding a plastic substrate, resulting in being transferred to the plastic substrate.

By the printing process and the transfer method, display panel fabrication up to A4 size has become possible. In Fig. 8.11, the display panel actually fabricated is demonstrated. Since the thin plastic substrates are rigidly bonded with a polymer composite structure, the displayed images are not disturbed even when the panel is bent.

8.1.5.2   Color Display Scheme

In order to colorize a flexible display, we have developed two panel-driving methods of micro color filter [9] and field sequential color. The former is based on mixing three-primary-color fine pixels that cannot be identified with the human eye. In most of the liquid crystal display existing, this method is used. Using the transfer method of the above, high-precision fine microfilter of three primary colors is fabricated on a plastic substrate.

Color scheme in another way is to switch the three-primary-color images in speed high enough where people cannot discriminate flicker, based on color-mixing visual effects by afterimage. In this method, in synchronization with the backlight of light-emitting diodes that emits three-primary-color lights sequentially, the liquid crystal panel is fast rewritten at 180 Hz rate. In this scheme, high-speed response is required for the liquid crystal panel. We have realized a full-color display panel using fast response ferroelectric liquid crystal so far. We obtained an advantage of high light efficiency because there is no light loss caused by the color filters with light absorption.

Fig. 8.11 Demonstration of A4-sized flexible liquid crystal panel made by printing and transfer techniques

8.1.5.3   Flexible Backlight

In reflective displays of cholesteric liquid crystal for electronic paper with power saving by using external ambient light, a backlight system is not needed. On the other hand, similar to the liquid crystal displays existing, in order to obtain a color image with excellent visibility with a high contrast ratio, the backlight system is indispensable. Currently, for a backlight for a liquid crystal display, the light-emitting diodes with high color purity have progressed, so we also developed two flexible backlight systems.

Our first backlight system is a direct illumination method, and a two-dimensional array of fine light-emitting diode chips with three primary colors is surface-mounted on a thin polyimide film used for flexible printed circuit board. In this case, via a light diffusion plastic film and a transparent optical spacer thick vinyl sheet, the light-emitting diode backlight and the flexible liquid crystal panel are stacked and laminated to obtain a uniform illumination light. This method has the advantage of good heat dissipation, and a dynamic local dimming control of the backlight is also possible to obtain high contrast and power saving.

In order to obtain a flexible backlight with high light usage efficiency, the light-guide plate [10] using a thin transparent silicone rubber is fabricated as shown in Fig. 8.12. As edge light source, we mounted thin light-emitting diode chips of three

Fig. 8.12 Flexible light-guide plate backlight using small light-emitting diodes
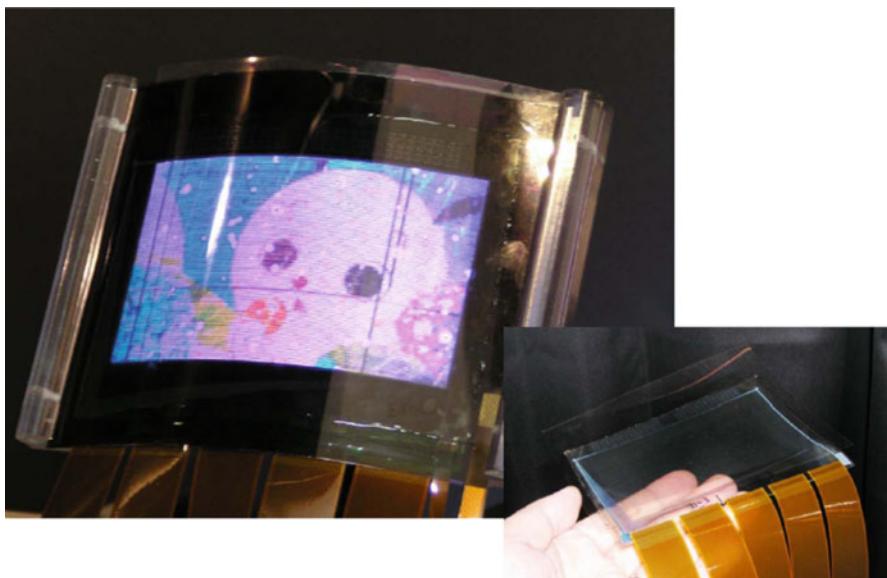
primary colors on the side surface of the light-guide plate. The backlight in this method is flexible and thin and has features such as high light efficiency and low cost with fewer light-emitting diode chips.

8.1.5.4   Thin-Film Transistor

In order to obtain a high-contrast display, a flexible liquid crystal display using plastic substrates requires an active matrix driving. The driving method is effective for simplifying driving circuit and reducing the panel electric connection and wiring. In scanning drive by the voltage pulse, an active electronic device like field-effect transistor having switch/memory functions is required in each pixel, which maintains the display state after the selected period finishes.

For realizing an image display with high contrast and high resolution, we have developed the thin-film transistor array for driving the liquid crystal polymer composite film. In the active matrix driving scheme, we introduced the polycrystal Si thin-film transistor technology of low-temperature formation (maximum process temperature, 150 °C or less) suitable for high-resolution high-speed driving with high mobility. As the result of the development of the flexible liquid crystal panel [11] using a heat-resistant substrate, color display operation has been successfully obtained (Fig. 8.13, 5.1 in. diagonal, 128 × 72 pixels).

To obtain the thin-film transistor array suitable to softening the panel, flexible 5 inch diagonal liquid crystal displays were also fabricated by lower-temperature vacuum deposition of the organic semiconductor (pentacene). The fabricated panel (QQVGA, 160 × 120 pixels) has confirmed the video display function [12].

Fig. 8.13 Fabricated flexible display driven by active matrix method with polycrystal Si thin-film transistors

In both the active matrix display panel using the fast response liquid crystal and the three-primary-color light-emitting diode backlight, full-color display operation is achieved by a field sequential color driving method.

As for the formation of fine thin-film transistor array, photolithography is often used now, but significant effort to continuously produce the panel by a roll-to-roll process with printing technique has also been made for the future. The steady progress in roll-to-roll manufacturing technology is expected for highly productive large-area screen flexible liquid crystal displays.

8.1.6   Development of the Future

Through the development of a plastic-substrate-based liquid crystal device stabilized by liquid crystal polymer composite film, a foundation of various techniques is established towards flexible displays. The features of small-sized displays are light weight and robustness not to crack. On the other hand, in a wide range of applications from medium-sized portable devices to stationary-usage large screen panels, flexible electronic device technology using plastic substrates has a huge impact.

To make rapid progress towards the practical use and commercialization of a small- and medium-sized flexible liquid crystal displays, the flexibility, tolerance, and screen size must be determined according to the specific applications.

Furthermore, in order to obtain large screen high-resolution flexible liquid crystal panel, novel fabrication technique for forming a fine pixel structure on a plastic substrate is essential.

To support it, these days, peripheral technology has also prepared. For example, organic electronics using organic semiconductors and conductors and printable electronics associated with high precision attract a great deal of attention for next-generation flexible displays.

We believe that it is important to continue to evolve a flexible display fabrication technology for the near-future information-oriented society.

## 8.2   Blue Phase Displays

Hirotsugu Kikuchi
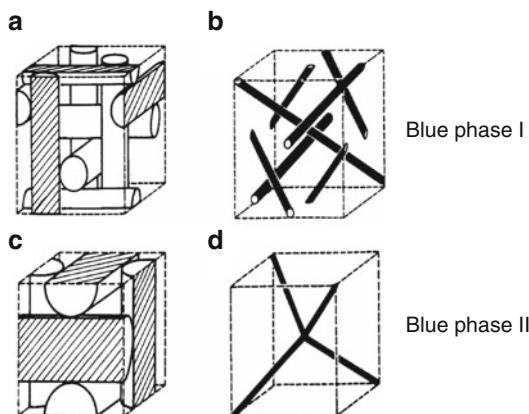
8.2.1   *Characteristic Properties of Blue Phases*

Blue phases appear in a small temperature range between the chiral nematic phase with a sufficiently short helical pitch length and the isotropic phase. The blue phase has very peculiar characteristics [13–15]:

1. It exists in a narrow temperature range (typically a few kelvin).
2. It is optically isotropic.
3. It is optically active.
4. There are three types, named blue phase I (body-centered cubic), blue phase II (simple cubic), and blue phase III (isotropic symmetry) with increasing temperature.
5. The lattice constants of the unit cells of blue phases I and II are typically a few hundred nm, and the phases show Bragg diffraction in the ultraviolet–visible range. The name "blue phase" originates from the color of the diffracted light; many actually appear bluish, but some do not.

There is a record of the observation of a blue phase in 1888 when a liquid crystal compound was discovered. However, serious research started in the 1970s and blue phases were recognized in the academic world as specific liquid crystal phases in the 1980s. Two major reasons for why these phases failed to catch the attention of

Fig. 8.14 Structure of blue phase I (**a**, **b**) and blue phase II (**c**, **d**). Blue phase I has body-centered cubic symmetry, and blue phase II has simple cubic symmetry. (**a**) and (**c**) show the chiral cylinder and (**b**) and (**d**) the disclination lines

Blue phase I

Blue phase II

researchers are that they did not exhibit birefringence and the stable temperature range was extremely narrow. It was unavoidable that the blue phase was misunderstood to be a transient phenomenon during a phase transition because the identification of the blue phase as an intrinsic liquid crystal phase was difficult only by polarizing microscopal observation. After the concept of frustration was introduced in blue phase studies in the 1980s, the understanding of the blue phase was further deepened. One of the characteristic properties of blue phases is the complicated and three-dimensional hierarchical structure that will be introduced in the next chapter.

8.2.2 Structure of Blue Phases

Blue phases I and II show cubic 3D lattice structures. Figure 8.14a–d shows the unit cell structures of blue phases 1 and II, respectively. Blue phases I and II have a body-centered cubic lattice structure and a simple cubic lattice structure, respectively, with lattice constants of several 100 nm.

Figure 8.14a, c shows double twist cylinders, and the bold black lines in Fig. 8.14b, d show disclinations (defect lines). In each double twist cylinder, the molecules are radially twisted towards each other through 90°. The molecules are parallel to the cylinder axis at the cylinder center and are tilted by 45° at the outer radial periphery. In other words, the molecules twist from −45° to +45° through the cylinder, which corresponds to a quarter pitch. The diameter of a double twist cylinder is typically about 100 nm, and a simple calculation shows that approximately 200 molecules with a diameter of 0.5 nm mildly twist against each other. The lattice constant for blue phase I corresponds to a one helical pitch, and the lattice constant for blue phase II corresponds to one half helical pitch. We generally see a very small mismatch in pitch length with that of the lower-temperature chiral nematic phase. Peculiar to soft matter, a complex hierarchical structure is formed in

a self-organized manner as a result of repetitively twisted molecular alignment. It is interesting to see that behind this structure is a frustration between space topologies that smoothly connect the doubly twisted geometry and space. I refer to review articles in textbooks [13, 15] about frustration. A disclination (a type of defect line), which stems from frustration, is formed as if to run through the corner where the three double twist cylinders orthogonally come close to one another. The symmetry of the disclination geometry is body-centered cubic in blue phase I and simple cubic in blue phase II. It is estimated that the diameter of a disclination core is about 10 nm and the inner molecular alignment is thought to be disordered. Although details are not yet certain, blue phase III has also been identified; it is presumed that its structure is amorphous and that there is only doubly twisted, short-range order.

Due to the giant periodic structure discussed above, the blue phase exhibits Bragg diffraction in the ultraviolet-to-visible range. Blue phase I mainly exhibits diffraction from the (110), (200), to (211) planes, and blue phase 2 shows diffraction from the (100) to (110) planes. Hence, there are several reflection peaks, which is not the case with the chiral nematic phase. Typically, the diffractions from the (110) and (200) planes in blue phase I and from the (100) plane in blue phase II are in the blue region, which is the origin of the name "blue phase."

8.2.3 Polymer-Stabilized Blue Phase
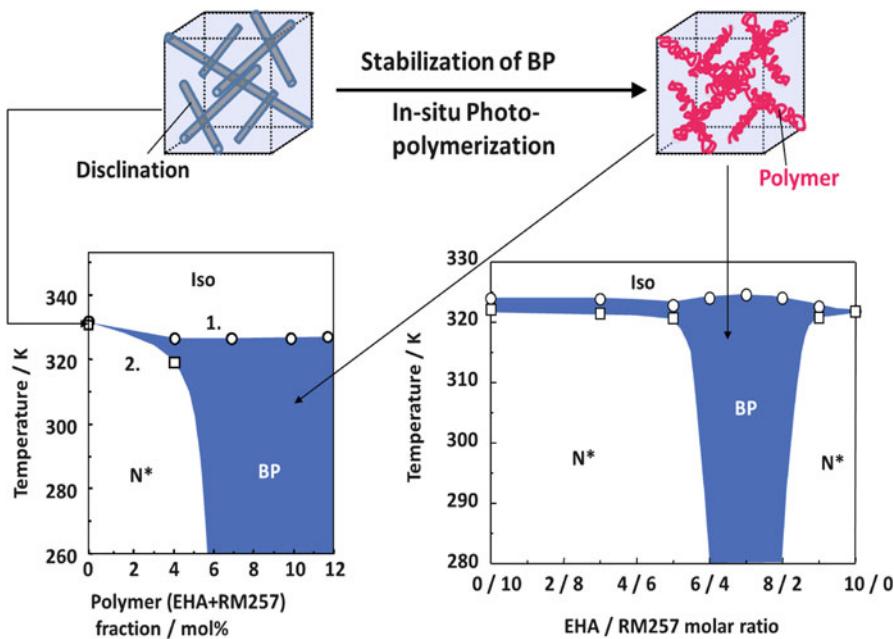
It has long been believed that the temperature range of the blue phase is small and cannot be extended. Recently, however, many attempts have been made to address this issue.

In 1993, Kitzrow et al. formed a blue phase with polymerizable crystal monomers: the monomers were polymerized in the blue phase, which immobilized the molecules, thus preserving the blue phase structure in the solid resin [16]. In this type of material, although the characteristics of the blue phase structure had been preserved, the dynamics of the liquid crystal had been lost because all molecules had been polymerized and thus immobilized to a certain extent.

Then in 2002, the author and coworkers reported that the temperature range of a blue phase could be increased to over 60 K by forming a small amount (7–8 wt%) of polymers in the blue phase; the material was named the "polymer-stabilized blue phase" (Fig. 8.15) [17]. The molecular dynamics are not lost in the polymer-stabilized blue phase, and moreover, the electro-optical response is very fast. It is believed that the polymers in the blue phase condense around disclinations and the blue phase is stabilized when the disclinations are thermally stabilized.

In 2005, Yoshizawa et al. synthesized T-shaped liquid crystal molecules and achieved a temperature range of 13 K for the blue phase [18]. They suggested that the biaxial nature played an important role.

In 2005, Coles et al. reported a temperature range as large as 44 K in the cooling process for a dimeric liquid crystal with strong flexoelectricity [19]. They suggested that flexoelectricity stabilizes disclinations. It is interesting, from an application

Fig. 8.15 Polymer-stabilized blue phases. The monomers were 2-ethyl hexyl acrylate and 2-methyl-1,4-phenylene-bis(4(3(acryloyloxy)propyloxy)benzoate) (RM257, Merck)

standpoint, that the diffraction wavelength of the blue phase lattice varies reversibly with the electric field.

As discussed above, technologies have recently been advanced in important ways to solve the problem of the narrow temperature range of the blue phase, and we now believe strongly in the prospective future for the blue phase.

Let us consider the role of the polymer in the polymer-stabilized blue phase (PSBP) from the viewpoint of the thermodynamic interaction between the liquid crystal and the polymer. A feature of the blue phase is that it must coexist with disclination lines, and the very existence of the disclinations is the reason why the temperature range of the blue phase is small. Looking at it from the opposite direction, the blue phase could be stabilized by the disclinations.

In general, the thermodynamic stability of a phase and the temperature range of a stable phase result from a competition with other phases on the higher- and lower-temperature sides. In the case of a PSBP, the thermodynamic balance between the blue phase and the chiral nematic phase can be changed by the polymer, because the temperature range of the PSBP is extended towards the lower-temperature side, that is, into the chiral nematic phase. In the blue phase and chiral nematic phase, double and simple twist alignments compete with each other. If the double twist alignment dominates, the blue phase occurs, and vice versa. Because the double twist alignment cannot continuously fill three-dimensional space, the blue phase must coexist with disclinations that form a regular network with cubic symmetry. Basically, the
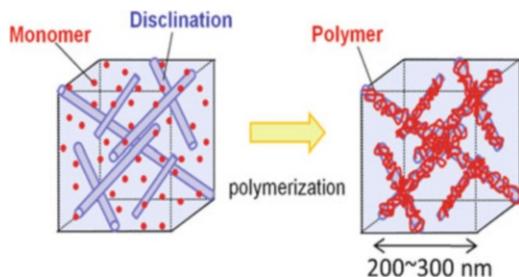
phase transition temperature of the lower side of the blue phase is determined by the relative stability of the single and double twist alignments. When the phase is heated up and the temperature comes close to the isotropic phase, the blue phase readily appears, because the coexistence of the disclinations becomes more allowable. As a result, blue phases appear in the temperature region just below the isotropic phase.

There is a contrast between liquid crystals and polymers with respect to entropy. In general, the entropy of soft matter can be separated into two parts corresponding to the translational and rotational motion of the molecules or chain segments. The orientational ordering of liquid crystals is based on an increase in the entropy of the translational freedom of the molecules, i.e., the packing entropy, while that of the random coils of the polymer is due to the maximized entropy of the rotational freedom of the chain segments. Therefore, the mixing of a liquid crystal with orientational order and a polymer forming random coil reduces the mutual entropy; as a result, the miscibility of both is generally very poor and phase separation readily occurs. Therefore, compositions comprised of liquid crystals and polymers induce varying competitive and/or cooperative interactions between them, resulting in unique behavior.

It has been suggested in a recent study that when polymers are generated and propagated in a blue phase, the resulting polymers are possibly concentrated in the areas of the disclinations [20]. The disclinations in the blue phase should be fixed by the polymer and should not disappear even when the phase transition into the chiral nematic phase takes place. Therefore, the disclination-free state, which is the only advantage of the chiral nematic phase over the blue phase, is lost. The balance between both the phases is changed, and the blue phase is stabile at a lower temperature. In other words, the blue phase is stabilized over the chiral nematic phase, because the disclination, which is a negative characteristic, becomes a common feature for both phases. Because the polymer has little influence on the phase transition between the blue phase and the isotropic phase, which is on the high-temperature side of the blue phase, it does not play a role in stabilizing the molecular orientational order as in other polymer-stabilized liquid crystals, such as in polymer-stabilized cholesteric textures.

It is also meaningful to discuss the phenomenon of polymer assembly in the disclination from the viewpoint of entropy. As mentioned above, the orientational order of liquid crystals is induced by the entropy of translation, while the random coils of polymers are due to the entropy of rotation. The coexistence of a liquid crystal and a polymer causes a conflict between the different entropies. The polymers in the liquid crystal phase thus assemble in the disclination region, where the orientational order is lowered and the polymers can maximize their conformational entropy. A satisfactory coexistence is then self-sufficiently achieved by cooperation between the blue phase (which must have disclinations) and the polymer (which tends to be excluded from the ordered region). The elastic energy of the liquid crystal orientational field that accumulates around the disclination also plays an important role in the diffusion of the polymer. The curvature of the director increases closer to the disclination core. The elastic energy, which is proportional

Fig. 8.16 The monomer is randomly distributed, but after polymerization, the polymer aggregates in the disclinations
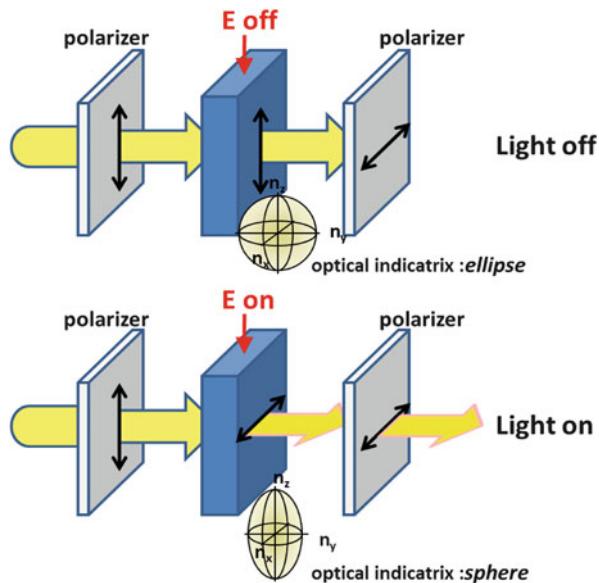

to the square of the director curvature, increases divergently near the disclination core. The orientational order should be small or zero at the areas being very close to the disclination core because the elastic energy exceeds the thermal energy to disorder, which is approximately the latent heat of the nematic–isotropic phase transition. If a random coil polymer or small particle with a certain volume comes closer to the distorted director field, it should be increasingly attracted towards the disclination core, because the elastic energy corresponding to its volume is reduced. Therefore, the polymers synthesized by in situ polymerization within a blue phase are drawn more to the disclination as the molecular weight increases, resulting in the fixation of the disclinations and stabilization of the blue phase (Fig. 8.16).

8.2.4 Electro-optical Effect and Driving Method

Because blue phases are optically isotropic without an electric field, a dark field can be obtained under crossed polarizers if the Bragg diffractions due to the lattice structure are shifted out of the visible wavelength range. The index ellipsoid is then a sphere. Therefore, initially there is no viewing angle dependence originating from the phase structure. However, when an electric field is applied, anisotropy or birefringence appears in the direction of the electric field as the optical axis. If the dielectric anisotropy of the host liquid crystal is positive, the index ellipsoid becomes stretched in the direction of the electric field. Conversely, a flattened ellipsoid contracted in the direction of the electric field is obtained if the dielectric anisotropy of the host liquid crystal is negative. Therefore, the blue phase exhibits electric field-induced birefringence of the type that can be switched between optical isotropy and anisotropy, i.e., from zero to finite birefringence, as shown in Fig. 8.17. The induced birefringence is proportional to the square of the electric field at small fields, which is known as the Kerr effect. This type of electro-optical effect is significantly different from that in conventional liquid crystals, where the initial state is anisotropic, and the optical axis changes with the electric field. Electric field-induced birefringence also exists and the Kerr effect has been confirmed in PSBPs, their related materials, and polymer-stabilized isotropic liquid crystals, which is referred to as the pseudo-isotropic phase. In the pure blue phase, i.e., free from polymers, a local reorientation of the molecules, a lattice distortion, and a

Fig. 8.17 The display mode of blue phases. *Upper figure*: dark state under crossed Nicols in the absence of an applied electric field, because the blue phase is optically isotropic. *Lower figure*: bright state, because the blue phase becomes optically anisotropic upon application of an electric field and an appropriate retardation is induced in the electric field direction
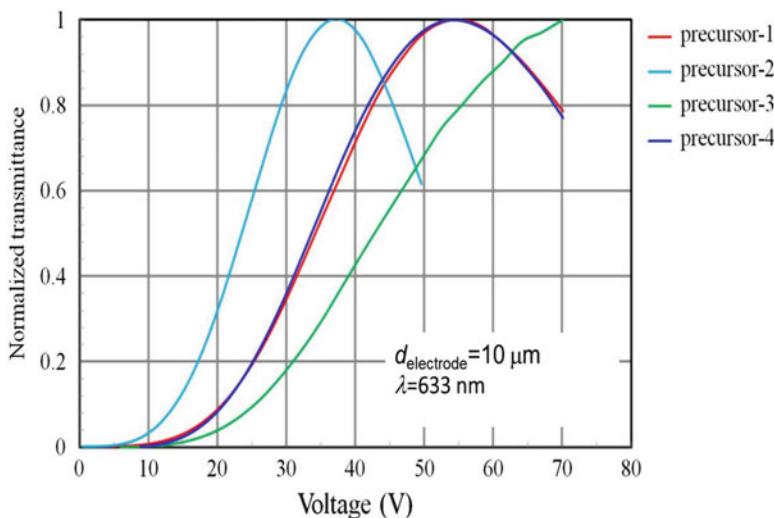

phase transition occur as the electric field increases. In the PSBP, the latter two effects are suppressed, and only the high-speed local reorientation of the molecules remains after polymer stabilization. Therefore, PSBPs show a fast electro-optical response of less than 1 ms.

To exploit the electric field-induced birefringence in display applications, the polarization of the incident light through the optical retardation produced by the induced birefringence is simply controlled in a manner similar to the mode of retardation control used for in-plane switching (IPS). If a simple comb-shaped IPS electrode is used for the device, the optical axis of the induced birefringence is parallel to the electric field, and the optical axes lie mainly in a plane perpendicular to the comb [21, 22]. A typical voltage–transmittance curve is shown in Fig. 8.18.

8.2.5 Current State of the Art and Challenges That Remain

The most significant possible problem with the polymer-stabilized blue and isotropic phases is the need for large driving voltages. The short correlation length in orientational order is the source of both the fast switching speed and the large driving voltage. In fact, several tens of volts are required across an electrode distance of 10 μm. Although the driving voltage could be reduced by decreasing the electrode distance, it would be difficult to fabricate such small electrodes. The driving voltage of the polymer-stabilized blue phase depends on the dielectric anisotropy, the birefringence and elastic modulus of the host liquid crystal [22], the fraction and structure of polymers, and the helix pitch, i.e., the chiral dopant

Fig. 8.18 Electro-optical response of polymer-stabilized blue phases. Precursor 1 is an acrylate monomer (11 %), precursor 2 is an acrylate monomer (8 %), precursor 3 is a methacrylate monomer (11 %), and precursor 4 is a methacrylate monomer (8 %). The liquid crystal was provided by JNC. The electrodes were simple interdigitated electrodes with a spacing of 10 mm

concentration. Although there could be some other parameters, it would be difficult to reduce the driving voltage to levels used by nematic liquid crystals merely through improvements to the material. It is very likely that improved electrode structures will be required for application requiring large electric fields.

Residual birefringence will become a serious problem if the dielectric anisotropy and the birefringence of the parent liquid crystal become greater. When the dielectric anisotropy is zero (initial state without zero electric field), the so-called printing phenomenon occurs: birefringence does not disappear after the electric field is removed. By improving the uniformity of the polymer network in the cell, the problem is partly, but not wholly, solved.

The light shield is an important factor in controlling display contrast. In the polymer-stabilized blue and isotropic phases, short wavelength light can easily leak through because while diffraction and scattering occur mainly in the ultraviolet range, the longest wavelength tail is still in the visible range. This problem would not occur if the lattice constant and the correlation length of short-distance ordering are sufficiently small, but there is a trade-off with the driving voltage.

In the manufacture of the polymer-stabilized blue and isotropic phases, a polymerization reaction occurs in the entire panel. Conventional liquid crystal display technology does not use this type of process, and hence a change will be required in the manufacturing process. Furthermore, we expect several other unknown adverse factors, especially long-term stability, from the use of liquid crystals containing polymers as impurities. The challenge will then be to remove unreacted monomer or eliminate the adverse effects of the residual monomer.

8.2.6 Summary

Although both polymer-stabilized blue and isotropic phases have truly excellent characteristics, they have innate problems stemming from their structures and driving mechanisms, not to mention many as yet unidentified factors. In the flat-panel display industry, with excellent products and heated competition, the barrier for introducing an entirely new mode could be considerably high. In order to put the technology to practical use, an essential requirement will be cooperation among the various organizations bearing responsibility for materials, fabrication processes, device design, drive circuits, and so on.

8.3 Polymer-Stabilized V-Shaped Ferroelectric Liquid Crystal Display PSV-FLCD
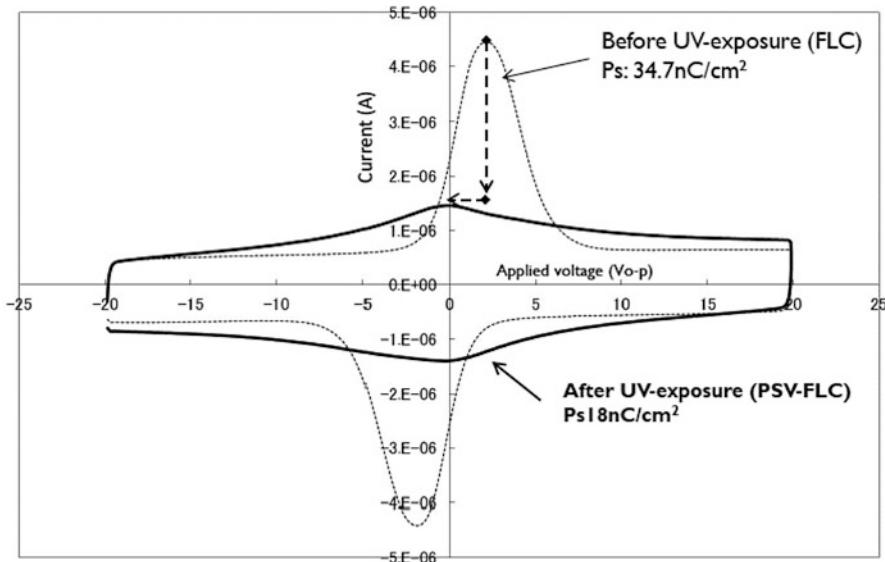
Toru Fujisawa and Shunsuke Kobayashi

8.3.1 Introduction

The development of the LCD has been actively carried out to improve a display performance in terms of high contrast and wide viewing angle. In recent years, there are strong demands for an LCD that is well capable of displaying full-color moving video image without blurring and with a high resolution and a high contrast ratio. The improvement of these subjects has been achieved from two sides: one is progress of liquid crystal material properties by reduction of rotational viscosity. The other is acceleration of switching speed by specific driving method such as an overdrive and a frame rate controlling. In such a background in view of a fast switching, the polymer-stabilized blue phase [17] and ferroelectric liquid crystal attract our attention, because those liquid crystal materials exhibit a high response speed.

Professor Clark and Lagerwall discovered surface-stabilized liquid crystal displays (SS-FLCDs) that show a fast switching with bistability in the 1980s [5]. However, there are several issues towards a full-color display application, which include the existing of zigzag defects causing the reduction of contrast ratio on the screen of display, the producing of grayscale capability for color reproduction, and the productivity of LCDs with a narrow gap less than 2 μm. Hence, FLCs were only practical uses for watches and ultrasmall viewfinders. In these applications of FLCDs, biaxial alignments in which exhibits two states to be switched between a dark state and a light state by applied electric filed are utilized.

The solution for these issues that we have adapted is the polymer stabilization of FLCs exhibiting a continuous grayscale V-shaped switching free from zigzag defects producing a high contrast ratio and a high-speed response below 400 μs

Fig. 8.19 Comparison of polarization reversal current before/after UV exposure

[23]. Polymer-stabilized liquid crystals are obtained by a formation of the polymer network made of the small amount of photo-curable liquid crystalline monomer added into a liquid crystalline host under the UV light exposure. In the case of using ferroelectric liquid crystals, the effect of polymer stabilization appeared remarkably by a UV light exposure for a formation of polymer networks stabilizing FLC alignment with an applying AC voltage. By the application of this process, a bistable switching in a biaxial alignment based on surface-stabilized ferroelectric liquid crystal display (SS-FLCDs) changes into uniaxial alignment to be possible to exhibit V-shaped switching to lead an analog gray scale, called polymer-stabilized V-shaped ferroelectric liquid crystal displays (PSV-FLCDs) discovered by Kobayashi [23–25]. In this chapter, the influence of the physical properties of the ferroelectric liquid crystal by polymer stabilization is discussed.

8.3.2 Switching Properties

Liquid crystalline monomers that are contained in the liquid crystals form three-dimensional polymer networks by UV curing. The alignment control force derived from the polymer network affects the electro-optical switching connected closely with the motion of liquid crystal molecules. The effect of the anchoring force coming from the polymer network leads to the change in the polarization reversal current and switching properties. The differences of polarization reversal current before and after UV exposure can clearly be seen in Fig. 8.19.

When the change of current was measured with applying a triangular wave, a polarity of polarization reversal current peak depended on a polarity of electric fields observed at the coercive electric field of voltage in the first and third quadrant on the graph of the current as a function of applied voltage before UV exposure as shown in Fig. 8.19. The polymer network has not yet been formed and liquid crystal molecules behave as a conventional ferroelectric liquid crystal having a spontaneous polarization of 34.7 nC/cm^2. UV curing was carried out while applying an alternating electric field of 1 kHz. After that, the area of the spontaneous polarization peak drops to 18 nC/cm^2, which is due to the anchoring force by the polymer network. The decrease of the polarization reversal current of the spontaneous polarization of the liquid crystal molecules reflects the movement of the liquid crystal molecules. The decreased spontaneous polarization by UV exposure polymerization means that the movement of liquid crystal molecules is suppressed by the anchoring force of the polymer network. In addition, another key feature is that the position of the peak shifted to the vicinity of zero voltage less than the coercive electric field. It is suggested that switching mechanism in FLCs is changed by the polymer stabilization. This can be described as the force of interaction between liquid crystal molecules and the polymer network. When there is no electric field, the molecules are in the ground state orientation exhibiting optical uniaxial alignments.

When an electric field is applied, a force to orient the molecules towards the electric field direction conflicts with the intermolecular interaction. The higher the electric field, the more the dipole of the liquid crystal molecules aligns towards the direction of the electric field. If the electric field is weakened, the effect to attempt the return of the molecules to the ground state becomes stronger and as a result, the polarization reversal current is maximum at the central position near zero voltage.

The force of the liquid crystal molecules to return to the ground state affect also obviously the switching characteristics. The optical switching characteristics of the device before and after UV exposure are shown in Fig. 8.20, which show the change in current flowing through the liquid crystal during switching. We can compare the optical response waveform and current waveform when a rectangular waveform is applied to the liquid crystal cell. The polarization reversal current appeared after the end of charging current of capacitor due to the polarity inversion of applied waveform. The optical response for this duration, which is the delay of optical response caused by the charging current and the polarization reversal current, is approximately 500 μs.

On the other hand, after the UV exposure, the response improved significantly to 25 μs. It can be seen that after UV exposure the polarization reversal current peak overlaps with the capacitor charging current peak. This is because the polarization reversal occurs at the same time as the polarity of the rectangular waveform is inverted, which has contributed greatly to faster relaxation times of the optical response. To describe this in terms of alignment force, the liquid crystal molecules begin to move and return to the ground state when the potential of the rectangular wave passes through zero volts. The switching by such a mechanism is a major feature of the PSV-FLCD.
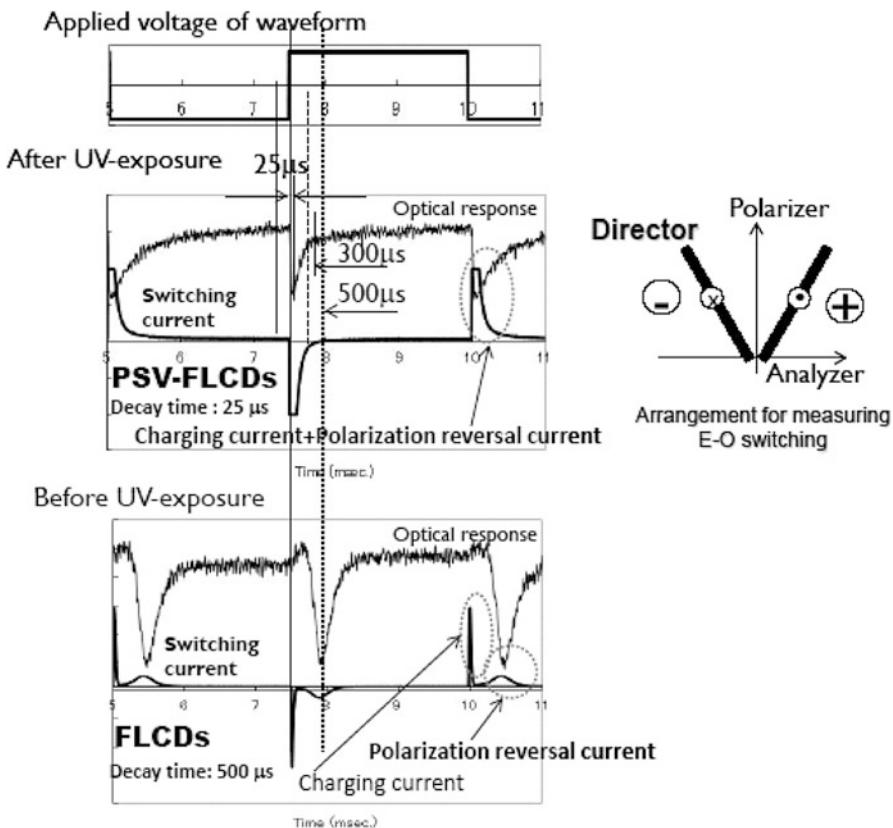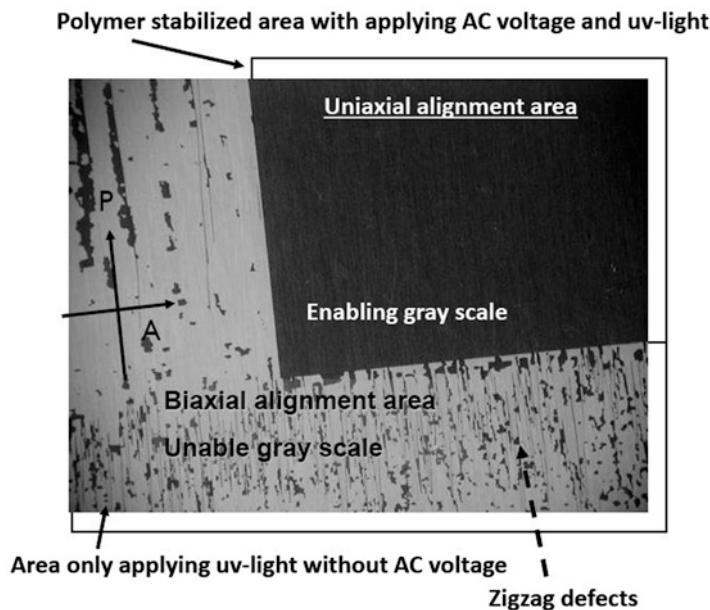
Fig. 8.20 Comparison of optical response and switching current before/after UV exposure
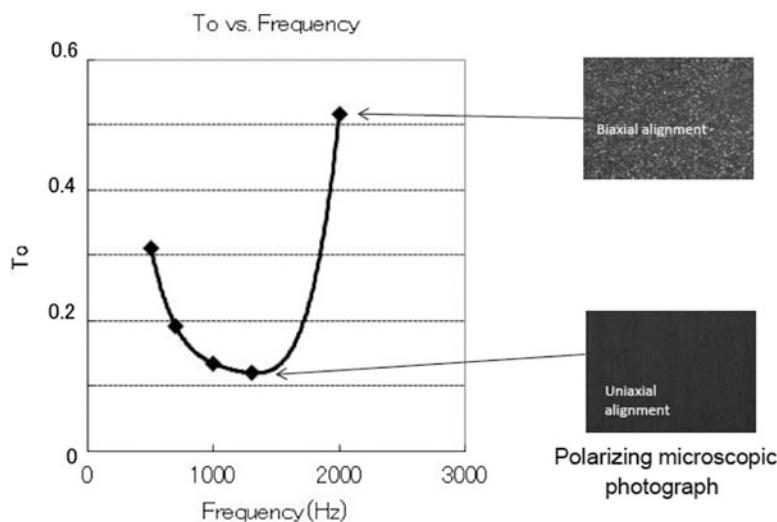
8.3.3   Uniaxial Orientation

Figure 8.21 shows the micrograph of PSV-FLCD under crossed polarizer. The device was obtained by UV exposure while applying a rectangular waveform to the oriented state of the SS-FLCD with a cell thickness of 1.4 μm. In the portion where the rectangular waveform is applied to the liquid crystal during UV exposure, the uniaxial orientation generated by the effect of polymer stabilization can be observed as a dark state. The biaxially oriented state around the electrodes is exhibited as a bright fleck dark spots. Uniaxial polarization properties along with a direction perpendicular to the layer structure of SmC* phase appear only in the portion of the cell where the electric field is switched by applying an AC voltage of about 1 kHz (see Fig. 8.21).

Figure 8.22 shows the relationship between the frequency of the rectangular waveform applied during the UV exposure and minimum transmittance (T_o). The lowest transmission (T_o) is determined by setting the transmission of crossed

Fig. 8.21 Polarization microscopic photograph of PSV-FLCDs at 1.8 μm of cell gap


Fig. 8.22 T_0 of minimum transmittance versus frequency of rectangular waveform

polarizers at 0 % and the transmission of parallel polarizers at 100 %. The minimum transmittance is measured with polarizing microscope equipped with a photomatter when the direction of uniaxial orientation is adjusted to the polarization axis of crossed polarizer. The uniaxial orientation obtained by the polymer-stabilized LC phase is greatly influenced by the frequency of the rectangular waveform applied during the UV exposure as shown in Fig. 8.22. If the frequency is below 1 kHz, a multi-domain fine grain of biaxial orientation is observed with a polarizing microscope. Between 1 and 1.5 kHz, the polarization properties of the uniaxial orientation improved and minimum transmittance decreases. A fine multi-domain structure appears again at a frequency of 2 kHz so as to increase the minimum transmittance. One of the reason for this phenomenon is that the liquid crystal molecules are no longer able to follow the square wave completely which may be the causes of T_o increase. Thus, the uniaxial orientation by polymer stabilization significantly affects the dynamic behavior of liquid crystal molecules during switching.
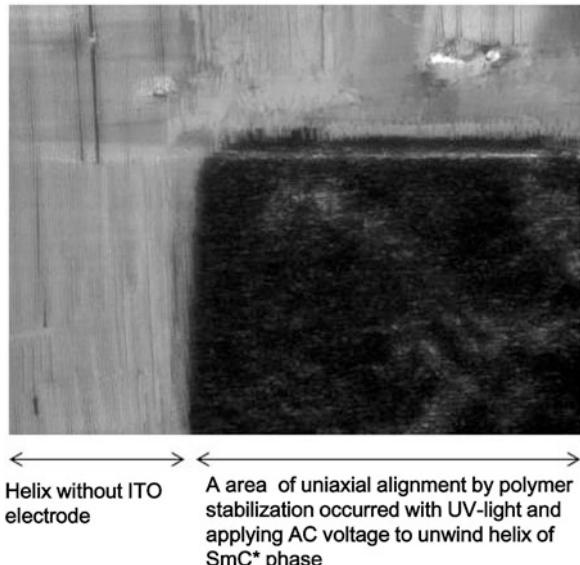
8.3.4 Effect of Cell Thickness

In order to establish a method to extend a cell thickness from a cell gap for a conventional FLCDs less than 2 μm to a cell gap to be suitable for mass production over a 3 μm, we should consider with the change of LC director configuration in smectic C* phase in which the configuration of liquid crystalline directors is depended on a relation between the length of helical pitch in smectic C* and the cell gap. The stripped pattern appeared at the cell gap more than the helical pitch. In this case, electro-optical properties are not suitable for a display application owing to a generating light scattering based on the helix. To avoid an influence of the helix, it is necessary to unwind the helical structure in smectic C* with a condition that the cell gap is a smaller than the helical pitch. For the solution of the helix, we examined a capability of polymer stabilization to retain the unwinding configuration of LC directors aligned by the electric field during UV exposure.

We have examined the method to stabilize unwinding helical structures in smectic C* phase. Experimental results are shown in Fig. 8.23. A cell gap in the photo shown in Fig. 8.23 is 5 μm with parallel alignment layers in which a liquid crystal with a 1.9 μm pitch of a chiral smectic C phase has been injected.

The stripped pattern derived from helical structures exists throughout LC cell with such cell gap before UV exposure, and then AC voltage is applied across the layer of FLCs containing UV curable monomers through ITO electrodes coated on glass substrates so that the helix is unwound at the area of electrode. After that, a 5 mW/cm^2 of UV light at 365 nm by using UV-LED array is exposed for 10 min with the applying AC voltage at the same time to attain uniaxial alignments at a portion of the electrode shown in Fig. 8.23. The area of the uniaxially oriented LC on the electrode portion becomes a dark state under crossed polarizers, as shown in Fig. 8.23. This result indicates that uniaxial alignment is formed by fixation of

Helix without ITO
electrode

A area of uniaxial alignment by polymer
stabilization occurred with UV-light and
applying AC voltage to unwind helix of
SmC* phase
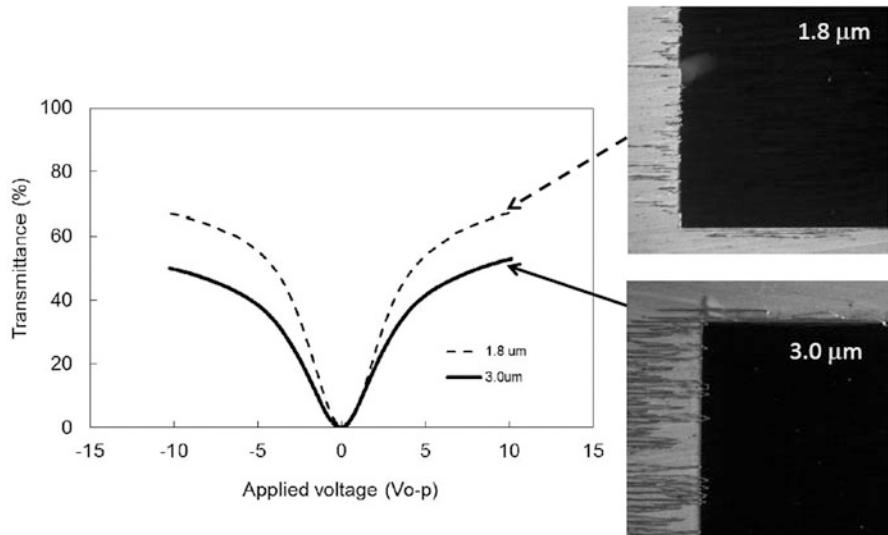
unwinding the helical structures with the applied AC electric field and polymer-stabilized alignment of liquid crystals. It is revealed that retaining of an unwound helix is not the effect of conventional surface stabilization but the effect of polymer stabilization with applying AC voltage.

We succeeded in fabricating polymer-stabilized ferroelectric liquid crystals exhibiting a transmittance as a function of applied voltage with a V-shaped switching with a 3 μm of cell gap as shown Fig. 8.24. The cell thickness was 1.8 and 3 μm. As shown in Fig. 8.24, the 3 μm cell does not show any inferior uniaxial alignment compared with the 1.8 μm cell. This means that production of PSV-FLCDs becomes possible for 3 μm cells. However, the maximum transmittance is lower for the 3 μm cell, because the retardation of the liquid crystal ($\pi d \Delta n / \lambda$) depends on Δn (refractive index anisotropy) and d (cell thickness). An improvement of the maximum transmittance in thicker cells is expected in the future because the development of ferroelectric liquid crystal with a low Δn is in progress.

8.3.5 Prototype of a TFT Drive Panel

We fabricated a field sequential full-color (FS-FC) LCD with 4 in. diagonal and SVGA (800 × 600, 254 ppi, 1.8 μm of cell gap) specification that makes it possible to display high-quality moving video images without blurring and without significant color break due to the fast response of our PSV-FLCDs as shown in Fig. 8.25 [26]. Materials used in the TFT-driven LCD are a ferroelectric liquid crystal composition containing a UV polymerizable liquid crystalline monomer with

Fig. 8.24   Transmittance as a function of applied voltage in PSV-FLCDs with different cell gap

Fig. 8.25   A photograph
of displayed image of the
prototype field sequential
full-color TFT-LCDs using
PSV-FLCD 4 in. diagonal
SVGA (800 × 600 pixels)
254 ppi

spontaneous polarization 33 nC/cm^2, tilt angle 27°, and phase sequence Iso
76.3 °C N* 70.6 °C SmA 66.2 °C · SmC* −12 °C Crystal.

The prepared mixture was injected into an empty cell at a temperature showing
a nematic phase via vacuum filling, because the viscosity of the smectic liquid
crystal is too high for vacuum filling. After the injection, the cell was cooled
gradually at a cooling rate of 2 °C/min to room temperature at which the SmC*
phase is observed. And then, the FLC mixture was photocured with a 5 mW/cm^2 of
UV light source at 365 nm for 10 min to form uniaxial alignments at electrode in
the SmC* phase. A square wave voltage of ±9 V$_{o-p}$ at a frequency of 1 kHz was

applied simultaneously to the data line of TFT array during the UV exposure in order to obtain V-shaped switching.

The panel is driven by voltage modulation to display a gray scale at a voltage of ± 9 V_{o-p} or less. Images were displayed with the frame frequency of 60 Hz as a default frequency, and a flashing LED array backlight system was used to emit three monochrome lights in the sequence of a red, green, and blue light at intervals of 1/180 s, where the frame period of 1/60 is divided into three sub frames: R, G, and B of monochrome images.

These emissions of monochrome lights were synchronized with the addressing period and erase period of images for PSV-FLCDs. The black frame was inserted as erase period to prevent a generating overlap of colors between the subframes. Thus we could demonstrate the potential of polymer-stabilized ferroelectric liquid crystal displays for application as full-color displays and analog grayscale displays. If it is possible to further improve the uniaxial orientation and the transmittance in the future, such displays could be used for excellent video display performance with high contrast.

References

 1. H. Fujikake, H. Sato, T. Murashige, Polymer-stabilized ferroelectric liquid crystal for flexible displays. Display **25**, 3–8 (2004)
 2. N.A. Vaz, G.W. Smith, G.P. Montgomery Jr., A light control film composed of liquid crystal droplets dispersed in a UV-curable polymer. Mol. Cryst. Liq. Cryst. **146**, 1–15 (1987)
 3. H. Fujikake, T. Murashige, J. Yonai, H. Sato, Y. Tsuchiya, H. Kikuchi, Y. Iino, M. Kawakita, K. Takizawa, Flexible ferroelectric liquid crystal devices with polymer fiber network supporting plastic substrates. Proc. Int. Display Res. Conf. **3.3**, 68–71 (2000)
 4. H. Sato, H. Fujikake, Y. Iino, M. Kawakita, H. Kikuchi, Flexible grayscale ferroelectric liquid crystal devices containing polymer walls and networks. Jpn. J. Appl. Phys. **41**(8), 5302–5306 (2002)
 5. N.A. Clark, S.T. Lagerwall, Submicrosecond bistable electro-optic switching in liquid crystals. Appl. Phys. Lett. **36**(11), 899–901 (1980)
 6. S. Kamata, H. Fujikake, H. Furue, H. Sato, H. Kikuchi, T. Kurita, Flexible twisted nematic liquid crystal devices containing molecular-aligned polymer walls and networks. IEICE Trans. Electron. **J92-C**(10), 561–566 (2009)
 7. H. Fujikake, T. Suzuki, H. Sato, H. Kikuchi, T. Kurita, F. Sato, Flexible reflective display devices using twisted-alignment guest-host liquid crystal and polymer walls. IEICE Trans. Electron. **J90-C**(3), 294–297 (2007)
 8. K. Sasagawa, H. Fujikake, H. Sato, M. Omodani, Cholesteric liquid crystal devices stabilized by polymer walls and networks. IEICE Trans. Electron. **J92-C**(1), 26–31 (2009)
 9. T. Eguchi, A. Sonehara, A. Sugizaki, T. Ito, A. Kumano, T. Takahashi, New color filter carried out by a roll-to-roll process. Proc. IDW. FMC3-3, 579–583 (2004)
10. H. Sato, H. Fujikake, Y. Fujisaki, S. Suzuki, D. Nakayama, T. Furukawa, H. Kikuchi, T. Kurita, A4-sized liquid crystal displays with flexible light guide plate. Proc. Int. Display. Workshops. LCT4-2, 605–608 (2006)
11. Y. Fujisaki, H. Sato, H. Fujikake, Y. Inoue, S. Tokito, T. Kurita, Liquid crystal cells fabricated on plastic substrate driven by low-voltage organic thin-film transistor with improved gate insulator and passivation layer. Jpn. J. Appl. Phys. **44**(6A), 3728–3732 (2005)

12. Y. Iwamoto, K. Motai, Y. Naitou, M. Kadowaki, K. Ichimura, H. Sato, Y. Fujisaki, T. Yamamoto, H. Fujikake and T. Kurita, Flexible field-sequential-color FLCD panels driven by poly-Si TFTs. Soc. Int. Display. Tech. Dig. **23.3**, 318–321 (2008)
13. D.C. Wright, N.D. Mermin, Rev. Modern Phys. **61**, 385 (1989)
14. P.P. Crooker, in *Chirality in Liquid Crystals*, ed. by H.S. Kitzerow, C. Bahr (Springer, New York, 2001)
15. H. Kikuchi, *Structure and Bonding*, vol. 128 (Springer, Berlin/Heidelberg, 2008), pp. 99–117
16. H.S. Kitzerow, H. Schmid, A. Ranft, G. Heppke, R.A.M. Hikmet, J. Lub, Liq. Cryst. **14**, 911–916 (1993)
17. H. Kikuchi, M. Yokota, Y. Hisakado, H. Yang, T. Kajiyama, Polymerstabilized liquid crystal blue phases. Nat. Mater. **1**, 64–28 (2002)
18. A. Yoshizawa, M. Sato, J. Rokunohe, J. Mater. Chem. **15**, 3285–3290 (2005)
19. H.J. Coles, M.N. Pivnenko, Nature **436**, 997–1000 (2005)
20. T. Iwata, K. Suzuki, N. Amaya, H. Higuchi, H. Masunaga, S. Sasaki, H. Kikuchi, Macromolecules **42**(6), 2002–2008 (2009)
21. Y. Hisakado, H. Kikuchi, T. Nagamura, Adv. Mater. **17**, 96 (2005)
22. Y. Haseba, H. Kikuchi, T. Nagamura, Adv. Mater. **17**, 2311–2315 (2005)
23. Y. Taguchi, Y. Iimura, S. Kobayashi, H. Hasebe, H. Takatsu, Liquid crystalline polymer stabilized FLCDs with conventional rubbed polyimide films or with photo alignment films of poly(vinyl cinnamate). Mol. Cryst. Liq. Cryst. **292**, 333–343 (1997)
24. Y. Miyazaki, H. Furue, T. Takahashi, M. Shikada, S. Kobayashi, Mesogenic polymer-stabilized FLCDs exhibiting asymmetric and symmetric (V-shape) electrooptic characteristics. Mol. Cryst. Liq. Cryst. **364**, 491–499 (2001)
25. S. Kawamoto, M. Oh-kochi, S. Kundu, H. Hasebe, H. Takatsu, S. Kobayashi, Polymer-stabilized V-mode FLCDs and their application to color sequential fullcolor LCDs. Display **25**, 45–47 (2004)
26. T. Fujisawa, I. Nishiyama, K. Hatsusaka, K. Takeuchi, H. Takatsu, S. Kobayashi, Field sequential full color LCDs using polymer-stabilized V-shaped ferroelectric liquid crystals. Ferroelectrics **364**, 78–85 (2008)

Part II
Liquid Crystal Research Leading the Field in the Twenty-First Century

Chapter 9
Liquid Crystalline Materials

Katsumi Yoshino, Hideo Takezoe, Takashi Kato, Junji Watanabe, Kazuo Akagi, and Isa Nishiyama

9.1 Ferroelectric Liquid Crystals

Katsumi Yoshino

9.1.1 Introduction

During the development of liquid crystals, there was an ongoing discussion if ferroelectricity could exist in LC materials. Until then, ferroelectricity only existed in solids with a specific crystal structure having no inversion symmetry center. Ferroelectricity was considered to be impossible in gases or liquids, but since liquid crystals have a regularity to some extent, the expression of a ferroelectric liquid in

K. Yoshino
Shimane Institute for Industrial Technology, Matsue, Japan
e-mail: yoshino@shimane-iit.jp

H. Takezoe • J. Watanabe
Tokyo Institute of Technology, Tokyo, Japan
e-mail: takezoe.h.aa@m.titech.ac.jp; jwatanab@polymer.titech.ac.jp

T. Kato
Department of Chemistry and Biotechnology, School of Engineering,
The University of Tokyo, Tokyo, Japan
e-mail: kato@chiral.t.u-tokyo.ac.jp

K. Akagi
Department of Polymer Chemistry, Kyoto University, Kyoto, Japan
e-mail: akagi@fps.polym.kyoto-u.ac.jp

I. Nishiyama
DIC Corporation, Saitama, Japan
e-mail: isa-nishiyama@ma.dic.co.jp

the liquid crystal was expected. In fact, there have been measurements of pulses of electric current in liquid crystals when applying the polarity inversion pulse voltage, which were similar to the currents observed in association with spontaneous polarization reversal of a ferroelectric to the liquid crystal, but this effect is not due to ferroelectricity. Meanwhile, the liquid crystal DOBAMBC showing the ferroelectric smectic C phase was reported by Meyer et al. in 1975 [1].

They found that an asymmetric carbon atom and a dipole moment in the molecular structure lead to a liquid crystal smectic C phase in which the molecular long axes are tilted from the layer normal of the smectic phase. Hence, ferroelectricity was expressed. The ferroelectric behavior definitely was confirmed by various measurements, including the D-E hysteresis [2].

Since the molecules have an asymmetric carbon atom, the molecular long axis is inclined at an angle from the smectic layer normal in the smectic C phase, but this inclination direction is rotated by an angle in each smectic layer. This phase is referred to as smectic C* phase, or chiral smectic C phase. The helical structure shows a pitch perpendicular to the chiral smectic layers. This spiral is unwound when a voltage is applied.

However, the spontaneous polarization of the molecules is much smaller as compared with the case where dipole moments are arranged ideally. In DOBAMBC, the spontaneous polarization of 3 nC/cm^2 is of orders of magnitude smaller than the ideal case. So, the development of ferroelectric liquid crystals with a large spontaneous polarization was carried out.

In order to have a large dipole moment, various atoms such as halogens were introduced into the molecular structure, the chiral group that carried the dipole moment was shortened, and plural asymmetric carbons and dipoles were introduced.

In other words, molecular design and the synthesis were carried to express various characteristics for the required purposes that depend on the specific application of the ferroelectric liquid crystal. For example, ferroelectric liquid crystals with large spontaneous polarization, a large tilt angle with small temperature dependence, a specific viscosity, a small rotational viscosity of the molecules along their long axis, a chiral smectic C phase over a wide temperature range, a characteristic anisotropy of the dielectric constant, a suitable phase sequence, a suitable helical pitch, photochemical stability, and so on have been newly synthesized [3–5].

The discovery of a ferroelectric liquid crystal by Meyer fueled a strong interest in basic science and in the physical properties such as the mechanism of the dielectric strength at first. Immediately after that, the particular relevance of ferroelectrics for display applications attracted attention [4, 5].

Examples are the electro-optical effect caused by helix distortion [6], the unwinding of the helix in thin cells that leads to the intense electro-optical effect utilizing the refractive index change upon polarization reversal associated with an applied voltage polarity reversal [7, 8], and the light scattering due to molecular motion during polarization inversion (transient scattering electro-optical effect) [9]. Devices have been proposed taking advantage of those various characteristics of ferroelectric liquid crystals, and synthesis of new compounds that exhibit excellent characteristics advanced more and more.

Along with the vigorous research on ferroelectric liquid crystals began subsequent active guidance of molecular design by classifying the features of the molecular structure of materials which has been developed at that time.

9.1.2 Classification by Core

9.1.2.1 Schiff-Base-Based Ferroelectric Liquid Crystals

DOBAMBC (*p*-(n-decyloxy)benzylidene-*p*-amino-(2-butyl)cinnamate) was the first reported ferroelectric liquid crystal which uses 2-methyl-1-butanol, the only noncentrosymmetric amylalcohol, as the chiral source at its molecular end [1]. Many different molecules with varying length of the alkoxy group or an alkyl group have been synthesized and investigated for ferroelectricity in the vicinity of room temperature [10].

Schiff bases are highly reactive and are easily hydrolyzed, but stability could be improved by the introduction of hydroxyl groups [11, 12]. The secondary alcohol 2-pentanol was used instead of 2-methyl-1-butanol in the synthesis of DOBA-1-MBC (*p*-decyloxy-benzylidene *p'*-amino-1-methylbutylcinnamate), which showed an increase of the spontaneous polarization by more than one order of magnitude than that of DOBAMBC. This effect stems from the shortening of the distance between dipole moment and chiral center [12, 13].

HOBACPC (*p*-hexyloxybenzylidene-*p'*-amino-2-chloropropyl-cinnamate) obtained by directly attaching a chlorine atom to the asymmetric carbon closes the distance of dipole and the asymmetric carbon atom even more, resulting in doubling the spontaneous polarization value as compared to DOBAMBC [3, 14, 15]. I suspect that this is the influence from the rotational motion of the entire molecule that offsets the effect of more than one dipole. Furthermore, lactate and amino acid derivatives with directly attached chlorine atoms, bromine atoms, and cyano groups as the chiral source have also been synthesized.

9.1.2.2 Azo- and Azoxy-Based Ferroelectric Liquid Crystals

P. Keller et al. had synthesized symmetric azoxy-type ferroelectric liquid crystals which led to the synthesis of various conjugated azo- and azoxy-type ferroelectric liquid crystals, but since they are colored, optical deterioration is problematic [16].

9.1.2.3 Biphenyl- and Ester-Based Ferroelectric Liquid Crystals

Chemically stable benzoic acid ester compounds and biphenyl-based ferroelectric liquid crystal have been synthesized as well. The spontaneous polarization is relatively low in these two-ring systems [17], but very interestingly, the

spontaneous polarization reverses its direction upon heating [18]. Generally speaking, in the liquid crystals of the two-ring system in the core structure, the temperature range of the liquid crystal is often narrow.

The liquid crystal properties can be improved by extending the core part to esters with three or four rings and ferroelectric liquid crystals with a wide temperature range have been synthesized [19, 20].

The spontaneous polarization in those ester and Schiff-base ferroelectric liquid crystals that contain a secondary alcohol as the asymmetric center shows a large value of several 10 nC/cm^2 or more [21].

Many ferroelectric liquid crystals have been obtained by substituting a cyano group, a halogen, a nitro group, or an OH group on one of the core benzene rings. These substitutions are effective to show ferroelectricity at room temperature regions, to increase the spontaneous polarization, or to expand the temperature range of the SmC* phase [22, 23].

9.1.2.4   Others

Ferroelectric liquid crystals having a heterocyclic pyrimidine, pyrazine, or pyridazine ring have been developed. Phenylpyrimidine systems show a characteristic low rotational viscosity, and fused aromatics, such as fluorene, fluorenone, or naphthalene, have been discussed from the viewpoint of dipole moment, spontaneous polarization, and orientability.

Further, many tolan (1,2-diphenylethyne) compounds have been synthesized, and among them several antiferroelectric compounds were found.

9.1.3   Classification by the Chiral Part

9.1.3.1   Ferroelectric Liquid Crystals Containing Amino Acids as Chiral Source

Amino acids that have a branched alkyl side chain, such as valin, leucine, and isoleucine, are preferred. Especially isoleucine derivatives can show a large spontaneous polarization in the range of 300 nC/cm^2 and more [24, 25].

9.1.3.2   Fluorine-Containing Ferroelectric Liquid Crystals

Ferroelectric liquid crystals containing a chiral unit fluorine, especially those that connect a trifluoromethyl group directly to the asymmetric carbon, show a large spontaneous polarization [25–28].

9.1.3.3 Ferroelectric Liquid Crystals with Lactic Acid as Asymmetric Source

Many ferroelectric liquid crystals with lactic acid as the chiral source have been developed from the early days of the ferroelectric liquid crystal research, and it was found that a large spontaneous polarization is obtained by attaching several dipoles in the vicinity of the asymmetric carbon [29, 30].

9.1.3.4 Ferroelectric Liquid Crystal Having Multiple Asymmetric Carbons

Ferroelectric liquid crystals containing several chiral groups, either on one end of the mesogen or on both ends, have been synthesized. Those compounds often have a large spontaneous polarization by themselves, but sometimes a chiral dopant has to be added [23, 31, 32].

9.1.3.5 Ferroelectric Liquid Crystal with Cyclic Chiral Sources

The first ferroelectric liquid crystal having an cyclic chiral group was an asymmetric epoxy derivative, which had paved the way for many similar compounds that are effective chiral dopants for nonchiral host liquid crystals [33].

9.1.3.6 Chiral Dopants for Host Liquid Crystals

It is possible to express ferroelectricity in a non-ferroelectric liquid crystal compound exhibiting a smectic phase with a tilt angle such as a smectic C phase by mixing with a chiral dopant. The first smectic C liquid crystal system was a phenyl pyrimidine compound. For the application in displays the following points need to be satisfied: small chiral dopant amount, large spontaneous polarization, low viscosity, and optimum temperature range.

As explained above, a ferroelectric liquid crystal is an elongated rod-like molecule containing an asymmetric carbon atom. By synthesizing a variety of compounds, this concept has been expanded significantly.

For example, a discotic ferroelectric liquid crystal was synthesized by introducing an asymmetric center in a discotic liquid crystal, which is a flat platelike molecule [34].

The polymer ferroelectric liquid crystals with the mesogen either in the main chain or as a side group of the polymer have been synthesized [35, 36]. Large spontaneous polarizations have been found in those polymers, and interestingly, even though the viscosity of polymers is higher than low molar mass compounds, a fast electro-optical switching has been found.

Furthermore, during the course of the study of ferroelectric LCs, the antiferroelectricMHPOBC(4-(l-methylheptyloxycarbonyl)phenyl-4-octyloxybiphenyl-4-carboxylate) has been found. The synthesis of a variety antiferroelectric compounds was fueled by display applications.

Furthermore, banana-shaped molecules are found to show ferroelectricity and antiferroelectricity, even though they do not contain an asymmetric center. The research of such type of liquid crystal has been actively carried out (see Sect. 9.4 in this book).

9.2 Antiferroelectric Liquid Crystals

Hideo Takezoe

9.2.1 Introduction
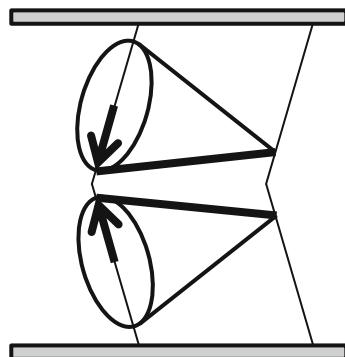
Antiferroelectric liquid crystals were first reported in 1989 [37], 14 years after the discovery of ferroelectric liquid crystals [38]. The first ferroelectric compound, Rochelle salt (potassium sodium tartrate), was discovered in 1921 [39], and the discovery of the first antiferroelectric (lead zirconate in 1951) [40] took 30 years. Compared to that, the road to the discovery of antiferroelectric liquid crystals was short. However, later in this chapter, I will describe that actually the first antiferroelectric LC was synthesized already in 1985 [41]. Even though antiferroelectricity was a phenomenon already known in the solid state, the road leading to antiferroelectric LCs was not so straightforward.

Actually, the first solid antiferroelectric material had been discovered at Tokyo Institute of Technology [40]. The discovery of the first antiferroelectric liquid crystal at the very same university was quite unintentional, but can be considered quite fortunate. In this chapter, I will introduce some details of what led to the discovery of antiferroelectric liquid crystals from the study of ferroelectric liquid crystals and also discuss the history of the discovery of the ferroelectric phase.

9.2.2 Road to Antiferroelectric Liquid Crystals

A.D.L. Chandani, who is the first author of our first paper on antiferroelectric liquid crystals, joined our lab as a PhD student in 1987. We were studying the switching of ferroelectric liquid crystals at this time [42]. Just at the same time, we also had proposed a new method to measure the viscosity coefficient of liquid crystals [43]. We asked Chandani to study the correlation of the viscosity coefficient and the

Fig. 9.1 Our first model
of antiferroelectric liquid
crystal (third stable state)
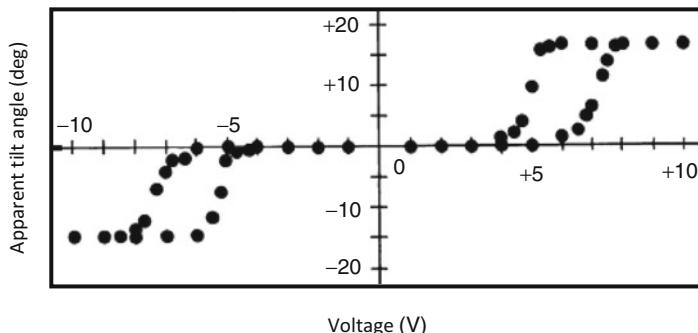
spontaneous polarization. One of the compound she used at this time was
MHPOBC (4-(1-methylheptyloxycarbonyl) phenyl 4′-octyloxybiphenyl-4-carbox-
ylate), which then became known as the first antiferroelectric liquid crystal [44].

MHPOBC was reported by Inukai et al. (Chisso Corp.) during the 11th Domestic
LC conference in 1985 and has the phase sequence Iso-SmA-SmC*. This com-
pound had also been studied as one component in a mixture of ferroelectric liquid
crystals for fast electro-optical devices by industry, but had never been of particular
interest as a pure compound.

We have measured the viscosity [43, 44] and the electroclinic effect [45] of
MHPOBC, but we did not mention a little abnormality of it in those papers.
However, we have mentioned that the SmC* may in fact be SmF* or SmI* in a
footnote of [43]. In addition, we had inferred a third stable state, such as the one
shown in Fig. 9.1, appears due to the effect of the polarization charge below a
certain temperature in [44]. This structure was proposed by us on the bases of
a chevron structure and was presented as a poster at the first international ferro-
electric liquid crystal conference in 1987 [46]. This structure, however, was later
replaced by the model of the antiferroelectric liquid crystal phase.
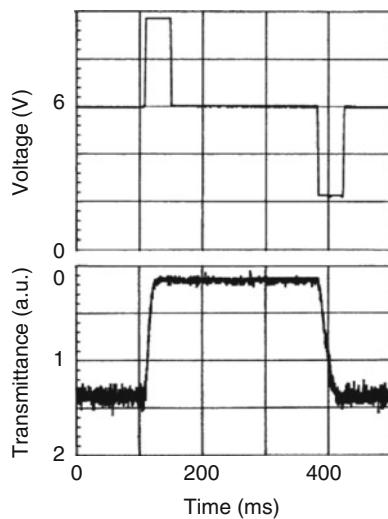
Here, I would like to go off on a tangent about the 1st international ferroelectric
liquid crystal conference. One of the most important moments for the discovery of
antiferroelectric liquid crystal was the presentation by Kenji Furukawa (Chisso
Corp.) on this conference [47]. The designated SmY* phase exists at the
low-temperature side of the SmC* phase of MHPOBC; it has an abnormally small
dielectric constant compared to the ferroelectric phase, indicating a threshold during
the direct current switching by an electric field. Thus, experimental facts pointed to
an antiferroelectric phase rather than a ferroelectric phase as early as 1987.

Despite this circumstantial evidence and in the absence of a final model for the
phase structure, we went into applied research to develop display devices. The basic
principle of the device, as reported in the Japanese Journal of Applied Physics [48],
is an electro-optical response that is based on a tristable switching, as shown in
Fig. 9.1. As shown in Fig. 9.2 the tilt angle of the molecules led to a tristable state
with two threshold values that show a double hysteresis. As shown in Fig. 9.3 it is
possible to switch to either of the bistable states from the third state by applying

Fig. 9.2 Voltage dependence of apparent tilt angle
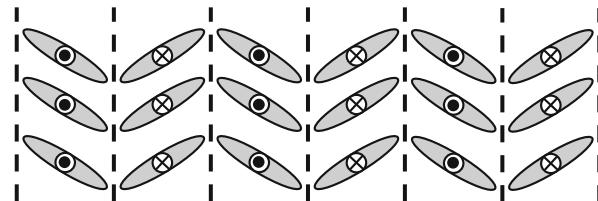
Fig. 9.3 Transmittance as a function of time by applying positive and negative pulses in addition to dc voltage


positive and negative pulses. In that paper, we have reported that the transmittance changes twice during one half cycle of an applied triangular wave. During these changes, switching currents had been observed. On these findings, MHPOBC appealed to us that this phase is antiferroelectric.

We were forced to conclude that this abnormal switching does not occur in the SmC* phase based on two facts that had been transpired by Chisso's Furukawa. One is the fact that a clear DSC peak appears at a temperature a few degrees below the SmA-SmC* phase transition, indicating a distinct phase below SmC*. The other fact is that the third stable state can also be seen in the racemic form. Around this time, we also have reported on the switching of the layer structure in tristable states [49]. In the introduction of this paper, we had pointed out the occurrence of this switching phenomenon in a new phase. Around this time, E. Gorecka joined our laboratory as a UNESCO Fellow from Poland. She, together with Chandani, started

Fig. 9.4 Local molecular orientation structure of antiferroelectric liquid crystal
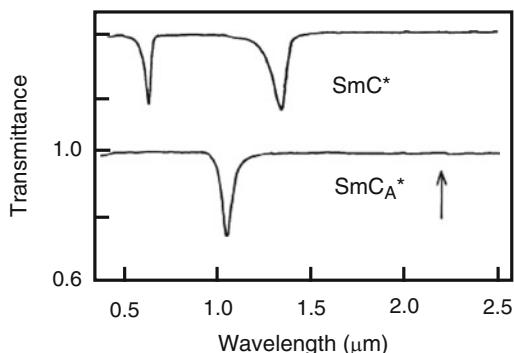

precise microscope observation of MHPOBC, and helical pitch, optical rotation, and conoscope measurements.

We discussed eagerly the various models based on these data. One of those models involved the rotation in a coherent molecular array structure in the SmC* phase. A uniaxial macroscopic helical structure with the optical axis in the layer normal direction that is rotated about its axis coherently is stable against an external electric field. Furthermore, we also added to the model that a flexible layer structure causes the switching of the layer structure under such conditions. Of course, around this time, we were also thinking about models based on the antiferroelectric liquid crystal, but we thought that the temperature dependences of the optical rotation and the helical pitch could not be explained by this model. Because the tilt angle increases with lowering temperature, we mistakenly thought that the optical rotation, which is proportional to the square of the anisotropy, should not become smaller with lowering temperature, and there must be a novel helical structure. As described in the textbook of Chandrasekar, the optical rotation is proportional to the pitch, and thus we should have immediately known that our results can be explained without any problem by the conventional helical structure of our sample.

In any case, after solving the problem of the optical rotation, we developed the model of the antiferroelectric liquid crystal SmC_A^* phase with the local structure shown in Fig. 9.4. The biggest challenge was how to confirm this structure experimentally. Previously, we had studied the light propagation in a helical structure both experimentally and theoretically. Optically, the antiferroelectric liquid crystal phase is the same as the cholesteric liquid crystal phase: without depending on the propagation direction of light, a half pitch of the helix corresponds to one optical period. In the SmC* structure, light behaves similar when the incident angle is perpendicular to the layer, and Bragg reflection occurs. On the other hand, for oblique irradiation, one pitch of the helix corresponds to one optical period. Thus, for the SmC* phase only, the Bragg reflection corresponding for one pitch (full-pitch band) should appear. Fortunately, the wavelength range for the transmission measurements is in the visible or in the near-infrared region; Bragg reflection can be easily observed as a dip in the spectrum. Figure 9.5 shows the obtained transmittance spectra. Two dips appear at high temperatures, which support the presence of the SmC* phase, but only one dip in the low-temperature phase could only be explained by the model of the SmC_A^* phase [37].

Our experiment could only show that the optical properties of our structure are different from the helical structure of the SmC* phase and that those properties

Fig. 9.5 Transmittance
spectra of the SmC* and
SmC$_A$* phases at oblique
incidence
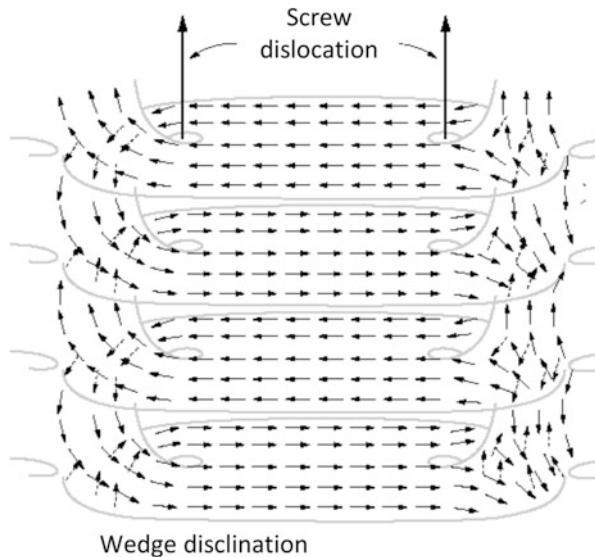
can be explained without contradiction by the model of the SmC$_A$* structure.
In addition, there are a lot of experimental methods to distinguish the ferroelectric
and antiferroelectric phases: (1) electro-optical and switching current observations,
(2) smaller dielectric constants in the SmC$_A$* phase than that in the SmC* phase,
(3) inversion of helix sense in the two phases, (4) biaxial conoscope image in the
SmC$_A$* phase, and (5) different birefringence in the two phases [50]. However,
neither could prove the model of Fig. 9.4.

The fact that the molecular orientation changes from layer to layer could be
inferred from the observation of dispirations [50, 51]. In the vertically aligned
SmC* phase, a c-director exists, and a schlieren texture similar to that in the
nematic phase is observed. However, since the formation of disclinations with
the strength 1/2 is inevitably associated with plane discontinuity of the tilt of the
molecules, such disclinations do not occur in the SmC* phase. However, in addition
to the four-brush disclinations, two-brush defects (1/2 disclinations) are observed in
the SmC$_A$* phase. We thought to be able to resolve the defect structure as shown in
Fig. 9.6 [51]. That is, the structure entangled twist dislocations with a strength of
1/2. You may find that the plane discontinuity is removed, i.e., a disclination (tilt
direction) is connected to that in the neighboring layer through a dislocation
without discontinuity. This model has received interest from L. Lejcek of Czech
Republic who had studied for many years the defect structure of liquid crystals. In
addition, we have received a letter of congratulations from the American
W.F. Harris, who had predicted such a displation in the 1970s that "this is the
first clear experimental observation" [52]. Nowadays, the identification of the
antiferroelectric phase by observation of displations is widely used. In addition to
the simplicity of the method, the major advantage is that the method can be applied
to racemic compounds (SmC$_A$ phase), which have no spontaneous polarization,
unlike the other methods mentioned above.

The structure shown in Fig. 9.4 has been verified experimentally by Gelerne
et al. [53] and Bahr et al. [54]. Using free surface of the liquid crystal and free films,
respectively, they showed that the orientation of the molecules and their inclination
reversed layer by layer.

Fig. 9.6 Structure of dispiration
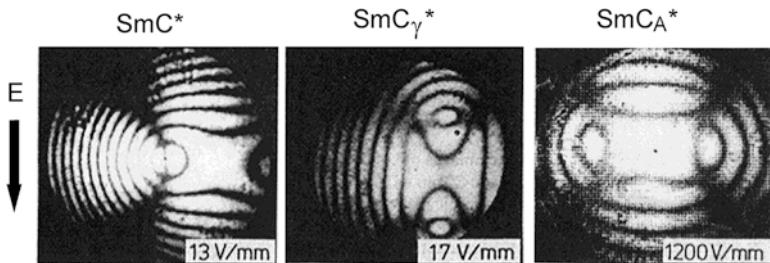
9.2.3 Deployment of the Ferroelectric Phases

MHPOBC was not only the first reported antiferroelectric liquid crystal, but it was also very useful for the discovery of other liquid crystal phases. It does exhibit not only SmC* and SmC$_A$* but also all of the now well-established secondary phases, SmC$_\alpha$*, SmC$_{FI2}$* (AF), and SmC$_{FI1}$* (SmC$_\gamma$*). The existence of several phases has been reported prior to the authors by Furukawa et al. [47] and Fukui et al. [55]. We have reported the existence of SmC$_\alpha$*, SmC$_\beta$*, and SmC$_\gamma$* between the SmA and SmC$_A$* phases. It was then claimed that SmC$_\beta$* is the same as SmC*. Thereafter, objections were raised by other groups [56–58] and experiments using a compound with high optical purity were used to confirm that SmC$_\beta$* is the same as SmC$_{FI2}$*.
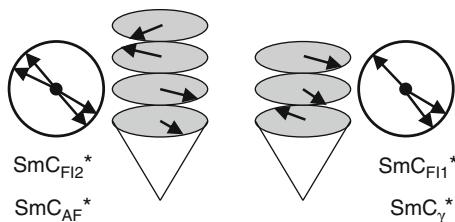
Rather than just doing research on the SmC$_A$* phase, we were also studying the secondary phases by X-ray diffraction, by conoscopy, and by measuring the electro-optical response as well as the polarization reversal current. Concerning the SmC$_\alpha$* phase, Takanishi et al. reported [59] that it was a phase, in which molecules tilted from the smectic layer normal, and showed a strange electro-optical response, although it appeared to be the SmA phase. But we could not get to the current model, i.e., a SmC*-like phase with a very short pitch [60]. Conoscopic image observation was very effective for the identification of the SmC$_\gamma$* phase structure in the initial stage. It was not possible to conclude that it has a three-layer period, but the conoscopic image (see Fig. 9.7) in an electric field showed that it is a ferro-electric phase [61]. From the investigation of the helical pitch, the SmC$_\gamma$* phase, which appears between SmC$_A$* and SmC* phases, has a three-layer period [62].

We have overlooked the SmC$_{FI2}$* phase of MHPOBC, but we found a phase of the same nature as the SmC$_A$* phase in a fairly wide temperature range immediately

Fig. 9.7 Conoscope images in the SmC*, SmCγ*, and SmC$_a$* phases under electric fields indicated

Fig. 9.8 Modified Ising model of the SmC$_{FI1}$* and SmC$_{FI2}$* phases

above the SmC$_{FI1}$* phase in a similar compound MHPBC (4-(1-methylheptyloxycarbony)phenyl 4′-octylbiphenyl-4-carboxylate) [63]. It was named AF phase because it is a novel antiferroelectric phase that exhibits a conoscopic image similar to the SmC$_A$* phase when a small electric field is applied, and the dielectric constant is small. Thereafter, from theoretical considerations concerning the "devil's staircase," we concluded that it is the antiferroelectric phase with a four-layer period [64]. As described above, it was not possible to propose an accurate model regarding the SmC$_α$* phase, but we could propose correctly the models with respect to the other phases ahead of other research groups.

The need to make modifications to these models comes out of the result of resonance X-ray diffraction experiments. In the first report, the SmC$_{FI2}$* phase was concluded to be a four-layer structure and the SmC$_{FI1}$* phase a three-layer structure [65]. This conclusion was similar to ours, but unlike our Ising model, the authors interpreted the data as a XY clock model [65]. However, characteristics such as the optical rotation cannot be explained by this, and we have proposed a deformed Ising model shown in Fig. 9.8 which fuses the XY and Ising models [66]. Further resonant X-ray diffraction experiments and optical analysis led to the current deformed clock model [67], which was equivalent to our deformed Ising model [68].

After that, the experimental observation of secondary phases with five- and even six-layer periods had been reported [68, 69]. Theoretical considerations are also important, but one needs to verify the authenticity of the experimental results in plural compounds, and there is a need for another researcher to reaffirm carefully using other experimental means.

9.2.4 Instead of a Conclusion: Facts and Future

I introduced the process leading to the discovery of the antiferroelectric SmC$_A$* phase and the structural determination of secondary phases by focusing our researches.

The discovery of the antiferroelectric phase had been a competitive endeavor. It has been recognized that the antiferroelectric liquid crystal phase was discovered by our group. However, some other groups were almost at the same position. Y. Galerne announced at the second international ferroelectric liquid crystal conference in 1989 that the direction of the molecular polarization changes with each smectic layer in MHTAC (1-(methyl)-heptyl-terephthalylidene-bis-amino cinnamate). At the same meeting, we announced the antiferromagnetic structure of MHPOBC. Just before the conference, in May 1989, we submitted a manuscript to the *Japanese Journal of Applied Physics* that was published in July the same year. The conference was held in the end of June 1986, just between those two dates. On the other hand, a homologue of MHTAC was synthesized in 1976 [70], soon after the discovery of ferroelectric liquid crystal. MHTAC itself had been published in 1983 [71]. However, it was in 1990 when Galerne published a paper describing the anticlinic structure (initially named the phase SmO*) [53]. Later it was reported by several groups that this SmO* phase is the same as the SmC$_A$* phase [72–74]. As of November 2011, our JJAP paper had been cited 535 times, whereas Galerne's Phys. Rev. Lett. Paper had been cited 93 times. This shows the importance of speedily publishing significant results.

During that time there was another antiferroelectric compound, which was announced by J.W. Goodby and E. Chin in 1988. They had found two phases at the low-temperature side of the SmC* phase, but they were reasoning the SmC* phase with another handedness, the SmF* phase, or the SmI* phase due to racemization. In 1992 they identified those as an antiferroelectric phase and a ferroelectric phase, respectively [75].

Let me here mention the nomenclature of the SmC$_A$* phase. The first one to name the antiferroelectric phase was Furukawa et al.: SmY*. However, the structure was not yet clear at this time, and we felt the need for a new name. Because the phase related to SmC*, canditaes were SmC*(3), SmC$_A$*, and SmC$_{AF}$*. But if SmC$_{AF}$* was the name for the antiferroelectric phase, SmC$_F$* should be the name of the corresponding ferroelectric phase. Thus, we settled on SmC$_A$*. Because the racemate, which does not have antiferroelectric properties, has the same structure, it is possible to assign the subscript A to mean "anticlinic," which now gives an even better reason for the name. However, for me it is not very pleasant that some researchers recommend to use a lowercase "a" (SmCa*) [76].

There are also several conventions to name the ferroelectric phases. When these phase structures are not exactly known, the names have Greek subscripts, α, β, or γ. The SmC$_\alpha$* phase is left as it is, but the ferroelectric phases have commonly FI1 and FI2 as subscript. They were proposed around the time when the clock model appeared, but there is a sense of incongruity because SmC$_{FI2}$* is basically

antiferroelectric. If the ferroelectric phases would be discovered now, it would be nice to indicate the value of the ferroelectric boundary per period in its name, as in SmC ($q = 0$, 1/2, 1/3, 1). The goal for the naming of LC phases should be to avoid confusion as much as possible.

There are two review commentaries about the antiferroelectric phase, one by Fukuda et al. in 1994 [77] and one by Takezoe et al. in 2010 [78]. There is a sense of maturity in this field both theoretically and experimentally. Also, the interest in other secondary phases seems to be endless. Applications for antiferroelectric phases are made in the field of fast switching displays, such as V-shaped switching displays, 45° orthoconic antiferroelectric liquid crystal displays, and so on. Even though speed is a great feature, research with the aim of display applications is declining.

Even though it might sound a little presumptuous, I want to convey my message to young scientists. I think one reason that the discovery of the antiferroelectric liquid crystal was delayed was because of the common sense that rod-like molecules align parallel in the liquid crystal state. Molecules are generally parallel to each other in both nematic and smectic phases before SmC_A^*. One of our important publications was the polar switching in bend-core liquid crystals, which reached more than 800 citations by now [79]. It was said that bent molecules were not suitable for liquid crystals until our discovery in 1996. But, in fact, many bent-core molecules form liquid crystal phases, and extremely interesting phenomena have been discovered in terms of polarity and chirality in particular. When you find an unexplained phenomenon, do not think of it as some mistake. Please have in mind that there is the possibility that this uncommon phenomenon may lead to a big discovery.

9.3 Supramolecular Liquid Crystals
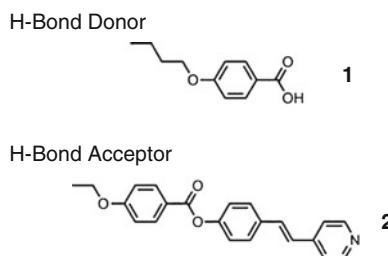
Takashi Kato

9.3.1 Introduction
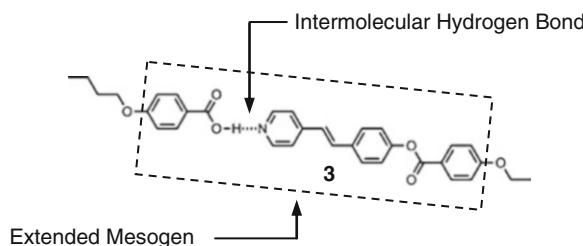
The molecular design of chemical building materials that express a variety of functions using molecules and non-covalent bonds is commonplace now. However, before 1989, when we reported for the first time a supramolecular liquid crystal [80] and supramolecular polymers [81–84] in which hydrogen bonds play an essential role, there was little knowledge about the active use of non-covalent bonds in the design of molecular material.

The research that I had conducted in the group of Prof. J.M.J. Frechet was a groundbreaking effort and the four earliest papers by us [80–83] had a total citation

Fig. 9.9 Molecular
structures of hydrogen
bond donor **1** and hydrogen
bond acceptor **2** used
in the formation
of supramolecular
liquid crystal

H-Bond Donor

1

H-Bond Acceptor

2

Fig. 9.10 Supramolecular
liquid crystal **3** formed by
the hydrogen bonding

Intermolecular Hydrogen Bond

3

Extended Mesogen
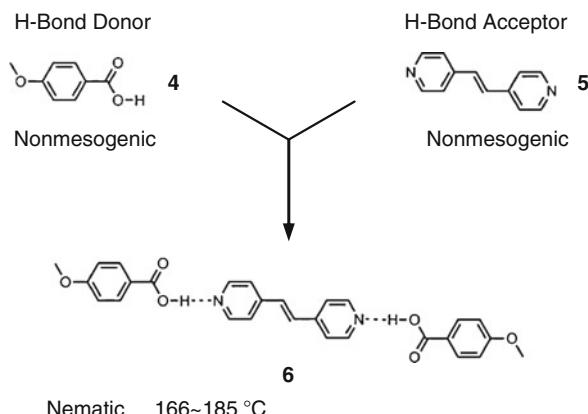
number of 1,100 as of December 2012 that shows their major impact in areas
related not only to the liquid crystal but also to supramolecular chemistry, polymer
chemistry, and materials chemistry in general.

Hydrogen bonds can be expressed as –X–H. . .Y (X, Y are large and electroneg-
ative atoms such as oxygen, nitrogen, and fluorine), and electrostatic interaction
plays a central role. It can be said the hydrogen bond is asymmetric and that it has a
direction. In the living body, independent multiple hydrogen bonding between
molecules for molecular recognition and information transfer plays a decisive
role. Compared to the outstanding performance in the natural world, I am hesitant
to say that using hydrogen bonds for the molecular design of organic functional
materials and polymer materials has being fully utilized.
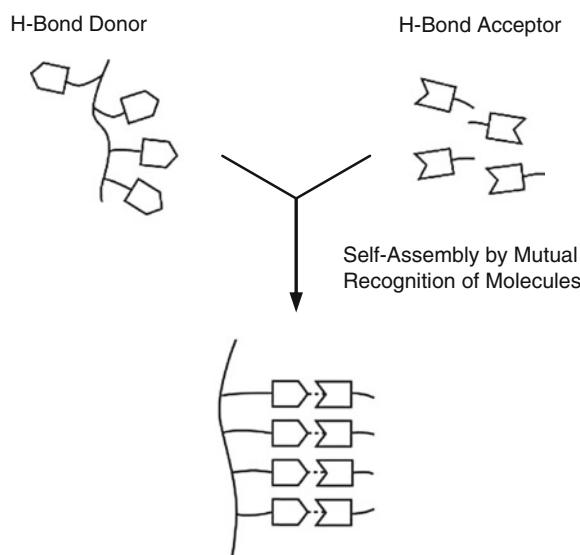
Together with J.M.J. Frechet, I could show that the combination of suitable
hydrogen-bonding molecules that can interact almost quantitatively leads to new
functional supramolecular structures (Fig. 9.9).

First, we used two kinds of different molecules, one having a carboxyl group at
the molecular terminal acting as a donor for hydrogen bonds (butoxy benzoic
acid **1**) and the other one having a pyridine ring acting as a hydrogen bond acceptor
(a stilbazole benzoate **2**). A supramolecular complex was formed almost quantita-
tively in a 1:1 mixture of both compounds, and the hydrogen-bonded complexes
became a new type of self-organized liquid crystalline mesogen **3** (Fig. 9.10) [80].
This hydrogen-bonding supramolecule shows a transition phase behavior as clear as
one molecule: the melting point and the nematic–isotropic liquid phase transition
point appear as a sharp endothermic peak in the DSC. In particular, compared to the
behavior of pure **1** and **2**, the liquid crystal phase was greatly stabilized towards the
high-temperature side, that is, this rigid structure connected by hydrogen bonds is
also working as a mesogen. In addition, even nonliquid crystalline compounds,

Fig. 9.11 Induction of liquid crystallinity for the supramolecular complex formed through the hydrogen bond between nonmesogenic components

H-Bond Donor

4

Nonmesogenic

H-Bond Acceptor

5

Nonmesogenic

6

Nematic   166~185 °C
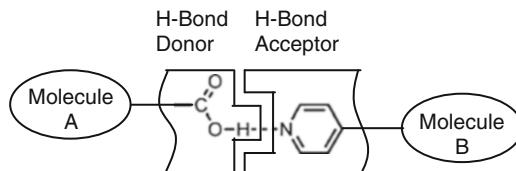
Fig. 9.12 Conceptual illustration of the formation of side-chain liquid crystalline supramolecular polymer by hydrogen bonding

H-Bond Donor

H-Bond Acceptor

Self-Assembly by Mutual Recognition of Molecules

such as methoxybenzoic acid **4** and bipyridine **5**, can build a supramolecular liquid crystal showing a nematic liquid crystal phase (Fig. 9.11) [85–87]. In the 1990s, various polymers that contain carboxylic acids as side groups were complexed with pyridine derivatives [81–84] to form liquid crystalline side-chain-type polymers, ferroelectric liquid crystals [84–88], host–guest liquid crystals [89], and so on (Fig. 9.12). Development of these compounds has been reported in detail in many comprehensive reviews [90–97].

I started this series of studies of constructing supramolecular liquid crystals as a postdoctoral fellow between 1988 and 1989 in the laboratory of Professor Frechet of Cornell University, Department of Chemistry. When I arrived, Prof. Frechet said to me, "I want to give you some time to think about the project by yourself."

Fig. 9.13 Conceptual illustration of the connection of molecules by the hydrogen bonding
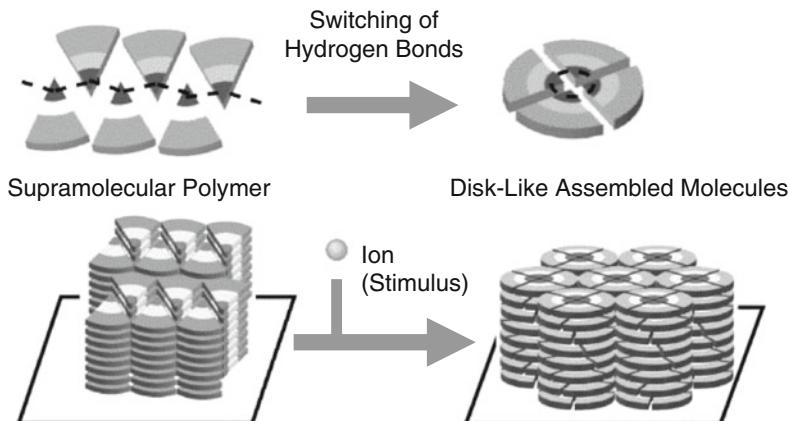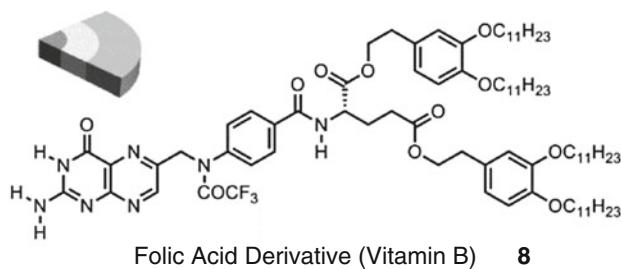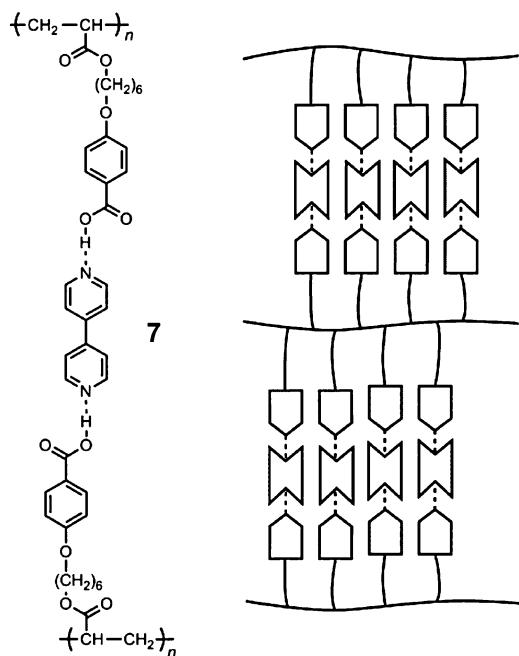
In a recent paper Prof. Frechet had published an attempt to increase the compatibility of polymer blends by hydrogen bonding [98]. In that study, polyvinyl pyridine, polyvinyl phenol, or polyvinyl benzoic acid had been used as a hydrogen-bonding polymer. Then, at the library, a report relating to a metal coordinating liquid crystal by Duncan W. Bruce et al. (now York University, UK) caught my eye. They produced a liquid crystal with a new type of metallomesogen with the pyridyl group of stilbazole as the ligand for the metal. In my head, a link between both stories, hydrogen-bonding polymer blend, and LC metal complex was made. In other words, I saw the pyridine group of stilbazole as a hydrogen bonding site. The initial trigger of supramolecular liquid crystal construction was born when I wanted to know what happens, or does not happen, when I combine molecules that allow for hydrogen bonds with stilbazole. There are many possible hydrogen bond pairs and my rationale was to use a pair of molecules that have a complementary shape. Finally I settled for the pair shown in Fig. 9.13: carboxylic acid and pyridine. Our first paper of this supramolecular liquid crystal was published in 1989, and in the same year Professor Jena Marie Lehn reported the construction of supramolecular liquid crystals using triple hydrogen bonds [99]. The dimer of benzoic acid was known as a liquid crystal by hydrogen bonds since the beginning of last century [100], but those were dimers of the same molecule, which limits the development of structures for supramolecular chemistry. The construction of liquid crystals from molecules of different types can stimulate the development of structures that could actively be used in the field of related materials chemistry [101].

Supramolecular liquid crystal molecules that are spontaneously formed by mixing several compounds that can form hydrogen bonds are fundamentally different from unimolecular mesogens. First, mixing molecules with simple molecular structure makes it possible to assemble more complex functional materials. Secondly, it is a structure which is formed by non-covalent bonds and hence has a dynamic nature. For example, molecules with more than one hydrogen bonding site can build liquid crystalline network structure (Fig. 9.14) [102]. Low molecular weight bipyridines and a polyacrylate having acid sites in the side chain form a liquid crystalline network structure that shows a smectic thermotropic liquid crystalline phase [102]. Polyfunctional low molecular weight hydrogen-bonding molecules can also build supramolecular liquid crystal networks [103, 104].

Another example is a new liquid crystalline molecular assembly that alters the structure and function in response to environmental stimuli (Fig. 9.15). The folic acid derivative **8** can, by hydrogen bond formation, be connected in series, taking a supramolecular polymer structure that shows a smectic liquid crystal phase. The introduction of salt changes the mode of hydrogen bonds by ion and dipole

Fig. 9.14 Liquid crystalline supramolecular network

7

Folic Acid Derivative (Vitamin B)   **8**

Switching of Hydrogen Bonds

Supramolecular Polymer

Disk-Like Assembled Molecules

Ion (Stimulus)

Fig. 9.15 Change of the liquid crystalline assembled structure of the folic acid derivative by the addition of salt

interactions, and the supramolecular aggregates become a cyclic tetramer, showing a columnar liquid crystal phase (Fig. 9.15) [105, 106]. This is a dynamic structural change in the liquid crystal formed by hydrogen bonds. Furthermore, folic acid derivatives with multiple amino acid side chains cannot form a smectic liquid crystal phase because of steric effects, and columnar liquid crystal phase and micellar cubic liquid crystal phase are formed [107, 108]. It is interesting to note that added salts cause a change in the balance between hydrogen bonds and dipole interactions that leads to a suppression of the rotation of the discotic supramolecules and results in a chiral liquid crystalline phase.

The design of the chemical structure and shape of the molecule should not be limited for the purpose to synthesize liquid crystals by hydrogen bonding. Using other interactions (ionic, charge-transfer, dipole–dipole, etc.), the arrangement and organization of molecules can also promote new functional materials of molecular aggregates [109–111]. By including those interactions, we developed micro-phase-separated structures and liquid crystal physical gels [112, 113]. Recently, by controlling the competing interactions of the aromatic ring and the intermolecular hydrogen bonds, an isothermal phase transition from a micellar cubic phase to columnar phase could be achieved by mechanical stimulation. With this, we obtained a new stimuli-responsive liquid crystal that changed its light emission by a mechanical force [114–117]. Now, the building of self-organized functional materials through the use of non-covalent interactions is widely accepted. Just two recent review articles received a total number of citations of over 1,000 times [105, 117] showing that our concepts have made a great impact in areas such as materials chemistry, supramolecular chemistry, and polymer chemistry.

9.4 Banana-Type Liquid Crystals: Shape-Induced Ferroelectric Structure, Chiral Structures, and Dissipative Structures

Junji Watanabe

9.4.1   Introduction

Ferroelectric liquid crystals were discovered about 35 years ago [118]. They gained interest, because of their chiral structure which provided optical activity, their fast response for display applications, and their bistable and polar structure. The fact that some of those compounds that are now used in LCDs are based on chiral pharmaceuticals and pesticides added to their fascination, and research flourished in the 1990s when around 40 domestic companies synthesized an amazing number of more than 1,000 compounds!
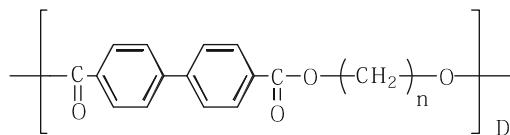
Chirality is introduced to manipulate the symmetry of the molecular aggregates. That is, chirality is intended to eliminate mirror symmetry. One specific example is the smectic C phase in which the symmetry is reduced from C_{2h} to C_2. As a result, a ferroelectric phase is formed with a twofold polar axis that can be inverted by an electric field.

However, it should be noticed here that the introduction of chirality is one of the simplest ways to reduce the packing symmetry. The research of banana-shaped liquid crystal is actually born from this fact. In other words, the attachment of a bent shape into a molecule could give rise to a smectic (Sm) structure which has the polar twofold axis along the bent direction and thus to ferroelectric and antiferro-electric Sm LCs without a chiral center. This was firstly suggested in the polymer molecules, successfully demonstrated in bent dimers and then in banana molecules.

The research for banana Sm LCs, however, did not stop there. As a by-product of this research, a number of achiral systems showed periodic chiral dissipative structures on the nanoscale. In this chapter, I will introduce this research trend and explain why a new "banana zone" has been claimed.
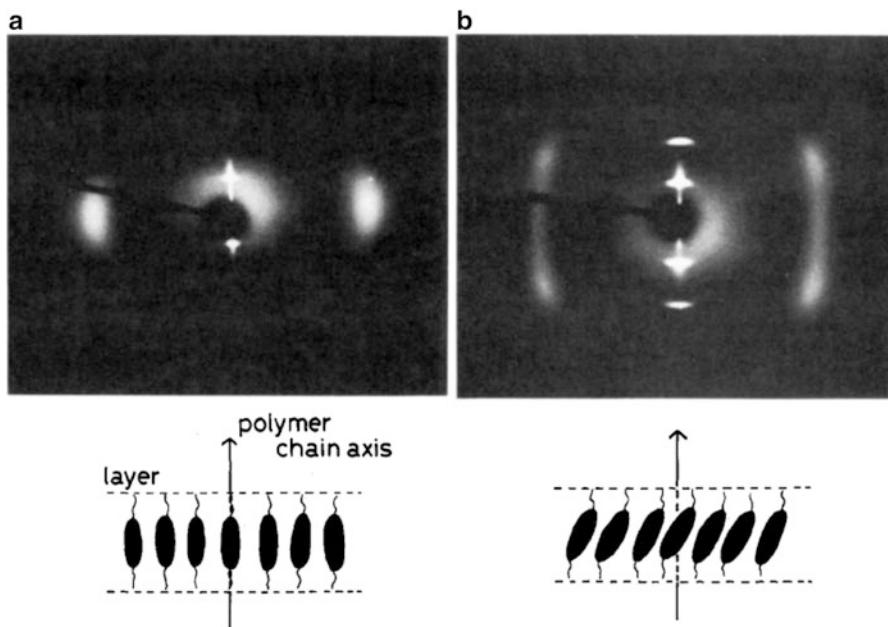
9.4.2   The Start from Main-Chain Liquid Crystal Polymers

The forerunner for the study of main-chain liquid crystalline polymers is shown below.

The mesogens (the part that forms the liquid crystal) are biphenyls that are connected with alkyl chains to form the flexible BB-n polyesters (where n is the number of carbon atoms in the alkyl chain). How would those polymers form a mesophase? For a nematic phase it is necessary that the director of the molecules align in one direction. For a smectic phase, in addition, the positional order of the mesogens to form layers is required. Unlike low molecular weight liquid crystals that have a single mesogen in one molecule, the answer is not simple for polymers with many linked mesogens in their backbone. In a mesogen, in order to acquire the orientational and positional orders of a mesophase, the liquid crystal structure may constraint greatly the polymer conformation. Or, on the opposite, the polymer chain orientation might affect the liquid crystal structure. Thus, the interplay of polymer and liquid crystal was an important problem that needed to be solved first [119–121].

Fortunately, the BB-n polyesters had the following important properties to solve this problem:
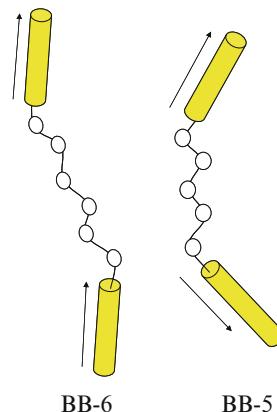
Fig. 9.16 Oriented X-ray patterns of fibrous smectic phases of (**a**) BB-6 and (**b**) BB-5 and packing structures of mesogenic groups within a layer elucidated from the X-ray patterns. Here, the oriented fibers were prepared by pulling the isotropic melt and the fiber axes placed in the vertical direction

1. BB-n polyesters form a smectic phase.
2. There is a clear odd–even effect: the smectic layer thickness d increases with increasing n, but with an odd–even oscillation in which d for even n is relatively larger than that for odd n.
3. The smectic phase structure is essentially different for even and odd n.

The consequence of this odd–even effect on the liquid crystal phase is shown in Fig. 9.16. The figure shows the X-ray diffraction patterns of fibers that have been spun from the isotropic phase. Figure 9.16a is an example for an even-numbered polyester, while Fig. 9.16b is an odd-numbered polymer. The fiber orientation is vertical for both samples. The even-numbered BB-6 shows a diffuse reflection on the equator of the pattern, indicating that the molecules are packed in a liquid manner in the smectic layer. For the odd-numbered BB-5, on the other hand, the diffuse reflections appear at an angle of about 25–30° from the equator. The lower part of Fig. 9.16 illustrates the molecular packing within a layer that corresponds to the diffraction pattern. The smectic layers are oriented perpendicular to the fiber direction for both polymers, but the mesogenic groups are tilted in the odd-numbered polymer. According to the conventional classification scheme of smectic phase liquid crystals, one would speculate that the even-numbered polymer forms a smectic A (S_A) phase and the odd-numbered polymer a smectic C (S_C) phase.
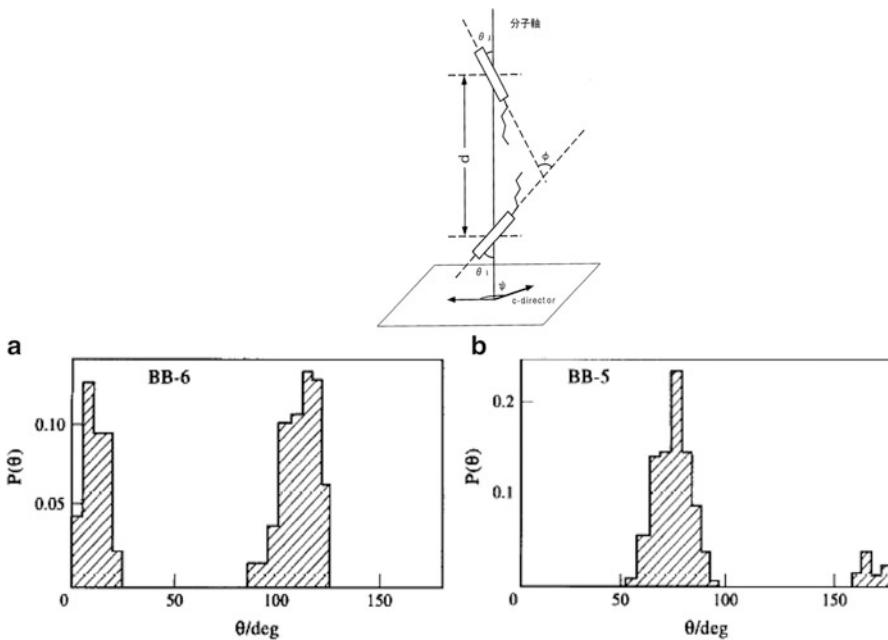
Fig. 9.17 Illustration of
BB-6 and BB-5 chains
in all-trans conformation

BB-6   BB-5

9.4.3 Nature of the Odd–Even Effect and Discovery of Novel Smectic Phase in the Odd-Numbered Polymer
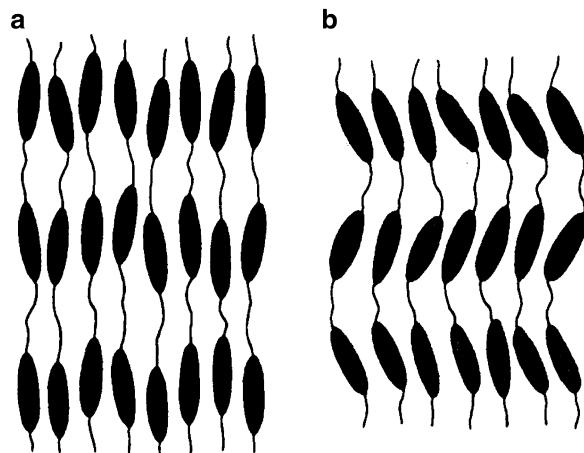
After we reported the above findings, a discussion of the conformation of polymers was promoted under the assumption that polymers take a conformation acceptable for isolated polymer chains. Results clearly show that in the even-numbered polymer there are many conformers that have the uniaxial orientation of mesogenic groups while in the odd-numbered polymer a uniaxial orientation of mesogens cannot be allowed. Most simply, this can be understood in the all-trans model of alkyl spacers shown in Fig. 9.17 [120, 121]. Of course, the mesogenic groups dynamically rotate and translate in the liquid crystal field, which is not considered in the hard all-trans conformation as such, but as a first-order approximation it is not a wrong model. In the odd-numbered polymers, adjacent mesogens are arranged in a zigzag fashion with a large angle of about 60° in contrast to a parallel alignment of mesogens in even-numbered polymers.

In more detail, by using the isomeric state approximation for the C–C bonds of alkylene chain, we can pick up all of possible conformers and thus can examine the angular distribution of adjacent mesogens within a polymer. The isomeric state approximation is a good approximation, because intermolecular interactions in the liquid crystal field are weak. The results in Fig. 9.18 show two different distributions. The chains with an even number of atoms have an angular distribution with two maxima at 0–30° and 90–130°. The odd-numbered spacer molecules show distribution maxima at 60–90° and 160–180°. Also, based on any set of orientations, small angle orientation corresponds to stretched conformers, whereas large angles correspond to folded conformers. It can be seen from the orientation distribution of the mesogens that in an even-numbered polymer there is a smaller angle orientation of the mesogens which conform to the S_A phase with a parallel mesogen orientation. However, there are no conformed ones that would satisfy a S_C phase presumed in the odd-numbered ones (in which the mesogens must be parallel, too) [119–121].

Fig. 9.18 Probability of conformers with two successive mesogens inclined by angle θ for BB-6 (**a**) and BB-5 (**b**)

Fig. 9.19 Illustration of (**a**) smectic A for even-numbered polymer and (**b**) smectic CA for odd-numbered polymer

In order to achieve consistency of the modeling and X-ray data results in the odd-numbered ones, a layered structure in which the tilted orientation of the mesogenic axis is reversed in adjacent layers (referred to as S_{CA} phase) was proposed (Fig. 9.19b) [120–122].

The S_{CA} phase proposed here is really new and hence the problem was how to distinguish the S_{CA} phase from the usual S_C phase. Both the S_C phase and the S_{CA}

phase have a c-director. However, there is a distinction between the head and the tail of the c-director in the S_C phase, which is the axis perpendicular to the layer normal orientation. On the other hand, the rotoreflection of the c-director in the S_{CA} phase leads to no distinction. From a crystallographic viewpoint, the former phase has a C_{2h} symmetry, whereas the latter has a repetition period of two smectic layers and thus a D_{2h} symmetry. This means that the optical properties of a spiral structure after doping with a chiral component are essentially different in both phases. Because of this difference in the phase structure, their defect structure is different as well. By giving these experimental evidences, we have demonstrated the correctness of this model of S_{CA} phase [122]. This new S_{CA} phase will be of importance for the later description of the antiferroelectric phase of banana molecules [37].

Again, let me summarize the characteristics of the smectic main-chain-type liquid crystal polymers here:
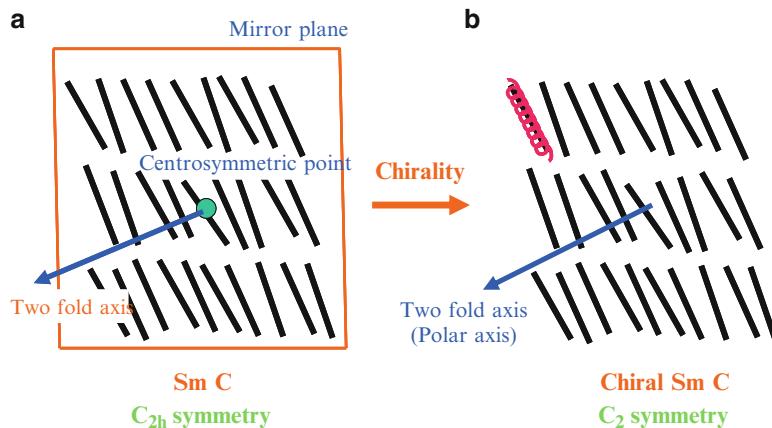
1. When n is even, a smectic liquid crystal with parallel mesogens is present, in which the axis is parallel as well.
2. When n is odd, a smectic liquid crystal in which adjacent mesogens have a tilt angle of about $60°$ is present, in which the polymer chains are inclined $30°$ to the molecular axis of the mesogens.

Surprisingly, the odd–even effect does not disappear even for alkyl chain length of $n = 20$ [123]. How far exactly this effect would continue is interesting to know, but there are limits to the synthesis of such polymers.
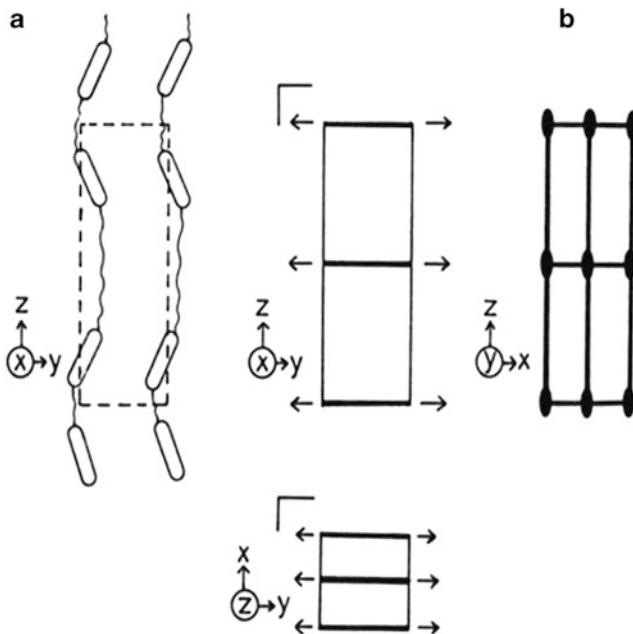
9.4.4 First Step Towards the Creation of an Achiral Ferroelectric Phase

Bearing in mind the odd–even effect, I tried to synthesize new polymer types in order to express the ferroelectric phase in an achiral system. The opportunity to study chiral ferroelectric liquid crystals was ripe at that time, as I already mentioned in the opening sentence. Their discoverer Mayer [118] argued that by introducing a chiral molecule into a S_C phase, the twofold axis of the S_C phase becomes the polar axis because of the extinction of a vertical mirror symmetry (Fig. 9.20). The reduction of the symmetry by the introduction of chirality into the system is in a sense conventional, simple, and straightforward.

Here, we decided to use the polymer effect to lower the packing symmetry of the system. Let's consider alternating copolymers with the two different alkyl chains having the odd carbon number and one common mesogen. When the two different units are segregated to form the bilayer, a Sm phase structure shown in Fig. 9.21 should be possible. In this phase, unlike in the simple S_{CA} structure, the rotation–reflection axis disappears, and the symmetry is reduced from D_{2h} to C_{2v}. Thus, a spontaneous polarization is generated in the twofold axis along the tilt direction of the mesogen and parallel to the layer (see Fig. 9.21). As a result, the liquid crystal becomes a ferroelectric phase [124, 125].
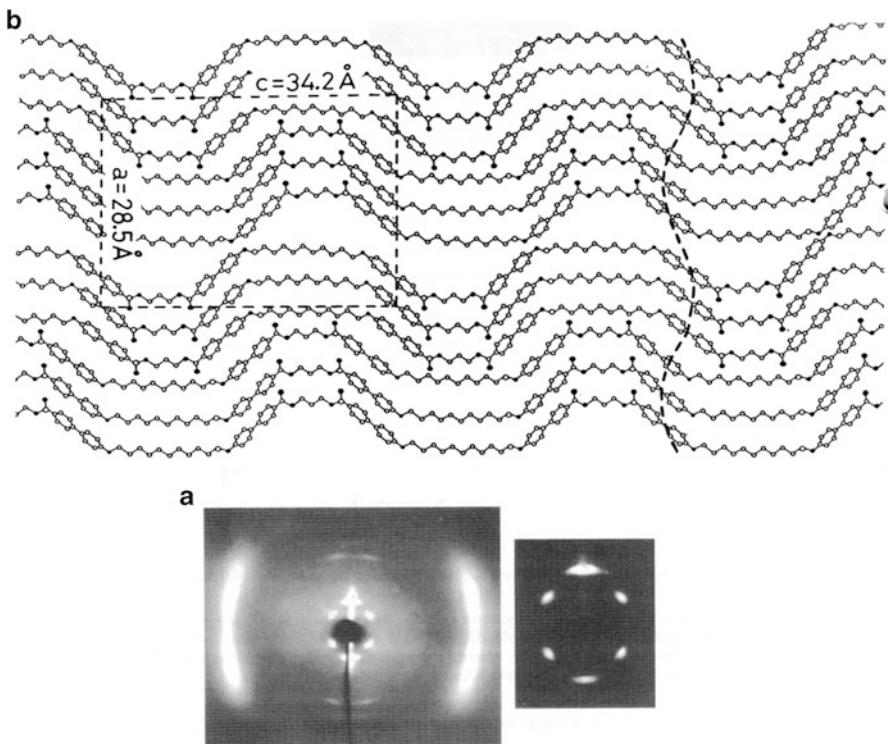
Fig. 9.20 Layer structures and their symmetry elements for smectic C and chiral smectic C*
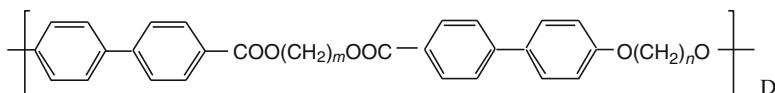
Fig. 9.21 Space-group symmetry for the bilayer smectic structure formed from alternate copolymer with two different alkyl spacers (see text). (**a**) alternate copolymer, (**b**) notation of symmetry element: spontaneous polarization is generated along the tilt direction of the mesogen

Such alternating copolymers were synthesized from a mesogenic hydroxy biphenyl carboxylic acid as described below, with one of the spacers (number of carbon atoms: m) linked by ester bonds and the other (number of carbon atoms: n) by ether bonds.
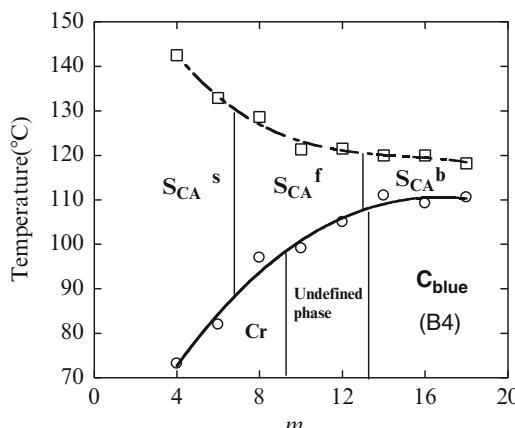
Fig. 9.22 (**a**) X-ray pattern of oriented smectic phase observed in BPCO3-011 fibers at 200 °C. The fiber specimen was prepared by pulling up the isotropic melt and its axis is placed in the vertical direction. It includes several other inner reflections except for the usual layer reflections, indicating the frustrated phase. (**b**) Tentative structural model of frustrated smectic phase. For convenience, the polymer chains in an all-trans conformation are illustrated

The goal of the synthesis was clear. The pair (m, n) should be both odd, and the system should cause segregation. Various combinations of m and n were possible, but we focused on polymers in which n and m were greatly different, specifically $(m, n) = (3,11)$, $(3,13)$, $(3, 15)$, $(3,17)$, and $(3,19)$.

In these copolymers, the segregation of two components into the bilayer really takes place; however, the formed phase was a dissipative (frustrated) structure as can be seen from the X-ray diffraction pattern in Fig. 9.22a. In addition to the ordered position of the mesogen in the smectic layer cycle, there is a periodic density fluctuation from the undulations parallel to the layers. Figure 9.22b expresses the structural model. The undulations of the layer are due to a reverse domain structure of the polar structure of Fig. 9.21. We expected it to emerge in one

Fig. 9.23 Phase transition behavior in dimer compounds, *m*OAM*n*AMO*m*. When the tail length, *m*, is larger than 14, antiferroelectric smectic phase, $S_{CA}{}^{b}$, is formed

domain, but it shifted by 1/2 cycle and inverted in relation to the molecular axis orientation in the adjacent domain. Thus, spontaneous polarization is canceled out in the two-dimensional lattice, and so the undulations may be considered to be caused by dissipation of interaction of the spontaneous polarization [124, 125]. This itself was interesting as mentioned below, but our purpose to produce a ferroelectric phase was not fulfilled.

In the frustrated smectic phase, the mesogens at the domain inversion boundaries have the energetically unfavorable contact with the alkyl groups. So, a larger difference between *m* and *n* means that the segregation strength should dominate to overcome the spontaneous polarization interaction. Thus, it may be possible to obtain the desired structure (i.e., without inversion domain) with other combinations of (*m*, *n*) in a largely different length. But synthetically, we had reached the limit for large *n*.

Our next aim was dimer compounds with two mesogens linked with an alkyl chain. The odd–even effect of the alkyl chain would basically be the same for polymers as well as for dimers. In the dimer case, the segregation, which is the reduction in symmetry, is made between the alkyl spacer and alkyl tail. Here, the terminal alkyl chains can be more freely chosen, which can induce the large difference in length between the terminal alkyl tail and connecting alkyl spacer so as to cause a strong segregation. A typical dimer system showing strong segregation is *m*OAM*n*AMO*m* shown below [126, 127].
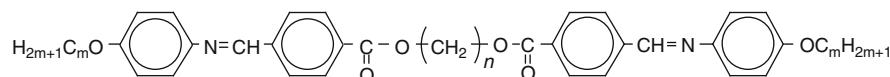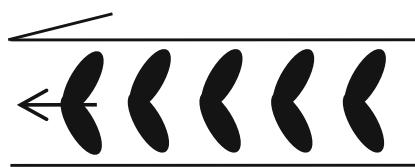

Figure 9.23 shows the phase behavior of compounds with the common spacer length of *n* = 5 carbons and with different terminal alkyl chain lengths of *m* = 4–18. As described above, the connecting spacer has to be an odd number of carbons, but the terminal groups can be both, odd or even. When *m* is short, the alkyl spacer and
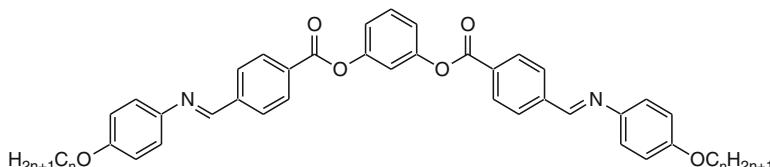
Fig. 9.24 The smectic layer structure formed by banana molecules. The banana molecules are packed into a layer with the same directionality, showing the spontaneous polarization along the bent direction
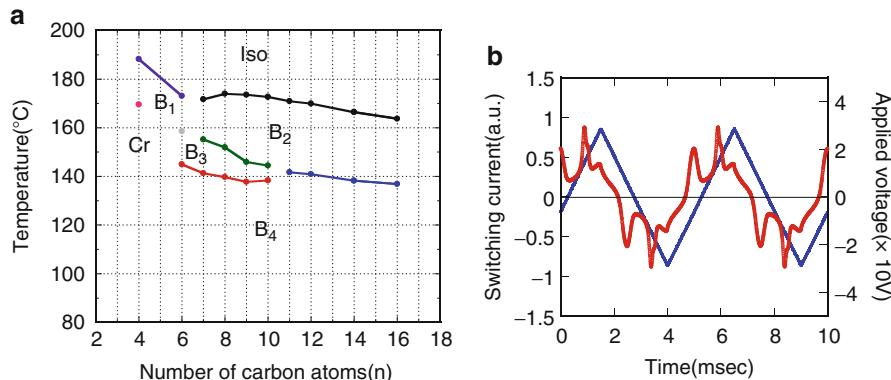
alkyl tail are compatible to each other and a conventional $S_{CA}{}^{s}$ phase is formed. On the other hand, medium-long terminal alkyl tail causes segregation and a frustrated smectic phase $S_{CA}{}^{f}$ phase is formed as observed in the polymer system. With further longer alkyl tails this changes to an inversion domain-free $S_{CA}{}^{b}$ phase [126, 127]. As a result, a phase sequence that beautifully followed our expectations was obtained [126, 127], resulting in an antiferroelectric $S_{CA}{}^{b}$ phase [127–129].

9.4.5 The Banana-Type Ferroelectric Phase

Through the studies of these dimer molecules, our research began to migrate to the banana-shaped molecule, as they were a natural extension of symmetry breaking along the longitudinal axis of the molecule. In other words, the constrained orientation of the bent mesogens that had been created in linear molecules by attaching them to an odd-numbered spacer was now achieved by the bent mesogen itself. Connecting two mesogens to the meta-positions of an aromatic ring led directly to bent mesogens. Even though it was a wacky idea, banana-type mesogens were simply fascinating.

If banana mesogens form a smectic phase, it is possible that each layer is polar. Because of the excluded volume effect (to increase the packing density) the mesogens should be facing in the same direction, as shown in Fig. 9.24. The story is quite simple here: the bent direction is the polar axis. Once an isolated layer is polar, it just depends on the adjacent layers if a ferroelectric (adjacent layers have the same orientation) or antiferroelectric phase (adjacent layers have opposite orientation) is formed. In 1966 [130], this fascinating banana smectic phase showing the polarization reversal was first reported in a high-temperature smectic B2 phases of the following compounds (PnO-PIMB), as can be seen in Fig. 9.25a.
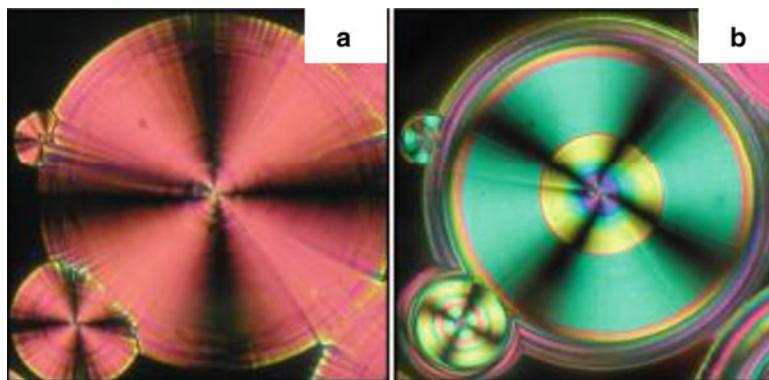
Fig. 9.25 (**a**) Phase transition behavior of banana molecules, P-n-O-PIMB, and (**b**) antiferro-electric switching behavior observed in B2 phase on the triangular-wave voltage application

9.4.6 Spontaneous Generation of "Banana Chirality"
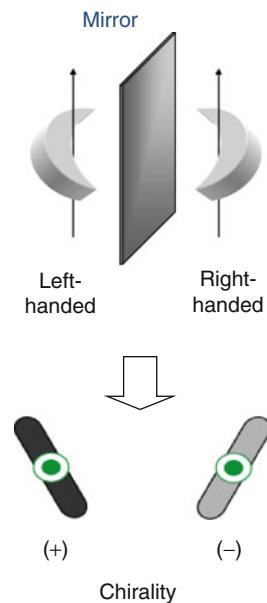
The banana molecules are too interesting to say "now since the ferroelectric phase has been demonstrated, let's move on." Their bizarre behavior sometimes leads to ferroelectric and sometimes to antiferroelectric phases. Their optical texture is also not uniform, but they exhibit a polydomain liquid crystal phase, as if they would contain a large amount of impurities (of course the compounds were as pure as possible). The reason for this erratic behavior was proposed at a Gordon conference in 1997: the complexity of the behavior stems from the tilting of the molecules with respect to the smectic layer. Initially, we considered the molecular tilting in the B2 phase because the measured thickness of the smectic layers was far less than the calculated molecular length [131]. This fact had always been in the back of my head, but I could not find a reason why the molecular axis must tilt.

The tilting of molecules in the B2 phase is clearly confirmed from the observation that the spherulites emerging from the isotropic phase show an electric field dependence of the position of the optical extinction lines (Fig. 9.26). Because of the tilting of banana molecules to the layer, chirality is spontaneously generated in addition to the polarity; this fact sounds shocking but is so simple to be understood [132, 133]. If the molecule is rotated around their polar axis (the orientation of the bent in the molecules), which is akin to tilting the molecules in the layer, the rotation operation cannot be achieved by a simple translation (see Fig. 9.27). That is, these two states are in a mirror relation with left-handed and right-handed chirality. This is called "the layer chirality." When the chirality couples with the polarity of the molecules, one would consider various smectic liquid crystal structures. There are two homochiral phases in which either (−) or (+) chiral molecules stack in the layers and a racemic phase in which layers are alternately stacked with layers of (−) and (+) chiral molecules. Each of those phases can be either ferroelectric or antiferroelectric, so that in total six different phases are present
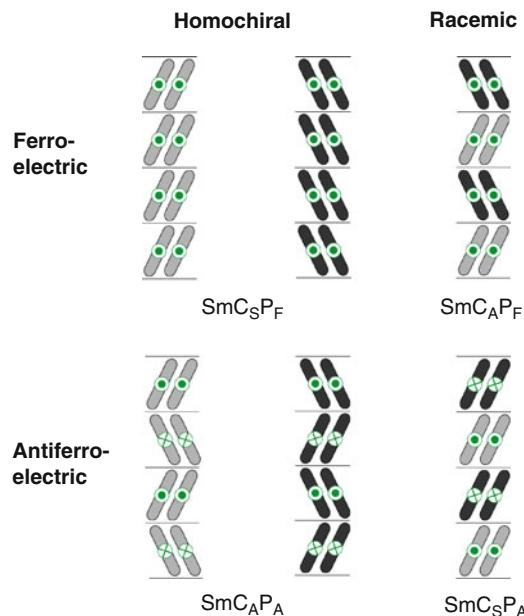
Fig. 9.26 (**a**) Polarized micrographs of the sphere-like domain of B2 phase between crossed polarizer and analyzer. When the external field is applied, the extinction brushes, which were parallel to the polarizer and analyzer, rotate as in (**b**)

Fig. 9.27 Illustration of the chiral symmetry breaking event by tilting of banana molecule to the layer normal
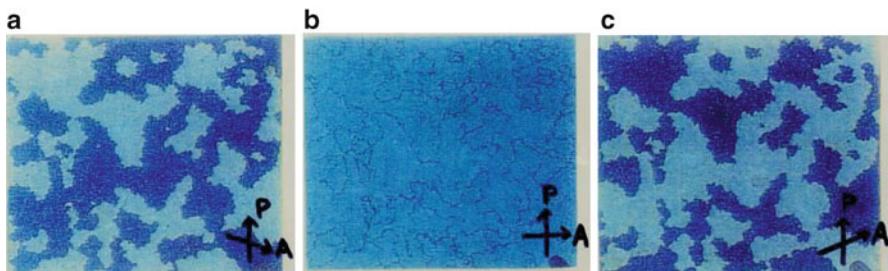
after all (Fig. 9.28). Because the energy difference between homogeneous and heterogeneous stacked layers is not so large, the emergence of innumerable phases is possible. The layers thus become irregular and look like a "devil's staircase," leading to the fact that nonuniform optical texture as observed. As stated in Sect. 9.4.4, our aim had been to create a ferroelectric phase with achiral molecules to avoid having to deal with chiral compounds. However, it has become a chiral ferroelectric phase, which is quite ironic.

Fig. 9.28 Six types of layer structures with different alignments of tilting (chirality) and polarity (see text)
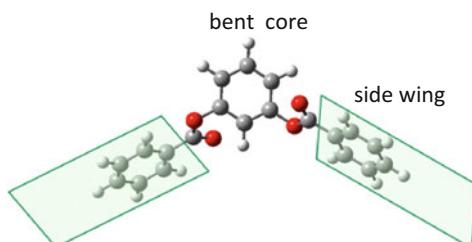
In practice, a chirality had been already discussed in low-temperature B4 phase [134], before it was in the B2 phase. The B4 is called "blue phase" because of its beautiful blue transparent color. It has a characteristic very low birefringence, which is hard to recognize under crossed Nicols. The blue color is due to the reflection of circularly polarized light, which is attributable to some spiral structure. This spiral structure has been proposed to be of twisted ribbons or twisted blocks in a twisted grain boundary phase [135, 136]. The B4 phase is transparent, because the spiral pitch is significantly smaller than the wavelength of light. Since the molecules themselves are not optically active, the left-handed and right-handed spiral structures should be equally formed, but a slight imbalance in their probability gives the positive or negative circular dichroism [137]. Because of the negligible birefringence and the opposite sign of optical rotations, the two chiral domains can be clearly detected by the optical microscopy under decrossed Nicols (see Fig. 9.29) [133, 135, 136].

It should be noted here that the size and shape of chiral B4 domains remained unchanged after the transformation between the B4 and B2 phases [138]. This means that there is a common origin of chirality. However, the problem is that one cannot avoid asking about the different origin of chirality in this B4 phase from that in the B2 phase because in this phase the molecules are not tilted [131, 138].

Fig. 9.29 Optical microscopic textures observed B4 phases. Under the cross Nicols, only a dark texture is observed as in (**b**), but two types of bright and dark domains can be distinguished by rotating the polarizer or analyzer from the cross-polarization position in (**a**) and (**c**). This means that there are two chiral domains with the opposite optical rotations

Fig. 9.30 Illustration of the chiral propeller-like conformation produced by the twisting of ester linkage between two aromatic rings in bent core and side wing

9.4.7 The Origin of Chirality

What is the common origin? Physicists say that chirality occurs because of the tilting of molecules to the layers, but chemists tend to argue the other way around: molecules become tilted in smectic phases because they are chiral. We then proposed that the chiral origin is due to the spiral conformation of molecule, according to two following points.

One of them is based on the calculated conformational energy of the isolated molecule, which shows two stable conformations. In these conformations, the ester groups at the bent core are twisted right ($60°$) or left ($120°$), so that the molecule adopts a chiral propeller-like conformation, as shown in Fig. 9.30 [139]. The calculation is credible, but the energy barrier between the left and right twist form is small, at most several hundred calories per unit bond. Therefore, in a liquid crystalline phase in which the molecules can rotate relatively freely, the chirality of the twist should be averaged over time.

Another interesting result is given by ^{13}C NMR measurement that the carbonyl emission in the ester linkage was split in two peaks in both of the B2 and B4 phases. Of course, the isotropic phase shows only one peak [140]. The presence of two

signals shows that two different conformations that exist are in the liquid crystal field, which is reasonable if the molecules assume chiral propeller type of conformation around the ester bonds as mentioned above.

If this is the case, the liquid crystal phase with maximum density is formed when molecules with the same twist form aggregate and form either (+) or (−) chirality in each layer of the B2 phase. Then, the tilted orientation (packing chirality) that is commensurate with the sense of the twist form is generated. To change the chiral twist within a layer then becomes almost impossible, because it would require a large cooperative movement of many molecules. As a result the energy barrier becomes very high and the chirality is preserved once the smectic layers are formed [138]. On the other hand, the molecular tilt disappears in the B4 phase, that is, the layer chirality disappears, but the chirality by the twisting conformation of molecules still remains. In my opinion, this is probably the mechanism by which a chiral TGB phase is built up in a blue phase probably.
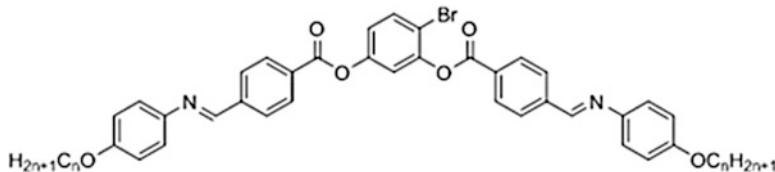
9.4.8 The Nematic Phase Including Banana Molecules Is Also Chiral?

There is an interesting experimental result that supports the evidence that twisted molecules create chirality. It is observed when achiral banana mesogens are mixed with a chiral nematic phase [141]. In general, the twisting force of the chiral nematic phase is reduced by the dilution of chiral molecules with achiral molecules and therefore the helical pitch increases. However, this trend is reversed when banana molecules are used; the twisting power increases. This suggests that the banana molecules are acting as a chiral molecule with strong twisting power. Here, we do not need to consider molecular packing symmetry leading to chirality in a nematic phase, unlike in the smectic phase. Thus, the chirality is attributed to individual molecules. Perhaps, the uniaxial anisotropic nematic phase leads to a biased distribution of conformers in which the twisted propeller form of the molecule, which is more flat than other conformations [139], is favored. Under the influence of the uniaxial anisotropic field of the chiral nematic molecule, the twisted conformation becomes more prevalent and the pitch of the nematic phase becomes amplified.

9.4.9 Various Frustrated Structures
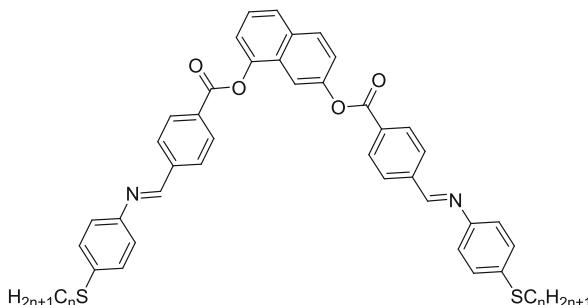
The third interesting characteristic of banana-shaped liquid crystals, besides polarity and chirality, is the frustrated (dissipative) phases B1, B5, B6, and B7. It is understood that all those phases have been produced by some kind of dissipation of the spontaneous polarization [142].

The chiral B4 phase as described above may also be considered one of the dissipative structures. It is believed that the B4 phase is a dissipative solid phase because it appears at temperatures below the crystalline B3 phase. In addition there are other phases that can be considered dissipative phases. The most typical are those formed in P*n*O-PIBM derivatives that contain a Br group on the central phenyl ring, 4Br-P*n*O-PIMB [143–146].
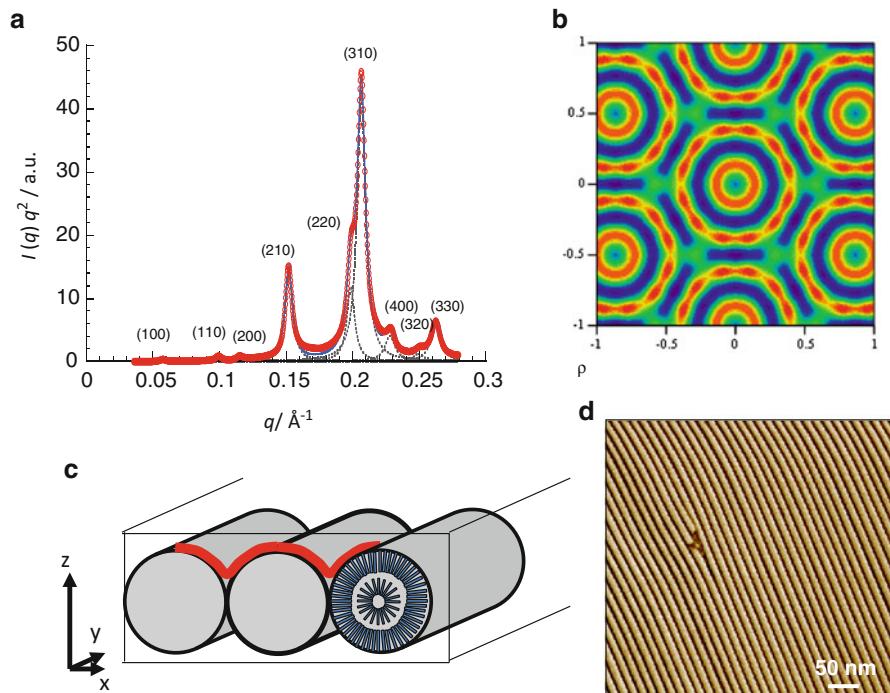
Depending on the length of the alkyl chains, three phases are formed: X1, X2, and X3. The X3 phase is formed with long alkyl chains and has an undulation of 17.5 nm. Short alkyl chain homologues form the X1 phase in which cylindrical structures with a diameter of 12.7 nm may arrange in a hexagonal lattice (Fig. 9.31).

Bent mesogens with the comparatively small bent-angle naphthalene core also show interesting dissipative structures [147–150]. (1,7)-*n*S-PIMB that has 1,7-dihydroxydiamine naphthalene as the central core is one example.

The mesogens are either packed in closed cylinders that arrange in a hexagonal smectic layer (columnar hexagonal (Col_h) liquid crystal phase), or they form a closed-sphere cubic (Cub) liquid crystal phase (Fig. 9.32a) [149, 150]. The Col_h phase has a spontaneous polarization that is in the column axis direction and shows an antiferroelectric response. Dissipative structures appear specifically in systems without molecular asymmetry. That is, as described in Fig. 9.32b, when asymmetric molecules are packed in layers, a difference in packing density occurs in the lower and upper halves of the layer [150].
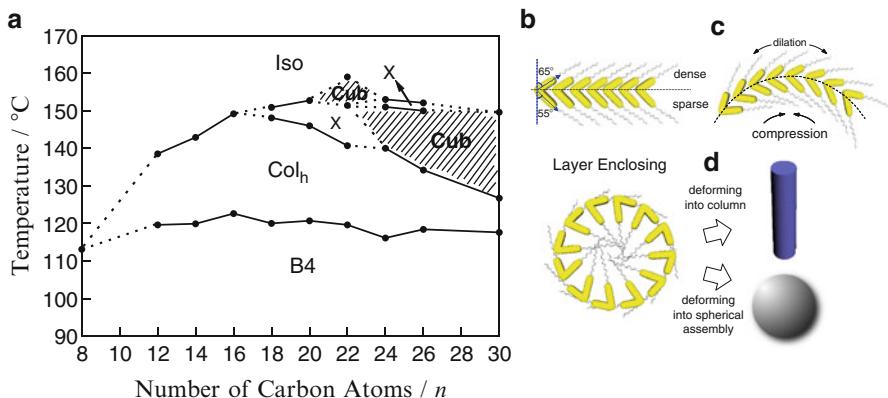
I just introduced a few examples of characteristic dissipative phases and they are splendid cases of nano-ordered structures in solids and liquid crystals that form an interesting branch of research about banana-shaped molecular systems.

Fig. 9.31 (**a**) Intensity profile of SR SAXS reflections with the Lorentz' correction (*red circle*) observed for the powder X3 sample. The numbers given on the figure are the (*hk0*) indexes. In (**b**), most probable reconstitution of the electron density map for the X3 phase by the nine reflections with the phase differences. The map indicates that the cylindrical rods packed into the hexagonal lattice are constructed of two concentric cylinders as illustrated in (**c**). The cylindrical association is also supported by AFM topography image of (**d**) observed on the surface of the fan-shaped domain in the X3 phase

9.4.10 Summary

Let me emphasize at the end of this chapter that there is nothing particular about the banana shape. What is inherent in the banana shape is that it reduces the symmetry of the molecule and thus was able to reduce the symmetry of the crystal structure, which is a collection of these molecules. Thus, molecules with other shapes, for example, similar to fans or hats, could be designed, too. These low-symmetry molecules can also form these unusual structures if they conform with the general requirements for liquid crystal orientation. Thus, it can be said that there is still room for the development liquid crystal molecules and liquid crystal materials.
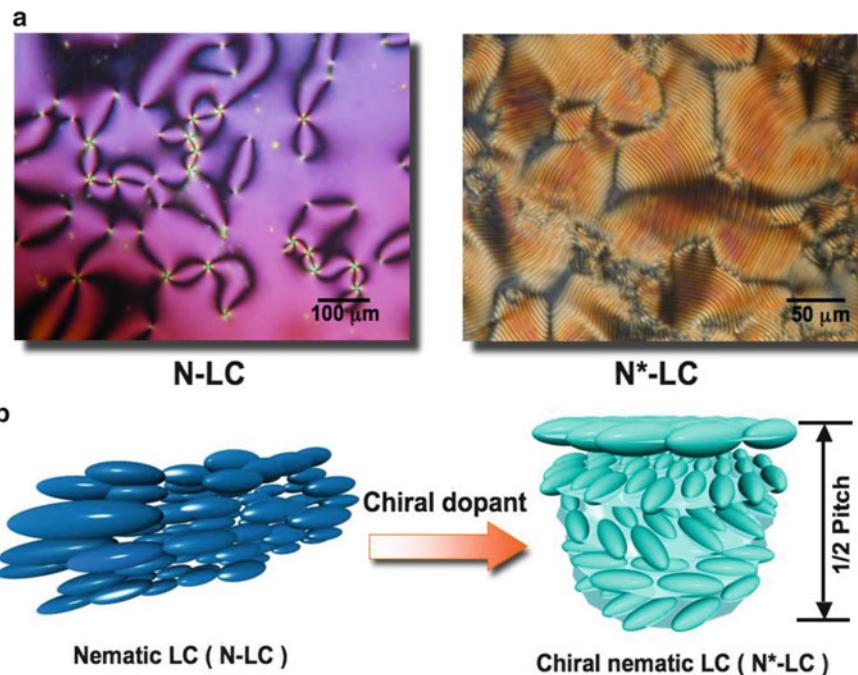
Fig. 9.32 (**a**) Phase transition behaviors of N (1,7)-S*n* including hexagonal columnar phase (Col$_h$) and optical isotropic cubic (Cub) as a function of carbon number of alkyl tail. (**b–d**) Schematic illustration of the column and cubic formation by the winding of the layer. (**b**) The asymmetric molecules are packed with the same directionality. Then, two rigid side arms of the banana molecule take a different orientation to the layer normal, producing a significant difference in the density if the layer is flat. Hence a dilation occurs in one half-layer (*upper part* divided by the *dotted line* in (**a**)) while a compression occurs in the other half (*lower part*) as in (**c**). This frustration can cause cylindrically and spherically enclosed deformations of the layer as in (**d**)

9.5 Polymer Synthesis in a Chiral Liquid Crystal Field

Kazuo Akagi

9.5.1 Introduction

Polyacetylene (PA) is one of the one-dimensionally conjugated compounds and a representative for conductive polymers [151]. The conductivity of PA is in the semiconductor region and its conductivity improves by 14 orders of magnitude by chemical doping [152, 153]. The highest reported conductivity is above 10^5 S/cm and comparable to the conductivity of copper and gold [154]. The PA backbone consists of strongly π-conjugated sp^2-hybridized carbon atoms, which takes a planar structure regardless of the conformer, *cis* or *trans*. However, it is possible to adopt a helical structure if a slight twist in one direction from the planar structure exists [155, 156]. Such a structure may express novel electromagnetic properties or second harmonic nonlinear optical properties [157, 158]. In this chapter, I will describe the acetylene polymerization in an asymmetric reaction field using chiral nematic liquid crystals (N*-LC), which also include cholesteric liquid crystals. The synthesized helical polyacetylenes have an ultra-hierarchical spiral form from the primary structure of the polymer chain to higher-ordered structures [156, 159, 160].
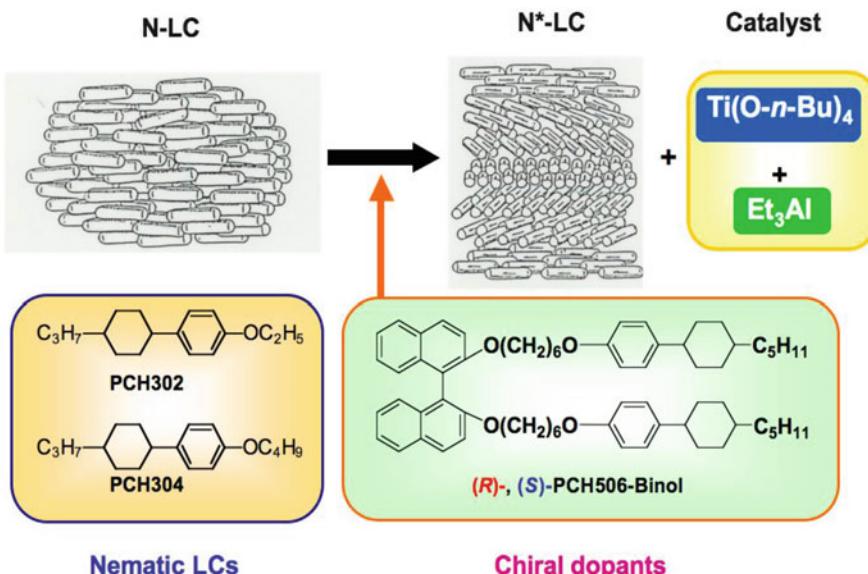
Fig. 9.33 Chiral nematic LC (N*-LC) induced by an addition of chiral dopant into nematic LC. Schlieren texture (*left*) and fingerprint texture (*right*) are observed for nematic and chiral nematic LCs, respectively, in polarized optical microscope

9.5.2 Chiral Dopants and Chiral Nematic Liquid Crystals (N *-LCs)

The N*-LC is used as an asymmetric liquid reaction field and it is prepared by adding a small amount of a chiral dopant to a nematic liquid crystal (N-LC). The formation of the N*-LC can be confirmed under the polarizing microscope (POM) by the change of the characteristic nematic Schlieren texture to a fingerprint-like or striated Schlieren texture of the chiral nematic phase. The distance between the fingerprint lines of the optical pattern is equivalent to half of the helical pitch of the N*-LC phase. Therefore, the stronger twisting power of the dopant can be observed by the shorter helical pitch of the optical pattern under the POM (Fig. 9.33).

There are two ways to adjust the helical pitch of the N*-LC phase: by varying the concentration of the chiral dopant or by changing the twisting power of the chiral dopant. In the former case, it is necessary to consider that the liquid crystal temperature range of N*-LC phase can be affected by the concentration of the chiral dopant. In other words, the liquid crystal temperature range is narrowing with increasing concentration of the chiral dopant and above a critical concentration might even disappear. Therefore, it is more practical to control the pitch of the

Fig. 9.34 Construction of asymmetric reaction field for acetylene polymerization by dissolving Ziegler–Natta catalyst, Ti(O-n-Bu)$_4$—AlEt$_3$, into the chiral nematic LC. The N*-LC contains an axially chiral binaphthyl derivative, (R)- or (S)- 2,2′-PCH506-Binol as a chiral dopant

N*-LC phase with the latter approach. Axially asymmetric chiral binaphthyl derivatives are known to have a larger twisting power than chiral compounds with an asymmetric carbon center [161, 162]. For our studies, we synthesized chiral (R)- and (S)-PCH506-Binol from the optically active (R) (+) and (S) (−) 1,1′-bi-2-naphtols by Williamson etherification reaction with a liquid crystalline phenylcyclohexyl (PCH) derivative (Fig. 9.34). The terminal alkyl chain was n-pentane, and the mesogen was linked to the binaphthyl with a hexamethylene spacer via ether bonds.

We prepared the N*-LC phase by adding a small amount (5–14 wt%) of PCH506-Binol to a two-component nematic liquid crystal mixture (PCH302, or PCH304). The liquid crystal group in PCH506 is essential in order to ensure compatibility with the chiral binaphthyl dopant and the nematic liquid crystal of the host material. PCH506 did not mix well with a host liquid crystal with a short methyl group (PCH503). Also, a mixture of an LC host with an alkyl-bearing chiral binaphthyl dopant did not result in an N*-LC phase.

9.5.3 Acetylene Polymerization in an Asymmetric Liquid Crystal Field

PCH304 and PCH302 are liquid crystals, but with a very narrow liquid crystal temperature range of 1–2 °C. Thus, they cannot be used as liquid crystalline
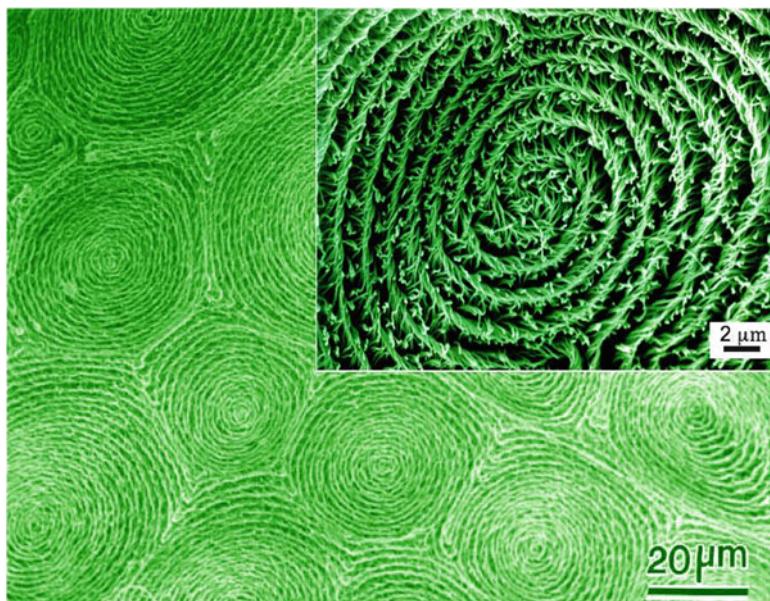
solvents for acetylene polymerization. Because acetylene polymerization is an exothermic reaction, the temperature within the Schlenk flask will rise during polymerization, and the liquid crystal phase turns into the isotropic phase. So, we prepared a nematic liquid crystal mixture with equimolar amounts of PCH304 and PCH302. The temperature of the nematic–isotropic transition (T_{N-I}) increases, while the crystal–nematic transition temperature (T_{C-N}) drops, resulting in a broadened nematic phase between 20 and 35 °C. Differential scanning calorimetry (DSC) measurements indicated that, also by taking a supercooling effect of the added catalyst $Ti(O-Bu)_4 - AlEt_3$ into consideration, chiral nematic liquid crystals containing a catalyst are suitable for the polymerization of acetylene at room temperature. Figure 1.34 shows a liquid crystal phase consisting of a nematic liquid crystal, the chiral dopant, and the catalyst $[(Ti(O-Bu)_4] = 15$ mmol/L; $[AlEt_3]/[Ti(O-Bu)_4] = 4$. The catalyst solution is aged at room temperature for 30 min, during which no change in the optical pattern of the N*-LC was observed, and the transition temperature decreased slightly by 2–5 °C. In other words, the T_{C-N} melting point was at 16–17 °C and the T_{N-I} clearing point was at 30–31 °C. Furthermore, the supercooling effect caused the catalyst solution to be fluid down to -7 °C. Furthermore, the chiral binaphthyl derivatives were found to be chemically stable with respect to the catalyst. Thereby, we confirmed that such a liquid crystal system can be used as a solvent for asymmetric acetylene polymerization.

High purity acetylene gas (99.9999 %) was used for the polymerization, and the temperature was maintained at 17–18 °C in order to maintain the N*-LC phase during polymerization. In order to achieve a constant temperature, cooled ethanol was circulated around the Schlenk flask. The initial acetylene pressure was 1.55–3.01 kPa (11.6–22.6 Torr), and the polymerization time was 10–43 min. After polymerization, the PA film was carefully peeled from the inner wall of the Schlenk flask and was washed several times with toluene at room temperature in an argon atmosphere. The film was transferred to a Teflon sheet, vacuum dried, and stored in a freezer at -20 °C.

9.5.4 Helical Polyacetylene (H-PA) Film

The surface of the H-PA film was observed by scanning electron microscope (SEM). In Fig. 9.35a, it can be seen that the film has a polydomain structure in which each domain is made up of helical fiber bundles that are all twisted in the same direction (Fig. 9.35b) [156]. The form of these H-PA spiral looks as if the optical pattern of the N*-LC has been copied by the interfacial polymerization.

The more detailed SEM observation revealed that the (R)-catalyst produced left-handed bundles of fibrils and the (S)-catalyst produced right-handed fibrils. This means that, as long as one uses the chiral dopant induced N*-LC phase, the winding direction of the twisted H-PA can be controlled by the helicity of the chiral dopant. The helical pitch of the N*-LC phase depends on the optical purity, twisting power, and concentration of the chiral dopant [163–165].
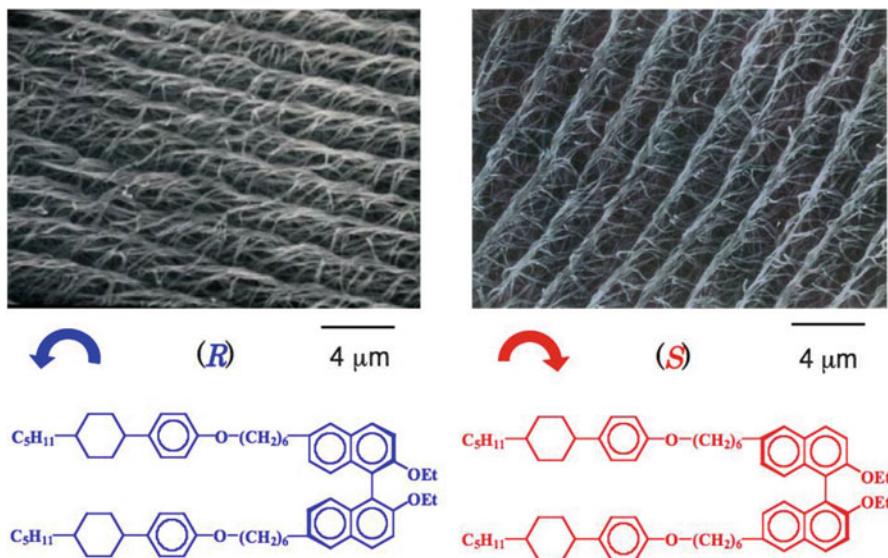
Fig. 9.35 Scanning electron microscope (SEM) photographs of helical polyacetylene (H-PA) film with hierarchical spiral morphology. The inset shows right-handed screwed bundles of fibrils in a domain of spiral morphology

Interestingly, the hierarchical conformation shown in Fig. 9.35 is very similar to the helical self-organized structures of organic compounds such as lipids, in living organisms, for which a synthetic counterpart has been missing. This suggested, in that sense, that the N*-LC phase is a versatile platform for helical conformation control of synthetic polymers, as well as templating for a polymerization medium.

Tetra-substituted binaphthyl derivatives that contain ethyl groups in the 2,2′ positions and PCH506 in the 6,6′ positions give a N*-LC helical pitch of less than 0.3 μm. Therefore, it induces a larger twist in the helical H-PA (Fig. 9.36). Here, it should be noted that the (R)- and (S)-N*-LC host show right- and left-handed helices, respectively. However, the bundles of H-PA fibrils synthesized in such an asymmetric reaction field produce helices with the opposite handedness. This result is the same for both types of binaphthyl derivatives, di-substituted as well as tetra-substituted ones [166, 167].

The circular dichroism (CD) spectra of H-PAs that were synthesized in the (R)-N*-LC phase show an absorption of 450–800 nm, corresponding to the PA chain π-π* transitions and a positive cotton effect and vice versa. This suggests that the PA chain itself is twisted in one direction. It should be noted that the cotton effect is not due to the binaphthyl derivatives, which only show a cotton effect in the short wavelength range of 240–340 nm, which is different from the absorption region of
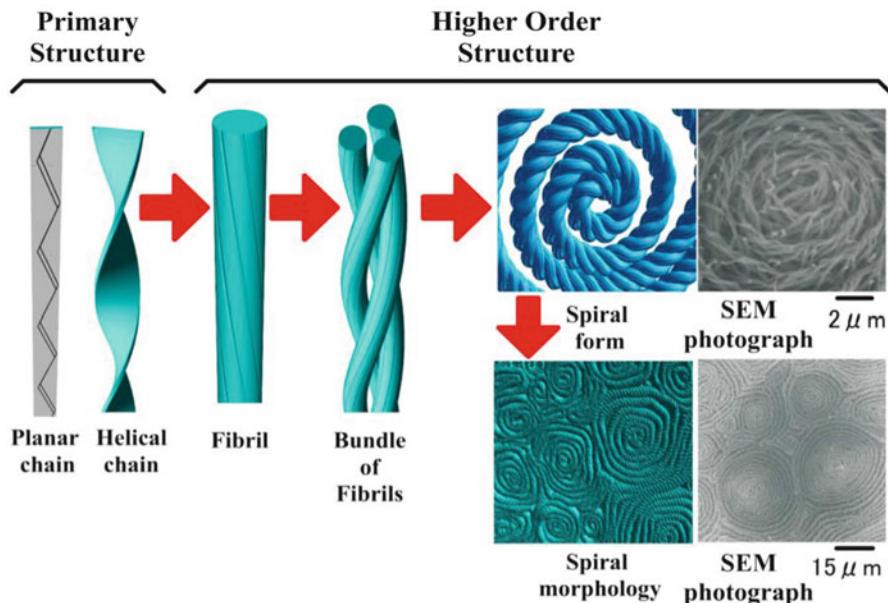
Fig. 9.36 SEM photographs of H-PA films synthesized in the N*-LCs containing (*R*)-6,6′-PCH506-2,2′-Et-Binol as a chiral dopant. The left- and right-handed screw directions of H-PAs are determined by the chirality of the chiral dopants with *R*- and *S*-configurations, respectively

the PA main chain. From these results we conclude that (*R*)–H-PA forms left-handed (counterclockwise) helices and vice versa. They then self-assemble by Van der Waals interactions to form helical fibrils that further aggregate into bundles that form spiral polydomains of various sizes (Fig. 9.37).

9.5.5   Helix Formation Mechanism of H-PA in the Asymmetric Liquid Crystal Reaction Field
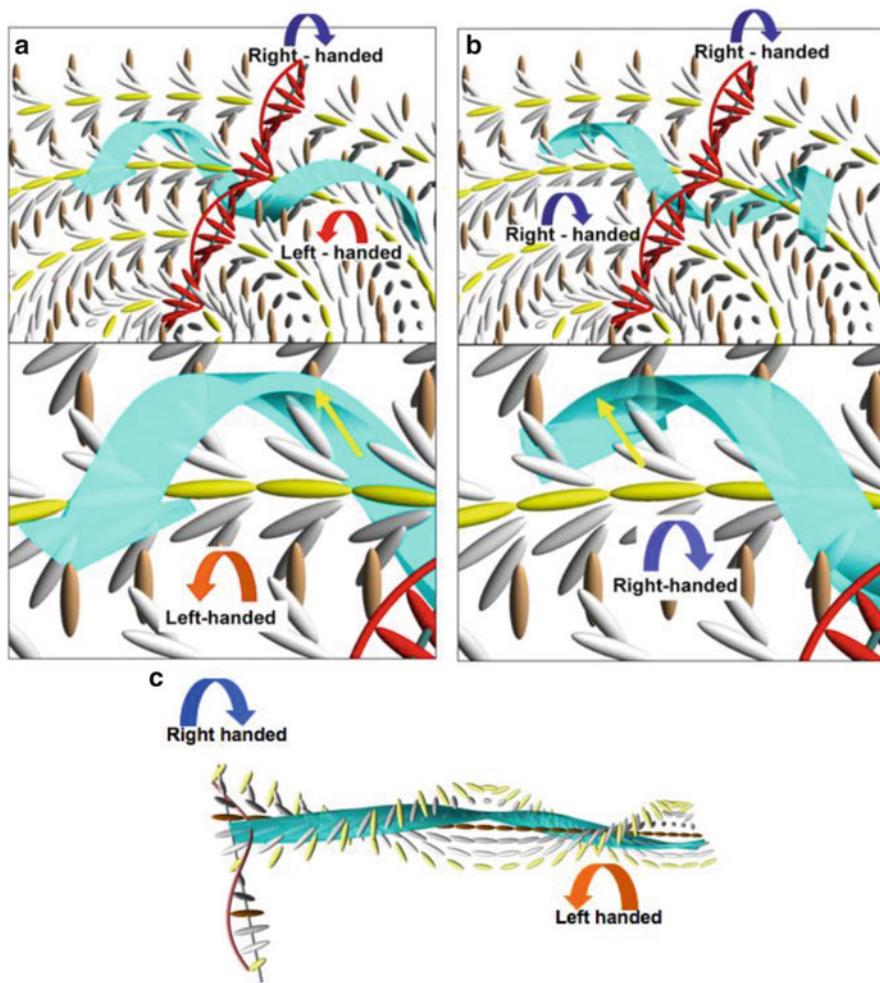
The discussion about the formation mechanism of the spiral structure of H-PA in the N*-LC phase can be found in the literature [168, 169]. When H-PA fibrils are synthesized by polymerization in a solvent, the polymer grows parallel to the substrate. In the case of the N*-LC phase as the solvent, the fibril formation depends on the surface of the liquid crystal. Therefore, in this system, the free surface of the liquid crystal alone may be considered for the formation mechanism of H-PA. The H-PA fibrils are grown along the director of the liquid crystal and grow while twisting along the fringes of the fingerprint-like LC pattern. Therefore, the portion where the liquid crystal molecules are oriented parallel to the substrate acts as an axis around which the director of the liquid crystal

Fig. 9.37 Super-hierarchical helical structures from primary to higher order in H-PA

molecules winds (Fig. 9.38). As a result, the right-hand twisted N*-LC phase leads to a spiral pattern in the H-PA in the bright part of the striped pattern of the fingerprint-like organization (Fig. 9.38a). Given the growth direction of the fibrils of the H-PA is the direction of the arrow, it is possible to explain the relationship between H-PA and N*-LC structure.

In other words, the winding direction of the spiral form of H-PA is consistent with that of the fingerprint-like pattern of the N*-LC phase and the H-PA fibrils are parallel to the stripes of the fingerprint pattern of the liquid crystal. That is, the helical axis of the H-PA is perpendicular to the helical axis of the N*-LC phase [226]. Furthermore, the distance between the fibril bundles of H-PA corresponds to half the length of the helical pitch of the N*-LC phase. The final conclusion is that the direction of the spiral of H-PA is opposite to the direction of the twist of the N*-LC phase. This last fact is shown in Fig. 9.38a, where the polyene chain grows in parallel to the liquid crystal molecules. In other words, if the liquid crystal molecules are twisted in the direction of the growing polyene chain, the polyene has to be twisted, too. At the same time, the twisting of the N*-LC phase will be transferred to a counter-wound form of the H-PA. On the other hand, if the polyene chain wants to grow in the same rotation direction as the liquid crystal (Fig. 9.38b), the polyene chain will collide at some point. Hence, this growth direction has a stereochemical disadvantage.

Fig. 9.38 Schematic representation of the mechanism for acetylene polymerization in N*-LC. (**a**) The H-PA chains that twist opposite to the helical sense of the N*-LC propagate smoothly along the LC molecules. (**b**) The H-PA chains with the same handedness as that of the N*-LC encounter the LC molecules and concurrently a sterically unfavorable polymerization occurs. (**c**) The helical sense of the N*-LC is transcribed to the H-PA with an opposite screw direction

9.5.6   Stability of the Helical Structure of H-PA

The H-PA film contains 90 % *trans*-double bonds and iodine doping leads to a metal-like conductivity of $1.5–1.8 \times 10^3$ S/cm at room temperature. After iodine doping, the absorption is slightly shifted to the short wavelength side as

compared to undoped H-PA, but it still exhibits the cotton effect with the same sign, indicating that the helical structure of H-PA is maintained even after doping. Furthermore, X-ray diffraction and CD spectra measurements show that the helical structure is retained even after heating to 150 °C, which is the *trans-cis* isomerization temperature [170]. The helical structure formed upon polymerization is stable even after washing with toluene or other solvents [167]. Even though the most stable form of PA has a planar structure, it can be said that, since PA is insoluble and does not melt, it is possible to maintain a metastable helical structure.

The polymerization processes described in this chapter may also impart a helical structure in heterocyclic conjugated polymers or aromatic systems that do not have chiral substituents in the side chain. In fact, in recent years various helical conjugated copolymers, such as polythiophenes, polyethylenedioxythiophenes, and phenylene–thiophene, have been synthesized by electrochemical or chemical polymerization using the N*-LC host phase [171–178].

Very recently, an iodine-doped precursor H-PA was carbonized by heat treatment at 800 °C, and the form was not only retained but at a carbonization degree of 80 % had even significantly improved. Furthermore, the material can be graphitized at 2,600 °C and the spiral morphology characteristic was retained, and helical ribbonlike graphite could be observed in the TEM [179–181].

9.5.7 Conclusion

In this chapter, I outlined recent developments of a new polymerization techniques using a asymmetric liquid crystal reaction field of the N*-LC phase, focusing on helical polyacetylene with a super-hierarchical spiral structure (H-PA). Chiral binaphthyl axially chiral derivatives are added as a chiral dopant to nematic liquid crystal to produce the chiral N*-LC phase.

This builds an asymmetric reaction field for Ziegler–Natta catalyst which was used for the interfacial polymerization of acetylene. Bundles of PA chains formed fibrils in a PA film, resulting in a hierarchical helical structure. Further, the winding direction could be precisely controlled by selecting the chirality of the chiral dopant. The direction of the twist in the fibril bundles has been found to be opposite to that of the N*-LC reaction field.

The use of the N*-LC as an asymmetric solvent enabled us to synthesize polymers having a hierarchical structure with a helical conformation of the molecular backbone primary structure. We can expect that this approach can be used to freely control the helical structure of various products to further progress in the field of polymer synthesis.
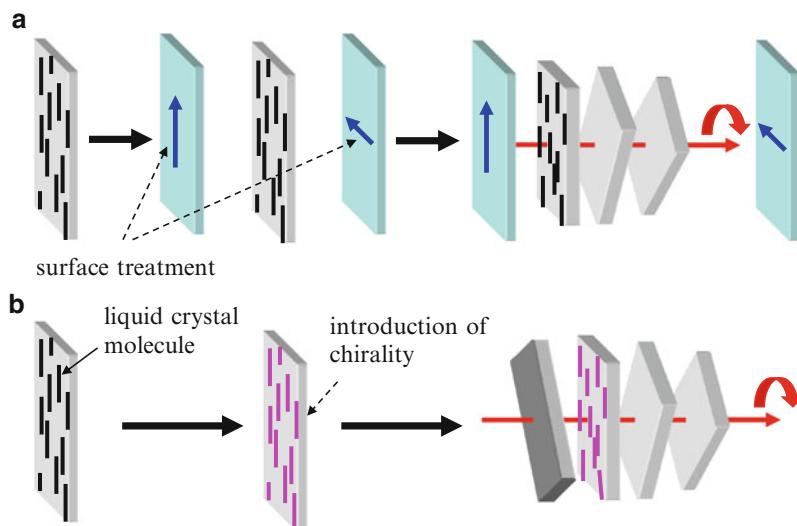
9.6   Frustration

Isa Nishiyama

9.6.1   Characteristics of Liquid Crystals and Frustrated States

It is one of the characteristics of a liquid crystal material, as a molecular assembly material, that there are two different origins determining the alignment styles, i.e., (a) the surrounding environment conditions such as surface treatments of the cell containing liquid crystal molecules define the alignment, and (b) liquid crystal molecules align spontaneously. Examples in the case of forming the twist alignment are shown in Fig. 9.39. It is schematically presented in Fig. 9.39a that liquid crystal molecules are sandwiched between two surfaces, which are treated in such a way that the molecules align in a direction indicated by the arrows. The alignment direction is twisted in 90° between two surfaces so that the molecules form a helical structure. In this molecular ordering, the directions of the molecules adjacent to both of the surfaces match the treatments. The resulting twisted structure is considered to be a kind of frustrated structure since the bulk molecules intrinsically have a desire to align in parallel.

Recent development of flat panels is largely owing to liquid crystal display technology. The key factor in realizing the great industrial success is the emergence and improvement of the display modes suitable for the large size TV display. There are different types of display modes for this purpose; however, the materials

Fig. 9.39 Two different characters for the determination of alignment, e.g., the helical structure is induced by the surface treatment of two surfaces (**a**), or is spontaneously emerged by the introduction of chirality (**b**)
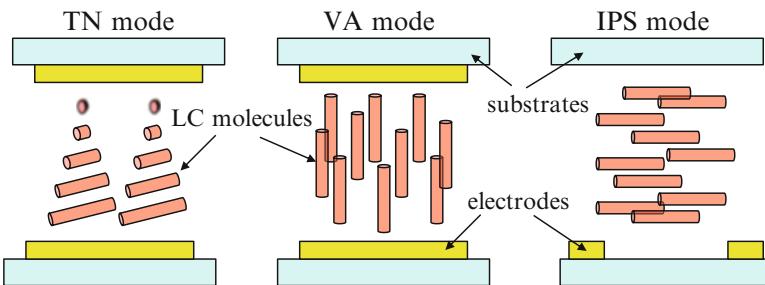
Fig. 9.40 LCD modes and the initial LC alignment

showing a certain kind of the liquid crystal phase, i.e., the nematic phase, are utilized for all of the modes. The difference between the display modes is characterized by the different initial alignment of the liquid crystal molecules as shown in Fig. 9.40. As such, the liquid crystal technology makes our life happy, thanks to the frustration, to some extent, of the liquid crystal molecules.

9.6.2 Frustrated Liquid Crystal Phase and the Origin

Frustrated liquid crystal phases are generated by two competitive factors [182, 183]. In this section, some examples of origins which are responsible for the emergence of frustration and resulting frustrated liquid crystal phases are introduced.

9.6.2.1 Frustration Between "Twisting in all Directions" and "Filling the Space"

The helical structure of the chiral nematic liquid crystals (Fig. 9.39b) is attributable to the fact that the molecules prefer to be at a slight angle to each other, rather than parallel. Thus, the resulting helical structure seemed to be most stable with respect to satisfying the desire for the molecules to twist each other. However, as far as the twist arrangement is concerned, another structure turned out to be more stable. Instead of the single helical axis shown in Fig. 9.39b, the director in this alternative structure rotates in a helical fashion about every axis perpendicular to the line (Fig. 9.41a). Such a structure has been coined "double twist" (Fig. 9.41b), although an infinite number of helical axes are really present. However, this double twist structure is more stable than the normal helical structure or the "single helical" structure only within a small distance from the line at the center. It is rather easy to understand this effect because one can imagine that the double twist structure cannot fill the space uniformly. The "blue phase" [184–186] is a special case where the double twist structure can fill a large volume of the space if the
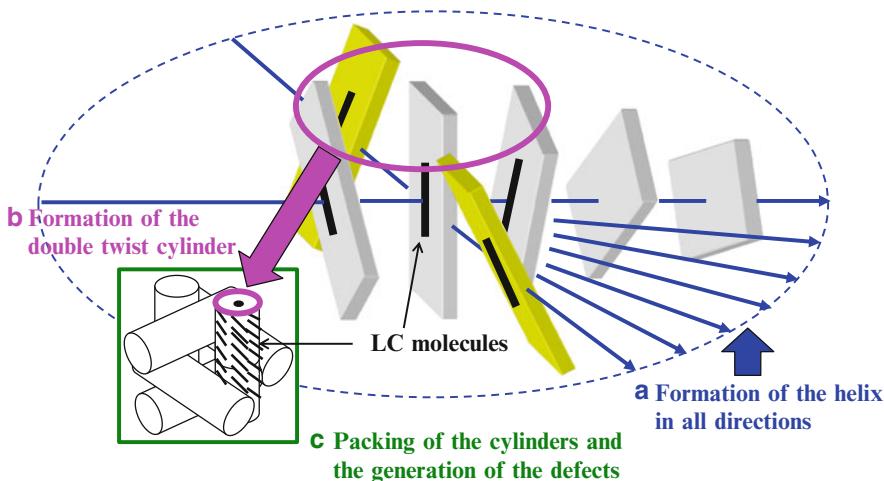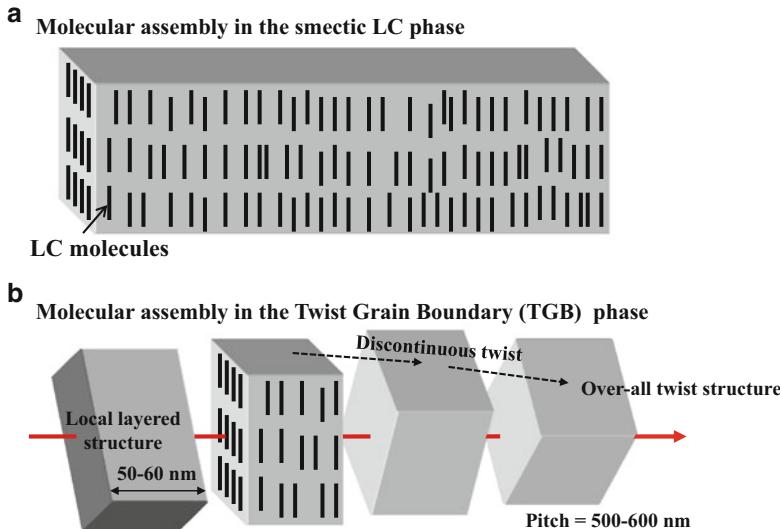
Fig. 9.41 Molecular assembly in the blue phase

occurrence of the defects at regular points between the cylinders is allowed (Fig. 9.41c). Thus, the defects do not just exist randomly in the blue phase, but the existence of the defects is in fact essential to the blue phase structure. The blue phase thus appears when the free energy gain of the formation of the double twist structures is larger than the free energy loss of the formation of the intrinsically generated defects.

As liquid crystalline materials showing or stabilizing the blue phase, dimers with an odd-numbered spacer [187], bend-shaped[188] and T-shaped [185] liquid crystals, and, more recently, dendrimers [189] have been reported. These materials do not possess a normal rod molecular shape but are expected to show lower elastic constant(s) which may decrease the free energy loss of the defect formation and thus may increase the stability of the blue phase. For example, it has been reported that the addition of bent-shaped liquid crystal into the normal rod-shaped nematic liquid crystal decreases the K_{33}/K_{11}, resulting in the stabilization of the blue phase [188]. Similar effect has also been reported in the case of doping dendrimer into the nematic liquid crystal [189]. This effect of decreasing K_{33}/K_{11} on the stabilizing the blue phase has theoretically been supported [190]. However, some contradictory experimental results have been reported on the correlation between the elastic constants and the stability of the blue phase. Thus, further experimental and theoretical considerations are needed. Flexoelectricity has also some effects on the elasticity of the material. It has been reported in the case of the dimer with an odd-numbered spacer that the flexoelectric effect reduces the apparent elastic constants and thus stabilizes the blue phase [187]. Biaxiality in the molecular shape is also another important point to be discussed. The relationship between the biaxiality of the molecular shape and that of the Q tensor has not well been described theoretically [191]. However, a theoretical treatment suggests the effect

a Molecular assembly in the smectic LC phase

LC molecules

b Molecular assembly in the Twist Grain Boundary (TGB) phase

Discontinuous twist

Over-all twist structure

Local layered structure

50-60 nm

Pitch = 500-600 nm
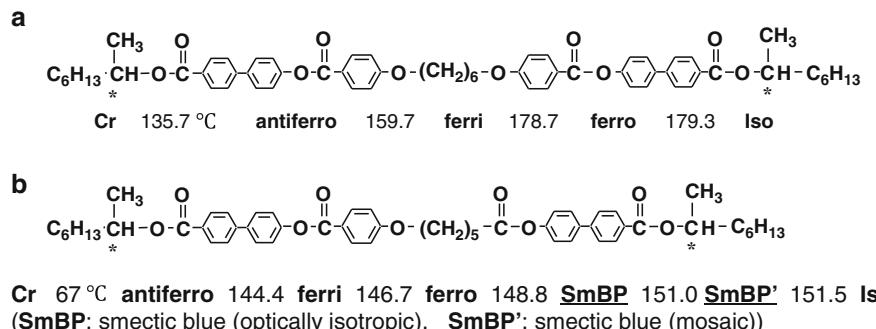
Fig. 9.42 Molecular assemblies in the smectic and TGB phases

of molecular biaxiality to some extent [192], and furthermore, the experimental results so far obtained strongly indicate the importance of the biaxial shape of the molecule on the emergence of the blue phase [193]. Further theoretical treatments relating the biaxiality of the molecular shape are expected. It should be noted that these properties, i.e., elasticity, flexoelectricity, and biaxiality, are closely related to each other and thus the total effects be taken into account to discuss the stabilization of the blue phase. Furthermore, the blue phase possesses a three-dimensional ordered or disordered structure which changes into usual liquid crystalline organization at the phase transition from the blue phase to the chiral nematic phase. If this re-arrangement in the molecular ordering is too slow to be occurred under the experimental conditions, the transition from the blue phase to the chiral nematic phase cannot be observed which results in the misunderstanding that the blue phase is stable [186]. This misunderstanding may happen when the viscosity of the material is high enough. The blue phase of the polymer system was also reported to be frozen.

9.6.2.2 Frustration Between "Helical" and "Layered" Structures [182, 183]

In contrast to the nematic phase, the smectic phase is more close to the crystalline phase in nature, because the smectic phase possesses an additional order, i.e., a layered structure, as shown in Fig. 9.42a. Usually a similar helical structure to the nematic phase (see Fig. 9.39b) is not generated in the smectic phase, because the

a

Cr 135.7 ℃ **antiferro** 159.7 **ferri** 178.7 **ferro** 179.3 **Iso**

b

Cr 67 ℃ **antiferro** 144.4 **ferri** 146.7 **ferro** 148.8 **SmBP** 151.0 **SmBP'** 151.5 **Iso**
(**SmBP**: smectic blue (optically isotropic), **SmBP'**: smectic blue (mosaic))

Fig. 9.43 Molecular design and the emergence of the smectic blue and TGB phases. Compound (**a**) shows only ordinary smectic phases, such as antiferroelectric (anti), ferrielectric (ferri) phases, whereas Compound (**b**) shows the Compound (**b**) with less phenyl ring exhibits the smectic blue and TGB phases.

layered structure itself does not favor a twist. For strongly chiral systems, however, there can be competition between the desire for the molecules to form a helical macrostructure and that for the formation of the smectic layers. This competition can result in frustrated structures containing a regular lattice of grain boundary; thus, the dislocation-driven twist grain boundary (TGB) phase can be obtained [194]. The TGB phase consists of smectic slabs which are separated by the defects, where the adjacent slabs are tilted forming a helical macrostructure as shown in Fig. 9.42b. The TGB phase has a similar helical structure to the chiral nematic phase, i.e., the helical axis is perpendicular to the molecular axis. The smectic blue phase possessing a similar overall structure to the blue phase of the nematic system but has a local layered order has also been reported [195].

Let me now introduce examples of the systematic investigation on the relationship between molecular structures and the emergence of the TGB and related phases. The introduction of chiral moieties at both ends of the twin molecular configuration (see Fig. 9.43a) is a promising molecular design for producing strong chiral interaction between the neighboring molecules [196]. In the smectic phases of chiral twin compound shown in Fig. 9.43a, various polar structures, such as ferroelectric, ferroelectric, and antiferroelectric, are obtained. However, no TGB structure appears. This experimental result suggests that the layered structure of this compound is not weak enough to produce the frustrated TGB helical structure, because the TGB structure results from the good balance between two competitive natures, i.e., the smectic layer formation and the chirality-originated helix formation. A molecular design that decreases the amphiphilic character is needed for obtaining a weak layered structure, thus for increasing the possibility of the emergence of the TGB phase. Elimination of one phenyl ring from one of the core parts of this chiral twin compound (Fig. 9.43a) produces an analogous non-symmetric compound (Fig. 9.43b) which was found to exhibit two kinds of smectic blue phases between the ferroelectric liquid crystal phase and the isotropic liquid phase. The smectic blue phases change

into the TGB phase with decreasing optical purity of the system. The smectic A phase, instead of the TGB phase, is observed for the racemic mixture [197]. Similar to the TGB phase, which is produced by the twist deformation on the layered structure, BGB (bend grain boundary) phase [198], produced by the bend deformation instead, has been reported to exist, which is a new type of frustrated phase. Further studies on this topic including the suggestion of the molecular design are needed.

9.6.2.3 Incompatibility and Segregation
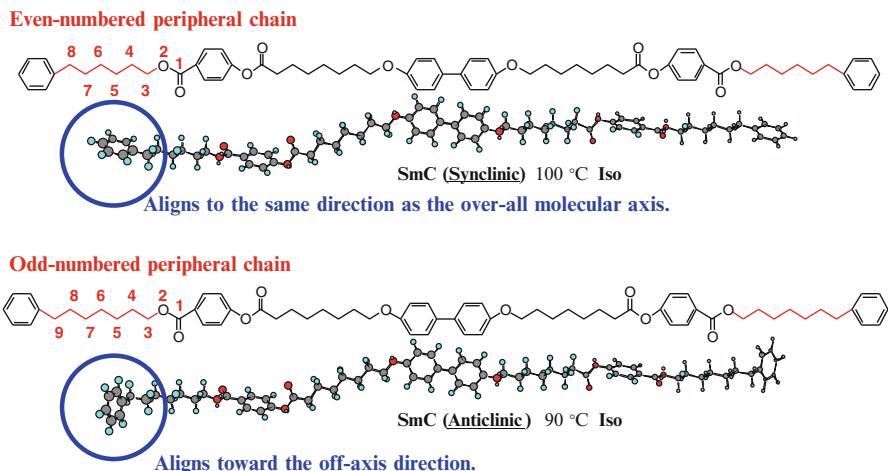
The lamellar phase of the lyotropic liquid crystals and the smectic phase of the thermotropic liquid crystals are similar in nature where the layered structure is formed in the molecular assemblies. However, the clarity of the periodicity of the layered structure is significantly different among them. For the lamellar phase, layers are made by the bilayer assemblies of the consisting molecules and are separated by the solvent, resulting in the well-defined layered structure. However, the smectic phase of the thermotropic liquid crystal is generally created as a result of just one-dimensional sine-wave modulation of the density and thus is not a well-defined layered structure. Degree of the segregation is so different among these two layered structures [182]. There have been lots of studies on the similarity between the thermotropic and lyotropic liquid crystals so that the common nature essential to build up the molecular assemblies can be clarified [199]. Materials showing the liquid crystal phase both by the addition of solvent and by changing temperature are called "amphotropic" liquid crystals [200]. Materials possessing structures characteristic to the thermotropic and lyotropic liquid crystals at the same time or mixtures between thermotropic and lyotropic liquid crystals are sometimes called "amphitropic" liquid crystals [201, 202]. At an earlier stage of works, amphotropic or amphitropic liquid crystals possess an ionic moiety as a hydrophilic part within their overall hydrophobic structures. In later stages of studies, however, there have been many studies on the amphiphilic thermotropic liquid crystals possessing a nonionic moiety as a hydrophilic part [203]; for example, it has been reported that for the liquid crystal system possessing a poly(propylene oxide) (PPO) unit at the peripheral end of the molecular structure, the smectic, cubic, and hexagonal columnar phases are observed when the number of the unit is 4, 5, and 6, respectively [204]. This change in the phase structure with respect to the change in the volume of the PPO moiety is quite similar to the phase change observed for the di-block copolymer system, indicating that incompatibility plays an important role in determining the style of molecular assembly. The other origins well studied so far are related to the incompatibility between the hydrocarbon and (semi)-perfluoro-hydrocarbon. The frustration between the intrinsic desire for the liquid crystal molecules to assemble each other and the incompatibility between the hydrocarbon and highly fluorinated moieties has been systematically studied [205].

9.6.2.4 Molecular Shape and Frustration

Molecular shape has a significant effect on the style or structure of the resulting molecular assembly; thus, the shape-originated frustration could occur [182]. For example, polycatenar molecules [206], which are made by introducing the rod-shaped moiety into the overall disk-shaped structure, have two competitive desires, i.e., the rod-shaped moiety favors the smectic order whereas the disk-shaped structure likes columnar packing. The columnar phase with lamellar structure or the cubic phase can be obtained by the well-designed polycatenar molecules. It is another important shape effect that the liquid crystal molecules with totally different molecular structures are immiscible with each other. For example, calamitic and discotic liquid crystals are generally immiscible, although it is theoretically predicted [207] that the mixtures between rod-shaped and disk-shaped molecules can show the "biaxial" nematic phase [208] which is expected to show fast switching useful for the display device application [209]. Some compounds, the so-called shape amphiphiles, have been reported [210]. Recently, a new strategy for the molecular design of the biaxial nematic has been proposed, in which arene–perfluoroarene interaction is utilized for breaking the symmetry [211]. This is a unique example of the frustration in which two competitive factors, i.e., free rotation around the molecular axis and molecular packing through the arene–perfluoroarene interaction, are well balanced. If the free rotation is much favored, the liquid crystal phase becomes uniaxial, or if the packing interaction is too strong, the crystal phase appears instead of the emergence of the biaxial nematic phase. In this case, it is also interesting to deal with the frustration between the dynamic properties of the system.

9.6.2.5 Clinicity and Frustration [76, 182, 183]

Liquid crystal molecules usually tilt in the same direction over the smectic layers (synclinic [212]) in the smectic C (SmC) phase. However, in one of the smectic A (SmA) phases, called de-Vries phase [213, 214], molecules tilt but the tile direction is random so that the overall molecular tilt cannot be recognized optically. Frustration can be produced between aligning and random orders [215]. There is another style of tilt, in which the tilting direction is aligning in one direction in each smectic layer; however, tilting direction alternates between the adjacent layers (anticlinic [212]). It has been well known that the introduction of chirality into the synclinic and anticlinic structures produces the ferroelectric and antiferroelectric properties, respectively. Frustration between the ferroelectric and antiferroelectric properties produces the ferroelectric structure in which the spontaneous polarization is partially canceled by the different magnitude between plus and minus polarization directions [216, 217]. The anticlinic order, NOT the antiferroelectric order, has been reported to be created by achiral systems [218, 219], indicating that the frustration between synclinic and anticlinic structures occurs, without any polar effects. The clinicity is determined by the style of the molecular order between the adjacent smectic layers, and therefore, the molecular structures at the peripheral

Fig. 9.44 Clinicity control in achiral rod-shaped LC

ends should have a significant effect on the clinicity. Usually liquid crystal molecules have methyl groups at the peripheral ends. Newly designed molecules possessing a phenyl ring at each peripheral end of the molecular structure show the synclinic and anticlinic structures when the peripheral alkyl chains are even and odd numbered, respectively (Fig. 9.44) [220, 221]. The direction of the terminal phenyl ring can be varied as a result of the odd–even effect of the peripheral alkyl chain. When the direction of the terminally attached phenyl rings is different from the molecular long axis, the anticlinic ordering is stabilized. Furthermore, it was found by the microscopic observation that there is a slight tilt, in some domains, even in the anticlinic phase, i.e., the coexistence of the anticlinic and synclinic structures. This result suggests that the clinicity is well balanced in this system producing the frustration between the anticlinic and synclinic orders.

9.6.2.6 Externally Induced Frustration

The examples described above are the so-called intrinsic frustration observed in the liquid crystals, whereas the frustration can be introduced externally as shown in Fig. 9.39a. For example, the intrinsic bistable alignment of the ferroelectric liquid crystal (FLC) in a thin cell can be changed into the monostable alignment which shows V-shaped fast switching with a gray scale [222], by doping a suitable monomer into FLC followed by the polymerization under the desired conditions. In this system, the frustration between intrinsic and polymer-stabilized alignments occurs. Introduction of the liquid crystal molecules into a thin microfiber has been reported to have a special effect on the liquid crystal properties [223]. The pitch length is varied due to the limited geometry determined by the diameter of the fiber, which resulted from the frustration between making a helix and filling the surrounding space. However, the cylindrical geometry imposes an unusual director

configuration to the chiral nematic phase making it degenerate with the blue phase, which is a rare example resolving the frustration produced in the blue phase as described earlier. Memory effects resulted from the frustration and topology in the nematic liquid crystals confined in the bicontinuous structure has also been reported [224, 225].

9.6.3 Summary

There are varieties of origins for the frustration, and thus many kinds of frustration can exist in the liquid crystal systems. Investigation on the effects based on the combination of different frustrations, especially of intrinsic and externally induced frustration, is important for the development of new materials. Nonuniformity with respect to time and space produced by the frustration and the stabilization of the resulting inhomogeneous frustrated structure would also be attractive subjects to be studied. Materials with the frustrated structure can be sensitive to the external stimulus and can show new function due to the instability intrinsically built in the frustrated structure. The origins of the frustrated structure can also be well controlled by the external stimulus, which may actively change the degree of frustration, which is most challenging but attractive for future studies.

References

1. R.B. Meyer, L. Liebert, L. Strzelecki, P. Keller, J. De Phys. (Paris) **36**, L-69 (1975)
2. K. Yoshino, T. Uemoto, Y. Inuishi, Jpn. J. Appl. Phys. **16**, 571 (1977)
3. K. Yoshino, Y. Iwasaki, T. Uemoto, S. Yanagida, M. Okahara, Oyo Butsuri **49**, 876 (1980) (in Japanese)
4. K. Yoshino, *High Speed Liquid Crystal Technology -Ferroelectric Liquid Crystal and Devices* (CMC, Tokyo, 1986) (in Japanese)
5. K. Yoshino, M. Ozaki, *Fundamental of Liquid Crystal and Display* (Corona, Tokyo, 1994) (in Japanese)
6. K. Yoshino, K.G. Balakrishnan, T. Uemoto, Y. Iwasaki, Y. Inuishi, Jpn. J. Appl. Phys. **17**, 597 (1978)
7. Y. Iwasaki, K. Yoshino, T. Uemoto, Y. Inuishi, Jpn. J. Appl. Phys. **18**, 2323 (1979)
8. N.A. Clark, S.T. Lagerwall, Appl. Phys. Lett. **36**, 899 (1980)
9. K. Yoshino, M. Ozaki, Jpn. J. Appl. Phys. **23**, L385 (1984)
10. P. Keller, L. Liebert, L. Strzelecki, J. De. Phys. (Paris) **37**, C3–27 (1976)
11. B.I. Ostrovskii, A.Z. Rabinovich, A.S. Sonin, E.L. Sorkin, B.A. Strukov, S.A. Taraskin, Ferroelectrics **24**, 309 (1980)
12. T. Sakurai, K. Sakamoto, M. Honma, K. Yoshino, M. Ozaki, Ferroelectrics **58**, 21 (1984)
13. K. Yoshino, M. Ozaki, T. Sakurai, K. Sakamoto, M. Honma, Jpn. J. Appl. Phys. **23**, L175 (1984)
14. P. Keller, S. Juge, L. Liebert, L. Strzelecki, C. R. Acad. Sci. (Paris) **282-C**, 639 (1976)
15. T. Sakurai, N. Mikami, M. Ozaki, K. Yoshino, J. Chem. Phys. **85**, 585 (1986)
16. P. Keller, Ann. Phys. **3**, 139 (1978)
17. M.V. Loseva, B.I. Ostrovskii, A.Z. Rabinovich, A.S. Sonin, B.A. Strukov, N.I. Chernova, JETP Lett **28**, 374 (1978)

18. N. Mikami, R. Higuchi, T. Sakurai, M. Ozaki, K. Yoshino, Jpn. J. Appl. Phys. **25**, L833 (1986)

19. G.W. Gray, D.G. McDonnell, Mol. Cryst. Liq. Cryst. **37**, 189 (1976)

20. J.W. Goodby, G.W. Gray, Mol. Cryst. Liq. Cryst. Lett. **41**, 145 (1978)

21. T. Inukai, S. Saitoh, H. Inoue, K. Miyazawa, K. Terashima, K. Furukawa, Mol. Cryst. Liq. Cryst. **141**, 251 (1986)

22. H. Taniguchi, M. Ozaki, K. Nakao, K. Yoshino, N. Yamasaki, K. Satoh, Mol. Cryst. Liq. Cryst. **167**, 191 (1989)

23. S. Kobayashi, S. Ishibashi, S. Tsuru, Mol. Cryst. Liq. Cryst. **202**, 103 (1991)

24. T. Sakurai, N. Mikami, R. Higuchi, M. Honma, M. Ozaki, K. Yoshino, Chem. Soc. Chem. Commun. 978 (1986)

25. M. Ozaki, K. Yoshino, T. Sakurai, N. Mikami, R. Highchi, J. Chem. Phys. **86**, 3648 (1987)

26. K. Yoshino, M. Ozaki, H. Taniuguchi, M. Ito, K. Satoh, N. Yamazaki, T. Kitazume, Jpn. J. Appl. Phys. **26**, L77 (1987)

27. Y. Yamada, K. Mori, N. Yamamoto, H. Hayashi, K. Nakamura, M. Yamawaki, H. Orihara, Y. Ishibashi, Jpn. J. Appl. Phys. **28**, L1606 (1989)

28. K. Yoshino, H. Taniguchi, M. Ozaki, Ferroelectrics **91**, 267 (1989)

29. K. Yoshino, M. Ozaki, K. Nakao, H. Taniguchi, N. Yamasaki, K. Satoh, Liq. Cryst. **5**, 1203 (1989)

30. H. Taniguchi, M. Ozaki, K. Yoshino, K. Satoh, N. Yamasaki, Ferroelectrics **77**, 137 (1988)

31. S. Saito, K. Miyazawa, M. Ushioda, K. Ohno, H. Inoue, K. Furukawa, T. Inukai, in *Proceedings of International Display Research Conference*, San Diego, U.S.A. vol. 107 (1988)

32. S. Arakawa, K. Nito, J. Seto, Mol. Cryst. Liq. Cryst. **204**, 15 (1991)

33. D.M. Walba, R.T. Vohra, N.A. Clark, M.A. Handschy, J. Xue, D.S. Parmar, S.T. Lagerwall, K. Skarp, J. Am. Chem. Soc. **108**, 7424 (1986)

34. A.M. Levelut, P. Oswald, A.G. Hanem, J. Malthete, J. Phys. (Paris) **45**, 745 (1984)

35. V.P. Shibaev, M.V. Kozlowsky, L.A. Beresnev, L.M. Blinov, A. Plate, Polym. Bull. **12**, 299 (1984)

36. G. Decobert, F. Soyer, J.C. Dubois, Polym. Bull. **14**, 179 (1985)

37. A.D.L. Chandani, E. Gorecka, Y. Ouchi, H. Takezoe, A. Fukuda, Jpn. J. Appl. Phys. **28**, L1265 (1989)

38. R.B. Meyer, L. Liebert, L. Strzelecki, P. Keller, J. Phys. (Paris) **36**, L69 (1975)

39. J. Valasek, Phys. Rev. **17**, 475 (1921)

40. E. Sawaguchi, G. Shirane, Y. Takagi, J. Phys. Soc. Jpn. **6**, 333 (1951)

41. T. Inukai, K. Furukawa, K. Terashima, S. Saito, M. Isogai, T. Kitamura, A. Mukai, in *11th Liquid Crystal Symposium*, Kanazawa, 1975, Abstract book 2N22

42. Y. Ouchi, H. Takezoe, A. Fukuda, Jpn. J. Appl. Phys. **26**, 1 (1987)

43. S. Kimura, S. Nishiyama, Y. Ouchi, H. Takezoe, A. Fukuda, Jpn. J. Appl. Phys. **26**, L255 (1987)

44. A.D.L. Chandani, Y. Ouchi, H. Takezoe, A. Fukuda, Jpn. J. Appl. Phys. **27**, L276 (1988)

45. S. Nishiyama, Y. Ouchi, H. Takezoe, A. Fukuda, Jpn. J. Appl. Phys. **26**, 1787 (1987)

46. N. Hiji, A.D.L. Chandani, S. Nishiyama, Y. Ouchi, H. Takezoe, A. Fukuda, Ferroelectrics **85**, 99 (1988)

47. K. Furukawa, K. Terashima, M. Ichihashi, S. Saitoh, K. Miyazawa, T. Inukai, Ferroelectrics **85**, 451 (1988)

48. A.D.L. Chandani, T. Hagiwara, Y. Suzuki, Y. Ouchi, H. Takezoe, A. Fukuda, Jpn. J. Appl. Phys. **27**, L729 (1988)

49. M. Johno, A.D.L. Chandani, Y. Ouchi, H. Takezoe, A. Fukuda, M. Ichihashi, K. Furukawa, Jpn. J. Appl. Phys. **28**, L119 (1989)

50. Y. Takanishi, H. Takezoe, A. Fukuda, H. Komura, J. Watanabe, J. Mater. Chem. **2**, 47 (1992)

51. Y. Takanishi, H. Takezoe, A. Fukuda, J. Watanabe, Phys. Rev. B **45**, 7684 (1992)

52. W.F. Harris, Philos. Mag. **22**, 949 (1970)

53. Y. Galerne, L. Liebert, Phys. Rev. Lett. **64**, 906 (1990)

54. C. Bahr, D. Fliegner, Phys. Rev. Lett. **70**, 1842 (1993)

55. M. Fukui, H. Orihara, Y. Yamada, N. Yamamoto, Y. Ishibashi, Jpn. J. Appl. Phys. **28**, L849 (1989)

56. T. Sako, Y. Kimura, R. Hayakawa, N. Okabe, Y. Suzuki, Jpn. J. Appl. Phys. **35**, L114 (1996)
57. J.F. Li, E.A. Shack, Y.K. Yu, X.Y. Wang, C. Rosenblatt, M.E. Neubert, S.S. Keats, H. Gleeson, Jpn. J. Appl. Phys. **35**, L1608 (1996)
58. A. Jakli, J. Appl. Phys. **85**, 1101 (1999)
59. Y. Takanishi, K. Hiraoka, V.K. Agrawal, H. Takezoe, A. Fukuda, M. Matsushita, Jpn. J. Appl. Phys. **30**, 2023 (1991)
60. V. Laux, V.N. Isaert, H.T. Nguyen, P. Cluseau, C. Destrade, Ferroelectrics **179**, 25 (1996)
61. E. Gorecka, A.D.L. Chandani, Y. Ouchi, H. Takezoe, A. Fukuda, Jpn. J. Appl. Phys. **29**, 131 (1990)
62. H. Takezoe, J. Lee, Y. Ouchi, A. Fukuda, Mol. Cryst. Liq. Cryst. **202**, 85 (1991)
63. N. Okabe, Y. Suzuki, I. Kawamura, T. Isozaki, H. Takezoe, A. Fukuda, Jpn. J. Appl. Phys. **31**, L793 (1992)
64. T. Isozaki, T. Fujikawa, H. Takezoe, A. Fukuda, T. Hagiwara, Y. Suzuki, I. Kawamura, Jpn. J. Appl. Phys. **31**, L1435 (1992)
65. P. Mach, R. Pindak, A.M. Levelut, P. Barois, H.T. Nguyen, C.C. Huang, L. Furenlid, Phys. Rev. Lett. **81**, 1015 (1998)
66. T. Akizuki, K. Miyachi, Y. Takanishi, K. Ishikawa, H. Takezoe, A. Fukuda, Jpn. J. Appl. Phys. **38**, 4832 (1999)
67. P.M. Johnson, D.A. Olson, S. Pankratz, H.T. Nguyen, J.W. Goodby, M. Hird, C.C. Huang, Phys. Rev. Lett. **84**, 4870 (2000)
68. A.D.L. Chandani, A. Fukuda, S. Kumar, J.K. Vij, Liq. Cryst. **38**, 663 (2011)
69. S. Wang, L. Pan, R. Pindak, Z.Q. Liu, H.T. Nguyen, C.C. Huang, Phys. Rev. Lett. **104**, 027801 (2010)
70. P. Keller, L. Liebert, L. Strzelecki, J. Phys. (France) **37**, C3–27 (1976)
71. A.M. Levelut, C. Germain, P. Keller, L. Liebert, J. Billard, J. Phys. (France) **44**, 623 (1983)
72. P. Cladis, H.R. Brand, Liq. Cryst. **14**, 1327 (1993)
73. G. Heppke, P. Kleineberg, D. Loetzsch, S. Mery, R. Shashidhar, Mol. Cryst. Liq. Cryst. **231**, 257 (1993)
74. Y. Takanishi, H. Takezoe, M. Johno, T. Yui, A. Fukuda, Jpn. J. Appl. Phys. **32**, 4605 (1993)
75. J.W. Goodby, J.S. Patel, E. Chin, J. Mater. Chem. **2**, 197 (1992)
76. J. Lagerwall, F. Giesselmann, ChemPhysChem **7**, 20 (2006)
77. A. Fukuda, Y. Takanishi, T. Isozaki, K. Ishikawa, H. Takezoe, J. Mater. Chem. **4**, 997 (1994)
78. H. Takezoe, E. Gorecka, M. Cepic, Rev. Mod. Phys. **82**, 897 (2010)
79. H. Takazoe, Y. Takanishi, Jpn. J. Appl. Phys. **45**, 597 (2006)
80. T. Kato, J.M.J. Fréchet, J. Am. Chem. Soc. **111**, 8533 (1989)
81. T. Kato, J.M.J. Fréchet, Macromolecules **22**, 3818 (1989)
82. T. Kato, H. Kihara, T. Uryu, A. Fujishima, J.M.J. Fréchet, Macromolecules **25**, 6836 (1992)
83. U. Kumar, T. Kato, J.M.J. Fréchet, J. Am. Chem. Soc. **114**, 6630 (1992)
84. U. Kumar, J.M.J. Fréchet, T. Kato, S. Ujiie, K. Iimura, Angew. Chem. Int. Ed. Engl. **31**, 1531 (1992)
85. T. Kato, J.M.J. Fréchet, P.G. Wilson, T. Saito, T. Uryu, A. Fujishima, C. Jin, F. Kaneuchi, Chem. Mater. **5**, 1094 (1993)
86. T. Kato, P.G. Wilson, A. Fujishima, J.M.J. Fréchet, Chem. Lett. **1990** (2003)
87. T. Kato, M. Fukumasa, J.M.J. Fréchet, Chem. Mater. **7**, 368 (1995)
88. T. Kato, H. Kihara, T. Uryu, S. Ujiie, K. Iimura, J.M.J. Fréchet, U. Kumar, Ferroelectrics **148**, 161 (1993)
89. T. Kato, N. Hirota, A. Fujishima, J.M.J. Fréchet, J. Polym. Sci. A Polym. Chem. **34**, 57 (1996)
90. T. Kato, Chem. Chem. Ind. **45**, 269 (1992)
91. T. Kato, Polymers **42**, 672 (1993)
92. T. Kato, Hyomen (Rev. Topics Surface Sci. Technol. Avant-Garde) **31**, 221 (1993)
93. T. Kato, in *Handbook of Liquid Crystals*, vol. 2B, ed. by D. Demus, J.W. Goodby, G.W. Gray, H.-W. Spiess, V. Hill (Wiley, Weinheim, 1998), p. 969
94. T. Kato, Struct Bond **96**, 95 (2000)
95. T. Kato, Ekisho **4**, 4 (2000)
96. T. Kato, J.M.J. Fréchet, Macromol. Symp. **98**, 311 (1995)

97. T. Kato, N. Mizoshita, K. Kanie, Macromol. Rapid Commun. **22**, 797 (2001)
98. M. Vivas de Meftahi, J.M.J. Fréchet, Polymer **29**, 477 (1988)
99. M.-J. Brienne, J. Gabard, J.-M. Lehn, I. Stibor, J. Chem. Soc. Chem. Commun. 1868 (1989)
100. D. Vorlander, Ber. Dtsch. Chem. Ges. **41**, 2033 (1908)
101. C. Weygand, R.Z. Gabler, Z. Phys. Chem. **B46**, 270 (1940)
102. T. Kato, H. Kihara, U. Kumar, T. Uryu, J.M.J. Fréchet, Angew. Chem. Int. Ed. **33**, 1644 (1994)
103. H. Kihara, T. Kato, T. Uryu, J.M.J. Fréchet, Chem. Mater. **8**, 961 (1996)
104. H. Kihara, T. Kato, T. Uryu, J.M.J. Fréchet, Liq. Cryst. **24**, 325 (1998)
105. T. Kato, Science **295**, 2414 (2002)
106. K. Kanie, M. Nishii, T. Yasuda, T. Taki, S. Ujiie, T. Kato, J. Mater. Chem. **11**, 2875 (2001)
107. T. Kato, T. Matsuoka, M. Nishii, Y. Kamikawa, K. Kanie, T. Nishimura, E. Yashima, S. Ujiie, Angew. Chem. Int. Ed. **43**, 1969 (2004)
108. K. Kumazawa, M. Yoshizawa, H. Liu, Y. Kamikawa, M. Moriyama, T. Kato, M. Fujita, Chem. Eur. J. **11**, 2519 (2005)
109. T. Kato, S. Kumar (ed.), Special Issue, Functional liquid crystals. Isr. J. Chem. **52**, 799–959 (2012)
110. T. Kato (ed.), *Liquid Crystalline Functional Assemblies and Their Supramolecular Structures, Structure and Bonding*, vol. 128 (Springer, 2008)
111. The Society of Polymer Science (ed.), *Self-Assembly and Functional Materials* (Kyoritsu Shuppan Co., Ltd., Japan, 2012)
112. T. Kato, Y. Hirai, S. Nakaso, M. Moriyama, Chem. Soc. Rev. **36**, 1857 (2007)
113. T. Kato, T. Kutsuna, K. Hanabusa, M. Ukon, Adv. Mater. **10**, 606 (1998)
114. Y. Sagara, T. Kato, Angew. Chem. Int. Ed. **47**, 5175 (2008)
115. Y. Sagara, S. Yamane, T. Mutai, K. Araki, T. Kato, Adv. Funct. Mater. **19**, 1869 (2009)
116. Y. Sagara, T. Kato, Angew. Chem. Int. Ed. **50**, 9128 (2011)
117. T. Kato, N. Mizoshita, K. Kishimoto, Angew. Chem. Int. Ed. **45**, 38 (2006)
118. R.B. Mayer, Mol. Cryst. Liq. Cryst. **40**, 33 (1977)
119. J. Watanabe et al., Prog. Polym. Sci. **22**, 1053 (1997)
120. J. Watanabe, M. Hayashi, Macromolecules **21**, 278 (1988)
121. J. Watanabe, M. Hayashi, Macromolecules **22**, 4083 (1989)
122. J. Watanabe et al., J. Phys. II France **4**, 581 (1994)
123. Y. Nakata, M. Hayashi, M. Tokita, K. Osada, J. Watanabe, High. Perform. Polym. **10**, 121 (1998)
124. J. Watanabe, Y. Nakata, J. Phys. II France **4**, 853 (1994)
125. J. Watanabe, Y. Nakata, Polym. J. **29**, 193 (1997)
126. J. Watanabe, T. Izumi, T. Niori, M. Zen-nyoji, Y. Takanishi, H. Takezoe, Mol. Cryst. Liq. Cryst. **346**, 77 (2000)
127. T. Izumi, S. Kang, T. Niori, Y. Takanishi, H. Takezoe, J. Watanabe, Jpn. J. Appl. Phys. **45**, 1506 (2006)
128. J. Watanabe, T. Niori, S.W. Choi, Y. Takanishi, H. Takezoe, Jpn. J. Appl. Phys. **37**, L401–L403 (1998)
129. T. Izumi, T. Niori, Y. Naito, J. Watanabe, Jpn. J. Appl. Phys. **45**, 4991 (2006)
130. T. Niori, T. Sekine, J. Watanabe, T. Furukawa, H. Takezoe, J. Mater. Chem. **6**, 1231 (1996)
131. T. Niori, T. Sekine, J. Watanabe, T. Furukawa, H. Takezoe, Mol. Cryst. Liq. Cryst. **301**, 337 (1997)
132. D.M. Link et al., Science **278**, 1924 (1997)
133. G. Heppke, D. Moro, Science **279**, 1872 (1998)
134. T. Sekine, Y. Takanishi, T. Niori, J. Watanabe, H. Takezoe, Jpn. J. Appl. Phys. **36**, L-1201 (1997)
135. J. Thisayukta, H. Takezoe, J. Watanabe, Jpn. J. Appl. Phys. **40**, 3277 (2001)
136. L.E. Hough et al., Science **325**, 452 (2009)
137. J. Thisayukta, Y. Nakayama, S. Kawauchi, H. Takezoe, J. Watanabe, J. Am, Chem. Soc. **122**, 7441–7448 (2000)

138. H. Niwano, M. Nakata, J. Thisayukta, D.R. Link, H. Takezoe, J. Watanabe, J. Phys. Chem. B **108**, 14889 (2004)
139. T. Imase, S. Kawauchi, J. Watanabe, J. Mol. Struct. **560**, 275 (2001)
140. H. Kurosu, M. Kawasaki, M. Hirose, M. Yamada, S. Kang, J. Thisayukta, M. Sone, H. Takezoe, J. Watanabe, J. Phys. Chem. **108**, 4674 (2004)
141. J. Thisayukta, H. Niwano, H. Takezoe, J. Watanabe, J. Am. Chem. Soc. **124**, 3354 (2002)
142. D.A. Coleman et al., Science **301**, 1204–1211 (2003)
143. S. Kang, J. Thisayukta, H. Takezoe, J. Watanabe, K. Ogino, T. Doi, T. Takahashi, Liq. Cryst. **31**, 1323 (2004)
144. S. Kang, J. Koki, M. Tokita, J. Watanabe, Jpn. J. Appl. Phys **46**, 3518 (2007)
145. S. Kang, R. Ishige, E.-W. Lee, M. Tokita, J. Watanabe, J. Mater. Chem. **22**, 21448 (2012)
146. S. Edo, S. Kang, M. Tokita, J. Watanabe, Jpn. J. Appl. Phys. **48**, 030215 (2009)
147. S.K. Lee, Y. Naito, L. Shi, M. Tokita, J. Watanabe, Liq. Cryst. **34**, 935 (2007)
148. S.K. Lee, X.D. Li, S. Kang, M. Tokita, J. Watanabe, J. Mater. Chem. **19**, 4517 (2009)
149. X. Li, S. Kang, S.K. Lee, M. Ito, M. Tokita, J. Watanabe, Jpn. J. Appl. Phys. **49**, 121701 (2010)
150. S. Kang, M. Harada, X. Li, M. Tokita, J. Watanabe, Soft. Matter **8**, 1916 (2012)
151. J.C.W. Chien, *Polyacetylene – Chemistry, Physics and Material Science* (Academic, Orlando, 1984)
152. H. Shirakawa, E. Louis, A.G. MacDiarmid, C.K. Chiang, A.J. Heeger, J. Chem. Soc. Chem. Commun. 578 (1977)
153. C.K. Chiang, C.R. Fincher, Y.W. Park, A.J. Heeger, H. Shirakawa, E.J. Louis, S.C. Gau, A.G. MacDiarmid, Phys. Rev. Lett. **39**, 1098 (1977)
154. H. Naarrmann, N. Theophilou, Synth. Met. **22**, 1 (1987)
155. I. Bozovic, Mod. Phys. Lett. B **1**, 81 (1987)
156. K. Akagi, G. Piao, S. Kaneko, K. Sakamaki, H. Shirakawa, M. Kyotani, Science **282**, 1683 (1998)
157. A.N. Aleshin, H.J. Lee, Y.W. Park, K. Akagi, Phys. Rev. Lett. **93**, 196601 (2004)
158. M. Oh-e, H. Yokoyama, S. Yorozuya, K. Akagi, M.A. Belkin, Y.R. Shen, Phys. Rev. Lett. **93**, 267402 (2004)
159. K. Akagi, Chem. Rev. **109**, 5354 (2009)
160. M. Goh, S. Matsushita, K. Akagi, Chem. Soc. Rev. **39**, 2466 (2010)
161. M. Goh, K. Akagi, Liq. Cryst. **35**, 953 (2008)
162. K. Akagi, I. Higuchi, G. Piao, H. Shirakawa, M. Kyotani, Mol. Cryst. Liq. Cryst. **332**, 463 (1999)
163. K. Akagi, S. Guo, T. Mori, M. Goh, G. Piao, M. Kyotani, J. Am. Chem. Soc. **127**, 14647 (2005)
164. M. Goh, T. Matsushita, M. Kyotani, K. Akagi, Macromolecules **40**, 4762 (2007)
165. M. Goh, M. Kyotani, K. Akagi, J. Am. Chem. Soc. **129**, 8519 (2007)
166. T. Mori, M. Kyotani, K. Akagi, Macromolecules **41**, 607 (2008)
167. T. Mori, T. Sato, M. Kyotani, K. Akagi, Macromolecules **42**, 1817 (2009)
168. T. Mori, M. Kyotani, K. Akagi, Macromolecules **43**, 8363 (2010)
169. T. Mori, M. Kyotani, K. Akagi, Chem. Sci. **2**, 1389 (2011)
170. M. Goh, G. Piao, M. Kyotani, K. Akagi, Macromolecules **42**, 8590 (2009)
171. H. Goto, K. Akagi, Macromol. Rapid Commun. **25**, 1482 (2004)
172. H. Goto, K. Akagi, Macromolecules **38**, 1091 (2005)
173. H. Goto, K. Akagi, Angew. Chem. Int. Ed. **44**, 4322 (2005)
174. Y.S. Jeong, K. Akagi, Macromolecules **44**, 2418 (2011)
175. Y.S. Jeong, K. Akagi, J. Mater. Chem. **21**, 10472 (2011)
176. S. Matsushita, K. Akagi, Isr. J. Chem. **51**, 1075 (2011)
177. H. Hayasaka, T. Miyashita, K. Tamura, K. Akagi, Adv. Funct. Mater. **20**, 1243 (2010)
178. B.A. San Jose, S. Matsushita, Y. Moroishi, K. Akagi, Macromolecules **44**, 6288 (2011)
179. M. Kyotani, S. Matsushita, M. Goh, T. Nagai, Y. Matsui, K. Akagi, Nanoscale **2**, 509 (2010)
180. M. Kyotani, S. Matsushita, T. Nagai, Y. Matsui, M. Shimomura, A. Kaito, K. Akagi, J. Am. Chem. Soc. **130**, 10880 (2008)

181. S. Matsushita, M. Kyotani, K. Akagi, J. Am. Chem. Soc. **133**, 17977 (2011)
182. I. Nishiyama, Ekisho **7**, 40 (2003)
183. I. Nishiyama, J. Yamamoto, A. Yoshizawa, Ekisyo **11**, 274 (2007)
184. H. Kikuchi, Struct. Bond. **128**, 99 (2007)
185. A. Yoshizawa, Mol. Cryst. Liq. Cryst. **516**, 99 (2010)
186. T. Seideman, Rep. Prog. Phys. **53**, 659 (1990)
187. F. Castles et al., Phys. Rev. Lett. **104**, 157801 (2010)
188. S.-T. Hur et al., Soft Matter **7**, 8800 (2011)
189. S. Shibayama et al., in *Proceedings of the IDW' 10*, 41 (2010)
190. G.P. Alexander, J.M. Yeomans, Phys. Rev. E **74**, 061706 (2006)
191. D.C. Wright, N.D. Mermin, Rev. Mod. Phys. **61**, 385 (1989)
192. L. Longa et al., Phys. Rev. E **50**, 3841 (1994)
193. M. Lee et al., in *Proceedings of IDW' 09*, 633 (2009)
194. J.W. Goodby et al., C. R. Chim **12**, 70 (2009)
195. E. Grelet, Mol. Cryst. Liq. Cryst. **412**, 1647 (2004)
196. I. Nishiyama, Chem. Rec. **9**, 340 (2009)
197. I. Nishiyama et al., J. Mater. Chem. **12**, 1709 (2002)
198. H.-S. Kitzerow, Mol. Cryst. Liq. Cryst. **412**, 1713 (2004)
199. C. Tschierske, Prog. Polym. Sci. **21**, 775 (1996)
200. H. Ringsdorf et al., Angew. Chem. Int. Ed. Engl. **27**, 113 (1988)
201. J. Corcoran et al., J. Mater. Chem. **2**, 695 (1992)
202. S. Fuller et al., Liq. Cryst. **12**, 521 (1992)
203. T. Kato, Ekisyo **4**, 4 (2000)
204. M. Lee, Y.S. Yoo, J. Mater. Chem. **12**, 2161 (2002)
205. G. Ungar et al., Adv. Funct. Mater. **21**, 1296 (2011)
206. D. Fazio et al., J. Mater. Chem. **11**, 2852 (2001)
207. J.J. Hunt et al., J. Am. Chem. Soc. **123**, 10115 (2001)
208. C. Tschierske, D.J. Photions, J. Mater. Chem. **20**, 4263 (2010)
209. G.R. Luckhurst, Thin Solid Films **393**, 40 (2001)
210. R.W. Date, D.W. Bruce, J. Am. Chem. Soc. **125**, 9012 (2003)
211. K. Kishikawa et al., Soft Matter **7**, 5176 (2011)
212. A. Fukuda, J.K. Vij, Ekisho **7**, 123 (2003)
213. A. de Vries, Mol. Cryst. Liq. Cryst. **41**, 27 (1977)
214. A. de Vries et al., Mol. Cryst. Liq. Cryst. **49**, 143 (1979)
215. J.C. Roberts et al., J. Am. Chem. Soc. **132**, 364 (2010)
216. A.D.L. Chandani et al., Phys. Rev. E **72**, 041705 (2005)
217. K.L. Sandhya et al., Liq. Cryst. **36**, 1101 (2009)
218. I. Nishiyama, J.W. Goodby, J. Mater. Chem. **2**, 1015 (1992)
219. Y. Ouchi et al., J. Mater. Chem. **5**, 2297 (1995)
220. I. Nishiyama et al., J. Mater. Chem. **13**, 1868 (2003)
221. I. Nishiyama et al., Mol. Cryst. Liq. Cryst. **439**, 1921 (2005)
222. S. Kobayashi, Ekisho **11**, 251 (2007)
223. E. Enz, J. Lagerwall, J. Mater. Chem. **20**, 6866 (2010)
224. T. Araki et al., Nat. Mater. **10**, 303 (2011)
225. I. Musevic, S. Zumer, Nat. Mater. **10**, 266 (2011)
226. M. Goh, T. Matsushita, H. Satake, M. Kyotani, K. Akagi, Macromolecules **43**, 5943 (2010)

Chapter 10
Physics of Liquid Crystals

Yuka Tabe, Kenji Urayama, Akihiko Matsuyama, Jun Yamamoto, and Makoto Yoneya

10.1 The Latest Studies in Physics of Liquid Crystals

Yuka Tabe

Over the 100 years since its discovery, liquid crystals have been the intriguing subject for both academia and industries. The textbook of de Gennes "*The Physics of Liquid Crystals*" published in 1974 is still the bible for many LC researchers, but new subjects unmentioned in the book have also risen for these years. This chapter describes the story of the recent developments and the future perspectives in physics of liquid crystals, especially focusing on the contributions by Japanese research groups for the last decade.

Recently, the role of computer simulations has rapidly increased in many fields including liquid crystals. Although there is a large-scale gap between the (sub) nanometer-size LC molecules and the macroscopic structures with micro- to

Y. Tabe
Faculty of Science and Engineering, Waseda University, Tokyo, Japan
e-mail: tabe@waseda.jp

K. Urayama
Kyoto Institute of Technology, Kyoto, Japan
e-mail: urayama@kit.ac.jp

A. Matsuyama
Kyusyu Institute of Technology, Fukuoka, Japan
e-mail: matuyama@bio.kyutech.ac.jp

J. Yamamoto
Kyoto University, Kyoto, Japan
e-mail: junyama@scphys.kyoto-u.ac.jp

M. Yoneya
National Institute of Advanced Industrial Science and Technology (AIST), Tsukuba, Japan
e-mail: makoto-yoneya@aist.go.jp

millimeter size in LC phases, the advances in the simulation techniques and the remarkable development of computer performances have gradually filled the gap. The connection between the nanoscale molecules and the macroscale structures by means of molecular dynamics simulations is expected to make a big contribution to both fundamental and industrial fields of liquid crystals.

To control the molecular alignment at the nanometer level is one of the new challenges that have attracted people's attention during the last decade, where the new trend is apparent in the increasing number of the papers published in these years. Generally, interfaces and surfaces are designed and used to uniformly align the direction of LC molecules. In contrast, Yokoyama and his coworkers proposed the new concept; if the LC molecules are set on the nano-patterned substrates, the director should possess bi- or tri- or even more easy-axes, which can be used for the new LC displays with the multi-stability. Their success gave a big impact to the community and now the nano-patterning is intensively studied beyond the LC field. When the modulation of the surface is in the nanoscale order, the director cannot be described by the general continuum theory and should be treated by meso-scopic physics. Thanks to the advancement of the probe microscopy and the related technologies, the further development is in progress in this field, which also stimulates the theoretical studies.

Nonuniform orientation of liquid crystals is not only given by the surface nano-patterning but also realized by the dispersion of colloids in liquid crystals. Usually the existence of orientational (topological) defects is a trouble to LC devices, but it gives us a lot of useful information about the physical properties of the media. In LC colloidal system, the various topological defects caused by the anchoring on colloid surfaces have been intensively studied during the last decade, in which the researchers found and revealed the fantastic defect structures, and moreover succeeded in the regular alignment of the colloidal particles one-, two-, or three-dimensionally by controlling the elasticity due to the defects. In another defect-induced LC structure, "blue phase," a Japanese group also made a major breakthrough about 10 years ago. Kikuchi and his coworkers succeeded in expanding the temperature region of the blue phase dramatically, which indicates the possible use of blue phases for new LC displays.

The hot topics on the physics of liquid crystals shown in this chapter have the keyword "nano" (molecular scale) in common. It has been a big challenge for us to build a bridge between the nanoscale molecules and their macroscopic properties. Hopefully the remarkable works introduced in this chapter will give us some clues on how we can contribute to the bridge construction, how fast and which direction the physics of liquid crystals will go in the future.

10.2 Stimulus-Response Characteristics of Liquid Crystal Elastomers and Gels
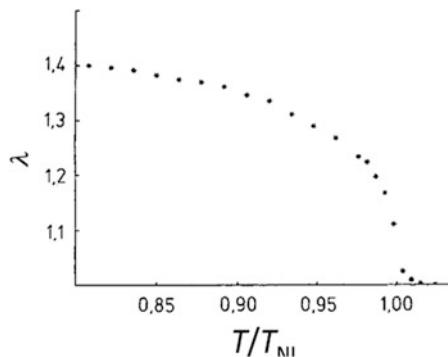
Kenji Urayama

10.2.1 Introduction

Liquid crystal elastomers (LCE) are hybrids of elastomers and liquid crystals that have both liquid crystalline and elastic properties [1, 2].
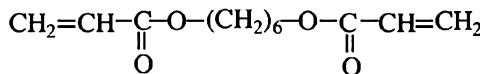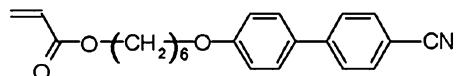
Neither does the microbrownian motion of the amorphous mesh inhibit the liquid crystal phase, nor does the positional order of the molecules interfere with the elasticity. Hence, as a hybrid material that combines LC and rubber characteristics, LCEs have unique properties in which the molecular orientation of the liquid crystal is strongly correlated with the macroscopic shape (deformation) which is unparalleled to other materials. The most prominent example in the physical properties derived from this property is the huge thermal deformation. Figure 10.1 shows an example of the thermal deformation behavior of side-chain nematic elastomers (NE) [3]. When the molecules transform from the random orientation in the isotropic phase to the macroscopic planar orientation in the nematic phase, the rubber extends in the direction of the liquid crystal orientation and increases with decreasing temperature as a result of an increase in the degree of liquid crystal orientation. This thermal deformation behavior is reversible, and LCEs can be even considered as a shape-memory material. Figure 10.1 is from a report of the early research on thermal deformation of LCEs, and a strain of about 40 % was observed [3]. It is said that LCEs show the largest thermal effect of all materials, and it has been reported that the thermal deformation reaches about 400 % in a main-chain type NE [4].

I was an undergraduate student, but I clearly remember that I was truly astonished when I read for the first time the paper that described the results in Fig. 10.1; the change in alignment of the liquid crystal molecules can be seen in the

Fig. 10.1 Thermal deformation behavior of a side-chain type nematic elastomer [3]. The quantity λ is the dimension along the director which is reduced by that in the isotropic phase, and T_{NI} denotes the nematic–isotropic phase transition temperature

Fig. 10.2 Monoacrylate
LC monomer and diacrylate
cross-linker

macroscopic world by the change of the rubber material dimensions. I was studying
the fundamental properties of rubber and gel at that time and the effect of the liquid
crystal imparting on the rubber looked very attractive. I thought that using the
coupling of liquid crystal alignment and macroscopic deformation would give rise
to interesting stimulus-responsive properties and that a variety of external fields,
such as temperature, electric fields, and magnetic fields could be used. In addition,
because I was dedicated to rheology, I was fascinated also by the changes in
mechanical properties that occur during the reorientation of liquid crystals. How-
ever, in the beginning, the threshold to make LCEs was high for me. The idea to
swell a non-LC rubber with low molecular weight liquid crystal solvent was a
simple idea, but must have already frustrated many researchers who have made
futile attempts to produce materials that should behave as LCEs. However, through
this futile attempt, I realized the need to produce the liquid crystalline network itself
in order to impose a significant effect of LC on the macroscopic physical properties
of elastomers. Even though it was a failed approach, by doing the experiments, I got
the "feel" to potentially understand the physical properties of the liquid crystal gel
through it. I learned later that de Gennes had submitted for the first time the
theoretical concepts of LCEs by cross-linking a nonliquid crystalline rubber in a
liquid crystal solvent [5]. He had asked the question if the cross-linking of nonliquid
crystalline rubber in an oriented liquid crystal would lead to an oriented rubber
network, even before it I had done the experiments [6]. The experimental results
will give "no" as the answer.

Then, thanks to the competent students in our group, we successfully synthe-
sized a side-chain type NE with mesogenic groups in the side chains of the network.
So far we have examined the stimulus-response behavior from various perspectives
in those NEs. In the following, I would like to introduce our research results.

10.2.2 Preparation of LCEs

LCEs forming nematic, cholesteric, and smectic phases have been synthesized,
with various chemical structures comprising of both side-chain and main-chain
types. Because of the multitudes of preparation techniques, I will here focus on our
synthetic methods [7]. Reactive cyanobiphenyl monoacrylate mesogens were
mixed with diacrylate cross-linkers to produce a photoinitiated side-chain acrylate
NE (Fig. 10.2). As it will be described later, the LCE fixes the liquid crystal
orientation at the time of cross-linking, and it can be said that this orientation
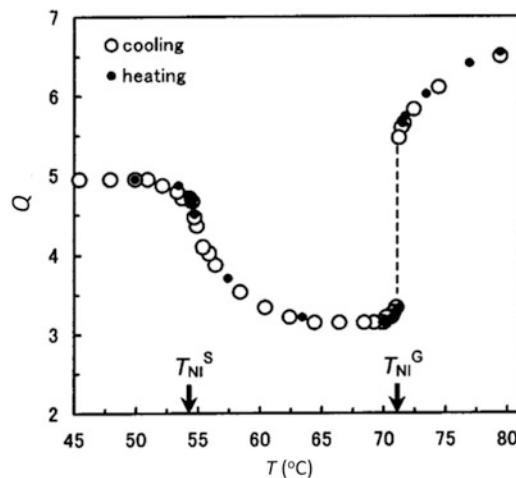
storage is the most important factor governing the physical properties of the gels. For this reason, the cross-linking reaction while controlling the liquid crystal alignment is an important point in the production of the LCE. The authors have carried out photopolymerization in glass cells which were coated with an alignment film of polyimide. By using various alignment layers, it is possible to realize a variety of planar orientation alignment state in the cell: vertical alignment, twisted alignment, and hybrid orientation. In addition, photopolymerization has the advantage that one can easier choose the reaction temperature for any liquid crystal phase. However, there is an upper limit for the film thickness by this type of orientation control, and the preparation of a sample with several hundred micrometers thickness or more is difficult. Orientation control methods using mechanical stress or magnetic fields that are not limited in thickness have been reported for the production of LCEs [8, 9].

10.2.3 Volume Phase Transition of Liquid Crystal Gels

The volume of the solvent-swollen polymer gel network is strongly dependent on the external environment such as temperature and solvent composition. In particular, the phenomenon called "volume phase transition" greatly changes the gel volume to changes in microenvironmental factors, and thus gels attracted attention as functional materials and at the same time became the target for physical measurements [10]. My first study of LCEs was to investigate the presence or absence of a volume phase transition driven by the nematic–isotropic phase transition. Even though uncross-linked polymer liquid crystals are isotropic in solution, they undergo phase separation driven by the orientational order when the liquid crystalline phase forms. This effect should lead to a swelling and shrinking in liquid crystalline gels and thus will appear as a volume phase transition. At that time, the boom of the research on volume phase transitions of gels had already passed, but there was no clear-cut experimental study whether the liquid crystal phase transition is the driving force for the volume phase transition. Initially, we examined a nonliquid crystalline swelling solvent, but we were struggling to select a suitable solvent. In the next step, we decided to use a low molecular weight liquid crystal as a swelling solvent that would keep its liquid crystal phase in the gel, thus enabling us to simultaneously measure the effect of each of the phase transitions of the gel and the surrounding solvent on the swelling behavior.

In the LCE/liquid crystal solvent system, two independent liquid crystal phase transition temperatures, one for the pure surrounding solvent (T_{NI}^S) and one for the gel (T_{NI}^G), are present. In our experiments T_{NI}^G was always higher than T_{NI}^S. During slow cooling, while maintaining the balance of swelling at each temperature from the isotropic phase ($T > T_{NI}^G$), a sudden and large volume phase transition was observed as soon as the transition to the liquid crystal phase was reached (Fig. 10.3) [11, 12]. The volume of the gel increased again as the temperature was lowered further and at T_{NI}^S the whole system changed to a continuous nematic phase. The volume at T_{NI}^S and T_{NI}^G is approximately the same and the shrinking and swelling
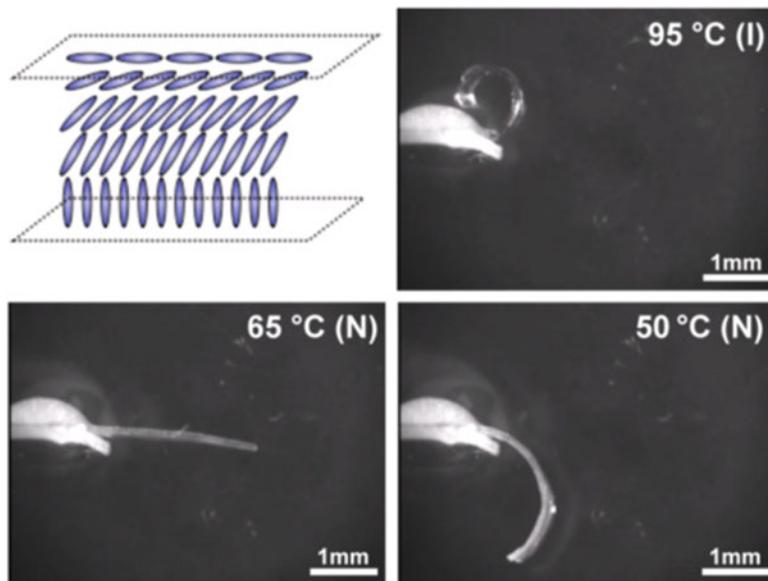
Fig. 10.3 Temperature (T) dependence of the degree of equilibrium swelling (Q) for a nematic elastomer in a nematic solvent [15]

is a completely reversible process. We were excited that the volume phase transition at T_{NI}^{G} occurred as expected, but we were scratching our heads about the interpretation of the complex swelling behavior at lower temperatures. Interestingly, around that time I attended a conference of the Japanese Society of Polymer Science, at which a theoretical study that corresponded to our experiment was presented by Matsuyama et al. (now Kyushu Institute of Technology; at that time Mie University) in which they predicted a temperature-dependent recursive swelling and a volume phase transition. At that time, we were disappointed to know that our experimental work had been preceded by the theories of Matsuyama et al. [13] and Warner et al. [14], but on the other hand, we were glad that our complex experimental results could be explained theoretically. Their mean field theory clearly showed that the dominant factor in the swelling of the nonliquid crystalline gel is the polymer-solvent affinity, whereas in the liquid crystal gel, it is the orientational order of the molecules. Later on, we observed the volume phase transition [15] in the nonliquid crystalline solvents and the tension effects [16] and could explain successfully the phenomena by the mean field theory.

The above-described results were for polydomain liquid crystalline gels having no macroscopic orientation, and thus the volume change during the liquid crystal phase transition does not cause an anisotropic shape change.

Later, the successful creation of monodomain LCEs that have a macroscopic orientation led to an anisotropic shape change by swelling. The gel expanded and contracted in the liquid crystal director direction during the volume increase or decrease [7, 17]. Furthermore, when examining the dynamics of swelling and shrinking of such a gel, the slow exponential relaxation towards the equilibrium value was commonplace for the volume change, but in a certain direction, the length change of the gel exhibited overshoot or undershoot [18]. This peculiar dynamics consists of two modes that are significantly different in the characteristic time. One is a very slow volume change due to the diffusion in the gel network, and
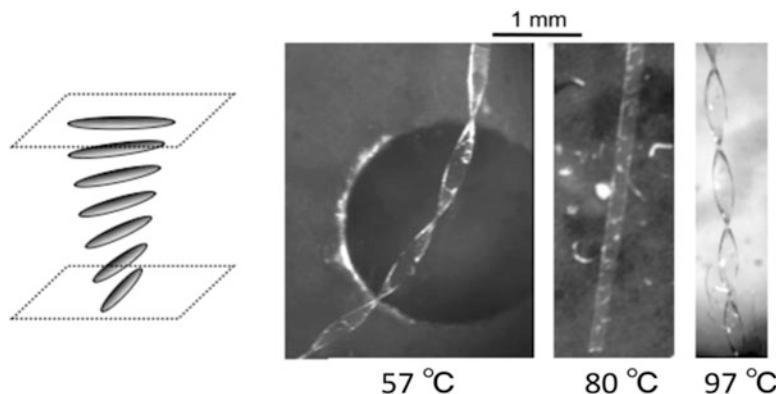
Fig. 10.4 Thermal bending behavior of HNE whose one end is fixed [19]

the other is a very fast shape change due to a change in the director direction. My experimental know-how and the knowledge that I inquired during my study for the physical properties of gels helped me in understanding the swelling behavior of liquid crystal gels. Until then I had the impression that the liquid crystal aspect dominated the LCE research, but the aspects of elastomers and networks came to light.

10.2.4   Various Thermal Deformation Behavior of Alignment-Controlled LCEs

Because, as mentioned above, we have used an alignment film for orientation control, the thought came quite naturally that hybrid alignment (Fig. 10.4) and twist alignment (Fig. 10.5) that both have been used in display applications should be investigated for LCEs as well. We expected that the distortion of LCE reflects the orientation pattern and that a complex deformation such as bending and twisting can be induced by using nonuniform alignment. NEs with hybrid orientation (HNE) can be prepared by using the alignment layers for inducing vertical and horizontal alignment on either side of the cell. HNE showed a huge bending deformation with respect to thermal changes (Fig. 10.4) [19]. Upon cooling, the degree of orientation of the liquid crystal increases and the length of the side with the vertical orientation shrinks, while the other side expands. Since the effect is proportional to the degree

Fig. 10.5 Temperature dependence of helical form of TNE. The ribbon specimen is immersed in oil bath and subjected to no mechanical constraint [22]

of orientation of the liquid crystal, the curvature depends significantly on the magnitude of strain and thus on the temperature change. This thermal bending behavior of HNE is similar to a bimetal, but HNE is a continuum phase, unlike bimetal which consists of two metals with a different coefficient of thermal expansion. By combining the liquid crystal alignment with rubber elasticity, the magnitude of the bending strain induced by the temperature change is very large and a large change in curvature can be reversibly induced (Fig. 10.4). According to linear elasticity theory, the difference in strain between the front and back surfaces $[\varepsilon(t) - \varepsilon(0)]$, normalized by the thickness (t) (t/r), governs the curvature. We calculated the quantity $[\varepsilon(t) - \varepsilon(0)]$ from the thermal strains in the direction parallel and normal to the director of a planar-oriented NE, and we could reproduce well the actual behavior of HNE. If we know the thermal deformation of a planar-oriented NE, we can easily predict with high accuracy the thermal bending behavior of the hybrid alignment NE [19].
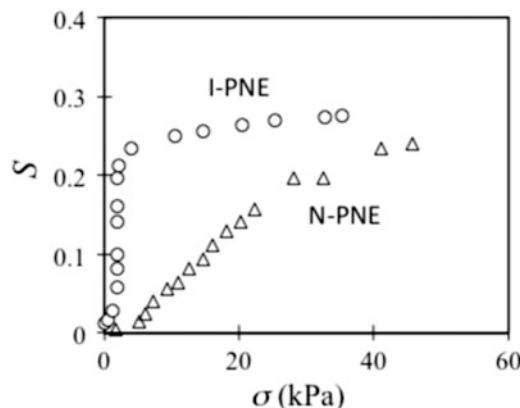
Control of the orientation of the helix and the twist angle is required for the fabrication of NE with a twisted orientation (TNE). The fabrication of a cholesteric LCE has been reported in which the helical structure has been conserved after the initially added, nonreactive chiral dopant had been extracted after cross-linking [20, 21]. Thus, such a chiral imprinting method can be used to produce a chiral structure with controlled twist angle even by starting from non-chiral liquid crystal monomer. A 90° twist-angle TNE film formed a macroscopic spiral over a wide temperature range (Fig. 10.5) [22]. When cooling down from the high-temperature nematic phase, the left-handed helix unwinds, forms a flat ribbon at a certain temperature, and then coils into a right-handed helix. This process is completely reversible. The cause of this morphological change is because the strain of the twisted film between the surfaces varies with temperature as in the bending deformation of the HNE described previously, but a very dramatic reversal of spiral chirality was completely unexpected. We also found that the type of spiral shape

(helicoid or spiral ribbon) and the sense of the helix depend on the direction of the liquid crystal director in the intermediate layers between the surfaces (parallel to either the major or minor axes of the ribbon) and the width-to-length ratio of the ribbon. Since we had not anticipated the various shape changes, it was difficult to explain our discovery. It was during the coffee break at an international conference when Dr. Ye, a theoretician at Illinois University, upon hearing about our results, remarked that interesting shape transitions should be obtained when using samples with different widths at a fixed temperature. Through the chatting with him, I knew that the formation of chiral ribbons was a hot issue for pure physical mathematics [23] and that the nanoscale assembly of chiral molecules takes a similar spiral form [24]. The spiral shapes of TNEs are also closely related to the problems of spiral structures that can be seen widely in nature [25]. We also carried out a theoretical calculation that described the experiment, and a paper coauthored with Ye et al. has been published [22]. Through this experience, I realized again the importance of collaboration and discussions with researchers of different research background to advance science and technology.

### 10.2.5   Soft Elasticity of Polydomain LCEs
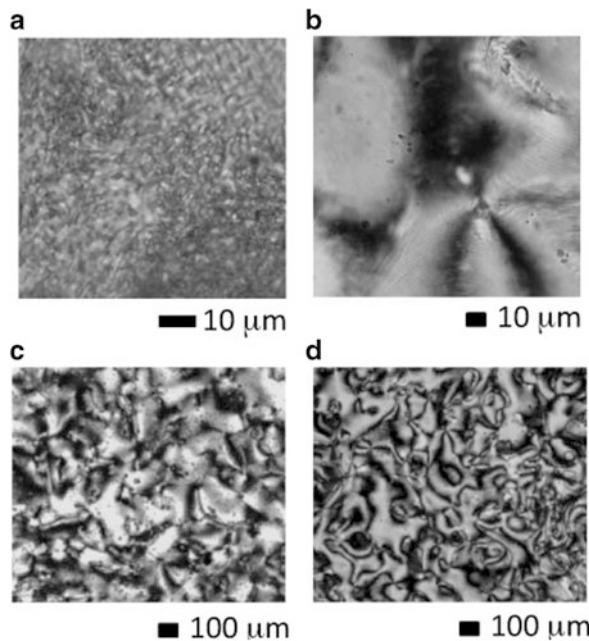
Without special care for the mesogen alignment in cross-linking reaction, LCEs form polydomains (so-called P-LCE) without macroscopic-oriented alignment. Thus, for example, the macroscopic deformation due to liquid crystal phase transition does not occur in P-LCEs, because the liquid crystal molecules are randomly oriented on a macroscopic scale in the liquid crystal phase. The macroscopic shape change due to the liquid crystalline character becomes apparent only when the LCE is oriented in a single monodomain. After the successful synthesis of monodomain LCEs, P-LCEs were drifting into the shadow. However, recently, polydomain NE (PNE) is getting attention because of its distinctive soft elastic properties. According to the concepts of soft elasticity, orientation energy of the director is the same regardless of the direction, and the director of the LCE is easily reoriented by very small external forces (according to some theorists, the external force is ideally zero) [26, 27]. This property not only is interesting from a basic physics standpoint but is indeed the keyfactor for the advancement of functional LCEs. A merit of PNE is that it does not require a monodomain during cross-linking, making the material much easier to produce. There are two different kinds of PNE depending on the temperature during cross-linking. The material obtained by cross-linking in the isotropic phase that is then cooled down to the nematic phase is called I-PNE. The other type, N-PNE, is cross-linked in the polydomain state of the liquid crystal phase. PNE showing a polydomain–monodomain transition upon stress has been reported quite some time ago [28], but the effect of thermal history during cross-linking has not been reported, even though it has been theoretically addressed by Uchida [29]. Uchida's prediction was that I-PNE should show a PM transition and soft elasticity upon stress,

Fig. 10.6 Dependence
of orientational order
parameter (S) on tensile
stress (σ) for PNE [31]

but that N-PNE should lack the soft elasticity because of the frozen
polydomain structure. We prepared both types of PNEs and found no difference
elastic modulus and phase transition temperature of both PNE. However, when
examining the response of the swollen LC gels to electric field (as described later
in this chapter), we noticed that the strain recovery time for the I-PNE was one
magnitude or more longer than for N-PNE and that there are some physical
properties due to such a difference in thermal history [30]. These results made
me return to the somewhat old-fashioned phenomenon of the PM transition and I
studied it from the viewpoint of cross-linking history.

Figure 10.6 shows the dependence of the order parameter of the mesogens in
side-chain I-PNE and N-PNE on the applied stress [31]. The macroscopic order
parameter S is zero at no extension, because the LCE exists in the polydomain
structure. The final stage of both gels is very similar at around $S = 0.25$, but in the
intermediate stress regime, S is quite different. I-PNE shows soft elasticity at a very
small force of about 2 kPa and a steep increase in order parameter, whereas N-PNE
shows a gradual increase in order upon stress, which is qualitatively consistent with
the theoretical predictions of Uchida. We found that the mechanical work necessary
for the PM transition is one order of magnitude smaller for I-PNE than for N-PNE.
Figure 10.7 shows that the texture of the structure for N-PNE remained after cross-
linking and is characterized by many defects [31]. In contrast, a more uniform
domain structure with very small features is formed in the I-PNE. Interestingly,
even though the organizational structure is very different for both PNEs, there is no
significant difference in the phase transition temperature, the initial modulus of
elasticity, and the order parameter S after the PM transition. Still, the reorientation
process of the director upon stress reveals large differences. All these findings not
only are closely related to the understanding of the origin of the soft elasticity, but
also show the potential of I-PNE as stimulus-responsive materials. One example is
the electric field response that I will explain in the next section. In addition, through
the comparison of the organizational structure of N-PNE before and after cross-
linking, we were able to understand clearly the memory effect of liquid crystal
alignment due to cross-linking.
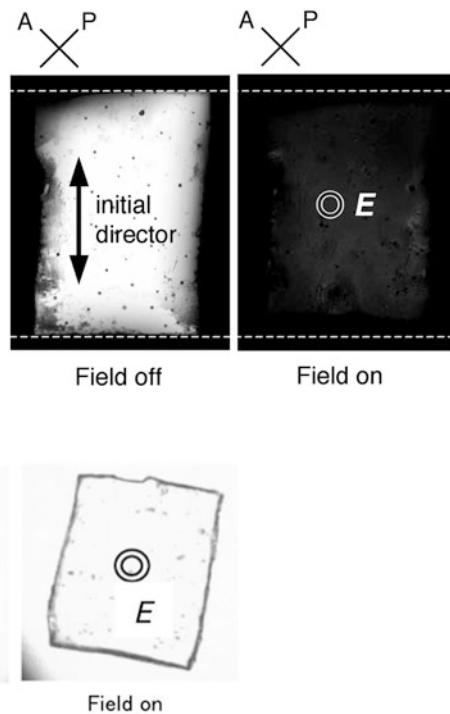
Fig. 10.7 Microphotographs of (**a**) I-PNE, (**b**), (**c**) N-PNE, and (**d**) N-PNE before cross-linking under crossed Nicols condition [31]

10.2.6   Electric Field Response of Liquid Crystal Gels and LCEs

It goes without saying that researchers in the LCE field have thought about by using the reorientation characteristic of LCs in an electric field, which is the typical application for LCDs, to deform an LCE. However, before I entered in this field it had been quite difficult to find such an example and it only had been reported for a LC gel that was swelled with a low molar mass LC [32, 33]. The observation of the deformation of such an LC gel previously was on a qualitative level, and the correlation between the reorientation of the LC and the deformation was left untouched. Since the gel sandwiched by rigid electrodes cannot distort in the direction of the electric field, the reorientation of the LCs is also severely restricted. We immersed the LC gels in a sealed, thick-gap cell filled with silicone oil, a non-solvent for the gels, to ensure the deformability of the gels [34–36]. In this setup, we were able to observe clearly a macroscopic deformation caused by the rotation of the director in unconstrained conditions (Fig. 10.8). The deformation is characterized by a shortening in the initial director axis, an extension in the field direction, and a nonappreciable dimensional variation in the axis of rotation of the director. We could also evaluate the

Fig. 10.8 Response of a monodomain LC gel film to electric field [34]. The gel-thickness and the cell gap are 34 and 40 μm, respectively. The voltage amplitude and frequency of the imposed AC electric field are 750 V and 1 kHz, respectively. Observation under crossed Nicols condition

Field off   Field on

Field off   Field on

Fig. 10.9 Response of a 42 μm-thick I-PNE film to electric field. The gap between electrodes was 58 μm and filled with silicone oil. The voltage amplitude and frequency of the imposed AC electric field are 1.3 kV and 1 kHz, respectively. Observation under natural light [39]

rotation angle of the director (θ) from the change in birefringence and found that the strain is proportional to $\sin^2\theta$ [35].

Then we asked ourselves if the electrical actuation would be impossible in the dry rubber state. The deformation of LCE rubber in an electric field has been observed only for chiral smectic elastomer ferroelectrics [37, 38]. The origin of this phenomenon is the electroclinic effect specific to ferroelectric liquid crystals and it is physically different from the deformation resulting from the reorientation of the director as described above. In public, we were told by a fellow researcher that unrealisitically high electric field is necessary to change the director direction in a non-ferroelectric rubber. As mentioned in the previous section [31], we knew that the polydomain structure of I-PNEs can easily lead to a director reorientation by just a little force, and we thought that a finite electrical actuation of I-PNEs in the rubber state might be possible. As shown in Fig. 10.9, a I-PNE changes to a monodomain alignment in the direction of the electric field and showed a large strain that reached 35 % at the same time [39]. The reasons why the elongation strain is generated in the vertical direction are not known at present, but this deformation is considerably larger than the previously reported value of the

deformation in ferroelectric LCEs. The threshold field strength for the onset of electrical actuation (ca. 10 MV/m) is still considerably high from the viewpoints of application, but the significance of our work is the observation of finite electrical actuation in the rubber state which has been considered unrealistic for a long time.

10.2.7   Summary

I introduced some of the various external field responses derived from the strong correlation of molecular orientation and macroscopic shape of LCEs. The response to temperature, electric field, and tension on the deformation behavior was described. Others, like the light-induced shape change of azobenzene-containing LCEs [40], could not be introduced in this paper, but also have attracted attention. Polymer liquid crystals can be spun into high strength fibers because of the rigidity and alignment of the liquid crystal molecules. LCE, on the other hand, is a soft material that uses the flexibility of the polymer network and the liquid crystal phase, resulting in a completely different character than the liquid crystal fiber. LCEs are becoming recognized as a new category of polymer liquid crystals that are increasingly used as a new type of functional rubber material.

The interest in LCEs is fueled by the fact that they have a multifaceted character and a hybrid nature, which makes an approach from a variety of viewpoints possible. When I look at the research of other researchers, I am surprised by the difference in ideas, even though their research uses the same material in many cases. It seems that those who delve more and more in the area of their own expertise, rather than combine the expertise of polymer science and liquid crystal science, fare better in finding new developments in the study of LCEs. The reason is that the character of the hybrid material made of rubber and liquid crystal is not a mere addition of properties. When more professional researchers with different backgrounds will enter the research field, the hidden potential of LCE will become more apparent.

Will LCEs be able to repeat the spectacular success of low molecular weight liquid crystals in applications as LCDs? This is a question that LCE researchers specializing in liquid crystals posed recently. Not few liquid crystal researcher veterans likened the early days of low molecular weight liquid crystal research to the current state of LCE research. LCE is an interesting system that suits very well as a subject of basic research, but it goes without saying that it would be a joy if unexpected results that spring up in basic research of LCEs will lead to applications as new materials. Thus I am hopeful for the expansion of study of LCE in the future.

10.3 Phase Separations of Liquid Crystalline Composites: Theoretical Perspectives for Liquid Crystalline Hybrid Matters
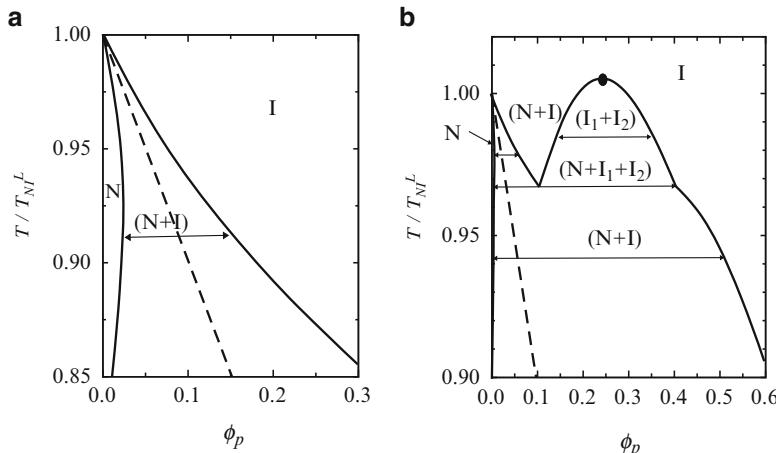
Akihiko Matsuyama

10.3.1 Introduction

Polymers and liquid crystals are important materials for various research fields. If the two substances are mixed, novel materials which combine the advantageous properties of both may be formed. I began to think about this around 1994. Already at that time, this mixed system had attracted attention as an electro-optical material, but from the perspective of basic physical properties, the center of the liquid crystal research up to that point was the phase transition and liquid crystal structure of novel low molecular weight liquid crystals. The physics of liquid crystals was based on the Onsager theory, the Maier–Saupe theory, and the elastic theory by Frank. However, the theoretical study of a liquid crystal mixed with other substances had not yet been developed. So, I began to think to build theories of phase separations and phase transitions in mixtures of liquid crystals and other substances. Our first paper on the theory of phase separations in the mixture of a polymer and a liquid crystal was published in 1996 [41]. I found at a later date that a paper on the same topic by Prof. Kyu of Akron University had been presented already in 1995 [42]. However, there was a difference between the two theories. Kyu's theory has dealt with low molecular weight liquid crystals in an attractive model, whereas our model considered both attractive and repulsive interactions between rodlike liquid crystal molecules and can handle also long rodlike molecules. After that, I had a variety of discussions with Kyu and it was a valuable experience for my research.

My original plan had been to develop theories for mixtures of liquid crystals with other materials, such as semiflexible polymers, spherical particles, rodlike polymers, nanotubes, surfactant molecules, or membranes. Currently, in 2011, the theoretical studies of the liquid crystal composites are almost completed up to nanotubes. Of course, there are various problems unresolved and it is likely to take about ten more years.

In the following two sections I will describe the dynamics and phase separation in mixtures of a flexible polymer and a liquid crystal, and the phase separation phenomenon in mixtures of a long rodlike polymer and a liquid crystal.

Fig. 10.10 Phase diagrams of polymer/liquid crystal mixtures

10.3.2   Mixtures of a Flexible Polymer and a Liquid Crystal

Mixtures of a flexible polymer and a liquid crystal are called a polymer-dispersed liquid crystal (PDLC) and are used as an electro-optical material in optical shutters and displays. Understanding the phase separation behavior and compatibility of the mixtures of two different components thus are important from the viewpoints of fundamental properties as well as in engineering.

10.3.2.1   Phase Separations

Figure 10.10 shows the phase diagram of a typical mixed system of a polymer and a liquid crystal [43]. The vertical axis shows the reduced temperature which is normalized by the nematic–isotropic phase transition temperature (T_{NI}^L) of the pure liquid crystal, and the horizontal axis is the polymer concentration (φ_p). The solid lines are the coexistence curves and the dashed line is the nematic–isotropic phase transition curve; on its left side is the nematic phase, and on its right side is the isotropic phase. Figure 10.10a shows a mixture that includes a nematic phase (N), an isotropic phase (I), and a two-phase region (N+I). The width of the coexistence curve becomes wide with decreasing temperature. Figure 10.10b shows the case in which two-phase coexistence ($I_1 + I_2$) and three-phase coexistence ($N + I_1 + I_2$) are present. We have the triple point temperature T_{TP}, where the three phases ($N + I_1 + I_2$) coexist. Such a phase diagram has been observed in mixed systems such as poly(acrylamide) (PAA)/n-alkane, polystyrene (PS)/4-Cyano-4′-heptylbiphenyl (7CB) and in a variety of liquid crystal/polymer mixtures. A flexible

polymer disturbs the molecular orientation of a nematic liquid crystal. As a result, the polymer is expelled from the nematic phase so as not to disturb the orientation field. The liquid crystalline phase is then the almost pure nematic compound, and the isotropic phase consists of mainly polymer. Depending on the stiffness of the polymer, it is sometimes distributed in the liquid crystalline phase [44].

The free energy of a mixture of a flexible polymer and a liquid crystal is given by

$$f = f_{mix} + f_{nem} \tag{10.1}$$

where n_p is the number of segments on the polymer and $n_r(=L/D)$ is the axial ratio of the liquid crystal molecule with the length L and diameter D.

The first term of the mixing free energy f_{mix} is given by

$$f_{mix} = \frac{\phi_p}{n_p} \ln \phi_p + \frac{\phi_r}{n_r} \ln \phi_r + \chi \phi_p \phi_r \tag{10.2}$$

where φ_p and φ_r indicate the volume fractions of the polymer and the liquid crystal molecules, respectively, $\varphi_p + \varphi_r = 1$. The parameter χ in the third term is the interaction parameter between the liquid crystal molecule and the polymer in an isotropic phase. Equation (10.2) is the Flory–Huggins theory of a polymer solution [41].

In fact, as a student, I had been very concerned about the relationship of the Flory theory of polymer solutions and the Onsager theory. Whereas the Onsager theory is about compressible liquids, the Flory theory is about incompressible liquids, and thus the so-called lattice theory. Later, it has been shown that the extension of the Onsager theory under incompressible assumptions results in the Flory theory of polymer solutions [41].
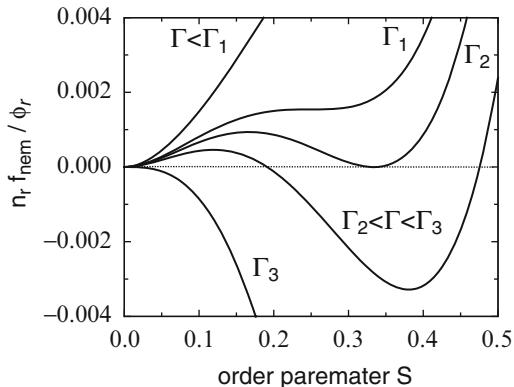
The second term of Eq. (10.1) is the free energy of a nematic phase of liquid crystal molecules. Let us consider the following equation that takes into account both the excluded volume and the attractive intermolecular interactions of the liquid crystal molecules [41, 43]:

$$f_{nem} = \left(v + \frac{5}{4} \right) \phi_r^2 \left[\frac{1}{2} \left(1 - \frac{\Gamma}{3} \right) S^2 - \frac{\Gamma}{9} S^3 + \frac{\Gamma}{6} S^4 \right] \tag{10.3}$$

$$\Gamma = (v + 5/4) n_r \phi_r \tag{10.4}$$

where S is the orientational order parameter of the liquid crystal molecules. The symbol v in the first term of Eq. (10.4) is the attractive interaction energy of the liquid crystal molecules (Maier–Saupe interaction parameter, which is inversely proportional to temperature). The second term 5/4 is the excluded volume (entropy term) [41]. Figure 10.11 shows the relationship between orientational order parameter S and the nematic free energy (f_{nem}) for different values of Γ. In the following,

Fig. 10.11 Free energy (2.3) plotted against the orientational order parameter S
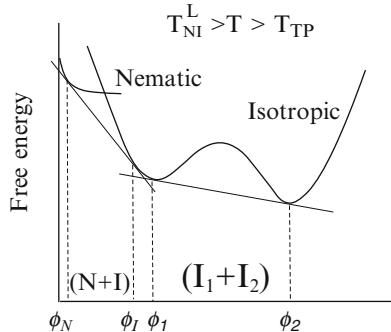
let consider the thermal equilibrium state or the minimum value of the free energy f_{nem}:

(i) When $\Gamma < \Gamma_1 \ (=8/3)$, f_{nem} has a unique minimum at $S=0$.

(ii) When $\Gamma_1 < \Gamma < \Gamma_2 \ (=2.7)$, there are two local minima, but the one at $S=0$ f_{nem} is lower. Therefore, from (i) and (ii) it follows that the isotropic phase is in the thermal equilibrium state when $\Gamma < \Gamma_2 \ (=2.7)$.

(iii) When $\Gamma = \Gamma_2$, for $S=0$ and $S=0.33$, $f_{nem}=0$ has two minima. The orientation order parameter jumps from 0 to 0.33 and the isotropic phase coexists with the nematic phase (in the Onsager theory this value is $\Gamma_2 = 4.55$).

(iv) When $\Gamma_2 < \Gamma < \Gamma_3 \ (=3)$, f_{nem} has two local minima, but the one at $S>0$ f_{nem} is lower.

(v) When $\Gamma > \Gamma_3$, $S=0$ corresponds to the maximum value of free energy and $S>0$ corresponds to the thermal equilibrium state. Therefore, on increasing Γ, the phase transition from the isotropic phase ($S=0$) to a nematic phase ($S=0.33$) occurs at $\Gamma=2.7$ and the orientation order parameter increases from 0.33 to 1 with Γ. The above discussion is called the Landau-de Gennes first-order phase transition theory. The nematic–isotropic (NI) phase transition temperature (T_{NI}) can be expressed by using $\Gamma=2.7$ and Eq. (10.4):
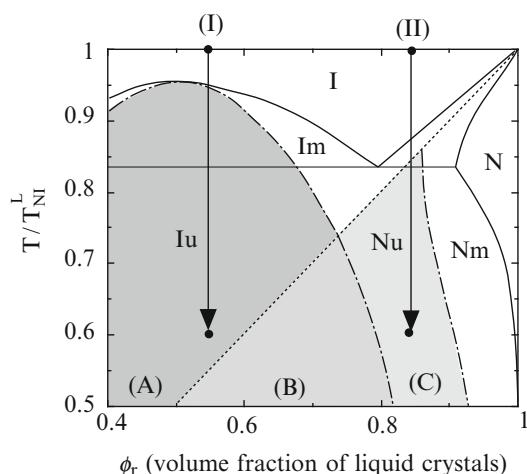
$$T_{NI}/T_{NI}^{L} = \frac{(2.7 - 1.25 n_r)(1 - \phi_p)}{2.7 - 1.25 n_r (1 - \phi_p)} \tag{10.5}$$

For $n_r > 2.16$, the phase transition temperature of the pure liquid crystal molecule ($\phi_p = 0$) shifts to higher temperature. For long rodlike molecules, the excluded volume effect is dominant over the attraction effect, and the NI phase transition increases by increasing the concentration. Figure 10.12 shows the free energy as a function of polymer concentration at a temperature that is between T_{TP} and T_{NI}^{L}. The concentration determined from a common tangent method corresponds to the concentration of the coexistence curve. In addition, I found that inside the phase-

Fig. 10.12 Free energy
(2.1) for $T_{TP} < T < T_{NI}^L$
in Fig. 2.10b

Fig. 10.13 Unstable
regions (A), (B), (C)
in the phase diagram

separated isotropic region, the free energy has a convex unstable region (spinodal region) with respect to the concentration. This area is important for the understanding of phase separation dynamics.

10.3.2.2 Phase Separation Dynamics

Quenching from the isotropic phase into the unstable region inside the coexistence curve, phase separation proceeds. Phase separation in an isotropic liquid is normally induced by concentration fluctuations. However, in addition to concentration, the orientational order should also affect the phase separation dynamics in liquid crystal systems.

In order to understand this, it is necessary to consider the time evolution of orientation order parameter and concentration. Figure 10.13 shows the phase diagram depicting both coexistence curve (solid line) and spinodal curve (dashed

line). The dotted line shows the NI phase transition curve. The vertical axis is temperature and the horizontal axis represents the volume fraction of the liquid crystal molecules. Thermodynamically unstable regions ((A), (B), and (C)) appear on the lower temperature side of the spinodal curves. The unstable region (A) of the isotropic phase has a negative second derivative of the concentration with respect to the free energy $(\partial^2 f/\partial \varphi^2)_T < 0$, but a positive one with respect to the orientation order parameter $((\partial^2 f/\partial S^2)_T > 0)$. Therefore, the driving force for the phase separation in area (A) is a concentration fluctuation. Region (C) is the unstable region of the nematic phase, and it has a negative second derivative of the orientational order parameter with respect to free energy $((\partial^2 f/\partial S^2)_T < 0)$, but is positive with respect to concentration $(\partial^2 f/\partial \varphi^2)_T > 0$. Therefore, orientation fluctuations become the driving force for phase separation in region (C). In region (B), $((\partial^2 f/\partial \varphi^2)_T < 0$ and $(\partial^2 f/\partial S^2)_T < 0)$, both orientation and concentration fluctuations become the driving force for phase separation.

In the following, consider the time evolution of the conserved order parameter (concentration) and the nonconserved one (orientational order). In order to describe the nematic phase, we consider the tensor order parameter

$$Q_{ij} = \frac{3}{2} S \left(n_i n_j - \frac{1}{3} \delta_{ij} \right) \tag{10.6}$$

that can handle simultaneously the average molecular orientation vector ($\boldsymbol{n}$) and the scalar order parameter (S). Here, n_i represents the component i of the orientation vector $\boldsymbol{n}$ (director) ($i = x$, y, z), and δ_{ij} is the Kronecker delta function (if $i = j$, $\delta_{ij} = 1$; if $i \neq j$, $\delta_{ij} = 0$). The free energy of a spatially nonuniform system, such as a phase-separated system, is given by the sum of the bulk free energy and the gradient terms of the two order parameters:

$$\beta F = \int dr \left[f(\phi_r, Q_{ij}) + f_g(\phi_r, Q_{ij}) \right] \tag{10.7}$$
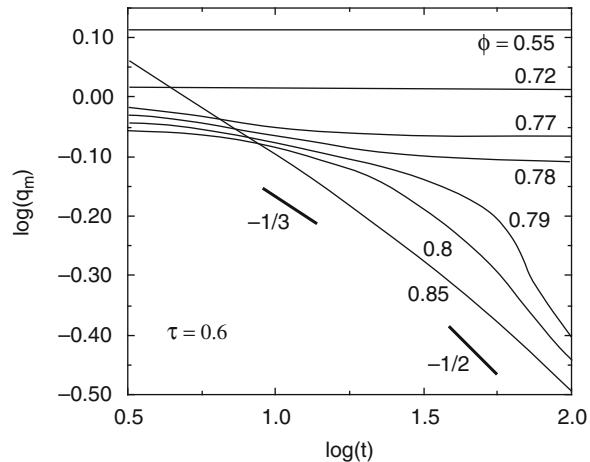
$$f_g = \frac{1}{2} K_\phi (\nabla \phi_r)^2 + \frac{1}{2} L_1 (\partial_k Q_{ij})^2 + \frac{1}{2} L_2 (\partial_i Q_{ik})(\partial_j Q_{jk}) + w(\partial_i \phi_r)(\partial_j Q_{ij}) \tag{10.8}$$

where K_φ, L_i are coefficients related to interfacial tension and the elastic Frank constant, respectively. The last term (ω) is the coupling term of the orientation field and concentration field, which means the anchoring energy of the director at the interface. The temporal evolution of the order parameters in the conserved system (concentration φ_r) and in the nonconserved system (orientation tensor Q_{ij}) is given by the following equations:

$$\partial \phi_r / \partial t = D_\phi \nabla^2 (\delta F/\delta \phi) \tag{10.9}$$

$$\partial Q_{ij} / \partial t = -D_Q (\partial F/\partial Q_{ij}) \tag{10.10}$$
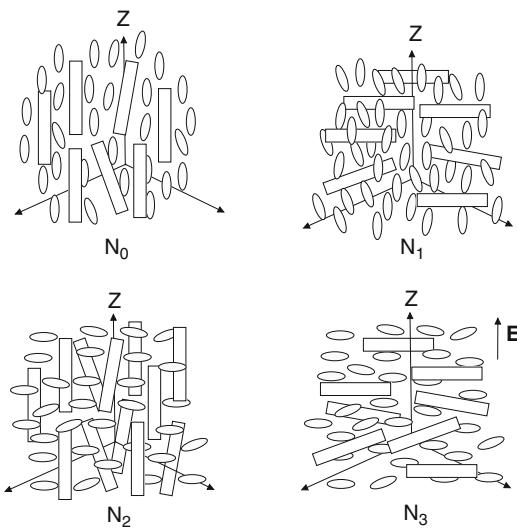
Fig. 10.14 Temporal evolutions of the scattering wave number q_m at which the compositional structure factor has a maximum. The initial concentration is varied at fixed temperature

where D_i $(i = \boldsymbol{\varphi}, \boldsymbol{Q})$ is the transport coefficient. In this case, hydrodynamic effects are ignored. By numerically solving Eqs. (10.9 and 10.10), the time evolution of the phase separation can be determined [44–50]. A detailed simulation that takes into account the viscoelastic effects has also been examined [46].

The time evolution of the initial stage of the phase-separated domains can be analyzed by linear approximation of Eqs.(10.9 and 10.10) [44]. Figure 10.14 shows the time dependence of the peak wave number (q_m) of the scattering function for a thermal quenching from the isotropic state into the unstable regions (A), (B), and (C) (the process shown by the arrows in Fig. 10.13) at the early stage of the spinodal decomposition for different concentrations (volume fractions φ) of the liquid crystal molecules. When quenched to (A) region ($\varphi = 0.55$), the scattering intensity increases at a constant peak frequency in the early stages of spinodal decomposition [44]. This result is the same as for the Cahn theory of spinodal decomposition of an initially isotropic liquid mixture. That is, the concentration fluctuation is causing a phase separation in this region. However, the peak wave number decreases with increasing concentration of the liquid crystal molecules ($\varphi = 0.72$). Because $(\partial^2 f/\partial \boldsymbol{\varphi}^2)_T > 0$ in region (C), concentration fluctuations weaken over time, but the orientation fluctuation grows since $(\partial^2 f/\partial \boldsymbol{S}^2)_T < 0$. This orientation fluctuation induces concentration fluctuations through the coupling term (w) in Eq. (10.8) and proceeds spinodal decompositions. In region (C), the peak position q_m in the compositional structure factor shifts to lower values of the wave number with time. The mean radius of domains initially grows as $t^{1/3}$. There is no longer the time stage predicted by the Cahn linearized theory for isotropic spinodal decompositions. With increasing concentration of the liquid crystal, the spinodal decomposition changes from concentration-induced to orientation-induced one. Such a spinodal decomposition that is caused by an orientation fluctuation was observed in an fd virus solution at a later time [50].

Fig. 10.15 Schematically illustrated four possible uniaxial nematic phases. The nematic phases are defined by using the orientational order parameter S_1 of the liquid crystal and that S_2 of the rod
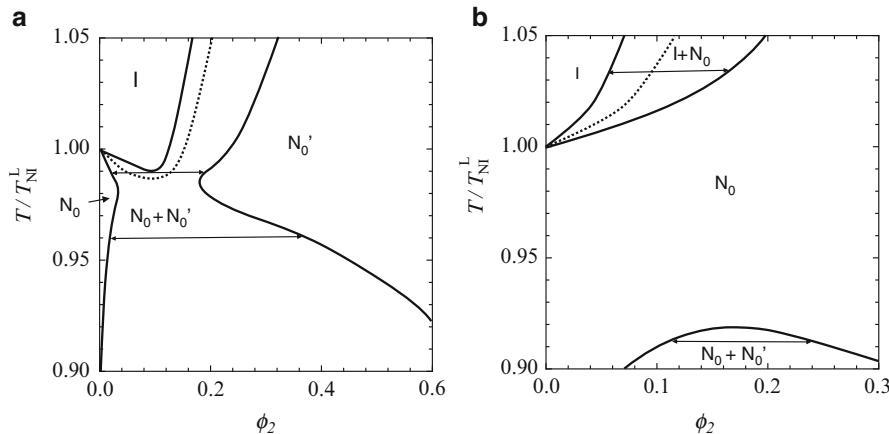
10.3.3   Mixtures of a Rigid Rodlike Polymer and a Liquid Crystal

I will introduce the phase separation of mixtures of rigid rodlike polymers and liquid crystal molecules in this section. Stiff, long liquid crystal polymers and carbon nanotubes are considered to be rodlike molecules. Because of the strong intermolecular van der Waals attraction, nanotubes aggregate and do not easily dissolve. However, they can be dispersed by modifications with surfactant-like molecules on the nanotube surface [51]. Such dispersed nanotubes can be aligned in a liquid crystal matrix.

10.3.3.1   Uniaxial Nematic Phases

Here, I introduce the phase separation of the mixed system of rodlike molecules and liquid crystal molecules. By using the orientational order parameter of the liquid crystal molecules and the rodlike molecules (S_1, S_2), it is possible to define four nematic phases as shown in Fig. 10.15. In particular, it is possible to define a new nematic phase that has $S_\alpha < 0$ ($\alpha = 1,2$). In the nematic phase N_0, rodlike molecules and liquid crystal molecules are oriented parallel to each other, and the orientational order parameter is defined as having positive value ($S_1 > 0$, $S_2 > 0$). In the nematic phase N_1 ($S_1 > 0$, $S_2 < 0$), the average orientation of the liquid crystal molecules describes the director and the rodlike molecules are randomly distributed in the plane perpendicular to that director. In the N_2 nematic phase ($S_1 < 0$, $S_2 > 0$), the rod-shaped molecules determine the director and the nematic liquid crystals are
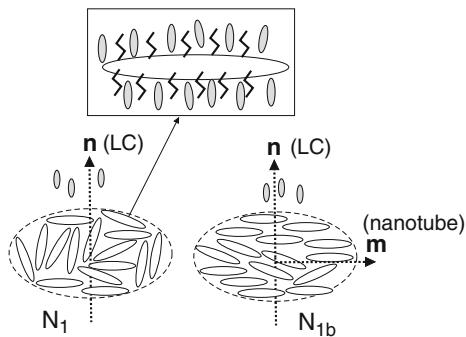
Fig. 10.16 Phase diagrams of mixtures of a rodlike molecule and a liquid crystal molecule

randomly distributed on average in a plane perpendicular to the orientational vector. Furthermore, it is also possible to define the orientational order parameter negative for both types of molecules in the N_3 nematic phase ($S_1 < 0$, $S_2 < 0$). There is the possibility that both, the rod-shaped molecules and the liquid crystal molecules, have a negative dielectric anisotropy when an external field such as an electric field is applied and all molecules are randomly distributed in the plane perpendicular to the direction of the electric field [52].

Figure 10.16 shows the phase diagram of the mean field theory calculations [52]. The vertical axis is temperature and the horizontal axis represents the volume fraction of rod-shaped molecules. The attractive interaction parameter c_{12} between the liquid crystal and the rod-shaped molecules is 0.3 (Fig. 10.16a) and 0.4 (Fig. 10.16b). The solid line is the coexistence curve and the dotted line shows the NI phase transition. Because of the excluded volume effect, there is a phase separation between an isotropic and a nematic phase ($I + N_0$) on the high-temperature side in Fig. 10.16. With the decrease of temperature, the concentration difference in the coexistence region of $I + N_0$ is reduced, and triple point of $N_0 + I + N_0'$ appears in Fig. 10.16a. On the low-temperature side of the triple point, the nematic phase splits into two nematic phases (N_0 and N_0') with different concentrations of liquid crystal molecules.

When the attractive interaction between the liquid crystal molecule and rodlike molecule becomes stronger, the coexistence curve splits into two nematic phases (N_0 and N_0') of the low-temperature side and a nematic phase and an isotropic phase (N_0 and I) on the high-temperature side (Fig. 10.16b). Phase separation between I and N_0 phase on the high-temperature side takes place because of the excluded volume between rodlike molecules, but with decreasing temperature, the attractive interaction between liquid crystal molecules and rodlike molecules becomes dominant, and phase separation curve disappears and the stable nematic phase

Fig. 10.17 Uniaxial planar nematic (N$_1$) and biaxial nematic (N$_{1b}$) phase in mixtures of a rod and a liquid crystal, where both components favor perpendicular orientations to each other

N$_0$ appears. Thus, in these phase diagrams, a lower critical phase solution temperature (LCST) exists above which the phase separation (I + N$_0$) occurs. Such an LCST has been observed in a mixed system of liquid crystal molecules and main-chain liquid crystal polymers with strong attractions caused by hydrogen bonding [53]. If the surface of the rodlike molecules would be modified with surfactant molecules, it is conceivable that the liquid crystal molecules and the rod-shaped molecules could align vertically [52] as described in Fig. 10.15. Such a two-phase separation of N$_1$ + N$_2$, or I + N$_2$ has been predicted theoretically [52].
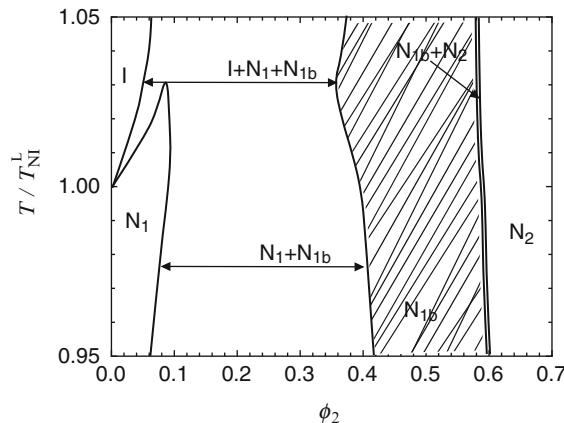
10.3.3.2   Biaxial Nematic Phases

If the liquid crystal molecules and the rodlike molecules are aligned vertically, there is a possibility that a novel biaxial nematic phase exists on the uniaxial nematic phases N$_1$ and N$_2$. So far, biaxial nematic phases have been attracting attention for molecules having a biaxial molecular shape (plate-shaped or disc-shaped molecules) [53, 54], but based on the above discussion, the novel biaxial phase can also be produced in the combinations of molecules with uniaxial symmetry.

Figure 10.17 shows schematically the biaxial nematic phase N$_{1b}$ and the uniaxial nematic phase N$_1$ [55]. The orientation of the rodlike molecules in a plane perpendicular to the direction of the major director ($\boldsymbol{n}$) is random in the uniaxial N$_1$ phase. However, with increasing concentration of the rodlike molecules, the rodlike molecules may orient by mutual attraction and the excluded volume effect in a second direction with the minor director ($\boldsymbol{m}$) as shown in the figure on the right. Thus, the novel biaxial nematic phase N$_{1b}$ may be possible. In the same fashion, in the N$_2$ phase, it may be possible to have a biaxial nematic N$_{2b}$ phase, where the additional ordering of liquid crystals appears in the minor director ($\boldsymbol{m}$) perpendicular to the major director ($\boldsymbol{n}$) of rodlike molecules.

Using Eq. (10.6), such a biaxial nematic phase is defined by two orientational order parameters: $S_\alpha = Q_{zz,\alpha}$ and $\Delta_\alpha = Q_{yy,\alpha} - Q_{xx,\alpha}$. Here, $\alpha = 1$ or 2 are used for the liquid crystal molecules and rodlike molecules, respectively. The uniaxial order

Fig. 10.18 Phase diagram
of biaxial nematic phases in
a rod/liquid crystal mixture

parameter S_α represents the major director (parallel to the z-axis) and defines the
degree of orientation of the molecules.

The biaxial order parameter Δ_α represents the minor director and defines the
degree of orientation along an axis that is perpendicular to the z-axis. In the
isotropic phase $S_\alpha = \Delta_\alpha = 0$, in the uniaxial nematic phase $S_\alpha \neq 0$, $\Delta_\alpha = 0$, and in
the biaxial nematic phase $S_\alpha \neq 0$, $\Delta_\alpha \neq 0$.

Figure 10.18 shows the results of the calculated phase diagram of a biaxial phase
that takes into account those two-order parameters [55]. The solid lines show the
coexistence curves depending on the volume fraction of rod-shaped molecules (the
phase transition curves are not drawn in this figure, because it would become too
complicated). At high temperature there is two-phase coexistence $(I + N_{1b})$ between
the isotropic phase (I) and biaxial nematic phase N_{1b}. At the lower temperature
there is a triple point $(I + N_1 + N_{1b})$, where three phases simultaneously coexist.
Below the triple point temperature there are two-phase-separated regions $(I + N_1)$
and $(N_1 + N_{1b})$. In the volume fraction range of $0.4 < \varphi_2 < 0.6$, there is a single,
stable biaxial phase N_{1b} (shaded area). At the volume fraction of $\varphi_2 > 0.6$, the
biaxial nematic phase changes to a uniaxial N_2 phase, and, on high-temperature
side, there is a narrow phase-separated region $(N_{1b} + N_2)$. When the attractive
interaction between the liquid crystal molecule and the rodlike molecule becomes
weak, the stable N_{1b} phase shifts to lower concentrations, and a thermodynamically
stable biaxial nematic phase is hidden inside bimodal lines. The biaxial nematic N_{1b}
phase has not been observed yet, but it should be a challenging subject for the future
from a theoretical and an experimental point of view.

10.3.4   Outlook

Liquid crystalline hybrid materials can be obtained by adding other molecules to a
pure liquid crystal. Material design using a liquid crystal matrix will become
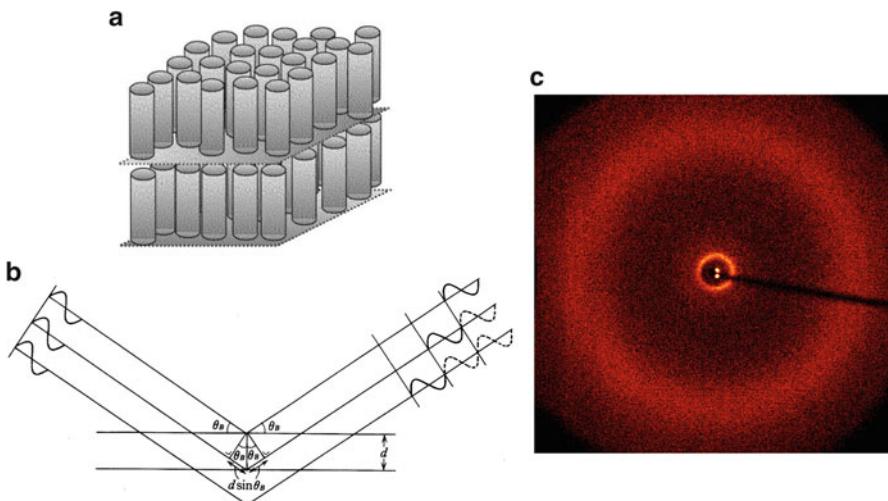
important in the future. Areas of interest in the future may be in totally different fields than the conventional liquid crystal display application and may include cosmetics, drugs, food, detergents, biomimetics, actuators, and drug delivery systems, in terms of liquid crystal science. It will be challenging subjects from both an experimental and theoretical point of view.

10.4   Static and Dynamic Inhomogeneities in New Hierarchical Liquid Crystal Structures Caused by Frustration

Jun Yamamoto

10.4.1   New Liquid Crystal Composite Hierarchy Can Be Induced by Frustration

Soft matter, such as liquid crystals, phospholipid membranes, surfactants, emulsions, gels, polymers, and colloids, are formed by the hierarchical self-assembly of molecules, and the structures can span over from the micro to macro length scales. For example, biological tissue is one of the hierarchical structures of soft matter that is more sophisticated and complex than others. State-of-the-art chemistry is able to design and produce new diverse and complex molecules by combining molecules with new functionalities. Furthermore, in the field of biology, it became possible to decipher the genome that contains a huge amount of information and to obtain a complex design view of the living body. However, the physical mechanisms of how the material is actually assembled into parts of that hierarchy are still insufficient. The biggest problem is that our knowledge of connecting the interactions on the molecular scale with those on the macroscopic length scale is largely missing. The Van der Waals force effectively governs the intermolecular interactions between molecules, but it works on a short distance only. Thus it cannot be the basic driving force for building the giant structures of soft matter. We believe that the low-dimensional order of liquid crystals can produce frustrated structures in composite systems that stabilize the hierarchical structure of the substance by new long-range interactions. In recent years, it was found that the elastic deformation of the liquid crystal orders produces ordered chain-like structures of particles or spheres in liquid crystals. I, on the other hand, had the idea that the scalar order parameter can mediate the long-range interactions and I proposed the principle of a new molecular manipulator [56].
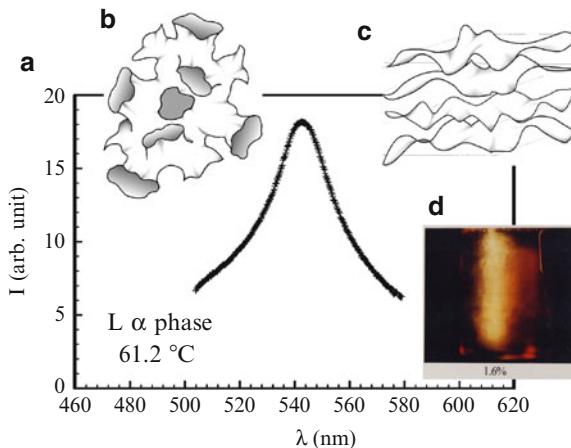
Fig. 10.19 (**a**) Schematic representation of layer structure of SmA. (**b**) Bragg condition. (**c**) Two-dimensional profile of Bragg scattering of the X-ray

10.4.2 Order (Spatial Regularity) and Structure (Spatial Heterogeneity)

10.4.2.1 Static Spatial Heterogeneity

The smectic phase has a one-dimensionally ordered structure (Fig. 10.19a). The molecules are arranged in regular (periodic) intervals. If the atoms or molecules are arranged periodically, the Bragg condition for X-rays with a wavelength of about 0.1 nm is satisfied at a specific orientation and angle (Fig. 10.19b) and Bragg scattering is observed (Fig. 10.19c). On the other hand, hyper swollen lamellar structures formed by surfactants and the like helical structure of the cholesteric liquid crystal phase satisfy the Bragg condition (Fig. 10.20) for visible light, leading to Bragg scattering of certain colors. Such a color is called iridescence or "structural color," it is produced by a type of photonic structure that became of interest in recent years.

On the contrary, the random arrangement of molecules in completely isotropic liquids, in the nematic phase, in sponge phases (Fig. 10.20b), or within the smectic layers leads to only diffuse scattering in X-ray diffraction experiments, which correspond to the average distance of the molecules. In addition, structures that have a characteristic length on a larger scale, such as polymer solutions and blends, aqueous surfactant solutions, sponge phases, consolidated phases, or micro-phase-separated structures, show a diffuse scattering with a small wave number that can be measured with long wavelength neutron scattering or visible light. By summarizing these properties, one can say that the "structure" within a material can be

Fig. 10.20 (**a**) Bragg scattering of visible light in swollen lamellar phase. (**b**) Schematic representation of sponge phase. (**c**) Schematic representation of lamellar phase. (**d**) Photograph of Bragg scattering of the visible light in sample container in swollen lamellar phase. (*Color* corresponds to the "structural color" depend on inter lamellar distance) [105]

paraphrased as a "spatial heterogeneity" of the spatial distribution of molecules and an "order" in which these inhomogeneities have a "regularity."
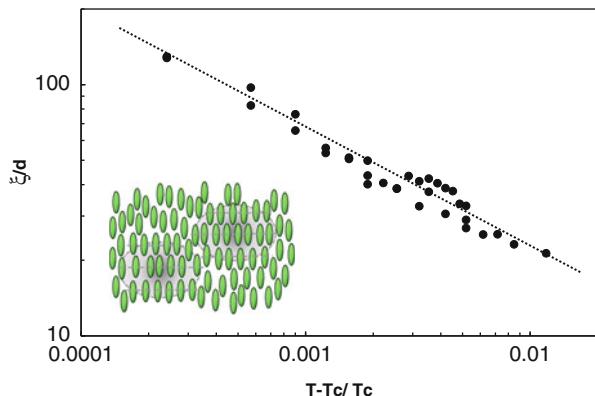
10.4.2.2 Transient Spatial Heterogeneity

Close to the phase transitions point (such as the weak first-order isotropic to nematic transition or the second-order nematic to smectic transition), the order of the low-temperature phase occurs transiently in the finite small size of fluctuations, which is called cybotactic clusters. When the correlation length of the fluctuation increases towards the transition point, the relaxation time diverges. For example, near the nematic–smectic phase transition point, it can be seen that the correlation length becomes longer towards the transition point by X-ray diffraction experiments (Fig. 10.21). In addition, the increase of the relaxation time of the fluctuations can be measured using dynamic light scattering method, which will be introduced in detail in Sect. 10.4.3.2.

10.4.2.3 Dynamic Heterogeneity

The order and the structure in the material are characterized as the spatial heterogeneity of the position of atoms and molecules as described above. In the glassy state, the center of gravity of molecules is random in all spatial direction as it is in a liquid, but a glass is hard as a solid, because molecular motions are frozen. When characterizing a material in the glass state by "static" X-ray scattering, the gravity center distribution of the molecules is equal to the distribution in a liquid, and there

Fig. 10.21 Normalized
temperature, $T-T_c/T$,
dependence of correlation
length of transient
cybotactic cluster of SmA in
nematic phase near nematic
to SmA phase transition.
(Data was obtained by
Y. Kimoto)

is almost no change in the scattering function. Thus, the two states (glass and liquid) cannot be distinguished. When the super-cooled liquid state is approaching the glass transition point, the viscosity increases by ten or more orders of magnitude. In recent years, it has been found that the molecular mobility is different for each part of the space [57]. In this way, "dynamic heterogeneity" depends on the spatial distribution of different mobility in the material and plays an important role in the origin of dynamics that characterize the physical properties of glassy materials.

10.4.2.4 Dynamic Heterogeneity Induced by Frustrated Order

In the new hierarchical structures of liquid crystal composite systems, this dynamic heterogeneity has a close relationship with the structure and dynamics of the composite. Even in the well-known micro-phase-separated structure of surfactants and in the mesoscale structures of polymer solutions, polymer blends, gels, and colloidal suspensions, molecular aggregates and polymer chain networks have a characteristic timescales, which are completely different from the surrounding medium, and thus static and dynamic spatial heterogeneity appears.

On the other hand, in a pure liquid crystal system, liquid crystalline order, such as orientation order in nematic or layer order in smectic, is created under phase transition point, and the symmetry of the system is reduced. At the same time, new hydrodynamic fluctuation motions appear to be associated with new degrees of freedom. The modes of hydrodynamic fluctuations are characterized by a dispersion relation that can be obtained by solving the constitutive hydrodynamic equations of the system, giving the angular frequency ω and the wave number q of the fluctuations. It can be said that in a uniform alignment of the pure liquid crystal, the system universally satisfies the dispersion relation from the micrometer scale up to the length of the sample chamber, which means that the material keeps spatial homogeneity for the dynamics in pure system.

In turn, in a liquid crystal composite system, the nano-interface at the boundary between the impurity or the micro-phase segregation leads to a loss of the spatial continuity of motion and now a different dispersion relation that depends both on

the actual size of the impurity and the distance between them. In some special case, the nano-interface may also be regularly aligned by the elasticity of the liquid crystalline, to form a cubic lattice space, such as the blue phase. However, it is randomly distributed in the space in general, and the higher symmetry is often restored on the macroscopic scale and may even look like an isotropic phase. Therefore, the quantitative structure analysis by electromagnetic wave scattering such as X-rays, even though it might be able to capture the scattering factor of the liquid crystal order, is difficult. However, even though the distribution of the interface is random, the dynamic heterogeneity changes abruptly to reflect the characteristic length of the spatial structure of the nano-interface. That is, if one measures the dynamic heterogeneity on how motions relate to the local order of a liquid crystal distributed in space, information on the spatial distribution of the nano-interface is obtained.
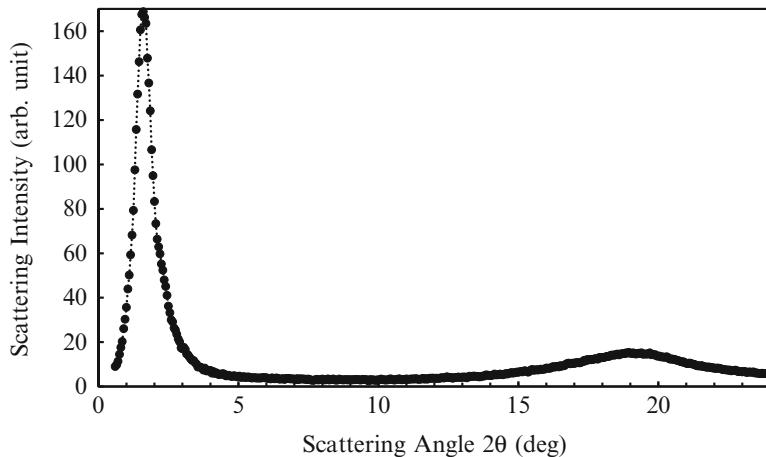
10.4.3 Observation of Static and Dynamic Heterogeneities

10.4.3.1 X-Ray Scattering Experiment for Observation of Static Heterogeneities

In the nematic phase, molecules are oriented along their long molecular axis, but the position of the center of gravity of the molecule is random without spatial regularity as in liquids. X-ray scattering from the molecular alignment in such a liquid state only shows diffuse, broad scattering (halo) at a scattering angle that reflects the average distance between molecules. However, if the nematic phase is uniformly oriented, the intensity of the halo depends on the orientation of the director. That is, the small angle scattering occurs along the director, whereas the wide angle scattering perpendicular to it. The smectic phase has a layered structure and a one-dimensional ordering of the position of molecular center of gravity. Therefore, unlike the nematic phase, Bragg diffraction occurs (Fig. 10.22). In the case of the smectic A phase, this is parallel to the molecular long axis. Furthermore, since the molecules in the layer plane take a random liquid-like arrangement, a diffuse scattering is observed in wide-angle X-ray region that is vertical to the direction in which the Bragg scattering appears. Corresponding to the interlayer spacing of the smectic layer structure, the wave number of the Bragg scattering from the layered structure is approximately the length of the molecular long axis.

10.4.3.2 Dynamic Electromagnetic Scattering Experiment for Dynamic Heterogeneities

First of all, because the whole concept of dynamic heterogeneities was new [57], there were no established specific measurement methods. Some examples were visualized by simulating the dynamic heterogeneity near the glass transition point near, but there were only few examples using experiments. A particular experiment
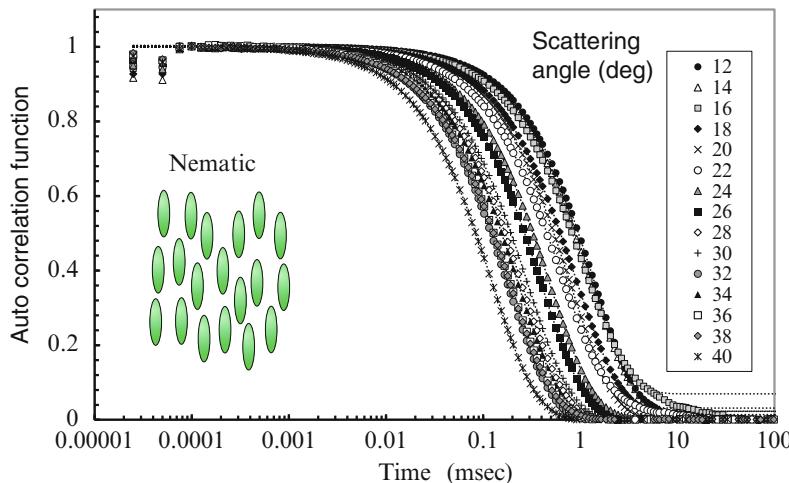
Fig. 10.22 Scattering profile of one-dimensional layer structure in SmA. Sharp peak in small angle region corresponds to the Bragg scattering of layer structure, whereas broad hallow represents the liquid-like molecular arrangement within layers

should be noted in which the dynamic heterogeneity of crystallization near colloidal particles was recorded in real-time by a high-speed laser confocal microscope [58]. In order to measure the dynamic nonuniformity, the principle of measuring the state of motion of the freedom of the material inside will be relevant. In the above case, the fluctuation of the refractive index of the medium can be measured by using laser-based dynamic light scattering, and the degree of freedom of the material can be calculated. From wave number dependence of the dispersion relation, one can obtain information about the spatial distribution of the dynamic heterogeneity. However, the experiment gives 2-dimensional data and in order to get a spatial resolution in three dimensions, it is necessary to measure at high speed at the same time the movement in a plurality of coordinates, which is difficult to achieve at present. On the other hand, by using a free electron laser or X-ray sources of high intensity, such as synchrotron radiation, a time-resolved method had been developed that could measure the dynamics on a molecular scale—something that is not possible with laser-based systems [59].

10.4.3.3 Dispersion Relation

By measuring the wave number dependence of the relaxation time, that is, the dispersion, information about the average spatial size of the dynamic heterogeneity can be obtained.

First, we can describe the dispersion relation of the hydrodynamics of the orientation fluctuation in a uniformly oriented nematic phase that is spatially uniform without dynamic heterogeneities. The modes of the orientation fluctuation

Fig. 10.23 Scattering angle dependence of autocorrelation function for the orientation fluctuation in nematic phase

of the liquid crystal phase can be described by continuity equations that combine the Navier–Stokes equation with others to describe the motion in liquid crystalline orders. Rigorous analysis is omitted here, but the orientation fluctuation becomes a motion mode called diffusion mode, and the dispersion relation represents the relationship between the wave number q and the frequency ω $(=2\pi/\tau)$ of the wave propagation, in which the wave number q is inverse proportional to the square of the relaxation time τ [60, 61]. With increasing Frank elastic constant or with decreasing rotational viscosity coefficient, the relaxation time becomes shorter. Figure 10.23 shows as an example the measurement of the autocorrelation function of the light scattering when the wave number q (determined by the scattering angle) is the parameter for the racemic mixture of the nematic CE5R which has been oriented horizontally on a glass substrate.

It can be seen from Fig. 10.24 how the relaxation time of the orientation fluctuations varies depending on the scattering angle q. The horizontal axis is the wave number q and the vertical axis is the relaxation time τ. The curve fits the inverse square relation of the dispersion relation of the diffusion mode well. The ratio of rotational viscosity and Frank elasticity is obtained from the intercept of the log–log graph representing the dispersion relation.

10.4.3.4   Critical Phenomena and Order Parameter Fluctuation Near the Isotropic–Nematic Phase Transition

Here, I will introduce another type of the fluctuation as an example for the isotropic–nematic phase transition, which is a weak first-order transition and large fluctuations of the order parameter appear as a critical phenomenon near
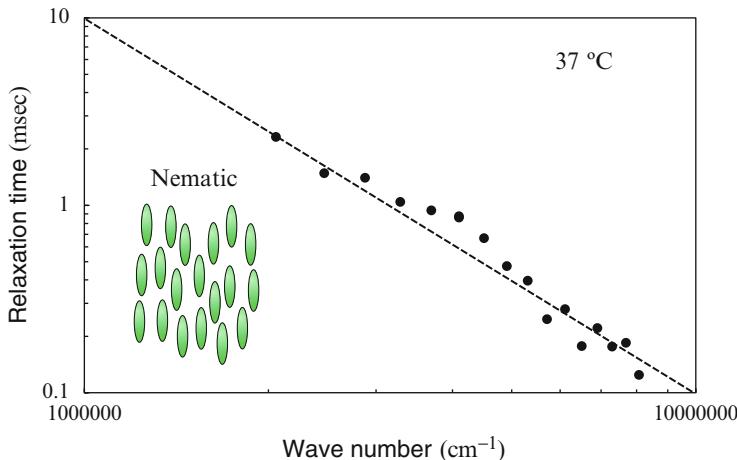
Fig. 10.24 Dispersion relation of orientation fluctuation in nematic phase
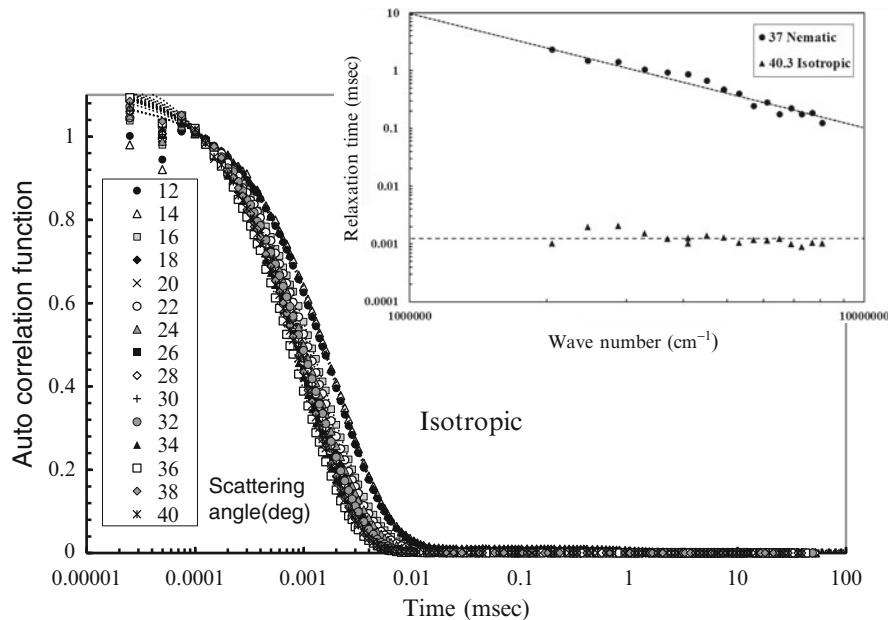
phase transition point. Namely, small clusters of the nematic phase with a finite order parameter are repeatedly generated and annihilated in the isotropic phase. In addition, the characteristic relaxation time of generation and annihilation of the fluctuations is decreasing when approaching the transition temperature due to a critical slowing down. The isotropic–nematic phase transition is a weak first-order transition, and commonly, the transition temperature and the critical temperature are separated by 1 K or more. That is why the fluctuation of the order parameter is slow, but even just before the transition temperature still has a frequency of 1 MHz. This is also due to the fact that the order parameter is a nonconserved quantity. According to the Landau general theory of phase transition, the free energy near a weak first-order phase transition can be expanded in the following equation:

$$f_L = \frac{1}{2}A(T - T^*)s^2 + \frac{1}{3}Bs^3 + \frac{1}{4}Cs^4 + \cdots$$

assuming that the change of the order parameter s can be linearized by the viscosity coefficient ζ. Thus the relaxation is expressed in the following form:

$$\Delta s(t) = \Delta s(0)\exp(-t/\tau), \quad \tau^{-1} = -\frac{2A}{\zeta} = \frac{2a}{\zeta}(T^* - T)$$
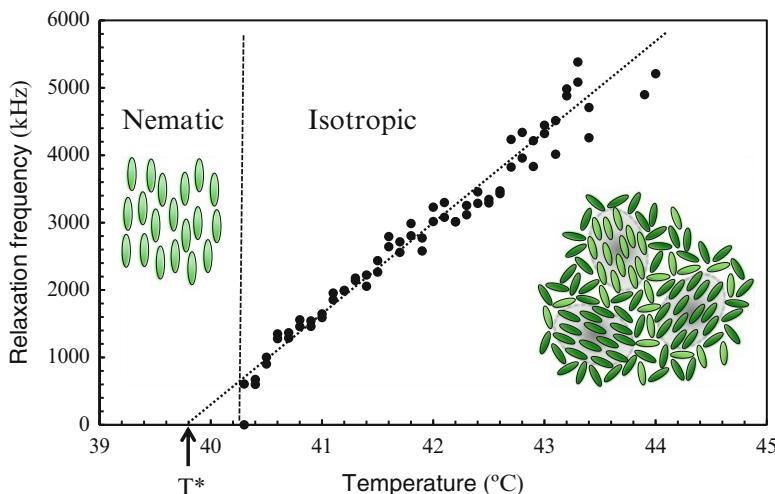
The relaxation time τ is directly related to the coefficient of the second-order term of the Landau free energy. For this reason, due to a decrease of the spring coefficient in the vicinity of the phase transition temperature, the relaxation time of the fluctuations shows a critical slowing down.

Fig. 10.25 Scattering angle dependence of autocorrelation function for the order parameter fluctuation in isotropic phase near isotropic–nematic phase transition temperature. *Inset*: Dispersion relation of the order parameter fluctuation, which is independent of the wave number, together with the orientation fluctuation

Figure 10.25 shows the experimental result of the fluctuation of the order parameter obtained by dynamic light scattering experiments in the isotropic phase close to the phase transition temperature. The relaxation time is very fast with about 1 μs which is about three orders of magnitude faster than the fluctuations in the orientation of the nematic phase. It should also be noted that the correlation length of the fluctuation (cluster size) just above the transition temperature is sufficiently smaller than the wavelength of visible light. Therefore, the relaxation time of the fluctuations observed by dynamic light scattering method is always the same irrespective of the scattering angle, which differs from the orientation fluctuation (the upper right part of Fig. 10.25 shows the dispersion relation of the orientation fluctuation of the nematic phase).

Figure 10.26 shows the temperature dependence of the relaxation time of the fluctuations. It can be seen that it is proportional to the temperature difference from the phase transition temperature, increases divergently, and shows a critical slowing down, which fits well with the prediction of the Landau theory. In the case of liquid crystal shown in the example, the critical temperature T^*, estimated by linear extrapolation of the data points, is approximately 1 K below the isotropic–nematic phase transition temperature.
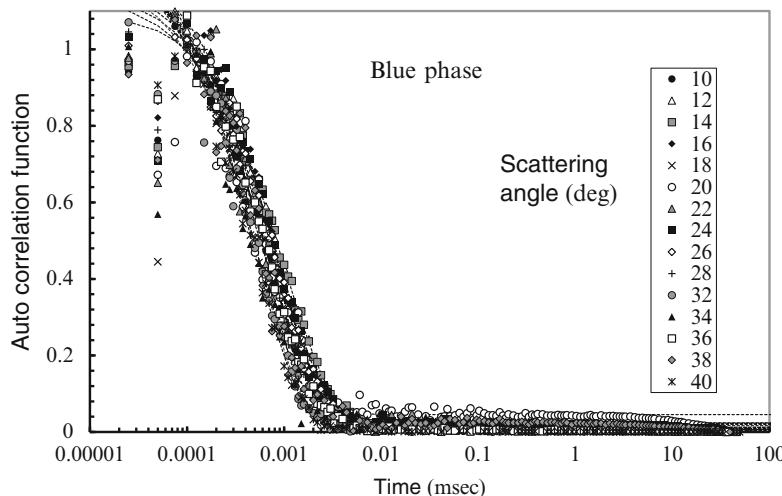
Fig. 10.26 Critical slowing down of order parameter fluctuation near isotropic to nematic phase transition temperature

10.4.4 Hierarchical Structures in Liquid Crystal Composite and Their Static and Dynamic Heterogeneity

As described in the previous section, the fact that the dynamics of the internal degrees of freedom in the wave number space satisfy predicted dispersion relation in a certain wave number space that are identical to that the "dynamic structure is uniform" in space. On the contrary, if there is a spatial dynamic heterogeneity, then that appears also in the dynamics of the internal degrees of freedom, and peculiarity appears in the dispersion relation. As of the origin of the dynamic heterogeneity in pure liquid crystal systems and composite systems, the following can be said:

1. Point, line, or plane defects are spontaneously created in the space. These structures can be either ordered or be distributed randomly having sizes in the range of the visible light wavelength or more.
2. The meso-structure induced by the introduction of other molecules or particles lead to spatially random static heterogeneities that also show dynamic one.
3. Fluctuations near the phase transition temperature or near the critical point lead to dynamic heterogeneity, whereas there is no static heterogeneity due to the absence of uniform long-range order.
4. Glasses and super-cooled liquids are spatially homogeneous as same as liquid state, but show spontaneous dynamic heterogeneities.
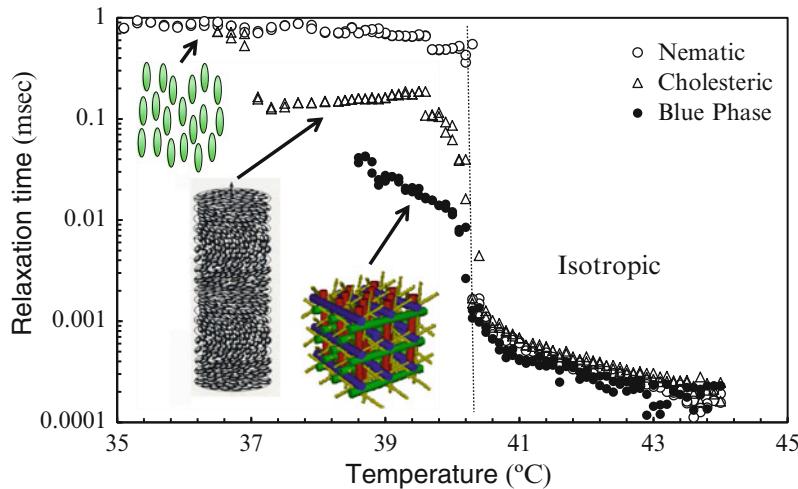
Fig. 10.27 Scattering angle dependence of the autocorrelation function for the orientation fluctuation in ChBP

10.4.4.1   Blue Phase

The cholesteric blue phase (ChBP) appears in a very narrow temperature range (usually within 1 °C) just below the isotropic phase in short helical pitch material. Recently it was found by Kikuchi et al. that the temperature range can be expanded by polymer stabilization [62], and application in high-speed displays is anticipated. In ChBP, the helices produced by the spontaneous twist of the director form a cubic lattice with a regular three-dimensional alignment. However, it cannot fill the space continuously, and defect lines called disclinations are embedded in the cubic lattice structure.

Upon examining the dispersion relation by observing the orientation fluctuation of ChBP by dynamic light scattering, the relaxation frequency of the orientation fluctuation is independent of the scattering angle and has a constant value, which is different from the behavior of the nematic phase described in the previous section (Fig. 10.27). This can be understood because the spatial continuity of the fluctuation is lost due to the existence of disclination lines in the cubic lattice. In fact, the relaxation frequency is very fast, because the fluctuation is confined in the cubic lattice of blue phase. This is also the principle of the speed of blue phase display.

On the other hand, the order parameter fluctuation is observed in the isotropic phase close to the ChBP phase transition temperature. As in the case of the previously described nematic–isotropic transition in Sect. 10.4.3.4, this fluctuation also does not depend on the scattering angle, but depends only on temperature (Fig. 10.28). In other words, the fluctuation of the ChBP near the isotropic phase is
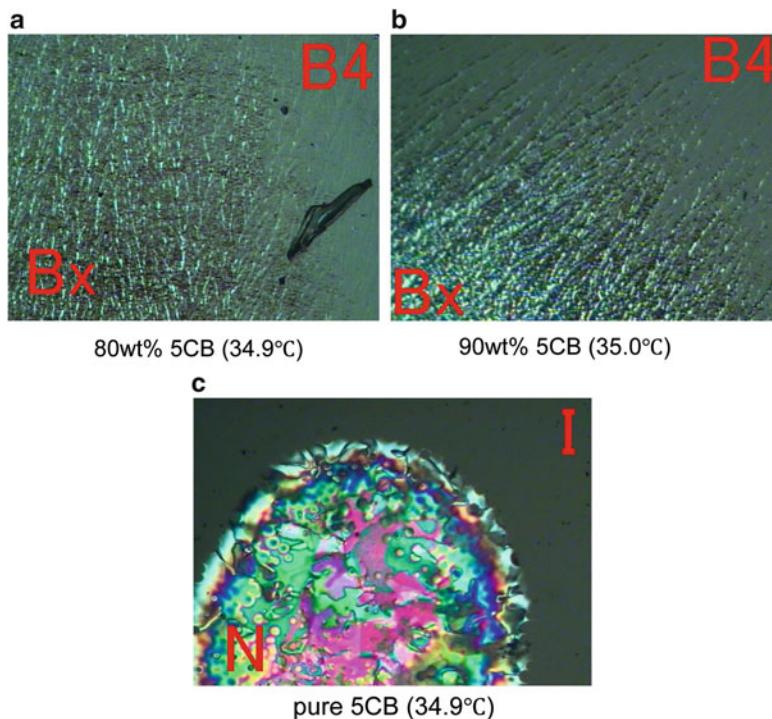
Fig. 10.28 Temperature dependence of relaxation frequency of the orientation fluctuation in nematic, cholesteric, and ChBP, respectively (*left side*), together with the order parameter fluctuation in the isotropic phase of each sample (*right side*)

due to a fluctuation of the scalar order parameter. Figure 10.28 compares the temperature dependence of the relaxation time of the fluctuations of a ChBP compound (CE5), with that of its racemic mixture that forms a nematic phase (CE5R) and low chirality mixture that forms the ChBP phase. The figure shows that although the order on the low-temperature side is different for the ChBP, cholesteric, and nematic phase, the same fluctuation of the order parameter is observed for the isotropic phase, and its temperature dependence is completely irrespective of the optical purity. On the contrary, fluctuations of specific hydrodynamic modes occur dependent on the different symmetry of the ordered low-temperature phases.

10.4.4.2 Swollen Banana Phases
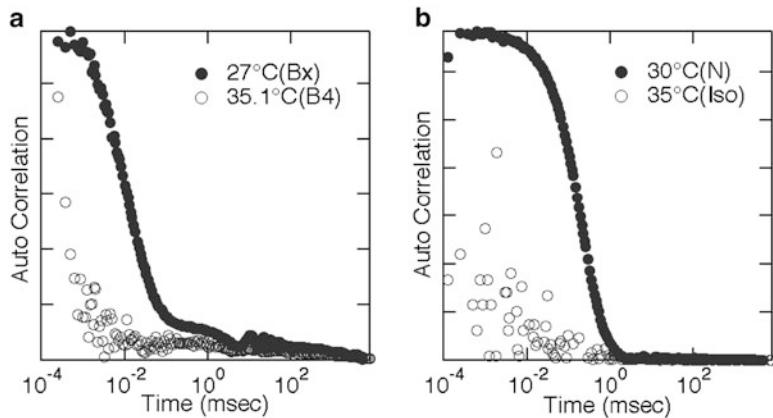
Another example is the swollen B4 phase of banana-type (bend-type) liquid crystals. The banana-type molecules form smectic liquid crystals in which the molecules are tilted with respect to the layer normal. This tilt and the orientation of the bow-shaped molecules have been of interest, because even achiral molecules can express a chiral structure. In addition, in the mixed system of pentylcyanobiphenyl (5CB), a typical nematic rodlike mesogen, and (P-8-O-PIMB), one of the banana-type liquid crystals, the specific B4 phase is formed in a wide mixing range of up to 107 wt% 5CB [63]. In addition, there is a new Bx phase in the low-temperature
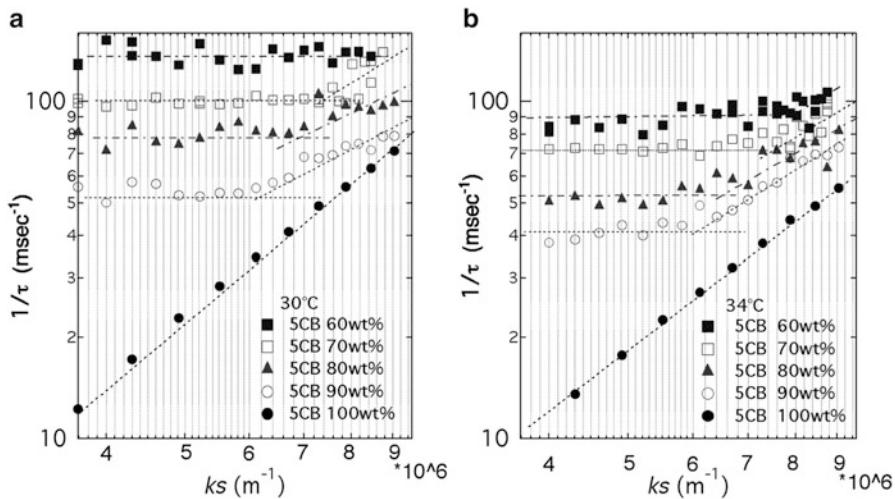
Fig. 10.29 Polarizing microscope photographs of B4 and Bx phase in swollen banana liquid crystal (concentration of 5CB 80 wt% (**a**) and 90 wt% (**b**), respectively), together with pure 5CB (**c**)

region (35 °C or less) of mixtures with at least 65 wt% 5CB. Figure 10.29 shows the polarized light micrographs of two mixtures and the pure 5CB. The nematic phase transition of the BX phase and B4 phase has been studied by DSC and X-ray diffraction, but there were many unclear points about its internal structure.

Here, I will show that the measurement of the dynamic heterogeneity revealed the characteristics of the random structure in the B4 phase [64]. Figure 10.30a shows the time autocorrelation function of the BX phase (at 27 °C) and the B4 phase (at 34 °C) of a mixed system of 80 wt% 5CB. Figure 10.30b shows the nematic and isotropic phases of pure 5CB for comparison. Large fluctuations are present around 0.1 ms in the Bx phase, but the corresponding fluctuation in the B4 phase has disappeared. In addition, the Bx–B4 transition temperature of the mixed system is almost the same as the phase transition temperature of pure 5CB, 34.10 °C. In the phase diagram, Bx–B4 transition temperature corresponds to the extrapolated isotropic–nematic phase transition temperature phase of 5CB. From these two experiments we reason that the fluctuations that had been observed in the Bx phase come from the orientation fluctuations of the 5CB nematic

Fig. 10.30 (**a**) Autocorrelation functions in swollen banana liquid crystal. *Closed symbols* are observed in B4 phase (27 °C) and *open symbols* in Bx phase (35.1 °C). (**b**) Autocorrelation functions in 5CB. *Closed symbols* are observed in nematic phase and *open symbols* in isotropic phase

Fig. 10.31 5CB concentration dependence of the dispersion relation in swollen banana liquid crystal at 30 °C (**a**) and 34 °C (**b**) respectively. Phase transition temperature between Bx and B4 phase is about 34.5 °C

phase. That is, 5CB molecules are in a nematic order in the Bx phase and have an isotropic orientation in the B4 phase, located between the chiral nanofilaments of the B4 phase.

Furthermore, Fig. 10.31a (at 30 °C) and Fig. 10.31b (at 34 °C) can give both temperature dependence of the dispersion relation of the orientation fluctuation.

The nematic phase of pure 5CB is indicated by black circles in both Fig. 10.31a, b. It can be seen that the dispersion relation has two linear sections that agree very well with the orientation fluctuation and the diffusion mode as described in the previous section. In contrast, the dispersion relation of the orientation fluctuations in the Bx phase mixed system has the following features: (1) There exists a boundary at a certain wave number k_c, which is dependent on the concentration that separates two regions with different dispersion relation. (2) In the region where the wave number is larger than k_c, the dispersion of the orientation fluctuation fulfills two linear relationships. (3) In the area where the wave number is smaller than k_c, the relaxation time does not depend on the wave number and is almost constant.

As has been described in the previous section of the blue phase, the continuity of the orientation fluctuation is disturbed by the meso-structure of cubic lattice of disclination lines. Thus, the diffusion mode of the fluctuation cannot be satisfied, and the relaxation time does not depend on the wave number. Having this in mind, it is reasonable to assume that the internal structure of the Bx phase of banana-shaped molecule disrupts the nematic phase, and the continuity of orientation fluctuation is lost. That is, the Bx phase is a random, but micro-phase-separated structure having certain block size close to k_c. It can be seen that k_c estimated from the graph of dispersion relation is highly dependent on concentration but hardly dependent on temperature. The nanofilaments are formed as a micro-phase-separated structure in the B4 phase. Regions rich in 5CB are present in the periphery and independently show a nematic–isotropic phase transition. In other words, by using dynamic light scattering to analyze the dynamic heterogeneity, we were able to conclude that nematic phase 5CB molecules exist in the micro-phase-separated structure of chiral nano-filament banana-type liquid crystal molecules.

Of the various origin of the dynamic nonuniformity described above, when it has a spatial regularity, is open to static structural analysis by light and X-rays, but in case of random, irregular heterogeneities, those methods give little useful information in static scattering experiments. Information obtained by scattering experiments is very limited in the case of glasses. Here, I introduced a new liquid crystal composite structure with a meso-structure as an example of a spatial structure analysis of dynamic heterogeneities by dynamic light scattering.

10.5   Simulation of Liquid Crystals

Makoto Yoneya

10.5.1   Introduction

Computer simulation is sometimes referred to as the third research approach, beside experiment and theory, but how could simulations contributes to liquid crystal research?

The first thing that comes to mind when thinking about liquid crystal simulations are molecular orbital (MO) simulations that target the electronic state calculation of isolated molecules, and molecular dynamics (MD) calculation to investigate the aggregation state of the molecular assemblies. Furthermore, continuum models can calculate the macroscopic liquid crystal alignment in an external electric field. Applications of simulations are also cover circuit simulations to calculate a range of driving characteristics of liquid crystal display panels. The value of the various contributions concerning liquid crystal simulations depends on the circumstance. For example, according to one position [65], the molecular (MO and MD) simulations are able to take into account chemical characteristics of a compound, then that can be used for scientific needs and for engineering applications. On the other hand, simulations by using the continuum approach unable to take into account the chemical character of the molecule, but can focus on the pure physical phenomena that can be applied to pure science.

In this section, I want to share my personal engagement, which stems from a different standpoint. Through this, I want to show how simulations have contributed to the liquid crystal science and technology during the last quarter of a century.

10.5.2   Continuum Simulation

Modeling of liquid crystals by a continuum approach has had a long history dating back to Ossen [66]. The continuum simulation is also almost the only tool that can simulate a liquid crystal device on the macroscale.

The major turning point for continuum simulation of liquid crystals as a tool for liquid crystal display research and development came when in-plane switching (IPS) mode had been developed and commercialized [106].[1] Before that, the common display mode was the so-called twisted nematic (TN) configuration, in which the liquid crystal layer is sandwiched between two indium tin oxide (ITO)

---

[1] The author had worked for Hitachi, Ltd. and conducted the continuum simulations in the original development group of the IPS-mode LCD.

electrodes and a vertical electric field is applied. This means that it was sufficient in most cases to just have a simple one-dimensional model parallel to the liquid crystal layer normal. Those one-dimensional models could be treated analytically, and demands for the simulation of those models had been very limited.

10.5.2.1   Simulation of the IPS Mode

As the name suggests, the in-plane switching (IPS) mode is a method that applies an in-plane transverse electric field that is generated by comb-shaped electrodes placed on the substrate, and the liquid crystal layer is switched in the in-plane direction [67]. The modeling of the IPS mode requires an at least two-dimensional model, for example, with respect to the arrangement of the various comb-shaped electrodes to obtain the two-dimensional distribution of the liquid crystal alignment and the transverse electric field described above. There is no alternative to a simulation to get a realistic model, which is totally different from the case of the TN display described above.

In the TN system, since the vertical electric field is applied to the upper and lower ITO electrodes sandwiching the liquid crystal layer, the field distribution is homogeneous in the in-plane direction, and one can calculate the electric field in the liquid crystal layer with a fixed potential boundary vertical to the ITO electrode. On the other hand, in the IPS case, there is no electrode at all on the upper substrate (color filter side), and also on the lower substrate (thin-film transistor side) in the parts between the comb electrodes. The electric field generated by the comb electrodes has to be calculated including the liquid crystal layer and thus portion includes a significant area of the upper and lower substrates as shown in Fig. 10.32 [68].[2]
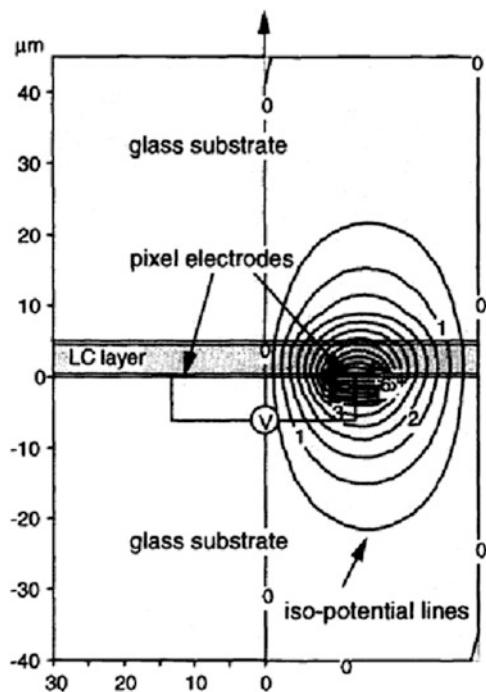
Calculations include upper and lower glass substrate areas with a sufficient area that revealed the asymmetry of the liquid crystal layer on the electric field comb electrodes is not so large. Then the in-plane switching of the liquid crystal layer also occurs in a nearly symmetrical distribution. This fact allows a one-dimensional model, which assumes a uniform horizontal electric field to approximate to some extent, to study the fundamental characteristics of this original IPS type comb electrodes devices [69].

The most prominent advantage of the IPS mode is the unprecedented wide viewing angle, and the importance of the simulation is also manifested in the sense of optical calculations of the viewing angle characteristics. The so-called 4×4 matrix had already been established as a method of calculating the optical properties in an oblique direction [70], but there was not much necessity of such a computation for the TN mode. But for the IPS mode, the calculations proved to be

---

[2] After the first IPS-mode paper at 1995, many research groups tried the simulation of the IPS-mode. However, almost all the groups did not calculate the electric fields within the glass substrates.

Fig. 10.32 Two-dimensional simulation model for the IPS-mode LCD (iso-potential lines are shown only in the right-hand side as these are symmetric)
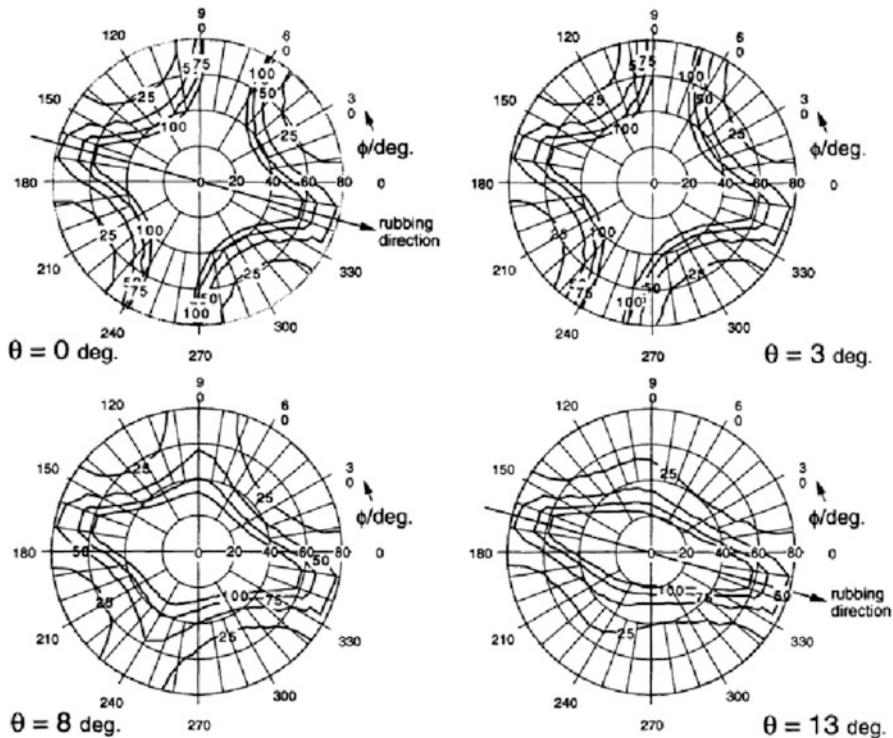
very useful to calculate the optical properties such as the relationship between the viewing angle characteristics and the pretilt angle due to the alignment layer (Fig. 10.33) [71].

As described above, the continuum simulation as a tool of research and development of the early IPS mode displays used both the two-dimensional model and the one-dimensional approximation model. In 1998, the two-dimensional model became mainstream when it was used in the fringe field switching (FFS) mode [72].

10.5.2.2 Simulation of the FFS Mode

In its original, the FFS configuration had transparent comb electrodes instead of metal electrodes in the IPS mode and a negative dielectric anisotropy liquid crystal material instead of a positive dielectric anisotropy liquid crystal material in the IPS-mode LCD. Thus, the transmittance of an FFS mode could be greatly improved as compared to the IPS system [73]. The distribution of the LC orientation field and the electric field is much more complex than in the IPS mode, as can be seen in Fig. 10.34, and the one-dimensional approximation was no longer possible. By combining the advantages of the FFS mode with the original IPS mode, we developed the advanced FFS prototype looked different from the original design.
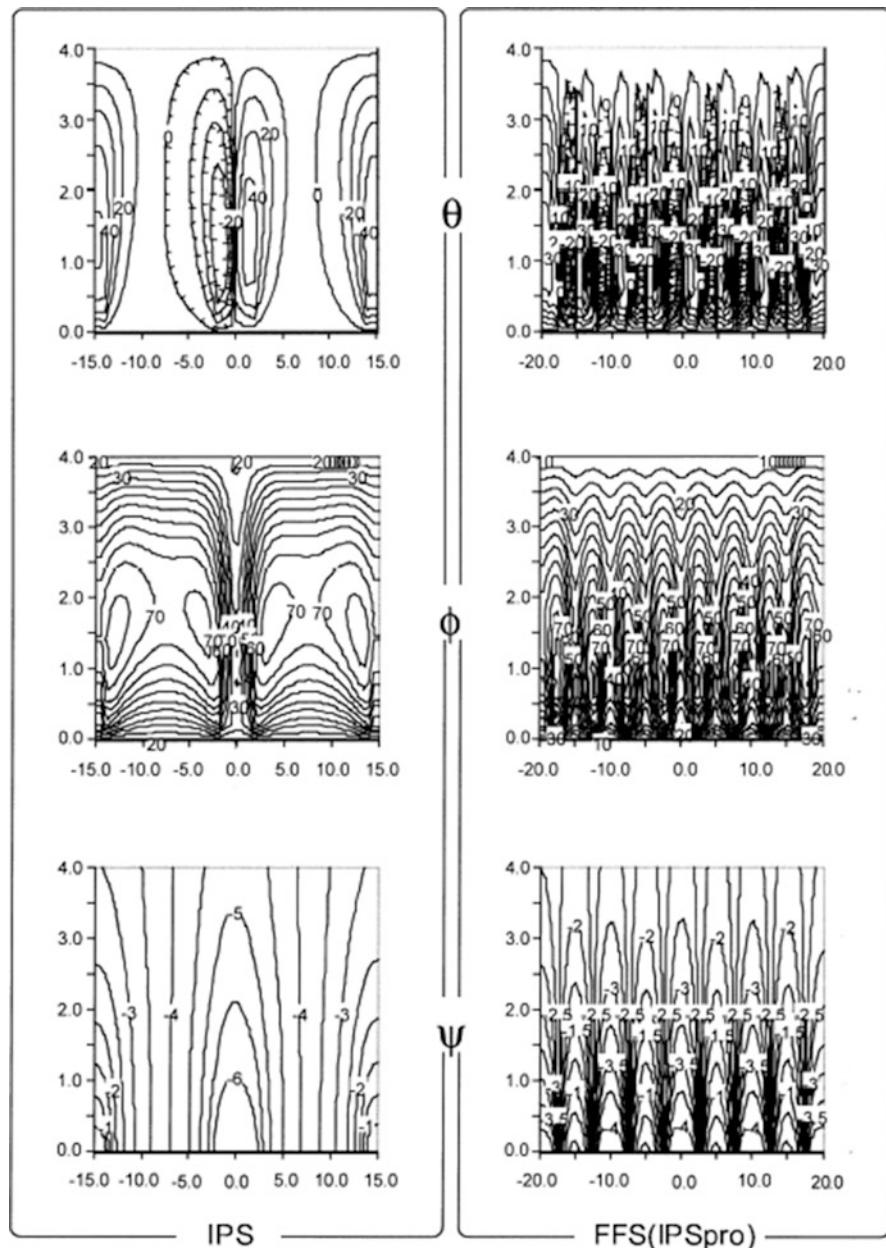
Fig. 10.33 Dependency on the surface pre-tilt angles of the viewing angle characteristics of the display contrasts of the IPS-mode LCD

Comblike electrodes were fabricated on a transparent electrode, separated by a dielectric layer in the so-called finger-on-plate (FOP) configuration [107].[3] A positive dielectric anisotropy liquid crystal material, as for the original IPS mode, was applied and it was commercialized as the IPSpro LCD [74].

From these days, the optical simulation of complex optical compensation films for designing high-quality displays became essential [75]. In the similar way, the design of the electrode slits and protrusions used in the pixel division method in the vertical alignment (VA) mode has been carried out by continuum simulation [76].

---

[3] During we had been evaluating the first FOP test cell results, one of our colleague who was attending the Society of Information Display (SID) 1999 e-mail us that there was presentation of the FOP configuration from the original FFS research group [107]. We're surprised the coincidence across the world.

Fig. 10.34 Comparison of simulation results for IPS-mode LCD and FFS (IPSpro)-mode LCD (*top*: tilt-angle distributions of LC, *middle*: azimuthal-angle distributions of LC and *bottom*: the electric potentials at their bright state)

10.5.3 Molecular Simulation

In the early 1970s, molecular simulation of liquid crystals started by Monte Carlo simulations of simple shaped models (rigid body ellipses, etc.) to estimate the excluded volume effect [77]. At the same time, there were already attempts to use the so-called Lennard–Jones potential to calculate the anisotropic potential in model liquid crystals [78]. This has developed into the nowadays well-known Gay–Berne potential [79].

Along with the above-mentioned simple model potentials, there was a detailed simulation by atomic detailed models that used the chemical structure of the molecules. The first molecular dynamics simulation of 4-*n*-pentyl-4′-cyanobiphenyl (5CB) had been reported in 1989 by a group at Groningen University [80].[4] There is a relatively recent review article that summarizes the MD calculation of liquid crystals [81].

10.5.3.1 Liquid Crystal Surface Alignment
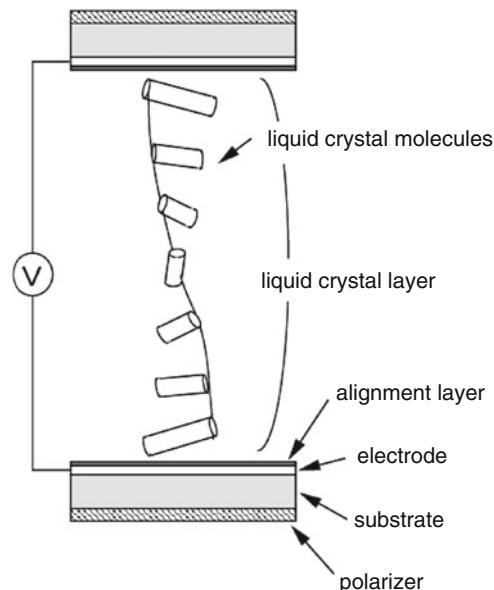
It is well known that the orientation state of the liquid crystal inside the liquid crystal display without external field is determined by the surface state of a glass substrate that is covered with the alignment layer, as shown in Fig. 10.35.

Even though the liquid crystal surface alignment is of great importance for liquid crystal displays, the alignment mechanism is not clear. One of the reasons is that it is necessary to analyze surface phenomena with molecular resolution. In this sense, molecular simulation is considered a powerful means analysis with molecular resolution, and even on the atomic level. With respect to the issue of liquid crystal surface orientation, simulation of liquid crystal molecules on a graphite surface has been started relatively early by an atomic detailed model with scanning tunneling microscopy images [82–84]. After that, we have used MD calculations to model the surface structure of polyamide [85] and polyimide [86] alignment film on graphite as a very primitive model interface. There, we were able to analyze the liquid crystal molecular orientation in a triple layer (graphite/polyimide/liquid crystal) structure [86]. The liquid crystal was 4-*n*-octyl-4′-cyanobiphenyl (8CB), and the alignment layer was a trimer with the pyromelltic dianhydride-*p*-phenylene diamine (PMDA-PPD) repeat unit. Figure 10.36a shows the initial state, and Fig. 10.36b shows the average structure after 300 ps. This simulation shows that 8CB molecules are approximately oriented in the direction of the oligomer chain (±10°) and have a tilt angle of 0° (±0.4°). The estimated adsorption energy was 122 kJ/mol, indicating that the 8CB molecule is strongly adsorbed.

---

[4] The contents of this paper [80] was already presented at the Tenth International Liquid Crystal Conference (1984). However, I know that when I visited the university of Groningen in 1989 as the preprint just before its publication. Thus, I'd stayed the university of Groningen from 1990 to 1991 to study the MD of liquid crystals.

Fig. 10.35 Sectional-view
of the LCD
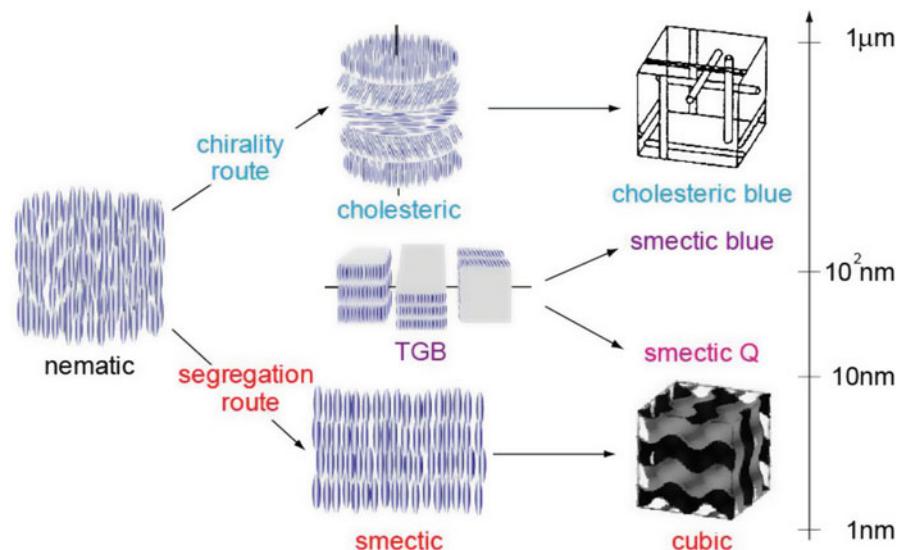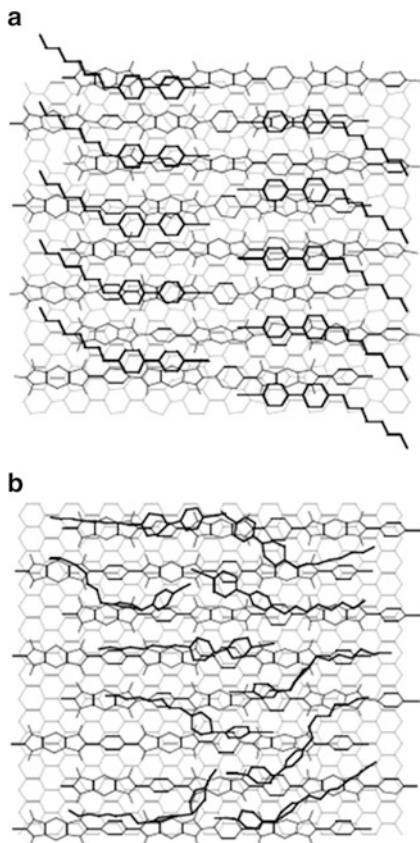
In a similar system, we simulated the effect of the chemical structure of the
polymer and the polymer chain density on the liquid crystal orientation [87]. To see
the effect on the orientation of the polymer structure, we compared the liquid
crystal orientation (out-of-plane tilting and in-plane orientation) on a polyamide
surface that had the same surface density as the above-described PMDA-PPD. Even
though the polyamide is similar to PMDA-PPD, the adsorption energy of the 8CB
molecules is only about 2/3 as high.

Polyimides are of great interest because of their display application and simu-
lations of large film areas have been carried out [88]. Furthermore, analysis of
different combination of surface molecules and liquid crystal molecules has been
carried out [89–92].

10.5.3.2 Nanostructured Liquid Crystalline Phase
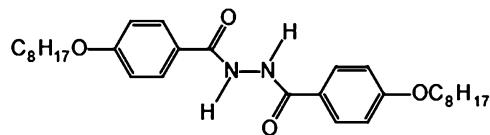
Nanostructured liquid crystalline phases, as shown on the right side of Fig. 10.37,
have a three-dimensional self-assembled structure. If the structure is in the range of
the optical wavelength, new applications in the field of photonic crystals [93] and
others can be envisioned. One route for obtaining a higher-order structure from the
nematic phase liquid crystal phase as the starting point is introducing chirality in the
molecule that will add a helical structure. Another route, segregation, will add a
layered structure, as shown in Fig. 10.37. Adding further higher structure to the
cholesteric phase will lead to the cholesteric blue phase [94]. On the other hand,

Fig. 10.36 Simulated 8CB molecules on the PMDA-PPD monolayer: (**a**) initial structure, (**b**) averaged structure
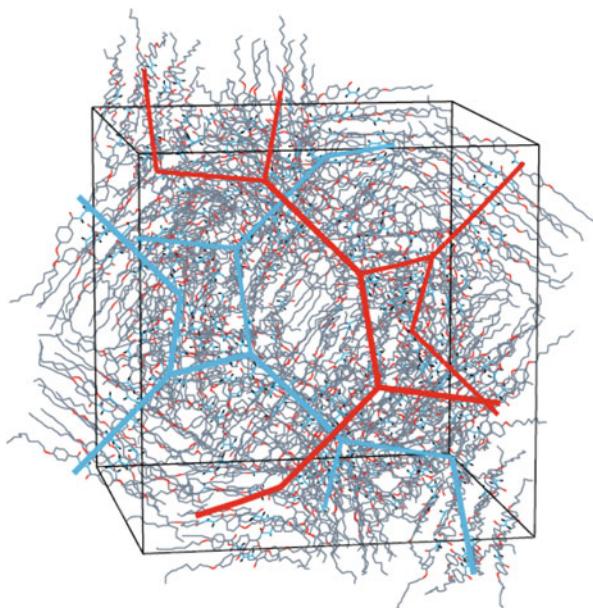
Fig. 10.37 Routes for the nanostructured liquid crystal phases

Fig. 10.38 Chemical
structure of BABH8
molecule
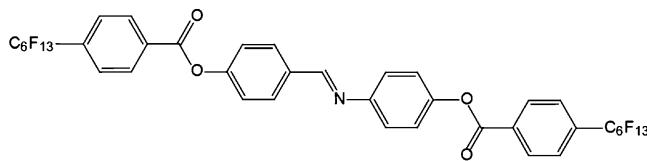
Fig. 10.39 Cubic phase
structure model for the
BABH8 molecular phase

adding a density fluctuation based on micro-phase separation will lead to a cubic
phase [95].

A realistic target for molecular simulation of the nanostructured liquid crystal
phases shown in Fig. 10.37 are the smectic Q (SmQ) and the cubic (Cub) phases. It
is virtually impossible to reveal the molecular level structure of these two phases
from experimental X-ray diffraction data, and thus we tried a molecular simulation
approach [96].

First, we used the simplest molecule that forms a cubic phase, BABH8 (see
Fig. 10.38 for the chemical structure) [97, 98]. We found that locally oriented
aggregates of molecular bundles exist. If the orientation distribution of the bundles
is along a two- or fourfold symmetry axis that can result in optically isotropic phase
at the global level while maintaining the local orientational order. The cubic phase
of BABH8 belongs to the Ia3d (double gyroid) and a rod-network model can be
proposed with twofold symmetry in which the molecular bundles are oriented along
a total of 24 rods that are orthogonal at their network points. Figure 10.39 shows this
model in which the bold lines are the rod-network.

Fig. 10.40 Chemical structure of PFMI6 molecule

The thermodynamic stability of the model was evaluated by MD simulations that use a three-dimensional periodic boundary condition. As a result, we found that the optical isotropy and the characteristic (211) reflection of the Ia3d space group of the model were maintained even after 60 ns. Thus we concluded that the above model is at least a promising candidate for Cub phase nanostructure of BABH8.

Based on those results we reasoned that a strong intramolecular phase separation is the origin of the Cub phase, and we tried the MD simulation of a liquid crystal with perfluorinated alkyl chains at both ends of a rodlike molecule, PFMI6 (the molecular structure is shown in Fig. 10.40) [108, 109]. We simulated a system composed of 256 PFMI6 molecules at two temperatures, in the smectic C (SmC) phase at 530 K, and in the cubic phase at 570 K.

Figure 10.41 shows snapshots after 60 ns. The results at 530 K show a clear SmC-like layered structure, while the 570 K structure is optically isotropic, but contains oriented clusters (which is difficult to see in Fig. 10.41). There are quite a number of experimental results, like small-angle scattering data, measurements of optical isotropy, and molecular diffusion that confirm the spontaneous structure that we had obtained with MD simulations was the Cub phase. These characteristics also correspond well to the Cub phase nanostructure model of Fig. 10.39, which suggests a three-dimensional arrangement of ordered clusters.
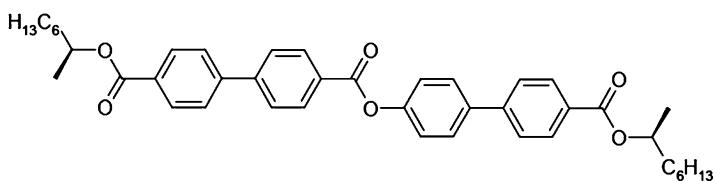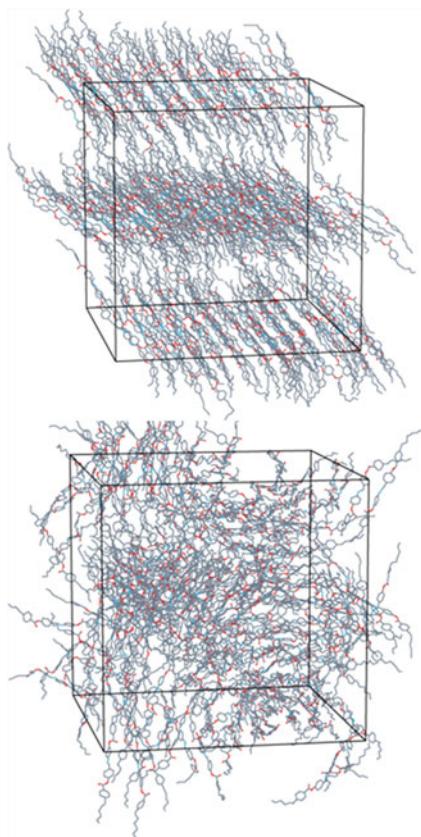
Also the above-described SmQ phase was object of molecular simulation studies by using the molecule shown in Fig. 10.42 [99]. Figure 10.43 shows the structure of the SmQ phase, which is also known as the $T*1$ phase. This structure is based on a model according to Levelut et al. (Fig. 10.40 in [100]), in which the local liquid crystal molecular alignment direction is tilted in respect to the layers of smectic blocks. In the case of a 45° tilt, this leads to a cubic phase with a threefold symmetry.

These research results on nanostructured liquid crystal phase structures strengthen my confidence that molecular simulation can advance the research on liquid crystal phases with a complex structure.

10.5.3.3   Chiral Liquid Crystal Molecular Motor

A report has shown that an interesting evidence of non-equilibrium dynamics that depends on the molecular chirality of the liquid crystal exists: a chiral liquid crystal molecular motor [101]. There is a water-permeation-driven motor that exists in a monolayer of a chiral liquid crystal, in which the molecules rotate around the

Fig. 10.41 Snapshots of
the MD simulations of the
PFMI6 system at 530 K
(*upper*) and 570 K (*lower*)
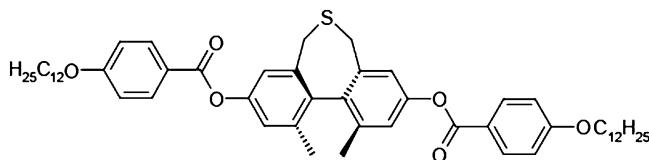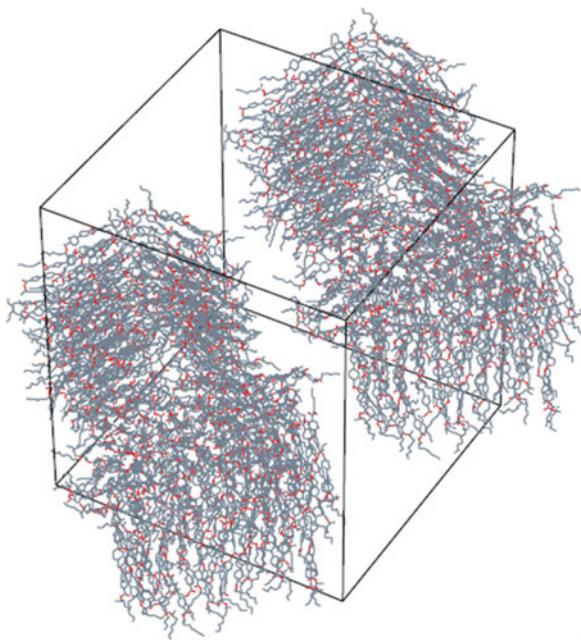
Fig. 10.42 Chemical structure of (*s,s*)-M7BBM7 molecule

so-called C director of the liquid crystal [102]. We examined the microscopic
mechanism of this phenomenon with the picture of a "chiral liquid crystal motor
molecule" in mind by MD simulation [103].

According to Solladie et al. [104], an axially asymmetric molecule with a
bridged biphenyl backbone (12BBT, Fig. 10.44) shows SmC* and N* phases.

The simulation was carried out by modeling a monolayer containing 200 mole-
cules of the (R) or (S) enantiomer in a noble gas at 350 K, a temperature of the bulk

Fig. 10.43 *T**1phase
structure model for the
M7BBM7 molecular phase
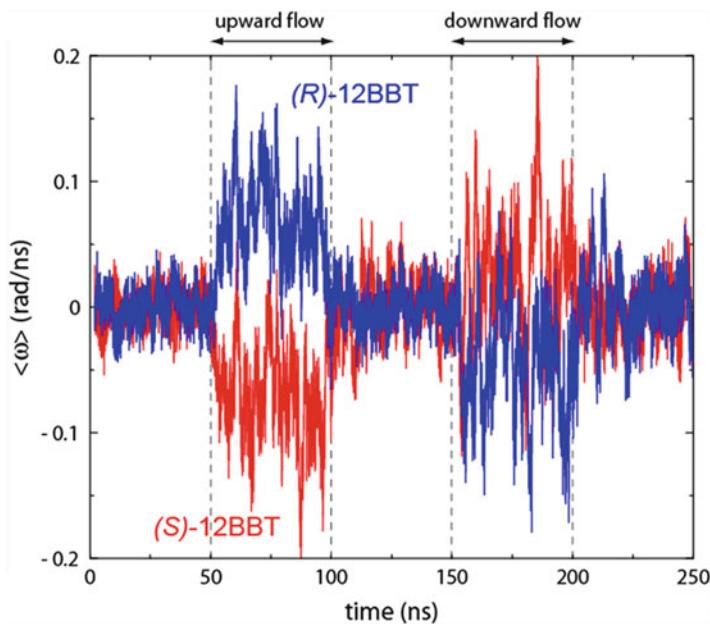
Fig. 10.44 Chemical structure of (*s*)-12BBT molecule
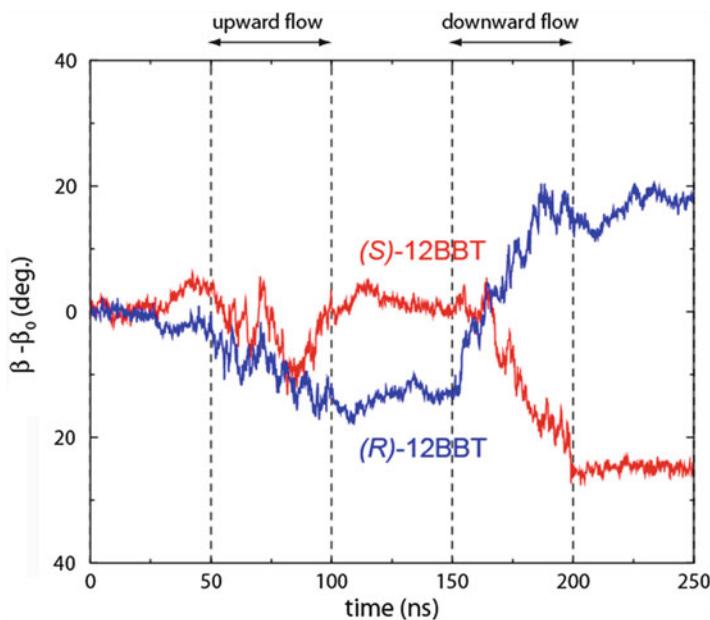
SmC* phase. Figure 10.45 shows the time variation of the average angular velocity of the rotation around the long axis of the smectic molecules the case of using argon as transmembrane species.

Only in two time-windows in the figure, the argon atoms exert an external force in the film normal direction and thereby permeate the monolayer in opposite directions. At those two time-windows, the baseline of the average angular velocity is biased from 0, and thus the rotation in the predominant direction depends of the twisting sense of the molecules (*R* or *S* enantiomers). That is, the rotation around the long axis of the axially asymmetric molecules is generated that biases in the direction depend uniquely on the twisting sense of the molecules and the transmission direction of the monolayer permeable molecule.

Next, behaviors of the C director azimuthal rotations, which correspond to the precession rotation observed experimentally using polarizing optical microscopy [101], are shown in Fig. 10.46. The rotational directions under the trans-monolayer

Fig. 10.45 Time evolutions of the averaged angular velocities around the molecular long axis of the 12BBT molecules

Fig. 10.46 Time evolutions of the C director azimuthal-angles of the 12BBT molecules

gas flow were opposite for the (R)- and (S)-12BBT and also their dependency on the directions of the gas flow (except for (S)-12BBT during the time period 50–80 ns where the direction was rather opposite to which we expected). We found that the periods of the rotation are 10^7 times different between the experiments (ca. 10 s) and the simulated one in Fig. 10.46 (10^{-6} s). However, this difference could be explained as the *trans*-monolayer gas rate was 10^6 times larger than the experimental condition.

As described above, the results of simulations using axially asymmetric molecular systems support the "chiral liquid crystal molecules propeller" picture in which the *trans*-monolayer diffusion driven by molecular rotation around the molecular long axis relates to the C director azimuthal rotation. Experimental measurements of nanosecond rotational dynamics on the molecular level are difficult, and the obtained knowledge also is limited. Molecular simulation can be an effective means to explore the molecular level dynamics of the liquid crystals.

10.5.4 Summary

In this chapter, I'd like to share my personal experience in the two areas of liquid crystal simulation: continuum simulation and molecular simulation. I showed one example, research and development of the IPS-mode LCD, for which the continuum simulation of liquid crystals contributed a lot in the latest quarter of a century. In contrast, the molecular simulation did not aid much in the material development in the same period. In this sense, the contribution of these two simulation approaches have to be evaluated differently from the viewpoint described in the introduction of this paper. Existence of a greatly differing perspective on the contributions of simulations for liquid crystal science itself shows that this field is still developing.

It is always a possibility that the future will bring about new liquid crystal materials and display types or liquid crystal applications that break the limits of the current systems, and I would be glad if the simulations could be used to achieve those goals. I hope that this chapter will increase the interest in simulations of liquid crystals in the reader.

References

1. M. Warner, E.M. Terentjev, *Liquid Crystals Elastomers (Revised Edition)* (Clarendon, London, 2007)
2. K. Urayama, Macromolecules **40**, 2277–2288 (2007)
3. J. Kupfer, H. Finkelmann, Macromol. Chem. Phys. **195**, 1353–1367 (1994)
4. H. Wermter, H. Finkelmann, e-Polym. 013 (2001)
5. P.G. de Gennes, C. R. Acad. Sci. Ser. B. **281**, 101 (1975)
6. P.G. de Gennes, Phys. Lett. A. **28**, 765 (1969)
7. K. Urayama, Y.O. Arai, T. Takigawa, Macromolecules **38**, 3469–3474 (2005)
8. J. Kupfer, H. Finkelmann, Makromol. Chem. Rapid. Commun. **12**, 717–726 (1991)
9. C.H. Legge, F.J. Davis, G.R. Mitchell, J Phys. II. **1**, 1253–1261 (1991)
10. T. Tanaka, Sci. Am. **244**, 124 (1981)
11. K. Urayama, Y. Okuno, T. Kawamura, S. Kohjiya, Macromolecules **35**, 4567–4569 (2002)
12. K. Urayama, Y. Okuno, T. Nakao, S. Kohjiya, J. Chem. Phys. **118**, 2903–2910 (2003)
13. A. Matsuyama, T. Kato, J. Chem. Phys. **114**, 3817–3822 (2001). K. Urayama, Macromolecules 40, 2277–2288 (2007)
14. M. Warner, X.J. Wang, Macromolecules **25**, 445–449 (1992)
15. K. Urayama, Y. Okuno, S. Kohjiya, Macromolecules **36**, 6229–6234 (2003)
16. K. Urayama, R. Mashita, I. Kobayashi, T. Takigawa, J. Chem. Phys. **127**, 144908 (2007)
17. K. Urayama, Y.O. Arai, T. Takigawa, Macromolecules **38**, 5721–5728 (2005)
18. K. Urayama, R. Mashita, Y.O. Arai, T. Takigawa, Macromolecules **39**, 8511–8516 (2006)
19. Y. Sawa, K. Urayama, T. Takigawa, A. DeSimone, L. Teresi, Macromolecules **43**, 4362–4369 (2010)
20. C.D. Hasson, F.J. Davis, G.R. Mitchell, Chem. Commun. 2515–2516 (1998)
21. S. Courty, A.R. Tajbakhsh, E.M. Terentjev, Phys. Rev. Lett. **91**, 085503 (2003)
22. Y. Sawa, F.F. Ye, K. Urayama, T. Takigawa, V. Gimenez-Pinto, R.L.B. Selinger, J.V. Selinger, Proc. Natl. Acad. Sci. U. S. A. **108**, 6364–6368 (2011)
23. R. Ghafouri, R. Bruinsma, Phys. Rev. Lett. **94**, 138101 (2005)
24. R. Oda, I. Huc, M. Schmutz, S.J. Candau, F.C. MacKintosh, Nature **399**, 566–569 (1999)
25. Y. Forterre, J. Dumais, Science **333**, 1715–1716 (2011)
26. L. Golubovic, T.C. Lubensky, Phys. Rev. Lett. **63**, 1082–1085 (1989)
27. P. Bladon, E.M. Terentjev, M. Warner, J Phys. II. **4**, 75–91 (1994)
28. J. Schatzle, W. Kaufhold, H. Finkelmann, Makromol. Chem. **190**, 3269–3284 (1989)
29. N. Uchida, Phys. Rev. E. **62**, 5119–5136 (2000)
30. K. Urayama, S. Honda, T. Takigawa, Phys. Rev. E. **74**, 041709 (2006)
31. K. Urayama, E. Kohmon, M. Kojima, T. Takigawa, Macromolecules **42**, 4084–4089 (2009)
32. R. Zentel, Liq. Cryst. **1**, 589–592 (1986)
33. R. Kishi, Y. Suzuki, H. Ichijo, O. Hirasa, Chem. Lett. 2257–2260 (1994)
34. K. Urayama, S. Honda, T. Takigawa, Macromolecules **38**, 3574–3576 (2005)
35. K. Urayama, S. Honda, T. Takigawa, Macromolecules **39**, 1943–1949 (2006)
36. K. Urayama, Adv. Polym. Sci. **250**, 119–146 (2012)
37. W. Lehmann, H. Skupin, C. Tolksdorf, E. Gebhard, R. Zentel, P. Kruger, M. Losche, F. Kremer, Nature **410**, 447–450 (2001)
38. C.M. Spillmann, B.R. Ratna, J. Naciri, Appl. Phys. Lett. **90**, 021911 (2007)
39. T. Okamoto, K. Urayama, T. Takigawa, Soft. Matt. **7**, 10585–10589 (2011)
40. Y.L. Yu, M. Nakano, T. Ikeda, Nature **425**, 145 (2003)
41. A. Matsuyama, T. Kato, J. Chem. Phys. **105**, 1654 (1996)
42. C. Shen, T. Kyu, J. Chem. Phys. **102**, 556 (1995)
43. A. Matsuyama, in *Encyclopedia of Polymer Blends*, ed. by A.I. Isayev, vol. 1 (Wiley-VCH, Weinheim, 2010) (Chapter 2)
44. A. Matsuyama, T. Kato, Phys. Rev. E. **59**, 763 (1999)
45. A. Matsuyama, R.E. Evans, M.E. Cates, Phys. Rev. E. **61**, 2977 (2000)

46. A.M. Lapena, S.C. Glotzer, S.A. Langer, A.J. Liu, Phys. Rev. E. **60**, R29 (1999)
47. T. Araki, H. Tanaka, Phys. Rev. Lett. **93**, 015702 (2004)
48. J. Fukuda, Phys. Rev. E. **59**, 3275 (1999)
49. S.K. Das, A.D. Ray, J. Chem. Phys. **121**, 9733 (2004)
50. M.P. Letting, K. Kang, P. Holmqvist, A. Imhof, D. Derks, K.G. Dhont, Phys. Rev. E. **73**, 011412 (2006)
51. S. Zhang, S. Kumar, Small **4**, 1270 (2008)
52. A. Matsuyama, J. Chem. Phys. **132**, 214902 (2010)
53. J.A. Ratto, F. Volino, R.B. Blumstein, Macromolecules **24**, 2862 (1991)
54. C. Tschierske, D.J. Photinos, J. Matt. Chem. **20**, 4263 (2010)
55. A. Matsuyama, Liq. Cryst. 38, 729 (2011); 38, 885 (2011)
56. S. Samitsu, Y. Takanishi, J. Yamamoto, Nat. Mater. **10**, 816–820 (2010)
57. R. Yamamoto, A. Onuki, Phys. Rev. Lett. **81**, 41015 (1998)
58. C.P. Royall et al., Nat. Mater. **7**, 556–561 (2008)
59. M. Saito et al., J. Phys. Soc. Jpn. **81**, 023001 (2012)
60. P.G. de Genne, J. Prost, *The Physics of Liquid Crystals*, 2nd edn. (Clarendon, Oxford/New York, 1993)
61. B.J. Berne, R. Pecora, *Dynamic Light Scattering* (Dover publication, New York, 1976)
62. H. Kikuchi et al., Nat. Mater. **1**, 64–68 (2002)
63. Y. Takanishi, G.J. Shin, J.C. Jung, S.W. Choi, K. Ishikawa, J. Watanabe, H. Takezoe, P. Toledano, J. Mater. Chem. **15**, 4020 (2005)
64. Y. Yamazaki, Y. Takanishi, J. Yamamoto, Europhys. Lett. **88**, 56004 (2009)
65. R. Yamamoto, M. Yoneuya, T. Okuzono, J. Fukuda. EKSHO **11**, 259 (2007)
66. C. Oseen, Trans. Faraday Soc. **29**(140), 883–899 (1933)
67. M. Oh-e, K. Kondo, Appl. Phys. Lett. **67**(26), 3895 (1995)
68. M. Yoneya, M. Ohta, M. Oh-e, K. Kondo, Proc. SPIE, No. 3014 40, SanJose (1997)
69. M. Yoneya, K. Kondo, Appl. Phys. Lett. **74**(23), 3478 (1999)
70. D. Berreman, JOSA **62**(4), 502–510 (1972)
71. M. Oh-e, M. Yoneya, M. Ohta, K. Kondo, Liq. Cryst. **22**(4), 391 (1997)
72. S.H. Lee, S.L. Lee, H.Y. Kim, Proc. Asia Display 371 (1998)
73. S.H. Lee, S.L. Lee, H.Y. Kim, Appl. Phys. Lett. **73**(20), 2881 (1998)
74. K. Ono, I. Mori, M. Ishii, Y. Ooishi, T. Furuhashi, SID2006 Digest, San Francisco 1954 (2006)
75. D. Kajita, I. Hiyama, Y. Utsumi, M. Ishii, K. Ono, J. Elec. Imag. **17**, 013019 (2008)
76. C. Lee, H. Yoon, S. Yoon, S. Yoon, M. Jung, D. Kim, T. Won, SID2005 Digest, Boston 982 (2005)
77. J.E. Vieillard-Baron, J. Chem. Phys. **56**, 4729 (1972)
78. B.J. Berne, P. Pechukas, J. Chem. Phys. **56**, 4213 (1972)
79. J.G. Gay, B.J. Berne, J. Chem. Phys. **74**, 3316 (1981)
80. S.J. Picken, W.F. van Gunsteren, P.T. van Duijnen, W.H. de Jeu, Liq. Cryst. **6**, 357 (1989)
81. M. Wilson, Chem. Soc. Rev. **36**(12), 1881–1888 (2007)
82. M. Hara, Y. Iwakabe, K. Tochigi, H. Sasabe, A.F. Garito, A. Yamada, Nature **344**, 228 (1990)
83. D.J. Cleaver, D.J. Tildesley, Mol. Phys. **81**(4), 781 (1994)
84. M. Yoneya, Y. Iwakabe, Liq. Cryst. **18**(1), 45 (1995)
85. M. Yoneya, Y. Iwakabe, Langmuir **11**(9), 3516 (1995)
86. M. Yoneya, Y. Iwakabe, Liq. Cryst. **21**(3), 347 (1996)
87. M. Yoneya, Y. Iwakabe, Liq. Cryst. **21**(6), 817 (1996)
88. M. Uehara, H. Kuwajima, S. Toyoda, K. Tanabe, EKISHO **2**, 36 (1998)
89. D.R. Binger, S. Hanna, Liq. Cryst. **28**, 1215 (2001)
90. N.F.A. van der Vegt, F. Müller-Plathe, A. Geleßus, D. Johannsmann, J. Chem. Phys. **115**, 9935 (2001)
91. M.B. Hamaneh, P.L. Talor, Phys. Rev. E. **77**, 021707 (2008)
92. M. Li, H. Lai, B. Chen, X. Liu, Y. Gu, Liq. Cryst. **37**(2), 149–158 (2010)

93. W. Cao, A. Munoz, P. Palffy-Muhoray, B. Taheri, Nat. Mat. **2**, 111 (2002)
94. E. Dubois-Violette, B. Pansu, Mol. Cryst. Liq. Cryst. **165**, 151 (1988)
95. K. Saito, M. Sorai, EKISHO **5**, 20 (2001)
96. M. Yoneya, EKISHO **7**, 32 (2003)
97. P. Göring, S. Diele, S. Fischer, A. Wiegeleben, G. Pelzl, Liq. Cryst. **25**(4), 467 (1998)
98. M. Yoneya, E. Nishikawa, H. Yokoyama, J. Chem. Phys. **120**, 3699 (2004)
99. M. Yoneya, T. Yamamoto, I. Nishiyama, H. Yokoyama, J. Phys. Chem. B **112**(29), 8452–8458 (2008)
100. A.-M. Levelut, E. Hallouin, D. Bennemann, G. Heppke, D. Lotzsch, J. Phys. II. Fr. **7**, 981 (1997)
101. Y. Tabe, H. Yokoyama, Nat. Mat. **2**, 806 (2003)
102. Y. Tabe, EKISHO **10**, 277 (2006)
103. M. Yoneya, Y. Tabe, H. Yokoyama, J. Phys. Chem. B **114**(25), 8320–8326 (2010)
104. G. Solladié, P. Hugelé, R. Bartsch, J. Org. Chem. **63**, 3895 (1998)
105. J. Yamamoto, H. Tanaka, Phys. Rev. Lett. **77**, 43100–43103 (1996)
106. M. Ohta, M. Oh-e, K. Kondo, Proc. 15th. Int. Display Res. Conf., Hamamatsu, p. 707 (1995)
107. S.H. Lee, S.L. Lee, H.Y. Kim, T.Y. Eom, SID99 Digest, San-Jose 202 (1999)
108. M.-A. Guillevic, D.W. Bruce, Liq. Cryst. **27**(1), 153 (2000)
109. M. Yoneya, E. Nishikawa, H. Yokoyama, J. Chem. Phys. **121**(15), 7520 (2004)

Chapter 11
Function of Liquid Crystals

**Junichi Hanna, Tomiki Ikeda, Toru Ube, Masanori Ozaki,
Takashi Kato, Masafumi Yoshio, and Atsushi Yoshizawa**

11.1 Liquid Crystalline Organic Semiconductors

Junichi Hanna

11.1.1 Background and Expectations

An organic semiconductor is material that is capable of transporting a charge, that is, electrons and holes. By this characteristic, that is, the property to support a current flow, they can be used in various electronic devices. In the early 1970s, organic semiconductors have been put to their first practical use in the photosensitive drum of copy machines. Thereafter, it began to be used as a practical material for organic

J. Hanna
Tokyo Institute of Technology, Tokyo, Japan
e-mail: hanna@isl.titech.ac.jp

T. Ikeda • T. Ube
Research and Development Initiative, Chuo University, Tokyo, Japan
e-mail: tikeda@tamacc.chuo-u.ac.jp; ube@tamacc.chuo-u.ac.jp

M. Ozaki
Graduate School of Engineering, Osaka University, Osaka, Japan
e-mail: ozaki@eei.eng.osaka-u.ac.jp

T. Kato • M. Yoshio
School of Engineering, The University of Tokyo, Tokyo, Japan
e-mail: kato@chiral.t.u-tokyo.ac.jp; yoshio@chembio.t.u-tokyo.ac.jp

A. Yoshizawa
Graduate School of Science and Technology, Hirosaki University, Hirosaki, Japan
e-mail: ayoshiza@cc.hirosaki-u.ac.jp

electroluminescent (EL) elements in the 1990s. In recent years, research and development has been actively aimed to practical use in organic solar cells and organic transistors.

In many cases, the material is used in the form of amorphous thin films in the organic semiconductor device. The reason is that such devices require large-area thin films that are at the same time morphologically homogeneous. However, amorphous materials cannot reach the mobility as high as that of crystalline materials, which is a measure of the semiconductor materials required of devices. Indeed, compared to crystalline materials, the mobility of amorphous materials is at least one thousand times smaller. Thus, in order to expand device applications of organic semiconductor beyond the state-of-the-art applications in the early 1990s, the development of a liquid crystalline organic semiconductor was envisioned that would increase charge mobility by several orders of magnitude. It needs to be noticed that at that time, the use of polycrystalline thin films of organic semiconductors for organic transistors had not been studied yet.
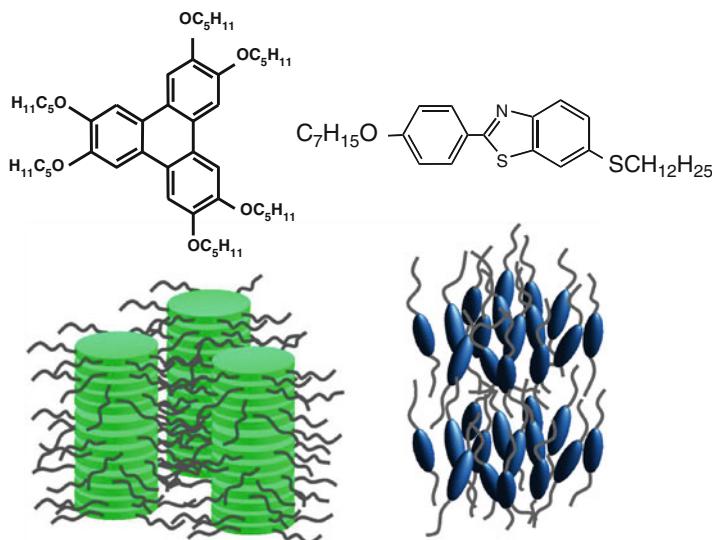
The conduction mechanism in organic semiconductors is hopping of the charge from molecule to molecule. Basically, the mobility depends on the distance between molecules and the distribution width of the density of states involved in charge transfer. Therefore, there is a limit to reducing the average intermolecular distance in amorphous materials to improve mobility. Meanwhile, the mobility in single crystals is high, but in terms of the critical parameter uniformity and large-area applicability, single crystal materials cannot satisfy the essential request of the devices. In polycrystalline materials, the deterioration of the charge transport by grain boundaries becomes a problem.

It is necessary to seek the answer to questions like "What substance can be an innovative materials?" and "What novel organic semiconductor can both have high mobility and be applied to a large area?" At one point, suddenly, I had the answer: "Liquid crystal materials!" Liquid crystals are substances that combine crystal-like molecular orientation with liquid-like fluidity. It is not difficult to imagine the changes that are necessary to a given material to realize new characteristics such as high mobility over a few orders of magnitude, which cannot be achieved by conventional materials and their extension. I imagined that the molecular aggregation of liquid crystals would be the right one to be the changes, and two years later started my research.

At the beginning of this research it was necessary to organize the basic facts of liquid crystalline materials and what to expect from them.

From the viewpoint of the particular energy levels associated with charge transport, molecules having a π- electron conjugated system can be used in principle. Looking at the structural characteristics, liquid crystal molecules can, in principle, facilitate charge transport properties because they consist of a flexible hydrocarbon chain and a rigid aromatic ring portion.

The average intermolecular distance of 0.7–1 nm is about as large as for an amorphous organic semiconductor thin film or a molecular-dispersion polymer-type organic semiconductor. On the other hand, liquid crystal molecules aggregate by self-assembly, and the intermolecular distance is reduced to 0.4–0.6 nm in the
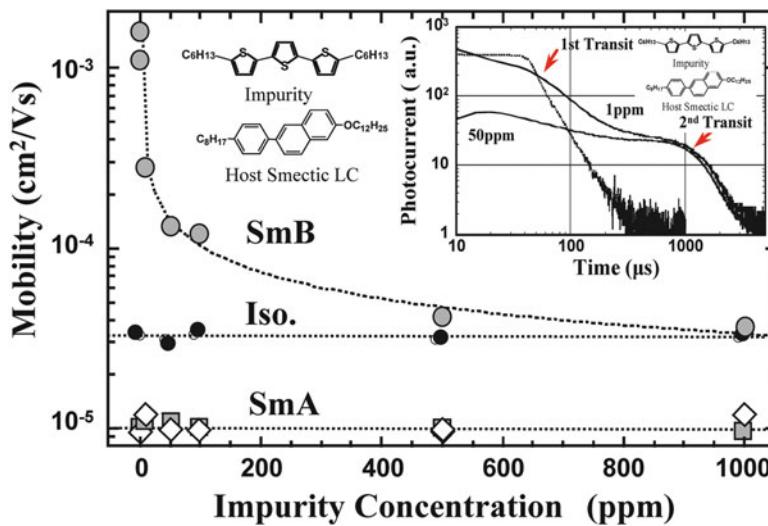
Fig. 11.1 Discotic and calamitic liquid crystals in which the electronic conduction was established firstly, hexapentyloxytriphenylene (H5T: *left*) and 2-(4′-heptyloxyphenyl)-6-dodecylthiobenzothiazole (7O-PBT-S12: *right*)

liquid crystal phase. Therefore, I thought that liquid crystal molecules should show electronic conduction because of a short intermolecular distance in the aggregated state. Furthermore, the liquid crystalline molecules are oriented in the liquid crystalline state that should lead to a high mobility that could not even be reached by amorphous materials, and a fluidity that ensures uniformity over a large area that cannot be achieved by crystalline materials. However, until I started my research in the early 1990s, there was the opinion that liquid crystals were only ionic conductors which were, in fact, backed up by many experimental results.

11.1.2 Discovery of Electron Conduction

The group of Prof. Haarer at Bayreuth University was the first to measure electron conduction in liquid crystal materials. Figure 11.1 shows the chemical structure and the discotic liquid crystal phase of a triphenylene derivative, which is a disk-shaped liquid crystal material. Using the time-of-flight method, they were able to measure the mobility of hexapentyloxytriphenylene (H5T) in 1993 [1]. Around that time, we had begun research with the aim to establish electronic conduction in a rodlike liquid crystal material. Initially, we examined a Schiff-base type of liquid crystal, which is easy to synthesize by time-of-flight measurements. However, the measurement result showed that the conduction is due to ion conduction. Therefore we changed to a more stable phenylbenzothiazole derivative that cannot be hydrolyzed, 2-(4′-heptyloxyphenyl)-6-dodecylthiobenzothiazole (7O-PBT-S12; see Fig. 11.1), and we were able to confirm

Fig. 11.2 Impurity effect of terthiophene (6-TTP-6) on positive charge mobility in smectic and isotropic phases of 2-phenylnaphthalene derivative, 8-PNP-O12. The *inset* shows transient photocurrents for positive carriers in Sm A phase pof non-doped 8-PNP-O12 and doped 8-PNP-O12 with 6-TTP-6 of 1 ppm and 50 ppm

the hole mobility of more than 5×10^{-3} cm^2/Vs in the SmA phase [2, 3]. In addition, 6-(4′-octylphenyl)-2-dodecyloxynaphthalene (8-PNP-O12) showed a conductivity of 2.5×10^{-4} cm^2/Vs in the SmA phase and 1.7×10^{-3} cm^2/Vs in the SmB phase [4]. These results show that the basic idea behind electronic conductivity is not wrong. So we decided to select liquid crystal materials that most likely show electronic conduction to further examine their characteristics. One of them was a dialkylterthiophene derivative, ω,ω′-dihexylterthiophene (6-TTP-6). However, the mobility characteristics pointed towards ionic conductivity. This was probably because the purity of the material used is not sufficient, and the following investigations proved electronic conduction. We used this terthiophene to investigate how a chemical impurity affects the charge transport in a 2-phenylnaphthalene derivative (8-PNP-O12), a liquid crystal that could be sufficiently purified, and then added trace amounts of the terthiophene as a chemical impurity. The experimental data, shown in Fig. 11.2, were very interesting. By adding a mere 1 ppm of the terthiophene, a slow component showed up in the measurement, and electronic conduction completely disappeared after the addition of several tens ppm [5, 6]. This slow component is due to ionic conduction. These results speak for themselves—the nature of conduction in the liquid crystal materials can be made clear.

That is, the actual reason for conduction in liquid crystals, including discotic liquid crystals, is electronic conduction, but ionic conduction due to impurities is

also observed. In addition, we have suggested that neutral impurities can act as trap sites for electrons and holes that contributes to the resistance of the material.

Later, electronic conduction by electrons in a discotic liquid crystal had been observed [7] and this finding was used to establish the electronic conductivity in a low molecular nematic liquid crystal phase [8]. Furthermore, these findings illustrate why until lately electronic conduction had not been found in liquid crystal material and why only ionic conduction in liquid crystals had been supported by the experimental results so far.
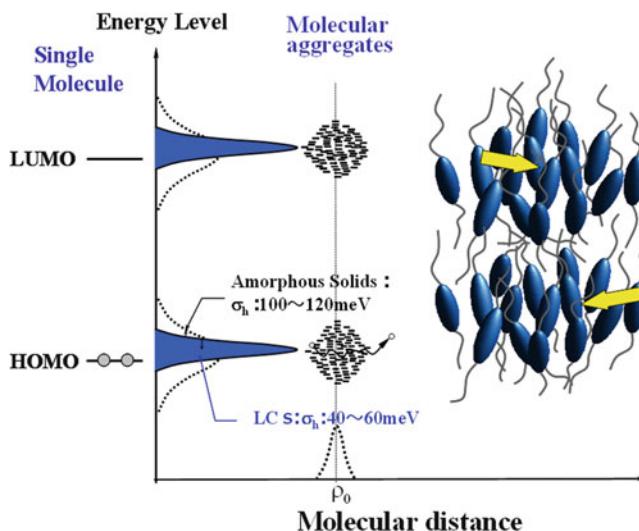
Reviewing the results of these studies on the conduction in the smectic phase, it became clear that conduction is closely related to the microphase-separated structure in the smectic phase. The ionic conduction channel is in the hydrocarbon chain layer that is flexible and liquid-like, so that ions can be transported, and the electronic conduction channel is in the core portion, the π-electron conjugated aromatic layer, resulting in 2-dimensional conduction within smectic layers.

11.1.3 Electronic Mobility and Nature of the Electron Conduction in the Liquid Crystal Phase

It is apparent from the results described above that the sufficient reduction of impurities that have electronic energy levels in the gap between electron and hole conduction levels of the liquid crystal material will hopefully make it possible to measure electron conduction.

The density of states involved in electronic conduction in the smectic liquid crystalline phase should show an energetic distribution, because there are fluctuations similar to the amorphous state that do not occur in crystalline materials. Those fluctuations change the density of energy states involved in charge transport. However, the conduction in the liquid crystal phase is different from conduction in the amorphous state. Basically it is a non-Poole–Frenkel type; in other words, the conduction characteristic mobility does not depend on the strength of the electric field nor on the temperature. Judging from the knowledge so far, the characteristic properties of liquid crystal molecules with a small dipole moment are shown in Fig. 11.3, which shows the distribution in the HOMO and LUMO energy levels that resulted from the reduced order in the liquid crystal phase due to thermal fluctuation [9]. In fact, since the value of the thermal energy is smaller than the distribution width of the conduction level at a very low temperature region, similarly to the conduction in the amorphous material, the mobility will show an electric field and temperature dependence. Our results on the electron conduction in the smectic phase of molecules with a strong dipole moment show a temperature-dependent mobility [10].

Liquid crystals are different from amorphous materials that have a random molecular orientation. Similar to crystalline materials, because liquid crystals have a molecular orientation, it is necessary to clarify the factors that affect the
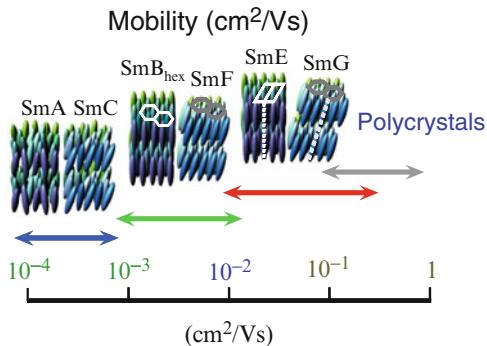
Fig. 11.3 Schematic illustration of the density of states in a liquid crystalline mesophase. A typical distribution width is 40–60 meV, which is a half of those of amorphous organic semiconductors

charge transport. One of them is the effect of anisotropic molecular orientation on charge transport. As already mentioned, in the case of smectic phases, reflecting the anisotropy of the molecular shape, interlayer conduction is significantly suppressed compared to the conduction within the two-dimensional smectic layer.

Similarly, columnar phase discotic liquid crystals show a one-dimensional conductivity along the liquid crystal column. However, unlike a uniform amorphous material, materials having a molecular orientation form different interfaces due to the difference in molecular orientation. For example, in a polydomain texture, it is necessary to look at the effect of the interface between the domains, which is similar to grain boundaries of polycrystalline materials. In general, smectic molecules align parallel to the substrate surface in a liquid crystal cell, even without applying an alignment layer. Generally, the domain size of smectic liquid crystals is in the range of tens of micrometers, which is even larger than the cell thickness, so that there are no domain boundaries in the thickness direction. Thus, the electronic conduction is the same as in a monodomain, and domain boundaries have no or almost no effect on the charge transport [11–13]. The problem that is unique to liquid crystals is that the type of liquid crystal has an effect on the charge transport. As is well known, various smectic phases exist that show different molecular orientation. When a liquid crystal material is used as an organic semiconductor, the relation between molecular design and charge transport properties becomes important. Since electronic conduction in a liquid crystal material is basically a hopping conduction, the charge transfer rate between molecules can be expressed as in Eq. (11.1). The charge transfer rate between two molecular sites i and j is v_{ij}, which depends on the distance between i and j, r_{ij}, and the difference of the energy

Fig. 11.4 Typical mobility in various smectic mesophases

levels ε_i and ε_j. Here, v_0 is a constant, T is the absolute temperature, and α is a constant which is a measure of the spatial extent of the wave function:

$$v_{ij} = v_0 \exp\left(-2\frac{r_{ij}}{\alpha}\right)\exp\left(-\frac{\varepsilon_j - \varepsilon_i}{kT}\right) \tag{11.1}$$

In smectic phases, the orderliness in the smectic layer improves with the ordering of the molecular orientation. The intermolecular distance within the smectic layer is reduced to about 0.4 nm from about 0.6 nm for amorphous materials. Therefore, as is apparent from Eq. (11.1), mobility improves essentially in accordance with the ordering of the molecular orientation in smectic phase. For liquid crystal material having a similar molecular structure, the mobility in the smectic A and C phases is in the order of 10^{-4} cm^2/Vs, as shown in Fig. 11.4. It can be improved by one order of magnitude to 10^{-3} cm^2/Vs in smectic B$_{hex}$ and F phases. When it comes to phases that show a high molecular orientational order, such as smectic E and G phases, mobility improves further to 10^{-2} cm^2/Vs. Mobility reflects differences in the structure of the core, but it is within roughly one order of magnitude, if it is. In general, substances with a large core structure and a less dipole moment show high mobility.

On the other hand, discotic liquid crystal material exhibits a column phase regardless of the difference in molecular orientation order. The intermolecular distance in the columns is generally about 0.35 nm, and the actual differences in observed mobility of over three orders of magnitude (ranging from 10^{-4} to 10^{-1} cm^2/Vs) cannot be explained by differences in the intermolecular distance in the columnar phase [10]. There is not enough empirical evidence about this problem, but perhaps orientational fluctuations of the molecules in the column could be the dominant factor.

The highest bulk mobility of liquid crystal materials reported so far are 0.3 cm^2/Vs [14], for both hole and electron conduction in calamitic liquid crystals, and 0.3 cm^2/Vs for electron conduction and 0.2 cm^2/Vs [15] for hole conduction in discotic liquid crystals. These values are comparable to the mobility in polycrystalline thin films of organic semiconductor materials.

11.1.4 Device Application
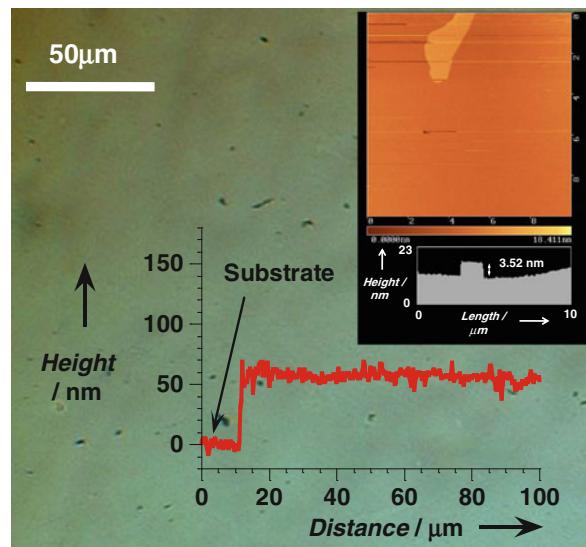
As described above, liquid crystals show not only a high mobility of over 0.1 cm^2/Vs but also the unique characteristic that the mobility is independent of the electric field and temperature. Those charge transport characteristics make liquid crystals excellent materials for large-area applications by using the polydomain texture. High-quality organic semiconductors that combine the advantages of crystalline and amorphous materials can now be achieved. A liquid crystal organic semiconductor can be used as thins films either in the crystal state or in the liquid crystal state, depending on the temperature range of the device. Therefore, the same material cannot be used in both the crystalline and the liquid crystalline state. Still, material design allows to adjust the phase transition temperatures and thus can tailor the phases in which the material is to be used.

Liquid crystal semiconductors are not limited to a specific device, and a wide variety of applications have been proposed, including organic electroluminescent (EL) devices, organic transistors, organic solar cells, optical sensors, or as an electrophotographic photosensitive material. There is a large interest for polarized emission [16] due to molecular orientation and low electric field driving that takes advantage of the large mobility in the organic EL element, but so far prototypes have not been reported. Meanwhile, the application closest to a practical break-through is the transistor (organic field-effect transistor (OFET)) that relies on the large charge mobility in liquid crystals. Both a liquid crystal [17] and a polycrystalline thin film [18] can act as the active layer of the transistor. Typically, charge mobility of liquid crystals is around 10–50 % of that of crystalline materials. When focusing only on the mobility values, crystalline thin films are advantageous, but in addition concern about the uniformity of the thin films and the ease of processing play a role for suppressing variations in the device characteristics for a large number of transistors. Here, liquid crystals clearly have the advantage over thin crystalline films.

Also from a processing point of view, liquid crystal materials show additional advantages. In many cases they are readily soluble in an organic solvent and can be applied by a wet process, such as ink-jet printing or coating. Not only this but also the preparation of a crystalline film can be achieved by going through a liquid crystal phase. Figure 11.5 shows the polarizing microscope image of a 50 nm thick polycrystalline thin film of 8-TTP-8, which is a liquid crystalline terthiophene derivative. The film was produced by spin coating at the liquid phase temperature. In addition, a confocal laser microscope image and an AFM surface profile are shown. The figure shows the formation of a very homogeneous film in which the only heterogeneity are the islands with a height of a single molecular step of 8-TTP-8 [19].
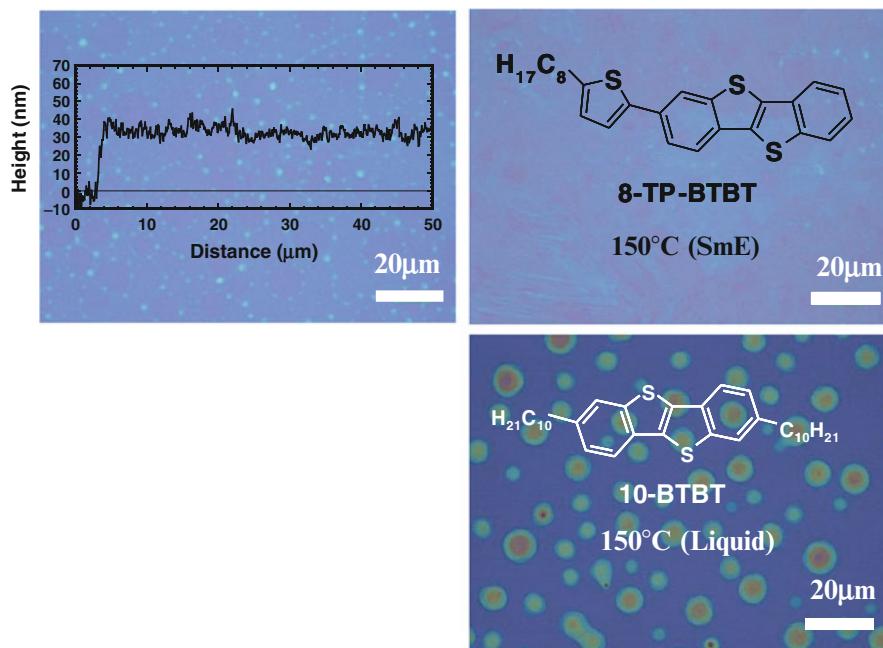
Currently, the core development of organic FET materials for the production of polycrystalline thin films by a solution process goes towards materials that are soluble in organic solvents. The approach we developed for such soluble materials is the chemical modification of widely used fused aromatic ring molecules that show high mobility by long-chain hydrocarbons. However, there is a trade-off

Typical film texture of polycrystalline thin films of a liquid crystalline terthiophene derivative, 8-TTP-8, observed by polarized optical microscope, atomic force microscope, and confocal laser microscope

between the crystallization temperature and solubility of the material causing a significant decrease in crystallinity by chemical modification. For example, pentacene is often used as a model material for FETs, and its melting point is lowered from over 300 °C to 50 °C by chemical modification with alkyl chains. FETs that were prepared by a solution process showed a high FET mobility of more than 1 cm^2/Vs [20]. Also dialkylbenzothienothiophene (BTBT) is an interesting compound and its crystallization temperature can be decreased from 216 °C to about 100 °C for some derivatives [21]. On the other hand, FETs made of such materials cannot withstand heat treatments required for passivation and wiring. For this problem, liquid crystal materials can give the essential solution. That is, in the temperature region above the crystal phase, there exists a highly ordered smectic phase, such as the smectic E or smectic G phase, and when the thin film is heated above the crystallization temperature, thin-film morphology is maintained and thus substantially improves the heat resistance of the material.

Figure 11.6 shows a liquid crystalline BTBT derivative (2-(4′-Octylphenyl) [1] benzothieno [3, 2-b] benzothiophene (8-Tp-BTBT) that has been designed to express the smectic E phase [22]. Upon cooling from the isotropic melt, it shows a smectic A phase from 198 to 180 °C and a smectic E phase until the crystal phase is reached at 102 °C. Meanwhile, the heating process shows a smectic E phase from 131 to 180 °C and a smectic A phase until 197 °C. By spin coating a solution of this compound at 110 °C in the smectic E phase, it is possible to obtain a uniform polycrystalline thin film, which is stable even after a 5-min heat treatment at 150 °C. The heat resistance is greatly improved as compared to the dialkyl derivatives. From Fig. 11.6 it can be seen that the FET mobility exceeds 1 cm^2/Vs and even though the mobility decreases, the FET characteristic is retained after heat treatment. On the other hand, heating of dialkyl BTBT derivatives to a temperature of 100 °C makes them lose their FET

Fig. 11.6 Texture and surface profile of polycrystalline thin film of 8-Tp-BTBT (30 nm) observed by optical microscope and confocal laser microscope (*upper left*), and microscope textures of the films of 8-Tp-BTBT (*upper right*) and 10-BTBT-10 (*bottom right*) after heating at 150 °C for 5 min

characteristics. These results show that liquid crystal materials, because they are suitable for semiconductor processes, can be applied to organic FETs and yield excellent characteristics as compared to nonliquid crystal materials [23].

Another interesting device application is the organic solar cell. Heterojunction solar cells, followed by the bulk heterojunction (BHJ) solar cell, used to have a very low conversion efficiency of less than 0.1 %, and in previous studies, organic solar cells were left out. However, in the 1990s, once a conversion efficiency of a few percent was reported for BHJ organic solar cells, their research and development was actively carried out [24]. BHJ solar cell are prepared by mixing a hole conducting (p-type, or donor-type) and an electron conducting (n-type, or acceptor-type) organic semiconductor in a certain ratio. The phase-separated film structure shows a large p-n junction interface area and thus an efficient photo-charge generation which is intended to achieve a highly efficient solar cell. It is well known that the orientation of liquid crystal molecules can be controlled at interfaces and that, depending on the properties of the interface, can be aligned either horizontally or vertically. In that way the vertical alignment required for FET applications as well as the horizontal alignment film required for organic EL devices and solar cells can much more easily be achieved in a liquid crystal material than in a nonliquid crystal material. Furthermore, liquid crystal molecules consist of aligned molecular aggregates by self-organization which can help

to improve the formation of a phase-separated structure necessary for BHJ solar cells. Perylenediimide derivatives and hexabenzocoronene are used as n-type and p-type organic semiconductors, respectively. It has been reported that those mixed systems of rodlike and disk-like molecules lead to effective phase separation by self-organizing [25]. Recently, a liquid crystalline phthalocyanine derivative, which shows strong absorption in the visible light region, 1,4,8,11,15,18,22,25-octahexylphthalocyanine (C6PcH2), has been used as a p-type material and was combined with a C60 derivative, [6, 6]-phenyl C61 butyric acid methyl ester (PC61BM), to give a conversion efficiency of 3.1 % [26]. Furthermore, changes in molecular orientation of the rodlike liquid crystal 1,4-diketo-N,N′-dimethyl-3,6-bis(4-dodecyloxyphenyl)pyrrolo[3,4-c]pyrrole (DmPP-O12) in a mixture with PC61BM by heating to 60 °C for 30 min increased the efficiency of a BHJ cell from 0.01 to 1.1 % [27]. These are examples in which the control of molecular orientation by the liquid crystal material was used efficiently to improve device characteristics. The conversion efficiency still leaves some room for improvement, but they are good examples for the potential expansion into solar cell applications of liquid crystal materials. I am confident that future research progress will be enjoyed.

11.1.5 Outlook

Electron conduction in liquid crystal materials has been discovered about 20 years ago. During this time, as described in this article, the nature of organic semiconductor in calamitic and discotic liquid crystals has been clarified and molecular design was effectively used to achieve high mobility. However, devices that use organic semiconductors are still in their infancy. Given their high potential, the high quality of the material properties is a major premise for future applications. One specific property is the control of molecular orientation in liquid crystals that is useful for the preparation of high-quality polycrystalline thin films. The liquid crystal state of the material is essential for the control of the crystal grain boundaries in those films [28]. At present, however, even after 20 years have passed, only a few research groups focus on the research on applications for organic semiconductor liquid crystal materials. One of the reasons may be that the evolving nature and importance of liquid crystal organic semiconductor materials have not been widely recognized yet. The often heard comments that "liquid crystals are display materials," "liquid crystals are liquids," "the molecular orientation changes in an electric field," and "liquid crystals are ionic conductors" are largely due to the misunderstanding that the nematic liquid crystals are the archetype. This misconception seems to delay and even limit new developments of liquid crystal materials.

Judging from the current state of research, the organic FET is the closest practical application for organic semiconductor devices. The expansion and promotion of research is necessary for the development of a new liquid crystal industry.

11.2   Photomobile Polymer Materials: From Nano to Macro

Tomiki Ikeda and Toru Ube

11.2.1   Introduction
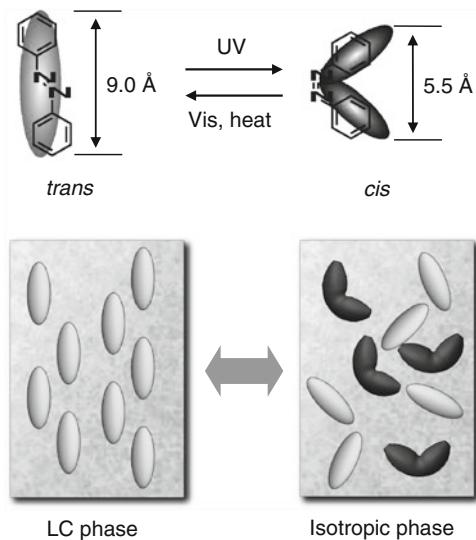
Fossil fuel is finite. We are using mainly fossil fuel as our energy source, but the development of alternative energy sources is a pressing issue for humanity. Studies that aim to produce a stable energy source by effectively using "renewable energy" have actively been conducted since the Fukushima nuclear accident.

It is reasonable to consider the photoelectric conversion of sunlight into electricity, because the base of our modern society is electronics. However, tools such as motors and gears are required to convert electric energy into mechanical work. On the other hand, by using materials that themselves absorb sunlight and convert it directly into work, it should be possible to build a new system of conversion devices that make gears or motors unnecessary. Such devices would also be advantageous for non-contact and remote operations. Polymers are lightweight, are easily processable and cheap, and thus are prime candidates for such a conversion material. The easy molding of polymers allows for the creation of arbitrary shapes from the nano- to the meter size. By controlling the optical alignment of the liquid crystals, polymeric photomechanical materials can be used to directly transform light energy into work. In this section we will describe how to control light-induced motion in all three dimensions at will.

11.2.2   Learning from Visual Phototransduction

Rhodopsin, a membrane protein in the photoreceptor cells of vertebrates, plays an important role in the initial process of light sensing in the retina [29]. It consists of a photosensitive dye and seven units of a helical retinal protein called opsin, and it is located in the cell membrane. Retinal, in its dark-state bent 11-cis conformation, is bound to the central space that is formed by the seven opsin helices. After light absorption it immediately isomerizes to the rod-shaped all-trans form. Because it is housed tightly in the central pocket of the opsins, the conformational change significantly affects the rhodopsin structure. This structural change activates G proteins that are present in the cell, and a second messenger cascade is induced. Thus, in the cell, the structural change of one molecule (cis-trans isomerization of retinal) by a single photon is causing the conformational change of the macromolecule opsin. A single photon has only enough energy to induce a molecular shape

Fig. 11.7 Photoinduced
isomerization and phase
transition of azobenzene

change in a small molecule, but through the combination with a macromolecule, it
can induce a significant shape change. Structural changes of the opsin may start
subsequent processes that induce a large change in the whole cell. This domino
effect amplifies a small trigger (the photon) into a large change that influences the
entire cell. In the end, the photon trigger is converted to a change in membrane
potential of the cell. Because of this built-in amplification, vision is extremely
sensitive.

   To convert the change of a molecule on the nanoscale to the macroscopic scale is
difficult in general. However, in the above-described retinal system in cells, such a
change on the nanoscale causes amplified structural changes.

11.2.3   Photoinduced Phase Transition of Liquid Crystals

Liquid crystals show cooperative phenomena. When the alignment of liquid crystal
molecules (mesogens) is varied by an external field in a portion of the molecules,
the alignment change spreads to the entire system and the orientation of the entire
system can be changed. Photochromic molecules change their molecular shape by
photon absorption similar to the visual retinal system. Azobenzene is a well-known
photochromic molecule in which the trans-cis isomerization is caused by ultraviolet
light irradiation and the reverse reaction by heat or visible light (Fig. 11.7).
When irradiated with ultraviolet light, trans-cis isomerization takes place and a
small amount of cis molecules are dispersed in the liquid crystalline trans-
azobenzene (Fig. 11.7), which leads to a lowering of the phase transition temper-
ature [30, 31]. Trans-azobenzene is a rod-shaped molecule that structurally matches

very well to calamitic liquid crystal molecules and thus liquid crystal phase is stabilized due to the interactions between trans-isomer molecules. On the other hand, molecules with a bent shape, such as cis-azobenzene, interact less with liquid crystal molecules. Those molecules even inhibit liquid crystal molecules from forming a liquid crystal phase. Irradiation with light causes trans-cis isomerization and the cis-azobenzene accumulates in the mixture, destabilizing the liquid crystal phase. The irradiation is an isothermal process, but it can induce the liquid crystal–isotropic phase transition. This process is reversible, of course, by visible light irradiation or by heat and the liquid crystal phase is restored if the concentration of the cis "impurity" is reduced by cis-trans reverse isomerization. That is, by selecting the correct irradiation wavelengths, it is possible to reversibly and isothermally induce an order–disorder transition in liquid crystals that contain azobenzene. Such a photoinduced isotropic phase is unstable in low molecular weight liquid crystal mixtures, because of diffusion of the cis form. Meanwhile, for liquid crystalline polymers containing mesogenic and photochromic molecules in the side chain (photochromic liquid crystalline polymers), diffusion is impossible because both moieties are attached to the same polymer, and a stable isotropic phase is formed [32, 33]. In exactly the same way as in the low molecular weight liquid crystal system, photochromic liquid crystalline polymers show an isothermal liquid crystal–isotropic phase transition by ultraviolet light irradiation that can be reversed by irradiation with visible light [34]. Furthermore, because of the glass transition temperature (Tg) of polymers, a stable isotropic phase can be achieved by irradiation with UV light above Tg and then cooling the polymer down below Tg [34].

11.2.4 Deformation of Crosslinked Liquid Crystalline Polymers

Liquid crystal elastomers can be obtained by the crosslinking of liquid crystalline polymers and show the nature of both an elastomer and a liquid crystal [35]. When the crosslinked liquid crystalline polymer is heated above the clearing temperature, the mesogens lose their orientational order and are in the isotropic phase with random orientation. According to the theory of de Gennes, crosslinked liquid crystalline polymers contract along the alignment direction of the mesogens during this phase transition [36, 37] and revert back to the original dimensions upon cooling. That is, in crosslinked liquid crystalline polymers, it is possible to extend or retract by simply changing the orientation of the mesogens. In 1989, Finkelmann et al. confirmed experimentally that a crosslinked liquid crystalline polymer shrinks up to 25 % along the direction of the mesogen orientation during the phase transition [38].

The combination of the photoinduced phase transition of photochromic liquid crystalline polymers described in Sect. 11.2.3 and the anisotropic distortion of the
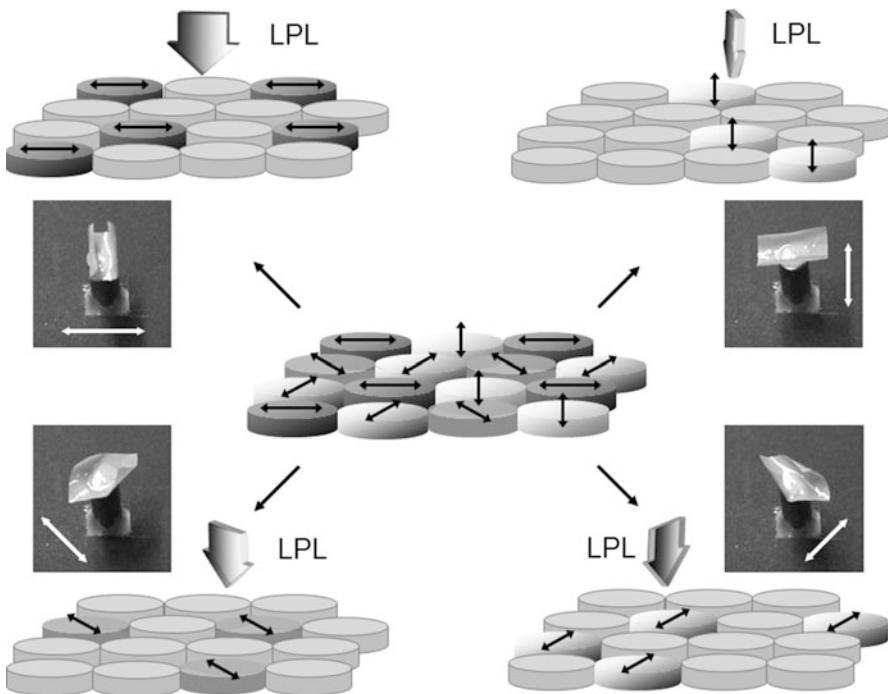
liquid crystal elastomers should result in the photoinduced deformation in a crosslinked photochromic liquid crystalline polymers. That is, as is happening in the visual system of the eye, structural changes of the photochromic molecules (photoisomerization) caused by one photon leads to the structural change of this one molecule (on the nanoscale) that, in turn, will induce a change in the alignment of the liquid crystal molecules in the entire system (on the macroscale). The conformation of the polymer chain and the orientation of the liquid crystal are strongly correlated in crosslinked liquid crystalline polymers and the change in mesogen order should influence the shape of the object. Finkelmann et al. found that a crosslinked liquid crystalline polymer that contains azobenzene in the crosslinks shrinks approximately by 20 % when it is irradiated with ultraviolet light [39].

The biggest advantage for using azobenzene derivatives as the photochromic molecule is their good compatibility with calamitic liquid crystals [31] and that it can express liquid crystal phases in itself. Thus azobenzene can fulfill both requirements, acting as the mesogen as well as the photochromic unit. This will lead to an elastomer that should show a high-speed response in the time range of the azobenzene trans-cis isomerization [31].

11.2.5 Three-Dimensional Photoinduced Motion of Crosslinked Liquid Crystalline Polymers

The expansion and contraction of the crosslinked photochromic liquid crystalline polymer described in the previous section is a motion in two dimensions, but a three-dimensional motion would be desirable from the standpoint of photomechanical material. When the surface of a crosslinked azobenzene liquid crystalline polymer film (The size of the films 10mm × 5 mm × 20∼50 micron (thickness). Slab means a bit thick slice or thick flat piece, so just 'film' is better in our case. The film is free-standing.) is irradiated with ultraviolet light, it bends towards the light source [40]. The molecular extinction coefficient of azobenzene is around 2×10^4 at 366 nm; thus, more than 99 % of incident photons are absorbed within the top 1 μm of the film. Hence, the trans-cis isomerization takes place in a thin layer and this surface layer contracts along the alignment direction of the azobenzene mesogens, resulting in a bending towards the light source. After irradiation with visible light, the sample returned to its original state.

According to the theory of de Gennes, crosslinked liquid crystalline polymers shrink along the alignment direction of the mesogens. The direction of the mesogens in the monodomain films and thus the direction of the bending or contraction is determined at the time of crosslinking. Is it then possible to bend in any free direction after synthesis of the film? This question has been answered by Yu et al. [41]. They reported that a film can be bent in any direction by irradiating a polydomain film having a large number of microdomains by linearly polarized light. The absorption transition moment of azobenzene is parallel to the molecular

Fig. 11.8 Direction-controlled bending of polydomain films induced by linearly polarized light (LPL)

long axis. When irradiated with linearly polarized light, only the azobenzene molecules that are aligned parallel to it will absorb the incident light (photoselection). When a polydomain film is irradiated with linearly polarized light, only the microdomains with the correctly aligned azobenzene absorb the incident light. Photoisomerization and orientation change occurs near the surface and the surface layer contracts along the alignment direction of the azobenzene mesogens. Since the polarization direction of linearly polarized light can be freely adjusted, it is possible to bend the film in any direction (Fig. 11.8) [41].

The combination of linearly polarized light and crosslinked azobenzene liquid crystalline polymers allows for a wide variety of 3-D photomechanical motions. We mentioned before that the absorption of linearly polarized light is determined by the direction of the absorption transition moment of azobenzene and light polarization by the photoselection principle. The orientation of the azobenzene mesogens decreases with ongoing trans-cis isomerization. After restoring the trans-azobenzene films, the mesogens could then very well orient in another direction, and subsequent deformation in a different direction can be induced [42]. Repeated azobenzene trans-cis isomerization cycles lead to the so-called Weigert effect, in which the molecules reorient in a direction perpendicular to the polarization plane of the incident light [31]. Molecules that are oriented in a direction perpendicular to

the plane of polarization have the lowest probability of absorbing the incident light, and thus, over time, azobenzene changes its orientation to a direction perpendicular to the polarization plane, and the film surface expands. As a result, the film will be bent away from the light source [42].
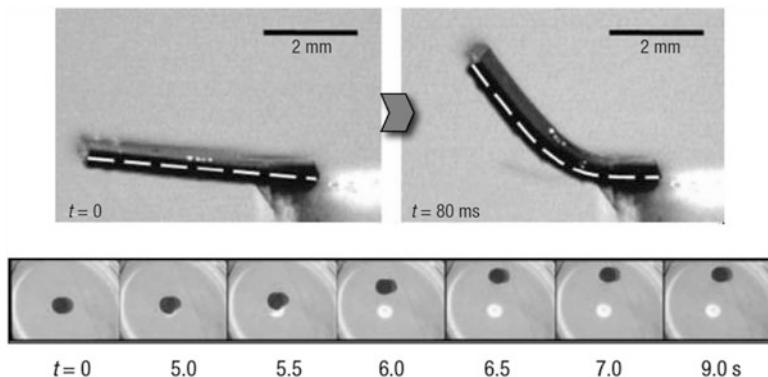
A similar behavior has been observed in films with a homeotropic orientation of the azobenzene mesogens [43]. In this case unpolarized light is used, which is selectively absorbed by the film surface. The orientation loss by photoisomerization takes place in the surface layer, but because the alignment direction of the mesogens is parallel to the incident direction, the volume increases in the irradiated area. According to the de Gennes theory, therefore, expansion occurs at the surface layer and the film bends away from the light source [43].

How large is the stress induced in the crosslinked liquid crystalline polymer film by light irradiation? Factors that affect the photoinduced stress are the degree of crosslinking, concentration of photoresponsive molecules, attachment site of the photoresponsive molecule, light penetration distance, sample thickness, and degree of orientation of the mesogens. Particularly important roles are the concentration and the attachment site of the photoresponsive molecules [44]. Photoresponsive molecules can either be attached to the polymer as a side group or incorporated into the crosslink. If present in the side groups, one end of the molecule is attached to the polymer backbone by chemical bonds and the other end is free, and such azobenzenes are easily isomerized. On the other hand, both ends of the molecule are coupled to the polymer main chain when the azobenzene is incorporated into the crosslinking sites. This also means that photoisomerization is more difficult. Trans-cis isomerization goes along with a large molecular shape change and the rate of isomerization is low in that case. However, even though the photoisomerization rate is small, it contributes significantly to photoinduced stress generation. In samples with an optimized concentration of azobenzene, the photoinduced stress can reach 2.6 MPa [44], which is much larger than the stress generated by the human muscle (about 300 Kpa).

According to the de Gennes theory, crosslinking is essential in order to strongly correlate the orientation of mesogens and the conformation of polymer chains, but it was found that crosslinking by covalent bonds is not necessary. Photoinduced bending in materials that are weakly crosslinked by hydrogen bonds has been reported, which is especially interesting, because hydrogen bonds can easily be cleaved and crosslinked materials can be recovered and reused [45].

11.2.6 Recent Photomobile Materials

Human muscles are composed of actin/myosin fibers, thereby realizing a precise motion by the sliding action of the fibers. Real applications of photomechanical systems should be possible if the material would be in a fibrous state, and thus the optical response of crosslinked photochromic liquid crystalline polymer fibers has

Fig. 11.9 Photoinduced deformation of a dye-doped CLCP and swimming behavior of the film like a flatfish

been investigated [46]. A mixed diisocyanate photochromic liquid crystalline polymer was obtained by introducing a hydroxyl group at the side chain terminal and spun in the liquid crystalline phase temperature to prepare crosslinked liquid crystalline polymer fibers of 10–80 μm diameter. Because of the flow alignment during spinning, the azobenzene mesogens show a high degree of orientation along the fiber axis. Fibers can be bent towards the light source with ultraviolet light and they return to their original state by irradiation with visible light. Controlling the irradiation direction can induce photoinduced motion in any direction [46].

Irradiation of an azo-dye-doped crosslinked liquid crystalline polymer with a strong argon ion laser induces a large bending [47]. Molded into a disk shape and floated on the water, this material is capable of escaping from the laser beam in a motion that is similar to a swimming fish (Fig. 11.9) [47]. Also artificial cilia have been successfully produced by ink-jet printing and a ciliary movement was induced by light irradiation (Fig. 11.10) [48]. In addition, by optimizing the laser irradiation conditions, a bird winglike flapping has been reported [49, 50].

The biggest problems of crosslinked polymers concern moldability and mechanical strength. They are brittle and cannot be formed after crosslinking. There have been attempts to produce laminate films using a polymer base material with excellent mechanical strength for the development of high-performance photomechanical polymer materials.

Low-density polyethylene is a robust and flexible polymer with a T_g of $-60\,^{\circ}$C. Laminated films of polyethylene and crosslinked photochromic liquid crystalline polymers were produced and the photoresponse was measured [51, 52]. We found that the bending and reversibility of the laminated film, in which the mesogens were aligned parallel to the film surface, was indistinguishable from that of the original free-standing azobenzene film. We prepared a belt from this homogeneous film, wrapped it around two pulleys (one large, one small), and irradiated the belt with ultraviolet light close to the small pulley and with visible light at the large pulley side. The experimental setup is shown in Fig. 11.11 and the belt rotated
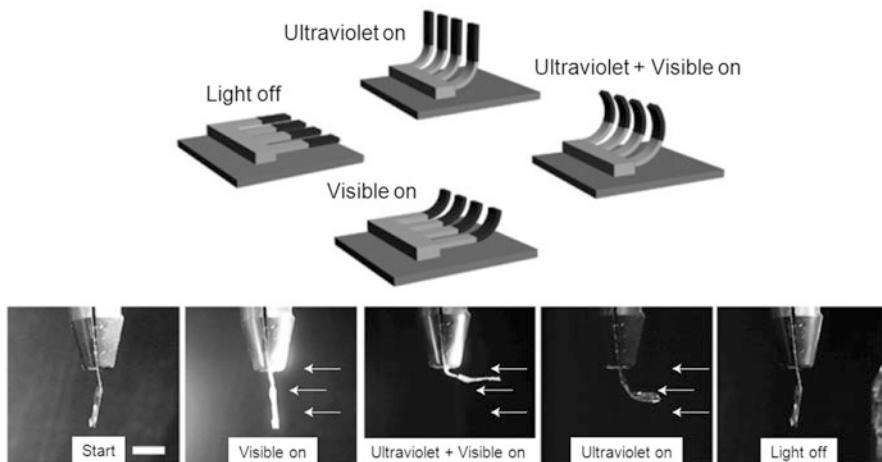
Fig. 11.10 Photoinduced motion of artificial cilia
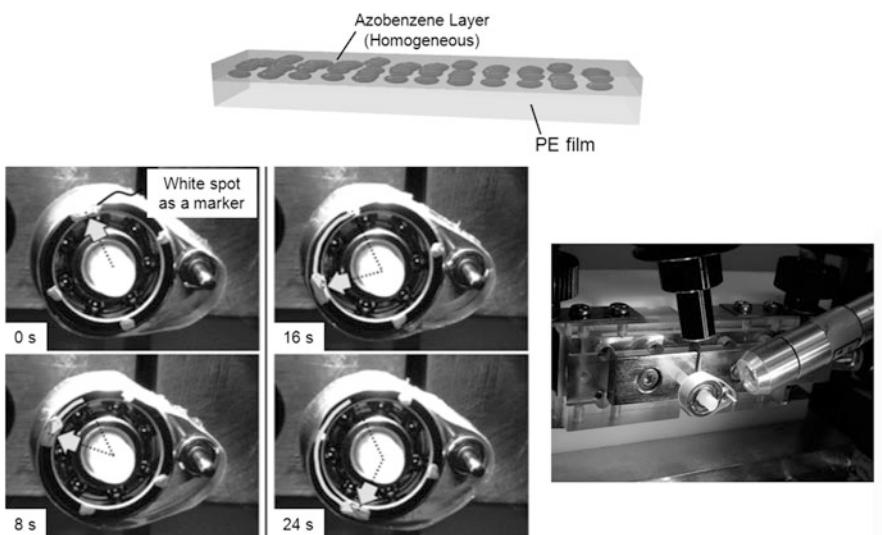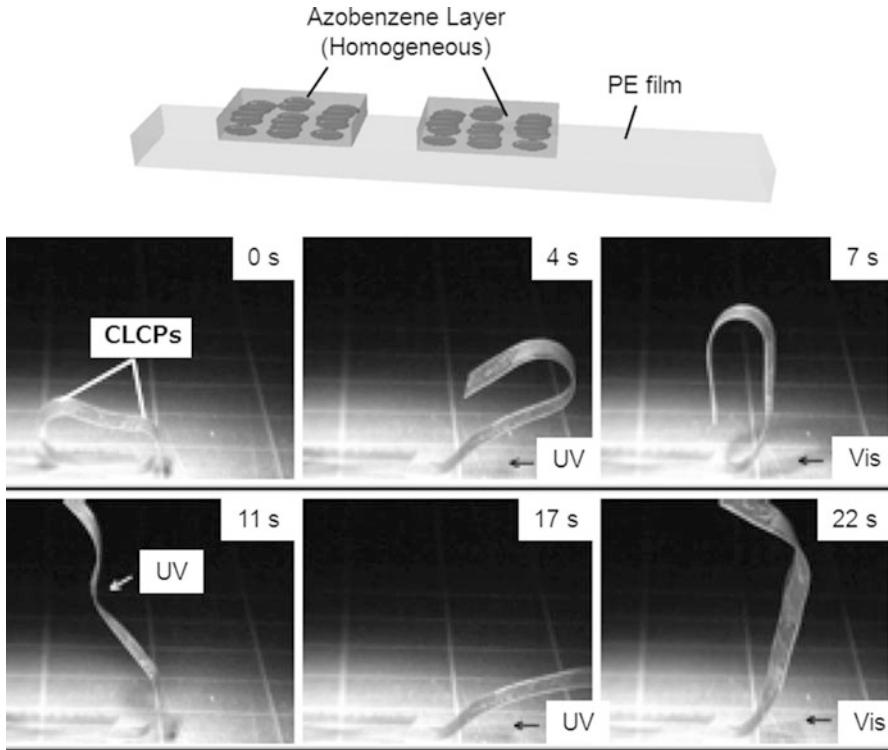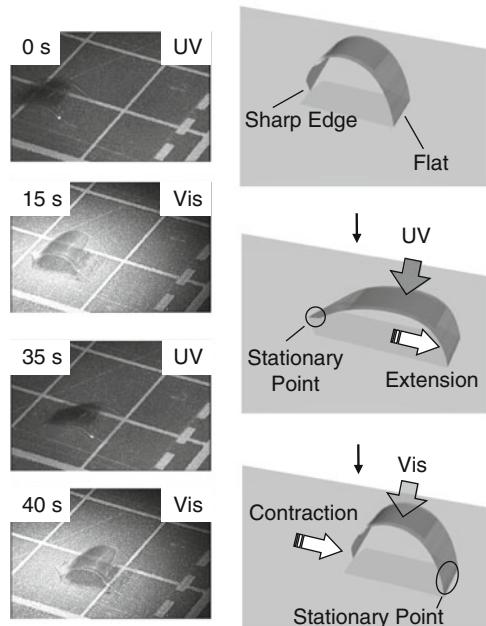
Fig. 11.11 Light-driven plastic motor

counterclockwise. The driving force for the rotation of this motor is the UV light. Furthermore, we designed a photomechanical drive for a robot arm by placing the photochromic elastomer at two sites (Fig. 11.12) and prepared an inchworm-like motion by pasting a photochromic elastomer in a laminated film, as shown in Fig. 11.13 [52].

Fig. 11.12 Robotic arm motion of the laminated film by photoirradiation

Fig. 11.13 Inchworm-like motion induced by alternate irradiation with UV and visible light

11.2.7 Summary

We were able to exhibit a variety of the three-dimensional motion in crosslinked photochromic liquid crystalline polymers by controlling the irradiation conditions and thus were able to convert light energy directly to mechanical work.

The photoinduced nanoscale changes at the molecular level induced by light (photoisomerization of the photochromic molecule) are amplified by the cooperative effect of the liquid crystal molecules with the conformation of the polymer chain. The macroscopic movement of these materials, which is characteristic for crosslinked liquid crystalline polymers, strongly correlates with the mesogen alignment. Since such polymer materials can be molded into a variety of shapes and sizes, it is possible to drive components remotely and without direct contact. No wires, electrodes, motors, or gears are necessary. Possible applications are micro actuators and microfluidic devices.

11.3 Development Towards Photonic Devices

Masanori Ozaki

11.3.1 Introduction

Photonics is often treated as a synonym for optoelectronics. In other words, it is said to be a scientific field that integrates optics and electronics, restricting it to the study of materials, devices, and systems involved in the conversion of light into electricity and vice versa. On the other hand, photonics can be broadened to include photochemistry and thus be related to chemical reactions such as photopolymerization and photochromism. That is, photonics covers a wide range of sciences that deal with photons themselves and their interaction with matter (electrons). The main applications of liquid crystals so far proposed were in optics, especially for displays and the control and modulation of light. This means that even in the field of optics, applications were restricted to control of the light beam in geometric optics and solving of Maxwell's equations. However, in recent years, new liquid crystal applications related to controlling the interaction of photons with electrons have been developed.

In addition, photonics was coupled with the development of microfabrication technology in the latter half of the twentieth century, and the academic field of nanophotonics emerged. The resulting photonic structures have dimensions of several hundred nanometers or less and play a role in the development of photonic crystals (PCs), plasmonic devices, and metamaterials. Analogous to the energy

band gap related to the propagation of electrons in a crystal, a photonic band gap (PBG) is present when photons propagate through a medium in which the dielectric constant (refractive index) changes periodically. Photons are localized at defects in PCs that disturb the PBG. Of course, even before the concept of PCs had been proposed, it was clear that interference of light waves in a periodic medium leads to Bragg reflection and threw development of dielectric multilayer mirrors, based on the idea of a stop band and that light cannot propagate in certain directions. In addition, the selective reflection band of cholesteric liquid crystal (ChLC) (a chiral smectic liquid crystal) can be said to be a one-dimensional (1D) PBG in the liquid crystal. However, the concept of the PC has come to draw a lot of attention after Yablonovich proposed the non-threshold laser and suppression of spontaneous emission in a three-dimensional (3D) PBG and John proposed the concept of a light localization [53, 54]. Meanwhile, plasmonics is based on a specific interaction with electrons and photons in a nanoscale space, such as fine metal particles and a metal surface, and interesting phenomena such as anomalous light transmission and optical field enhancement have been noted. Furthermore, metamaterials, which are nano-sized arrays of resonators which can be seen as "artificial atoms" and "molecules," can be used to control the optical properties in such a way that even a negative refractive index can be achieved, resulting in materials that do not exist in nature.

There are two methods to employ liquid crystals for nanophotonics. The first one is to impart functionality to a plasmonics or PC by using the external field response and anisotropy of the liquid crystal. The other is to use the structure-forming ability of self-organized liquid crystal molecules to build nanoscale structures, trying to achieve metamaterials and 3D PCs. The latter can be a very powerful tool to contract metamaterials and PCs in the visible light region, which is difficult in top-down approaches, such as photolithography. In this section, first I focus on our efforts to realize the PCs based on a synthetic opal infiltrated with liquid crystal. This will allow us to control the characteristics of PCs by external fields. I also introduce the laser action in the PCs based on chiral liquid crystals having a helical periodic structure.

11.3.2 Artificial Opals and Tunable Photonic Crystals

The photonic crystal (PC) has a structure in which the dielectric constant (the refractive index) changes with a period of about the wavelength of light. In the case of visible light, it is necessary to make a material having a periodic structure with dimensions of around 200–300 nm. To prepare a 3D structure in this size region is not easy. In fact, the first PBG has been confirmed in experiments using microwaves and a periodic structure in millimeter range. Thereafter, research on PBGs at the wavelength of visible light has been carried out using synthetic opal structures [55–57]. Synthetic opals can be produced relatively easily by precipitating suspensions of monodispersed nanospheres. The biggest challenge is that
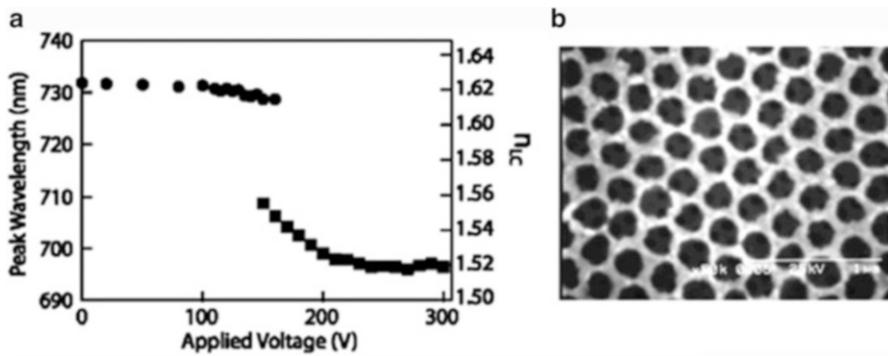
there are two close-packed structures of those spheres with the same density, the hexagonal close-packed and face-centered cubic structures. So, two different PBGs are obtained simultaneously in the macroscopic sample. But for the time being, we have to be content that such structures can be made.

In our laboratory at that time (Yoshino group at Osaka University), research on synthetic opals started around 1995 as a joint research with Dr. Anvar A. Zakhidov (now at University of Texas). We jointly study the light-induced charge transfer in conducting polymer/C_{60} composites for organic solar cells. First, Masanori Ozaki measured the optical reflectance spectra of bulk-like synthetic silica opal prepared by Dr. Zakhidov. Silica spheres with a diameter of about 200 nm gave a strong white scattering, but by dipping the opal in a liquid with a similar refractive index as silica, vivid colors that resembled the natural opal jewelry appeared [55].

The PBG characteristics of opal depend on the crystal structure (symmetry), size (periodicity and aspect ratio), and refractive index. By combining such synthetic opals with functional organic materials, Professor Katsumi Yoshino proposed the concept of "tunable photonic crystal (TPC)" in which the optical properties of synthetic opal, PBG, can be controlled [58]. That is, if synthetic opal is made of a material having an electronic or optical function, or the pores of a synthetic opal are filled with such materials with the aim to control the refractive index and structure, the TPC can be realized [59–62]. Particularly interesting materials are the so-called inverted opals, which can be produced by using a synthetic opal as a template, because they widen the degree of freedom for material selection [63–65]. For example, phenolic resin-filled silica opals give inverted graphite opals after heating to 2,800 °C and removing the original by hydrofluoric acid treatment [65]. Such a black or blue graphite can be alkali-doped to change the electronic state of the graphite. This leads to a refractive index change and thus the reflected color changes. In addition, by filling the voids of the opal with photochromic dyes or conductive polymers, it is possible to control the reflection band by light, heat, or electrochemical doping. Of course, by filling with a liquid crystal, the 1D PBG can be controlled by temperature and electric field and thus the position of the stop band can be changed as well [66–72]. In this case, because of the large anisotropy of the liquid crystal, phenomenon such as the resolution of the band degeneracy is also being observed [73]. This new concept is called "anisotropic photonic crystal" [73].

A thin film of an inverted opal has been obtained by infiltrating an opal (made from 200 nm silica spheres) with a photopolymer. This inverted opal was then filled with a liquid crystal. Figure 11.14a shows the electro-optical response in which the reflection peak (corresponding to the stop band) shifts due to the change of the refractive index of the liquid crystal [72]. Figure 11.14b shows the electron microscope image of the film itself. The discontinuous peak shift is due to the resolution of the degeneracy of the band caused by the introduction of the aniso-tropic medium. Furthermore, a memory effect due to the interface between liquid crystal and the opal pores can also be seen.

The principle is simple, but it is important to completely remove residue from the porous medium. Keizo Nakayama, who was a doctoral student in our group at that time (now at Kinki University), started this research around 1997 and spend

Fig. 11.14 (**a**) Reflection peak wavelength of polymer inverse opal infiltrated with 5CB as a function of applied voltage. (**b**) SEM image of polymer inverse opal

many trial-and-error runs for this study. Yuki Shimoda, a master course student at that time (now at Ricoh), took four years to successfully measure the electric field response of inverted opals.

We introduced tunable PCs using opals as a PC medium in the above, but there is another method to produce TPCs in a combination of liquid crystal and PC fabricated by a multi-beam optical interference. For example, one can realize tunable PCs by means of an infiltration of liquid crystal into the periodic polymer structure which is forehead fabricated by the interference exposure of photopolymer [74, 75]. TPC can also be realized in a so-called holographic polymer-dispersed liquid crystal (HPDLC). Namely, when a mixture of liquid crystal and UV-curable monomer is illuminated with interfered light beams, periodically aligned array of liquid crystal droplets is formed because of the phase separation during photopolymerization [76, 77]. A 3D HPDLC can be also fabricated by using four-beam interference configuration [78, 79]. Moreover, there is no need to create a permanent periodic structure by optical interference. It was reported that transient periodic structures also show these effects. That is, color-tunable lasing based on a transient distributed feedback (DFB) laser is possible using the periodic excitation by interfered pump beams [80–82].

11.3.3 Photonic Crystals Made by Self-Assembly of Nano-spiral Periodic Structures of Chiral Liquid Crystals

11.3.3.1 Liquid Crystal Band-Edge Laser
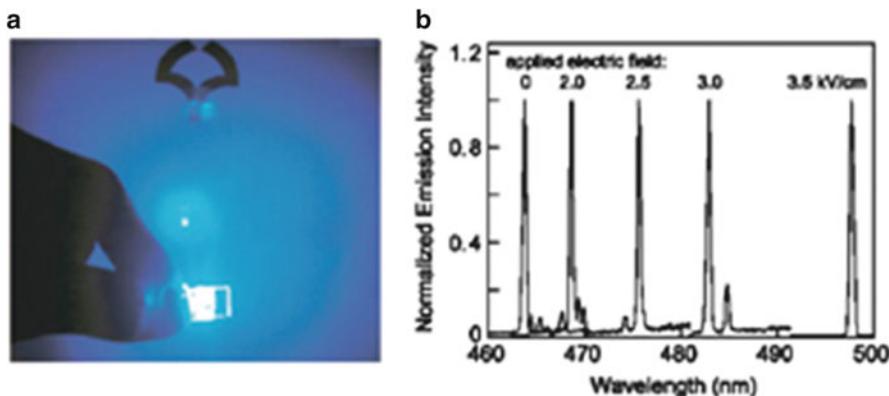
There are many examples in which liquid crystals form nanostructures by self-organization. Chiral liquid crystals, such as ChLCs, form a one-dimensional

nano-helical periodic structure in which the rodlike molecules are twisted at a pitch of the order of the wavelength of light. There has been ongoing research to use such structures as wavelength- and polarization-selective laser mirrors or optically anisotropic laser media [83]. Also, the idea to use the helical structure of ChLCs as a distributed feedback laser cavity is quite old [84, 85].

1D and two-dimensional (2D) PBGs, which mean incomplete PBGs, suppress only the spontaneous emission in a certain direction and do not increase the excitation lifetime that is expected in complete PBGs, and thus there is little contribution of 1D or 2D periodic structures for the realization of the inverted population necessary for lasing. Near edges of PBG, however, since the photon group velocity decreases, the interaction of generated photons with laser medium becomes effective and a decrease in the lasing threshold can be expected [86, 87]. In other words, the emitted light is standing wave at the band edge. In this case, there are two types of circularly polarized standing waves with zero group velocity at the edges of the stop band. For one of the standing waves, the polarization direction of the light is always parallel to the molecular long axis (in-phase standing wave). This light feels a larger refractive index (extraordinary refractive index) of the LC and has lower energy with respect to a travelling wave, which corresponds to the longer edge of the stop band. If we dope laser dye having a transition moment parallel to the long axis of liquid crystal, the polarization of the in-phase standing wave is parallel to the transition moment of the doped dye. This circularly polarized standing wave with lower energy effectively interacts with the laser medium and we can expect the low threshold laser action at the longer wavelength edge of the band gap.

Lasing from the PBG edge was first reported by Kopp et al. using a ChLC doped with a laser dye [88]. The emitted laser light is circularly polarized with the same handedness as the spiral sense of the ChLC. With temperature increases, the lasing wavelength shifts towards a shorter wavelength, which corresponds to the shift of the stop band originating from the temperature dependence of the helical pitch of CLC [89]. Laser action can also be induced in undoped ChLCs. Here, the UV lasing is based on the fluorescence of the ChLC molecules themselves. The laser actions based on an energy transfer from an antenna molecule to emissive dyes and on two-photon excitation have been reported [90–94].

On the other hand, the greatest advantage of the liquid crystal laser is that it should be possible to control the lasing wavelength by an external field and here an electric field in particular. However, the first trials showed that the laser action disappears when an electric field is applied, because the cholesteric helix is unwound [95], and there have not been reports about continuous color-tuning upon applying a field perpendicular to the helical axis. However, control of the lasing wavelength by changing the helical pitch by an electric field has been reported by Kahn et al. [96] in the focal conic state of the ChLC, and we were able to confirm that finding [97]. We reasoned that ChLCs in their planar orientation show no change of the pitch by applying an electric field in the direction perpendicular to the helical axis because the liquid crystal structure is regulated by strong anchoring forces at the substrate interface. Thus we were considering the electric field response of ferroelectric liquid crystals (FLCs).

Fig. 11.15 (**a**) Far-field pattern of laser emission from FLC cell. (**b**) Lasing spectra of FLC cell as a function of applied electric field

A large torque acts on the FLC molecules under an electric field because the FLC has a spontaneous polarization, and thus the reaction to an electric field should be stronger than for ChLCs. In addition, it is generally known that anchoring forces of the FLC molecules on the substrate surfaces are weak in the homeotropic configuration in which the helix axis is normal to the substrates, because the director in the smectic C phase is not perpendicular to the helical axis as in a ChLC but rather forms an angle of 20–30 °. In the early 2000s, we had been studying the high-speed response of the electrooptic modulation of short-pitched FLCs with Professor Haase (Darmstadt Technical University). Fortunately, in response to the offer of a FLC sample from Professor Haase, I started to study the electric-field-driving tunable laser.

FLCs also have a stop band in the same manner as ChLCs. When the helical axis is aligned perpendicular to the glass substrates (homeotropic alignment), the stop band can be seen as a dip in the spectrum of the transmitted light. In the same manner as with ChLCs, the wavelength of the dip shifts with temperature. However, since the director is not perpendicular to the helical axis and the modulation of refractive index for the light travelling along the helix axis is smaller than for ChLCs, the width of the stop band is relatively narrow. Moreover, because the direction of the transition moment of the added laser dye is not perpendicular to the helical axis, the interaction of the dye with light propagating in the helix axis direction is not effective. Thus, no laser action can be observed by using the common Q-switched Nd-YAG laser with nanosecond pulse widths. Finally, by switching to a femtosecond mode-locked laser, Masahiro Kasano, a graduate student, was able to observe laser action in a FLC doped with a coumarin dye, as shown in Fig. 11.15 [98]. Furthermore, as originally intended, we could easily distort the helical structure by an electric field and hence could control the lasing wavelength [99]. In this case, the response time of the wavelength shift is estimated to be less than 100 μs. This shows that high-speed modulation of the lasing wavelength is possible. We have also

proposed a waveguide device configuration, in which the helix axis is parallel to the glass substrates, in order to efficiently excite doped dye and elongate the length of an active area along the helix [100].

Lasing wavelength easily shifts as the spiral pitch of the ChLC strongly depends on the temperature, which is a disadvantage in terms of stable oscillation. One possible solution for this problem is photopolymerization after the helical structure has been formed. Tatsunosuke Matsui (now at Mie University), a doctoral student, fabricated a thin-film flexible liquid crystal laser by using the photopolymerizable ChLC called "reactive mesogen" from Merck. The polymerization indeed made it possible to stabilize the lasing wavelength, since the helical pitch is nearly independent of temperature [101]. Furthermore, laser action from free-standing flexible films is also possible, and thus we can expect various applications [101]. In addition, it is also possible to make a film with a distribution of the spiral pitch in the film plane by applying a temperature gradient in the film plane prior to polymerization. Hence, depending of the position of the excitation laser spot, lasing at different wavelengths is observed.

The blue phase (BP) liquid crystal forms a 3D periodic structure. Cao et al. added a laser dye to a BP and have successfully demonstrated lasing by photoexcitation [102]. Currently, three types of BPs have been reported: BP I is body centered cubic, BP II is simple cubic, and BP III is said to be amorphous. None of the three phases meet the criteria for a complete PBG, but multi-directional lasing is very interesting. In addition, the working temperature range for lasing has been expanded by polymer stabilization [103, 104].

11.3.3.2 Defect Mode

One of the important properties of a PC is the defect mode. In other words, when there are disturbances in the uniform periodic structure, they act as localization centers for light in the PBG. On the other hand, there are defect mode characteristic for the spiral periodic structure of chiral liquid crystals [105–107]. They do not only disturb the periodicity of the structure, but they produce defect modes based on the phase mismatch of the helical twist angle, which was theoretically proposed by Kopp. This is an interesting characteristic of the properties of a helical periodic structure [106, 108].

We made attempts to use photopolymerized ChLC films to demonstrate the presence of twist defects experimentally [109]. However, even though the principle is straightforward, the realization is not easy. Ryotaro Ozaki, a doctoral student at that time (now at Ehime University) spent half a year to fix the films with a good enough precision to see the localized defects in the transmission spectrum. Furthermore, he could also confirm a laser action from this defect mode, which is interesting because it is a different mechanism to produce laser action [109–111].

On the other hand, Tatsunosuke Matsui proposed a theory that the partial change in the helical pitch of a ChLC should show up in the localized state of the stop band [107]. For example, a partial modulation of a right-handed helix with a pitch of
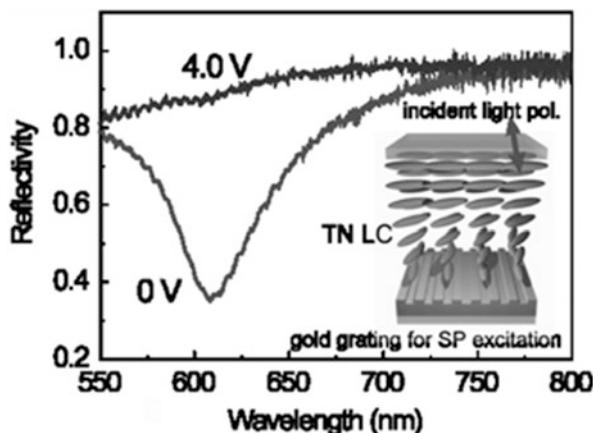
400 nm (400 m - > 300 nm) should lead to the appearance of a defect mode at 660 nm within the stop band (600–700 nm). Furthermore, by adding multiple modulations, the defect modes should couple each other and lead to a localized band [112]. The experimental verification of the theory was not easy because of the difficulty to obtain those structures in a fluid system. Therefore, a doctoral student Hiroyuki Yoshida (now at Osaka University) prepared a photopolymerizable ChLC and used direct laser writing to produce a tunable spiral defect mode [113–115]. He employed the two-photon photopolymerization technique by using 800 nm femtosecond laser and a high aperture ratio lens. First, he aligned the helical axis of the photopolymerizable ChLC to be perpendicular to the glass substrates. He then photopolymerized the ChLC near the substrate of one side of the cell and then, by inverting the cell, the other side. As a result, an unpolymerized ChLC layer sandwiched between two polymerized cholesteric structures is achieved. In this case, since the helical pitch changes during the polymerization, a 1D PC structure that includes defects with different helical pitches in the unpolymerized portion can be produced.

By using such a defect in a 1D PC structure in a ChLC, one can make a resonator with an extremely high Q-value. Since around 2002, we have introduced a nematic liquid crystal into the defect of a 1D PC composed of dielectric multilayers, and we were able to control the localized states by temperature and electric field [116–119]. These studies have been carried out by Ryotaro Ozaki, and in the process, he found very interesting characteristics by introducing a periodic structure into the defect layer of PC. In particular, the introduction of the helical periodic structure of the ChLC into the dielectric multilayer PC reduces the line width of the defect mode by one or two orders of magnitude as compared to the dielectric multilayer PC with a nonperiodic defect, and results in films with a very high Q-value [120–126]. Then, another doctoral student, Yuko Matsuhisa (now at Panasonic), took over and developed a new defect mode laser. This new mode allowed a lower-threshold laser oscillation than the band-edge laser in normal ChLCs [123, 124].
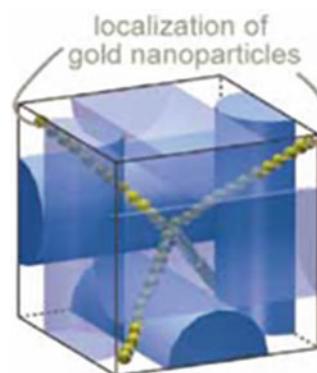
11.3.3.3 Outlook

So far, I have outlined the deployment of our initial research with respect to the applications of liquid crystal PCs. They are described in detail in references [127–130]. Starting from there, the progress of research related to liquid crystal lasers has advanced remarkably. In the early studies, it was necessary to excite samples with large Q-switched pulse lasers, but the research results led to a constant improvement of materials and device structures that reduced lasing threshold and improved slope efficiency [131–136]. This made it possible to excite those PCs with semiconductor lasers. Furthermore, it has even come possible to excite with a CW laser also shown in [137]. In addition, control of the lasing wavelengths by modulation of the helical pitch (by temperature and electric field) in the early days of development led to effective refractive index modulation and fast stability control [138]. In 2000 it was quite a surprise that laser actions occur even in a system containing fluctuation such as liquid crystals, but by now, it can be said that

Fig. 11.16 Applied voltage dependence of reflection spectrum of gold grating with twisted nematic layer for TE-mode incident light

Fig. 11.17 Schematic explanation of gold nanoparticle alignment in the defect of cholesteric blue phase liquid crystal

the interest has shifted from a purely scientific one, and practical application finally come into view.

Also, in the field of nanophotonics itself, starting from PCs, plasmonics, and metamaterials, the use of liquid crystals has been extended to the control of function in those metamaterials and plasmon [139–143]. For example, Fig. 11.16 shows the control of a plasmon excited on a gold grating by a twisted nematic liquid crystal [139]. The polarization direction of the light must be parallel to the grating vector in order to excite plasmons, but here, the polarization direction can be controlled by the rearrangement of the liquid crystal orientation. We have to say, though, that such applications are a mere extension of existing liquid crystal optical device applications because they are based on the control of the refractive index by the electric field response and the anisotropy of the liquid crystal. A completely new development would be the use of molecules and nanoparticles that self-assemble on the nanoscale to build a metamaterial by the bottom-up method (Fig. 11.17). I believe that liquid crystal molecules have an inherent high potential which can greatly advance the field of nanophotonics.

11.4   Mass Transport in Liquid Crystals

Takashi Kato and Masafumi Yoshio

11.4.1   Poly(Ethylene Oxide)-Based Liquid Crystals
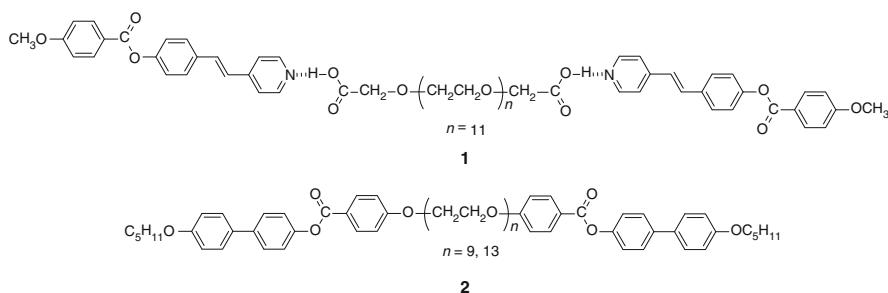
The question arises if liquid crystals can be used as new nano-structured functional materials. One avenue we explored since the late 1990s at Tokyo University, together with Professor Hiroyuki Ohno at Tokyo University of Agriculture and Technology, was ion conduction. Ions are an impurity in liquid crystal display elements.

However, we turned this fact on its head and developed the idea to use the nano-level phase-separated structure and the anisotropy of the liquid crystal as a material having a channel structure for carrying ions actively and efficiently so as to function as a battery electrolyte. From thereon we were able to construct ion-conducting material based on various liquid crystal structures [144–149].

The initial trigger for studying this was that Kato and Ohno were members of the "Polymer Nano Organization," a Scientific Research Priority Research of MEXT that was headed by Prof. Toyoki Kunitake from 1996 to 1998. At that time, Kato had built various supramolecular hydrogen-bonded liquid crystals [150–152]. Among them was one that had an oxyethylene chain [153]. In the past, Ohno had studied polymer electrolyte, poly(ethylene oxide), complexed with lithium salts. The combination of these two concepts, i.e., lithium salt liquid crystals having oxyethylene chains, should lead to liquid electrolytes having ion channels that anisotropically carry ions.

Kato started the molecular design immediately after joining the project. First, two liquid crystals were synthesized by attaching rigid mesogens on both sides of an oligo(ethylene oxide) (Fig. 11.18).

The polyoxyethylene chains in those liquid crystals can complex lithium salts, for example, lithium trifluoromethane sulfonate salt, and form a uniform liquid crystal phase. Furthermore, we found that the liquid crystal phase is formed in a wide temperature range by adding salt. (Comment by Karthaus: without salt, they do not form LC phases? This is not clear from the text, but it is important to know. Answer: The twin mesogenic compounds containing oligo(ethylene oxide)s form LC phases in the absence of lithium salts.). We were also aware of associated studies by Percec et al. who complexed liquid crystal having crown ether or oligooxyethylene groups [154]. However, their liquid crystal samples were unoriented, and they reported only a few data points, giving the impression that this was not a study focused on the development of liquid crystalline ionic conductors.
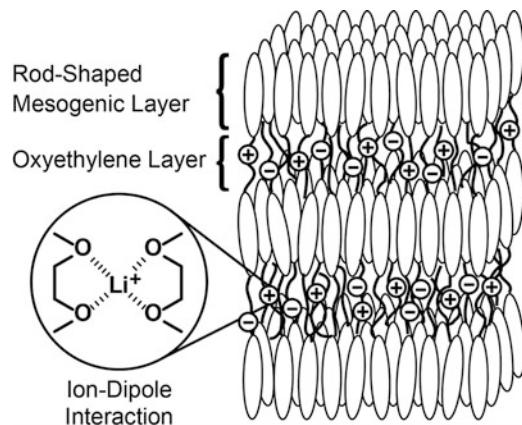
Fig. 11.18 Supramolecular hydrogen-bonded liquid crystalline dimer and covalently bonded liquid crystalline dimers, both of which contain oligo(ethylene oxide) spacers

There were other studies of added salt to improve ionic conductivity in liquid crystals, but they also did not investigate the orientation control, which is an important characteristic of liquid crystals [149].

The first presentation related to a lithium salt complex with a hydrogen-bonded supramolecular liquid crystal (compound **1** in Fig. 11.18) took place at the 72nd Spring Meeting of the Chemical Society of Japan in March 1997 and it had the title "The effect of metal salt addition to hydrogen-bonded supramolecular liquid crystals" and was the result of research conducted jointly by the University of Tokyo (Takahiro Amemiya, Hideyuki Kihara, Takashi Kato) and Tokyo University of Agriculture and Technology (Hiroyuki Ohno). The lithium salt of the even more stable dimeric oligooxyethylene group-containing covalent liquid crystal **2** shifts the temperature range of the smectic liquid crystal towards higher temperatures (Masumi Ogasawara, Toshihiro Ohtake, Takashi Kato, Hiroyuki Ohno, "The nature of the liquid crystal phase stabilization behavior of liquid crystal/lithium salt complex").

With this section, we aim to prove that liquid crystals can be anisotropic ion conductors, which was our original research target, after all. In order to do this, we used a macroscopically oriented sample of smectic liquid crystals on a substrate and measured ion conductivity in the horizontal and vertical directions, that means parallel and perpendicular to the smectic layers. For this, electrodes suitable for the liquid crystal material are required and Kaori Akita and Naoko Nishina of the Ohno group prepared liquid crystal cells with either gold interdigitated electrodes or indium tin oxide (ITO) electrodes for the measurement of the anisotropic conduction. The lithium salts of compounds **1** and **2** form both smectic phases that spontaneously orient parallel to the glass substrate and thus it was possible to measure the in-plane conductivity with comb-shaped electrodes. On the other hand, the complexes form a polydomain structure between the ITO electrodes. Thus, it was only possible to measure the average conductivity in the smectic polydomain sample. Still, by comparing the conductivity values of the two measurements, we could show that a uniform alignment gives higher conductivity. Furthermore, in the single-domain sample, we found that the isotropic liquid phase

Fig. 11.19 Smectic liquid crystalline structure formed by the complexes of rod-shaped molecules containing oxyethylene chains and lithium salts
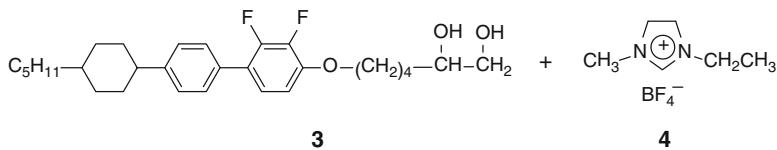
shows a greatly decreased conductivity. Thus, an effective ion transport in the two-dimensional smectic layers can be inferred. Even though we were not able to unequivocally prove anisotropic conduction, the finding that the liquid crystal phases of **1** and **2** are stabilized by increased dipole interactions between the mesogens in itself is interesting (Fig. 11.19). In addition, we thought at that time that the relatively high ion conductivity 10^{-4}–10^{-5} S/cm at around 150 °C may lead to a new ion-conducting material. As a result, the Polymer Journal published our peer-reviewed paper in a special issue of "Polymer nano organization" in 1999 [155]. After that, we designed other dimeric covalent liquid crystalline mesogenic with different structures and examined their ionic conductivity [156–158]. Other than that, we were also developing photopolymerizable liquid crystal electrolyte films [159, 160] and monomeric smectic liquid crystal [161].

11.4.2 Ionic Liquid-Containing Liquid Crystals

In 2001, I embarked on the development of new liquid crystalline ion conductors consisting of a two-component system of amphiphilic molecules and ionic liquids. Ionic liquids, organic liquids consisting only of ions, began attracting worldwide attention as nonvolatile solvents with high ionic conductivity [162, 163]. Professor Ohno had focused on ionic liquids from early on and was considering their applications in biotechnology and electrochemistry [164].

We, on the other hand, developed the idea to use ionic liquids to produce a new functional liquid crystal material with anisotropic conductivity [149, 165–168]. The head of the research team was graduate student Masafumi Yoshio (now associate professor at Tokyo University). Other members were Research Associate Kiyoshi Kanie (now associate professor at Tohoku University) from Kato's group and Masahiro Yoshizawa (now Masahiro Fujita, associate professor at Sophia University) from Ohno's group. The results led to the filing of a patent ("A method

Fig. 11.20 Liquid crystalline complexes composed of rod-shaped mesogenic molecule containing hydroxyl groups and ionic liquid

of manufacturing a liquid crystal ion conductor") in March 2001 [169] and a 2002 publication in Advanced Materials [170] in which the anisotropic conduction of an equimolar complex of the hydroxyl group bearing calamitic liquid crystal **3** and ionic liquid **4** was reported (see Fig. 11.20). Our choice of compound **3** was based on our knowledge that hydrogen bonding tends to stabilize liquid crystal phases [171]. By the interaction between the hydroxyl group and imidazolium ionic liquid, a smectic liquid crystal having a nanophase separated structure consisting of an insulating layer consisting of the mesogens, and an ionic liquid layer was obtained.
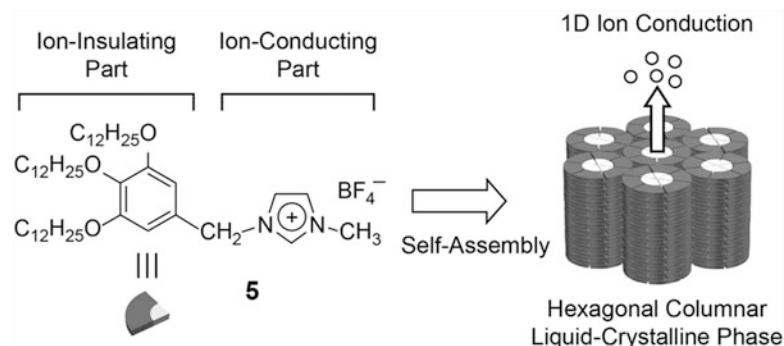
Furthermore, we succeeded in the uniform alignment between the ITO electrodes and gold comb electrodes in this two-component system liquid crystal and found that the ion conductivity parallel to the smectic layer structure is about 3,000 times higher than in the perpendicular direction. We could also easily adjust the ionic conductivity and the phase transition temperature by changing the composition mixture [172]. It is a great advantage to use such mixtures that form assembled structures by non-covalent intermolecular interactions.

11.4.3   Columnar Ionic Liquid Crystals

A completely different molecular design is used for one-dimensional ionic conductor. Here, a fan-shaped molecule having a hydroxyl group was complexed with an ionic liquid, resulting in a columnar liquid crystal in which the ionic liquid that is organized in the column center is obtained [173].

Furthermore, we proceeded to covalently attach mesogenic groups to the ionic liquid to obtain a liquid crystalline ionic liquid with anisotropic conductivity. Alkylated pyridinium and ammonium salts are well known to form smectic liquid crystals [174, 175]. Furthermore, at the time when ionic liquid came into the limelight, smectic liquid crystal of long-chain alkylated imidazolium salts had been reported by the groups of Prof. Bruce and Prof. Seddon in the United Kingdom [176–178], and they pointed out the potential of anisotropic solvent for chemical reactions. However, there was no report about their use as an ion conductor.

We investigated the liquid crystalline phases and the ion conductivity of mixtures of a long-chain alkylated imidazolium salt and a room temperature ionic liquid [179]. The ionic liquid provided the high ionic mobility in the smectic layer
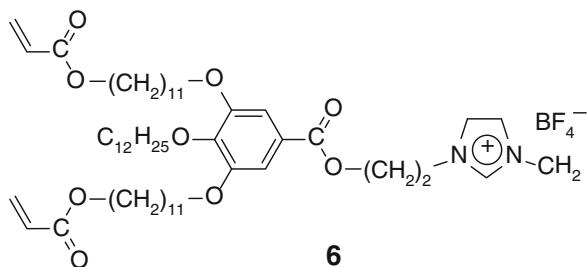
Fig. 11.21 Columnar liquid crystalline imidazolium salt
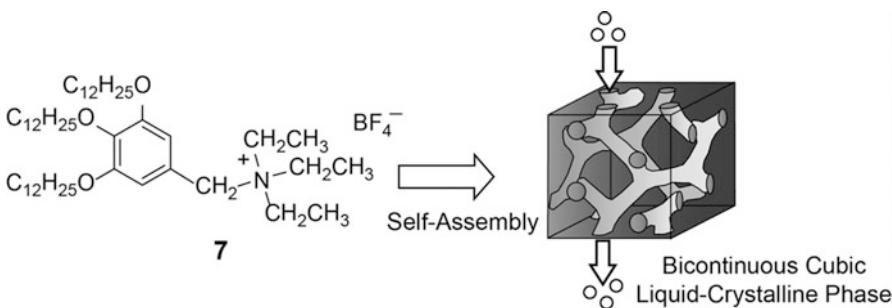
structure formed by the long-chain imidazolium salt. Thus, the conjugate showed a high ionic conductivity, even though with barely any anisotropy.

Then, we aimed at building a one-dimensional ion conductor by imidazolium salt columnar liquid crystals. Molecules such as **5** can form an ion channel structure by self-assembly (Fig. 11.21) [180, 183]. Our hope was that the wedge-shaped molecule leads to a nano-phase separation of nonionic sites and ionic sites and that the ionic sites would organize in the center of the column. Compound **5** shows a hexagonal columnar liquid crystal phase between 17 and 183 °C. By cooling from the isotropic liquid phase, a multi-domain liquid crystal phase with domain sizes of about 50 μm and different degrees of columnar orientation towards the glass substrate was formed. After mechanical shearing along the horizontal direction, the columns of the liquid crystal sandwiched between the two glass substrates could be horizontally oriented with respect to the substrate. As a result, a high ionic conductivity along the column axis could be measured [181].

Then, we aimed at the fabrication of polymer films with a one-dimensionally oriented ion channel structure. The photo-radical polymerization of acrylate group-containing derivatives of **5** was examined, in order to immobilize the liquid crystal columnar structure. Contrary to our expectations, it took quite some time to design a polymerizable columnar liquid crystal. The compound containing three acrylate groups at the alkyl chain end was a liquid at room temperature. At the end of a series of synthetic trials in which we changed the substitution position and the number of acrylate groups, we could achieve the reactive imidazolium salt **6**, which showed a columnar liquid crystal phase at room temperature (Fig. 11.22) [182]. By applying lateral shear in the columnar liquid crystal phase, columns could be oriented horizontally to the cell substrates. Furthermore, using a glass substrate that was surface-modified with a silane coupling agent having an amino group, the columns spontaneously aligned vertically to the substrate. By UV irradiation the vertically aligned columnar liquid crystal formed a transparent self-supporting film that showed a high ionic conductivity perpendicular to the film direction [183].

Fig. 11.22 Columnar liquid crystalline imidazolium salt containing polymerizable groups

Fig. 11.23 Bicontinuous cubic liquid crystalline ammonium salt

11.4.4 Bicontinuous Cubic Ionic Liquid Crystals

Because of the complex molecular interaction in those binary complexes, it was necessary to experiment with various techniques to achieve uniform molecular orientation, which is different from aligning liquid crystal molecules in liquid crystal displays. Therefore, we focused on the development of bicontinuous cubic liquid crystals that potentially can be used as an ion conductor without worrying too much about the molecular orientation. By switching from the columnar imidazolium salts to ammonium salts, we could synthesize various interesting derivatives with the desired liquid crystal structure, and among them was compound **7** that shows a bicontinuous cubic liquid crystal phase (Fig. 11.23) [184]. This study was conducted in 2006 by the fourth grade student Takahiro Ichikawa (now assistant professor at Tokyo University of Agriculture and Technology). After synthesizing the compound, he observed the phase transition behavior by polarizing microscopy and found that the columnar fan texture changes to a black state when the temperature is lowered. Professor Yoshio, who was with Ichikawa at that time, concluded that this must be a bicontinuous cubic phase. This was a distinct event in the study of liquid crystalline ion conductors in ionic liquid systems, and the three of us were very excited. We were thus able to publish a paper in the Journal of the American

Chemical Society in 2007 that showed that a relatively high ionic conductivity could be obtained in a liquid crystal without macroscopic alignment control [184]. This study was followed by producing a polymer film of a bicontinuous cubic liquid crystalline ion conductor [185]. We also, jointly with Ungar professor in the United Kingdom, analyzed the three-dimensional nano-channel structure by synchrotron X-ray studies [186] and recently built a two-component cubic liquid crystal consisting of amphiphilic liquid crystal molecules and ionic liquids [187].

11.4.5 Perspective

We expect that the development of anisotropic materials that conduct ions in a desired direction as next-generation nanomaterials for devices to transmit energy and information or as molecular switches will continue. By using the dynamic ordered structure of liquid crystals to control the orientation, such materials could also act to control the aggregation state of the ions themselves. In the future, it should be possible to achieve selective transport, high ionic conductivity, and high anisotropy of target ions [188].

11.5 Pharmaceutical Applications of Liquid Crystals

Atsushi Yoshizawa

11.5.1 Introduction

Liquid crystals were discovered in Europe in the nineteenth century by the Austrian botanist Friedrich Reinitzer. In order to determine the structure of cholesterol that he extracted from carrots, he synthesized several derivatives. He found that cholesteryl benzoate becomes an opaque liquid at 145.5 °C that becomes clear at 178.5 °C, and he reported his findings at a congress of Vienna Chemical Society in 1888. The German physicist Otto Lehmann received a request from Reinitzer to investigate the sample and he found that the turbid state is homogeneous and has the fluidity of a liquid and the optical anisotropy of a crystal. From their very discovery, researchers including Lehmann himself were interested in the relationship between life and liquid crystals [189]. Thereafter, basic research that supported the development of liquid crystals focused on phase structure studies, the correlation of molecular structure and liquid crystallinity, and the change of molecular orientation in external fields. This led to the development of the calculator display (LCD) in the 1970s. Since then, LCDs have been widely used in laptops, mobile phones, and large screen TVs that are indispensable to our lives. Innovations in display

technology led to high-definition, low power consumption, thin, light, and large displays. Taking advantage of their characteristics, liquid crystal displays are also used in the medical field.

Meanwhile, cell membranes in living tissue are known to be in a liquid crystal state. Dynamic membrane having both order and fluidity makes material transport and information exchange throughout the membrane possible [190]. During the transmission of information, signaling molecules such as membrane proteins enhance the transmission efficiency by self-assembling in the fluid membrane and thus localizing the transmission site. The fluid membrane separates the inside and outside of the cellular environment and maintains homeostasis in cells; the primary goal of the cell membrane is the transmission of substance with a high selectivity.

In recent years, liquid crystalline drugs have become interesting. Tomoyuki Tani and Kazuchika Ohta reported at a conference of the Japanese Liquid Crystal Society in 2004 that the molecular structure of the immunosuppressant FTY720 is similar to that of a liquid crystal and that they synthesized liquid crystalline derivatives of FTY20 having different alkyl chain lengths [191]. Liquid crystallinity in pharmaceutical compounds is thought to influence their functions, i.e., stability in vivo, solubility, elution rate, and metabolism. In addition, there is a review about the thermotropic and lyotropic liquid crystalline character of existing drugs [192]. In this section, I will describe the current state of liquid crystalline drugs while reviewing my own research.

11.5.2   Relations with Pharmaceutical Research

I received my doctoral degree in engineering from the department of synthetic chemistry of Kyoto University in 1986 under the guidance of Professor Iwao Tabushi on the topic of uranium recovery from seawater. I designed suitable molecules and studied their binding kinetics and equilibrium constants. The Tabushi lab was involved in biomimetic chemistry—the attempt to express the ability to mimic the biological functions by constructing simpler systems. Around 1985, the lab also started liquid crystal research. I joined Nippon Mining Co., Ltd. (later, the company name changed to Japan Energy Corporation, and after that it was integrated with Nippon Oil Corporation. Now it is JX Holdings) in September 1985 and until 2000 I was involved in the research of smectic liquid crystal and especially ferroelectric liquid crystals. I studied the molecular motion of the liquid crystal using ^{13}C NMR, and in 1995 I was allowed to lecture on solid-state NMR as a part-time lecturer at Ochanomizu University under the care of Professor Kayako Hori. I was interested in the behavior of lipid molecules in thin films at that time. A major overhaul of the research direction in Japan Energy Corporation took place in 1999 and as an unfortunate result the liquid crystal research was abolished. Fortunately, I found employment in the Faculty of Science and Technology of Hirosaki University in April 2000, and I was able to transfer chemical compounds and research equipment to Hirosaki with the assistance from Japan Energy Corporation.

In 2001, the JST selected "The creation of high-definition large-screen flat panel display," headed by Professor Tatsuo Uchida of Tohoku University, as a five-year project for the Aomori regional joint research project, and I participated as a group leader to develop nematic display materials. I could allocate research funding, and with the research equipment from Japan Energy Corporation, I could launch my research at Hirosaki University.

Parallel to the development of display materials I was studying the molecular design of materials that produce liquid crystalline phases with hierarchical structure. One of the results was a material that could stabilize the liquid crystalline blue phase. After meeting with Ikuo Kashiwakura who was appointed Professor at Hirosaki University Graduate School of Health Sciences in 2002, I started to work on drug discovery. In particular, I screened liquid crystals and their intermediates during the search of the compounds involved in platelet regeneration.

We observed the desired effects in several compounds and students started to work on this topic for their undergraduate thesis starting in 2004. This topic was popular with female students who wanted to do laboratory research in the medical field. Rie Terasawa, Yuka Takahashi, Yukako Fukushi, Aoi Sasaki, Saori Fukushi, and Rina Tanaka helped with progressing this work. Those students synthesized and evaluated the physical properties of the liquid crystals in my lab and investigated the pharmacological activity in the lab of Professor Kashiwakura.
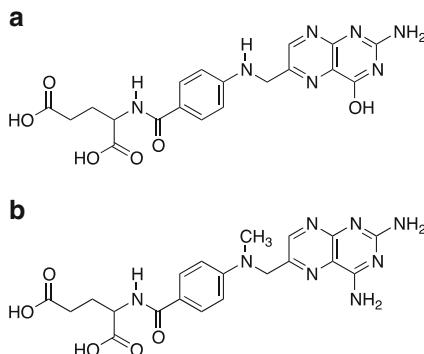
This kind of "double degree" is quite hard for the students. So, it is better for students who desire to continue to graduate school to have an undergraduate research topic from the medical field. Dr. Hiroshi Yokoyama (now professor at Liquid Crystal Institute, Kent State University) was the project leader of the ERATO Yokoyama Liquid Crystal Project and in the final project meeting in 2004 he pointed out that a new development of liquid crystal research would be in the medical field. Each cell in the body contains liquid crystals, but there was no research to correlate pharmacological activity and liquid crystallinity. This was a major motivation for me to earnestly start drug discovery research. Ms. Terasawa played a central role in the investigation of liquid crystalline compounds for platelet regeneration, but since the blood from umbilical cords had to be processed as soon as possible, the measurements were quite challenging. Nevertheless, two publications were published after Yukako Fukushi took over the research topic. Soon after that we moved to the study of antitumor effects of liquid crystal compounds at the suggestion of Professor Kashiwakura.

11.5.3 Antitumor Effect of Liquid Crystals
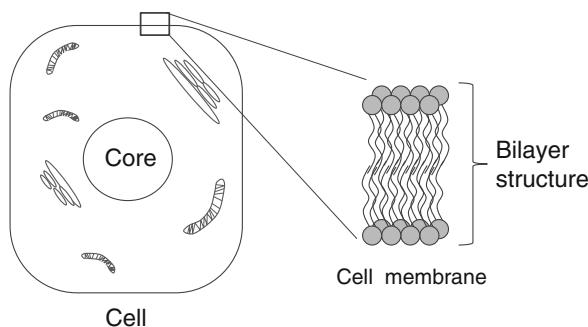
11.5.3.1 Liquid Crystalline Drugs

Chemotherapy for cancer treatment is widespread, and a wide range of natural as well as synthetic materials are known. One of the effective chemotherapies is the treatment with molecular targeting drugs. They are designed to bind to a specific

Fig. 11.24 Molecular structures of (a) folic acid and (b) methotrexate
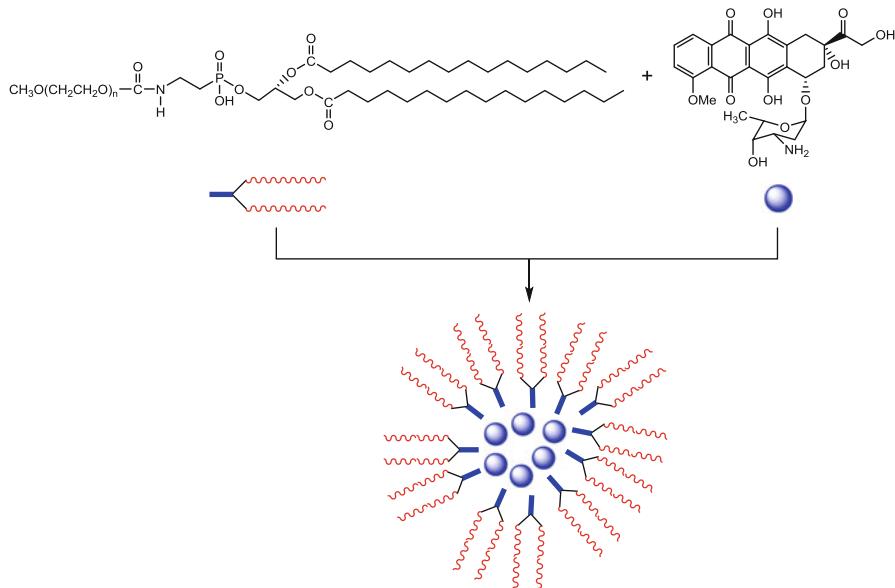
Fig. 11.25 Schematic illustration of a cell

receptor protein and have features that act specifically on cancer cells. Toxicity to normal cells is small and they are effective at nanomolar concentrations. The targeted agents are monoclonal antibodies that bind to a particular antigen on the surface of cancer cells, or inhibitors of tyrosine kinase, an enzyme involved in cell differentiation and proliferation. One example of such a molecular targeted agent is methotrexate, which is used to treat leukemia. Methotrexate is known to exhibit a nematic phase [193]. The molecular structure of methotrexate is similar to folic acid (see Fig. 11.24) and it prevents the folate to bind to the enzyme necessary for DNA synthesis in cancer cells.

On the other hand, it is not a valid chemotherapeutic agent for solid cancers such as lung cancer. It has been found that one of the reasons is that it cannot pass through a multi-layered cell membrane and thus cannot reach the cancer cells. Also, the intracellular distribution of the drug is insufficient [194]. A cell membrane is a bilayer membrane formed by phospholipids, and thus has a hydrophobic inside (Fig. 11.25). For example, the hydroxy groups of the clinically applied doxorubicin make the drug hydrophilic, which hampers permeability through the hydrophobic interior of the cell membrane. Therefore, as shown in Fig. 11.26, we designed a nanocarrier having both hydrophilic and hydrophobic moieties that can incorporate doxorubicin to the inner hydrophilic part. Tang et al. reported that such a nanocarrier forms aggregates with a diameter of 10 to 20 nm in which the

Fig. 11.26 Polyethylene glycol-phosphatidylethanolamine based nanocarrier of doxorubicin
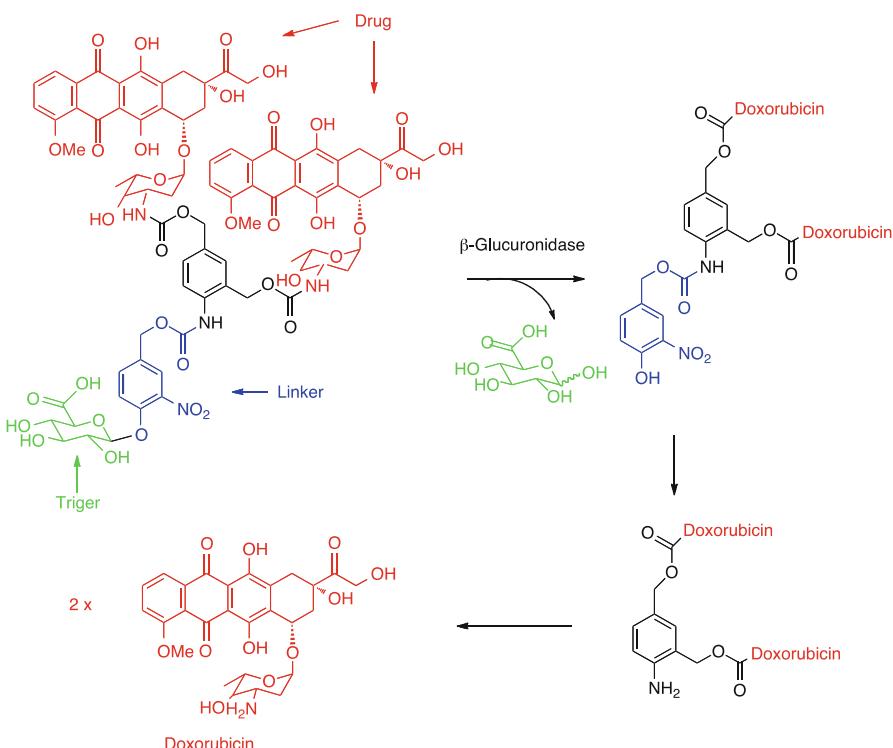
hydrophobic moiety is directed outwards. This increases the membrane permeability and improves antitumor effect compared with doxorubicin alone [195].

Meanwhile, there are the so-called prodrugs, which are drug precursors that are chemically modified and converted to active compounds with the desired pharmacological effect after reaching the target site. Figure 11.27 shows an example of a prodrug of doxorubicin [196]. Upon reaching the target site, it is converted to doxorubicin by hydrolytic enzymes.
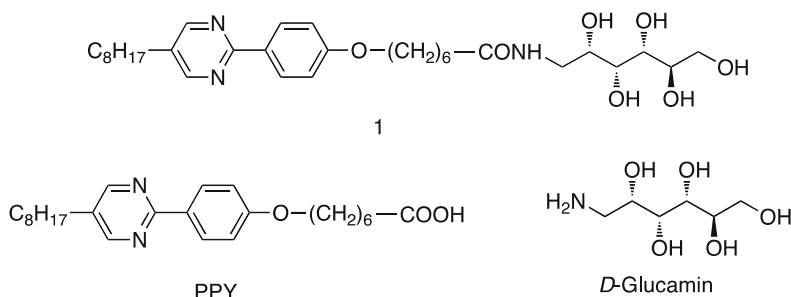
As I have described above, cell membrane permeability is important in solid tumors. I expect that liquid crystals that are derived from amphiphilic compounds show an affinity to the plasma membrane by their self-assembly and thus exhibit a high anticancer effect.

11.5.3.2 *D*-Glucamine Derivative Inhibits the Cell Growth of A549 Human Lung Cancer Cells

Cell membranes are covered with various sugar chains. We investigated the pharmacological activity of a *D*-glucamine-containing phenyl pyrimidine liquid crystal compound **1** with the A549 lung cancer cell line [197]. For comparison, we also evaluated in the same way both precursor compounds, *D*-glucamine and PPY (Fig. 11.28).
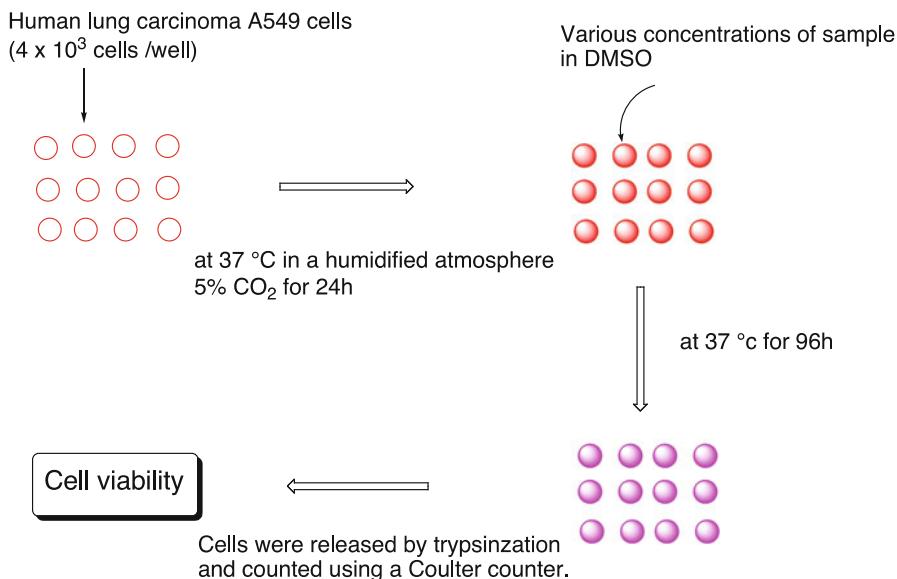
Fig. 11.27 β−Glucuronidase-catalyzed drug release mechanism of a dendritic glucuronide prodrug of doxorubicin [8]

Fig. 11.28 Molecular structures of compound **1**, **PPY**, and *D*-glucamine

Figure 11.29 shows the pharmacological activity of these compounds dissolved in DMSO and cultured in a cell liquid medium. Cell viability was evaluated by the Coulter cell count system. In comparison with the DMSO control, *D*-glucamine, and PPY, only compound **1** showed significant cytostatic effect at concentrations of 20 µM, as can be seen in Table 11.1.

Human lung carcinoma A549 cells
(4 x 10³ cells /well)

Various concentrations of sample
in DMSO

at 37 °C in a humidified atmosphere
5% CO₂ for 24h

at 37 °c for 96h

Cell viability

Cells were released by trypsinzation
and counted using a Coulter counter.

Fig. 11.29 Cell growth inhibition assay
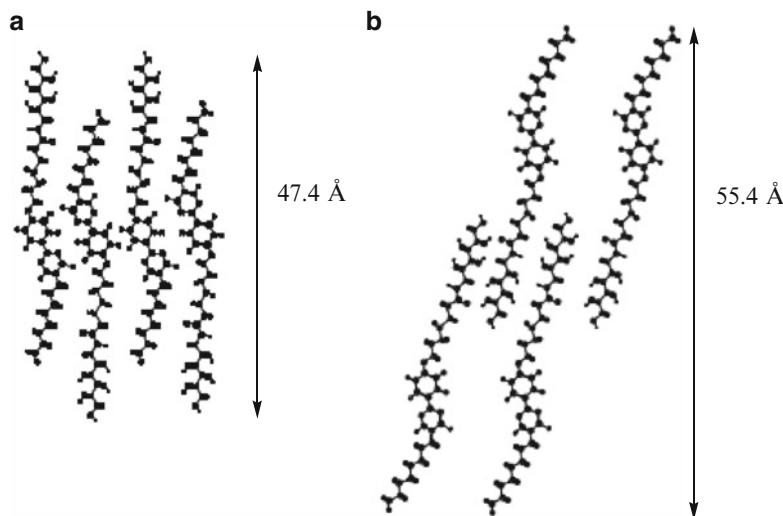
Table 11.1 Cell viability expressed as a percentage (%) relative to solvent (DMSO)-treated control incubations

Conc./μM	1	PPY	D-Glucamine	Mixture[a]
1	102 ± 4	105 ± 4	110 ± 3	103 ± 5
10	66 ± 0	91 ± 5	93 ± 1	86 ± 6
20	31 ± 10	89 ± 2	101 ± 3	80 ± 5
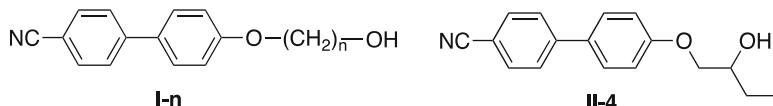
[a]An equimolar mixture of **PPY** and D-glucamine

   Upon cooling from the isotropic melt, compound **1** forms a smectic A phase at 194 °C, followed by an unidentified biaxial smectic X phase at 141 °C. On the other hand, the equimolar mixture and D-glucamine and PPY did not show liquid crystallinity. The layer spacing of the smectic phase of compound **1** decreases with decreasing temperature from 4.9 to 4.3 nm in the SmA phase. The SmX phase has a layer spacing of 5.5 nm. The molecular length is estimated to be about 3.7 nm and Fig. 11.30 shows the layer structure model of the SmX and SmA phases.

   Based on the interaction of the phenyl pyrimidine hydrophobic groups, the sugar moiety of the hydrophilic faces towards the outside of the SmA layer. On the other hand, the sugar moiety interactions in the SmX phase lead to a bilayer structure in which the molecular long axis is inclined and the hydrophobic moiety faces outward. We assume that the compound shows a high membrane permeability by switching from a hydrophilic to a hydrophobic aggregate while passing throughout the cell membrane.

Fig. 11.30 Molecular organization model for the SmA phase (**a**) and for the SmX phase (**b**)

Fig. 11.31 Molecular structures of compounds **I-n** and **II-4**

11.5.3.3 A549 Lung Cancer Cell Growth Inhibition Effect of a Cyanobiphenyl Derivative
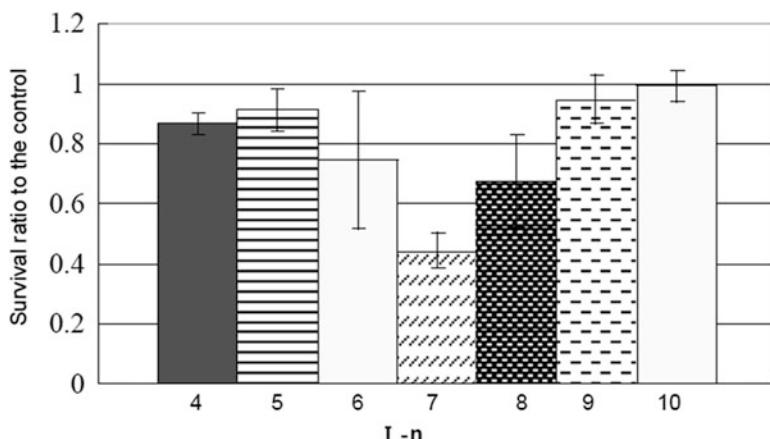
We investigated the effect of alkyl chain length of cyanobiphenyl compounds that had a primary alcohol end group (compounds I-*n*, where *n* is the number of carbon atoms of the alcohol) on the growth inhibition of A549 cells [198]. In addition, a compound bearing a secondary alcohol was synthesized (compound II-4) for comparison. Figure 11.31 shows the structure of the compounds, and their phase transition temperatures are shown in Table 11.2. All compounds except I-1 and II-4 show an enantiotropic nematic phase [199–201]; I-1 and II-4 are monotropic nematic.

The viability of A549 cells at 5 μM concentrations of each compound is shown in Fig. 11.32, as compared to the DMSO control. The highest antitumor activity was found for I-7, which also had the widest temperature range of the nematic phase. Then, we evaluated the lyotropic liquid crystal phase of I-7 (antitumor activity) and I-10 (no antitumor activity) in DMSO–water mixtures by polarizing microscopy. Both compounds did not show a liquid crystalline phase at 5 μM concentration. In the range of 0.1–5 mM, I-7 showed a liquid crystal phase, but I-10 did not. This suggests that there is a correlation between liquid crystallinity and antitumor activity against A549.

Table 11.2 Transition temperatures (°C) of compounds I-n and II-4 at a rate of 5 °C min^{-1a}

Compound	Cry	N	Iso	ΔT_N/K
I-4	• 132	(• 120)	•	0
I-5	• 90	• 104	•	14
I-6	• 97	• 109	•	12
I-7	• 78	• 100	•	22
I-8	• 89	• 102	•	13
I-9	• 85	• 96	•	11
I-10	• 96	• 97	•	1
II-4	• 85	(• 68)	•	0

[a]Brackets denote a monotropic transition. ΔT_N: Temperature range of the enantiotropic nematic phase

Fig. 11.32 Inhibition of cell proliferation by each cyanobiphenyl derivative **I-n** at a concentration of 5 µM in A549 human lung cancer cell lines for 96 h. Cell viability was expressed as a percentage relative to solvent (DMSO)-treated control incubations

Table 11.3 Inhibition of cell proliferation by compounds I-4 and II-4 at 10 µM in A549 human lung cancer cell lines for 96 h or in WI-38 fibroblast cell lines for 168 h. The survival ratio as a percentage (%) to solvent (DMSO)-treated control culture is shown

Compound	A549	WI-38
I-4	56 ± 9	140 ± 32
II-4	55 ± 5	47 ± 20

Next, we examined the effects on normal cells (fibroblast WI-38). Primary alcohol compound (I-4 to I-7) did not affect the proliferation of normal cells, but the secondary alcohol compound II-4 showed inhibition. The difference on the cell growth of I-4 and II-4 is shown in Table 11.3. The secondary alcohol inhibited the cell growth of both WI-38 and A549, while the primary alcohol compound
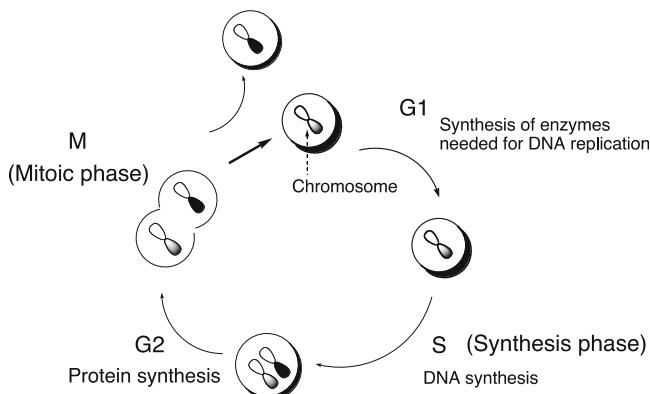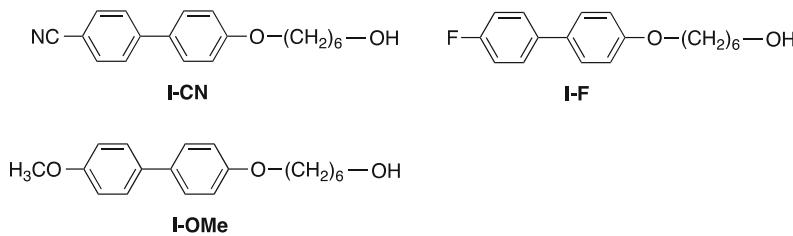
Fig. 11.33 Cell cycle

inhibited only the growth of A549 and had no effect on normal cells. There is a possibility that cancer cells and normal cells can recognize the difference in the position of the hydroxyl group.
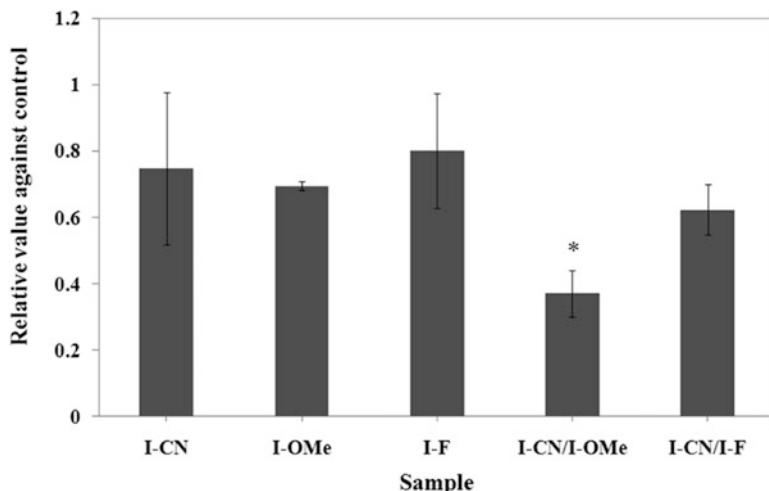
We also investigated the effect of I-7 compounds on the cell cycle (Fig. 11.33). The synthesis of enzymes for DNA replication takes place in the G1 phase, the replication of DNA in the S phase, the synthesis of proteins in the G2 phase, and finally, the cell division in the M phase. Cancer cells proliferate when the regulation of this cell cycle malfunctions. There are two paths in which antitumor agents act on cells: one is associated with cell death, and the other one simply slows cell growth. Cell death is classified into apoptosis and necrosis. The spontaneous removal of unwanted cells is called apoptosis, and necrosis refers to cell death related to inflammation caused by burns and poison. After the addition of I-7, 78.6 % of cells were in the G1 phase compared to 59.8 % in the control group. On the other hand, the rate of apoptosis was not different. Thus, I-7 slows the transition to the S phase from G1 phase, but it does not induce apoptosis.

11.5.3.4 Effect of Molecular Assembly

Since there was a correlation between the liquid crystalline state and the antitumor activity in cyano biphenyl derivatives, we vigorously designed molecules based on intermolecular interactions [202]. Figure 11.34 shows the molecular structures of the compounds we investigated. They are characterized by having a hydroxyl group at the end of the hydrocarbon side chain of a biphenyl that is substituted by an electron-donating or electron-withdrawing group. Figure 11.35 shows the effect of the three compounds and two of their equimolar mixtures on the proliferation of A549 cells. Mixed systems of the electron-donating I-OMe compound with the electron-withdrawing I-CN compound shows a significant inhibition. We found that

Fig. 11.34 Mesogenic compounds possessing an electron-withdrawing group or an electron-donating group

Fig. 11.35 Effects of mesogenic materials on the growth of the A549 human lung cancer cell line. The culture was conducted in liquid media containing 5 μM of each sample for 96 h. The binary mixtures contained 2.5 μM of each component. *$p < 0.05$ using Student's *t*-test
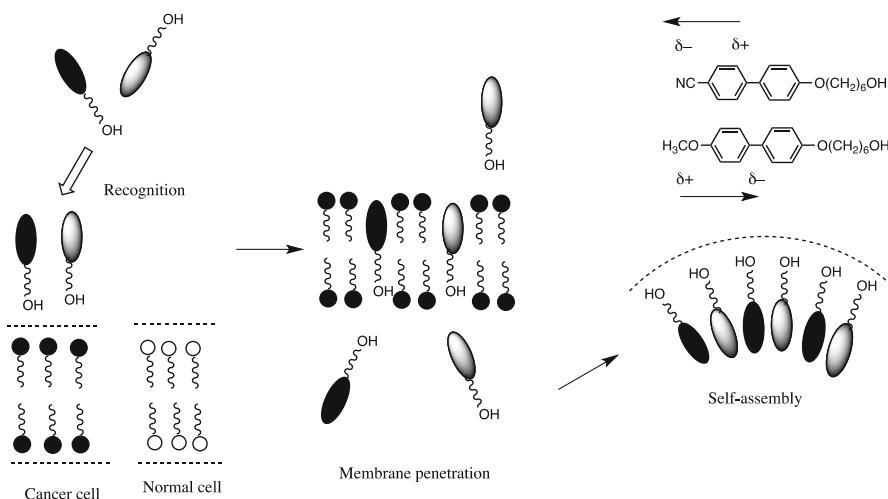
this system also slows down the transition from the G1 phase to the S phase, but did not induce apoptosis. On the other hand, the mixture did not affect the growth of normal cells.

The I-CN shows a nematic phase with a phase transition temperature to the isotropic phase at 109 °C, but I-OMe and I-F are not liquid crystalline. Furthermore, the nematic phase that is induced in the I-CN/I-OMe mixture has a clearing point that is 16 K higher, at 125 °C, which suggests the existence of intermolecular interactions in the equimolar mixture. Meanwhile, the equimolar mixture of both electron-withdrawing compounds I-CN and I-F has no special interaction between its components, and the clearing temperature drops to 87 °C, which is 22 K less than the pure I-CN.

Using DMSO–water as a mixed solvent, a 500 μM equimolar mixture of I-CN/I-OMe showed a liquid crystal texture specific to a spherical lamellar structure.

Table 11.4 Critical aggregation concentration (CAC) of each sample

Sample	CAC/μM
I-CN	30 ± 8
I-OMe	30 ± 11
I-F	57 ± 38
Equimolar mixture of **I-CN** and **I-OMe**	8 ± 5
Equimolar mixture of **I-CN** and **I-F**	44 ± 10
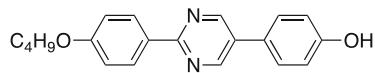
Fig. 11.36 Model for recognition, membrane penetration, and self-assembly of a **I-CN/I-OMe** mixture

The minimum concentration required for aggregate formation (CAC) in water can be obtained by UV turbidity measurements. The lower the CAC, the higher the aggregate formation. Table 11.4 shows that the equimolar mixed system of I-CN/I-Ome has the lowest CAC and thus forms the most stable aggregates in water.

Figure 11.36 explains the process of antitumor activity of the I-CN/I-OMe mixed system based on the above results. Aggregation in pure I-OMe and I-CN is caused by dipole–dipole interaction and microphase separation based on hydrophilic/hydrophobic interaction. Microphase separation will lead to a parallel alignment, while the dipole–dipole interaction will produce an antiparallel alignment of the molecules. In the pure compounds, parallel and antiparallel orientations are in equilibrium, but in the mixture of both, the dipole–dipole interaction leads to a parallel array. Those aggregates have the hydroxyl groups at one side, and they can recognize the difference in surface structure of normal cells and cancer cells, which leads to a penetration of the small molecules through the cell membrane.

Fig. 11.37 Mesogenic
compound inducing
apoptosis

C_4H_9O —⟨ ⟩— (pyrimidine) —⟨ ⟩— OH

11.5.4 Future Development [203]

In the medical field, liquid crystal display is used to display diagnostic imaging and electronic medical records. Liquid crystal tunable filters have been developed for the observation of biological tissue with higher contrast. Thus, the optical function of liquid crystal materials is widely used in the medical field in this way. Beyond this, some studies detected liquid crystal interactions between biological molecules [204]. The molecular-level intermolecular interactions between ligand and receptor molecules in vivo can be visualized by converting it to a change in alignment of liquid crystal molecules that can be visualized macroscopically. I expect that this new tool in the detection of interactions in biological systems will be expanded in the future.

Then, there are liquid crystalline drug delivery systems (DDS). Anticancer drugs that enclose the water-soluble doxorubicin hydrochloride in a bilayer membrane phospholipid liposomes modified with polyethylene glycol [205] were approved in Japan in 2007.

Furthermore, DDS that react to pH change in diverse sites as the stomach or the oral cavity were made from glyceryl linoleic ester, linoleic acid, and phloroglucinol as a hydrophilic model drug. Depending on the pH, it was possible to control the liquid crystal structure of the mixtures [206]. Considering that the liquid crystal cell membrane plays an important role in the uptake of drugs, liquid crystal DDS, including the cubic phase, have been studied actively.

Under these circumstances I began to study the pharmacological activity and membrane permeability to liquid crystalline molecules, and I designed new type of low molecular weight drugs. There was no induction of apoptosis in cancer cells in the compounds discussed in this paper, but the phenol derivative shown in Fig. 11.37 induces apoptosis in solid cancers, such as lung cancer A549 cells [207] and leukemia K562 cells [208]. The correlation between apoptosis and liquid crystallinity is not made clear yet, and thus it was not introduced in this paper. The mechanism of the antitumor effect was different in a compound with a slightly different molecular structure.

In this section I showed that liquid crystalline molecular assemblies have the potential to identify the surface structure of normal and cancer cells, because of the differences in the environment inside and outside of the bilayer membrane. Furthermore, I believe that new molecular targeted agents can be obtained by introducing an interaction site with a target protein. The study of liquid crystals in the pharmaceutical field has just begun, and I expect future developments.

References

1. D. Adam, F. Closs, T. Frey, D. Funhoff, D. Haarer, J. Ringsdorf, P. Schuhmacher, K. Siemensmeyer, Phys. Rev. Lett. **70**, 457–460 (1993)
2. M. Funahashi, J. Hanna, Phys. Rev. Lett. **78**, 2184 (1997)
3. K. Tokunaga, J. Hanna, J. Phys. Chem. B **111**, 12041 (2007)
4. M. Funahashi, J. Hanna, Appl. Phys. Lett. **71**, 602 (1997)
5. M. Funahashi, J. Hanna, Chem. Phys. Lett. **397**, 319 (2004)
6. H. Ahn, A. Ohno, J. Hanna, Jpn. J. Appl. Phys. **44**, 3764 (2005)
7. H. Iino, J. Hanna, D. Haarer, Phys. Rev. B **72**, 193203 (2005)
8. K. Tokunaga, Y. Takayashiki, H. Iino, J. Hanna, Phys. Rev. B **79**, 033201 (2009)
9. A. Ohno, J. Hanna, Appl. Phys. Lett. **82**, 751 (2003)
10. K. Tokunaga, H. Iino, J. Hanna, Mol. Cryst. Liq. Cryst. **510**, 241 (2009)
11. H. Maeda, M. Funahash, J. Hanna, Mol. Cryst. Liq. Cryst. **366**, 369 (2001)
12. H. Maeda, M. Funahashi, J. Hanna, Mol. Cryst. Liq. Cryst. **346**, 193 (2000)
13. H. Zhang, J. Hanna, Appl. Phys. Lett. **85**, 51–5253 (2004)
14. Y. Takayashiki, H. Iino, T. Kobori, T. Usui, J. Hanna, Annual Meeting of the Japanese Liquid Crystal Society (Tokyo, 2011), 3c01
15. H. Iino, J. Hanna, R.J. Bushby, B. Movaghar, B.J. Whitaker, M.J. Cook, Appl. Phys. Lett. **87**, 132102 (2005)
16. K. Kogo, T. Goda, M. Funahashi, J. Hanna, Appl. Phys. Lett. **73**, 1595 (1998)
17. M. Funahashi, N. Tamaoki, Chem. Phys. Chem. **7**, 1193 (2006)
18. H. Meng, F. Sun, M.B. Goldfinger, G.D.J.Z. Li, W.J. Marshall, G.S. Blackman, J. Amer. Chem. Soc. **127**, 2406 (2005)
19. H. Iino, J. Hanna, Adv. Mater. **23**, 1748 (2011)
20. H. Ebata, T. Izawa, E. Miyazaki, K. Takimiya, M. Ikeda, H. Kuwabara, T. Yui, J. Am. Chem. Soc. **129**, 15732 (2007)
21. B. KosĬata, V. Kozmik, J. Svoboda, A.V. Novotana, P. VanaÂk, A.M. Glogarva, Mol. Cryst. Liq. Cryst. **30**, 603 (2003)
22. J. Hanna, Y. Takayashiki, H. Iino, T. Kobori, T. Usui, Autumn Meetings of Japanese Liquid Crystal Society (Tokyo, 2011), 1p-R-11
23. H. Iino, T. Kobori, T. Usui, Y. Takayashiki, H. Iino, A. Ohno, 72th Autumn Meetings of Japanese Society of Applied Physics (Yamagata, 2011), 1p-R-13
24. N.S. Sariciftci, L. Smilowitz, A.J. Heeger, F. Wudl, Science **258**, 1474 (1992)
25. L. Schmidt-Mende, A. Fechtenkotter, K. Mullen, E. Moons, R.H. Friend, J.D. MacKenzie, Science **293**, 1119 (2001)
26. T. Hori, Y. Miyake, N. Yamasaki, H. Yoshida, A. Fujii, Y. Shimizu, M. Ozaki, Appl. Phys. Express **3**, 101602 (2010)
27. K. Nakano, H. Iino, T. Usui, J. Hanna, 72th Autumn Meetings of Japanese Society of Applied Physics (Yamagata, 2011), 1p-L-3
28. H. Iino, J. Hanna, Jpn. J. Appl. Phys. Express Letter **46**, L867 (2006)
29. A. G. Lee, *Rhodopsin and G-Protein Linked Receptors, Part A* (JAI Press, Greenwich, 1996)
30. S. Tazuke, S. Kurihara, T. Ikeda, Chem. Lett. **16**, 911 (1987)
31. T. Ikeda, J. Mater. Chem. **13**, 2037 (2003)
32. T. Ikeda, S. Horiuchi, D.B. Karanjit, S. Kurihara, S. Tazuke, Macromolecules **23**, 42 (1990)
33. T. Ikeda, S. Kurihara, D.B. Karanjit, S. Tazuke, Macromolecules **23**, 3938 (1990)
34. T. Ikeda, O. Tsutsumi, Science **268**, 1873 (1995)
35. M. Warner, E. Terentjev, *Liquid Crystal Elastomers* (Clarendon, Oxford, 2003)
36. P.G. de Gennes, C. R. Acad. Sci. Ser. B **281**, 101 (1975)
37. P.G. de Gennes, M. Hébert, R. Kant, Macromol. Symp. **113**, 39 (1997)
38. H. Finkelmann, H. Kock, G. Rehage, Makromol. Chem. Rapid Commun. **2**, 317 (1981)
39. H. Finkelmann, E. Nishikawa, G.G. Pereira, M. Warner, Phys. Rev. Lett. **87**, 015501–1 (2001)

40. T. Ikeda, M. Nakano, Y. Yu, O. Tsutsumi, A. Kanazawa, Adv. Mater. **15**, 201 (2003)
41. Y. Yu, M. Nakano, T. Ikeda, Nature **425**, 145 (2003)
42. N. Tabiryan, S. Serak, X.-M. Dai, T. Bunning, Opt. Express **13**, 7442 (2005)
43. M. Kondo, Y. Yu, T. Ikeda, Angew. Chem. Int. Ed. **45**, 1378 (2006)
44. M. Kondo, M. Sugimoto, M. Yamada, Y. Naka, J. Mamiya, M. Kinoshita, A. Shishido, Y. Yu, T. Ikeda, J. Mater. Chem. **20**, 117 (2010)
45. J. Mamiya, A. Yoshitake, M. Kondo, Y. Yu, T. Ikeda, J. Mater. Chem. **18**, 63 (2008)
46. T. Yoshino, M. Kondo, J. Mamiya, M. Kinoshita, Y. Yu, T. Ikeda, Adv. Mater. **22**, 1361 (2010)
47. M. Camacho-Lopez, H. Finkelmann, P. Palffy-Muhoray, M. Shelley, Nat. Mater. **3**, 307 (2004)
48. C.L. van Oosten, C.W.M. Bastiaansen, D.J. Broer, Nat. Mater. **8**, 677 (2009)
49. T.J. White, N. Tabiryan, S.V. Serak, U.A. Hrozhyk, V.P. Tondiglia, H. Koerner, R.A. Vaia, T.J. Bunning, Soft Matter **4**, 1796 (2008)
50. S. Serak, N. Tabiryan, R. Vergata, T.J. White, R.A. Vaia, T.J. Bunning, Soft Matter **6**, 779 (2010)
51. M. Yamada, M. Kondo, J. Mamiya, Y. Yu, M. Kinoshita, C.J. Barrett, T. Ikeda, Angew. Chem. Int. Ed. **47**, 4986 (2008)
52. M. Yamada, M. Kondo, R. Miyasaka, Y. Naka, J. Mamiya, M. Kinoshita, A. Shishido, Y. Yu, C.J. Barrett, T. Ikeda, J. Mater. Chem. **19**, 60 (2009)
53. E. Yablonovitch, Phys. Rev. Lett. **58**, 2059 (1987)
54. S. John, Phys. Rev. Lett. **58**, 2486 (1987)
55. K. Yoshino, K. Tada, M. Ozaki, A.A. Zakhidov, R.H. Baughman, Jpn. J. App. Phys. **36**, L714 (1997)
56. V.N. Bogomolov, S.V. Gaponenko, I.N. Germanenko, A.M. Kapitonov, E.P. Petrov, N.V. Gaponenko, A.V. Prokofiev, A.N. Ponyavina, N.I. Silvanovich, S.M. Samoilovich, Phys. Rev. E **55**, 7619 (1997)
57. K. Busch, S. John, Phys. Rev. E **58**, 3896 (1998)
58. K. Yoshino, Manufacturing and Technology (in Japanese). **50**, 26 (1998)
59. K. Yoshino, S. Tatsuhara, Y. Kawagishi, M. Ozaki, A.A. Zakhidov, Z.V. Vardeny, Jpn. J. Appl. Phys. **37**, L1187 (1998)
60. K. Yoshino, S.B. Lee, S. Tatsuhara, Y. Kawagishi, M. Ozaki, A.A. Zakhidov, Appl. Phys. Lett. **73**, 3506 (1998)
61. K. Yoshino, S. Tatsuhara, Y. Kawagishi, M. Ozaki, A.A. Zakhidov, Z.V. Vardeny, Appl. Phys. Lett. **74**, 2590 (1999)
62. S. Sato, H. Kajii, Y. Kawagishi, A. Fujii, M. Ozaki, K. Yoshino, Jpn. J. Appl. Phys. **38**, L1475 (1999)
63. A.A. Zakhidov, R.H. Baughman, Z. Iqbal, C. Cui, I. Khayrullin, S.O. Dantas, J. Marti, V.G. Ralchenko, Science **282**, 897 (1998)
64. K. Yoshino, H. Kajii, Y. Kawagishi, M. Ozaki, A.A. Zakhidov, R.H. Baughman, Jpn. J. Appl. Phys. **38**, 4926 (1999)
65. H. Kajii, Y. Kawagishi, H. Take, K. Yoshino, A.A. Zakhidov, R.H. Baughman, J. Appl. Phys. **88**, 758 (2000)
66. K. Yoshino, S. Satoh, Y. Shimoda, Y. Kawagishi, K. Nakayama, M. Ozaki, Jpn. J. Appl. Phys. **38**, L961 (1999)
67. K. Yoshino, Y. Shimoda, Y. Kawagishi, K. Nakayama, M. Ozaki, Appl. Phys. Lett. **75**, 932 (1999)
68. K. Busch, S. John, Phys. Rev. Lett. **83**, 967 (1999)
69. Y. Shimoda, M. Ozaki, K. Yoshino, Appl. Phys. Lett. **79**, 3627 (2001)
70. D. Kang, J.E. Maclennan, N.A. Clark, A.A. Zakhidov, R.H. Baughman, Phys. Rev. Lett. **86**, 4052 (2001)
71. Q.-B. Meng, C.-H. Fu, S. Hayami, Z.-Z. Gu, O. Sato, A. Fujishima, J. Appl. Phys. **89**, 5794 (2001)

72. M. Ozaki, Y. Shimoda, M. Kasano, K. Yoshino, Adv. Mater. **14**, 514 (2002)
73. H. Takeda, K. Yoshino, J. Appl. Phys. **92**, 5658 (2002)
74. M. Campbell, D.N. Sharp, M.T. Harrison, R.G. Denning, A.J. Turberfield, Nature **404**, 53 (2000)
75. T. Kondo, S. Matsuo, S. Juodkazis, H. Misawa, Appl. Phys. Lett. **79**, 725 (2001)
76. R.L. Sutherland, L.V. Natarajan, V.P. Tondiglia, T.J. Bunning, Chem. Mater. **5**, 1533 (1993)
77. K. Tanaka, K. Kato, S. Tsuru, S. Sakai, J. SID **2**, 37 (1994)
78. V.P. Tondiglia, L.V. Natarajan, R.L. Sutherland, D. Tomlin, T.J. Bunning, Adv. Mater. **14**, 187 (2002)
79. M.J. Escuti, J. Qi, G.P. Crawford, Opt. Lett. **28**, 522 (2003)
80. T. Matsui, M. Ozaki, K. Yoshino, Appl. Phys. Lett. **83**, 422 (2003)
81. T. Matsui, M. Ozaki, K. Yoshino, Jpn. J. Appl. Phys. **42**, L1462 (2003)
82. T. Matsui, M. Ozaki, K. Yoshino, J. Opt. Soc. Am. B **21**, 1651 (2004)
83. I.P. Il'chishin, E.A. Tikhonov, V.G. Tishchenko, M.T. Shpak, Sov. J. Quant. Electron. **8**, 1487 (1978)
84. L. S. Goldberg, J. M. Schnur, U. S. Patent 3,771,065 (1973)
85. I.P. Il'chishin, E.A. Tikhonov, V.G. Tishchenko, M.T. Shpak, JETP Lett. **32**, 24 (1980)
86. J. Martorell, N.M. Lawandy, Phys. Rev. Lett. **6**, 1877 (1990)
87. J.P. Dowling, M. Scalora, M.J. Bloemer, C.M. Bowden, J. Appl. Phys. **75**, 1896 (1994)
88. V.I. Kopp, B. Fan, H.K. Vithana, A.Z. Genack, Opt. Lett. **23**, 1707 (1998)
89. K. Funamoto, M. Ozaki, K. Yoshino, Jpn. J. Appl. Phys. **42**, L1523 (2003)
90. B. Taheri, A.F. Munoz, P. Palffy-Muhoray, R. Twieg, Mol. Cryst. Liq. Cryst. **358**, 73 (2001)
91. A. Munoz, F.P. Palffy-Muhoray, B. Taheri, Opt. Lett. **26**, 804 (2001)
92. E. Alvarez, M. He, A.F. Munoz, P. Palffy-Muhoray, S.V. Serak, B. Taheri, R. Twieg, Mol. Cryst. Liq. Cryst. **369**, 75 (2001)
93. K. Shirota, H.B. Sun, S. Kawata, Appl. Phys. Lett. **84**, 1632 (2004)
94. F. Araoka, K.C. Shin, Y. Takanishi, K. Ishikawa, H. Takezoe, Z. Zhu, T.M. Swager, J. Appl. Phys. **94**, 279 (2003)
95. S. Furumi, S. Yokoyama, A. Otomo, S. Mashiko, Appl. Phys. Lett. **82**, 16 (2003)
96. F.J. Kahn, Phys. Rev. Lett. **24**, 209 (1970)
97. M. Ozaki, M. Kasano, K. Funamoto, R. Ozaki, T. Matsui, K. Yoshino, Proc. SPIE **5213**, 111 (2003)
98. M. Ozaki, M. Kasano, D. Ganzke, W. Haase, K. Yoshino, Adv. Mater. **14**, 306 (2002)
99. M. Ozaki, M. Kasano, T. Kitasho, D. Ganzke, W. Haase, K. Yoshino, Adv. Mater. **15**, 974 (2003)
100. M. Kasano, M. Ozaki, D. Ganzke, W. Haase, K. Yoshino, Appl. Phys. Lett. **82**, 4026 (2003)
101. T. Matsui, R. Ozaki, K. Funamoto, M. Ozaki, K. Yoshino, Appl. Phys. Lett. **81**, 3741 (2002)
102. W. Cao, A. Munoz, P. Palffy-Muhoray, B. Taheri, Nat. Mater. **1**, 111 (2002)
103. H. Kikuchi, M. Yokota, Y. Hisakado, H. Yang, T. Kajiyama, Nat. Mater. **1**, 64 (2002)
104. S. Yokoyama, S. Mashiko, H. Kikuchi, K. Uchida, T. Nagamura, Adv. Mater. **18**, 48 (2006)
105. Y.-C. Yang, C.S. Kee, J.E. Kim, H.Y. Par, J.C. Lee, Y.J. Jeon, Phys. Rev. E **60**, 6852 (1999)
106. V.I. Kopp, A.Z. Genack, Phys. Rev. Lett. **89**, 033901 (2002)
107. T. Matsui, M. Ozaki, K. Yoshino, Phys. Rev. E **69**, 061715 (2004)
108. V.I. Kopp, R. Bose, A.Z. Genack, Opt. Lett. **28**, 349 (2003)
109. M. Ozaki, R. Ozaki, T. Matsui, K. Yoshino, Jpn. J. Appl. Phys. **42**, L472 (2003)
110. J. Schmidtke, W. Stille, H. Finkelmann, Phys. Rev. Lett. **90**, 083902 (2003)
111. M.H. Song, B. Park, K.-C. Shin, T. Ohta, Y. Tsunoda, H. Hoshi, Y. Takanishi, K. Ishikawa, J. Watanabe, S. Nishimura, T. Toyooka, Z. Zhu, T.M. Swager, H. Takezoe, Adv. Mater. **16**, 779 (2004)
112. H. Yoshida, R. Ozaki, K. Yoshino, M. Ozaki, Thin Solid Films **509**, 197 (2006)
113. H. Yoshida, C.H. Lee, A. Fujii, M. Ozaki, Appl. Phys. Lett. **89**, 231913 (2006)
114. H. Yoshida, C.H. Lee, Y. Matsuhisa, A. Fujii, M. Ozaki, Adv. Mater. **19**, 1187 (2007)
115. H. Yoshida, C.H. Lee, Y. Miura, A. Fujii, M. Ozaki, Appl. Phys. Lett. **90**, 071107 (2007)

116. R. Ozaki, T. Matsui, M. Ozaki, K. Yoshino, Jpn. J. App. Phys. **41**, L1482 (2002)
117. R. Ozaki, T. Matsui, M. Ozaki, K. Yoshino, Appl. Phys. Lett. **82**, 593 (2003)
118. R. Ozaki, M. Ozaki, K. Yoshino, Jpn. J. Appl. Phys. **42**, L669 (2003)
119. R. Ozaki, Y. Matsuhisa, M. Ozaki, K. Yoshino, Appl. Phys. Lett. **84**, 1844 (2004)
120. R. Ozaki, T. Sanda, H. Yoshida, Y. Matsuhisa, M. Ozaki, K. Yoshino, Jpn. J. Appl. Phys. **45**, L493 (2006)
121. R. Ozaki, Y. Matsuhisa, H. Yoshida, K. Yoshino, M. Ozaki, J. App. Phys. **100**, 023102 (2006)
122. J. Hwang, M.H. Song, B. Park, S. Nishimura, T. Toyooka, J.W. Wu, Y. Takanishi, K. Ishikawa, H. Takezoe, Nat. Mater. **4**, 383 (2005)
123. Y. Matsuhisa, R. Ozaki, M. Ozaki, K. Yoshino, Jpn. J. Appl. Phys. **44**, L629 (2005)
124. Y. Matsuhisa, R. Ozaki, K. Yoshino, M. Ozaki, Appl. Phys. Lett. **89**, 101109 (2006)
125. Y. Matsuhisa, R. Ozaki, Y. Takao, M. Ozaki, J. Appl. Phys. **101**, 033120 (2007)
126. Y. Matsuhisa, W. Haase, A. Fujii, M. Ozaki, Appl. Phys. Lett. **89**, 201112 (2007)
127. M. Ozaki, K. Yoshino, EKISHO **8**, 143 (2002)
128. M. Ozaki, OYO BUTURI **75**, 1445 (2006)
129. M. Ozaki, Y. Matsuhisa, H. Yoshida, R. Ozaki, A. Fujii, in *Nanophotonic Materials Photonic Crystals, Plasmonics, and Metamaterials* ed. by R. B. Wehrspohn, H.-S. Kitzerow, K. Busch, Weimheim (Wiley, 2008), Chapter 14
130. L. M. Blinov, R. Bartelino (ed.), *Liquid Crystal Microlasers* (Transworld Research Network, Kerala, 2010)
131. H. Yoshida, Y. Inoue, T. Isomura, Y. Matsuhisa, A. Fujii, M. Ozaki, Appl. Phys. Lett. **94**, 093306 (2009)
132. Y. Inoue, H. Yoshida, Kenta Inoue, A. Fujii, M. Ozaki. Appl. Phys. Express **3**, 102702 (2010)
133. Y. Inoue, H. Yoshida, K. Inoue, T. Kumagai, H. Kubo, A. Fujii, M. Ozaki, Jpn. J. Appl. Phys. **50**, 072702 (2011)
134. C. Mowatt, S.M. Morris, T.D. Wilkinson, H.J. Coles, Appl. Phys. Lett. **97**, 251109 (2010)
135. Y. Takanishi, Y. Ohtsuka, G. Suzaki, S. Nishimura, H. Takezoe, Opt. Express **18**, 12909 (2010)
136. M. Uchimura, Y. Watanabe, F. Araoka, J. Watanabe, H. Takezoe, G. Konishi, Adv. Mater. **22**, 4473 (2010)
137. A. Muñoz, M.E. McConney, T. Kosa, P. Luchette, T.J. Bunning, L. Sukhomlinova, B. Taheri, Opt. Lett. **37**, 2904 (2012)
138. Y. Inoue, H. Yoshida, K. Inoue, Y. Shiozaki, H. Kubo, A. Fujii, M. Ozaki, Adv. Mater. **23**, 5498 (2011)
139. M. Ojima, N. Numata, Y. Ogawa, K. Murata, H. Kubo, A. Fujii, M. Ozaki, Appl. Phys. Express **2**, 086001 (2009)
140. Y. Ogawa, M. Ojima, K. Murata, Y. Fujiwara, H. Kubo, H. Yoshida, A. Fujii, M. Ozaki, Mol. Cryst. Liq. Cryst. **545**, 85 (2011)
141. I.C. Khoo, D.H. Werner, X. Liang, A. Diaz, B. Weiner, Opt. Lett. **31**, 2592 (2006)
142. H. Yoshida, T. Matsui, A. Miura, N. Ikeda, M. Ochiai, Y. Sugimoto, H. Fujikawa, M. Ozaki, Opt. Mater. Express **2**, 893 (2012)
143. H. Yoshida, Y. Tanaka, K. Kawamoto, H. Kubo, T. Tsuda, A. Fujii, S. Kuwabata, H. Kikuchi, M. Ozaki, Appl. Phys. Express **2**, 121501 (2009)
144. T. Kato, Angew. Chem. Int. Ed. **49**(43), 7847 (2010)
145. T. Kato, N. Mizoshita, K. Kishimoto, Angew. Chem. Int. Ed. **45**(1), 38 (2006)
146. T. Kato, Science **295**, 2414 (2002)
147. T. Kato, Chemistry Today (July 2001), p. 24
148. M. Funahashi, H. Shimura, M. Yoshio, T. Kato, Struct. Bond. **128**, 151 (2008)
149. T. Kato, M. Yoshio, in *Electrochemical Aspects of Ionic Liquids*, ed. by H. Ohno, (Wiley 2005), Chapter 25, p. 307
150. T. Kato, Struct. Bond. **96**, 95 (2000)
151. T. Kato, Macromol. Symp. **98**(1), 311 (1995)
152. T. Kato, Chem. Chem. Ind. **58**, 561 (2005)

153. H. Kihara, T. Kato, T. Uryu, J.M.J. Fréchet, Chem. Mater. **8**(4), 961 (1996)
154. V. Percec, G. Johansson, J. Heck, G. Ungar, S.V. Batty, J. Chem. Soc. Perkin Trans. **1**, 1411 (1993)
155. T. Ohtake, K. Ito, N. Nishina, H. Kihara, H. Ohno, T. Kato, Polym. J. **31**(11–2), 1155 (1999)
156. T. Ohtake, M. Ogasawara, K. Ito-Akita, N. Nishina, S. Ujiie, H. Ohno, T. Kato, Chem. Mater. **12**(3), 782 (2000)
157. T. Ohtake, Y. Takamitsu, K. Ito-Akita, K. Kanie, M. Yoshizawa, T. Mukai, H. Ohno, T. Kato, Macromolecules **33**(21), 8109 (2000)
158. K. Hoshino, K. Kanie, T. Ohtake, T. Mukai, M. Yoshizawa, S. Ujiie, H. Ohno, T. Kato, Macromol. Chem. Phys. **203**, 1547 (2002)
159. K. Kishimoto, M. Yoshio, T. Mukai, M. Yoshizawa, H. Ohno, T. Kato, J. Am. Chem. Soc. **125**(11), 3196 (2003)
160. K. Kishimoto, T. Suzawa, T. Yokota, T. Mukai, H. Ohno, T. Kato, J. Am. Chem. Soc. **127**(44), 15618 (2005)
161. Y. Iinuma, K. Kishimoto, Y. Sagara, M. Yoshio, T. Mukai, I. Kobayashi, H. Ohno, T. Kato, Macromolecules **40**(14), 4874 (2007)
162. H. Ohno, in *Ionic Liquid II-Marvelous Developments and Colorful Near Future*, Tokyo (CMC Publishing Co., Ltd., 2006); H. Ohno, in *Ionic Liquids: The Front and Future of Material Development*, (CMC Publishing Co., Ltd., 2003)
163. H. Ohno, in *Electrochemical Aspects of Ionic Liquids* (Wiley, 2005)
164. H. Ohno, Bull. Chem. Soc. Jpn. **79**(11), 1665 (2006)
165. T. Kato, Chemistry Today (March 2007), p.52
166. M. Yoshio, T. Kato, J. Surf. Sci. Soc. Jpn. **28**, 318 (2007)
167. M. Yoshio, T. Katoin *Ionic Liquid II-Marvelous Developments and Colorful Near Future*, ed. by H. Ohno, (Tokyo CMC Publishing Co., Ltd., 2006) Chapter 22, p. 266; H. Ohno (ed.) *Ionic Liquids: The Front and Future of Material Development* (CMC Publishing Co., Ltd., 2003), Chapter 5, p. 161
168. T. Mukai, M. Yoshio, H. Ohno, T. Kato, Expected materials for the future, **6**(2), 2 (2006)
169. T. Kato, K. Kanie, M. Yoshio, H. Ono, M. Yoshizawa, Japanese Unexamined Patent Application Publication No. 2002-358821 (Priority Date: 30 March, 2001); T. Kato, K. Kanie, M. Yoshio, H. Ohno, M. Yoshizawa, US 7,166,238 B2
170. M. Yoshio, T. Mukai, K. Kanie, M. Yoshizawa, H. Ohno, T. Kato, Adv. Mater. **14**(5), 351 (2002)
171. T. Kato, T. Kawakami, Chem. Lett. **26**(3), 211 (1997)
172. M. Yoshio, T. Mukai, M. Yoshizawa, H. Ohno, T. Kato, Mol. Cryst. Liq. Cryst. **413**, 99 (2004)
173. H. Shimura, M. Yoshio, K. Hoshino, T. Mukai, H. Ohno, T. Kato, J. Am. Chem. Soc. **130**(5), 1759 (2008)
174. S. Ujiie, Ekisho **10**(2), 121 (2006)
175. K. Binnemans, Chem. Rev. **105**(11), 4148 (2005)
176. C. J. Bowlas, D. W. Bruce, K. R. Seddon, Chem. Commun. 1625 (1996)
177. C.M. Gordon, J.H. Holbrey, A.R. Kennedy, K.R. Seddon, J. Mater. Chem. **8**(12), 2627 (1998)
178. J. D. Holbrey, K. R. Seddon, J. Chem. Soc. Dalton Trans. 2133 (1999)
179. M. Yoshio, T. Mukai, K. Kanie, M. Yoshizawa, H. Ohno, T. Kato, Chem. Lett. **31**(3), 320 (2002)
180. M. Yoshio, T. Mukai, H. Ohno, T. Kato, J. Am. Chem. Soc. **126**(4), 994 (2004)
181. K. Hoshino, M. Yoshio, T. Mukai, K. Kishimoto, H. Ohno, T. Kato, J. Polym. Sci. Part A Polym. Chem. **41**(22), 3486 (2003)
182. M. Yoshio, T. Kagata, K. Hoshino, T. Mukai, H. Ohno, T. Kato, J. Am. Chem. Soc. **128**(16), 5570 (2006)
183. M. Yoshio, T. Ichikawa, H. Shimura, T. Kagata, A. Hamasaki, T. Mukai, H. Ohno, T. Kato, Bull. Chem. Soc. Jpn. **80**(9), 1836 (2007)

184. T. Ichikawa, M. Yoshio, A. Hamasaki, T. Mukai, H. Ohno, T. Kato, J. Am. Chem. Soc. **129** (35), 10662 (2007)
185. T. Ichikawa, M. Yoshio, A. Hamasaki, J. Kagimoto, H. Ohno, T. Kato, J. Am. Chem. Soc. **132**(28), 9555 (2011)
186. T. Ichikawa, M. Yoshio, A. Hamasaki, S. Taguchi, F. Liu, X. Zeng, G. Unger, H. Ohno, T. Kato, J. Am. Chem. **134**, 2634 (2012)
187. T. Ichikawa, M. Yoshio, S. Taguchi, J. Kagimoto, H. Ohno, T. Kato, Chem. Sci. **3**(6), 2001 (2012)
188. M. Henmi, K. Nakatsuji, T. Ichikawa, H. Tomioka, T. Sakamoto, M. Yoshio, T. Kato, Adv. Mater. **24**(17), 2238 (2012)
189. D. Dunmur, T. Sluckin, *Soap, Science, and Flat-screen TVs: A History of Liquid Crystals* London (Oxford University Press, 2011)
190. S. R. Goodman, *Medical Cell Biology* (Academic, 2007)
191. T. Tani, K. Ohta, in *Proceedings of 2004 Conference of The Japanese Liquid Crystal Society*, vol 390 (2004)
192. L. Stevenson, D.B. Bennet, D. Lechuga-Ballesteros, J. Pharmaceutic. Sci. **94**, 1861 (2005)
193. A. Fatta, J. Zhang, D.B. Bennett, D. Lechuga, Pharm. Sci. **4**, M1286 (2003)
194. A.J. Primeau, A. Rendon, D. Hedley, L. Ligle, F. Tannock, Clin. Cancer Res. **11**, 8782 (2005)
195. N. Tang, G. Du, N. Wang, C. Liu, H. Hang, W. Liang, J. Natl. Cancer Inst. **99**, 1004 (2007)
196. M. Grinda, J. Clarhaut, B. Renoux, I. Tranoy-Opalinski, S. Papot, Med. Chem. Commun. **3**, 68 (2012)
197. A. Yoshizawa, Y. Takahashi, R. Terasawa, S. Chiba, K. Takahashi, M. Hazawa, I. Kashiwakura, Chem. Lett. **38**, 310 (2009)
198. A. Yoshizawa, Y. Takahashi, R. Terasawa, A. Nishizawa, K. Takeuchi, M. Sagisaaka, K. Takahashi, M. Hazawa, I. Kashiwakura, Chem. Lett. **38**, 530 (2009)
199. V. Percec, M. Lee, C. Ackerman, Polymer **22**, 703 (1992)
200. A. Griffin, S.R. Vidya, Mol. Cryst. Liq. Cryst. **173**, 75 (1989)
201. V. Percec, M. Lee, Macromolecules **24**, 1017 (1991)
202. Y. Takahashi, M. Hazawa, K. Takahazhi, M. Sagisaka, I. Kashiwakura, A. Yoshizawa, Med. Chem. Commun. **2**, 55 (2011)
203. Y. Fukushi, A. Yoshizawa, EKISHO **16**, 21 (2012)
204. V.K. Gupta, J.J. Skaife, T.B. Dubrovsky, N.L. Abbott, Science **279**, 2077 (1998)
205. A. Gabizon, R. Catane, B. Uziely, Cancer Res. **54**, 987 (1994)
206. R. Negrini, R. Mezzenga, Langmuir **27**, 5296 (2011)
207. T. Wakasaya, H. Yoshino, Y. Fukushi, A. Yoshizawa, I. Kashiwakura, Int. J. Oncology **42**, 1205 (2013)
208. Y. Fukushi, M. Hazawa, K. Takahashi, A. Yoshizawa, I. Kashiwakura, Invest. New Drugs **29**, 827 (2011)

Appendix: Liquid Crystal Chronology

LC Milestone Chart

Publication

1963	Williams domain	R. Williams	J. Chem. Phys. **39**, 384 (1963)
1964	GH (guest-host) mode	G.H. Heilmeier, L.A. Zanoni	Appl. Phys. Lett. **13**, 91 (1968)
	Thermography using cholesterics	J.A.F. Fergason	Sci. Am. **211**(2), 76 (1964)
1966	DS (dynamic scattering) mode	G.H. Heilmeier et al.	Proc. IEEE **56**, 1162 (1968)
1967	Room temp, apolar Schiff base LC mixtures	J.A. Castellano	(US Patent)
	Concept of eutectic LC mixture formulation	D. Demus (Halle Univ.)	Naturforsch. **22**, 285 (1967)
1968	Electric-field-induced cholesteric-nematic transition	J.J. Wysocki et al.	Phys. Rev. Lett. **20**, 1024 (1968)
	ditto	R.B. Meyer	Appl. Phys. Lett. **12**, 281 (1968)
	ditto	P.G. de Gennes	Solid State Commun. **6**, 163 (1968)
	Demonstration of first LCDs	RCA	(Press Conference, New York)
1969	Room temp, DS-LCD use LC compounds (MBBA, EBBA, BBBA)	H. Kelker, B. Scheurle	Angew. Chem. **81**, 903 (1969)
1970	DS-LCD use ester compounds	Halle Univ.	(German Patent)
	DS-LCD use azoxy compounds	H. Kelker et al.	Angew. Chem. **82**, 984 (1970)
	DAP (deformation of vertically aligned phse) effect	W. Hass et al.	Phys. Rev. Lett. **25**, 1326 (1970)

(continued)

(continued)

1971	VA (vertically alignment) mode	M.F. Schiekel, K. Fahrenschon	Appl. Phys. Lett. **19**, 391 (1971)
	ditto	G. Assoulin et al.	Electronics Lett. **7**, 699 (1971)
	TN (twisted nematic) mode	M. Schadt, W. Helfrich	Appl. Phys. Lett. **18**, 127 (1971)
	TFT-array addressed DSM-LSD	B.J. Lechner et al.	Proc. IEEE **59**, 1566 (1971)
1972	4×4 matrix to model LCD configurations	D.W. Berreman	J. Opt. Soc. Am. **62**, 502 (1972)
	Alignment by oblique evaporation	J. Janning	Appl. Phys. Lett. **21**, 173 (1972)
	Concept of mosaic color filters for color LCDs	A.G. Fisher	IEEE Conference on Display Devices, vol. 64 (1972)
1973	Clock CMOS driving circuit for pocket calculators	Y. Suzuki et al.	Proceedings of International Solid State Circuit Conference, vol. 58 (1973)
	Demus alkyl-alkoxy cyclo-hexane ester LC compounds	J. Malthete et al.	Mol. Cryst. Liq. Cryst. **23**, 233 (1973)
	Biphenyl LC compounds	G.W. Gray et al.	Electronics Lett. **9**, 130 (1973)
	Inter-digital-electrode LCD configuration	R.A. Soref	Appl. Phys. Lett. **22**, 165 (1973)
1974	White-Taylor cholesteric GH mode	D.L. White, G.N. Taylor	J. Appl. Phys. **45**, 4718 (1974)
	1st and 2nd minimum conditions of TN mode, understood	C.H. Gooch, H.A. Tarry	Electron. Lett. **10**, 2 (1974)
	Suppressing reverse-twist/ tilt of TN-LCD	A. Sussman	IEEE Transactions on Parts, Hybrids, Packaging. PHP-8, vol. 24 (1972)
	ditto	E.P. Raynes	Electron. Lett. **10**, 141 (1974)
	Optimized multiplex driving	H. Kawakami	(US Patent)
	ditto	P.M. Alt, P. Pleshko	IEEE Transactions on Electron Devices, 146 (1974) ED-21
	Field-sequential color LCD	I.A. Shanks	Electron. Lett. **10**, 90 (1974)
1975	Ferroelectric LC compound (DOBAMBC)	R.B. Meyer et al.	J. de Phys. Lett. **36**, 69 (1975)
1977	Cyano-phenylcyclohexane LC compounds	R. Eidenschink et al.	Angew. Chem. **89**, 103 (1977)
	Electro-clinic effect of ferroelectric LCs	S. Garoff, R.B. Meyer	Phys. Rev. Lett. **38**, 848 (1977)
1978	Image generation by CdSe-TFT LCD	F.C. Luo et al.	Proceedings of SID, vol. 94 (1978)
1979	Trial-production and application-proposal of a-Si TFT	P.G. Le Comber et al.	Electron. Lett. **15**, 179 (1979)
1980	Surface-stabilized ferroelectric LC (SSFLC) mode	N.A. Clark, S.T. Lagerwall	Appl. Phys. Lett. **36**, 899 (1980)
1981	$360°$ bistable TN LC cell	Berreman, Heffner	J. Appl. Phys. **52**, 3032(1981)

(continued)

	a-Si TFT-Array addressed 5 × 7 dots LCD	A.I. Snell et al.	ESS-DERC Europhysics Conf. (1980) 99
	Additive-mixture color LCD by color filter array	T. Uchida (Tohoku Univ.)	Europian Display Conference, vol. 39 (1981)
1982	Super-twisted GH mode	Waters and Raynes	UK Patent, Proceedings of 3rd IDRC, vol. 396 (Kobe, Japan, 1983)
	a-Si TFT Addressed 96 mm × 96 mm, 240 × 240 dots LCD	Y. Okubo, et al. (Canon)	
1983	Te TFT-Array addressed 2inx2in, 50 × 50 dots LCD	M. Matsuura et al. (Sharp)	Proceedings of SID, vol. 148 (1982)
	2.13in Full-color LCD addressed by poly-Si array on quartz substrate	S. Morozumi et al. (Seiko-Epson)	Proceedings of SID, vol. 156 (1982)
	a-Si TFT Addressed 40 mm × 60 mm, 240 × 220 dots LCD	K. Suzuki et al. (Toshiba)	Proceedings of SID (1982)
1984	STN (super twisted nematic) mode	T.J. Scheffer, J. Nehring	Appl. Phys. Lett. **45**, 1021 (1984)
	π-Cell (bend alignment cell)	P.J. Bos et al.	Mol. Cryst. Liq. Cryst. **113**, 329 (1984)
1986	a-Si TFT Addressed 3in, 378 × 240 dots full-color LC-TV	S. Hotta et al. (Matsushita)	Proceedings of SID, vol. 296 (1986)
1987	Double-layer STN-LCD with optical retarder film	K. Katoh et al. (Asahi Glass)	Jpn. J. Appl. Phys. **26**, L1784 (1987)
	Flexoelectric effect of short-pitch cholesterics	J.S. Patel, R.B. Meyer	Phys. Rev. Lett. **58**, 1538 (1987)
1988	Color image by double-layer STN-LCD	N. Kimura et al. (Sharp)	Proceedings of SID, vol. 49 (1988)
	ditto	H. Koh et al. (Asahi Glass)	Proceedings of SID, vol. 53 (1988)
	ditto	H. Watanabe et al. (Seiko-Epson)	Proceedings of SID, vol. 416 (1988)
	Anti-ferroelectric LC, discovered	A.D.L. Chandani et al. (TIT)	Jpn. J. Appl. Phys. **27**, L729 (1988)
	Concept of AF (anti-ferroelectric) LCD	N. Hiji et al. (TIT)	Ferroelectrics **85**, 99(1988)
1991	Two-domain TN/VA mode	K.H. Yang	Proceedings of IDRC, vol. 68
	LC photo-alignment	W. Gibbons	Nature **351**, 49(1991)
1992	MLA (multi-line addressing) scheme	S. Ihara et al. (Asahi Glass)	Proceedings of SID, vol. 232 (1992)
	Active addressing scheme	T.J. Scheffer et al.	Proceedings of SID, vol. 228 (1992)
	Overdrive addressing scheme	H. Okumura, H. Fujiwara (Toshiba)	Proceedings of SID, vol. 601 (1992)
	Principle of wide-view IPS (in-plane switching)	R. Kiefer et al.	Proceedings of Japan Display'92, vol. 547 (1992)

(continued)

Year			
1993	OCB (optically compensated bend) mode	Y. Yamaguchi et al. (Tohoku Univ.)	Proceedings of SID, vol.277 (1993)
1994	Threshold-less AF-LCD	A. Fukuda et al. (TIT)	J. Mater. Chem. **4**, 997(1994)
1995	a-Si TFT Addressed IPS-LCD	M. Oh-e et al. (Hitachi)	Proceedings of Asia Display'95, vol. 707 (1995)
1997	a-Si TFT Addressed MVA-LCD	K. Ohmuro et al. (Fujitsu)	Proceedings of SID, vol. 845 (1997)
	Polymer-stabilized V-shape F-LCD	S. Kataoka et al. (TUS-Yamaguchi)	Mol. Cryst. Liq. Cryst. **292**, 333(1997)
	ditto	H. Furue et al. (TUS-Yamaguchi)	Jpn. J. Appl. Phys. Part 2 **36**, L1517 (1997)
1998	PVA (patterned VA) LCD	K.H. Kim et al. (samsung)	Proceedings of Asia Display'98, vol. 383 (1998)
	FFS (fringe field switching) LCD	S.H. Lee et al. (Hyundai)	Appl. Phys. Lett. **73**, 2881 (1998)
2002	Polymer stabilization choresteric BP (blue phase)	H. Kikuchi et al. (Kyushu Univ.)	Nat. Mater. **1**, 64(2002)
2007	180Hz Addressed IPS-Pro LCD-TV	I. Mori et al. (Hitachi)	Proceedings of IDW, vol. 79 (2007)
2008	Characterization of nanoparticle doped LCDs	S. Kobayashi et al. (TUS-Yamaguchi)	J. SID **16**, 871 (2008)
2009	240Hz Addressed full-HD LCD-TV	S.S. Kim et al.	Proceedings of SID, vol. 424 (2009)
	USH (uniformly-standing-helix) mode	H.H. Lee et al. (Kyushu Univ.)	J. Appl. Phys. **106**, 014503 (2009)
2011	Field-sequential color image generation by narrow-gap TN LCD	S. Kobayashi et al. (TUS-Yamaguchi)	J. SID, **19/11**, 787 (2011)
	Polymer-stabilized ULH (uniformly-lying-helix) mode	D.J. Gardiner et al.	Appl. Phys. Lett. **99,** 261903 (2011)
	Polymer-stabilized USH mode	V.P. Panov et al.	Appl. Phys. Lett. **98**, 263508 (2011)
2012	ULH mode	D.J. Gardiner et al.	Appl. Phys. Lett. **100**, 063501 (2012)

TIT: Tokyo Institute of Technology, *TUS-Yamaguchi*: Tokyo University of Science in Yamaguchi

Product

1971	First commercial of TN-LCD use cyano LC mixturees	Roche
1973	Pocket calculator using DSM-LCD	Sharp
	Wrist watch using TN-LCD	Seiko, Casio
1974	Commercial production of biphenyl LC mixtures	BDH

(continued)

(continued)

1976	Pocket calculator using TN-LCD	Sharp
1978	1/16 Duty addressed TN-LCDs	Hitachi
1982	1/32 Duty addressed TN-LCDs	Shinshu-seiki, Sharp, Hitachi
	Wrist watch TV using cryst-Si TFT addressed 152×210 dots GH-LCD	Seiko
1983	1/64 Duty addressed TN-LCDs	Sharp, Optrex, etc.
	Simple matrix 2.7-size B/W LCD-TV	Casio
1984	Poly-Si TFT addressed 2-size color LCD-TV	Seiko
1985	1/200 Duty addressed STN-LCD	Sharp, Hitachi, Daini-Seiko, etc.
	Simple matrix 2.6-/2.7-size color LCD-TV	Casio/Citizen
1986	Word processor using large-size STN-LCD	Fujitsu, Matsushita, etc.
	Portable PC using 640×400 dots LCD	NEC
1987	DSTN (double STN)/NTN (neutralized TN) B/W LCD	Sharp/Seiko-Epson, etc.
	Mechanically stretched optical retarder films	Nitto Denko, Sumitomo Chem.
	a-Si TFT Addressed 6-size color LCD-TV	Hitachi
1988	640×400 Dots blue-mode STN-LCDs, commercialized	
	STN-LCDs (FTN, FSTN, TSTN) using mechanically stretched optical retarder films	Sharp, Seiko-Epson
	Commercial production of pigment-based color filters	DNP
	1120×1120 Dots 14-size FLCD, developed	Canon
1989	Commercial production of fluorinated LC mixtures	Chisso, Merck
1990	Fluorinated LC mixtures with large negative dielectric anisotropy	Merck
	Subtractive-mixture LCD projector using stacked STN-LCDs	
	Lap-top PC using a-Si TFT addressed 640×400 color-pixels LCD	NEC
1992	Dual-scanning color STN-LCD, developed for Note-PC use	
	LTPS-array fabrication on large-size glass substrate	Xerox
	Application of AM-LCD to Note-PC	IBM
1993	Cholesteric bistable reflective LCD	KSU/KDI
1995	Commercial production of IPS-LCD	Hitachi
	Multi-layer brightness enhancement films (BEF, DBEF)	3M
1996	Commercialization of 2.6-size LTPS-TN LCD for VTR use	Sanyo
1997	15-size MVA (multi-domain vertical alignment) LCD monitor	Fujitsu
	Discotic-LC wide-view film for TFT-TN LCDs	Fujifilm
1998	Mass-production of 10.4-size XGA-format LTPS-LCD for Note-PC use	
	PVA-LCD	Samsung
	FFS-LCD	Hyundai
	ASV (axially symmetric vertical alignment) LCD	Sharp
	Super-IPS LCD with reduced color shift	Hitachi
	Commercialization of 15-size LCD-TV	
1999	Commercialization of 20-size LCD-TV	Sharp

(continued)

2000	Transflective AM-LCD	Sharp
2001	LC one-drop filling and cell mating in vacuum for large-size LCDs	
	Commercialization of 30-size LCD-TV	
2002	Commercialization of 37-size LCD-TV	
	AS (advanced-super) IPS-LCD with improved transmittance	Hitachi
2003	BiNem LCD for e-book application	
2004	OCB-LCD	Matsushita
	IPS-Pro (provectus) LCD with improved contrast ratio	Hitachi
2005	65-size LCD-TV	
2007	LCD-TV over 100-size	
	Commercialization of ASV-LCD for mobile devices	Sharp
	H(horizontal)-IPS LCD with improved contrast ratio	LG
2008	Demonstration of polymer-stabilized BP-LCD	Samsung
	Wide use of LED back-lights	
	Commercialization of LC mixtures for PS(polymer-stabilized)-VA LCD use	Merck
2009	Photo-alignment applied in 10-generation plant	Sharp
	E(enhanced)-IPS LCD with improved transmittance	LG
2010	Commercialization of 3D LCD-TV	
	Commercialization of LCD-TV using color filter with 4 primary colors	Sharp
	P(professional)-IPS LCD with 1.07 million colors	LG
2011	Commercialization of LCDs using IGZO semi-conductors	Sharp
	Super-PLS (plane to line switching) LCD monitor	Samsung
	AH(advanced high performance)-IPS LCD with improved resolution	LG

KSU/*KDI* Kent State Univ./Kent Displays Inc